Medical Radiology · Diagnostic Imaging
Series Editors: Hans-Ulrich Kauczor · Paul M. Parizel · Wilfred C. G. Peh

Mizuki Nishino *Editor*

Therapy Response Imaging in Oncology

Springer

Medical Radiology

Diagnostic Imaging

For further volumes:
http://www.springer.com/series/4354

Mizuki Nishino
Editor

Therapy Response Imaging in Oncology

Springer

Editor
Mizuki Nishino
Dana-Farber Cancer Institute
and Brigham and Women's Hospital
Harvard Medical School
Boston, MA
USA

ISSN 0942-5373 ISSN 2197-4187 (electronic)
Medical Radiology
ISBN 978-3-030-31170-4 ISBN 978-3-030-31171-1 (eBook)
https://doi.org/10.1007/978-3-030-31171-1

This Springer imprint is published by the registered company Springer Nature Switzerland AG
The registered company address is: Gewerbestrasse 11, 6330 Cham, Switzerland

“To Julica, Ayaka, and Hiroto”.

Contents

Part I

Imaging as a "Common Language" for Treatment Response Evaluations in Oncology

Conventional Tumor Response Criteria and Limitations

Mizuki Nishino

Contents

Abstract

Objective evaluation of tumor response to therapy has been a basis for advances of effective cancer therapies, and has contributed significantly to marked progress in the treatment approaches for cancer patients in the past decades. Imaging plays a key role in objectively characterizing tumor response and progression during therapy, thus providing trial endpoints that help to determine regulatory approvals of new agents and informing treating physicians for their treatment decisions. Several conventional tumor response criteria based on imaging have been proposed and utilized in the past few decades, and have been updated to meet the needs for the current era of cancer treatment. This chapter will (1) review the concept and goals of tumor response criteria, (2) describe introduction and revisions of Response Evaluation Criteria for Solid Tumors (RECIST) as a major standardized criteria to date, and (3) discuss the limitations of RECIST. This chapter focuses on the tumor response criteria for solid tumors, and criteria for lymphoma and other hematologic malignancies are discussed separately in the subsequent chapter in the book (chapter "Therapy Response Imaging in Lymphoma and Hematologic Malignancies").

M. Nishino (✉)
Department of Imaging, Dana-Farber Cancer Institute, Boston, MA, USA

Department of Radiology, Brigham and Women's Hospital, Boston, MA, USA
e-mail: mizuki_nishino@dfci.harvard.edu

M. Nishino (ed.), *Therapy Response Imaging in Oncology*, Medical Radiology, Diagnostic Imaging,
https://doi.org/10.1007/978-3-030-31171-1_1

1 The Concept and Goals of Tumor Response Criteria

The origin of tumor response criteria using imaging dates back to 1981, when Miller et al. described the essentials of tumor response assessment in the publication of World Health Organization (WHO) criteria (Miller et al. 1981). In the article, the importance of a "common language" to describe the results of lung cancer treatment is emphasized, and the need for internationally acceptable general principles for reporting and assessing data is highlighted (Miller et al. 1981). For this purpose, the essential elements of tumor response criteria to serve as a common language were described, including (1) the concept of measurability of the disease, in which malignant disease can be measured in metric system, (2) definitions of objective response categories using the thresholds of quantitative tumor burden changes and the qualitative changes, and (3) guidance to determine overall response and duration of response (Miller et al. 1981). The concept of tumor response criteria and the definitions of essential terminology introduced by the article have contributed significantly to standardize the methods for tumor response evaluations and the description of cancer treatment results (Nishino et al. 2014a). Notably, though published nearly 40 years ago, the message by Miller et al. remains pertinent in the current practice of clinical oncology and oncologic imaging, and helps to remind us that the goal of tumor response evaluations is to provide a common language to address the results of cancer therapy that forms the basis for advances of treatment approaches for cancer patients (Miller et al. 1981; Nishino et al. 2014a).

2 RECIST as Standardized Tumor Response Criteria: Introduction and Revisions

WHO criteria for tumor response assessment have introduced the important concepts, and defined the measurability of the tumor burden using the product of the longest diameter and the longest perpendicular diameter of the lesion. It also defined the four categories of response and progression that formed a basis of the tumor response categorization that remains in use today (Table 1) (Nishino et al. 2010a). However, due to advances of cancer treatment and rapid progress of imaging technology over time, the shortcomings of WHO criteria have become apparent. In particular, WHO criteria did not mention the types of the imaging modality to be used, did not clearly define the minimal size of the lesions for measurements, and did not determine the number of lesions to be measured (Nishino et al. 2010a; Therasse et al. 2000). To meet the increasing needs, Response Evaluation Criteria for Solid Tumors (RECIST) was introduced by the international working party in 2000 to simplify and standardize tumor response evaluations. The original RECIST, currently referred as RECIST version 1.0 (RECIST 1.0), has been quickly incorporated into the majority of solid tumor clinical trials after 2000, and has provided trial endpoints and the basis for approvals of new cancer therapies. RECIST was revised in 2009 to further update the methods with several important modifications, which is known as RECIST version 1.1 (RECIST 1.1). RECIST 1.1 again readily became the standard to describe results of cancer treatment after 2009, and currently serves as the major, generalized criteria to define response and progression during therapy for advanced solid tumors (Nishino et al. 2010a; Therasse et al. 2000). The details of WHO criteria, RECIST 1.0, and RECIST 1.1 are summarized in Table 1.

The original RECIST introduced in 2000 had several key features, including definitions of the minimum size of measurable lesions, instructions about how many lesions to follow, and the use of unidimensional measures for evaluation of overall tumor burden (Nishino et al. 2010a; Therasse et al. 2000). "Measurable" lesions were defined as lesions with a longest diameter of ≥10 mm on CT with a slice thickness of ≤5 mm (or a longest diameter of ≥20 mm on nonhelical CT with a slice thickness of >10 mm) or a longest diameter of ≥20 mm on chest radiography (Figs. 1 and 2). "Nonmeasurable" lesions were defined as lesions that do not meet the criteria for

Table 1 Summary of tumor response assessment by WHO criteria, RECIST 1.0, and RECIST 1.1 (Miller et al. 1981; Nishino et al. 2014a, 2012; Therasse et al. 2000; Eisenhauer et al. 2009)

	WHO (1979)	RECIST 1.0 (2000)	RECIST 1.1 (2009)
Measurement Strategies			
Imaging modality	No particular mention of imaging modality	CT, MR imaging, and chest radiography are recommended	CT, MR imaging, and chest radiography are recommended FDG-PET scan is included in detection of new lesions
Measurement	LD × SD (cm^2)	LD (cm)	LD (cm) for non-nodal lesions SD for lymph nodes
Measurable lesions	No mention of minimal size of the lesion	LD ≥ 10 mm on CT[a]	LD ≥ 10 mm on CT for non-nodal lesions[c] SD ≥ 15 mm for lymph nodes
Number of target lesions	Not mentioned	Up to 5 per organ Up to 10 in total	Up to 2 per organ Up to 5 in total
Criteria for response categories			
CR	Disappearance of all known disease	Disappearance of all target and nontarget lesions	Disappearance of all target and nontarget lesions, except that lymph nodes are <10 mm in SD
PR[b]	≥50% decrease	≥30% decrease	≥30% decrease
SD	Neither CR, PR or PD	Neither CR, PR or PD	Neither CR, PR or PD
PD[c]	≥25% increase of target lesions, new lesion, or nontarget PD	≥20% increase of target lesions, new lesion, or nontarget PD	≥20% and ≥ 5 mm increase of target lesions, new lesion, or nontarget PD

LD longest diameter, *SD* short-axis diameter (the longest perpendicular diameter), *CR* complete response, *PR* partial response, *PD* progressive disease

[a]With a section thickness of ≤5 mm. Measurable lesions have to be ≥20 mm at nonhelical CT with a section thickness of 10 mm, and LD ≥ 20 mm at chest radiography

[b]The percent change is calculated in comparison with the measurements at baseline

[c]The percent change is calculated in comparison with the measurements at the nadir (the smallest tumor burden since baseline)

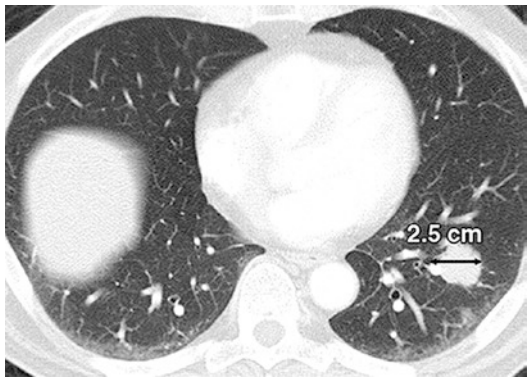

Fig. 1 Measurable lesions according to RECIST. CT scan of chest in 64-year-old man with colon cancer. Lobulated nodule in left lower lobe representing metastasis measures 2.5 cm in longest diameter (arrow), meeting criteria for measurable lesion on CT (longest diameter ≥ 10 mm). (Reprinted with permission from AJR Am J Roentgenol. 2010;195: 281–289)

measurable lesions, such as small lesions measuring less than 10 mm on CT, skeletal metastases without a soft-tissue component, ascites, pleural effusion, lymphangitic spread of tumor, leptomeningeal disease, inflammatory breast disease, cystic or necrotic lesions, lesions in an irradiated area, and an abdominal mass not confirmed by imaging (Figs. 3–6) (Nishino et al. 2010a; Therasse et al. 2000).

Once measurable and nonmeasurable lesions are identified on the baseline imaging prior to therapy, target lesions are selected at baseline based on the size (the longest diameter) and suitability for accurate measurements on the follow-up imaging studies during therapy. Up to 5 per organ and 10 total target lesions can be selected at baseline per RECIST 1.0 (Nishino et al. 2010a; Therasse et al. 2000). The sum of the longest

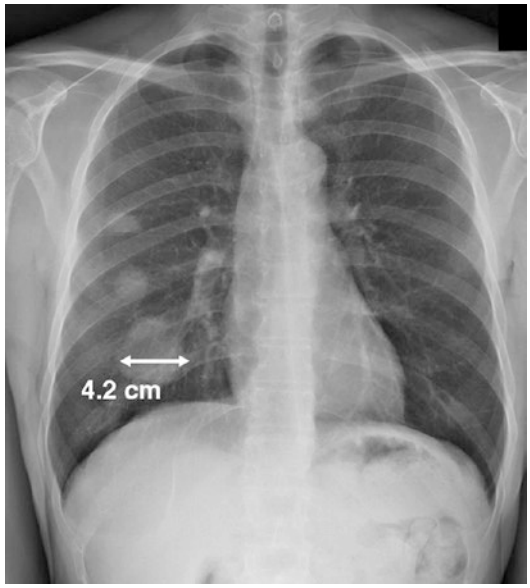

Fig. 2 Measurable lesions according to RECIST. Frontal chest radiograph in 52-year-old woman shows mass with longest diameter of 4.2 cm (arrow) representing lung cancer, which meets criteria for measurable lesion on chest radiography (longest diameter ≥ 20 mm). (Reprinted with permission from AJR Am J Roentgenol. 2010;195: 281–289)

Fig. 3 Nonmeasurable lesions according to RECIST. CT scan of chest in 52-year-old woman with lung cancer shows multiple small nodules in lungs measuring less than 10 mm; these nodules are miliary metastases. (Reprinted with permission from AJR Am J Roentgenol. 2010;195: 281–289)

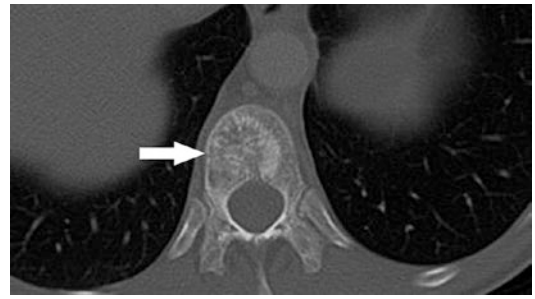

Fig. 4 Nonmeasurable lesions according to RECIST. CT scan at level of lung bases in 59-year-old woman with breast cancer shows sclerotic osseous metastasis (arrow). (Reprinted with permission from AJR Am J Roentgenol. 2010;195: 281–289)

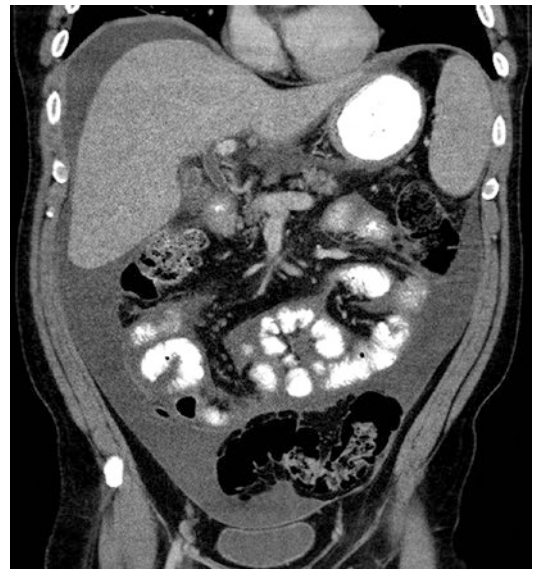

Fig. 5 Nonmeasurable lesions according to RECIST. CT scan of abdomen in 45-year-old man with gastric cancer shows large amount of ascites. Cytology of fluid was positive for malignant cells, confirming malignant nature of fluid. (Reprinted with permission from AJR Am J Roentgenol. 2010;195: 281–289)

diameters for all target lesions is recorded at baseline and at the follow-up study to represent quantitative tumor burden. The percent change of the sum of the measurements on the follow-up study compared to baseline contributes to define response, and the percent change compared to the nadir (the smallest tumor measurements since baseline during therapy) contributes to define tumor progression. Nontarget lesions include all other lesions or sites of disease, and their presence or absence is recorded without measurements at baseline and follow-up examinations (Nishino et al. 2010a; Therasse et al. 2000). Four categorical responses, including complete response (CR), partial response (PR), stable disease (SD), and progressive disease (PD), are

Fig. 6 Nonmeasurable lesions according to RECIST. CT scan of chest in 70-year-old woman with lung cancer shows irregular thickening of interlobular septum and bronchovascular bundles in lower lobes; these findings are consistent with lymphangitic spread of lung cancer. (Reprinted with permission from AJR Am J Roentgenol. 2010;195: 281–289)

assigned according to RECIST (Table 1) (Fig. 7) (Nishino et al. 2010a; Therasse et al. 2000). Overall response is assigned at each follow-up imaging study, and best overall response (BOR) is assigned based on the best response among all follow-up time points during therapy (Nishino et al. 2010a; Therasse et al. 2000).

The revised RECIST guidelines, RECIST 1.1, were published by the RECIST Working Group in 2009, based on the assessment of a database consisting of more than 6500 patients with greater than 18,000 target lesions (Nishino et al. 2010a; Eisenhauer et al. 2009). Major changes in RECIST 1.1 related to imaging included (1) reduction of the number of target lesions to be measured, (2) definition of the assessment of

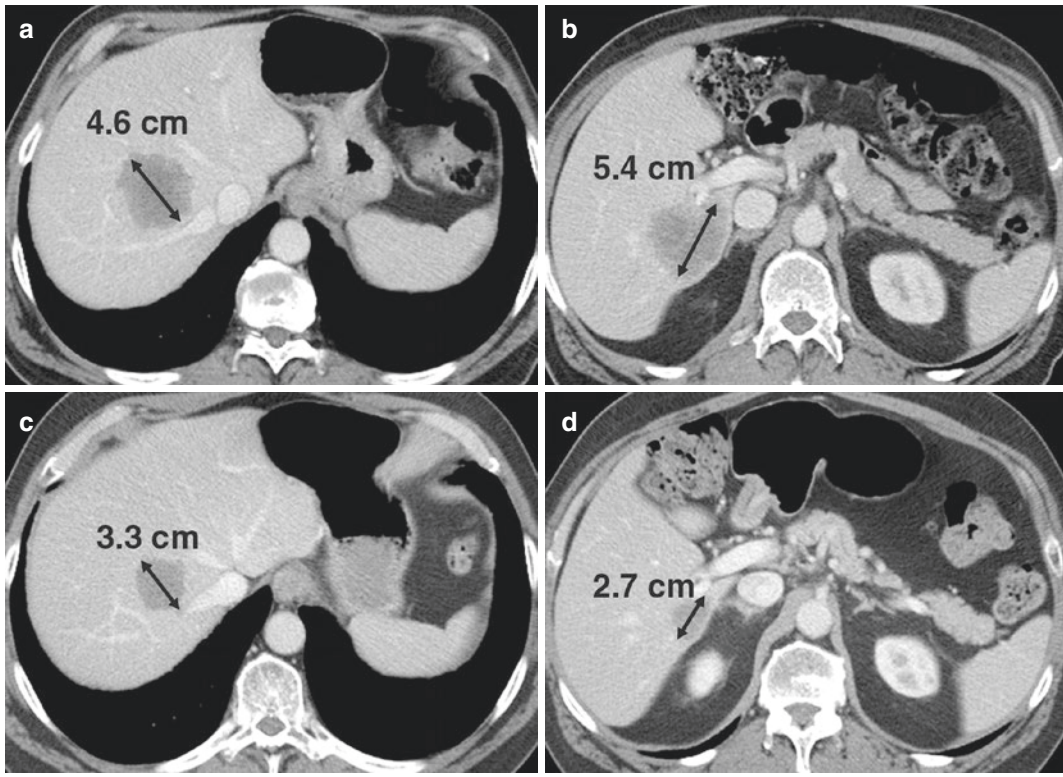

Fig. 7 (**a**, **b**) Baseline CT scans of abdomen in 68-year-old man with colon cancer show two target lesions (arrow) in liver. Measurements according to RECIST are 4.6 cm (**a**) and 5.4 cm (**b**), totaling 10.0 cm. (**c**, **d**) Follow-up CT scans obtained after initiation of therapy show decrease in size of target lesions (arrow). RECIST measurements are 3.3 cm (**c**) and 2.7 cm (**d**), totaling 6.0 cm. Given 40% decrease in sum of measurements of target lesions relative to baseline [(6–10 cm)/10 cm × 100], assessment of target lesions by RECIST is partial response. (Reprinted with permission from AJR Am J Roentgenol. 2010;195: 281–289)

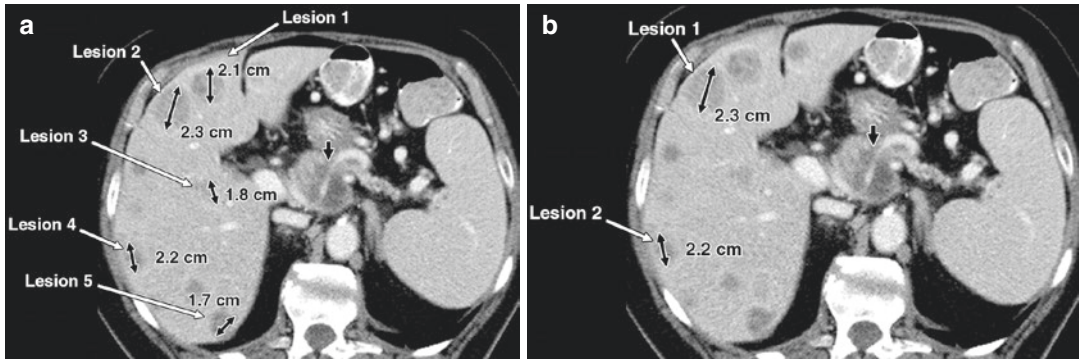

Fig. 8 Number of target lesions according to RECIST 1.1 has been reduced to up to two target lesions per organ. CT scan of abdomen in 72-year-old woman with pancreatic cancer shows dominant pancreatic mass (single-headed black arrow) with multiple metastatic lesions in liver. (**a**) Using RECIST 1.0, up to five lesions per organ (white arrows) could be selected. Double-headed black arrows show longest diameter of each lesion. (**b**) Using RECIST, version 1.1, which allows only up to two lesions per organ, only two liver lesions should be selected as target lesions (white arrows). Double-headed black arrows show longest diameter of each lesion. (Reprinted with permission from AJR Am J Roentgenol. 2010;195: 281–289)

pathologic lymph nodes, (3) clarification of disease progression, (4) clarification of unequivocal progression of nontarget lesions, and (5) inclusion of 18F-FDG PET in the detection of new lesions.

The number of target lesions to be assessed was reduced from maximum of 5 per organ to 2 per organ, and from a maximum of 10 in total to 5 in total (Figs. 8 and 9) (Nishino et al. 2010a; Eisenhauer et al. 2009). The change was based on the analysis of a large prospective database from 16 clinical trials that demonstrated that the assessment of 5 lesions per patient did not influence the overall response rate with minimal impact on progression-free survival (Nishino et al. 2010a; Eisenhauer et al. 2009).

RECIST 1.1 also defined the assessment of the lymph nodes, which was not clearly defined by RECIST 1.0 (Nishino et al. 2010a; Eisenhauer et al. 2009). According to RECIST 1.1, lymph nodes are measured using a short axis (the longest perpendicular diameter), and lymph nodes that are ≥15 mm in short axis are considered to be measurable and included as target lesions. Lymph nodes with a short axis of ≥10 mm but <15 mm are considered to be nontarget lesions (Fig. 10a) (Nishino et al. 2010a; Eisenhauer et al. 2009). Lymph nodes with a short axis of <10 mm are considered to be nonpathologic (Fig. 10b), which also affect the definitions of CR by RECIST 1.1 in that it requires all pathologic lymph nodes (whether target or nontarget) to be less than 10 mm in short axis (Nishino et al. 2010a; Eisenhauer et al. 2009).

PD for target lesions was modified by RECIST 1.1 and requires a 5-mm absolute increase of the sum of the target lesion measurement in addition to a 20% increase (Fig. 11) (Nishino et al. 2010a; Eisenhauer et al. 2009). The new criterion of a 5-mm absolute change in size was introduced to meet the needs to accurately define PD in patients with small tumor burden particularly after response to effective therapy, which is often encountered in the setting of precision cancer therapy using molecular targeting agents, which will be discussed further in chapter "Response Evaluations for Precision Cancer Therapy and Immunotherapy". In patients with small tumor burden at nadir (2 cm for example), a very small increase in size can be noted due to measurement variability without a true increase in tumor burden yet could meet the criterion of ≥20% increase by RECIST 1.0 (Nishino et al. 2010a; Eisenhauer et al. 2009). The absolute increase of 5 mm was introduced with an intention to better characterize tumor progression in such clinical scenarios.

"Unequivocal progression" of nontarget lesions was also clarified by RECIST 1.1. In patients with measurable tumor burden by target lesions, the overall level of substantial worsening in nontarget lesions leading to an increase of overall tumor burden even with SD or PR in

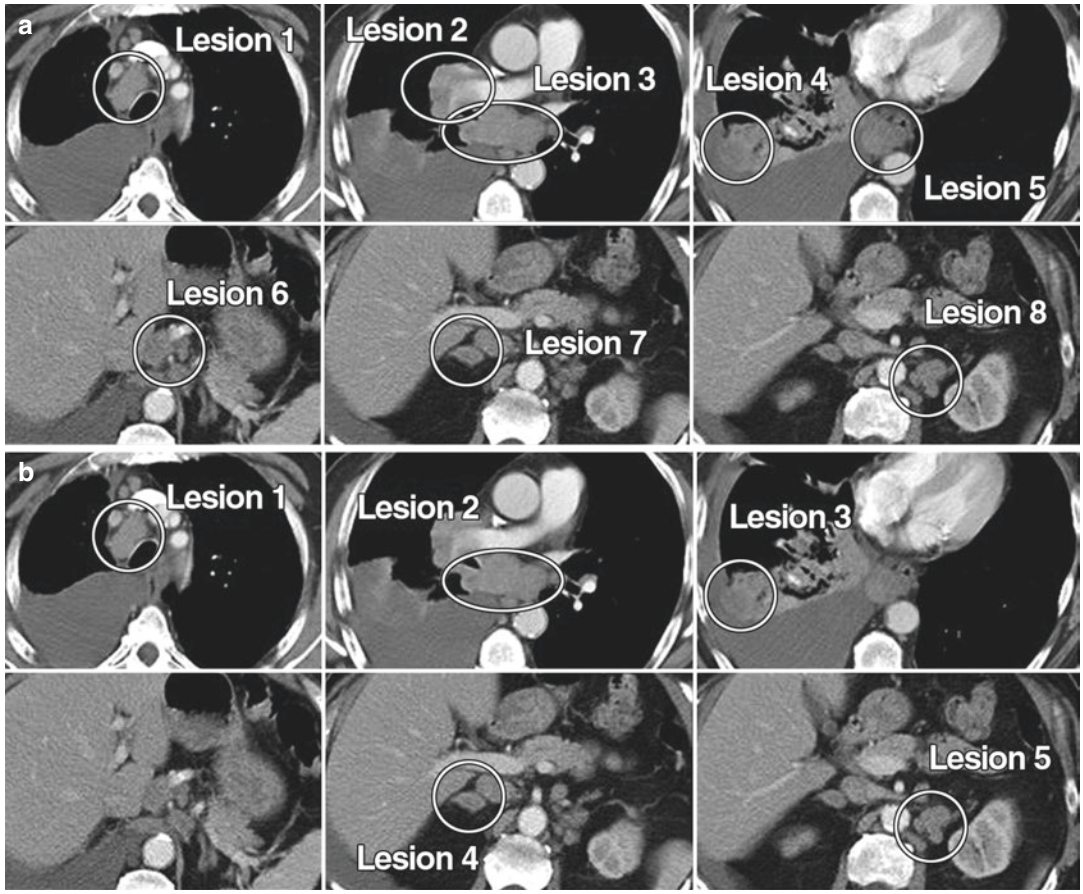

Fig. 9 Number of target lesions according to RECIST 1.1 has been reduced to up to five total. CT scans of chest in 74-year-old man with advanced NSCLC show multiple enlarged thoracic and upper abdominal lymph nodes, lesion in right lower lobe of lung, and bilateral adrenal metastases. (**a**) Using RECIST 1.0, which allows up to 10 lesions total, all eight lesions (circles) could be selected as target lesions. (**b**) Using RECIST 1.1, maximum of five lesions (circles) total can be selected to adhere to rule of up to two target lesions per organ. (Reprinted with permission from AJR Am J Roentgenol. 2010;195: 281–289)

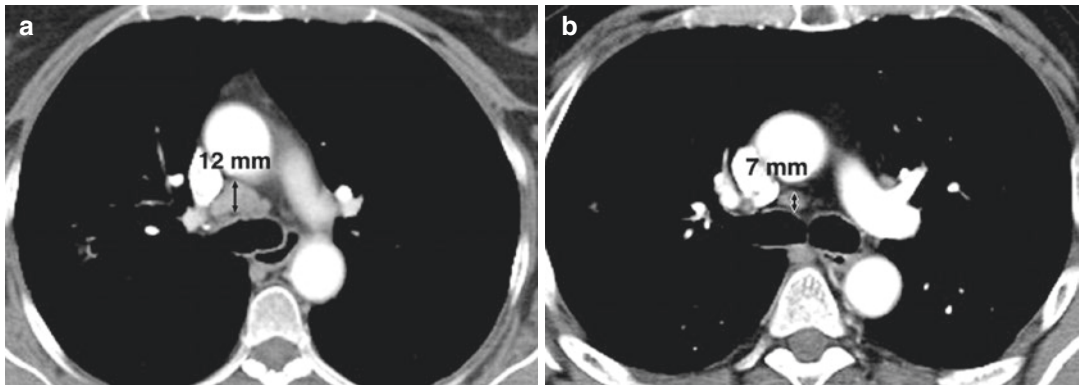

Fig. 10 Assessment of pathologic lymph nodes by RECIST 1.1 on CT scan of patient with lung cancer. (**a**) Subcarinal lymph node measures 12 mm in short axis (arrow) on chest CT, so it should be considered as nontarget lesion according to RECIST 1.1. (**b**) Precarinal lymph node measures 7 mm in short axis (arrow). Given that short-axis diameter is less than 10 mm, lymph node is nonpathologic according to RECIST 1.1. (Reprinted with permission from AJR Am J Roentgenol. 2010;195: 281–289)

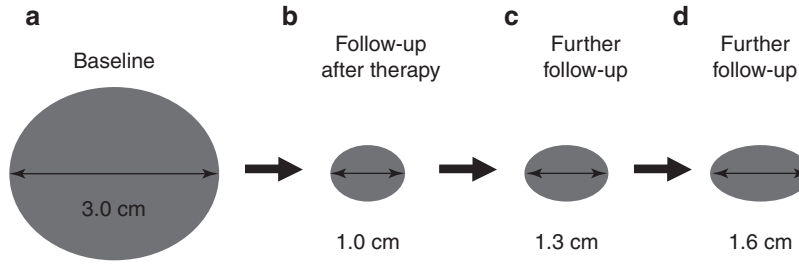

Fig. 11 Clarification of disease progression by RECIST 1.1. Target lesion at baseline (**a**) has longest diameter of 3.0 cm. On follow-up study after initiation of therapy (**b**), lesion measures 1.0 cm—showing 67% decrease in size compared with baseline. This finding is consistent with partial response. On further follow-up study (**c**), lesion has slightly increased in size and measures 1.3 cm. Because 30% increase in size of lesion since smallest diameter (nadir) of 1.0 cm, assessment category according to RECIST 1.0 would be progressive disease and therapy would be terminated. However, using RECIST 1.1, which requires 5-mm absolute increase in size in addition to ≥20% increase, assessment would be stable disease and therapy would be continued. If further follow-up showed increase to diameter of 1.6 cm (**d**), then criteria for progressive disease according to RECIST 1.1 would be met—that is, ≥5 mm absolute increase in size in addition to ≥20% increase compared with nadir. (Reprinted with permission from AJR Am J Roentgenol. 2010;195: 281–289)

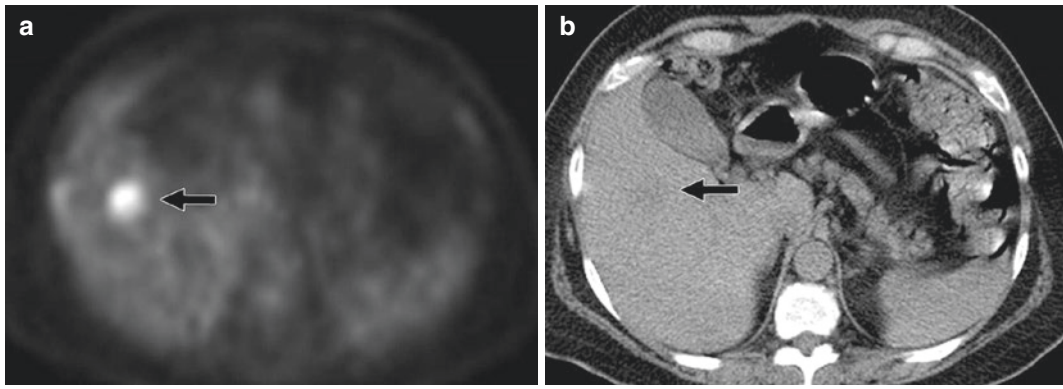

Fig. 12 FDG PET in detection of new lesions in 48-year-old woman with breast cancer who had negative FDG PET/CT findings at baseline. Follow-up FDG PET/CT images (**a**, **b**) show new FDG-avid liver lesion (arrows) representing metastasis. Finding meets criteria for progressive disease using Response Evaluation Criteria in Solid Tumors 1.1 because new lesion has been detected on FDG PET. (Reprinted with permission from AJR Am J Roentgenol. 2010;195: 281–289)

measurable tumor burden is required to assign PD by nontarget lesions (Nishino et al. 2010a; Eisenhauer et al. 2009). However, assigning PD by nontarget lesion increase in the setting of SD or PR of target lesions is considered to be extremely rare (Nishino et al. 2010a; Eisenhauer et al. 2009). In patients without measurable tumor burden, the general concepts as in the settings with measurable disease are applied, and an increase of tumor burden that would be required to assign PD for measurable tumor burden should be present. Examples of PD by nontarget lesions in this scenario include an increase in pleural effusion from trace to large, or an increase in lymphangitic disease from localized to widespread (Nishino et al. 2010a; Eisenhauer et al. 2009).

Another major change in RECIST 1.1 is the inclusion of FDG-PET in the detection of new lesions that define PD (Nishino et al. 2010a; Eisenhauer et al. 2009). In patients with negative FDG-PET at baseline, a positive FDG-PET at follow-up defines PD due to a new lesion by RECIST 1.1 (Fig. 12). The algorithm in cases

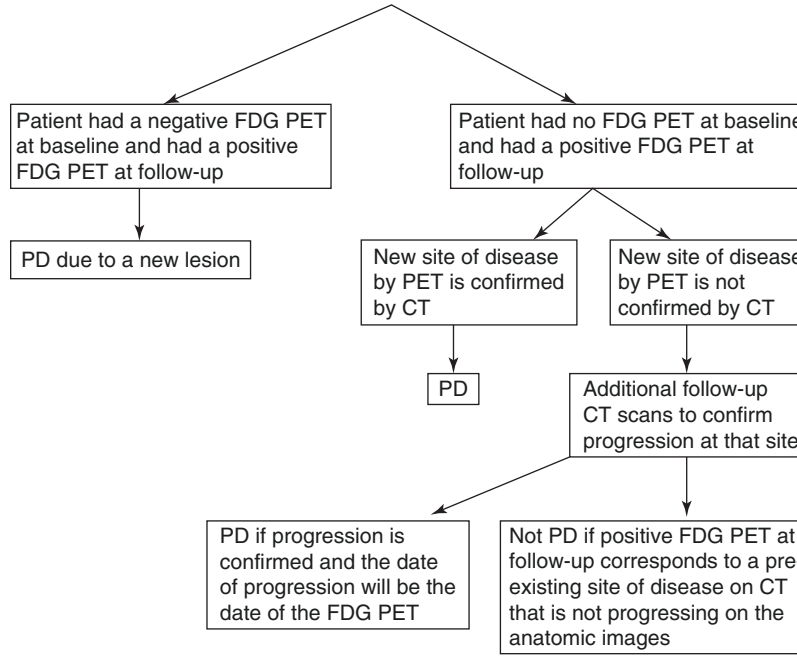

Fig. 13 Summary of guideline for including FDG PET in detection of new lesions according to RECIST 1.1. *PD* progressive disease. (Reprinted with permission from AJR Am J Roentgenol. 2010;195: 281–289)

without baseline FDG-PET is also defined in detail (Fig. 13) (Nishino et al. 2010a; Eisenhauer et al. 2009). Inclusion of FDG-PET in the detection of new lesions added a new dimension to RECIST by incorporating functional imaging. In a study of advanced NSCLC patients treated with epidermal growth factor receptor (EGFR) inhibitor that compared the response assessment by RECIST 1.0 and RECIST 1.1, the inclusion of FDG-PET was a major factor that influenced the difference in best response assessment by two criteria, indicating the impact of the revision in defining trial endpoints and progression-free survival (Nishino et al. 2010b).

After the introduction of RECIST 1.1, several studies have evaluated the response assessment by RECIST 1.1 in comparison with RECIST 1.0, with different types of tumors treated with different anticancer systemic agents (Nishino et al. 2010b, 2013a; Krajewski et al. 2015). Overall, these studies demonstrated that RECIST 1.1 can provide response assessments that are highly concordant with RECIST 1.0, with decreased number of target lesions requiring less efforts and time for measurements.

3 General Limitations of RECIST: Measurement Variability and Tumor Heterogeneity

Although RECIST guidelines have been the most widely accepted standardized method of tumor response evaluations with the advantages of simplicity and practicality, the limitations of RECIST have been increasingly acknowledged, even after the revisions introduced in RECIST 1.1. Limitations of RECIST can be classified into two groups, namely, general limitations that universally affect the assessment results regardless of tumor types or agents, and limitations specific to the era of precision cancer therapy and immunotherapy (Nishino et al. 2012; Nishino 2018). The present section of this chapter describes the general limitations of RECIST, focusing on (1) variability of tumor size measurements and (2) tumoral heterogeneity within a lesion as well as among different lesions in a patient (Nishino 2018). Emerging limitations specific to precision cancer therapy and immunotherapy will be discussed in detail in the following chapter (chapter "Response Evaluations for Precision Cancer Therapy and Immunotherapy").

Measurement variability, including both intraobserver and interobserver variability, is an inherent limitation of quantitative imaging methods including RECIST and other tumor response criteria. In a study of 40 lung tumors evaluated on CT by Erasmus et al., the probability of misclassifying a tumor progression was 43% for WHO criteria and 30% for RECIST. Although RECIST using unidimensional measurements had a lower misclassification rate compared to WHO criteria using bidimensional measurements, the results indicate that nearly one-third of patients can be classified as having progressive disease due to the measurement variability rather than true tumor growth (Erasmus et al. 2003). In a study of the same-day repeat CT scans of 32 non-small cell lung cancer (NSCLC) patients by Zhao et al., the 95% limits of agreement of tumor size measurements ranged from (−18.3%, 15.5%) to (−22.8%, 23.0%) for unidimensional measurements used in RECIST (Zhao et al. 2010). In spite of considerable variability, the results indicated that the RECIST-based unidimensional size measurements were reproducible within the partial response category (≥30% decrease); however, the cutoff value for progression (≥20% increase) is within the range of measurement variability and thus can misclassify patients into PD category (Zhao et al. 2010). Revisions in RECIST 1.1 may have contributed to reduce measurement variability. In a study of advanced NSCLC patients treated with EGFR inhibitor, RECIST 1.1 had narrower 95% limits of interobserver agreement (−18.6%, 25.4%) compared to RECIST 1.0 (−30.8%, 30.4%), which may be due to the reduction of number of target lesions and the use of short axis measurements for lymph nodes (Nishino et al. 2014a, 2010b).

In a study of 29 patients with metastatic colorectal cancer treated in a trial, three independent radiologists selected and measured the lesions, according to RECIST 1.0. Of 198 target lesions total, 33% were selected by all three, 28% by two, and 39% by one radiologist. With independent selection, the variability in relative change of unidimensional tumor measurements was 11%. The variability decreased to 8% when measuring the same lesions (Zhao et al. 2014). Another recent study also looked at the relationship between target lesion selection and response assessment results using RECIST 1.1 in 316 patients with metastatic solid tumors (Kuhl et al. 2019). Three readers evaluated the imaging of each patient. The same set of target lesions was selected in 41% (128/316) of the patients, whereas a different set of lesions was selected in 59% (188/316). High agreement of treatment response categories (κ = 0.97) was noted when target lesion selection was concordant; however, the agreement was much lower when target lesion selection was discordant (κ = 0.58). Though the fundamental solution for the issues demonstrated by these studies remain to be established, the results indicated the importance of target lesions selection at baseline that best represent the tumor burden by radiologist's interpretation. It is also important to evaluate nontarget lesions and new lesions/sites of disease on follow-up scans in addition to measuring target lesions, in order to accurately reflect overall tumor burden changes to the response assessments (Kuhl et al. 2019).

Tumoral heterogeneity in terms of both within a lesion and among different lesions in a patient is another important issue when considering the limitations of RECIST. RECIST relies on unidimensional size measurements for quantification of tumor burden, assuming that three-dimensional tumor volume burden is simply related to a planar measurement. However, in reality, tumors can be heterogeneous in terms of growth rates and patterns within the same lesion (Fig. 14), or among different lesions in one patient where some lesions show increase while other lesions may decrease during therapy (Nishino et al. 2014a; Nishino 2018; Gavrielides et al. 2009; Longo 2012). Application of tumor volume measurements for the evaluation of therapeutic response may help to address the issue, at least in part (Nishino et al. 2014a, 2013b, 2016, 2011, 2014b; Zhao et al. 2010; Mozley et al. 2012, 2010). With the current multi-detector row computed tomography (MDCT) technology, volumetric acquisition of large anatomic volumes with isotropic voxels can be performed in clinical oncology CT

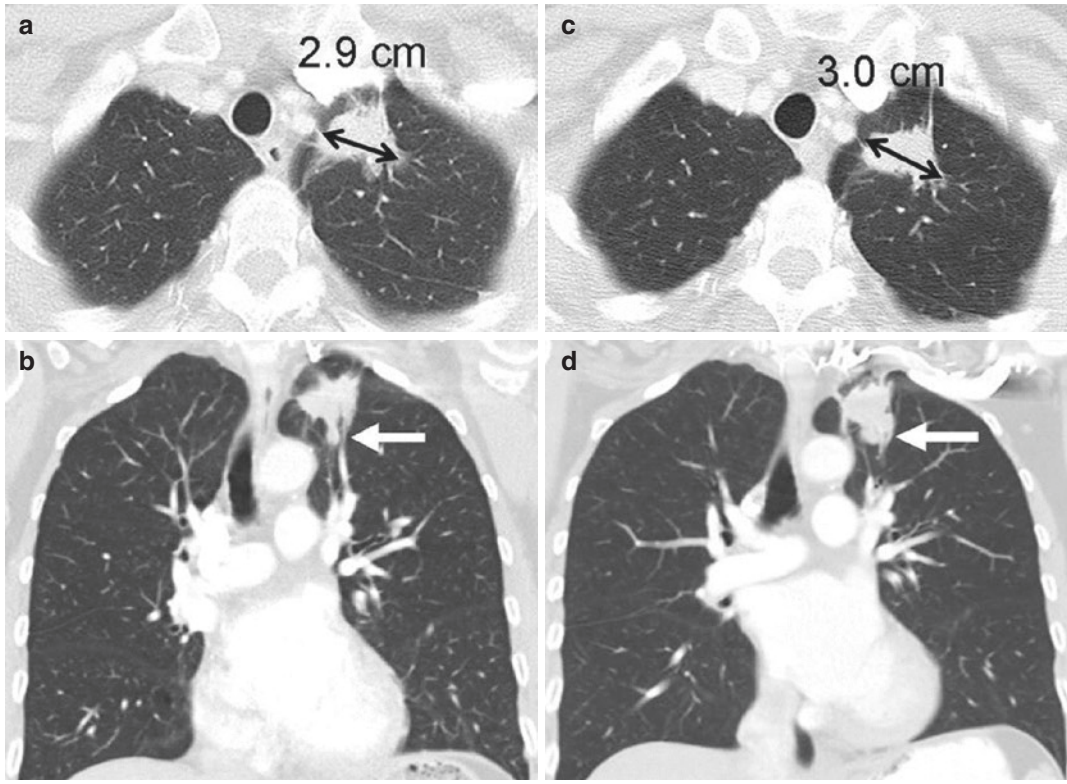

Fig. 14 Limitations of response assessment using RECIST in a 58-year-old woman with stage IV adenocarcinoma of the lung. (**a**, **b**) Contrast-enhanced axial and coronal CT images of the chest during pemetrexed and cisplatin therapy demonstrate a spiculated mass in the left upper lobe. The measurement of the dominant mass according to RECIST was 2.9 cm, measured in the longest diameter on an axial plane. Note a small nodular component of the mass at its inferior portion on coronal view (arrow, **b**). (**c**) At follow-up CT during therapy, the axial plane at the level of the longest diameter of the mass demonstrated a similar appearance and size of mass, 3.0 cm in the longest diameter. (**d**) However, on a coronal reformatted image at the level of the mass, the inferior component of the mass (arrow, **d**) has increased compared with the prior study, indicating increase of tumor burden, which is not captured by either RECIST or World Health Organization (WHO) measurements. (Reprinted with permission from Radiology. 2014;271(1):6–27)

scans, allowing the segmentation and measurement of tumor volumes as a marker for tumor response and clinical outcome (Nishino et al. 2014a; Nishino 2018). Tumor volume measurements have an advantage for decreasing measurement variability and thus improving reproducibility, as shown in many prior studies that have consistently reported less measurement variability of tumor volume compared to tumor size measurements used in RECIST (Zhao et al. 2010; Mozley et al. 2012, 2010; Nishino et al. 2013b, 2016, 2011, 2014b). The thought of moving from unidimensional assessment to volumetric or functional assessment was mentioned at the time of introduction of RECIST 1.1 by the RECIST Working Group, which concluded that sufficient standardization and widespread availability were needed before recommending the alternative methods (Nishino et al. 2010a; Eisenhauer et al. 2009; Nishino 2018). Almost a decade has passed since then, and robust solutions for the increasing needs for standardization and technology transfer need to be established via multidisciplinary collaborations among oncology and radiology communities (Nishino 2018).

References

Eisenhauer EA, Therasse P, Bogaerts J et al (2009) New response evaluation criteria in solid tumours: revised RECIST guideline (version 1.1). Eur J Cancer 45:228–247

Erasmus JJ, Gladish GW, Broemeling L et al (2003) Interobserver and intraobserver variability in measurement of non-small-cell carcinoma lung lesions: implications for assessment of tumor response. J Clin Oncol 21:2574–2582

Gavrielides MA, Kinnard LM, Myers KJ, Petrick N (2009) Noncalcified lung nodules: volumetric assessment with thoracic CT. Radiology 251:26–37

Krajewski KM, Nishino M, Ramaiya NH, Choueiri TK (2015) RECIST 1.1 compared with RECIST 1.0 in patients with advanced renal cell carcinoma receiving vascular endothelial growth factor-targeted therapy. AJR Am J Roentgenol 204:W282–W288

Kuhl CK, Alparslan Y, Schmoee J et al (2019) Validity of RECIST version 1.1 for response assessment in metastatic cancer: a prospective, multireader study. Radiology 290(2):349–356

Longo DL (2012) Tumor heterogeneity and personalized medicine. N Engl J Med 366:956–957

Miller AB, Hoogstraten B, Staquet M, Winkler A (1981) Reporting results of cancer treatment. Cancer 47:207–214

Mozley PD, Schwartz LH, Bendtsen C, Zhao B, Petrick N, Buckler AJ (2010) Change in lung tumor volume as a biomarker of treatment response: a critical review of the evidence. Ann Oncol 21:1751–1755

Mozley PD, Bendtsen C, Zhao B et al (2012) Measurement of tumor volumes improves RECIST-based response assessments in advanced lung cancer. Transl Oncol 5:19–25

Nishino M (2018) Tumor response assessment for precision cancer therapy: response evaluation criteria in solid tumors and beyond. Am Soc Clin Oncol Educ Book 38:1019–1029

Nishino M, Jagannathan JP, Ramaiya NH, Van den Abbeele AD (2010a) Revised RECIST guideline version 1.1: what oncologists want to know and what radiologists need to know. AJR Am J Roentgenol 195:281–289

Nishino M, Jackman DM, Hatabu H et al (2010b) New Response Evaluation Criteria in Solid Tumors (RECIST) guidelines for advanced non-small cell lung cancer: comparison with original RECIST and impact on assessment of tumor response to targeted therapy. AJR Am J Roentgenol 195:W221–W228

Nishino M, Guo M, Jackman DM et al (2011) CT tumor volume measurement in advanced non-small-cell lung cancer: performance characteristics of an emerging clinical tool. Acad Radiol 18:54–62

Nishino M, Jagannathan JP, Krajewski KM et al (2012) Personalized tumor response assessment in the era of molecular medicine: cancer-specific and therapy-specific response criteria to complement pitfalls of RECIST. AJR Am J Roentgenol 198:737–745

Nishino M, Cardarella S, Jackman DM et al (2013a) RECIST 1.1 in NSCLC patients with EGFR mutations treated with EGFR tyrosine kinase inhibitors: comparison with RECIST 1.0. AJR Am J Roentgenol 201:W64–W71

Nishino M, Dahlberg SE, Cardarella S et al (2013b) Tumor volume decrease at 8 weeks is associated with longer survival in EGFR-mutant advanced non-small-cell lung cancer patients treated with EGFR TKI. J Thorac Oncol 8:1059–1068

Nishino M, Hatabu H, Johnson BE, McLoud TC (2014a) State of the art: response assessment in lung cancer in the era of genomic medicine. Radiology 271: 6–27

Nishino M, Jackman DM, DiPiro PJ, Hatabu H, Janne PA, Johnson BE (2014b) Revisiting the relationship between tumour volume and diameter in advanced NSCLC patients: an exercise to maximize the utility of each measure to assess response to therapy. Clin Radiol 69:841–848

Nishino M, Dahlberg SE, Fulton LE et al (2016) Volumetric tumor response and progression in EGFR-mutant NSCLC patients treated with erlotinib or gefitinib. Acad Radiol 23:329–336

Therasse P, Arbuck SG, Eisenhauer EA et al (2000) New guidelines to evaluate the response to treatment in solid tumors. European Organization for Research and Treatment of Cancer, National Cancer Institute of the United States, National Cancer Institute of Canada. J Natl Cancer Inst 92:205–216

Zhao B, Oxnard GR, Moskowitz CS et al (2010) A pilot study of volume measurement as a method of tumor response evaluation to aid biomarker development. Clin Cancer Res 16:4647–4653

Zhao B, Lee SM, Lee HJ et al (2014) Variability in assessing treatment response: metastatic colorectal cancer as a paradigm. Clin Cancer Res 20:3560–3568

Response Evaluations for Precision Cancer Therapy and Immunotherapy

Mizuki Nishino

Contents

Abstract

Since the original introduction of RECIST in 2000 and the revision in 2009, the treatment approaches for advanced cancers have made considerable progress. Notably, the recent advances of the understanding of genomic abnormalities specific to cancer and its clinical application have transformed the way how oncologists approach cancer patients, enabling the era of effective precision cancer therapies using molecular targeting agents. Furthermore, the recent success in cancer immunotherapy has brought another paradigm shift, using immune-checkpoint blockade to activate host immune defense mechanism and fight against cancer. Given these advances of cancer therapies, additional limitations of RECIST apart from the general limitations discussed in "Conventional Tumor Response Criteria and Limitations" have been increasingly recognized, especially in patients treated with precision therapy and immunotherapy (Nishino 2018; Nishino et al. 2012). This chapter discusses these therapy-specific limitations of RECIST, including (1) CT tumor density changes in response to antiangiogenic therapy, (2) slow tumor progression during molecular targeted therapy, and (3) immune-related response in patients treated with immunotherapy (Nishino 2018; Nishino et al. 2012).

M. Nishino (✉)
Department of Imaging, Dana-Farber Cancer Institute, Boston, MA, USA

Department of Radiology, Brigham and Women's Hospital, Boston, MA, USA
e-mail: mizuki_nishino@dfci.harvard.edu

M. Nishino (ed.), *Therapy Response Imaging in Oncology*, Medical Radiology, Diagnostic Imaging,
https://doi.org/10.1007/978-3-030-31171-1_2

1 CT Tumor Density Changes in Response to Antiangiogenic Therapy

In cancer patients treated with molecular targeting agents with antiangiogenic activity, decrease of CT tumor density has been noted as a marker to indicate response to therapy, even in the absence of tumor size reduction (Choi et al. 2005, 2007; Benjamin et al. 2007). CT density changes have been initially described by Choi et al. as a sign of tumor response in patients with gastrointestinal stromal tumor (GIST) treated with tyrosine kinase inhibitor, imatinib (Fig. 1) (Nishino et al. 2012; Choi et al. 2005, 2007; Benjamin et al. 2007). Similar observations of CT density decrease in the setting of tumor response to therapy have been noted in other solid tumors including other sarcomas, renal cell carcinomas, and hepatocellular carcinomas (Nishino et al. 2012; Faivre et al. 2011; Smith et al. 2010a, b).

The Choi response criteria defines tumor response as a 10% decrease of unidimensional tumor size or a 15% decrease in CT density (or CT attenuation measured in Hounsfield units (HU)), rather than a 30% decrease of unidimensional tumor size per RECIST (Choi et al. 2004, 2007). The Choi response criteria are based on several studies in patients with GIST treated with imatinib, which evaluated the association between CT density changes versus FDG PET response and clinical outcome. In the initial study in 2004, 173 tumors from 36 patients with GIST were studied for the changes of tumor size and density on CT and FDG uptake measured by SUVmax at 2 months of imatinib therapy in comparison with the baseline pretherapy scans (Choi et al. 2004). In these patients, both tumor density and SUVmax demonstrated significant decrease after 2 months of imatinib therapy. Though tumor size also showed significant decrease after therapy, 75% of the patients was categorized as having stable disease (SD) according RECIST using size criteria alone (Choi et al. 2004).

On the basis of the initial results, another study evaluated 172 lesions in 40 patients with metastatic GIST treated with imatinib for tumor changes on CT and FDG PET at 2 months of therapy. Tumor size decrease >10% or tumor density decrease >15% on CT at 2 months of therapy demonstrated had a higher sensitivity in identifying PET responders compared to RECIST (97% by Choi criteria vs. 52% by RECIST), which is now known as Choi response criteria. The prognostic value of Choi response criteria was shown in a study of 58 patients with GIST treated with imatinib (Benjamin et al. 2007). Patients with response by Choi criteria after 2 months of imatinib therapy had significantly longer time to progression than those who did not ($p = 0.0002$). On the other hand, RECIST response did not have significant correlation with time to progression ($p = 0.74$). In addition, disease-specific survival was also significantly longer in responders by Choi criteria ($p = 0.04$), but not in responders by RECIST ($p = 0.45$) (Benjamin et al. 2007).

After CT density decrease as a sign of initial response to therapy, tumor progression may also be noted with radiographic appearance that are different from simple increase of tumor size or appearance of separate new lesions as defined by RECIST (Fig. 1) (Choi et al. 2005, 2007; Benjamin et al. 2007; Shankar et al. 2005). Progression in this setting is defined by Choi criteria as (1) appearance of new lesions, (2) appearance or increase in size of intratumoral nodules, or (3) tumor size increase of >20% without post-treatment hypodense change (Choi et al. 2005, 2007). The concept of CT density changes described by Choi has been widely recognized and sometimes used as an additional guideline to supplement RECIST, in order to accurately capture tumor response and progression in patients receiving agents with antiangiogenic activity (Nishino 2018; Nishino et al. 2012).

2 Slow Tumor Progression During Molecular Targeted Therapy

Advances in knowledge of genomic abnormalities specific to cancer in the past decade have enabled precision medicine approaches to cancer patients, where patients can be treated with molecular targeting agents that are specifically

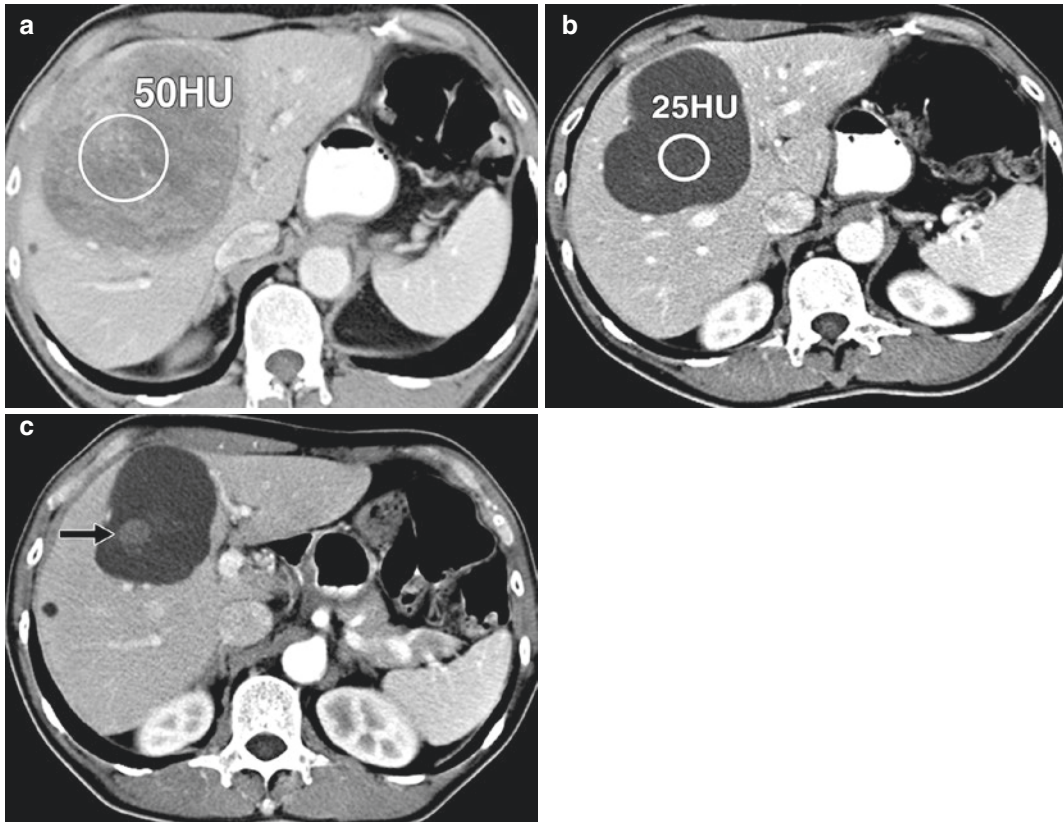

Fig. 1 A 58-year-old man with advanced gastrointestinal stromal tumor with liver metastasis, treated with imatinib mesylate. (Reprinted with permission from AJR Am J Roentgenol. 2012;198: 737–745). (**a**) Baseline contrast-enhanced CT of abdomen before therapy shows heterogeneously enhancing mass in liver representing metastasis, measuring 10 cm in longest diameter and 50 HU in CT attenuation (circle). (**b**) Follow-up CT scan obtained 8 weeks after initiation of imatinib mesylate therapy shows significant decrease in CT attenuation of tumor (circle; 25 HU), meeting criteria for response by Choi criteria, with minimal decrease in size (9.5 cm in longest diameter). (**c**) Patient continued receiving imatinib mesylate therapy. Follow-up CT scan at 2 years revealed new intratumoral tumor nodule (arrow), meeting criteria for progression by Choi criteria. Note measurement of longest diameter alone by Response Evaluation Criteria in Solid Tumors (7.5 cm) fails to detect progression. Adjacent small lesion in anterior segment of liver remained unchanged since baseline, most likely representing a benign lesion

designed to target the oncogenic genomic abnormalities of their tumors. The approach has been used widely in different tumor types, and contributed to increase the response rates to therapy among subgroups of patients selected for treatment based on the genomics analyses of their tumors (Nishino 2018; Nishino et al. 2011a, 2014a). However, most of the patients who respond markedly with significant initial tumor burden reduction eventually experience tumor regrowth, due to the development of the acquired resistance to therapy (Nishino 2018; Nishino et al. 2011a, 2014a). Tumors after initial response in these patients tend to grow slowly over time, and patients often remain on therapy. In this clinical scenario of precision cancer therapy, RECIST has a limited value in evaluating tumor progression and guiding treatment decisions.

As described in "Conventional Tumor Response Criteria and Limitations", RECIST defines the response categories based on the proportional changes of tumor measurements.

Because of this feature, the measurement variability has more impact on the results of response assessment in patients with smaller tumor burden. For example, 3 mm increase due to measurement variability contributes to only 5% increase for a tumor measuring 6 cm on the reference scan; however, it results in 30% difference for a tumor measuring 1 cm on the reference scan (Nishino et al. 2013a, 2014a). The issue is particularly relevant in the setting of effective precision cancer therapy where patients experience marked initial decrease of their tumor size, therefore achieving very small tumor size at the nadir (the smallest tumor size since baseline) which serves as a reference to define subsequent progression when tumors start to grow. Given small tumor size at the nadir, which is often only a few centimeters or less, only a few millimeter size increase may result in ≥20% increase compared to the nadir. To complement this limitation, the revision in RECIST 1.1 requires at least 5 mm increase of absolute size compared with the nadir to define PD, in addition to ≥20% increase (Fig. 2) (Eisenhauer et al. 2009; Nishino et al. 2010). However, in two prior studies of advanced non-small cell lung cancer (NSCLC) patients treated with EGFR inhibitors, the ≥5 mm absolute size

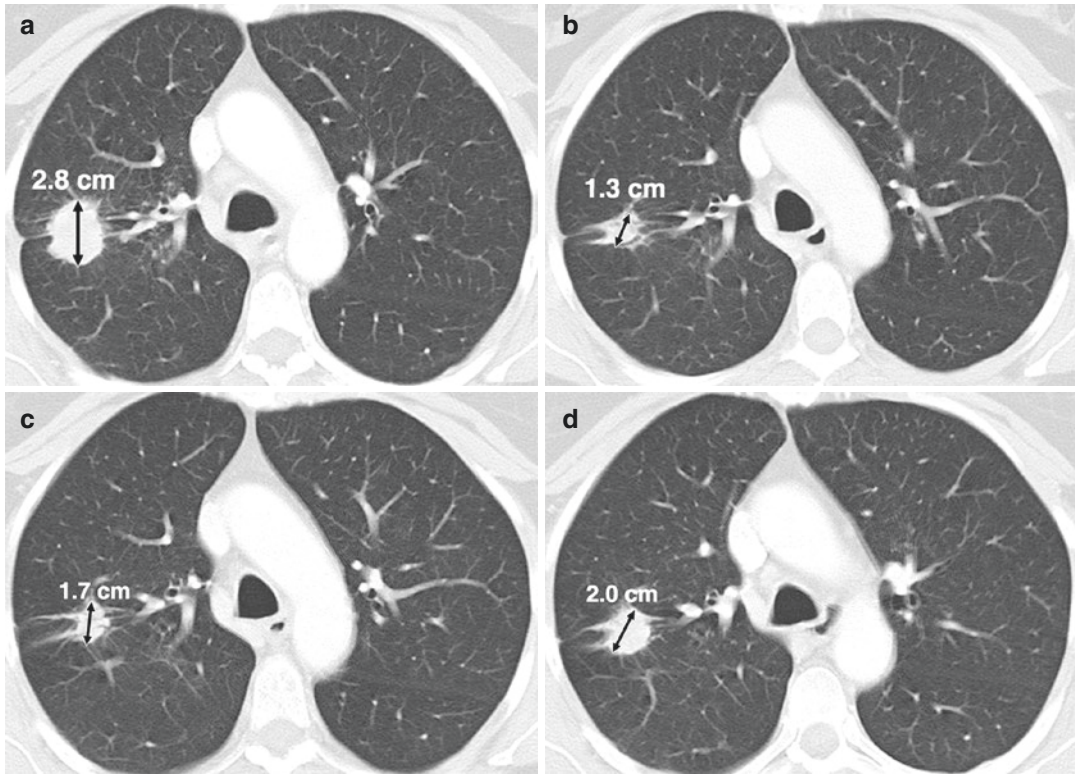

Fig. 2 Disease progression in 55-year-old woman with NSCLC treated with EGFR inhibitor erlotinib. (**a**) CT scan of chest shows spiculated right lung lesion, which is the only target lesion, has longest diameter of 2.8 cm (arrow). (**b**) After one cycle of therapy, lesion measures 1.3 cm (arrow), showing 54% decrease in size compared with baseline. This change is consistent with partial response. (**c**) After initial response, small residual tumor slowly increased in size and measured 1.7 cm (arrow) on a further follow-up study. Given 30% increase compared with nadir (1.3 cm), assessment using RECIST 1.0 would be progressive disease and therapy would be terminated. However, using RECIST 1.1, assessment is stable disease because absolute increase in size is less than 5 mm. (**d**) Another follow-up CT scan shows further increase in size of residual tumor with longest diameter of 2.0 cm (arrow), which meets criteria for progressive disease by RECIST 1.1 given 54% increase and 6-mm absolute increase in size compared with nadir. (Reprinted with permission from AJR Am J Roentgenol. 2010;195: 281–289)

increase rule resulted in longer time to progression only in a minority of patients (6% (4/70) in one study (Nishino et al. 2013a) and 1% (1/104) in the other study (Sun et al. 2010). These results indicate the needs for additional strategies using more accurate and less variable measurement methods to overcome the issue.

As an additional strategy to complement the limitations of RECIST for the evaluation of slow tumor progression after effective molecular targeted therapy, the concept of tumor growth rate during therapy has been investigated as a marker for defining treatment endpoints and clinical benefits in different types of advanced solid tumors (Ferte et al. 2014; Gomez-Roca et al. 2011; Levy et al. 2013; Nishino et al. 2013b, 2016; Stein et al. 2011, 2012). In the cohorts of renal cell carcinoma and prostate cancer, Stein et al. used the tumor growth rate constant, obtained as $\log_e 2$/doubling time (days) using tumor size measurements during trials, and demonstrated a negative correlation with overall survival. The results indicated that slow tumor growth can be a marker of better clinical outcome (Stein et al. 2011, 2012). Tumor growth rate was also tested in advanced NSCLC patients harboring EGFR mutations treated with EGFR inhibitors using tumor volume analysis, which provided a reference value for slow tumor progression after initial response in these patients (Nishino et al. 2013b, 2016). Further efforts are necessary to validate these findings and translate the approach into the clinical setting of oncologic imaging (Nishino 2018).

3 Immune-Related Response in Patients Treated with Immunotherapy

Another paradigm shift in treatment of cancer has been brought by the successful clinical application of cancer immunotherapy using immune-checkpoint inhibitors in the past few years (Hodi et al. 2010; Nishino et al. 2017a, 2015; Ott et al. 2013). As acknowledged by the Nobel Prize in Physiology or Medicine in 2018 that was awarded to James P. Allison and Tasuku Honjo "for their discovery of cancer therapy by inhibition of negative immune regulation," the discovery of immune-checkpoint inhibitors as antitumor agents has opened a new arena of cancer therapy (https://www.nobelprize.org/prizes/medicine/2018/summary/; Ishida et al. 1992; Leach et al. 1996).

The mechanism of antitumor action of immune-checkpoint inhibitors is based on the blockade of immune inhibition by tumors, as opposed to the direct cytotoxic or targeted effects to tumor cells (Nishino et al. 2015, 2017a, 2019; Ott et al. 2013). In the tumor microenvironment in cancer patients, a number of ligand–receptor pairs between tumor cells, T cells, dendritic cells, and macrophages are expressed. These molecules are called "immune-checkpoints" and regulate T cell activation specific to tumor cells as immune-responses of the host against tumor (Figs. 3 and 4) (Nishino et al. 2012, 2017a; Ott et al. 2013; Allison 1995; Hodi et al. 2003, 2008; Wolchok 2012; Lenschow et al. 1996). Using the signaling from immune-checkpoints in the microenvironment, tumor cells mediate immune suppression so that they can escape from T cell-mediated host immune responses, to survive and proliferate (Ott et al. 2013; Nishino et al. 2019; Lenschow et al. 1996; Zielinski et al. 2013; Pardoll 2012). Immune-checkpoint inhibitors, such as cytotoxic T-lymphocyte antigen-4 (CTLA-4) inhibitors and programmed cell death-1 (PD-1) and PD-ligand 1 (PD-L1) inhibitors, block the interaction and interfere the immune inhibition by tumors, thereby activating the immune response against cancer (Figs. 3 and 4) (Nishino et al. 2019; Zielinski et al. 2013; Pardoll 2012; Chen et al. 2012; Okazaki et al. 2013).

The first breakthrough using immune-checkpoint blockade was made in 2010, when a phase 3 trial of CTLA-4 inhibitor, ipilimumab, demonstrated a significantly improved overall survival in advanced melanoma (Hodi et al. 2010). Since then, many clinical trials have shown promising activity of immune-checkpoint inhibitor therapy using CTLA-4 inhibitors and PD-1/PD-L1inhibitors in a variety of advanced cancers. As the results, these immune-checkpoint inhibitors and their combination

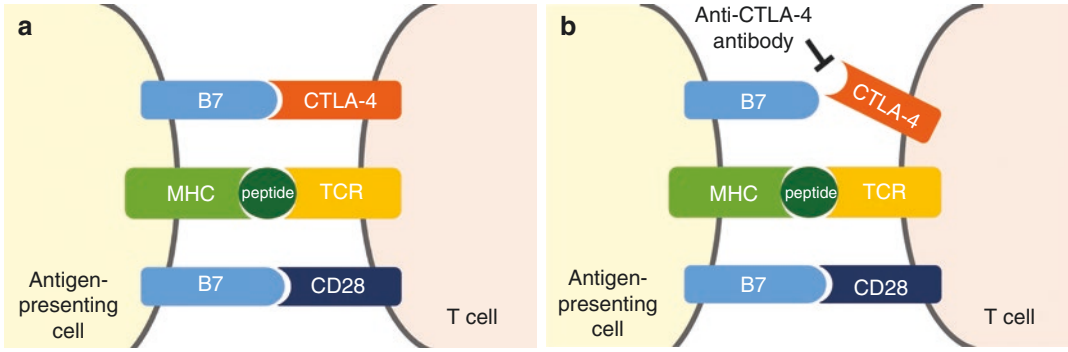

Fig. 3 Molecular mechanisms for immune inhibition by tumors and its blockade by anti-CTLA-4 antibody. (Reprinted with permission from Eur J Radiol. 2015 Jul;84(7):1259–68). (**a**) Interaction between CTLA-4 on T cell and its ligand (B7) on antigen-presenting cell inhibits the T cell immune response against tumor, allowing tumor cells escape from immune attack. (**b**) Anti-CTLA-4 antibodies, such as ipilimumab, block the interaction between CTLA-4 and its ligand, causing blockade of the T cell immune inhibition and thus activating immune response against cancer

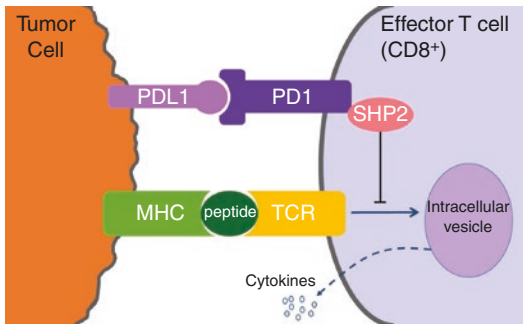

Fig. 4 Mechanism of PD-1 immunosuppression as a target for cancer therapy. (Reprinted with permission from Eur J Radiol. 2015 Jul;84(7):1259–68). PD-1 is expressed on the surface of effector T cells upon activation, and its ligand, PD-L1 is expressed on the tumor cells either by constitutive oncogenic signaling or by the induction in response to inflammatory signals as a response to tumor. The binding of PD-L1 to PD-1 delivers an inhibitory signal, through the phosphatase SHP2, which reduces cytokine production and proliferation of T cells, thus enabling tumor cells to evade the host immune response. Antibodies against PD-1 or PD-L1 prevent the binding and block immune inhibition by tumor, inducing antitumor immune response. Multiple additional receptor-ligand interactions that regulate T cell responses in the tumor microenvironment have been identified, such as KIR (killer cell immunoglobulin-like receptor), LAG3 (lymphocyte activation gene 3), and TIM3 (T cell membrane protein 3), and are currently under active investigation as possible targets for cancer immunotherapy

have been approved for a variety of tumors and indications, and has become the major treatment option for advanced cancers in clinical oncology (Table 1).

Because of unique mechanism of immune-checkpoint inhibitors, unconventional response patterns are noted in patients treated with these agents, including (1) response after an initial increase of tumor burden and (2) response during or after appearance of new lesions (Figs. 5 and 6) (Nishino 2018; Nishino et al. 2019). These response patterns are often called pseudoprogression, because patients meet the criteria for RECIST progression at the time of the initial increase of tumor burden or appearance of new lesions (Nishino et al. 2012, 2017a, 2019; Hodi et al. 2016; Wolchok et al. 2009; Chiou and Burotto 2015). Several sets of modified response criteria designed to capture these atypical immune-related response patterns have been proposed in the past decade to accurately characterize tumor response and progression in patients treated with immune-checkpoint inhibitors (Table 1) (Nishino et al. 2019).

The first set of criteria to characterize immune-related responses was proposed in 2009, based on the discussion among approximately 200 oncologists, immunotherapists, and regulatory experts at the series of workshops on their experience with immunotherapeutic agents in cancer patients (Wolchok et al. 2009). The criteria, known as immune-related response criteria (irRC), has key features that are very important when evaluating results of cancer immunotherapy (Wolchok et al. 2009). First, irRC requires confirmation of PD on two consecutive scans at least 4 weeks apart. This

Table 1 Summary of conventional tumor response criteria and modified strategies for immune-related response evaluations (Reprinted with permission from Radiology. 2019 Jan;290(1):9–22)

Type of criteria and criteria	Measurement	PR criteria[a]	PD criteria[b]	Confirmation of PD	New lesion
Conventional tumor response criteria					
Miller et al. 1981	Bidimensional (LD × LPD)	≥50% reduction	≥25% increase, new lesion, or nontarget PD	Not required	Defines PD
Therasse et al. 2000	Unidimensional (LD)	≥30% reduction	≥20% increase, new lesion, or nontarget PD	Not required	Defines PD
Eisenhauer et al. 2009	Unidimensional (LD for nonnodal lesions; LPD for lymph nodes)	≥30% reduction	≥20% and ≥5 mm increase, new lesion, or nontarget PD	Not required	Defines PD
Modified strategies for immune-related response evaluation					
irRC (2009), Wolchok et al. 2009	Bidimensional (LD × LPD)	≥50% reduction	≥25% increase	Required on consecutive studies at least 4 weeks apart	Does not define PD; measurements of new lesions included in the total tumor burden
irRECIST (2013) Nishino et al. 2013c, 2014b, 2016	Unidimensional (LD for nonnodal lesions; LPD for lymph nodes)	≥30% reduction	≥20% and ≥5 mm increase, new lesion, or nontarget PD	Required on a consecutive scan at least 4 weeks apart	Does not define PD; measurements of new lesions included in the total tumor burden
iRECIST (2017), Seymour et al. 2017	Unidimensional (LD for nonnodal lesions; LPD for lymph nodes)	≥30% reduction	≥20% and ≥5 mm increase, new lesion, or nontarget PD	Required at the next assessment 4–8 weeks later	Defines unconfirmed PD; confirms PD if additional new lesions or size increase (≥5 mm for the sum of new target or any increase in new nontarget lesions) are noted on the next assessment

irRC immune-related response criteria, *irRECIST* immune-related RECIST, *LD* longest diameter, *LPD* longest perpendicular diameter, *PD* progressive disease, *PR* partial response, *RECIST* Response Evaluation Criteria in Solid Tumors, *WHO* World Health Organization

[a]In reference to the baseline measurements

[b]In reference to the nadir (the smallest measurement since the baseline)

is to avoid prematurely declaring PD at initial tumor burden increase on one scan, because such increase may represent pseudoprogression and may be followed by subsequent tumor burden reduction. Second, irRC include new lesion measurements in the entire tumor burden, rather than defining PD at the appearance of new lesions, because response to immunotherapy can be seen after the appearance of new lesions in cases of pseudoprogression (Wolchok et al. 2009). The irRC has become quickly known as a novel set of criteria for cancer immunotherapy, and was used to define trial endpoint for immunotherapy (Lynch et al. 2012).

The irRC, however, was primarily based on the WHO criteria in terms of the measurement methods and response category definitions, and therefore used bidimensional measurements by multiplying the longest diameter and the longest perpendicular diameter (or shot axis) to quantify tumor burden (Nishino 2018; Nishino et al. 2012; Wolchok et al. 2009). This methodology of irRC was somewhat problematic, because most of the clinical trials of solid tumors in the past two

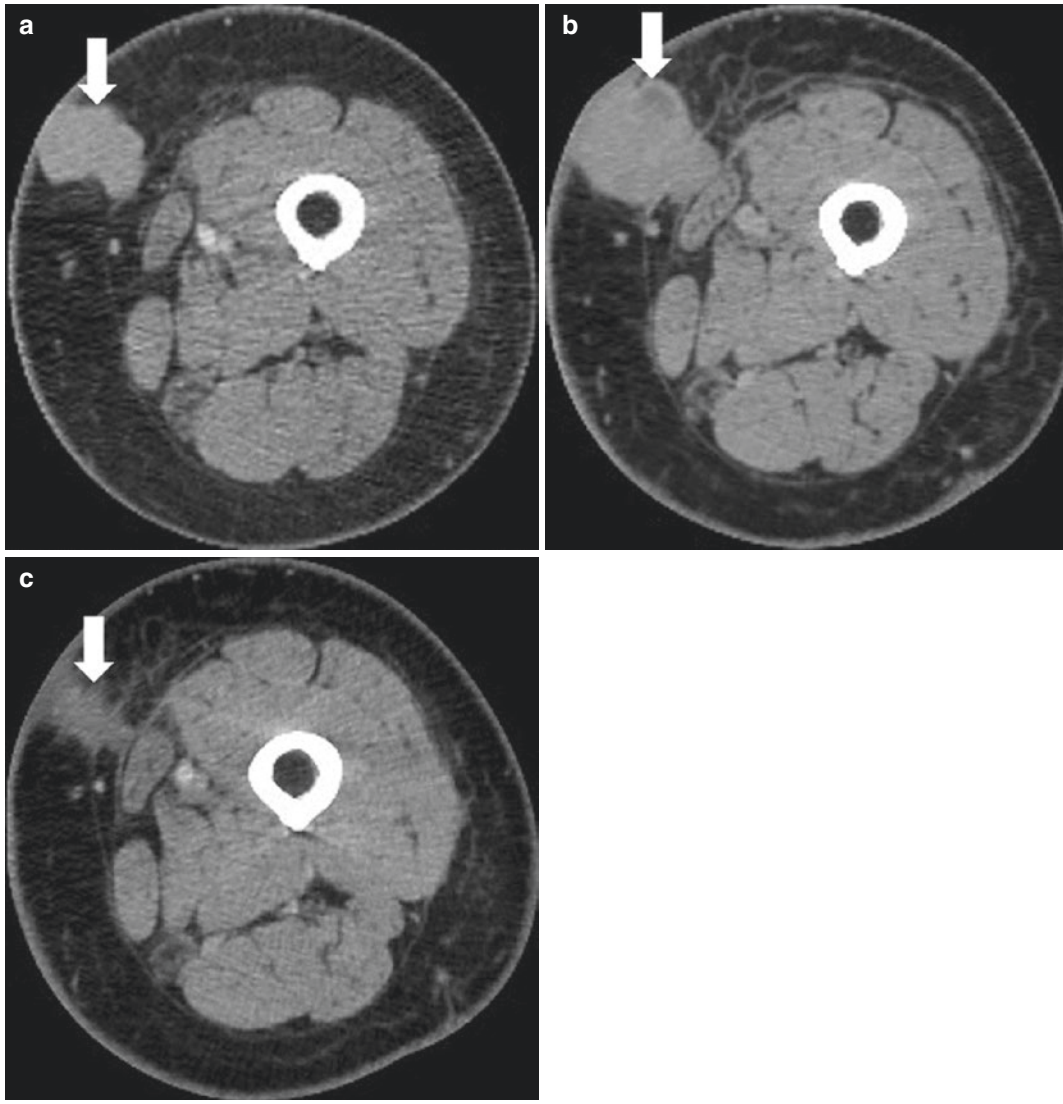

Fig. 5 Pseudoprogression with initial increase in tumor burden followed by subsequent tumor shrinkage due to immune-related response in a 66-year-old woman with metastatic melanoma treated with nivolumab and ipilimumab. (Reprinted with permission from Radiology. 2019 Jan;290(1):9–22). (**a**) Baseline contrast material-enhanced axial CT image obtained before therapy shows a metastatic nodule (arrow) in the left upper medial thigh measuring 4 cm in the longest diameter. (**b**) Follow-up axial CT image at 3 months of therapy shows an increase in the lesion, which now measures 5 cm (arrow), indicating progressive disease according to the Response Evaluation Criteria in Solid Tumors, or RECIST. (**c**) Further follow-up axial CT image at 6 months of therapy shows a decrease in size of the lesion, which now measures 2.5 cm (arrow), representing immune-related tumor response

decades used RECIST since its introduction in 2000 and thus used unidimensional measurements to quantify tumor burden changes (Nishino et al. 2019). Therefore, the results obtained by irRC using bidimensional measurements cannot be directly compared with the results of trials defined by RECIST using unidimensional measurements. In addition, many studies have shown that unidimensional measurements have less measurement variability and thus are more reproducible than bidimensional measurements (Erasmus et al. 2003; Nishino et al. 2011b; Zhao

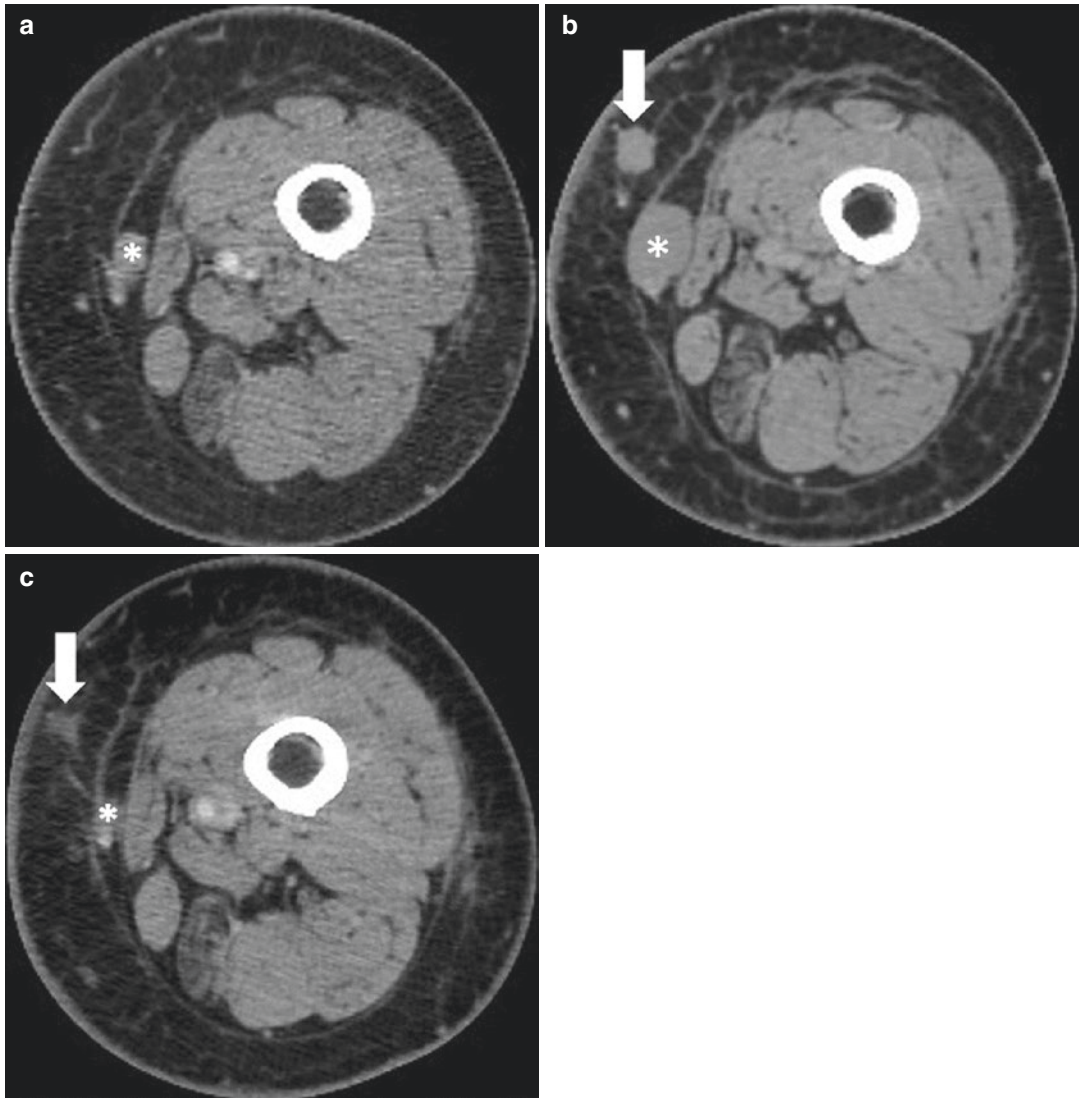

Fig. 6 Pseudoprogression with appearance of a new lesion followed by subsequent immune-related response in a 66-year-old woman with metastatic melanoma treated with nivolumab and ipilimumab. (Reprinted with permission from Radiology. 2019 Jan;290(1):9–22). Compared with (**a**) a baseline axial CT image obtained prior to the initiation of therapy, (**b**) a follow-up axial CT image obtained after 3 months of therapy shows a new subcutaneous lesion (arrow), indicating progressive disease according to the Response Evaluation Criteria in Solid Tumors, or RECIST; however, (**c**) a further follow-up axial CT image obtained after 6 months of therapy shows shrinkage of the new lesion (arrow), representing immune-related response. Note that another lesion in the deep subcutaneous tissue (∗) increased at 3-month follow-up, followed by subsequent shrinkage of the lesion, also indicating immune-related response after initial increase in tumor burden

et al. 2009). To address this issue and propose to develop a "common language" to assess tumor response to cancer immunotherapy, Nishino et al. conducted a series of studies that demonstrated that RECIST-based unidimensional measurements can characterize immune-related responses with higher reproducibility, while maintaining the important features of irRC regarding progression confirmation and new lesion assessment (Nishino et al. 2013c, 2014b, 2019). The results of these studies provided a scientific rationale to use RECIST-based unidimensional

measurements for immune-related response evaluations. The approach has become known as immune-related RECIST (irRECIST) among the investigators of immuno-oncology, and was used to define endpoint of many clinical trials of immunotherapeutic agents (Table 1) (Nishino 2018; Nishino et al. 2015, 2017a, 2019).

There has been another recent development from RECIST working group, which introduced iRECIST that is specifically designed for cancer immunotherapy trials (Seymour et al. 2017). Following the direction shown by irRECIST, iRECIST also uses unidimensional RECIST-based strategy, while it requires confirmation for PD; however, iRECIST proposed a slightly different approach for new lesion assessment (Seymour et al. 2017). Per iRECIST, new lesion measurements are not to be included in the sum; rather, new lesions should be recorded and measured separately. PD can be confirmed if additional new lesions or increase of new lesions are noted on the next imaging in 4–8 weeks (Seymour et al. 2017). Additionally, iRECIST introduced the concept of "unconfirmed PD," which is PD by RECIST 1.1 that remains to be confirmed. PD can be confirmed if the next scan in 4–8 weeks shows further increase (≥5 mm for the sum of target lesions) (Seymour et al. 2017). The concept of "unconfirmed PD" is particularly important because some patients do not undergo a confirmatory scan after their first scan demonstrating PD, and it is meaningful to differentiate these patients from those who are achieving stable disease on multiple follow-up scans. Although there are further steps needed to clarify the details of these criteria and validate their utility in defining treatment benefits and clinical outcome, the strategy for immune-related response evaluations has evolved quickly in the past decade toward establishing a common language which is primarily based on RECIST while implementing necessary modifications specific to the setting of immune-checkpoint inhibitor therapy.

In addition to the progress in the development of tumor response criteria for immunotherapy, several important observations have been made in terms of the patterns of tumor responses in patients treated with immunotherapy. One of such observations is the low incidence of pseudoprogression, which should be recognized by both treating physicians and radiologists interpreting the imaging studies (Nishino 2016, 2018; Nishino et al. 2017a; Chiou and Burotto 2015). In melanoma patients treated with immune-checkpoint inhibitors, the incidence of pseudoprogression has been known to be approximately 10% or lower (Nishino 2018; Hodi et al. 2016; Wolchok et al. 2009; Nishino et al. 2017b). The incidence is even lower in patients with advanced NSCLC, ranging from 1% to 5% (Gettinger et al. 2015; Nishino et al. 2017c). Moreover, patients with pseudoprogression may experience tumor burden decrease after PD was confirmed on two or more consecutive scans, as reported in two recent studies in cohorts of advanced melanoma and NSCLC treated with PD-1 inhibitors (Fig. 7) (Nishino 2018; Nishino et al. 2017b, c). The observation indicated the limitation of the current approaches of immune-related response evaluations, and emphasize the need for further studies including novel functional imaging techniques (Nishino 2018; Nishino et al. 2019).

Another novel observation include "hyperprogressive disease," which was described by Champiat et al. as a novel aggressive pattern of immune-related tumor behavior. Hyperprogressive disease is defined as a RECIST progression at the first evaluation and a ≥2-fold increase of the tumor growth rate after starting PD-1/PD-L1 inhibitor therapy compared to that during the period before initiating PD-1/PD-L1 inhibitor therapy (Champiat et al. 2017). In the initial study describing the phenomenon, hyperprogressive disease was noted in 9% (12/131) of the patients with various advanced malignancies treated in phase 1 trials of PD-1/PD-L1 inhibitors (Champiat et al. 2017). The observations call for a need for further development of biomarkers that can allow better patient selection, in order to achieve precision immunotherapy.

Finally, in addition to the unconventional response patterns and tumor behaviors on imaging, cancer immunotherapy is also associated with a variety of toxicities that can involve organs

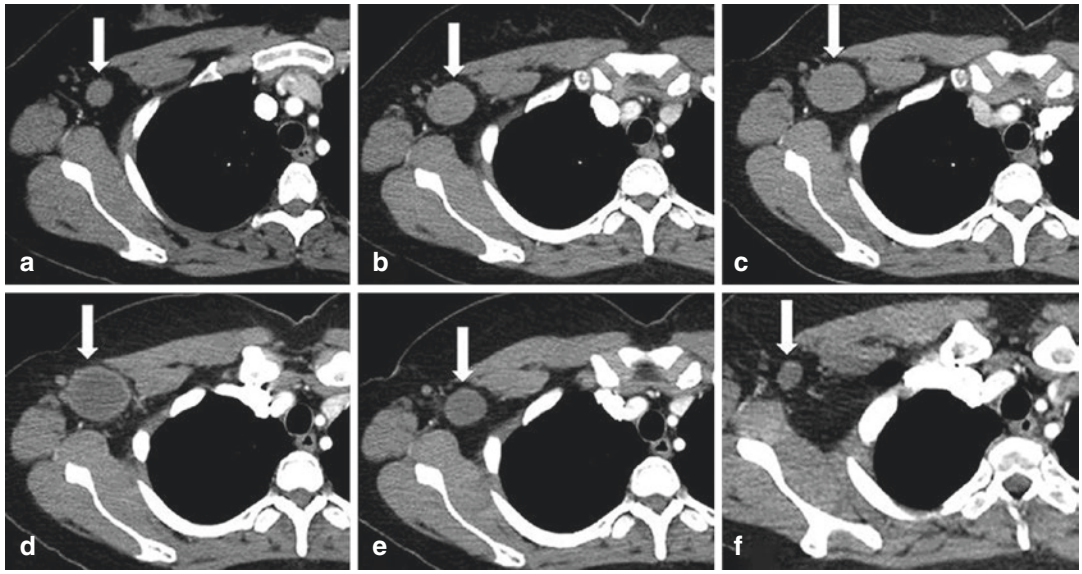

Fig. 7 A 38-year-old female with advanced melanoma with pseudoprogression. (Reprinted with permission from Clin Cancer Res. 2017;23:4671–4679). A baseline scan showed a right axillary lymph node measuring 1.7 cm in short axis (**a**, arrow). The lesion increased in size on the first at 2.7 months (**b**) and second follow-up scans at 4.1 months (**c**), demonstrating increase in size of the lesion more than 20% from baseline, confirming irPD. The lesion reached its maximal size at the third follow-up scan at 5.5 months (**d**), and then started to decrease in size on the fourth scan at 6.7 months (**e**). The lesion further decreased in size gradually, and met the criteria for response at 22.3 months of therapy (**f**). Since then, the lesion remained small and maintained durable response over 19 months

from head to toe, which are termed immune-related adverse events (irAEs). Some of these irAEs may require careful differentiation from tumor progression, and thus have implications on accurate therapy monitoring and tumor response evaluations. The topic of drug toxicities including irAE is discussed in detail in chapter "Drug Toxicity, Approach to Cancer as a Systemic Disease, and Imaging Modality-Specific Considerations".

In summary, strategies for tumor response evaluation for precision cancer therapy and immunotherapy have markedly evolved in the past decade, in response to rapid advances of novel cancer therapies. Tumor response criteria should continue to evolve in parallel with the advances of cancer treatment, in order to provide objective endpoints for trials and evaluations of efficacy and effectiveness in the new era of precision oncology and immuno-oncology.

References

Allison JP, Krummel MF (1995) The Yin and Yang of T-cell costimulation. Science 270:932–933

Benjamin RS, Choi H, Macapinlac HA et al (2007) We should desist using RECIST, at least in GIST. J Clin Oncol 25:1760–1764

Champiat S, Dercle L, Ammari S et al (2017) Hyperprogressive disease is a new pattern of progression in cancer patients treated by anti-PD-1/PD-L1. Clin Cancer Res 23:1920–1928

Chen DS, Irving BA, Hodi FS (2012) Molecular pathways: next-generation immunotherapy—inhibiting programmed death-ligand 1 and programmed death-1. Clin Cancer Res 18:6580–6587

Chiou VL, Burotto M (2015) Pseudoprogression and immune-related response in solid tumors. J Clin Oncol 33:3541–3543

Choi H, Charnsangavej C, de Castro Faria S et al (2004) CT evaluation of the response of gastrointestinal stromal tumors after imatinib mesylate treatment: a quantitative analysis correlated with FDG PET findings. AJR Am J Roentgenol 183:1619–1628

Choi H, Charnsangavej C, Faria SC et al (2007) Correlation of computed tomography and positron emission

tomography in patients with metastatic gastrointestinal stromal tumor treated at a single institution with imatinib mesylate: proposal of new computed tomography response criteria. J Clin Oncol 25:1753–1759

Choi JH, Ahn MJ, Rhim HC et al (2005) Comparison of WHO and RECIST criteria for response in metastatic colorectal carcinoma. Cancer Res Treat 37:290–293

Eisenhauer EA, Therasse P, Bogaerts J et al (2009) New response evaluation criteria in solid tumours: revised RECIST guideline (version 1.1). Eur J Cancer 45:228–247

Erasmus JJ, Gladish GW, Broemeling L et al (2003) Interobserver and intraobserver variability in measurement of non-small-cell carcinoma lung lesions: implications for assessment of tumor response. J Clin Oncol 21:2574–2582

Faivre S, Zappa M, Vilgrain V et al (2011) Changes in tumor density in patients with advanced hepatocellular carcinoma treated with sunitinib. Clin Cancer Res 17:4504–4512

Ferte C, Fernandez M, Hollebecque A et al (2014) Tumor growth rate is an early indicator of antitumor drug activity in phase I clinical trials. Clin Cancer Res 20:246–252

Gettinger SN, Horn L, Gandhi L et al (2015) Overall survival and long-term safety of nivolumab (anti-programmed death 1 antibody, BMS-936558, ONO-4538) in patients with previously treated advanced non-small-cell lung cancer. J Clin Oncol 33: 2004–2012

Gomez-Roca C, Koscielny S, Ribrag V et al (2011) Tumour growth rates and RECIST criteria in early drug development. Eur J Cancer 47:2512–2516

Hodi FS, Hwu WJ, Kefford R et al (2016) Evaluation of immune-related response criteria and RECIST v1.1 in patients with advanced melanoma treated with pembrolizumab. J Clin Oncol 34:1510–1517

Hodi FS, Mihm MC, Soiffer RJ et al (2003) Biologic activity of cytotoxic T lymphocyte-associated antigen 4 antibody blockade in previously vaccinated metastatic melanoma and ovarian carcinoma patients. Proc Natl Acad Sci U S A 100:4712–4717

Hodi FS, Oble DA, Drappatz J et al (2008) CTLA-4 blockade with ipilimumab induces significant clinical benefit in a female with melanoma metastases to the CNS. Nat Clin Pract Oncol 5:557–561

Hodi FS, O'Day SJ, McDermott DF et al (2010) Improved survival with ipilimumab in patients with metastatic melanoma. N Engl J Med 363:711–723

Ishida Y, Agata Y, Shibahara K, Honjo T (1992) Induced expression of PD-1, a novel member of the immunoglobulin gene superfamily, upon programmed cell death. EMBO J 11:3887–3895

Leach DR, Krummel MF, Allison JP (1996) Enhancement of antitumor immunity by CTLA-4 blockade. Science 271:1734–1736

Lenschow DJ, Walunas TL, Bluestone JA (1996) CD28/B7 system of T cell costimulation. Annu Rev Immunol 14:233–258

Levy A, Hollebecque A, Ferte C et al (2013) Tumor assessment criteria in phase I trials: beyond RECIST. J Clin Oncol 31:395

Lynch TJ, Bondarenko I, Luft A et al (2012) Ipilimumab in combination with paclitaxel and carboplatin as first-line treatment in stage IIIB/IV non-small-cell lung cancer: results from a randomized, double-blind, multicenter phase II study. J Clin Oncol 30:2046–2054

Miller AB, Hoogstraten B, Staquet M, Winkler A (1981) Reporting results of cancer treatment. Cancer 47:207–214.

Nishino M (2016) Immune-related response evaluations during immune-checkpoint inhibitor therapy: establishing a “common language” for the new arena of cancer treatment. J Immunother Cancer 4:30

Nishino M (2018) Tumor response assessment for precision cancer therapy: response evaluation criteria in solid tumors and beyond. Am Soc Clin Oncol Educ Book 38:1019–1029

Nishino M, Cardarella S, Jackman DM et al (2013a) RECIST 1.1 in NSCLC patients with EGFR mutations treated with EGFR tyrosine kinase inhibitors: comparison with RECIST 1.0. AJR Am J Roentgenol 201:W64–W71

Nishino M, Dahlberg SE, Adeni AE et al (2017c) Tumor response dynamics of advanced non-small cell lung cancer patients treated with PD-1 inhibitors: imaging markers for treatment outcome. Clin Cancer Res 23:5737–5744

Nishino M, Dahlberg SE, Cardarella S et al (2013b) Volumetric tumor growth in advanced non-small cell lung cancer patients with EGFR mutations during EGFR-tyrosine kinase inhibitor therapy: developing criteria to continue therapy beyond RECIST progression. Cancer 119:3761–3768

Nishino M, Dahlberg SE, Fulton LE et al (2016) Volumetric tumor response and progression in EGFR-mutant NSCLC patients treated with erlotinib or gefitinib. Acad Radiol 23:329–336

Nishino M, Gargano M, Suda M, Ramaiya NH, Hodi FS (2014b) Optimizing immune-related tumor response assessment: does reducing the number of lesions impact response assessment in melanoma patients treated with ipilimumab? J Immunother Cancer 2:17

Nishino M, Giobbie-Hurder A, Gargano M, Suda M, Ramaiya NH, Hodi FS (2013c) Developing a common language for tumor response to immunotherapy: immune-related response criteria using unidimensional measurements. Clin Cancer Res 19: 3936–3943

Nishino M, Giobbie-Hurder A, Manos MP et al (2017b) Immune-related tumor response dynamics in melanoma patients treated with pembrolizumab: identifying markers for clinical outcome and treatment decisions. Clin Cancer Res 23:4671–4679

Nishino M, Guo M, Jackman DM et al (2011b) CT tumor volume measurement in advanced non-small-cell lung cancer: performance characteristics of an emerging clinical tool. Acad Radiol 18:54–62

Nishino M, Hatabu H, Hodi FS (2019) Imaging of cancer immunotherapy: current approaches and future directions. Radiology 290(1):9–22

Nishino M, Hatabu H, Johnson BE, McLoud TC (2014a) State of the art: response assessment in lung cancer in the era of genomic medicine. Radiology 271: 6–27

Nishino M, Jackman DM, Hatabu H, Janne PA, Johnson BE, Van den Abbeele AD (2011a) Imaging of lung cancer in the era of molecular medicine. Acad Radiol 18:424–436

Nishino M, Jagannathan JP, Krajewski KM et al (2012) Personalized tumor response assessment in the era of molecular medicine: cancer-specific and therapy-specific response criteria to complement pitfalls of RECIST. AJR Am J Roentgenol 198:737–745

Nishino M, Jagannathan JP, Ramaiya NH, Van den Abbeele AD (2010) Revised RECIST guideline version 1.1: what oncologists want to know and what radiologists need to know. AJR Am J Roentgenol 195:281–289

Nishino M, Ramaiya NH, Chambers ES et al (2016) Immune-related response assessment during PD-1 inhibitor therapy in advanced non-small-cell lung cancer patients. J Immunother Cancer 4(1):84

Nishino M, Ramaiya NH, Hatabu H, Hodi FS (2017a) Monitoring immune-checkpoint blockade: response evaluation and biomarker development. Nat Rev Clin Oncol 14:655–668

Nishino M, Tirumani SH, Ramaiya NH, Hodi FS (2015) Cancer immunotherapy and immune-related response assessment: the role of radiologists in the new arena of cancer treatment. Eur J Radiol 84:1259–1268

Okazaki T, Chikuma S, Iwai Y, Fagarasan S, Honjo T (2013) A rheostat for immune responses: the unique properties of PD-1 and their advantages for clinical application. Nat Immunol 14:1212–1218

Ott PA, Hodi FS, Robert C (2013) CTLA-4 and PD-1/PD-L1 blockade: new immunotherapeutic modalities with durable clinical benefit in melanoma patients. Clin Cancer Res 19:5300–5309

Pardoll DM (2012) The blockade of immune checkpoints in cancer immunotherapy. Nat Rev Cancer 12: 252–264

Seymour L, Bogaerts J, Perrone A et al (2017) iRECIST: guidelines for response criteria for use in trials testing immunotherapeutics. Lancet Oncol 18:e143–e152

Shankar S, vanSonnenberg E, Desai J, Dipiro PJ, Van Den Abbeele A, Demetri GD (2005) Gastrointestinal stromal tumor: new nodule-within-a-mass pattern of recurrence after partial response to imatinib mesylate. Radiology 235:892–898

Smith AD, Lieber ML, Shah SN (2010b) Assessing tumor response and detecting recurrence in metastatic renal cell carcinoma on targeted therapy: importance of size and attenuation on contrast-enhanced CT. AJR Am J Roentgenol 194:157–165

Smith AD, Shah SN, Rini BI, Lieber ML, Remer EM (2010a) Morphology, Attenuation, Size, and Structure (MASS) criteria: assessing response and predicting clinical outcome in metastatic renal cell carcinoma on antiangiogenic targeted therapy. AJR Am J Roentgenol 194:1470–1478

Stein WD, Gulley JL, Schlom J et al (2011) Tumor regression and growth rates determined in five intramural NCI prostate cancer trials: the growth rate constant as an indicator of therapeutic efficacy. Clin Cancer Res 17:907–917

Stein WD, Wilkerson J, Kim ST et al (2012) Analyzing the pivotal trial that compared sunitinib and IFN-alpha in renal cell carcinoma, using a method that assesses tumor regression and growth. Clin Cancer Res 18:2374–2381

Sun JM, Ahn MJ, Park MJ et al (2010) Accuracy of RECIST 1.1 for non-small cell lung cancer treated with EGFR tyrosine kinase inhibitors. Lung Cancer 69:105–109

Therasse P, Arbuck SG, Eisenhauer EA et al (2000) New guidelines to evaluate the response to treatment in solid tumors. European Organization for Research and Treatment of Cancer, National Cancer Institute of the United States, National Cancer Institute of Canada. J Natl Cancer Inst 92:205–216.

Wolchok J (2012) How recent advances in immunotherapy are changing the standard of care for patients with metastatic melanoma. Ann Oncol 23(Suppl 8):15–21

Wolchok JD, Hoos A, O'Day S et al (2009) Guidelines for the evaluation of immune therapy activity in solid tumors: immune-related response criteria. Clin Cancer Res 15:7412–7420

Zhao B, James LP, Moskowitz CS et al (2009) Evaluating variability in tumor measurements from same-day repeat CT scans of patients with non-small cell lung cancer. Radiology 252:263–272

Zielinski C, Knapp S, Mascaux C, Hirsch F (2013) Rationale for targeting the immune system through checkpoint molecule blockade in the treatment of non-small-cell lung cancer. Ann Oncol 24:1170–1179

Part II

Practical Pitfalls in Therapy Response Imaging in Cancer Patients

Drug Toxicity, Approach to Cancer as a Systemic Disease, and Imaging Modality-Specific Considerations

Hyesun Park and Mizuki Nishino

Contents

Abstract

In addition to the limitations and pitfalls of tumor response criteria and strategies, there are practical pitfalls for therapy response imaging in cancer patients that should be recognized for accurate characterization of tumor response and progression. Drug toxicity in major organs can be noted on imaging with an appearance of unique radiologic characteristics, and should be distinguished from tumor progression. Approaching cancer as a systemic disease is another important concept, because treating physicians need to know the systemic tumor burden changes to make treatment decisions, rather than the changes in individual body parts. Finally, the choice of imaging modality is a key to maximize the contributions of imaging for therapy response assessment, and the strengths and weaknesses in each modality in specific clinical settings need to be acknowledged.

1 Drug Toxicity on Imaging as a Pitfall for Therapy Response Imaging

Systemic cancer therapy is associated with toxicities in various organs, and many of the toxicities involving major organs present with imaging findings that are newly apparent on follow-up

H. Park · M. Nishino (✉)
Department of Imaging, Dana-Farber Cancer Institute, Boston, MA, USA

Department of Radiology, Brigham and Women's Hospital, Boston, MA, USA
e-mail: hpark29@bwh.harvard.edu; mizuki_nishino@dfci.harvard.edu

M. Nishino (ed.), *Therapy Response Imaging in Oncology*, Medical Radiology, Diagnostic Imaging,
https://doi.org/10.1007/978-3-030-31171-1_3

scans during treatment monitoring. Notably, with the increasing use of precision cancer therapy and immune-checkpoint inhibitor therapy, unique sets of drug-related toxicities are noted that are often specific to the "class" of therapeutic agents used. It is important to be aware of the class-specific toxicities of these anticancer agents and be familiar with their imaging manifestations, to make an accurate diagnosis to guide patient management. Moreover, some of these toxicities may be mistaken for tumor progression on imaging, requiring careful interpretation. This section of the chapter focuses on the class-specific toxicities and their imaging manifestations, including (1) immune-checkpoint inhibitors, (2) antiangiogenic inhibitors, and (3) other molecular targeting agents such as mTOR inhibitors and EGFR inhibitors.

1.1 Immune-Related Adverse Events (irAE) During Immune-Checkpoint Inhibitor Therapy

Immune-checkpoint inhibitor therapy is associated with unique toxicities, termed immune-related adverse events (irAEs) that present a spectrum of imaging manifestations in various organs from head to toe (Weber et al. 2017; Michot et al. 2016; Nishino et al. 2017a, 2019; Tirumani et al. 2015a; Bronstein et al. 2011). The irAEs that are detected by imaging include hypophysitis, thyroiditis, sarcoid-like lymphadenopathy, pneumonitis, colitis, hepatitis, and pancreatitis, to name a few (Tirumani et al. 2015a; Nishino et al. 2019). Many of the irAEs are clinically significant and require immediate attention and management, which emphasizes the importance of early detection and accurate diagnosis on imaging. Some of the irAEs may be mistaken for a manifestation of tumor progression, emphasizing the need for expert interpretation of therapy response imaging.

Sarcoid-like lymphadenopathy is one of the irAEs that can be commonly mistaken for new lymph node metastases on imaging indicative of disease progression, and thus requires careful evaluation both clinically and radiologically. Sarcoid-like lymphadenopathy is noted in up to 5–7% of the patients treated with immune-checkpoint inhibitors, and most commonly involves mediastinal and hilar lymph nodes (Tirumani et al. 2015a; Bronstein et al. 2011; Berthod et al. 2012). Most cases are clinically silent and asymptomatic, and are often self-limited and resolve without specific treatment, while symptomatic cases respond well to corticosteroids (Berthod et al. 2012). Imaging manifestations include the appearance of mediastinal and hilar lymphadenopathy after initiation of immune-checkpoint inhibitor therapy, with distributions similar to sarcoidosis (Fig. 1). FDG-avidity of lymph nodes may be noted on PET-CT (Fig. 2) (Tirumani et al. 2015a; Nishino et al. 2019). Lung parenchymal changes of sarcoidosis can also be noted, which helps differentiating this entity from new metastatic lymphadenopathy. Histologic findings consist of granulomatous inflammation resembling sarcoidosis (Tirumani et al. 2015a; Bronstein et al. 2011; Berthod et al. 2012). Sarcoid-like granulomatosis can also occur as an isolated finding in the lung, as focal lung consolidation without accompanying lymphadenopathy (Fig. 3) (Nishino et al. 2018), mimicking progression. To accurately differentiate sarcoid-like lymphadenopathy and granulomatosis from progressive metastatic cancer, familiarity with the clinical and radiographic presentation of this entity and correlation with the pattern and onset of imaging findings in relation to the detailed course of immunotherapy are essential. It is also important to pay particular attention to the systemic tumor burden changes in organs beyond the lymph nodes and lungs. In addition, dialogue with clinical providers about the symptoms and overall disease status may provide important clues (Nishino et al. 2017a, 2019; Tirumani et al. 2015a).

Pneumonitis is another irAE that may require attention when interpreting treatment monitoring scans in patients undergoing immune-checkpoint inhibitor therapy. Pneumonitis related to immune-checkpoint inhibitors is relatively rare, but clinically serious and potentially life-threatening (Nishino et al. 2017a, 2019, 2016a, b, 2015a, 2016c). It has a wide spectrum of clinical and

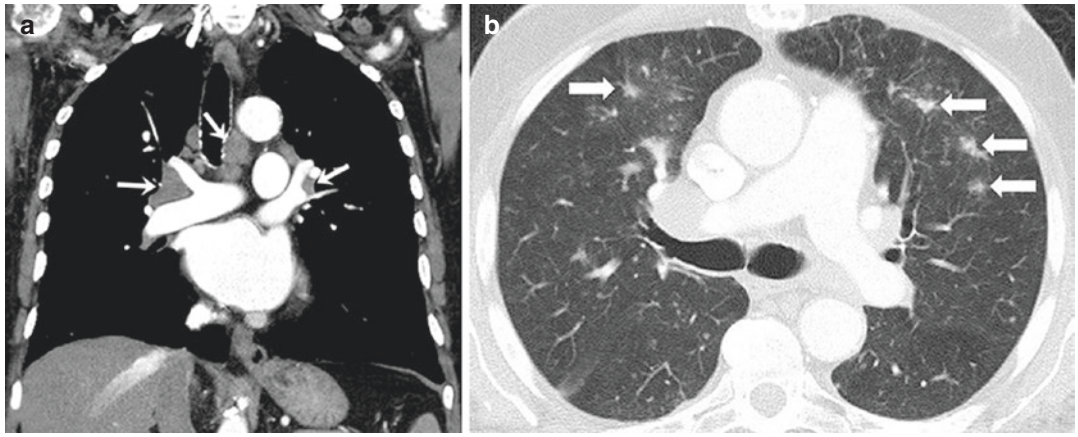

Fig. 1 Sarcoid-like lymphadenopathy in an asymptomatic 81-year-old man with metastatic melanoma treated with ipilimumab. (Reprinted with permission from Cancer Immunol Res. 2015 Oct;3(10):1185–92). (**a**) Coronal reformatted contrast-enhanced chest CT performed 4.9 months after the initiation of ipilimumab therapy showed new bilateral symmetric mediastinal and hilar lymphadenopathy, resembling sarcoidosis. (**b**) Axial CT image of the lungs showed bilateral irregular and nodular parenchymal opacities in upper and middle lung predominance (arrows), with peribronchovascular involvement, which falls in the spectrum of lung parenchymal manifestations of pulmonary sarcoidosis

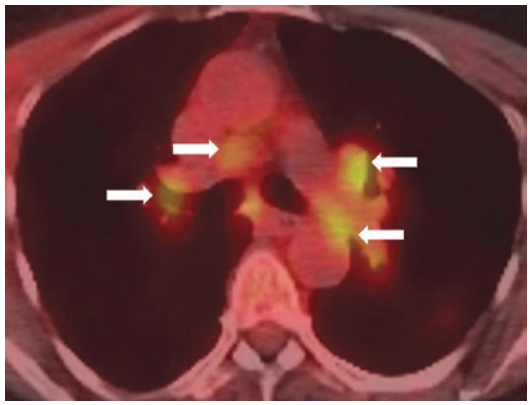

Fig. 2 Sarcoid-like lymphadenopathy in an asymptomatic 55-year-old woman with metastatic melanoma treated with ipilimumab. (Reprinted with permission from Cancer Immunol Res. 2015 Oct;3(10):1185–92). Axial fused FDG-PET/CT images at 3 months of ipilimumab therapy show new FDG-avid mediastinal and bilateral hilar lymphadenopathy (arrows) mimicking sarcoidosis. A follow-up PET/CT performed 5 months later showed resolution of FDG-avid lymphadenopathy (data not shown)

radiographic manifestations, ranging from mild respiratory symptoms that can be treated with oral corticosteroids in an outpatient setting with subtle interstitial changes of the lungs on CT, to rapidly worsening respiratory symptoms that require intensive care unit admission and intubation with extensive lung involvement on CT (Nishino et al. 2015a). Radiographic patterns of pneumonitis can be classified according to American Thoracic Society/European Respiratory Society (ATS/ERS) classifications of idiopathic interstitial pneumonias and related disorders, and include acute interstitial pneumonia (AIP)/acute respiratory distress syndrome (ARDS) pattern, cryptogenic organizing pneumonia (COP) pattern, nonspecific interstitial pneumonia (NSIP) pattern, and hypersensitivity pneumonitis (HP) pattern (Nishino et al. 2016a). Among them, COP pattern is the most common pattern across all tumors and therapeutic regimens, noted in 80% or more of the patients treated with immune-checkpoint inhibitors (Nishino et al. 2016a). Pneumonitis with COP pattern typically presents with multifocal bilateral parenchymal consolidations with accompanying ground glass opacities, often in peripheral and basilar distributions (Fig. 4) (Nishino et al. 2017a, 2019, 2016a, 2017). Development of new lung consolidative opacities may be misinterpreted as progression of lung tumor burden by treating physicians, especially in patients with thoracic malignancies. To avoid

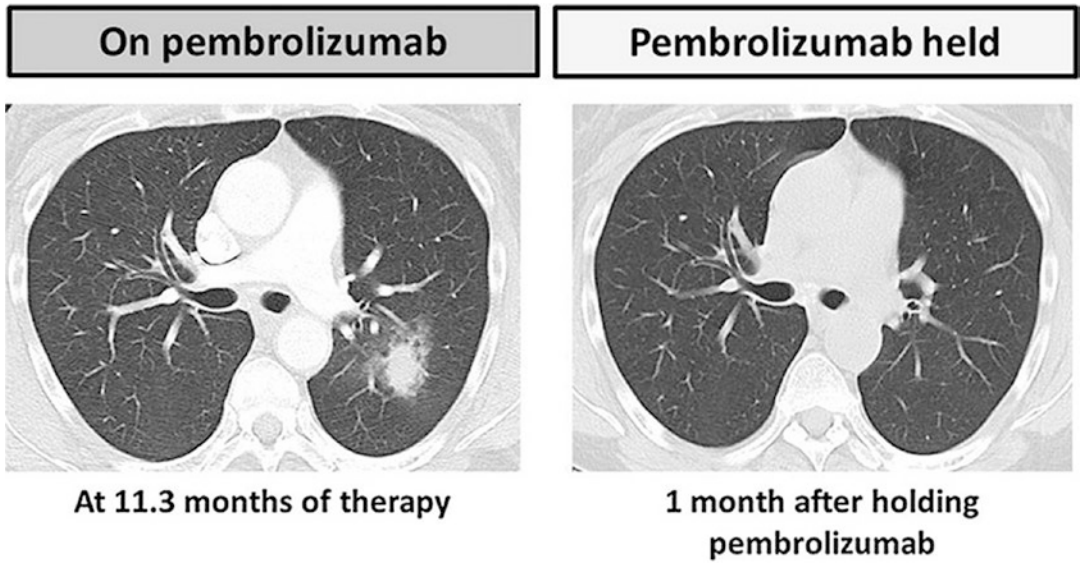

Fig. 3 A 65-year-old asymptomatic woman with melanoma treated with pembrolizumab. At 11 months of therapy, the patient developed a focal round consolidation with GGO halo in the left upper lobe, which resolved on the follow-up scan performed 1 month after holding pembrolizumab. The finding and the clinical course are characteristic for sarcoid-like granulomatosis isolated to the lung. (Reprinted with permission from Cancer Immunol Res. 2018 Jun;6(6):630–635)

such misinterpretation, familiarity with the manifestations of different radiographic patterns of immune-related pneumonitis is extremely important.

Recognition of irAEs can also be important for therapy response imaging because several recent reports indicate that the development of irAEs is associated with higher response rates and longer survival in patients treated with immune-checkpoint inhibitors (Haratani et al. 2018; Sato et al. 2018; Toi et al. 2018; Freeman-Keller et al. 2016). One of these studies evaluated 134 patients with advanced or recurrent NSCLC treated with nivolumab in the second-line setting (Haratani et al. 2018). Using the 6-week landmark analysis, patients with irAE had median progression-free survival (PFS) of 9.2 months compared to 4.8 months in those without irAE ($p = 0.04$). Median overall survival (OS) was not reached for patients with irAEs and was 11.1 months in patients without irAEs ($p = 0.01$). In multivariable analyses, irAEs were associated with better survival outcome, with hazard ratios of 0.525 (95% CI, 0.287–0.937; $p = 0.03$) for PFS and 0.282 (95% CI, 0.101–0.667; $p = 0.003$) for OS (Haratani et al. 2018). These observations indicate that the radiographic detection and diagnosis of irAEs may provide aid for accurate characterization of treatment responses in challenging cases with atypical manifestation of tumor burden changes on imaging.

1.2 Antiangiogenic Inhibitors

Antiangiogenic therapy using vascular endothelial growth factor (VEGF) inhibitors such as bevacizumab and tyrosine kinase inhibitors such as sorafenib and sunitinib is also associated with a variety of class-effect toxicities, including hemorrhage and thromboembolic events in various organs (Nishino et al. 2017a; Tirumani et al. 2014, 2015b; Viswanathan et al. 2014). In the gastrointestinal tract, these agents interfere the bowel microvasculature and cause mucosal ulceration, ischemia, and thrombosis of the vessels, leading to bowel perforation and fistula formation, and delayed anastomotic leak (Viswanathan et al. 2014). Bowel perforation is noted up to 4% of patients treated with

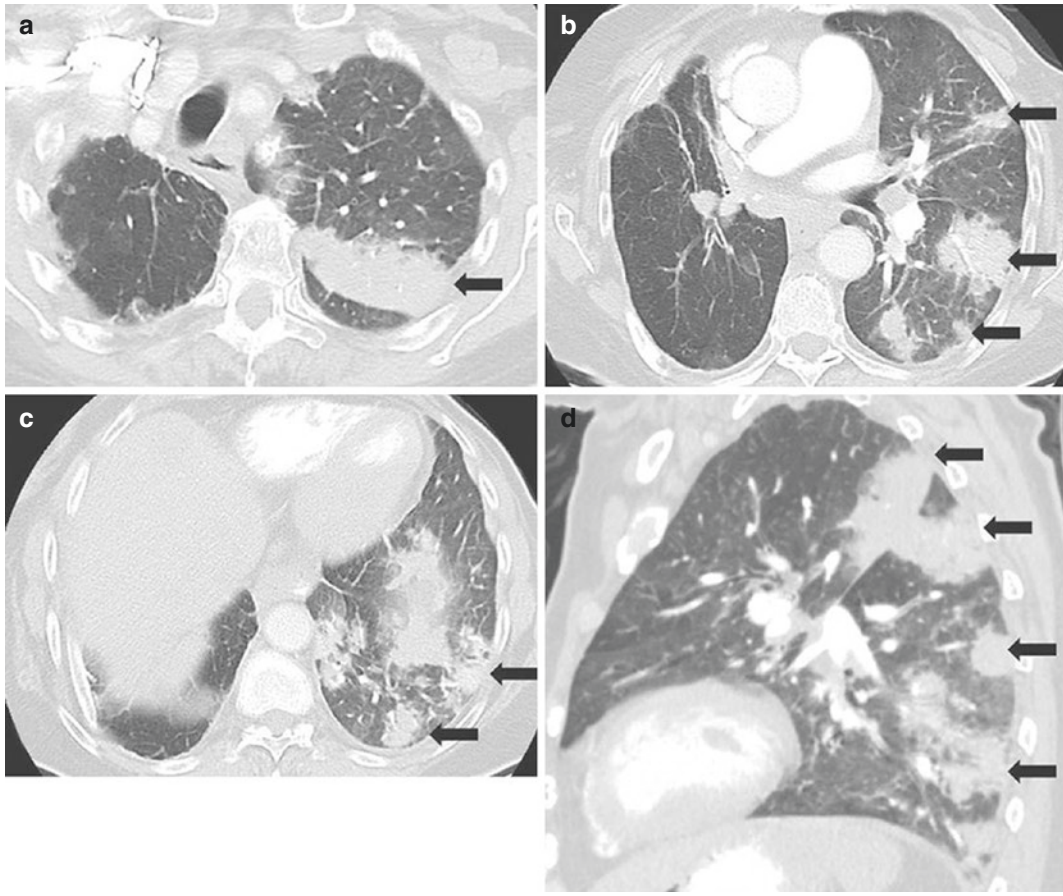

Fig. 4 An 83-year-old woman with recurrent NSCLC treated with nivolumab, presenting with an increasing dry cough, dyspnea, and hypoxemia after 4 weeks of therapy. (Reprinted from Cancer Immunol Res. 2016 Apr;4(4):289–93). (**a**–**d**) Axial (**a**–**c**) and sagittal (**d**) images of chest CT scan at 4 weeks of therapy demonstrated multifocal areas of GGO, reticular opacities, and extensive consolidation in the left lung with a peripheral distribution, demonstrating a COP pattern (arrows)

bevacizumab, and the risk factors include recent colonoscopy or bowel surgery, radiation treatment, the presence of primary tumor, peritoneal carcinomatosis, and high dose of antiangiogenic agents (Fig. 5) (Tirumani et al. 2015b; Viswanathan et al. 2014). Special attention is needed when considering the use of antiangiogenic inhibitors in patients who have serosal implants, preexisting bowel ulceration with adjacent implants, and weakened bowel walls due to underlying conditions such as inflammatory bowel disease, adjacent tumor, and tumor necrosis (Viswanathan et al. 2014), which should be carefully evaluated on pre-therapy imaging. Tumor-bowel fistula refers to a fistulous communication between the bowel loop and an extraluminal malignant tumor, either primary or metastatic, that abuts the bowel loop (Fig. 6) (Tirumani et al. 2014). Drug-related tumor-bowel fistula can be asymptomatic in approximately half of the cases, and can be seen in the setting of either treatment response or progression (Tirumani et al. 2014). Tumor-bowel fistula can be often managed conservatively with discontinuation of therapy (Tirumani et al. 2014).

Delayed anastomotic leak is another condition related to antiangiogenic therapy that requires attention on treatment monitoring scans (Viswanathan et al. 2014). Anastomotic leaks typically occur within 3 months after surgery,

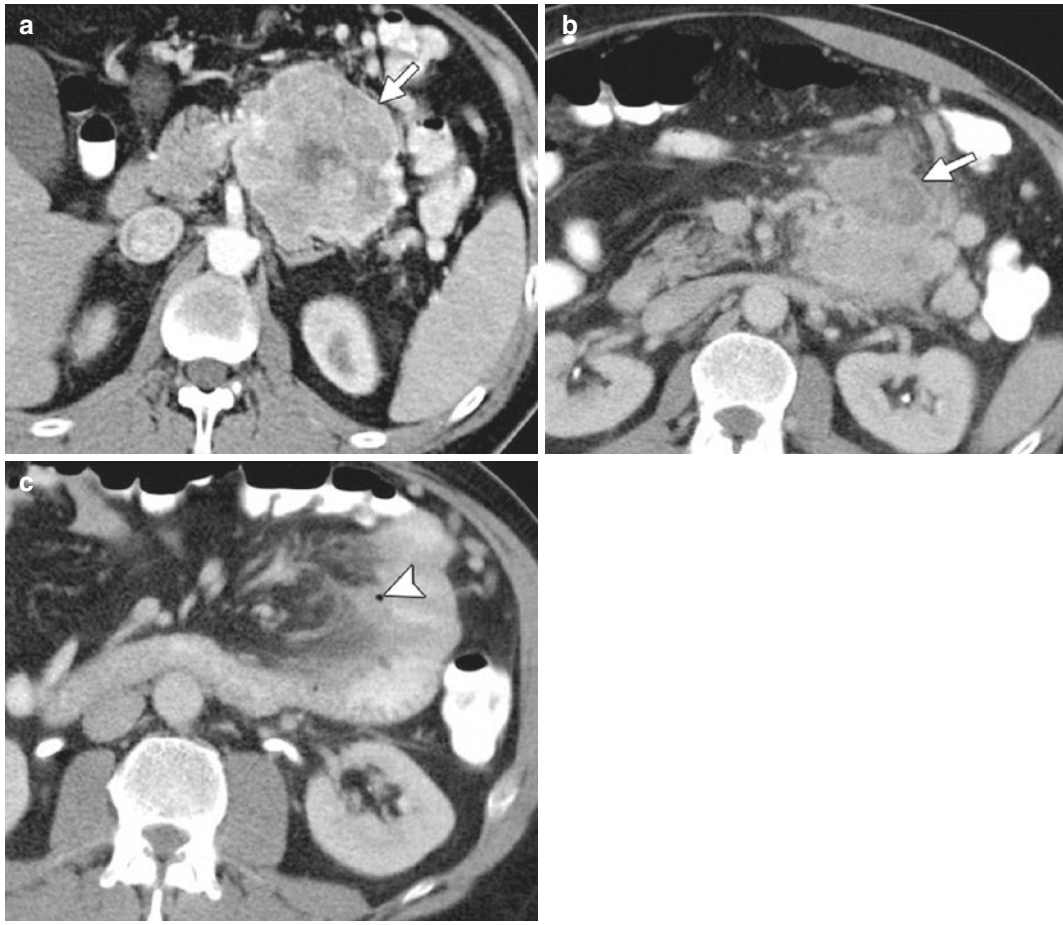

Fig. 5 Neuroendocrine tumor of the pancreas treated with 5-fluorouracil, leucovorin, and bevacizumab in a 49-year-old man who presented to the emergency department with acute abdominal pain. (Reprinted with permission from Radiographics. 2015 Mar-Apr;35(2):455–74). (**a**) Baseline contrast-enhanced CT image shows a large, hypervascular, exophytic pancreatic mass (arrow). (**b**, **c**) Axial contrast-enhanced CT images at the time of acute presentation show a decrease in tumor size (arrow in **b**) with new peritumoral stranding due to jejunal perforation (arrowhead in **c**)

and leaks occurring more than 1 year after surgery raise a suspicion for tumor recurrence. However, delayed anastomotic leaks can be noted more than 1 year after surgery when antiangiogenic therapy is used, in the absence of recurrent tumor. Anastomotic leak is noted on CT with a dehiscence near the surgical clips, increased fluid adjacent to the anastomosis site, and colonic wall thickening, which may be associated with abscess and extraluminal air (Viswanathan et al. 2014). The site of the leak should be carefully evaluated on imaging for the presence of mass that may be splaying the sutures, to differentiate drug-related delayed anastomotic leaks from those due to tumor recurrence (Viswanathan et al. 2014).

1.3 Other Molecular Targeting Agents

mTOR is a critical component of PI3K/Akt/mTOR pathway and is one of the major oncogenic drivers in human cancers (Nishino et al. 2017a, 2015b; Holmes 2011). mTOR inhibitors, including everolimus and temsirolimus, have been approved for treatment of certain types of

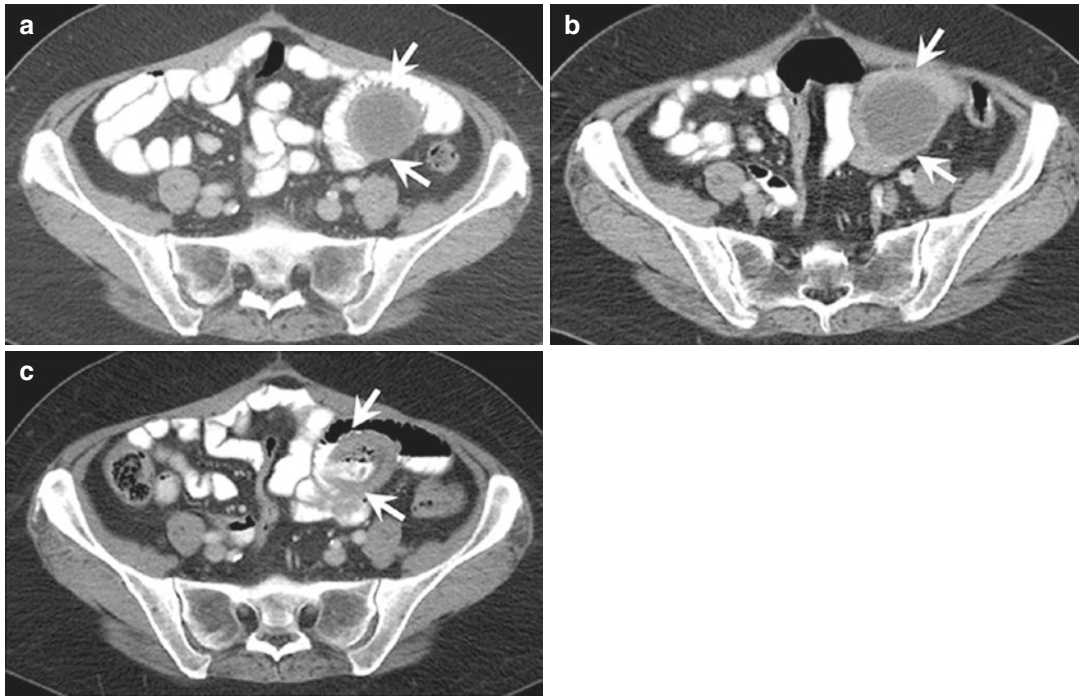

Fig. 6 A 73-year-old woman with metastatic leiomyosarcoma on sunitinib. (**a**, **b**) Axial contrast-enhanced CT images obtained at baseline and 1 month after the start of treatment demonstrate a decrease in the thickness of the enhancing wall of the metastatic deposit in the small bowel mesentery (arrows) in spite of slight increase in size, suggestive of partial response to treatment. (**c**) Axial contrast-enhanced CT images obtained 2 months after start of treatment demonstrates perforation of the adjacent small bowel with a fistulous tract/communication, oral contrast medium, and gas in the mesenteric deposit suggestive of tumor-bowel fistula. (Reprinted with permission from Clin Radiol. 2014 Feb;69(2):e100–7)

advanced cancers such as renal cell carcinomas (RCC) and neuroendocrine tumors. Pneumonitis has been recognized as the class-effect toxicity of mTOR inhibitors, and noted up to 30% in patients with RCC, 25% in NSCLC patients treated in trials, and 21% in patients with advanced neuroendocrine tumor (Dabydeen et al. 2012; Maroto et al. 2011; Soria et al. 2009; Nishino et al. 2016d). The most frequent CT findings of mTOR pneumonitis are bilateral GGOs and reticular opacities, with or without consolidation, in peripheral and lower lung distributions, representing COP pattern or NSIP pattern (Fig. 7) (Nishino et al. 2017a, 2015b, 2016d). Better tumor response and disease control rates have also been reported among patients with mTOR inhibitor pneumonitis compared to those without pneumonitis (Dabydeen et al. 2012), indicating

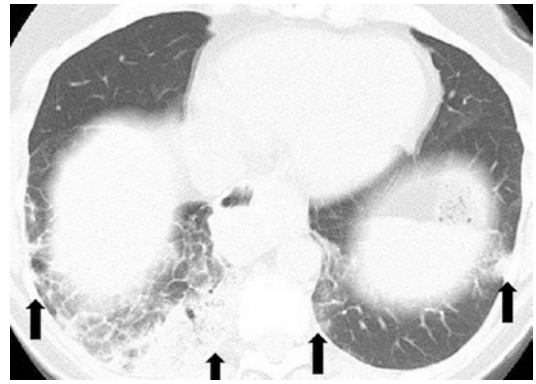

Fig. 7 Pneumonitis in a 66-year-old woman with Waldenström macroglobulinemia treated with mTOR inhibitor therapy. (Reprinted with permission from Radiographics. 2017 Sep-Oct;37(5):1371–1387). Axial CT image at 6 months of therapy shows consolidation, GGOs, and reticular opacities (arrows) that represent a COP pattern

the value of recognition of toxicity to facilitate therapy response imaging.

EGFR inhibitors are also associated with pneumonitis, which is infrequent in the US population; however, a higher incidence rate of 4–5% has been reported among the Japanese population, with high mortality rates of 30–35% (Burotto et al. 2015; Gemma et al. 2014; Kudoh et al. 2008; Suh et al. 2018). A newer EGFR inhibitor, osimertinib, that targets T790M second-site EGFR in acquired resistance NSCLC cases is also associated with pneumonitis with an incidence rate of 3–4% in the overall population of clinical trials (Suh et al. 2018; Soria et al. 2018). Additionally, in NSCLC patients treated with osimertinib, a new type of drug-related pulmonary phenomena termed "transient asymptomatic pulmonary opacities (TAPOs)" have been described (Noonan et al. 2016; Lee et al. 2018). TAPOs were noted in up to 35% of NSCLC patients treated with osimertinib, with the radiological patterns consisting of GGOs with or without nodular consolidation, which resolves during continued osimertinib treatment with a median duration of 6 weeks (Fig. 8). Longer PFS and OS were noted in patients with TAPOs compared to those without (Lee et al. 2018), again emphasizing the relationship between the drug-related toxicity/phenomenon and therapeutic benefit.

2 Approach to Cancer as a Systemic Disease

It has been more than four decades that cancer has been acknowledged as a systemic disease that may present with a local manifestation (Zajicek 1978). Though it may sound like common sense in the current medical practice, the recognition of cancer as a systemic disease is particularly important when performing therapy response imaging. Most patients who are evaluated for therapy response are receiving systemic therapy for their advanced metastatic cancers, except for a minority of patients who receive adjuvant or neoadjuvant therapy. Therefore, patients often have disease involvement in multiple organs or systems that can be beyond the divisions of organ systems that are typically used in radiology specialty practice, such as chest, abdomen, and pelvis. When performing therapy response imaging for advanced cancers, it is often necessary to comprehensively evaluate all the possible sites of involvement to generate an overall evaluation of treatment results. This approach is performed routinely in the clinical trial settings that follow the protocol-defined scan sites and intervals and utilize tumor response criteria such as RECIST. However, in the daily clinical practice, the comprehensive assessments may be missing especially when different body parts are interpreted by different groups of specialists who

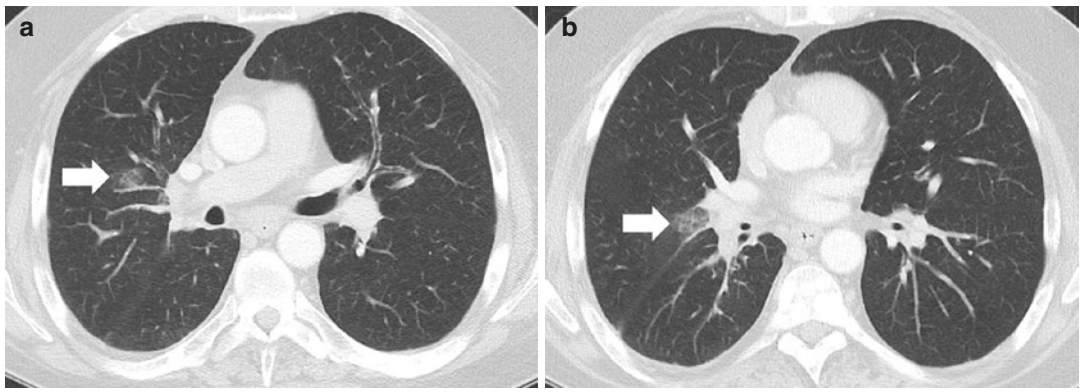

Fig. 8 Transient asymptomatic pulmonary opacities (TAPOs) in a 55-year-old man with advanced NSCLC treated with osimertinib. (**a**, **b**) CT scan of the chest at 2 months of therapy represented a several foci of new ground-glass opacities that are consistent with TAPOs in this asymptomatic patient. The overall tumor burden has decreased compared to the baseline, representing response to therapy (not shown)

focus on one system, leaving the important task of "putting everything together into the context" for the treating physicians. The examples of the solutions for this issue include interpretation of "body" CT including chest, abdomen, and pelvis as one report for oncology cases. Implementation of the radiology consultation service has also been described where radiologists are physically present in the midst of the oncology clinic to discuss the imaging studies of all body parts comprehensively with the multidisciplinary cancer care providers including medical oncologists, radiation oncologists, and surgeons at the tertiary cancer center (Van den Abbeele et al. 2016).

While optimal solutions might differ depending on the practice patterns and logistic barriers, it is important that the individual radiologists regardless of the area of specialty become aware of the concept that cancer is a systemic disease, and try to be prepared to review the imaging studies outside of their core practice when necessary. The approach is particularly important when faced with challenging cases and diagnostic dilemmas that require differentiation of tumor progression versus others including drug toxicity. For example, in the setting of new mediastinal and hilar lymphadenopathy on chest CT in a patient undergoing immune-checkpoint inhibitor therapy, the evaluation of tumor response or progression in the existing sites of the disease, which might be in the abdomen, can be helpful to determine if new lymphadenopathy is more likely due to irAE in the form of sarcoid-like lymphadenopathy or due to progressive metastatic tumor (Fig. 9) (Nishino et al. 2017a). Knowing the overall change in systemic tumor

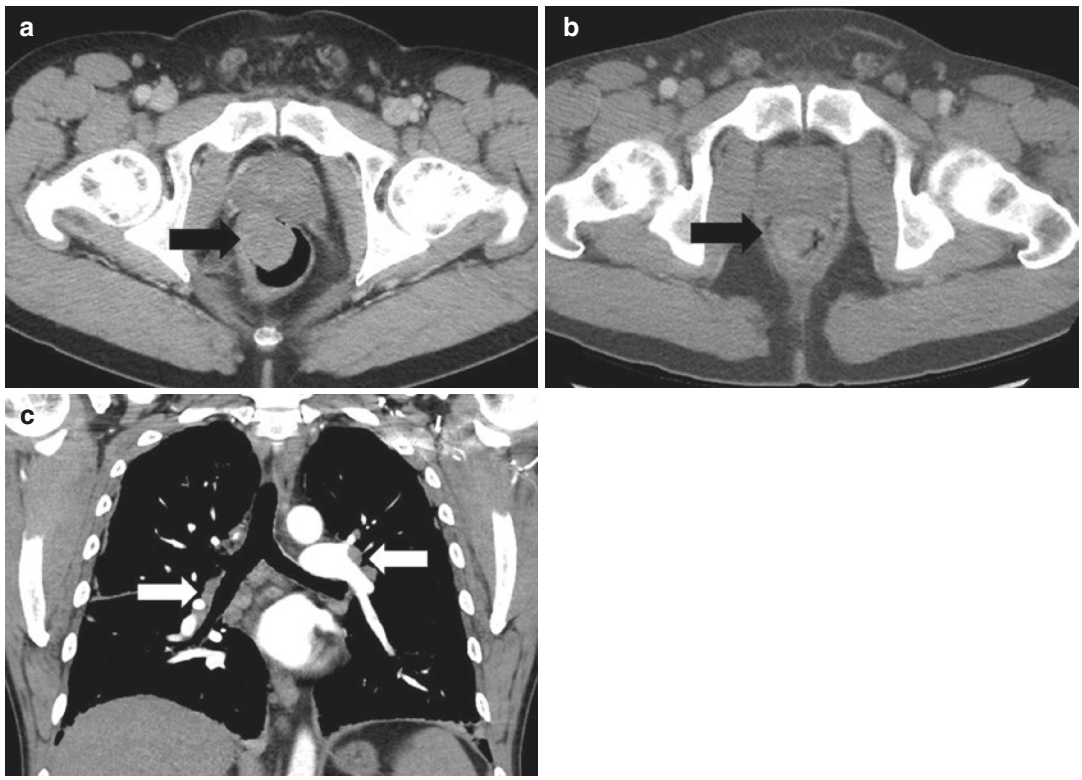

Fig. 9 A 51-year-old man with rectal melanoma treated with ipilimumab and nivolumab combination therapy. (**a**) Baseline CT shows a large intraluminal mass in the rectum (arrow) representing rectal melanoma. (**b**) Follow-up CT after 1 month of therapy shows significant decrease of the rectal mass (arrow). (**c**) However, chest CT after 1 month of therapy demonstrated a development of new bilateral mediastinal and hilar lymphadenopathy. In the light of responding tumor, the findings are most consistent with sarcoid-like lymphadenopathy as a form of irAE rather than progressing tumor

burden is essential to have a meaningful dialogue with treating physicians to discuss the most optimal patient management. In addition, tumors can be heterogeneous among different metastatic sites in one patient, which may lead to different treatment results in different organs or systems (Nishino et al. 2014). In such cases, it is important to document the treatment results according to the different sites. Special emphasis is needed if one of the lesions shows progression while others are responding or remain stable, because the lesion may have acquired different biological characteristics leading to drug resistance and may require molecular and genomic testing from targeted tissue sampling.

3 Modality-Specific Considerations

The choice of imaging modalities is an important component of all types of imaging including therapy response imaging. For most of the solid malignancies undergoing therapy response imaging, CT is by far the most frequently used modality for this purpose, based on its practicality, availability, and reproducibility on serial scans during therapy. It is also relatively easy to implement essentially same CT imaging protocols across different institutions for multicenter trials. With the advances of multi-detector row CT (MDCT) technology, the CT scanning has achieved faster speed and lower radiation exposure, further ensuring its suitability for serial scans for treatment monitoring and response evaluations in patients with systemic tumor burden. In addition to the regular CT scans, advanced techniques including dynamic contrast-enhanced (DCE) CT and dual-energy CT have also been used in the clinical setting. Studies have evaluated the use of CT tumor perfusion assessments on DCE-CT especially in the setting of antiangiogenic therapy (Nishino et al. 2014). However, DCE-CT is not yet used as a standardized routine method for tumor response evaluations in oncology patients. A few recent studies evaluated iodine quantification on dual-energy CT for its supplemental value in response assessment in advanced cancers (Uhrig et al. 2013; Ren et al. 2018); however, further studies are needed to determine its role in routine therapy response imaging.

MRI is another major modality used in therapy response imaging, especially in central nervous system (CNS) malignancies as discussed in chapter "Therapy Response Imaging in Central Nervous System (CNS) Malignancy", and in the setting of neoadjuvant therapy response evaluations in breast cancer that is discussed in chapter "Therapy Response Imaging in Breast Cancer". MRI using diffusion-weighted imaging (DWI) and DCE-MRI is also under active investigation in hepatocellular carcinoma (HCC) undergoing trans-arterial chemoembolization (TACE), which is described in chapter "Therapy Response Imaging in Hepatobiliary and Pancreatic Malignancies". In addition, whole-body MRI is noted as an emerging technique for early diagnosis, staging, and treatment response evaluations in cancer patients especially with bone marrow disease (Morone et al. 2017). In patients with multiple myeloma, whole-body MRI is used as a technique for initial diagnosis and staging, and has shown higher sensitivity for early detection of bone lesions compared to whole-body skeletal survey, whole-body low-dose CT, and FDG-PET/CT (Morone et al. 2017). Whole-body MRI with DWI has high sensitivity and capability for differentiating active from inactive sites of multiple myeloma. (Morone et al. 2017; Messiou and Kaiser 2015). Though the value of whole-body MRI in therapy response evaluations in multiple myeloma is still ongoing, in bone marrow transplant patients, residual bone marrow disease noted on whole-body MRI has shown to be associated with poorer patient outcome and increased risk of disease relapse (Morone et al. 2017; Hillengass et al. 2012). In patients with metastatic bone disease, whole-body MRI including DWI is tested for the evaluation of therapy response including a combination of size, morphologic features, number of lesions, MR signal intensity on T1- and T2-weighted images, and characteristics on DWI (Morone et al. 2017). In addition to these specific indications, MRI can also be useful as a problem-solving tool in cancer

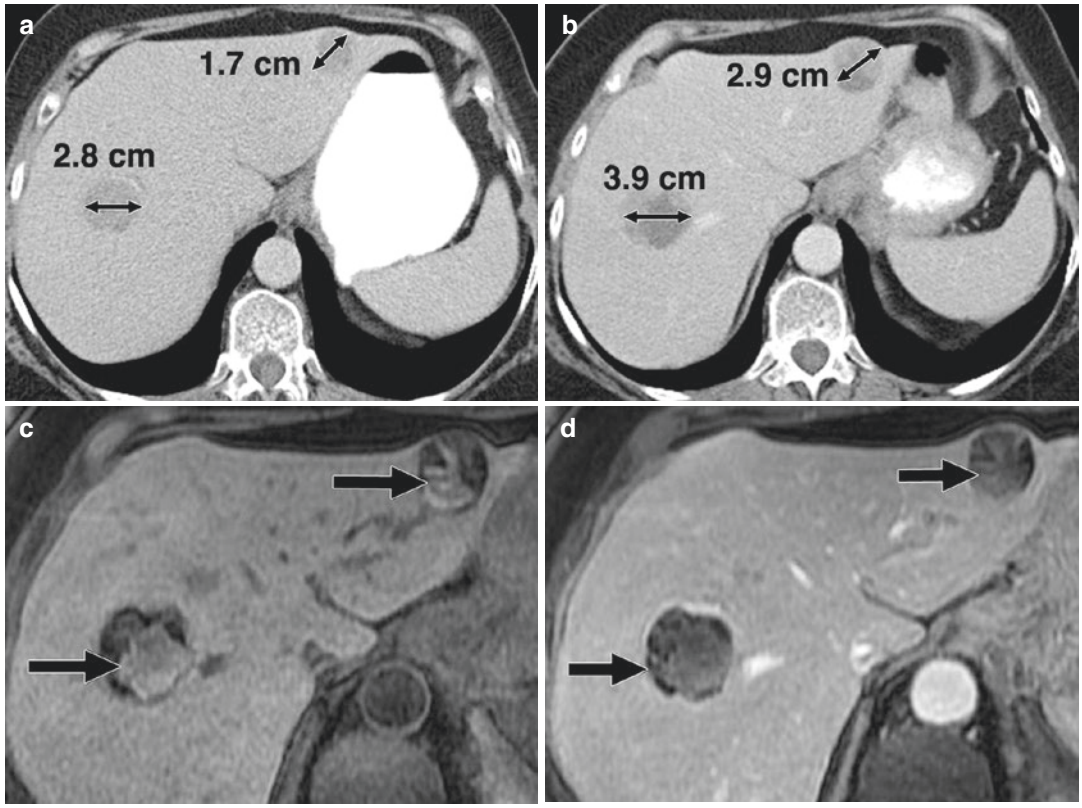

Fig. 10 Paradoxical increase in size of target lesions after targeted therapy in a 69-year-old woman with melanoma. (**a**) Baseline CT scan of abdomen shows two metastatic lesions in liver. (**b**) Follow-up CT scan obtained after treatment with tyrosine kinase inhibitor, sorafenib, shows increase in size of metastatic liver lesions, measuring 3.9 cm at follow-up compared with 2.8 cm at baseline and 2.9 cm compared with 1.7 cm at baseline. Note heterogeneous CT attenuation within liver lesions. (**c**, **d**) MR images of abdomen show central high signal intensity of lesions (arrows) with surrounding hypointense rim on unenhanced T1-weighted image (**c**) and without enhancement on contrast-enhanced T1-weighted image (**d**). (Reprinted with permission from AJR Am J Roentgenol. 2010 Aug;195(2):281–9)

patients undergoing systemic therapy. For example, patients treated with antiangiogenic therapy may present with a paradoxical increase of tumor size despite response to therapy because of hemorrhage or necrosis (Nishino et al. 2010a). In this setting, MRI can be performed to confirm the presence of these intratumoral changes and to clearly distinguish the phenomenon from tumor progression (Fig. 10) (Nishino et al. 2010a).

FDG-PET/CT is a leading modality that helps to implement a component of functional imaging in tumor response evaluations. RECIST1.1 has added FDG-PET for detection of new lesions, which was shown to impact response assessment results in patients with lung cancer (Nishino et al. 2010b; Eisenhauer et al. 2009). FDG-PET/CT is also an essential modality in therapeutic response evaluations in patients with lymphoma, which is discussed in detail in chapter "Therapy Response Imaging in Lymphoma and Hematologic Malignancies". PET/CT can also visualize and quantify different molecular functions beyond glucose metabolism by FDG, and a number of novel tracers are tested for specific indications such as cancer immunotherapy, as discussed in chapter "Molecular and Functional Imaging in Oncology Therapy Response". Emerging observations of the utility of novel PET tracer imaging in individual cancer types treated with specific therapy are also covered in the corresponding

chapters in Part III. The accumulating data indicate the value of PET/CT in therapy response imaging and outcome prediction, which emphasize the need to overcome logistic barriers and establish standardized methods for imaging and interpretation of the novel tracer imaging by PET/CT for oncology patients. It is also important to strategically implement novel tracer PET imaging to address unmet clinical needs that remain unsolved by conventional response evaluation strategies using RECIST.

4 Conclusions

Awareness of common and emerging drug-related toxicities as a pitfall for therapy response imaging is essential to perform accurate tumor response evaluations. Approach to cancer as a systemic disease should be emphasized as an important concept for therapy response imaging, which should provide comprehensive assessment of tumor behavior during therapy. The utility and value of each modality help to optimize imaging strategies for cancer patients and provide answers to clinical questions in the setting of therapy response imaging.

References

Berthod G, Lazor R, Letovanec I et al (2012) Pulmonary sarcoid-like granulomatosis induced by ipilimumab. J Clin Oncol 30:e156–e159

Bronstein Y, Ng CS, Hwu P, Hwu WJ (2011) Radiologic manifestations of immune-related adverse events in patients with metastatic melanoma undergoing anti-CTLA-4 antibody therapy. AJR Am J Roentgenol 197:W992–W1000

Burotto M, Manasanch EE, Wilkerson J, Fojo T (2015) Gefitinib and erlotinib in metastatic non-small cell lung cancer: a meta-analysis of toxicity and efficacy of randomized clinical trials. Oncologist 20:400–410

Dabydeen DA, Jagannathan JP, Ramaiya N et al (2012) Pneumonitis associated with mTOR inhibitors therapy in patients with metastatic renal cell carcinoma: incidence, radiographic findings and correlation with clinical outcome. Eur J Cancer 48:1519–1524

Eisenhauer EA, Therasse P, Bogaerts J et al (2009) New response evaluation criteria in solid tumours: revised RECIST guideline (version 1.1). Eur J Cancer 45:228–247

Freeman-Keller M, Kim Y, Cronin H, Richards A, Gibney G, Weber JS (2016) Nivolumab in resected and unresectable metastatic melanoma: characteristics of immune-related adverse events and association with outcomes. Clin Cancer Res 22:886–894

Gemma A, Kudoh S, Ando M et al (2014) Final safety and efficacy of erlotinib in the phase 4 POLARSTAR surveillance study of 10 708 Japanese patients with non-small-cell lung cancer. Cancer Sci 105:1584–1590

Haratani K, Hayashi H, Chiba Y et al (2018) Association of immune-related adverse events with nivolumab efficacy in non-small-cell lung cancer. JAMA Oncol 4:374–378

Hillengass J, Ayyaz S, Kilk K et al (2012) Changes in magnetic resonance imaging before and after autologous stem cell transplantation correlate with response and survival in multiple myeloma. Haematologica 97:1757–1760

Holmes D (2011) PI3K pathway inhibitors approach junction. Nat Rev Drug Discov 10:563–564

Kudoh S, Kato H, Nishiwaki Y et al (2008) Interstitial lung disease in Japanese patients with lung cancer: a cohort and nested case-control study. Am J Respir Crit Care Med 177:1348–1357

Lee H, Lee HY, Sun JM et al (2018) Transient asymptomatic pulmonary opacities during osimertinib treatment and its clinical implication. J Thorac Oncol 13(8):1106–1112

Maroto JP, Hudes G, Dutcher JP et al (2011) Drug-related pneumonitis in patients with advanced renal cell carcinoma treated with temsirolimus. J Clin Oncol 29:1750–1756

Messiou C, Kaiser M (2015) Whole body diffusion weighted MRI—a new view of myeloma. Br J Haematol 171:29–37

Michot JM, Bigenwald C, Champiat S et al (2016) Immune-related adverse events with immune checkpoint blockade: a comprehensive review. Eur J Cancer 54:139–148

Morone M, Bali MA, Tunariu N et al (2017) Whole-body MRI: current applications in oncology. AJR Am J Roentgenol 209:W336–w349

Nishino M, Jagannathan JP, Ramaiya NH, Van den Abbeele AD (2010a) Revised RECIST guideline version 1.1: what oncologists want to know and what radiologists need to know. AJR Am J Roentgenol 195:281–289

Nishino M, Jackman DM, Hatabu H et al (2010b) New Response Evaluation Criteria in Solid Tumors (RECIST) guidelines for advanced non-small cell lung cancer: comparison with original RECIST and impact on assessment of tumor response to targeted therapy. AJR Am J Roentgenol 195:W221–W228

Nishino M, Hatabu H, Johnson BE, McLoud TC (2014) State of the art: response assessment in lung cancer in the era of genomic medicine. Radiology 271:6–27

Nishino M, Sholl LM, Hodi FS, Hatabu H, Ramaiya NH (2015a) Anti-PD-1-related pneumonitis during cancer immunotherapy. N Engl J Med 373:288–290

Nishino M, Boswell EN, Hatabu H, Ghobrial IM, Ramaiya NH (2015b) Drug-related pneumonitis during mammalian target of rapamycin inhibitor therapy: radiographic pattern-based approach in Waldenstrom macroglobulinemia as a paradigm. Oncologist 20:1077–1083

Nishino M, Chambers ES, Chong CR et al (2016a) Anti-PD-1 inhibitor-related pneumonitis in non-small cell lung cancer. Cancer Immunol Res 4:289–293

Nishino M, Giobbie-Hurder A, Hatabu H, Ramaiya NH, Hodi FS (2016b) Incidence of programmed cell death 1 inhibitor-related pneumonitis in patients with advanced cancer: a systematic review and meta-analysis. JAMA Oncol 2(12):1607–1616

Nishino M, Ramaiya NH, Awad MM et al (2016c) PD-1 inhibitor-related pneumonitis in advanced cancer patients: radiographic patterns and clinical course. Clin Cancer Res 22:6051–6060

Nishino M, Brais LK, Brooks NV, Hatabu H, Kulke MH, Ramaiya NH (2016d) Drug-related pneumonitis during mammalian target of rapamycin inhibitor therapy in patients with neuroendocrine tumors: a radiographic pattern-based approach. Eur J Cancer 53:163–170

Nishino M, Hatabu H, Sholl LM, Ramaiya NH (2017a) Thoracic complications of precision cancer therapies: a practical guide for radiologists in the new era of cancer care. Radiographics 37:1371–1387

Nishino M, Hatabu H, Hodi FS, Ramaiya NH (2017) Drug-related pneumonitis in the era of precision cancer therapy. JCO Precis Oncol – published online May 26. https://doi.org/10.1200/PO.17.00026

Nishino M, Sholl LM, Awad MM, Hatabu H, Armand P, Hodi FS (2018) Sarcoid-like granulomatosis of the lung related to immune-checkpoint inhibitors: distinct clinical and imaging features of a unique immune-related adverse event. Cancer Immunol Res 6(6):630–635

Nishino M, Hatabu H, Hodi FS (2019) Imaging of cancer immunotherapy: current approaches and future directions. Radiology 290:9–22

Noonan SA, Sachs PB, Camidge DR (2016) Transient asymptomatic pulmonary opacities occurring during osimertinib treatment. J Thorac Oncol 11:2253–2258

Ren Y, Jiao Y, Ge W et al (2018) Dual-energy computed tomography-based iodine quantitation for response evaluation of lung cancers to chemoradiotherapy/radiotherapy: a comparison with fluorine-18 fluorodeoxyglucose positron emission tomography/computed tomography-based positron emission tomography/computed tomography response evaluation criterion in solid tumors. J Comput Assist Tomogr 42:614–622

Sato K, Akamatsu H, Murakami E et al (2018) Correlation between immune-related adverse events and efficacy in non-small cell lung cancer treated with nivolumab. Lung Cancer 115:71–74

Soria JC, Shepherd FA, Douillard JY et al (2009) Efficacy of everolimus (RAD001) in patients with advanced NSCLC previously treated with chemotherapy alone or with chemotherapy and EGFR inhibitors. Ann Oncol 20:1674–1681

Soria JC, Ohe Y, Vansteenkiste J et al (2018) Osimertinib in untreated EGFR-mutated advanced non-small-cell lung cancer. N Engl J Med 378:113–125

Suh CH, Park HS, Kim KW, Pyo J, Hatabu H, Nishino M (2018) Pneumonitis in advanced non-small-cell lung cancer patients treated with EGFR tyrosine kinase inhibitor: meta-analysis of 153 cohorts with 15,713 patients: meta-analysis of incidence and risk factors of EGFR-TKI pneumonitis in NSCLC. Lung Cancer 123:60–69

Tirumani SH, Shinagare AB, Jagannathan JP, Krajewski KM, Ramaiya NH (2014) Multidetector-row CT of tumour-bowel fistula: experience at a tertiary cancer centre. Clin Radiol 69:e100–e107

Tirumani SH, Ramaiya NH, Keraliya A et al (2015a) Radiographic profiling of immune-related adverse events in advanced melanoma patients treated with ipilimumab. Cancer Immunol Res 3:1185–1192

Tirumani SH, Fairchild A, Krajewski KM et al (2015b) Anti-VEGF molecular targeted therapies in common solid malignancies: comprehensive update for radiologists. Radiographics 35:455–474

Toi Y, Sugawara S, Kawashima Y et al (2018) Association of immune-related adverse events with clinical benefit in patients with advanced non-small-cell lung cancer treated with nivolumab. Oncologist 23(11):1358–1365

Uhrig M, Sedlmair M, Schlemmer HP, Hassel JC, Ganten M (2013) Monitoring targeted therapy using dual-energy CT: semi-automatic RECIST plus supplementary functional information by quantifying iodine uptake of melanoma metastases. Cancer Imaging 13:306–313

Van den Abbeele AD, Krajewski KM, Tirumani SH et al (2016) Cancer imaging at the crossroads of precision medicine: perspective from an academic imaging department in a Comprehensive Cancer Center. J Am Coll Radiol 13:365–371

Viswanathan C, Truong MT, Sagebiel TL et al (2014) Abdominal and pelvic complications of nonoperative oncologic therapy. Radiographics 34:941–961

Weber JS, Hodi FS, Wolchok JD et al (2017) Safety profile of nivolumab monotherapy: a pooled analysis of patients with advanced melanoma. J Clin Oncol 35:785–792

Zajicek G (1978) Cancer as a systemic disease. Med Hypotheses 4:193–207

Part III

Disease-Specific Approach for Therapy Response Imaging

1 Overview of Disease-Specific Approach

Based on the basic concept and strategies for conventional and emerging criteria for tumor response evaluations described in Part I and the practical pitfalls in therapy response imaging described in Part II, Part III describes therapy response imaging for individual tumors stratified according to the organ systems and cell origins, featuring "disease-specific approach."

The chapters in Part I reviewed the basics of conventional and emerging tumor response criteria and their limitations, and Part II described the practical pitfalls in therapy response imaging, including drug toxicity, approach to cancer as a systemic disease, and modality-specific considerations. Building on the knowledge, therapy response imaging of individual tumor types is discussed in Part III, emphasizing the importance of "disease-specific approach." The following nine chapters in Part III represent major types of cancer according to the organ systems or cell origins, and each chapter includes several subtypes of cancer within the group. The discussion includes advances in therapeutic approaches, strategies and pitfalls for tumor response evaluations, and emerging approaches and challenges that are specific to individual cancer types.

When performing therapy response imaging, it is important to be familiar with the characteristics of tumor response and progression and their pitfalls for each type of cancer, because tumoral behavior during therapy can be distinctly different among different types of cancers. In addition, cancer types and subtypes are the primary determinant of anticancer therapeutic agents to be used, which are also associated with specific characteristics and challenges. Each type of cancer represents a different disease, and it is essential to be aware of the types of cancers and types of agents in each case when performing therapy response imaging.

Therapy Response Imaging in Central Nervous System (CNS) Malignancy

Peter Abraham and Jason Handwerker

Contents

P. Abraham · J. Handwerker (✉)
Department of Radiology, University of California San Diego, La Jolla, CA, USA
e-mail: jhandwerker@health.ucsd.edu

Abstract

The wide spectrum of central nervous system (CNS) neoplasms and treatment-related changes makes imaging evaluation of treatment response challenging. In this chapter, we provide an overview of disease-specific approaches for therapy-response imaging. First, we review relevant background, such as classic MRI characteristics of pre- and post-treatment changes in CNS malignancy, the WHO brain tumor classification, and novel therapeutic approaches for CNS malignancy. Next, we discuss CNS therapy-response imaging strategies and pitfalls, including a discussion of RANO, pseudoprogression, pseudoresponse, and radiation necrosis. Lastly, we review emerging approaches for CNS therapy-response imaging, such as iRANO and radiomics. Understanding posttreatment imaging changes of CNS malignancies is crucial to help direct clinical management.

1 Background

Brain tumors remain a significant global health problem, with a broad array of pathology and often with high morbidity and mortality. The most common pathologies include malignant gliomas and metastases. In 2016, the World Health Organization Classification of Tumors of the Central Nervous System updated its overview

M. Nishino (ed.), *Therapy Response Imaging in Oncology*, Medical Radiology, Diagnostic Imaging,
https://doi.org/10.1007/978-3-030-31171-1_4

of tumor classification in an attempt to define tumor entities using both molecular parameters and histology (Louis et al. 2016).

Malignant glioma is the most common type of primary adult malignant brain tumor accounting for disproportionate morbidity and mortality due to its poor prognosis (Wen and Kesari 2008). Glioblastoma multiforme (GBM) accounts for 60–70% of malignant gliomas, with especially poor median survival of only 10 and 12 months (Fig. 1) (Ostrom et al. 2016). Treatment of newly diagnosed malignant gliomas typically involves maximal safe resection followed by radiotherapy and chemotherapy. Genetic mutations and syndromes are increasingly understood in the development of gliomas, with mutations in the p53 gene especially implicated in the development of low-grade astrocytomas and the secondary glioblastomas derived from them (Ohgaki 2009). Ionizing radiation is a proven environmental exposure predisposing to brain tumors.

Even more common, CNS metastatic disease occurs in up to 25% of adult cancer patients. The risk of brain involvement varies by primary cancer, with lung (40%), breast (20%), and melanoma (10%) primaries posing the highest risk (Fig. 2) (Barajas and Cha 2016). While arising from the meninges rather than the brain, the common benign intracranial tumor is a meningioma, which is typically slow growing although an atypical meningioma may be fast growing and invade the brain.

MRI is the mainstay for imaging assessment. Principal goals of imaging are to establish a diagnosis, define the baseline extent of disease, and follow change over time. Technical considerations including establishing a consistent brain tumor imaging protocol that typically includes a high-resolution volumetric post-contrast T1-weighted sequence and stable timing of contrast administration. Given the myriad of CNS tumor pathologies and varied imaging appearances, a comprehensive imaging description of each tumor subtype is beyond the scope of this chapter. When evaluating a suspected tumor, one of the first considerations in establishing a differential diagnosis is to determine the anatomic location, especially whether a lesion is intra-axial or extra-axial.

Although not entirely specific, contrast enhancement remains one of the most helpful biomarkers to evaluate brain tumors, as normal brain tissue excludes contrast due to an intact

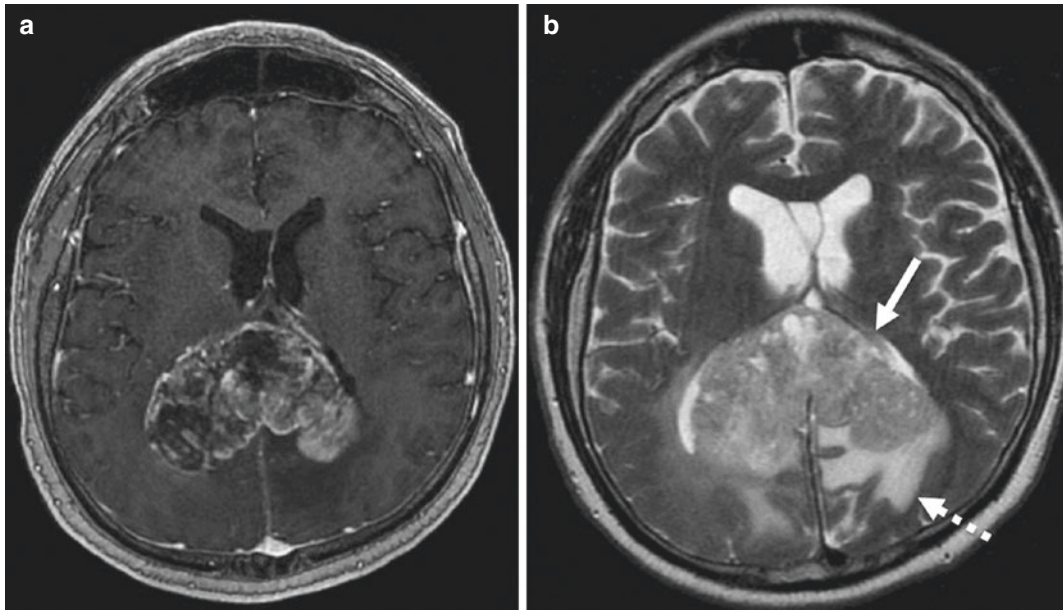

Fig. 1 Glioblastoma (GBM). (**a**) Post-contrast T1-weighted image demonstrates avid heterogenous enhancement with a "butterfly" pattern crossing the splenium of the corpus callosum. (**b**) T2-weighted image demonstrates heterogeneous mass-like signal (arrow) with surrounding hyperintense signal that may reflect a combination of infiltrative tumor and vasogenic edema (dashed arrow)

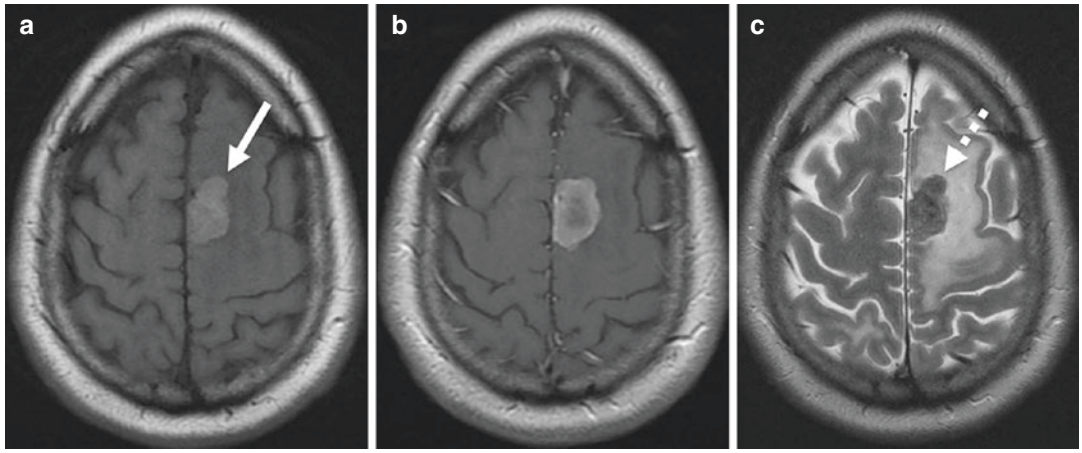

Fig. 2 Melanoma metastasis. (**a**) Pre-contrast T1-weighted image demonstrates intrinsic hyperintense signal due to melanin (arrow). (**b**) Post-contrast T1-weighted image demonstrates accompanying avid peripheral enhancement with central hypoenhancement. (**c**) T2-weighted image demonstrates hyperintense signal in the mass (dashed arrow) with surrounding hyperintense vasogenic edema

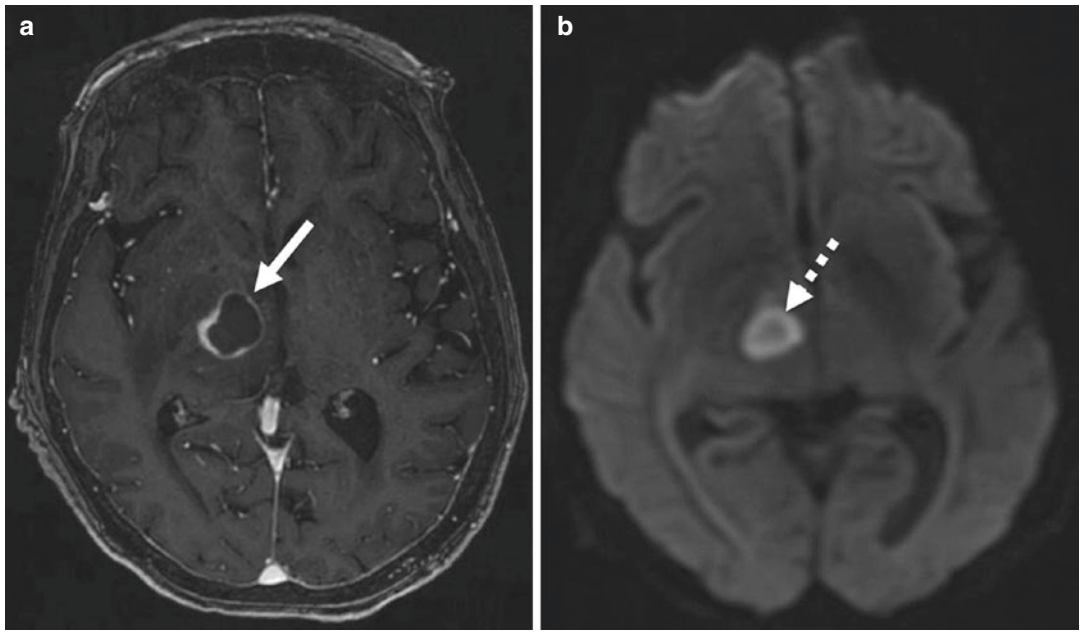

Fig. 3 Cerebral abscess. (**a**) Post-contrast T1-weighted image shows smooth rim-enhancement (arrow) in the right thalamus that is thinner towards the third ventricle medially, where the blood supply is less abundant. (**b**) DWI shows central diffusion restriction associated with internal purulent material (dashed arrow)

blood-brain barrier. In addition, tumors may be manifested by mass-like or infiltrative T2 FLAIR signal, although this may be confounded by vasogenic edema secondary to the tumor. The combination non-enhancing T2 FLAIR hyperintense tumor and vasogenic edema may especially challenge precise measurement of tumor extent. Finally, identifying complications of CNS malignancies such as hemorrhage, herniation, and hydrocephalus is critical to guide timely therapy.

A tissue biopsy is often required, except in the cases of compelling clinical suspicion, characteristic radiographic appearance, and location of the tumor, such as in the case of a brainstem glioma. It is also critical to understand imaging pitfalls that mimic CNS malignancy (Fig. 3). In

particular, the differential diagnosis of a rim-enhancing lesion includes primary neoplasm, metastasis, lymphoma, tumefactive demyelination, abscess, and encephalitis (Al-Okaili et al. 2006). If tissue is obtained, a final diagnosis requires radiologic and pathologic correlation.

2 Advanced Imaging

Given overlap of convention imaging findings and tissue sampling error, advanced MR techniques have been developed to help improve diagnostic accuracy and suggest tumor grade. Advanced MR techniques include MR spectroscopy, perfusion imaging, and diffusion-weighted imaging. MR spectroscopy compares the chemical composition of normal brain with abnormal tissue by comparing the relative concentrations of metabolites based on their resonant frequencies. Most commonly, neoplasms demonstrate decreased *N*-acetyl aspartate (NAA), increased choline, and decreased creatine (Fig. 4). Perfusion imaging can quantitatively assess tumor hemodynamics, which can be performed by non-contrast ASL techniques or contrast-enhanced techniques, such as dynamic contrast-enhanced (DCE) or dynamic susceptibility contrast (DSC) MR perfusion. One of the most common parameters calculated is the cerebral blood volume (CBV), which is calculated from an area under the concentration-time curve. Diffusion-weighted imaging can provide insight regarding the cellular density of the lesion, which is typically inversely related to the freedom of water molecule movement (Fig. 5) (Al-Okaili et al. 2006).

2.1 Baseline and Immediate Postoperative Changes

The goal of postoperative imaging is to define the extent of resection, to evaluate for complications, and to establish a baseline for follow-up imaging. Early postoperative imaging is helpful to avoid the possibility of confounding enhancement,

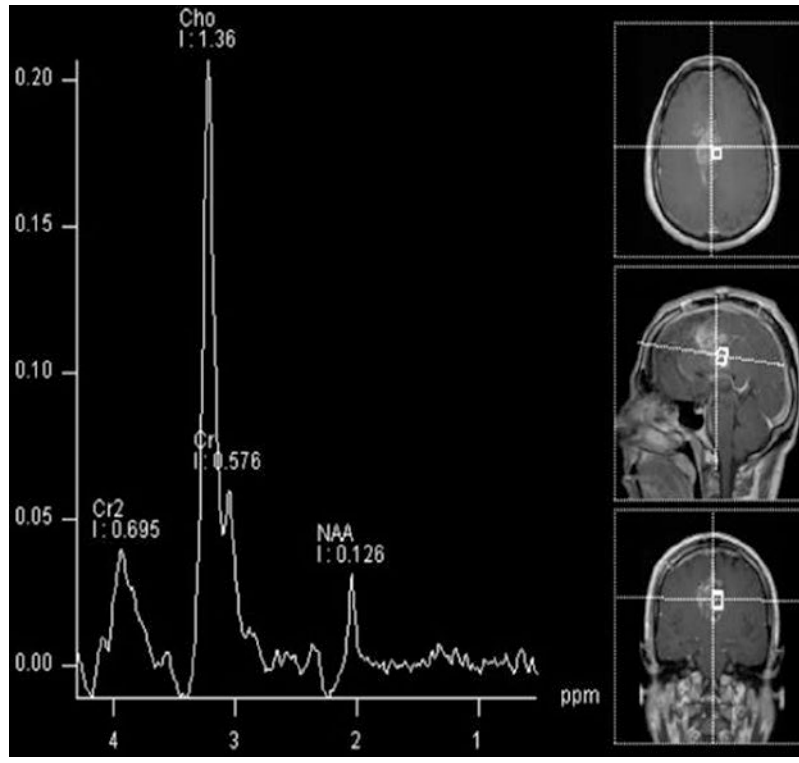

Fig. 4 Single-voxel spectroscopy (TE 144 ms) demonstrating high choline (Cho), low creatine (Cre), and low *N*-acetylaspartate (NAA) peaks associated with a high-grade glioma

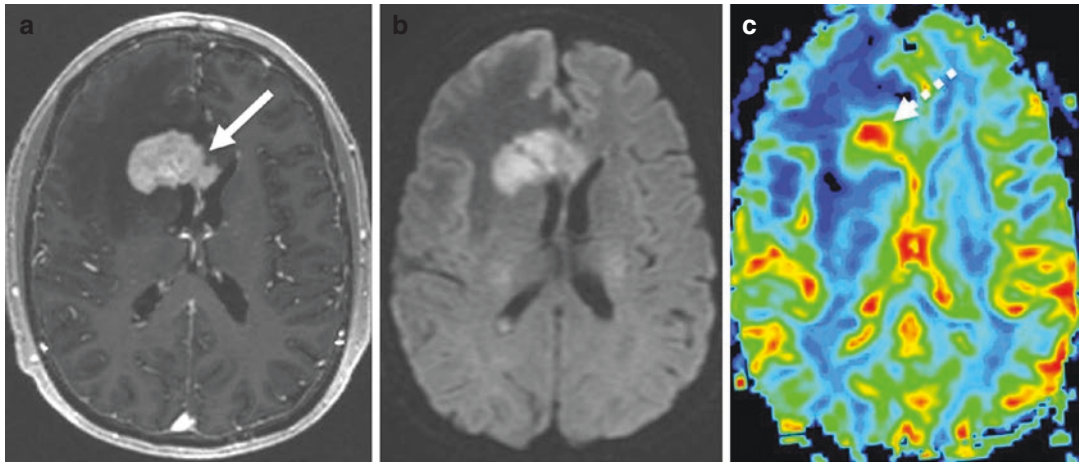

Fig. 5 CNS lymphoma. (**a**) Pre-contrast T1-weighted image demonstrates a homogeneously enhancing right frontal lobe periventricular mass crossing the genu of the corpus callosum (arrow). (**b**) DWI demonstrates corresponding restricted diffusion due to hypercellularity. (**c**) Cerebral blood volume (CBV) map perfusion image demonstrates hyperperfusion associated with the mass (dashed arrow)

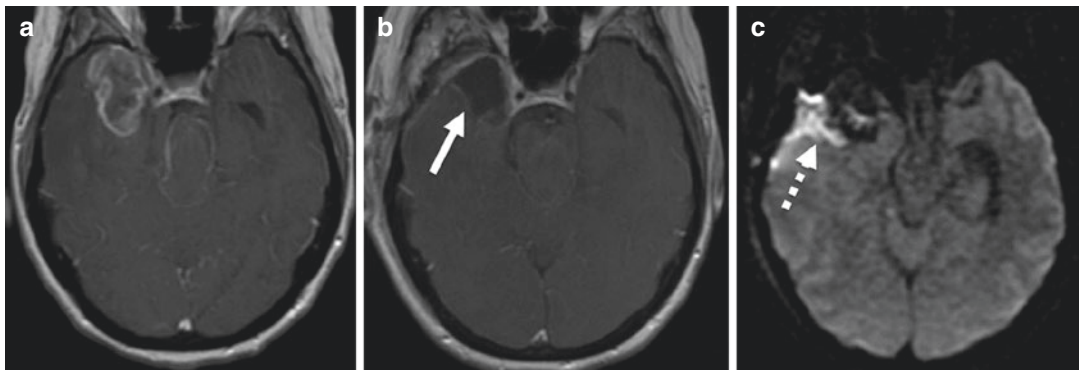

Fig. 6 Early postoperative changes. (**a**) Preoperative post-contrast T1-weighted image shows a right temporal lobe rim-enhancing tumor. (**b**) Postoperative post-contrast T1-weighted image within 48 h shows resection of the enhancing tumor (arrow). (**c**) DWI shows restricted diffusion in the adjacent brain, compatible with cytotoxic edema and which may enhance on follow-up imaging due to blood-brain barrier breakdown

which typically occurs after 48 h and may be associated with areas of cytotoxic edema due to blood-brain barrier breakdown (Fig. 6).

3 Therapy Response Imaging: Strategies and Pitfalls Specific to Brain Tumors

Several assessment criteria have been developed to define tumor progression, with early criteria suffering from interobserver variability. In 1990, MacDonald et al. posited three criteria to define tumor progression: a 25% increase in the two-dimensional size of enhancing tumor on CT or MRI, presence of new tumor on imaging, or clinical deterioration (Fig. 7). The MacDonald criteria were considered the standard for decades, but a growing understanding that tumor enhancement represents blood-brain barrier disruption, rather than tumor activity, paved the way for newer assessment criteria. Several scenarios demonstrate the limitations of the MacDonald criteria. First, imaging following resection and

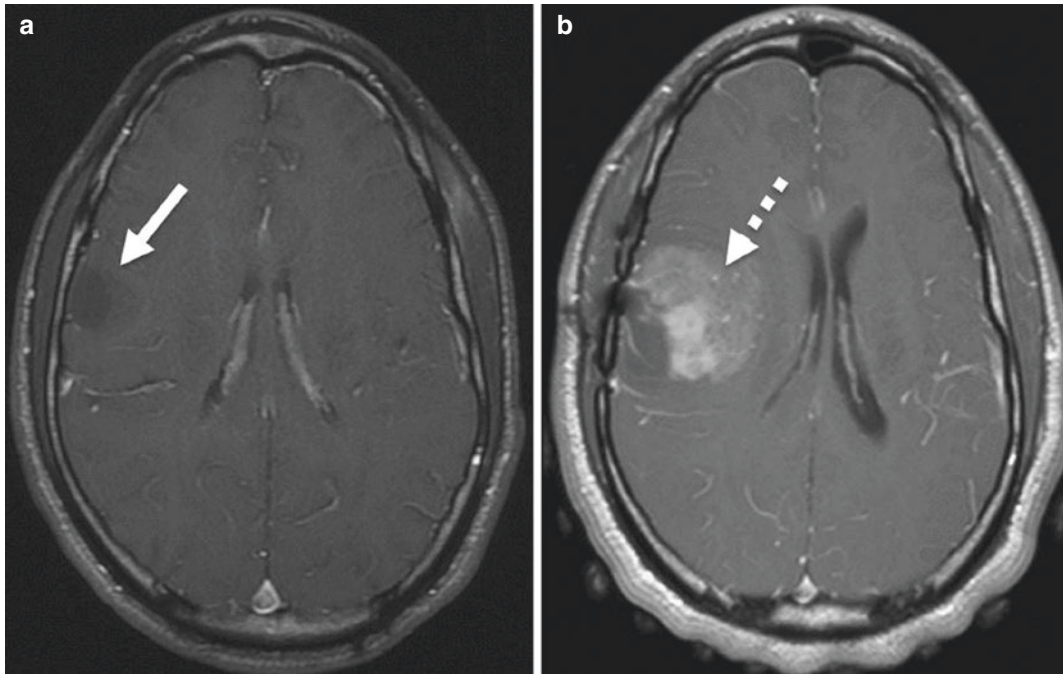

Fig. 7 Tumor progression. (**a**) Preoperative contrast T1-weighted image demonstrates a small non-enhancing mass (arrow) with pathology showing grade II diffuse astrocytoma. (**b**) Follow-up contrast T1-weighted image demonstrates increased size of the mass with new contrast enhancement compatible with higher-grade progressive (dashed arrow)

chemoradiotherapy may frequently demonstrate contrast enhancement that is unrelated to tumor. Thus, differentiating this so-called psuedoprogression from true progression is crucial in order to prevent inappropriate reoperation, premature discontinuation of effective adjuvant therapies, and inappropriate implementation of salvage therapies (Delgado-Lopez et al. 2018). Further, radiation necrosis can lead to an increase in mass effect, enhancement, or signal abnormalities following stereotactic or fractionated radiation therapy (Shah et al. 2012). The pattern of contrast enhancement seen in radiation necrosis is classically described as resembling soap bubbles, lace-like, or "Swiss cheese." Correlation with the radiation treatment plan and special attention to the timing of prior radiation can inform this diagnosis. Conversely, a primary brain tumor can demonstrate rapid decrease in contrast enhancement, with simultaneous increase in T2 infiltration following administration of antiangiogenic therapy (e.g., bevacizumab), leading to a phenomenon known as pseudoresponse (Hygino da Cruz et al. 2011). In pseudoresponse, imaging suggests a tumor appears to respond to a specific treatment, though the tumor actually remains stable or has progressed.

Due to these limitations of the MacDonald criteria, in 2010, the Response Assessment in Neuro-Oncology (RANO) Working Group suggested novel assessment criteria which attempted to integrate MRI measurements with clinical factors, while taking into consideration the timing of chemoradiation. According to the RANO criteria, within the first 12 weeks following chemoradiation, a diagnosis of progressive disease requires new enhancement outside the radiation field or demonstration of tumor via histopathological sampling. Crucially, clinical deterioration alone cannot define progression within 12 weeks

Table 1 Summary of Response Assessment in Neuro-Oncology (RANO) response criteria (Wen et al. 2010)

Criterion	Complete response	Partial response	Stable disease	Progressive disease
T1 gadolinium-enhancing disease	None	≥50% Reduction	<50% Reduction but <25% increase	≥25% Increase
T2/FLAIR	Stable or decreased	Stable or decreased	Stable or decreased	Increased
New lesion	None	None	None	Present
Corticosteroids	None	Stable or decreased	Stable or decreased	Not applicable
Clinical status	Stable or improved	Stable or improved	Stable or improved	Worsened
Requirement for response	All	All	All	Any

Modified from reference Wen et al. (2010): J Clin Oncol 2010;28(11):1963–1972

Table 2 Summary of Immunotherapy Response Assessment in Neuro-Oncology (iRANO) criteria (Okada et al. 2015)

	If ≤6 months after start of immunotherapy	If >6 months after start of immunotherapy
Is repeat scan required to confirm imaging progressive disease (PD) without clinical decline?	Yes	No
Minimal time interval for confirmation of progressive disease without clinical decline	≥3 months	N/A
Is further immunotherapy treatment allowed after imaging PD (if clinically stable) pending progression confirmation?	Yes	N/A
Does a new lesion define PD?	No	Yes

Modified from reference Okada et al. (2015): Lancet Oncol 2015;16(15):e534–e542

of initiation of chemoradiation, but is sufficient to explain progression after 12 weeks, if medications and comorbid conditions do not explain the deterioration fully. Greater than 12 weeks after chemoradiation, disease progression can be defined by the aforementioned unexplained clinical deterioration or any one of the additional three criteria: presence of a new enhancing lesion outside the radiation field, a 25% or greater increase in enhancing lesion (by perpendicular diameter area) compared to the first post-radiotherapy scan on stable or increasing steroids, or, in patients treated with antiangiogenic agents whose steroids have been stable or increased, a significant increase in non-enhancing T2 FLAIR hyperintense lesions not fully explained by postoperative changes, radiotherapy, demyelination, ischemia, infection, or seizures (Table 1) (Wen et al. 2010).

In 2015, the RANO criteria were applied to patients receiving immunotherapy. The resultant iRANO criteria posited that neuro-oncology patients undergoing immunotherapy could experience transient new enhancing lesions at local or distant sites (Okada et al. 2015, 2018). For this reason, within 6 months of starting immunotherapy, if patients do not demonstrate clinical worsening but demonstrate a new lesion on MRI, a repeat MRI 3 months later is required to diagnose disease progression. After 6 months of immunotherapy, patients do not require repeat MRI to confirm progression; in other words, after 6 months on immunotherapy, any new lesion is sufficient to define progressive disease (Table 2).

4 Pitfalls in Therapy-Response Imaging

4.1 Pseudoprogression

Simulating progressive disease, the combination of radiotherapy and temozolomide is often associated with increased contrast enhancement due to inflammation and necrosis. This phenomenon has been termed “pseudoprogression” and most

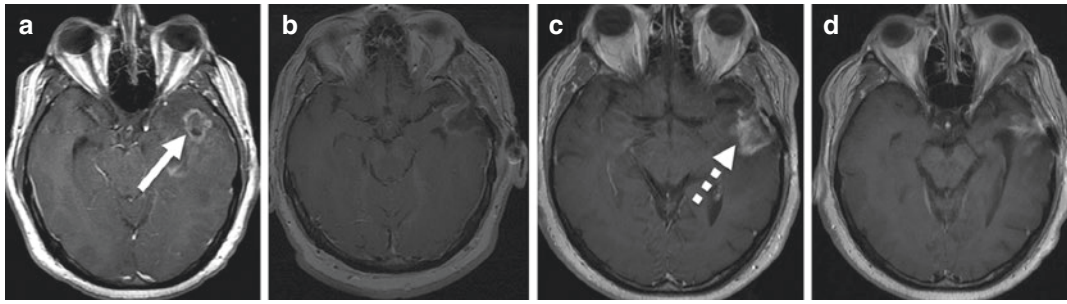

Fig. 8 Pseudoprogression involving MGMT-methylated glioblastoma. (**a**) Preoperative contrast T1-weighted image demonstrates a rim-enhancing left temporal lobe mass (arrow). (**b**) Postoperative contrast T1-weighted image demonstrates milder enhancement before the initiation of XRT/TMZ therapy. (**c**) At 2-month follow-up after chemoradiation, contrast T1-weighted image demonstrates increased indistinct contrast enhancement (dashed arrow), with associated increased vasogenic edema and decreased perfusion (image not shown). (**d**) At 1-year follow-up, contrast T1-weighted image demonstrates decreased contrast enhancement and volume loss in the left temporal lobe

often occurs within 3 months after such therapy (Fig. 8). Most shortly following radiation therapy, glioma patients may demonstrate increases in the size of their contrast-enhancing lesion (Fig. 8). Although the precise mechanism is not fully understood, endothelial cell damage leading to edema and abnormal vessel permeability may play a role. The hallmark of this entity is an increasing enhancing component with decreased perfusion and elevated ADC. Patients are typically asymptomatic and demonstrate pseudoprogression within 3 months of treatment. Methylated MGMT promoter status has been associated with pseudoprogression and better outcomes (Mamlouk et al. 2013).

4.2 Pseudoresponse

Pseudoresponse is typically associated with anti-angiogenic agents such as bevacizumab, which is a monoclonal antibody targeting vascular endothelial growth factor A (VEGF-A) (Fig. 9). Decreased permeability of the blood-brain barrier causes a rapid decrease in the contrast-enhancing component of the tumor, while simultaneously providing a reduction in symptoms due to a reduction in vasogenic edema. Crucially, tumors can undergo true progression despite decreased enhancement, evidenced by increased mass-like or infiltrative T2 hyperintense signal.

4.3 Radiation Necrosis

Months to years after radiation, the damage undergone by blood vessels during treatment may lead to parenchymal edema and necrosis (Fig. 10). Understanding the timeline of a patient's tumor care prior to the appearance of this lesion is crucial to correctly diagnosing this new lesion as radiation necrosis. Radiation necrosis can occur in radiation for head and neck cancer, extra-axial tumors, or primary or metastatic intra-axial tumors (radiation for these intra-axial tumors includes stereotactic radiosurgery). Knowledge of the time since initial radiation therapy, the radiation plan, the tumor type treated, extent of parenchyma radiated, and type of radiation can help make the diagnosis. Advanced MR techniques such as perfusion imaging (specifically calculating ADC ratios, percent signal recovery, and relative peak height), diffusion-weighted imaging, MR spectroscopy, and positron-emission tomography (PET) can help

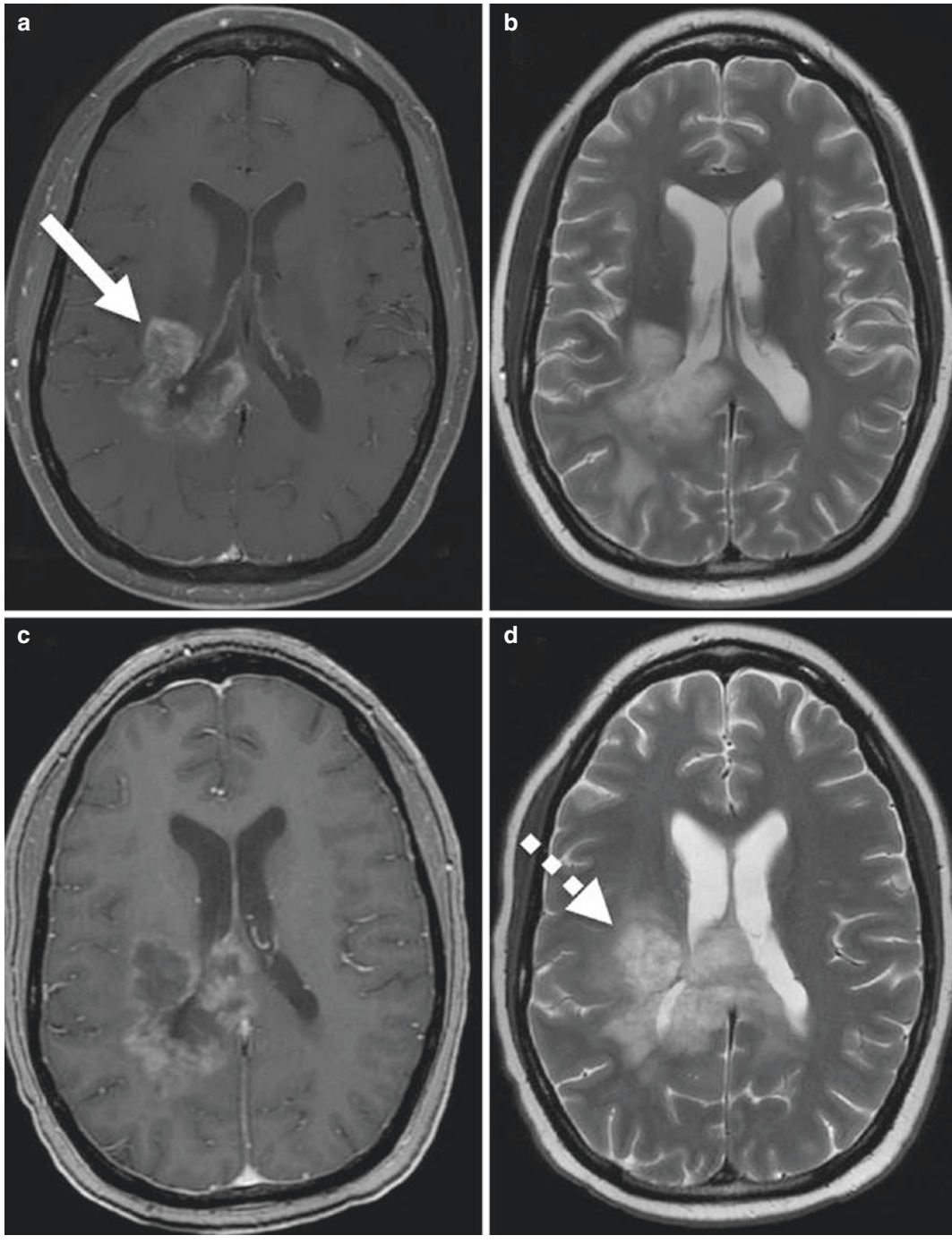

Fig. 9 Pseudoresponse. (**a**) Pretreatment contrast T1-weighted and (**b**) T2-weighted images shows avid contrast enhancement (arrow) with mass-like T2 hyperintensity associated with glioblastoma. (**c**) Follow-up contrast T1-weighted and (**d**) T2-weighted images after initiation of bevacizumab shows decreased intensity of contrast enhancement but increased size of mass-like T2 hyperintensity (dashed arrow)

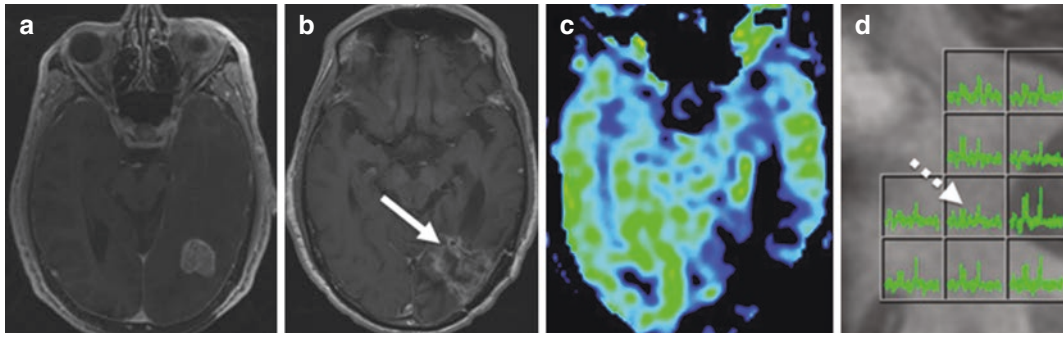

Fig. 10 Radiation necrosis involving a lung cancer metastasis. (**a**) Pretreatment contrast T1-weighted sequence demonstrates an avidly enhancing mass in the posterior left temporal-occipital lobe region. (**b**) Follow-up 1-year after resection and radiation therapy demonstrates "Swiss-cheese" enhancement along the resection cavity, with corresponding (**c**) decreased CBV on perfusion imaging and (**d**) global decreased metabolites on multi-voxel spectroscopy (dashed arrow) relative to adjacent voxels. These findings were stable on multiple subsequent studies

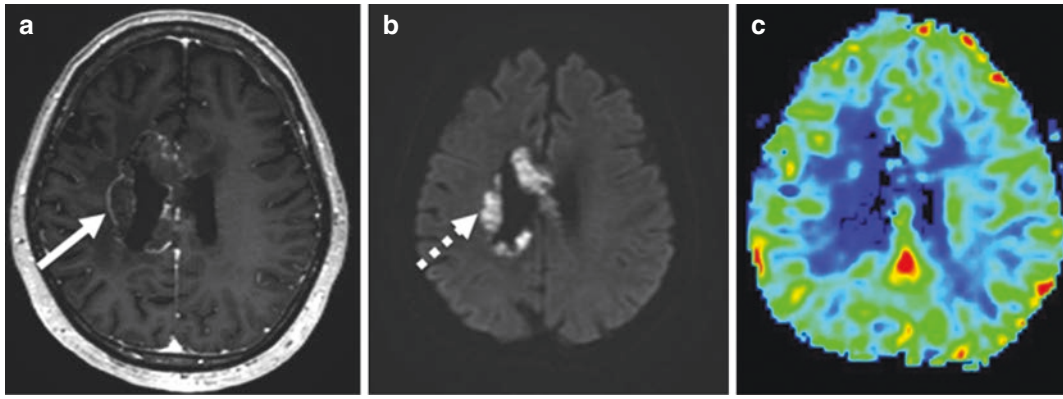

Fig. 11 Bevacizumab-related imaging abnormality (BRIA) associated with glioblastoma necrosis. Following treated with bevacizumab, (**a**) contrast T1-weighted image demonstrates thin rim-enhancement, (**b**) marked internal diffusion restriction on DWI (dashed arrow), and (**c**) decreased CBV on perfusion-weighted imaging. These findings were stable on multiple subsequent MRI studies

differentiate radiation necrosis from tumor recurrence. Figures 5 and 6 demonstrate radiation necrosis in two patients and emphasize the utility of perfusion imaging, spectroscopy, and PET.

4.4 Bevacizumab-Related Imaging Abnormality (BRIA)

Like radiation necrosis, antiangiogenic agents can cause delayed necrosis. In particular, bevacizumab-related imaging abnormality (BRIA) can demonstrate persistent marked restricted diffusion (Fig. 11). Combining restriction-spectrum imaging, an advanced diffusion-weighted imaging technique that more reliably estimates restricted diffusion using multiple *b*-values and diffusion times to separate restricted and hindered water components (White et al. 2013), with cerebral blood volume has improved differentiation of antiangiogenic necrosis from recurrence (Farid et al. 2014, 2013).

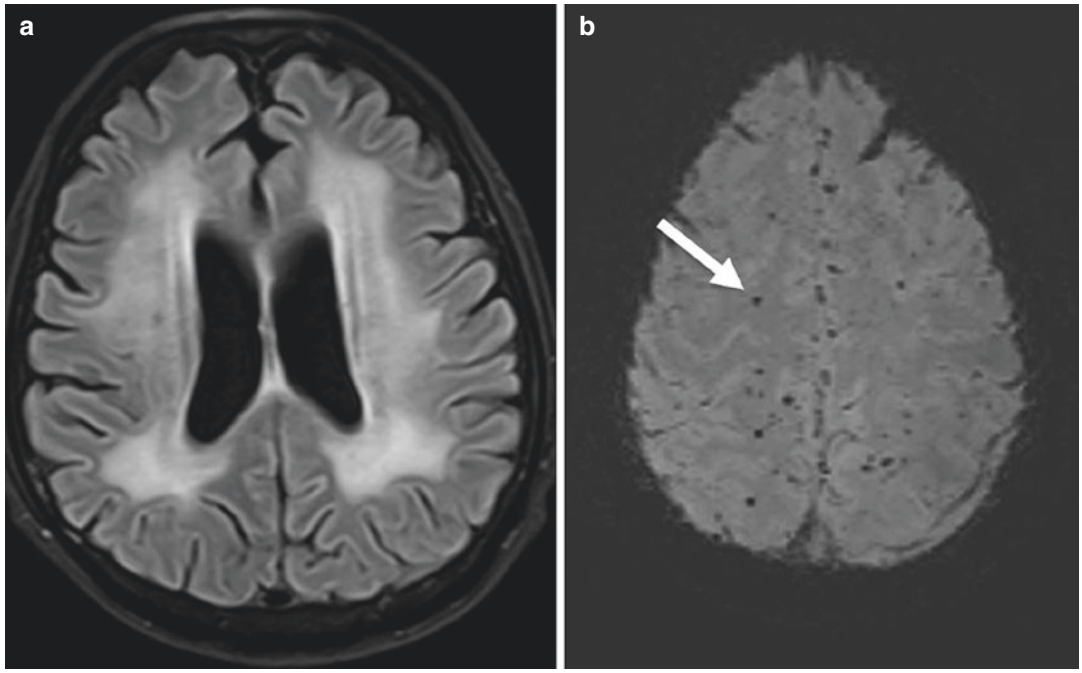

Fig. 12 Delayed diffuse white matter injury following radiation therapy. (**a**) T2 FLAIR image demonstrates confluent white matter hyperintense abnormality without mass effect. (**b**) Susceptibility-weighted imaging (SWI) demonstrates numerous microhemorrhages (arrow)

4.5 Postradiation Leukoencephalopathy and White Matter Injury

Postradiation leukoencephalopathy and white matter injury are long-known radiation effects that warrant discussion (Fig. 12). Pathology ranges from demyelination to coagulative necrosis and imaging typically demonstrates periventricular signal increase on T2 imaging, SWI microhemorrhages, and signal decrease on CT. Mass effect and advanced imaging techniques can help differentiate focal white matter change from recurrence (Valk and Dillon 1991).

4.6 Radiation-Induced Neoplasia

Radiation-induced neoplasia and secondary neoplasms should be considered in both pediatric and adult patients with new neoplasms in the area of previous radiotherapy. Though modern radiotherapy delivery methods, such as intensity-modulated radiation therapy, utilize three-dimensional anatomical software to target neoplasms, while sparing healthy tissues, failure to recognize that a new enhancing lesion in the area of radiation could represent radiation-induced neoplasia could lead to the improper conclusion of tumor recurrence. Radiation-induced neoplasia typically demonstrates long latency, with meningioma or sacrcomas typically occurring 10–20 years after radiation (Fig. 13).

4.7 SMART Syndrome

Stroke-like migraine attacks after radiation (SMART) syndrome is an uncommon delayed complication of cerebral radiation that can occur up to 30 years following radiation therapy. This syndrome typically presents with gyral enhancement involving a region of previously irradiated brain. Associated with migraine aura, attacks can

Fig. 13 Delayed radiation-induced meningiomas (arrows) following radiotherapy for nasopharyngeal cancer

take the form of seizures or stroke symptoms and are generally self-limited. Though uncommon, mistaking this delayed complication for tumor recurrence is another late pitfall.

5 Recent Advances in Novel Therapeutic Approaches for CNS Malignancy and Radiographic Implications

5.1 Intraoperative MRI

Though radiotherapy is the mainstay of treatment for patients with CNS malignancies, several studies have demonstrated the importance of the extent of tumor resection. Simply put, these studies demonstrate significantly improved survival for patients whose postoperative imaging demonstrates no enhancing residual tumor remnants (gross total resection, GTR) (Brown et al. 2016; Trifiletti et al. 2017). To improve resection of infiltrating tumors, particularly those infiltrating crucial structures, while avoiding damaging normal tissue, neuronavigation systems have commonly been utilized. These interactive devices attempt to show the real-time position of surgical instruments by calibrating positions on the patient's anatomy with preoperative scans. Since they do not provide surgeons with real-time intraoperative image feedback, shifts in structures, due to edema or disease evolution, can complicate this calibration. Thus, prospective data suggest these intraoperative devices may not improve the extent of resection or survival in patients with solitary cerebral tumors (Willems et al. 2006). To combat these shortcomings, several adjunctive intraoperative modalities, including intraoperative MRI, have been developed to improve real-time localization of tumor remnants (Eljamel and Mahboob 2016). Several randomized trials (Zhang et al. 2015; Roder et al. 2014; Napolitano et al. 2014; Senft et al. 2011a, b; Tsugu et al. 2011) have demonstrated intraoperative MRI improves rates of gross-total resection and progression-free survival compared to traditional neuronavigation technology (Li et al. 2017). A newer real-time intraoperative imaging technique is MR thermography, which monitors intraoperative temperature changes during thermoablation of cerebral tumors. Another important implication of intraoperative imaging is improved resection following surveillance imaging. This is especially important, given overall survival can be maximized by GTR at the time of recurrence for patients with initial STR (Bloch et al. 2012).

5.2 Immunotherapy

Immunotherapy offers promising options for treating brain tumors. However, assessment of new enhancing lesions in the context of treatment with immunotherapy represents a particular diagnostic challenge. For example, immunotherapy has been associated with autoimmune hypophysitis (Fig. 14) (Carpenter et al. 2009). In this condition, there is enlargement and enhancement of the pituitary gland, which reverses after discontinuation of the immunotherapy and steroid administration.

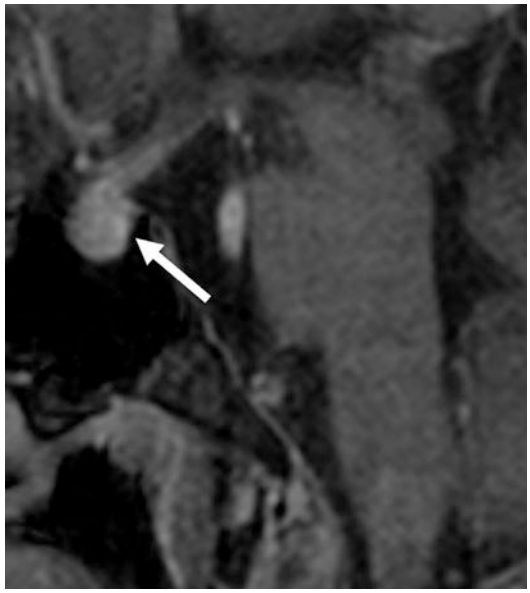

Fig. 14 Immunotherapy-related hypophysitis in a patient with renal cell carcinoma (RCC) treated with ipilmumab and nivolumab. Sagittal T1-contrast image demonstrates enlargement of the pituitary gland (arrow). The patient presented with new headache and hyponatremia, which improved after treatment with steroids

5.3 Antiangiogenic Agents

Antiangiogenic agents restore blood-brain-barrier integrity and improve outcomes for brain tumor patients, though these agents may be complicated by necrosis. A discussion of bevacizumab-related imaging abnormality (BRIA), which shows persistent marked diffusion following bevacizumab treatment, is discussed above.

5.4 Modalities with Mounting Evidence

Several advanced treatment options for CNS metastases have demonstrated trends towards improving outcomes, though insufficient evidence was found during meta-analyses to definitively recommend use. The Congress of Neurological Surgeons tumor section has extensively summarized the data surrounding these modalities (Elder et al. 2019), which include high-intensity focused ultrasound, laser interstitial thermal therapy, radiation sensitizers, interstitial modalities (such as chemo- or brachytherapy), immune modulators, and molecular targeted agents. In general, these modalities have not demonstrated sufficient evidence to gain more widespread utilization. Despite this, familiarity with the mechanisms of action of these therapies will be crucial if they are adopted more widely after sufficient evidence is collected. Careful attention to the regions in which these therapies are applied could improve diagnosis of a new lesion in this region in subsequent years (much like radiation therapy today). Immediate postoperative changes associated with these modalities must be studied further to improve immediate recognition of these treatment changes.

6 Emerging Approaches for Therapy Response Imaging for CNS Malignancy

A deeper understanding of imaging features of tumors has further motivated the updated 2016 WHO classification. Unlike its 2007 predecessor, this classification combines histology, WHO Grade, and molecular information, such as isocitrate dehydrogenase (IDH) status, 1p/19q, and other genetic factors, along with imaging features, to define an "integrated" diagnosis for diffuse gliomas (Fig. 15) (Johnson et al. 2017).

Radiomics is the use of computational methods to extract quantitative features from imaging. When linked to qualitative features recognized by radiologists, these quantitative data can help predict clinical outcomes such as prognosis and resistance in CNS malignancy (Zhou et al. 2018). Radiomic analysis assumes imaging reflects smaller-scale biological phenomena, including gene expression and the proliferation of tumor cells and blood vessels. Utilizing multiparametric algorithms to characterize imaging data, radionomic analysis can detect subtle quantitative changes. For example, as discussed previously, scoring criteria in CNS tumors often rely on contrast-enhancing tumor

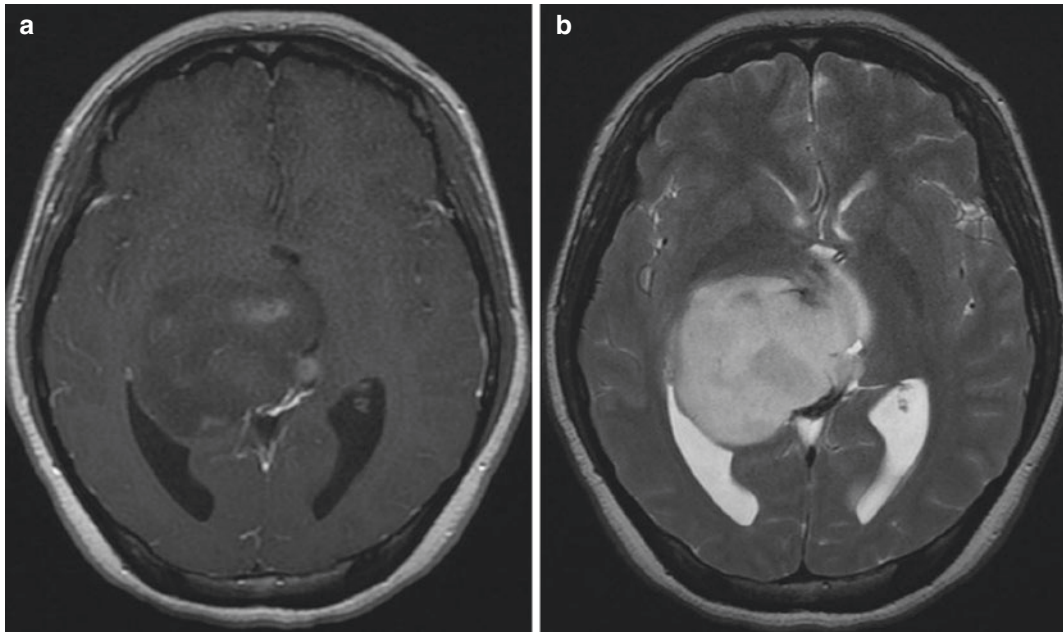

Fig. 15 Diffuse midline glioma with histone H3-K27M mutation centered involving the right thalamus. (**a**) Post-contrast T1-weighted image demonstrates heterogenous areas of enhancement. (**b**) T2-weighted image demonstrates mass-like hyperintense signal abnormality and early entrapment of the occipital horns of the lateral ventricles

volume, which is a descriptive endeavor fraught with potential pitfalls. Radiomic analyses rely on so-called "computer vision" to translate the contrast-enhancing image into local binary patterns that are eventually translated to detailed volumetric data that can detect subtle changes. By comparing each pixel to those in its immediate area, this technology can provide insights into tumor niche areas within a large tumor, potentially leading to better-informed assessment of changes in tumor volume. Radiomics can also be used to associate imaging features with genomic signatures in GBM. The growth of this research is supported by the need for radiomic signatures that inform treatment decisions. For example, though biopsy is the gold standard for genomic analysis of GBM, surgical planning and pathologic assessment could delay treatment and genetic analysis of the lesion is limited to the region sampled. Radiogenomics could offer genetic characterization rapidly, and efforts are ongoing to characterize genetic heterogeneity in GBM lesions (Chow et al. 2018).

Other emerging techniques in therapy response imaging include non-contrast perfusion imaging, MRI PET and single-photon emission computed tomography (SPECT) imaging, amide proton transfer weighted imaging, and restriction-spectrum imaging. An example of non-contrast perfusion imaging is arterial spin labeling (ASL), a noninvasive method to measure tumor blood flow which could reduce cost and intracranial contrast deposition. In ASL, magnetically labeled water is utilized in place of a contrast agent. This technique reliably estimates cerebral blood flow and correlates with tumor grade. Correlating survival with this noninvasive measurement could provide a low-risk, low-cost method to guide tumor treatment (Kim and Kim 2016). Restriction-spectrum imaging (RSI), a type of diffusion-weighted imaging, improves tumor conspicuity compared to surrounding normal white matter. Using aquisitions with multiple *b* values and diffusion times, this technique time acquisitions, this technique probes separated hindered and restricted water compartments to

create a cellularity map which can help discriminate between treatment-related changes in tumor from edema by increasing the discrepancy of ADC values of gliomas (which are typically similar to surrounding white matter) from that of surrounding tissues (White et al. 2013). Used with perfusion imaging, RSI can help differentiate recurrent tumor from bevacizumab-related imaging abnormality (Farid et al. 2013).

MRI PET combines detailed soft tissue anatomical assessment with radioactive-tracer data to provide high-resolution visualization of tumors with superimposed metabolic data. Similar to scintigraphy, SPECT imaging measures radionuclide emissions using a gamma camera. Brain imaging with SPECT is used to provide functional, metabolic information at lower cost than PET imaging. Future applications of these imaging modalities could guide treatment of tumors. Amide proton transfer-weighted (APTw) MRI provides indirect measurements of proteins and peptides using chemical exchange saturation transfer (CEST) of contrast to predict the cellular proliferation of gliomas. This measurement of biological relevance could help differentiate low- from high-grade gliomas and is superior to MR spectroscopy in assessing treatment-related change in tumor progression (Suh et al. 2019).

7 Conclusion

CNS malignancy remains a clinically challenging and morbid disease. Treatment is especially guided by neuroimaging, mainly MRI. While there are many types of primary and metastatic CNS malignancies, noninvasive neuroimaging can accurately diagnose and establish a baseline extent of disease for follow-up. In this work, we focused on the highly variable imaging findings of primary CNS neoplasms, particularly following treatment. We reviewed necessary background, reviewed classic MRI characteristics of pre- and posttreatment changes in CNS malignancy, and provided an overview on disease-specific approaches for therapy-response imaging, with special attention to potential diagnostic pitfalls and novel therapeutics that may affect posttreatment imaging. Lastly, we touched on emerging approaches that may improve diagnostic accuracy in the future. Ultimately, understanding therapy response imaging of CNS malignancies is crucial to guide therapy and to improve patient outcomes.

References

Al-Okaili RN, Krejza J, Wang S, Woo JH, Melhem ER (2006) Advanced MR imaging techniques in the diagnosis of intraaxial brain tumors in adults. Radiographics 26(Suppl 1):S173–S189. https://doi.org/10.1148/rg.26si065513

Barajas RF, Cha S (2016) Metastasis in adult brain tumors. Neuroimaging Clin N Am 26(4):601–620. https://doi.org/10.1016/j.nic.2016.06.008

Bloch O, Han SJ, Cha S, Sun MZ, Aghi MK, McDermott MW, Berger MS, Parsa AT (2012) Impact of extent of resection for recurrent glioblastoma on overall survival: clinical article. J Neurosurg 117(6):1032–1038. https://doi.org/10.3171/2012.9.jns12504

Brown TJ, Brennan MC, Li M, Church EW, Brandmeir NJ, Rakszawski KL, Patel AS, Rizk EB, Suki D, Sawaya R, Glantz M (2016) Association of the extent of resection with survival in glioblastoma: a systematic review and meta-analysis. JAMA Oncol 2(11):1460–1469. https://doi.org/10.1001/jamaoncol.2016.1373

Carpenter KJ, Murtagh RD, Lilienfeld H, Weber J, Murtagh FR (2009) Ipilimumab-induced hypophysitis: MR imaging findings. AJNR Am J Neuroradiol 30(9):1751–1753. https://doi.org/10.3174/ajnr.A1623

Chow D, Chang P, Weinberg BD, Bota DA, Grinband J, Filippi CG (2018) Imaging genetic heterogeneity in glioblastoma and other glial tumors: review of current methods and future directions. AJR Am J Roentgenol 210(1):30–38. https://doi.org/10.2214/ajr.17.18754

Delgado-Lopez PD, Rinones-Mena E, Corrales-Garcia EM (2018) Treatment-related changes in glioblastoma: a review on the controversies in response assessment criteria and the concepts of true progression, pseudoprogression, pseudoresponse and radionecrosis. Clin Transl Oncol 20(8):939–953. https://doi.org/10.1007/s12094-017-1816-x

Elder JB, Nahed BV, Linskey ME, Olson JJ (2019) Congress of neurological surgeons systematic review and evidence-based guidelines on the role of emerging and investigational therapies for the treatment of adults with metastatic brain tumors. Neurosurgery 84(3):E201–E203. https://doi.org/10.1093/neuros/nyy547

Eljamel MS, Mahboob SO (2016) The effectiveness and cost-effectiveness of intraoperative imaging in high-grade glioma resection; a comparative review of intraoperative ALA, fluorescein, ultrasound and

MRI. Photodiagn Photodyn Ther 16:35–43. https://doi.org/10.1016/j.pdpdt.2016.07.012

Farid N, Almeida-Freitas DB, White NS, McDonald CR, Muller KA, Vandenberg SR, Kesari S, Dale AM (2013) Restriction-spectrum imaging of bevacizumab-related necrosis in a patient with GBM. Front Oncol 3:258. https://doi.org/10.3389/fonc.2013.00258

Farid N, Almeida-Freitas DB, White NS, McDonald CR, Kuperman JM, Almutairi AA, Muller KA, VandenBerg SR, Kesari S, Dale AM (2014) Combining diffusion and perfusion differentiates tumor from bevacizumab-related imaging abnormality (bria). J Neuro-Oncol 120(3):539–546. https://doi.org/10.1007/s11060-014-1583-2

Hygino da Cruz LC Jr, Rodriguez I, Domingues RC, Gasparetto EL, Sorensen AG (2011) Pseudoprogression and pseudoresponse: imaging challenges in the assessment of posttreatment glioma. AJNR Am J Neuroradiol 32(11):1978–1985. https://doi.org/10.3174/ajnr.A2397

Johnson DR, Guerin JB, Giannini C, Morris JM, Eckel LJ, Kaufmann TJ (2017) 2016 updates to the WHO brain tumor classification system: what the radiologist needs to know. Radiographics 37(7):2164–2180. https://doi.org/10.1148/rg.2017170037

Kim M, Kim HS (2016) Emerging techniques in brain tumor imaging: what radiologists need to know. Korean J Radiol 17(5):598–619. https://doi.org/10.3348/kjr.2016.17.5.598

Li P, Qian R, Niu C, Fu X (2017) Impact of intraoperative MRI-guided resection on resection and survival in patient with gliomas: a meta-analysis. Curr Med Res Opin 33(4):621–630. https://doi.org/10.1080/03007995.2016.1275935

Louis DN, Perry A, Reifenberger G, von Deimling A, Figarella-Branger D, Cavenee WK, Ohgaki H, Wiestler OD, Kleihues P, Ellison DW (2016) The 2016 World Health Organization classification of tumors of the central nervous system: a summary. Acta Neuropathol 131(6):803–820. https://doi.org/10.1007/s00401-016-1545-1

Mamlouk MD, Handwerker J, Ospina J, Hasso AN (2013) Neuroimaging findings of the post-treatment effects of radiation and chemotherapy of malignant primary glial neoplasms. Neuroradiol J 26(4):396–412. https://doi.org/10.1177/197140091302600405

Napolitano M, Vaz G, Lawson TM, Docquier MA, van Maanen A, Duprez T, Raftopoulos C (2014) Glioblastoma surgery with and without intraoperative MRI at 30T. Neurochirurgie 60(4):143–150. https://doi.org/10.1016/j.neuchi.2014.03.010

Ohgaki H (2009) Epidemiology of brain tumors. Methods Mol Biol 472:323–342. https://doi.org/10.1007/978-1-60327-492-0_14

Okada H, Weller M, Huang R, Finocchiaro G, Gilbert MR, Wick W, Ellingson BM, Hashimoto N, Pollack IF, Brandes AA, Franceschi E, Herold-Mende C, Nayak L, Panigrahy A, Pope WB, Prins R, Sampson JH, Wen PY, Reardon DA (2015) Immunotherapy response assessment in neuro-oncology: a report of the RANO working group. Lancet Oncol 16(15):e534–e542. https://doi.org/10.1016/s1470-2045(15)00088-1

Okada HD, Reardon KM, David A (2018) Chapter 59—Immunotherapy response assessment in neuro-oncology (iRANO). In: Handbook of brain tumor chemotherapy, molecular therapeutics, and immunotherapy, 2nd edn. Academic Press, Cambridge, MA

Ostrom QT, Gittleman H, Xu J, Kromer C, Wolinsky Y, Kruchko C, Barnholtz-Sloan JS (2016) CBTRUS statistical report: primary brain and other central nervous system tumors diagnosed in the United States in 2009–2013. Neuro Oncol 18(suppl_5):v1–v75. https://doi.org/10.1093/neuonc/now207

Roder C, Bisdas S, Ebner FH, Honegger J, Naegele T, Ernemann U, Tatagiba M (2014) Maximizing the extent of resection and survival benefit of patients in glioblastoma surgery: high-field iMRI versus conventional and 5-ALA-assisted surgery. Eur J Surg Oncol 40(3):297–304. https://doi.org/10.1016/j.ejso.2013.11.022

Senft C, Bink A, Heckelmann M, Gasser T, Seifert V (2011a) Glioma extent of resection and ultra-low-field iMRI: interim analysis of a prospective randomized trial. Acta Neurochir Suppl 109:49–53. https://doi.org/10.1007/978-3-211-99651-5_8

Senft C, Bink A, Franz K, Vatter H, Gasser T, Seifert V (2011b) Intraoperative MRI guidance and extent of resection in glioma surgery: a randomised, controlled trial. Lancet Oncol 12(11):997–1003. https://doi.org/10.1016/s1470-2045(11)70196-6

Shah R, Vattoth S, Jacob R, Manzil FF, O'Malley JP, Borghei P, Patel BN, Cure JK (2012) Radiation necrosis in the brain: imaging features and differentiation from tumor recurrence. Radiographics 32(5):1343–1359. https://doi.org/10.1148/rg.325125002

Suh CH, Park JE, Jung SC, Choi CG, Kim SJ, Kim HS (2019) Amide proton transfer-weighted MRI in distinguishing high- and low-grade gliomas: a systematic review and meta-analysis. Neuroradiology 61(5):525–534. https://doi.org/10.1007/s00234-018-02152-2

Trifiletti DM, Alonso C, Grover S, Fadul CE, Sheehan JP, Showalter TN (2017) Prognostic implications of extent of resection in glioblastoma: analysis from a large database. World Neurosurg 103:330–340. https://doi.org/10.1016/j.wneu.2017.04.035

Tsugu A, Ishizaka H, Mizokami Y, Osada T, Baba T, Yoshiyama M, Nishiyama J, Matsumae M (2011) Impact of the combination of 5-aminolevulinic acid-induced fluorescence with intraoperative magnetic resonance imaging-guided surgery for glioma. World Neurosurg 76(1–2):120–127. https://doi.org/10.1016/j.wneu.2011.02.005

Valk PE, Dillon WP (1991) Radiation injury of the brain. AJNR Am J Neuroradiol 12(1):45–62

Wen PY, Kesari S (2008) Malignant gliomas in adults. N Engl J Med 359(5):492–507. https://doi.org/10.1056/NEJMra0708126

Wen PY, Macdonald DR, Reardon DA, Cloughesy TF, Sorensen AG, Galanis E, Degroot J, Wick W, Gilbert MR, Lassman AB, Tsien C, Mikkelsen T, Wong ET,

Chamberlain MC, Stupp R, Lamborn KR, Vogelbaum MA, van den Bent MJ, Chang SM (2010) Updated response assessment criteria for high-grade gliomas: response assessment in neuro-oncology working group. J Clin Oncol 28(11):1963–1972. https://doi.org/10.1200/jco.2009.26.3541

White NS, McDonald CR, Farid N, Kuperman JM, Kesari S, Dale AM (2013) Improved conspicuity and delineation of high-grade primary and metastatic brain tumors using "restriction spectrum imaging": quantitative comparison with high B-value DWI and ADC. AJNR Am J Neuroradiol 34(5):958–964, s951. https://doi.org/10.3174/ajnr.A3327

Willems PW, Taphoorn MJ, Burger H, van der Sprenkel JW B, Tulleken CA (2006) Effectiveness of neuronavigation in resecting solitary intracerebral contrast-enhancing tumors: a randomized controlled trial. J Neurosurg 104(3):360–368. https://doi.org/10.3171/jns20061043360

Zhang J, Chen X, Zhao Y, Wang F, Li F, Xu B (2015) Impact of intraoperative magnetic resonance imaging and functional neuronavigation on surgical outcome in patients with gliomas involving language areas. Neurosurg Rev 38(2):319–330; . discussion 330. https://doi.org/10.1007/s10143-014-0585-z

Zhou M, Scott J, Chaudhury B, Hall L, Goldgof D, Yeom KW, Iv M, Ou Y, Kalpathy-Cramer J, Napel S, Gillies R, Gevaert O, Gatenby R (2018) Radiomics in brain tumor: image assessment, quantitative feature descriptors, and machine-learning approaches. AJNR Am J Neuroradiol 39(2):208–216. https://doi.org/10.3174/ajnr.A5391

Therapy Response Imaging in Breast Cancer

Masako Kataoka

Contents

Abstract

In the management of breast cancer, imaging as a tool to evaluate therapy response by imaging is becoming more important. Chemotherapy and hormonal therapy are used in combination with surgical and radiation therapy for the primary breast cancer. For metastatic breast cancer, response assessment by imaging plays a vital role in optimized personalized management. Mammography (MMG), ultrasonography (US), magnetic resonance imaging (MRI), computed tomography (CT), bone scintigram, and FDG-PET are the major tools widely used in the clinics. Essential knowledge of breast cancer treatment including subtypes, treatment options, and response-guided approach are covered. Increasing data on neoadjuvant chemotherapy, in particular the estimation and prediction of pathological complete response (pCR) by imaging, is discussed. Magnetic resonance imaging (MRI) and FDG-PET are the two main modalities which can provide quantitative imaging data. Limited evidence on metastatic breast cancer and challenges in evaluation response specific to the metastatic location is reviewed.

M. Kataoka (✉)
Department of Diagnostic Imaging and Nuclear Medicine, Kyoto University Hospital, Kyoto, Japan
e-mail: makok@kuhp.kyoto-u.ac.jp

M. Nishino (ed.), *Therapy Response Imaging in Oncology*, Medical Radiology, Diagnostic Imaging,
https://doi.org/10.1007/978-3-030-31171-1_5

1 Introduction

Chemotherapy and hormonal therapy are the two fundamental therapies for breast cancer. They are used in combination with surgical and radiation therapy for the primary breast cancer either as a postoperative adjuvant treatment or as a preoperative neoadjuvant treatment. For metastatic treatment, chemotherapy and hormonal therapy play major roles in improving patients' outcome. In both contexts, evaluating therapy response of a specific treatment by imaging plays an important role in determining treatment response and selecting appropriate treatment options.

Imaging modalities used in therapy response includes mammography (MMG), ultrasonography (US), magnetic resonance imaging (MRI), computed tomography (CT), bone scintigram, and FDG-PET. Their importance depends on target lesions; MMG, US, and MRI tend to be used in neoadjuvant treatment for primary breast cancer, while CT, FDG-PET, and bone scintigram covers wider areas of the body and mainly used for metastatic breast cancer.

Neoadjuvant treatment, or preoperative systemic treatment (PST), is playing a vital role in the treatment of breast cancer. PST is defined as a systemic therapy initiated before the locoregional treatment. Neoadjuvant chemotherapy (NAC) was initially offered to patients with locally advanced breast cancer who may need extensive procedure if surgically treated. Then, NSABP B-18 study demonstrated in a randomized trial that no significant differences were seen for overall survival (OS) and disease-free survival (DFS) between preoperative neoadjuvant chemotherapy and postoperative adjuvant chemotherapy (Rastogi et al. 2008). Neoadjuvant hormonal therapy may be considered for hormone receptor-positive breast cancer. The purposes of neoadjuvant treatment are (1) shrinkage of primary tumor leading to the less-invasive surgery, i.e., de-escalating surgery (Curigliano et al. 2017), (2) estimation of the effectiveness of specific treatment regimen preoperatively so that the best postoperative regimen can be identified, and (3) prediction of the long-term survival of the patients, often using pathological complete response (pCR) as a surrogate marker of survival. There are increasing number of evidence showing the value of imaging in the above context, in particular for MRI.

In comparison, studies of imaging in metastatic breast cancer is limited. CT is the basic methods to evaluate metastatic disease including bone, liver, and brain metastasis, yet nuclear medicine is increasingly used for metastatic breast cancer. Efforts have been made to obtain information beyond RECIST-based evaluation.

In this chapter, basic knowledge of breast cancer subtype and general treatment option are reviewed. Neoadjuvant systemic treatment and the role of imaging are discussed. Considering that this is one of the active research topic, I will focus on the emerging evidence in the recent years. Imaging for metastatic breast cancer are also discussed.

2 Neoadjuvant Therapy

2.1 Basics of Treatment Options for Breast Cancer According to the Intrinsic Subtype

Treatment of breast cancer had been determined based on tumor size, presence of axillary lymph node metastasis, pathological grades, estrogen receptor (ER)/progesterone receptor (PgR) status, and HER2 status. Classification of intrinsic subtype based on gene expression profiling using cDNA microarray intrinsic subtype, reported by Perou et al. in 1990 (Perou et al. 2000), was associated with biological feature and changed our understanding of the breast cancer. Since performing gene-expression profiling is not feasible in the clinical setting, alternative intrinsic subtype based on ER, PgR, HER2, and Ki-67 index was proposed (Goldhirsch et al. 2011) (Table 1). The subtype classification has developed since then incorporating gene expression signature (Curigliano

Table 1 Subtypes of breast cancer

Subtypes	Detailed definition
Triple negative	ER-, PgR- and HER2-
HR− and HER2+	
HR+ and HER2+	
HR+ and HER2−	ER and/or PgR + ≥1%
✓ High receptor, low proliferation, low grade (luminal A-like)	High ER/PgR and low Ki-67 or grade
✓ Intermediate	
✓ Low receptor, high proliferation, high grade (luminal B-like)	Low ER/PgR and high Ki-67 or grade

HR hormone receptor, *ER* estrogen receptor, *PgR* progesterone receptor
Modified from Table 3, Curigliano et al. (2017)

et al. 2017), although limited availability. Tumor size and stage are taken into consideration in deciding treatment. The recommended primary systemic treatment for triple-negative or HER2-positive breast cancer with stage II or III are neoadjuvant chemotherapy including anthracycline and taxane. Trastuzumab will be added concurrently to taxane for HER2-positive cancer and endocrine therapy will be added for ER-positive /HER2-positive cancer. Endocrine therapy using tamoxifen or aromatase inhibitor is offered to ER-positive HER2-negative cancer. Depending on tumor burden (size), nodal involvement, higher Ki-67, neoadjuvant or adjuvant chemotherapy is added.

Advancement of experimental, genetic, and clinical research revealed that breast cancer consists of heterogeneous subpopulations. For example, cancers with the same "alternative intrinsic subtype" show wide variation in treatment response. Therefore, treatment should be personalized to individual patients to maximize treatment benefit while minimizing adverse effect. This led to the idea of response-guided approach; the treatment response is assessed by measuring the size or volume of tumor by physical examination or on imaging (von Minckwitz et al. 2013). These treatment options are summarized in Table 2.

2.2 Pathologic Complete Response (pCR) After Neoadjuvant Treatment

Pathologic complete response (pCR) after NAC can be achieved more frequently with better treatment regimens. A meta-analysis of 30 studies showed pCR rate of triple-negative subtype as 39% and HER2-positive subtype as 27% (Houssami et al. 2012). The benefit of pCR is not limited to the downstage of the surgical procedure. von Minckwitz et al. demonstrated that patients who achieved pCR experienced better disease-free survival (DFS), particularly for triple-negative, luminal B/HER2-negative, and HER2-positive subtype (von Minckwitz et al. 2013). Since then pCR has become widely used as a surrogate marker of better survival outcome and many imaging studies predicting pCR are motivated by the impact of this surrogate new biomarker. In their data, pCR was not associated with better DFS among luminal B/HER2-positive or luminal A tumors.

The abovementioned study also pointed out the impact of variable definition of pCR. The strictest criteria is no invasive cancer, no in situ residuals in breast and nodes (ypT0ypN0). No invasive cancer, in situ allowed (ypT0/is ypN0) is also used. Other definitions allowing positive lymph node involvement (ypT0/is yp any N) or minimally invasive component (ypT0/is/1mic yp any N) can be used but less frequently as positive lymph node involvement or invasive component is linked to the worse outcome. At least checking the definition of pCR is essential in comparing and combining data from the different sources.

2.3 Treatment Response Evaluated by Imaging

RECIST can be used for imaging-based evaluation of treatment response; the longest diameter of the target lesions is measured and summed up. The initial values are compared to the value after treatment. Mammography (MMG) is the basic

Table 2 Recommended (neo)-adjuvant systemic treatment for early breast cancer

Subtypes	Recommended treatment	
	Endocrine therapy	Chemotherapy
ER+ and HER2−		
High receptor Low tumor burden (pT1a, pT1b) No nodal involvement (pN0) Low proliferation Low grade or low "genomic risk"	+TAM/AI	–
High/intermediate ER and PgR expression Intermediate tumor burden (pT1c, pT2, pN0/1) Intermediate/high proliferation or grade and/or intermediate "genomic risk"	+TAM/AI/ exemestane	+Adjuvant chemotherapy
Intermediate to low ER and PgR expression Higher tumor burden (typically T3 and/or N2-3) More proliferative/higher Ki67 Intermediate to high "genomic risk"	+AI	+Adjuvant chemotherapy
Triple negative		
pT1a node negative		No routine adjuvant chemotherapy for stage pT1a pN0
Higher T and N stage		Neoadjuvant therapy for stage II/III (AC + taxane)
ER− and HER2+		
pT1a node negative	No systemic therapy	
pT1 b, c, node negative		Chemotherapy + trastuzumab
Higher T and N stage		Neoadjuvant therapy for stage II/III AC followed by taxane with concurrent trastuzumab ~12 m.o
ER+ and HER2+	As above +endocrine therapy[a]	

OFS ovarian function suppression, *HR* hormone receptor, *ER* estrogen receptor, *PgR* progesterone receptor, *AC* anthracycline

Modified from Tables 4 and 5, Curigliano et al. (2017)

[a]Endocrine therapy is selected according to menopausal status; Tamoxifen (TAM) for premenopausal women, Aromatase inhibitor (AI) for postmenopausal women

imaging for breast cancer and easily accessible, although it tends to underestimate residual tumor (Yeh et al. 2005). On the other hand, ultrasonography (US) is considered more accurate in evaluating lesion size than MMG. US can be frequently and easily conducted. Operator dependency is a drawback. Despite limited access and relatively high cost, breast MRI is the preferred method for evaluating treatment response after NAC. MRI demonstrated best correlation with pathology (Yeh et al. 2005). Perfusion data obtained by dynamic contrast-enhanced MRI can provide vascular information related to tumor angiogenesis. Diffusion-weighted images, magnetic resonance spectroscopy, and other emerging techniques can be applied to breast MRI.

Nuclear imaging can be used to evaluate treatment response to breast cancer patients undergoing NAC. Different from the abovementioned morphology-based imaging, nuclear medicine, in particular FDG-PET, is metabolic imaging identifying metabolically active spots. FDG-PET cannot provide exact size of the target lesion. However, changes in uptake of FDG is considered to reflect cytotoxic effect by chemotherapy earlier than morphological changes or even

Table 3 Comparison of clinical examination and imaging modalities in evaluating tumor response of (neo)adjuvant systemic therapy

	Accuracy (size)	Vascularity evaluation	Cost	Accessibility
Clinical examination	△	×	Low	Easy
MMG/DBT	△	×	Medium	Easy
US	○	△	Low-medium	Easy
MRI	○	○	High	Limited
FDG-PET	–[a]	×	High	Limited
Dedicated breast PET	–[a]	×	High	Very limited

MMG mammogram, *DBT* digital breast tomosynthesis
Modified from Personalized Treatment of Breast cancer p297 Table 18.1 Springer
[a]Size on PET image is influenced by metabolic activity of the lesion and does not correspond to the lesion size

perfusion changes. In that sense, FDG-PET can be used as response prediction at an early stage of the treatment (Rosen et al. 2007; Groheux et al. 2013). FDG-PET findings are used as an evidence of new lesion (PD) in RECIST 1.1 (Eisenhauer et al. 2009). New development of dedicated breast PET enables detailed metabolic changes of breast cancer (Masumoto et al. 2018). Comparison of imaging modalities are summarized in Table 3 (Kanao and Kataoka 2016).

2.4 Treatment Response to NAC by Mammography and Ultrasonography

Simple and the most convenient method for evaluating treatment response to NAC is clinical (physical) examination. This involves tumor size measurement using calipers before and during the treatment. Although clinical examination is inexpensive, noninvasive, and can be performed frequently, drawbacks include posttreatment fibrosis or inflammation leading to overestimation and non-palpable small residual tumor leading to underestimation. Lack of objective measurement is not ideal as a method to assess treatment response.

Mammography (MMG) and ultrasonography (US) are the basic imaging methods for breast cancer. Evaluating treatment response by MMG showed better results compared to physical examination. However, lesion size measurement using MMG is not accurate if the margin of the lesion is ill-defined, indistinct, or spiculated. The reliability of mammography also depends on surrounding breast tissue. If the margin of the tumor is definable in more than 50% of the lesion, diameter of the tumor on mammography showed relatively good correlations ($r = 0.77$) with that on histopathology (Huber et al. 2000). Obviously, dense breast can mask target lesions and prevent accurate size measurement. Digital breast tomosynthesis (DBT) can provide better accuracy by reducing masking effect (Fornvik et al. 2010). In a recent study comparing MMG, DBT, automated breast US (ABUS), and MRI, DBT performed better than MMG and ABUS in estimating tumor size (Park et al. 2018). Calcification, although associated with malignancy, may remain after viable tumor diminishes (Li et al. 2014), and new calcification may emerge during treatment, which makes interpretation difficult. Calcifications after NAC were more frequently found among estrogen receptor-positive tumors (Adrada et al. 2015).

US is more accurate than MMG in evaluating treatment response of breast cancer. In a retrospective review of primary breast cancers with NAC, tumor size measured on ultrasound was within 1 cm accuracy in 60% of cases, while that measured on MMG was accurate in only 32% of cases (Keune et al. 2010). In a study on triple-negative breast cancer, US was more accurate than MMG and equivalent to MRI in evaluating residual tumor size following NAC (Atkins et al. 2013). In a meta-analysis, US showed accuracy, comparable to MRI (Marinovich et al. 2013). In a

clinical aspect, US can be combined with US-guided biopsy when tissue sampling during the course of treatment is needed. Operator dependency and lack of reproducibility of measurement are the drawbacks of US. Parameters from strain elastography and shear-wave elastography obtained at pretreatment and after two cycles of NAC can predict favorable responses based on residual breast burden (Ma et al. 2017).

2.5 Technical and Practical Aspect of Evaluating NAC by MRI

Technical advancement in recent years contributes an increasing role of MRI in evaluating treatment response. Clinical scanners with higher magnetic field with dedicated breast coil contributed to improve image quality. In the setting of monitoring treatment response, better delineation of tumor with identification of small foci of residual tumor leads to accurate assessment of the target lesions. Software development to support radiologists such as kinetic or perfusion maps was another important step. EUSOBI guideline for breast MRI protocol proposed a practical guide to obtain images with sufficient quality to diagnose and evaluate breast lesions (Mann et al. 2008). If access to MRI scanner is limited, it would be recommended to perform MR before treatment, and after treatment, particularly when other imaging modality showed inconsistent results. If possible, avoid tissue sampling before MRI since biopsy-related hematoma may disturb the area surrounding the target lesion and making accurate evaluation difficult.

2.6 Evaluating Residual Tumor After NAC by MRI

Evaluating residual tumor after the completion of NAC, i.e., before surgical treatment, is important in determining optimal surgical planning as well as evaluating treatment efficacy of a specific regimen. In specific subtype, achievement of pCR can be used as a surrogate marker of long-term outcome. With its accuracy and objectiveness, dynamic contrast-enhanced MRI (DCE-MRI) is ideal for pre-op assessment. Ultrasound may be as accurate (Atkins et al. 2013; Marinovich et al. 2015), yet lacking objectiveness and reproducibility.

Data of patients with stage II or III breast cancer receiving NAC in American College of Radiology Imaging Network (ACRIN) 6657 study in conjunction with I-SPY TRIAL demonstrated that change in breast tumor size measured at MR imaging is superior to clinical assessment with areas under the receiver operating characteristic curve (AUCs) as 0.75, compared to clinical size with AUCs of 0.68 in predicting pCR (Hylton et al. 2012). Residual tumor size measured on MRI showed good agreement with pathologic tumor size, yet overestimation or underestimation can occur, with a medial correlation coefficient of 0.70 based on a systematic review (Lobbes et al. 2013). Subtype also affects accuracy of MRI. MRI can estimate residual tumor volume more accurately in triple-negative and HER2-positive tumors while less accurately in luminal type (Mukhtar et al. 2013). Causes of overestimation by MRI may be chemotherapy-induced fibrosis, reactive inflammation by tumor response and healing (Marinovich et al. 2013), or resorptive inflammation. On the other hand, possible reasons for underestimation included very small foci of cancer and cancers with lobular features (Yeh et al. 2005), multifocal or diffuse fragmented foci, or lesions presenting as non-mass enhancement.

Shrinkage pattern during or after NAC may affect accuracy in treatment response. Two types of tumor shrinkage pattern on MRI have been described: a concentric shrinkage and a dendritic shrinkage. The latter is associated with high risk of positive margins after a lumpectomy (Tozaki et al. 2006). Takeda et al. analyzed patients who underwent NAC or neoadjuvant endocrine therapy and found that dendritic shrinkage was associated with underestimation when compared to surgical specimen (Takeda et al. 2012a) (Fig. 1). Morphology of the primary tumor is another factor in affecting accuracy in residual tumor. Data

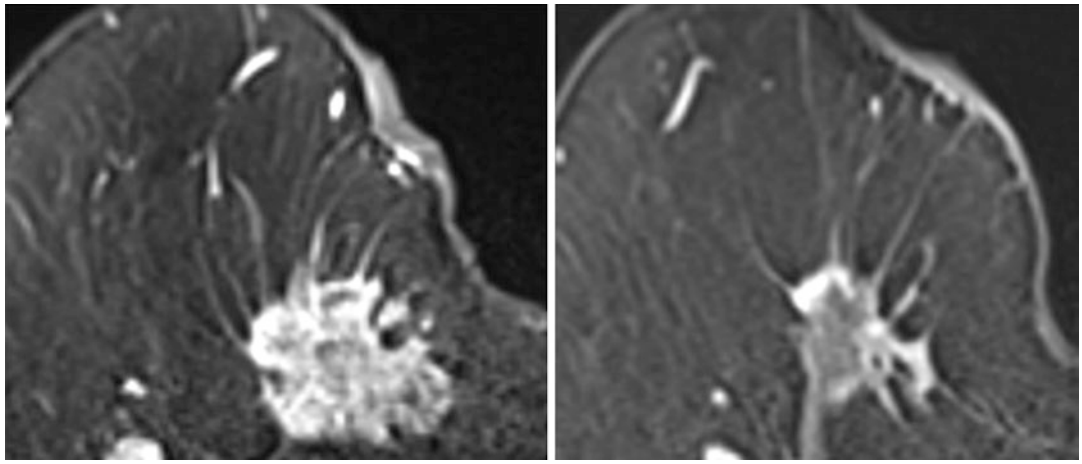

Fig. 1 Typical changes of treatment response in breast cancer on contrast-enhanced MRI. Contrast-enhanced MRI of breast cancer before (Left) and after (Right) chemotherapy. There was an oval-shaped mass with spiculated margin in the right inner area of the breast (Left). After chemotherapy, the mass diminished in size. However, long spicula remains, showing dendritic shrinkage pattern (Right). Central portion of the mass becomes poorly enhanced after chemotherapy

from previously mentioned ACRIN 6657 trial also reported higher concordance between MRI-based tumor size and tumor size on surgical pathology among well-defined tumors, especially with those with a triple-negative subtype (Mukhtar et al. 2013).

In order to solve the discrepancy related to lesion morphology, volumetry is attracting attention. Conventional RECIST size criteria are based on lesion diameter and affected by morphology of the target lesion. Volumetry can measure the amount of tumor in the 3-D direction and is less influenced by tumor morphology. Sophisticated viewing software is needed to measure volume easily, adding thresholding by degree of contrast enhancement. Value of the enhancing tumor volume was highlighted by the study by Partridge et al. that early change of MR tumor volume was significantly correlated with the final MRI volume change and more predictive of recurrence-free survival than tumor diameter. Volumetric changes measured using MRI may provide a more sensitive assessment of treatment efficacy. Their threshold was at least 70% enhancement from baseline at 2.5 min after injection of a contrast agent (Partridge et al. 2005). Computer-aided tumor volume can provide total enhancing volumes and washout volumes—i.e., enhanced areas with more than 100% signal increase on early DCE and signal reduction by 10% or more on delayed DCE phase. Using this CAD-generated volume, significantly higher inter-observer concordance than conventional RECIST-based longest diameter measurement was achieved. The results also showed that washout volume measurement after the completion chemotherapy is significantly better in differentiating patients with pCR and those with non-pCR (Takeda et al. 2012b). The enhancement threshold may vary among studies and may be adjusted to scanner. Henderson et al. used enhancing tumor volumes (ETVs) based on 2 min post-contrast subtraction series and demonstrated that ETVs can predict pCR and residual tumor burden better than functional tumor volume (FTV) they used (Adrada et al. 2015). This evidence suggests value of volume-based evaluation in treatment response in case of clinical trials.

Treatment regimen may affect evaluation of residual tumor by MRI. Therapeutic agent might affect vascularity or causing reactions mimicking disease progression. For example, residual disease was frequently underestimated in patients treated with taxane-containing regimens and in

Table 4 Factors affecting accuracy of MRI in estimating pCR/residual tumor volume

Factors	Comments
Definition of pCR	No invasive (in situ allowed)/no in situ cancer
MRI unit field strength	1.5T/3T
Size of invasive tumor	Difficult in lesions in predominantly intraductal component
Subtype Pathology type Treatment-related change Shrinkage pattern	More accurate in triple-negative/less accurate in ER+ HER2– (Kim et al. 2018) Less accurate in lobular type (Kim et al. 2018) Fibrosis Reactive inflammation (Partridge et al. 2005) Resorptive inflammation Less accurate in dendritic shrinkage (Takeda et al. 2012a)
Measurement methods	Volume more accurate than diameter (Adrada et al. 2015; Takeda et al. 2012a)
Neoadjuvant chemotherapy regimen	Tend to be underestimated in taxane-based treatment

pCR pathological complete response, *ER* estrogen receptor

HER-2-negative patients treated with bevacizumab. Schrading et al. examined the influence of taxanes on response assessment of DCE-MRI and showed that almost complete suppression of contrast enhancement occurred in cancers, benign enhancing lesions, and normal fibroglandular tissue after taxane-containing chemotherapy, while lower reduction of enhancement after non-taxane containing chemotherapy (Schrading and Kuhl 2015).

A recent more realistic study of 1274 patients who were examined by MRI and second-look US pre- and post-NAC, then breast-conserving surgery revealed that PPV of predicting pCR using MRI alone was 79.4%, increased to 86.8% when US was added. MRI combined with second-look US was useful in predicting pCR compared with MRI alone, especially for ER-negative /HER2-positive cancer. However, it was difficult to predict for the presence of a residual in situ component. They suggested adding vacuum-assisted biopsy to MRI plus second-look US is warranted to improve the prediction of pCR sufficiently high for omitting breast surgery (Hayashi et al. 2019).

Another recent publication examined 487 consecutive patients. Their results suggest smaller residual tumor size discrepancy using delayed-phase images. They investigated factors affecting residual tumor size discrepancy between MRI and histopathologic examination. Factors associated with larger discrepancy (underestimation of residual tumor size by MRI) were lobular histologic features and ER-positive/HER2-negative subtype (Kim et al. 2018). Interestingly, early-phase MRI performed better than delayed-phase or late delayed-phase MRI in determining pCR. The abovementioned factors are summarized in Table 4.

2.7 Prediction of Treatment Response by MRI

This is the area with hot topics. Pretreatment MRI, MRI after a few cycles of NAC, or changes between them have been used to predict pCR. More than 65% reduction in the tumor volume after two cycles of chemotherapy was associated with a major histopathological response (small cluster of dispersed residual cancer cells or no residual viable cancer cell) at surgery (Martincich et al. 2004). The data of 216 women from ACRIN 6657 trial showed that volumetric measurement of tumor response early in treatment showed better predictor of pCR than other measurements including the longest diameter, signal enhancement ratio, and clinical examination (Hylton et al. 2012). More sophisticated analysis based on texture analysis (Henderson et al. 2017; Chamming's et al. 2018), machine learning (Cain et al. 2019), and parametric maps (Cho et al. 2014) has been tried to show improvement in predicting pCR, often based on better AUC value. Some studies investigated beyond treatment response; MRI findings of pre- and/or

post-NAC can be used to predict local recurrence or recurrence-free survival (Partridge et al. 2005; Bae et al. 2016; Hylton et al. 2016; Wu et al. 2018; Shin et al. 2018).

2.8 Diffusion-Weighted Imaging and Other MRI Sequence

Diffusion-weighted imaging (DWI) is increasingly used in treatment assessment. DWI uses motion sensitizing gradients to measure the mobility of water molecules in tissues. DWI reflect cellularity of the tissue and the most sensitive non-contrast MR imaging for cancer. Chemotherapy induces various tissue changes, leading to a decrease in apparent diffusion coefficient (ADC) values. Increase of ADC values precedes morphological changes captured by conventional imaging or MRI. Post-NAC ADC is predictive of pCR with accuracy of 94.02 in luminal A subtype (Liu et al. 2015). Responders can be differentiated from nonresponders based on ADC values and its changes early in the treatment course (Galban et al. 2015; Li et al. 2012; Sharma et al. 2009; Fangberget et al. 2011; Iacconi et al. 2010; Park et al. 2010). The recent most-solid evidence has just come off from ACRIN 6698 multicenter trial that changes in breast tumor ADC after 12 weeks of treatment predicts pCR (Partridge et al. 2018). On the other hand, results from ACRIN 6657 MRS trial were rather disappointing, indicating technical challenges in using MRS in the multi-institutional setting (Bolan et al. 2017) .

2.9 Evaluation and Prediction of Tumor Response by ^{18}FDG-PET and Other Molecular Imaging

Nuclear medicine visualizes metabolic or functional aspect of the target. In the context of imaging breast cancer, the main malignant tumor shows higher uptake compared to the background, considered to reflect active metabolism in the growing cancer cells. The mainstream of nuclear medicine in oncology is ^{18}F-fluorodeoxyglucose (FDG)-PET/CT, whereas breast scintigraphy using 99mTc-sestamibi may be preferred in assessing breast cancer treatment response due to lower cost (Tiling et al. 2001). A new agent like ^{18}F-fluciclovine or ^{18}F-fluorothymidine (FLT) is also used for breast cancer imaging. These agents can be combined with CT or MRI.

^{18}F-FDG consists of ^{18}F as a positron-emitting radionuclide and FDG that is taken into the cells by glucose transporters. In general, cancer cells overexpress glucose transporters and uptake ^{18}F-FDG. Standard uptake value (SUV) is now widely used as a quantitative index to measure tumor metabolic function (Groheux et al. 2013).

For measuring residual tumors post-NAC and identifying pCR, studies have demonstrated that residual FDG uptake predicts residual disease. It should be noted, however, that lack of FDG uptake does not necessarily mean pCR (Lee et al. 2009; Bassa et al. 1996; Burcombe et al. 2002; Kim et al. 2004). Difference in threshold SUV (Dose-Schwarz et al. 2010), certain types of breast cancer known to have low SUV (DCIS, luminal A), limited spatial resolution are possible reasons of false negative diagnosis. The spatial resolution issue can be solved by using dedicated breast PET scanner (Miyake et al. 2014; Iima et al. 2012).

Prediction of tumor response earlier in the course of treatment is increasingly important with the wider use of response-guided treatment. Evaluating FDG-PET at early or mid-therapy suggested that changes in FDG uptake from the baseline scan is a good predictor to identify responder and nonresponders. SUV decrease in 50% or more at mid-therapy is associated with good response and lesser reduction indicated poor response (Rosen et al. 2007; Lee et al. 2009). Rapid drop of uptake in responders at day 8 and no reduction in nonresponders were observed, while tumor diameter showed no significant change (Wahl et al. 1993). Similar results were reported from other groups (Masumoto et al. 2018; Schelling et al. 2000; Rousseau et al. 2006) (Fig. 2). Dedicated breast scanner is not limited to FDG/PET. Recent publication using

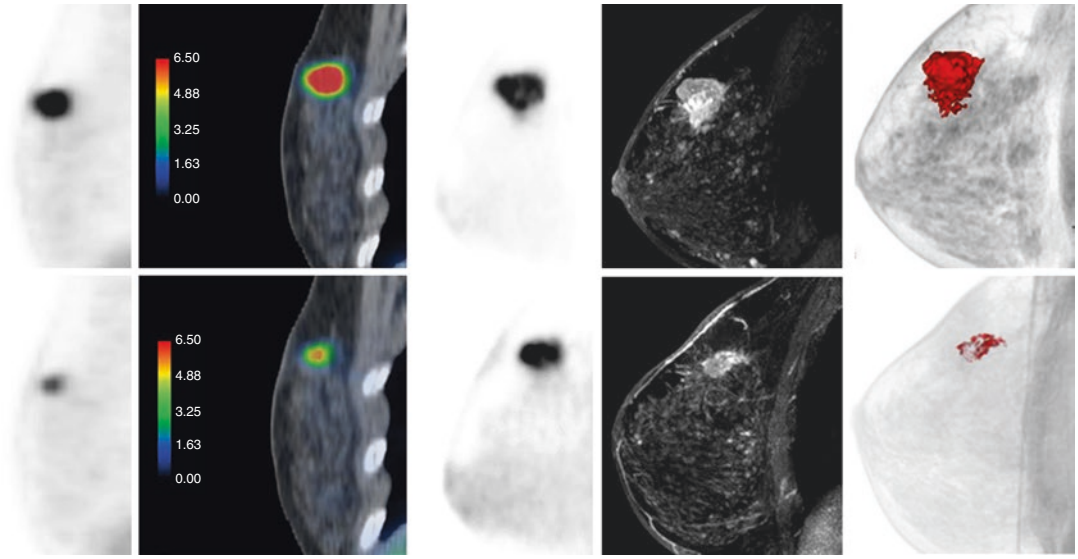

Fig. 2 Whole body ^{18}F-FDG PET/CT, dedicated breast PET, DCE-MRI, MRI volumetry in invasive breast cancer patients before (upper row) and after (lower row) neoadjuvant chemotherapy. Whole body ^{18}F FDG PET (left) image and fused image with CT showed intense uptake of ^{18}F FDG to the cancer. Dedicated breast PET revealed rim-like uptake, corresponding to the rim on contrast-enhanced MRI. Contrast-enhanced MRI and volumetry revealed detailed structure of the lesion including spiculated margin. After neoadjuvant chemotherapy (lower row), the uptake of ^{18}F FDG decreased both on whole body FDG PET and dedicated breast PET. On MRI, the diameter of the cancer remains the same, yet the volume is obviously decreased

breast-specific gamma imaging using ^{99m}Tc-sestamibi showed sensitivity and higher specificity compared to MRI in accurately determining pCR (Kim et al. 2004).

3 Evaluation of Treatment Response in Metastatic Breast Cancer

Breast cancer may metastasize to the bone, lung, liver, brain, and other organs of the body. Chemotherapy, endocrine therapy, molecular-targeted therapy, or immunotherapy is a treatment option for these patients with metastatic breast cancer. This means increasing needs in evaluating treatment response. CT is commonly used for metastasis to solid organ, while MRI and FDG-PET are increasingly used in evaluating treatment response.

Bone metastasis is very common among advanced breast cancer patients. Bone is after the first and the only organ involved in breast cancer metastasis. Effective treatment options contribute to improve survival of the patients. However, diagnosing bone metastasis from breast cancer is challenging for its complex changes; it can be lytic, sclerotic, or lytic-sclerotic mixed. Treatment-related changes can modify the appearance. RECIST criteria treat bone lesions as "non-measurable," due to difficulty in identifying and evaluating response using bone-scintigraphy. Response assessment of bone metastasis using bone scintigraphy need to wait for several months. In contrast, cancer-oriented tracers like FDG perform better in detecting new lesions or progression earlier, although nonspecific (Lecouvet et al. 2014). FDG-PET has a quantifiable parameter like SUV_{max}, and both qualitative and quantitative treatment response have been described. By combining metabolic information from FDG-PET and morphologic information from CT, PET/CT enables earlier response assessment that might be applicable in the context

of response-guided treatment. Currently two criteria—European Organisation for Research and Treatment of Cancer (EORTC) criteria and PET response criteria in solid tumors (PERCIST) criteria (Depardon et al. 2018; Wahl et al. 2009)—have been advocated to classify response into complete metabolic response (CMR), partial metabolic response (PMR), stable metabolic disease (SMD), and progressive metabolic disease (PMD) with slightly different definition. Both criteria turned out to be predictive of prognosis (Depardon et al. 2018). Another important point in using metabolic imaging is "flare" phenomenon observed early in the course of the endocrine therapy of metastatic patients that is predictive of a better outcome.

MRI has aspects of both morphologic imaging (T1-weighted image) and functional imaging (DWI, perfusion). T1WI MRI is useful in detecting bone metastasis and predicted disease progression in 79%, while it shows poor performance for identifying response (Brown et al. 1998). Using DWI for evaluating response based on ADC value is attracting attention, yet mixed results so far. Response to treatment involves return of marrow fat, as well as fibrosis, causing increase/decrease in ADC values (Lecouvet et al. 2014). Morphology-based MRI performs better in identifying and evaluating bony metastasis. PET/MRI has become commercially available and may be a one-for-all modality for therapeutic assessment of bone metastasis.

Hepatic metastasis is also common among advanced breast cancer patients in a later stage. It may be life-threatening as liver metastasis is often multiple or diffuse. Prognosis is not favorable for those who developed liver metastasis and clinical trials targeting patients in this stage are ongoing. Imaging assessment of hepatic metastasis is also challenging in routine assessment of treatment response. Metastatic lesions are often poorly enhanced on contrast-enhanced CT and non-contrast CT may perform better in identifying liver metastasis. Although CT is the major imaging tool in evaluating hepatic metastasis, drug-induced fatty changes of the background liver parenchyma (Nishino et al. 2003) add complexity in interpretation. PET/CT may be of limited value due to background FDG uptake. At the moment, MRI with DWI or EOB MRI is the most sensitive method to identify and evaluate hepatic metastasis.

Occasionally multiple liver metastasis from breast cancer may appear as cirrhotic, described as pseudo-cirrhosis. It occurs with patients with multiple liver metastasis after chemotherapy. Blood test shows all signs of hepatic dysfunction, associated with signs of portal hypertension. Nodular regeneration of the liver or desmoplastic reaction surrounding the tumor is reported to be a possible cause (Nascimento et al. 2001; Kashyap et al. 2018). The pseudo-cirrhosis is associated with increased mortality and morbidity (Adike et al. 2016).

Thoracic involvement is very common in advanced metastatic breast cancer. It should be noted that solitary pulmonary nodule may be a primary lung cancer in more than half of the cases. Multiple pulmonary nodules are more frequent form of lung metastasis from advanced breast cancer. They are typically oval or spherical shape with smooth margin. These types of thoracic metastasis are relatively easy to evaluate based on RECIST criteria. On the other hand, other forms of metastasis or treatment-related changes may coexist in the lung. Air-space or bronchoalveolar pattern (Jung et al. 2004) mimics infectious or inflammatory disease. Radiation-induced pneumonitis or fibrosis is another common thoracic complication that makes metastatic disease less visible on CT. Lymphangitic metastasis is difficult to recognize on conventional chest X-ray and high-resolution CT is often required for diagnosis. These manifestations are classified as "non-measureable" yet indicate unfavorable condition. Other thoracic involvement including pleural metastasis are often classified as "non-measurable" unless they present as "masses."

In conclusion, evaluating therapy response by imaging is increasingly used in the management of breast cancer. Evidence on NAC evaluation and prediction support the importance of imaging in decision-making of optimized/personalized treatment.

References

Adike A, Karlin N, Menias C, Carey EJ (2016) Pseudocirrhosis: a case series and literature review. Case Rep Gastroenterol 10(2):381–391

Adrada BE, Huo L, Lane DL, Arribas EM, Resetkova E, Yang W (2015) Histopathologic correlation of residual mammographic microcalcifications after neoadjuvant chemotherapy for locally advanced breast cancer. Ann Surg Oncol 22(4):1111–1117

Atkins JJ, Appleton CM, Fisher CS, Gao F, Margenthaler JA (2013) Which imaging modality is superior for prediction of response to neoadjuvant chemotherapy in patients with triple negative breast cancer? J Oncol 2013:964863

Bae MS, Shin SU, Ryu HS, Han W, Im SA, Park IA et al (2016) Pretreatment MR imaging features of triple-negative breast cancer: association with response to neoadjuvant chemotherapy and recurrence-free survival. Radiology 281(2):392–400

Bassa P, Kim EE, Inoue T, Wong FC, Korkmaz M, Yang DJ et al (1996) Evaluation of preoperative chemotherapy using PET with fluorine-18-fluorodeoxyglucose in breast cancer. J Nucl Med 37(6): 931–938

Bolan PJ, Kim E, Herman BA, Newstead GM, Rosen MA, Schnall MD et al (2017) MR spectroscopy of breast cancer for assessing early treatment response: results from the ACRIN 6657 MRS trial. J Magn Reson Imaging 46(1):290–302

Brown AL, Middleton G, MacVicar AD, Husband JE (1998) T1-weighted magnetic resonance imaging in breast cancer vertebral metastases: changes on treatment and correlation with response to therapy. Clin Radiol 53(7):493–501

Burcombe RJ, Makris A, Pittam M, Lowe J, Emmott J, Wong WL (2002) Evaluation of good clinical response to neoadjuvant chemotherapy in primary breast cancer using [^{18}F]-fluorodeoxyglucose positron emission tomography. Eur J Cancer 38(3):375–379

Cain EH, Saha A, Harowicz MR, Marks JR, Marcom PK, Mazurowski MA (2019) Multivariate machine learning models for prediction of pathologic response to neoadjuvant therapy in breast cancer using MRI features: a study using an independent validation set. Breast Cancer Res Treat 173(2):455–463

Chamming's F, Ueno Y, Ferre R, Kao E, Jannot AS, Chong J et al (2018) Features from computerized texture analysis of breast cancers at pretreatment MR imaging are associated with response to neoadjuvant chemotherapy. Radiology 286(2):412–420

Cho N, Im SA, Park IA, Lee KH, Li M, Han W et al (2014) Breast cancer: early prediction of response to neoadjuvant chemotherapy using parametric response maps for MR imaging. Radiology 272(2):385–396

Curigliano G, Burstein HJ, PW E, Gnant M, Dubsky P, Loibl S et al (2017) De-escalating and escalating treatments for early-stage breast cancer: the St. Gallen International Expert Consensus Conference on the Primary Therapy of Early Breast Cancer 2017. Ann Oncol 28(8):1700–1712

Depardon E, Kanoun S, Humbert O, Bertaut A, Riedinger JM, Tal I et al (2018) FDG PET/CT for prognostic stratification of patients with metastatic breast cancer treated with first line systemic therapy: comparison of EORTC criteria and PERCIST. PLoS One 13(7):e0199529

Dose-Schwarz J, Tiling R, Avril-Sassen S, Mahner S, Lebeau A, Weber C et al (2010) Assessment of residual tumour by FDG-PET: conventional imaging and clinical examination following primary chemotherapy of large and locally advanced breast cancer. Br J Cancer 102(1):35–41

Eisenhauer EA, Therasse P, Bogaerts J, Schwartz LH, Sargent D, Ford R et al (2009) New response evaluation criteria in solid tumours: revised RECIST guideline (version 1.1). Eur J Cancer 45(2):228–247

Fangberget A, Nilsen LB, Hole KH, Holmen MM, Engebraaten O, Naume B et al (2011) Neoadjuvant chemotherapy in breast cancer-response evaluation and prediction of response to treatment using dynamic contrast-enhanced and diffusion-weighted MR imaging. Eur Radiol 21(6):1188–1199

Fornvik D, Zackrisson S, Ljungberg O, Svahn T, Timberg P, Tingberg A et al (2010) Breast tomosynthesis: accuracy of tumor measurement compared with digital mammography and ultrasonography. Acta Radiol 51(3):240–247

Galban CJ, Ma B, Malyarenko D, Pickles MD, Heist K, Henry NL et al (2015) Multi-site clinical evaluation of DW-MRI as a treatment response metric for breast cancer patients undergoing neoadjuvant chemotherapy. PLoS One 10(3):e0122151

Goldhirsch A, Wood WC, Coates AS, Gelber RD, Thurlimann B, Senn HJ et al (2011) Strategies for subtypes—dealing with the diversity of breast cancer: highlights of the St. Gallen International Expert Consensus on the Primary Therapy of Early Breast Cancer 2011. Ann Oncol 22(8):1736–1747

Groheux D, Espie M, Giacchetti S, Hindie E (2013) Performance of FDG PET/CT in the clinical management of breast cancer. Radiology 266(2):388–405

Hayashi N, Tsunoda H, Namura M, Ochi T, Suzuki K, Yamauchi H et al (2019) Magnetic resonance imaging combined with second-look ultrasonography in predicting pathologic complete response after neoadjuvant chemotherapy in primary breast cancer patients. Clin Breast Cancer 19(1):71–77

Henderson S, Purdie C, Michie C, Evans A, Lerski R, Johnston M et al (2017) Interim heterogeneity changes measured using entropy texture features on T2-weighted MRI at 3.0 T are associated with pathological response to neoadjuvant chemotherapy in primary breast cancer. Eur Radiol 27(11):4602–4611

Houssami N, Macaskill P, von Minckwitz G, Marinovich ML, Mamounas E (2012) Meta-analysis of the association of breast cancer subtype and pathologic complete response to neoadjuvant chemotherapy. Eur J Cancer 48(18):3342–3354

Huber S, Wagner M, Zuna I, Medl M, Czembirek H, Delorme S (2000) Locally advanced breast carcinoma: evaluation of mammography in the prediction of residual disease after induction chemotherapy. Anticancer Res 20(1B):553–558

Hylton NM, Blume JD, Bernreuter WK, Pisano ED, Rosen MA, Morris EA et al (2012) Locally advanced breast cancer: MR imaging for prediction of response to neoadjuvant chemotherapy—results from ACRIN 6657/I-SPY TRIAL. Radiology 263(3):663–672

Hylton NM, Gatsonis CA, Rosen MA, Lehman CD, Newitt DC, Partridge SC et al (2016) Neoadjuvant chemotherapy for breast cancer: functional tumor volume by MR imaging predicts recurrence-free survival-results from the ACRIN 6657/CALGB 150007 I-SPY 1 TRIAL. Radiology 279(1):44–55

Iacconi C, Giannelli M, Marini C, Cilotti A, Moretti M, Viacava P et al (2010) The role of mean diffusivity (MD) as a predictive index of the response to chemotherapy in locally advanced breast cancer: a preliminary study. Eur Radiol 20(2):303–308

Iima M, Nakamoto Y, Kanao S, Sugie T, Ueno T, Kawada M et al (2012) Clinical performance of 2 dedicated PET scanners for breast imaging: initial evaluation. J Nucl Med 53(10):1534–1542

Jung JI, Kim HH, Park SH, Song SW, Chung MH, Kim HS et al (2004) Thoracic manifestations of breast cancer and its therapy. Radiographics 24(5): 1269–1285

Kanao S, Kataoka M (2016) Imaging tumor response by preoperative systemic treatment. In: Toi M, Winer E, Benson J, Klimberg S (eds) Personalized treatment of breast cancer. Springer, Tokyo

Kashyap R, Reddy R, Voona MK (2018) Pseudocirrhosis of the liver in setting of metastatic carcinoma breast: an ominous sign to be remembered. Indian J Nucl Med 33(1):86–87

Keune JD, Jeffe DB, Schootman M, Hoffman A, Gillanders WE, Aft RL (2010) Accuracy of ultrasonography and mammography in predicting pathologic response after neoadjuvant chemotherapy for breast cancer. Am J Surg 199(4):477–484

Kim SJ, Kim SK, Lee ES, Ro J, Kang S (2004) Predictive value of [18F]FDG PET for pathological response of breast cancer to neo-adjuvant chemotherapy. Ann Oncol 15(9):1352–1357

Kim SY, Cho N, Park IA, Kwon BR, Shin SU, Kim SY et al (2018) Dynamic contrast-enhanced breast MRI for evaluating residual tumor size after neoadjuvant chemotherapy. Radiology 289(2):327–334

Lecouvet FE, Talbot JN, Messiou C, Bourguet P, Liu Y, de Souza NM et al (2014) Monitoring the response of bone metastases to treatment with magnetic resonance imaging and nuclear medicine techniques: a review and position statement by the European Organisation for Research and Treatment of Cancer imaging group. Eur J Cancer 50(15):2519–2531

Lee JH, Rosen EL, Mankoff DA (2009) The role of radiotracer imaging in the diagnosis and management of patients with breast cancer: part 2—response to therapy, other indications, and future directions. J Nucl Med 50(5):738–748

Li XR, Cheng LQ, Liu M, Zhang YJ, Wang JD, Zhang AL et al (2012) DW-MRI ADC values can predict treatment response in patients with locally advanced breast cancer undergoing neoadjuvant chemotherapy. Med Oncol 29(2):425–431

Li JJ, Chen C, Gu Y, Di G, Wu J, Liu G et al (2014) The role of mammographic calcification in the neoadjuvant therapy of breast cancer imaging evaluation. PLoS One 9(2):e88853

Liu S, Ren R, Chen Z, Wang Y, Fan T, Li C et al (2015) Diffusion-weighted imaging in assessing pathological response of tumor in breast cancer subtype to neoadjuvant chemotherapy. J Magn Reson Imaging 42(3):779–787

Lobbes MB, Prevos R, Smidt M, Tjan-Heijnen VC, van Goethem M, Schipper R et al (2013) The role of magnetic resonance imaging in assessing residual disease and pathologic complete response in breast cancer patients receiving neoadjuvant chemotherapy: a systematic review. Insights Imaging 4(2): 163–175

Ma Y, Zhang S, Li J, Li J, Kang Y, Ren W (2017) Comparison of strain and shear-wave ultrasonic elastography in predicting the pathological response to neoadjuvant chemotherapy in breast cancers. Eur Radiol 27(6):2282–2291

Mann RM, Kuhl CK, Kinkel K, Boetes C (2008) Breast MRI: guidelines from the European Society of Breast Imaging. Eur Radiol 18(7):1307–1318

Marinovich ML, Macaskill P, Irwig L, Sardanelli F, von Minckwitz G, Mamounas E et al (2013) Meta-analysis of agreement between MRI and pathologic breast tumour size after neoadjuvant chemotherapy. Br J Cancer 109(6):1528–1536

Marinovich ML, Houssami N, Macaskill P, von Minckwitz G, Blohmer JU, Irwig L (2015) Accuracy of ultrasound for predicting pathologic response during neoadjuvant therapy for breast cancer. Int J Cancer 136(11):2730–2737

Martincich L, Montemurro F, De Rosa G, Marra V, Ponzone R, Cirillo S et al (2004) Monitoring response to primary chemotherapy in breast cancer using dynamic contrast-enhanced magnetic resonance imaging. Breast Cancer Res Treat 83(1):67–76

Masumoto N, Kadoya T, Sasada S, Emi A, Arihiro K, Okada M (2018) Intratumoral heterogeneity on dedicated breast positron emission tomography predicts malignancy grade of breast cancer. Breast Cancer Res Treat 171(2):315–323

Miyake KK, Nakamoto Y, Kanao S, Tanaka S, Sugie T, Mikami Y et al (2014) Journal club: diagnostic value of (18)F-FDG PET/CT and MRI in predicting the clinicopathologic subtypes of invasive breast cancer. AJR Am J Roentgenol 203(2):272–279

Mukhtar RA, Yau C, Rosen M, Tandon VJ, I-Spy T, Investigators A et al (2013) Clinically meaningful tumor reduction rates vary by prechemotherapy MRI phenotype and tumor subtype in the I-SPY 1 TRIAL

(CALGB 150007/150012; ACRIN 6657). Ann Surg Oncol 20(12):3823–3830

Nascimento AB, Mitchell DG, Rubin R, Weaver E (2001) Diffuse desmoplastic breast carcinoma metastases to the liver simulating cirrhosis at MR imaging: report of two cases. Radiology 221(1):117–121

Nishino M, Hayakawa K, Nakamura Y, Morimoto T, Mukaihara S (2003) Effects of tamoxifen on hepatic fat content and the development of hepatic steatosis in patients with breast cancer: high frequency of involvement and rapid reversal after completion of tamoxifen therapy. AJR Am J Roentgenol 180(1):129–134

Park SH, Moon WK, Cho N, Song IC, Chang JM, Park IA et al (2010) Diffusion-weighted MR imaging: pretreatment prediction of response to neoadjuvant chemotherapy in patients with breast cancer. Radiology 257(1):56–63

Park J, Chae EY, Cha JH, Shin HJ, Choi WJ, Choi YW et al (2018) Comparison of mammography, digital breast tomosynthesis, automated breast ultrasound, magnetic resonance imaging in evaluation of residual tumor after neoadjuvant chemotherapy. Eur J Radiol 108:261–268

Partridge SC, Gibbs JE, Lu Y, Esserman LJ, Tripathy D, Wolverton DS et al (2005) MRI measurements of breast tumor volume predict response to neoadjuvant chemotherapy and recurrence-free survival. AJR Am J Roentgenol 184(6):1774–1781

Partridge SC, Zhang Z, Newitt DC, Gibbs JE, Chenevert TL, Rosen MA et al (2018) Diffusion-weighted MRI findings predict pathologic response in neoadjuvant treatment of breast cancer: the ACRIN 6698 multicenter trial. Radiology 289(3):618–627

Perou CM, Sorlie T, Eisen MB, van de Rijn M, Jeffrey SS, Rees CA et al (2000) Molecular portraits of human breast tumours. Nature 406(6797):747–752

Rastogi P, Anderson SJ, Bear HD, Geyer CE, Kahlenberg MS, Robidoux A et al (2008) Preoperative chemotherapy: updates of National Surgical Adjuvant Breast and Bowel Project Protocols B-18 and B-27. J Clin Oncol 26(5):778–785

Rosen EL, Eubank WB, Mankoff DA (2007) FDG PET, PET/CT, and breast cancer imaging. Radiographics 27(Suppl 1):S215–S229

Rousseau C, Devillers A, Sagan C, Ferrer L, Bridji B, Campion L et al (2006) Monitoring of early response to neoadjuvant chemotherapy in stage II and III breast cancer by [18F]fluorodeoxyglucose positron emission tomography. J Clin Oncol 24(34):5366–5372

Schelling M, Avril N, Nahrig J, Kuhn W, Romer W, Sattler D et al (2000) Positron emission tomography using [(18)F]Fluorodeoxyglucose for monitoring primary chemotherapy in breast cancer. J Clin Oncol 18(8):1689–1695

Schrading S, Kuhl CK (2015) Breast cancer: influence of taxanes on response assessment with dynamic contrast-enhanced MR imaging. Radiology 277(3):687–696

Sharma U, Danishad KK, Seenu V, Jagannathan NR (2009) Longitudinal study of the assessment by MRI and diffusion-weighted imaging of tumor response in patients with locally advanced breast cancer undergoing neoadjuvant chemotherapy. NMR Biomed 22(1):104–113

Shin SU, Cho N, Lee HB, Kim SY, Yi A, Kim SY et al (2018) Neoadjuvant chemotherapy and surgery for breast cancer: preoperative MRI features associated with local recurrence. Radiology 289(1):30–38

Takeda K, Kanao S, Okada T, Ueno T, Toi M, Ishiguro H et al (2012a) MRI evaluation of residual tumor size after neoadjuvant endocrine therapy vs. neoadjuvant chemotherapy. Eur J Radiol 81(9):2148–2153

Takeda K, Kanao S, Okada T, Kataoka M, Ueno T, Toi M et al (2012b) Assessment of CAD-generated tumor volumes measured using MRI in breast cancers before and after neoadjuvant chemotherapy. Eur J Radiol 81(10):2627–2631

Tiling R, Linke R, Untch M, Richter A, Fieber S, Brinkbaumer K et al (2001) ^{18}F-FDG PET and 99mTc-sestamibi scintimammography for monitoring breast cancer response to neoadjuvant chemotherapy: a comparative study. Eur J Nucl Med 28(6):711–720

Tozaki M, Kobayashi T, Uno S, Aiba K, Takeyama H, Shioya H et al (2006) Breast-conserving surgery after chemotherapy: value of MDCT for determining tumor distribution and shrinkage pattern. AJR Am J Roentgenol 186(2):431–439

von Minckwitz G, Blohmer JU, Costa SD, Denkert C, Eidtmann H, Eiermann W et al (2013) Response-guided neoadjuvant chemotherapy for breast cancer. J Clin Oncol 31(29):3623–3630

Wahl RL, Zasadny K, Helvie M, Hutchins GD, Weber B, Cody R (1993) Metabolic monitoring of breast cancer chemohormonotherapy using positron emission tomography: initial evaluation. J Clin Oncol 11(11):2101–2111

Wahl RL, Jacene H, Kasamon Y, Lodge MA (2009) From RECIST to PERCIST: evolving considerations for PET response criteria in solid tumors. J Nucl Med 50(Suppl 1):122S–150S

Wu J, Cao G, Sun X, Lee J, Rubin DL, Napel S et al (2018) Intratumoral spatial heterogeneity at perfusion MR imaging predicts recurrence-free survival in locally advanced breast cancer treated with neoadjuvant chemotherapy. Radiology 288(1):26–35

Yeh E, Slanetz P, Kopans DB, Rafferty E, Georgian-Smith D, Moy L et al (2005) Prospective comparison of mammography, sonography, and MRI in patients undergoing neoadjuvant chemotherapy for palpable breast cancer. AJR Am J Roentgenol 184(3):868–877

Therapy Response Imaging in Thoracic Malignancy

Mizuki Nishino

Contents

Abstract

Lung cancer remains to be the leading cause of cancer death. More than half of patients with lung cancer present with advanced disease requiring systemic therapy. Remarkable advances of systemic therapy approaches have been made for patients with advanced lung cancer in the past decade, first with molecular targeting therapy that can specifically target genomic driver mutations of the tumor, and more recently with immune-checkpoint inhibitors that activate host T cell immune response against tumor. The strategies for radiographic tumor response evaluations for lung cancer have also evolved in parallel with the advances of treatment approaches for the disease. This chapter will discuss (1) recent advances of therapeutic approaches for lung cancer, (2) imaging for treatment monitoring for lung cancer in the era of precision cancer therapy, and (3) treatment monitoring of thoracic malignancies other than lung cancer, focusing on thymic tumors and malignant pleural mesothelioma.

M. Nishino (✉)
Department of Imaging, Dana-Farber Cancer Institute, Boston, MA, USA

Department of Radiology, Brigham and Women's Hospital, Boston, MA, USA
e-mail: mizuki_nishino@dfci.harvard.edu

M. Nishino (ed.), *Therapy Response Imaging in Oncology*, Medical Radiology, Diagnostic Imaging,
https://doi.org/10.1007/978-3-030-31171-1_6

1 Recent Advances of Therapeutic Approaches for Lung Cancer

1.1 Molecular Targeted Therapy

Lung cancer remains to be the leading cause of cancer death both in men and in women, accounting for more than 140,000 deaths per year in the USA (Siegel et al. 2019). Approximately 85% of patients with lung cancer have non-small cell lung cancer (NSCLC), and more than half of patients with NSCLC present with advanced disease, and thus require systemic therapy. Cytotoxic chemotherapy has been the main systemic therapy approach for NSCLC. However, it is marginally effective, as indicated in the analysis of 33 phase III trials between 1973 and 1994 that demonstrated the improvement of median survival by only 2.6 weeks (Breathnach et al. 2001). In response to the needs for new effective agents for systemic therapy of lung cancer, the efforts have been made to identify novel tumor genomic abnormalities specific to lung cancer that can be targeted by molecular targeting agents, and to translate the precision medicine approaches to clinical care of lung cancer patients (Nishino et al. 2011a, 2014).

The most representative example of precision medicine approaches to lung cancer is epidermal growth factor receptor (EGFR) tyrosine kinase inhibitors (TKIs), including erlotinib, gefitinib, afatinib, and more recently osimertinib, for NSCLC harboring sensitizing EGFR mutations (Fig. 1). EGFR is a transmembranous receptor tyrosine kinase that regulates cell proliferation, apoptosis, angiogenesis, and invasion (Nishino et al. 2014; Gazdar 2009; Herbst et al. 2008). EGFR mutations are more common in female, never-smokers with adenocarcinoma histology, and are noted in about 15% of lung adenocarcinomas in patients from northern European background and up to 50% of patients from East Asia (Nishino et al. 2014; Gazdar 2009; Herbst et al. 2008; Janne et al. 2004; Lynch et al. 2004; Paez et al. 2004; Pao et al. 2004). Certain types of EGFR mutations, including exon 19 deletions or L858R point mutation in exon 21, are associated with sensitivity and response to EGFR inhibitor therapy, and thus referred as "sensitizing mutations" (Nishino et al. 2014). EGFR inhibitor treatment in patients with NSCLC harboring sensitizing EGFR mutations results in a dramatic initial decrease of tumor burden, with a response rates up to 70–80% (Zhou et al. 2011; Mok et al. 2009).

Another example of precision therapy for lung cancer is anaplastic lymphoma kinase (ALK) rearrangements, which is noted in 3–7% of patients with NSCLC and is also more common in younger patients, women, never or light smokers with adenocarcinomas histology (Kwak et al. 2010). The ALK inhibitor, crizotinib, received the first FDA approval for advanced NSCLC with ALK rearrangements in 2011, and demonstrated a response rate of 65–74% and a median progression-free survival (PFS) of 7.7–10.9 months (Fig. 2) (Shaw et al. 2013; Solomon et al. 2014). Given the remarkable efficacy and effectiveness of EGFR inhibitors and ALK inhibitors in the subsets of patients with specific tumor genomic abnormalities, precision medicine approaches based on genome-based therapy selection have joined the mainstream of treatment for patients with advanced lung cancer (Nishino et al. 2011a, 2014). Molecular and genomic testing for EGFR mutations and ALK rearrangements are included in the management of advanced NSCLC patients with non-squamous histology in the NCCN guideline as Category 1 (Recommended based upon high-level evidence, there is uniform NCCN consensus that the intervention is appropriate) (https://www.nccn.org/professionals/physician_gls/pdf/nscl.pdf). More targetable mutations are being identified and novel agents are developed and evaluated. Precision therapy agents that have been approved by U.S. Food and Drug Administration (FDA) for the treatment of NSCLC with specific genomic abnormalities are listed in Table 1 (Park et al. 2019).

Precision lung cancer therapy using molecular targeting agents demonstrated marked initial activity. However, virtually all patients with initial response eventually experience tumor progression, due to the development of acquired resistance to these agents, which is the major

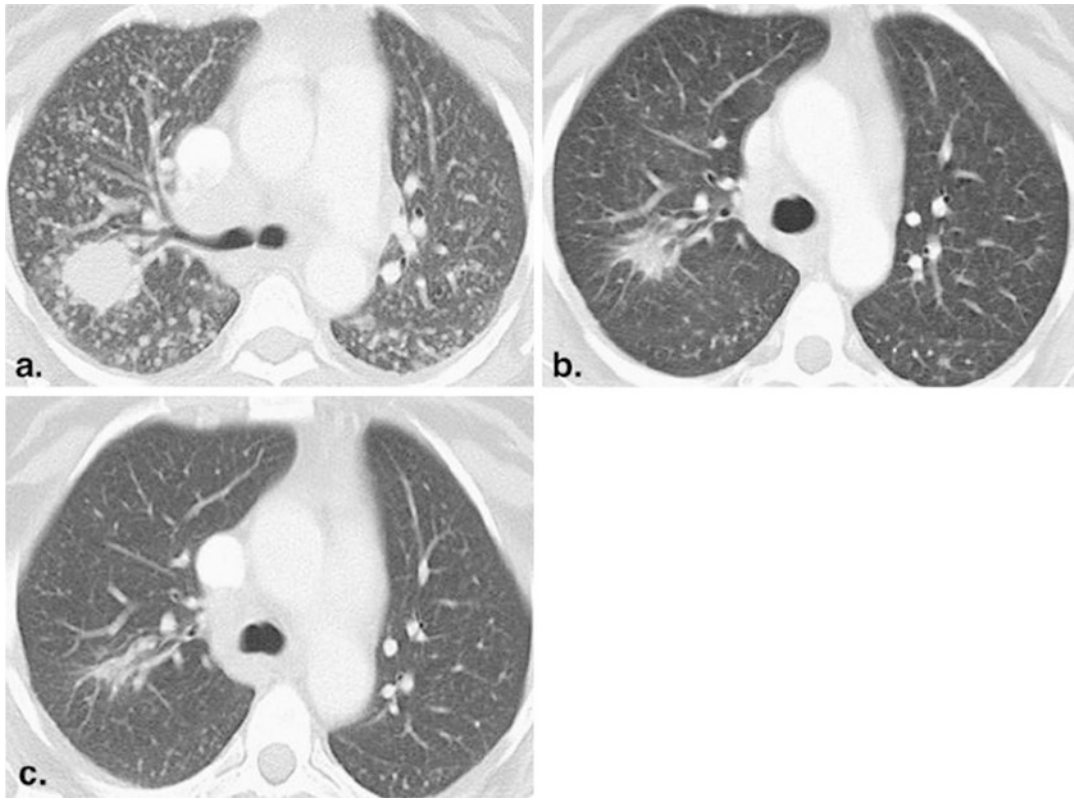

Fig. 1 A 52-year-old female nonsmoker with lung adenocarcinoma treated with erlotinib. (**a**) Baseline computed tomographic scan prior to erlotinib therapy demonstrated a dominant mass in the right upper lobe with innumerable metastatic nodules. Epidermal growth factor receptor (EGFR) gene sequencing of the tumor showed EGFR mutation with exon 19 deletion. (**b**) After one cycle (2 months) of therapy, the mass was significantly decreased in size, and the nodules were markedly decreased in size and number, representing partial response. (**c**) After two cycles (4 months) of therapy, a further decrease in size of the mass was noted. The nodules had mostly resolved. The patient remained progression free after 2.5 years, with a minimal amount of residual disease at the site of the dominant mass. (Reprinted with permission from Acad Radiol. 2011;18: 424–436)

limitation of precision cancer therapy in general (Nishino et al. 2011a, 2014). Some of the genomic mechanisms of acquired resistance mutations have been identified, and the efforts in lung cancer precision therapy in the past decade have focused on the strategy to overcome acquired resistance.

In EGFR-mutant NSCLC patients treated with the conventional EGFR inhibitors such as erlotinib or gefitinib, the development of a second-site EGFR T790M mutation is the most common mechanism of acquiring resistance, noted up to 50–60% of the acquired resistance cases. A mutant-selective EGFR inhibitor, osimertinib, has been developed, which targets both sensitizing EGFR mutations and T790M resistance mutations, while relatively sparing wild-type EGFR. Osimertinib showed the response rates of 60–70% in patients with EGFR T790M mutation in the clinical trials, and received accelerated FDA approval in 2015 for treatment for advanced NSCLC patients with T790M mutation who progressed on EGFR inhibitor therapy (Fig. 3) (Goss et al. 2016; Janne et al. 2015). More recently, osimertinib also showed a superior efficacy and better clinical outcome as the first-line treatment for EGFR-mutant advanced NSCLC compared to the conventional EGFR inhibitors including erlotinib and gefitinib. Based on the results, osimertinib has also been approved

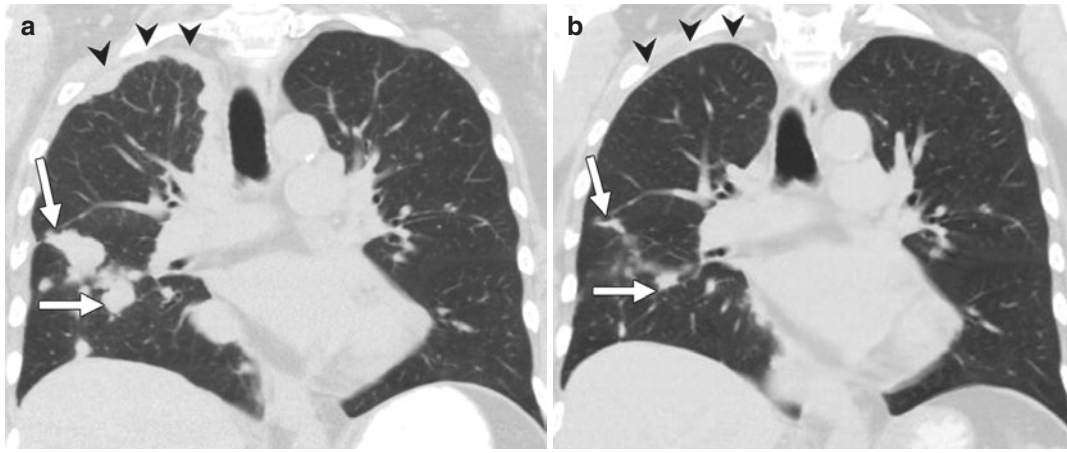

Fig. 2 Images in a 70-year-old woman with stage IV adenocarcinoma harboring ALK (anaplastic lymphoma kinase) translocation treated with ALK inhibitor, crizotinib. (**a**) Coronal reformatted image from baseline chest CT demonstrates multiple nodules in the right lung (arrows) with nodular thickening of the right apical pleura (arrowheads), representing significant tumor burden. (**b**) The patient was treated with crizotinib. After 4 months of therapy, follow-up chest CT scan demonstrates marked decrease of the right lung nodules (arrows) and resolution of pleural tumor burden in the right apex (arrowheads). (Reprinted with permission from Radiology. 2014 Apr;271(1):6–27)

Table 1 Precision therapy agents for NSCLC with corresponding genomic abnormalities (Park et al. 2019)

Oncogenic driver mutations/rearrangements	Precision therapy agents approved by United States FDA[a]
ALK rearrangements	Crizotinib, Alectinib[b], Ceritinib[b], Brigatinib[c], Lorlatinib[d]
BRAF mutations	Dabrafenib and trametinib combination
EGFR mutations	Erlotinib, Gefitinib, Afatinib, Osimertinib[e]
NTRK rearrangements	Larotrectinib[f]
ROS1 rearrangements	Crizotinib

NSCLC non-small cell lung cancer, *FDA* Food and Drug Administration, *EGFR* epidermal growth factor receptor mutation, *ALK* anaplastic lymphoma kinase, *ROS-1* ROS proto-oncogene 1, *BRAF* v-Raf murine sarcoma viral oncogene homolog B1, *NTRK* neurotrophic receptor tyrosine kinase

[a]The table lists approvals by U.S. FDA as of January 2019

[b]Approved as the first-line therapy and after progression on crizotinib therapy

[c]Approved after progression on crizotinib

[d]Approved after progression on crizotinib and at least one other ALK inhibitor or progression on alectinib or ceritinib as the first ALK inhibitor

[e]Approved as the first-line therapy, and after progression on previous EGFR tyrosine kinase inhibitor therapy with the development of T790M mutation

[f]Approved for the treatment of adult and pediatric patients with solid tumors including NSCLC that harbor NTRK gene fusion without a known acquired resistance mutation, that are either metastatic or where surgical resection is likely to result in severe morbidity, and who have no satisfactory alternative treatments or whose cancer has progressed following treatment

for the first-line treatment for EGFR-mutant NSCLC in 2018, further changing the landscape of precision medicine approaches for subsets of lung cancer patients harboring sensitizing EGFR mutations (Table 1) (Soria et al. 2018).

Similarly, acquired resistance to crizotinib in ALK-rearranged NSCLC patients has been noted, which develops within 12 months of crizotinib therapy in most cases. Additionally, in ALK-rearranged patients treated with crizotinib, central nervous system (CNS) is the most common site of disease progression, reflecting the poor blood-brain-barrier penetration of crizotinib (Costa et al. 2015). Newer ALK inhibitors are

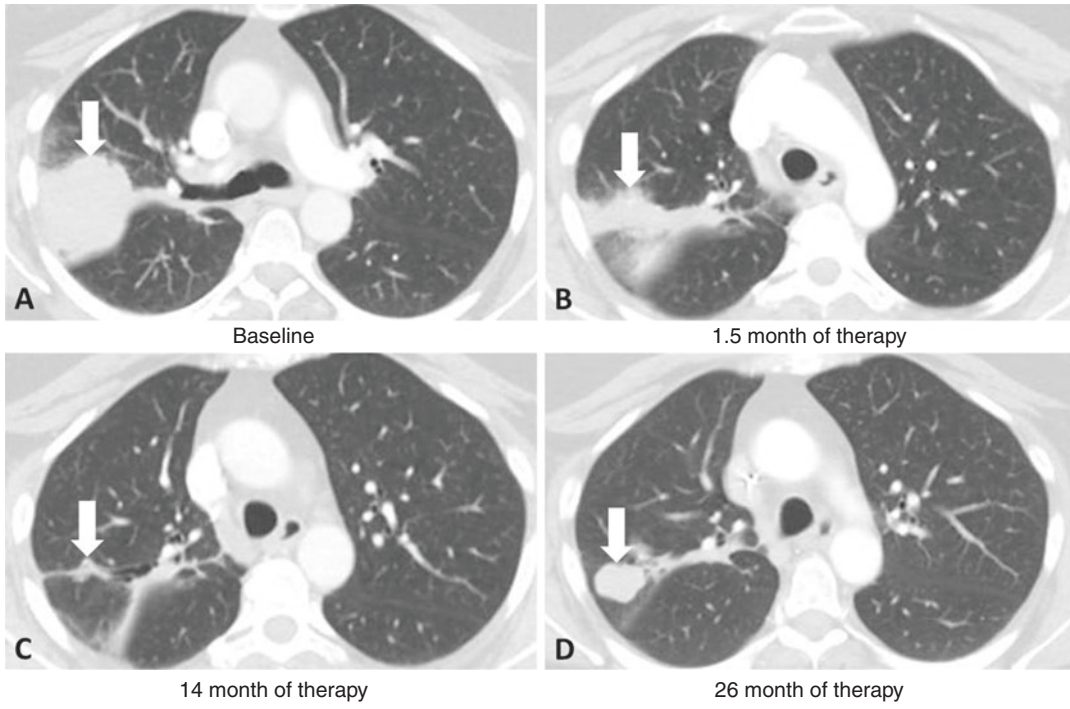

Fig. 3 A patient with stage IV NSCLC with EGFR exon 19 deletion who progressed on erlotinib due to the development of T790M acquired resistance mutation, subsequently treated with osimertinib. (**a**) Baseline CT prior to osimertinib therapy showed a dominant mass (arrow) in the right upper lobe demonstrating tumor progression during erlotinib therapy. (**b**) At 1.5 months of osimertinib therapy, significant reduction of the right upper lobe mass was noted (arrow). (**c**) The tumor continued to respond to osimertinib, with a minimal residual tumor burden noted at 14 months of therapy. (**d**) However, at 26 months of osimertinib therapy, tumor regrowth is noted due to acquired resistance to osimertinib (arrow)

developed to overcome resistance to crizotinib, including alectinib, ceritinib, brigatinib, and lorlatinib, which have been approved for the treatment of ALK-rearranged NSCLC (Table 1). Of note, alectinib showed a response rate of 48–50% and a median PFS of 8.1–8.9 months in ALK-rearranged patients who progressed on crizotinib. Alectinib also showed a superior efficacy and improved survival as the first-line treatment for ALK-rearranged NSCLC patients compared to crizotinib, with better CNS disease control (Fig. 4) (Ou et al. 2016; Peters et al. 2017; Shaw et al. 2016). Alectinib, as well as another second-generation ALK inhibitor ceritinib, have been approved as the first-line therapy for ALK-rearranged advanced NSCLC.

Although these newer molecular targeting agents are effective in patients who developed acquired resistance to the conventional agents, development of further acquired resistance to these new agents including osimertinib and alectinib has already been noted (Ortiz-Cuaran et al. 2016). Further efforts are ongoing to develop novel agents and test combination regimen to overcome acquired resistance to these newer agents.

1.2 Immune-Checkpoint Inhibitor Therapy

Cancer immunotherapy using immune-checkpoint inhibition has brought another paradigm shift in treatment of many advanced cancers, as discussed in chapter "Response Evaluations for Precision Cancer Therapy and Immunotherapy". Immune-checkpoint inhibitor therapy, especially using programmed death-1

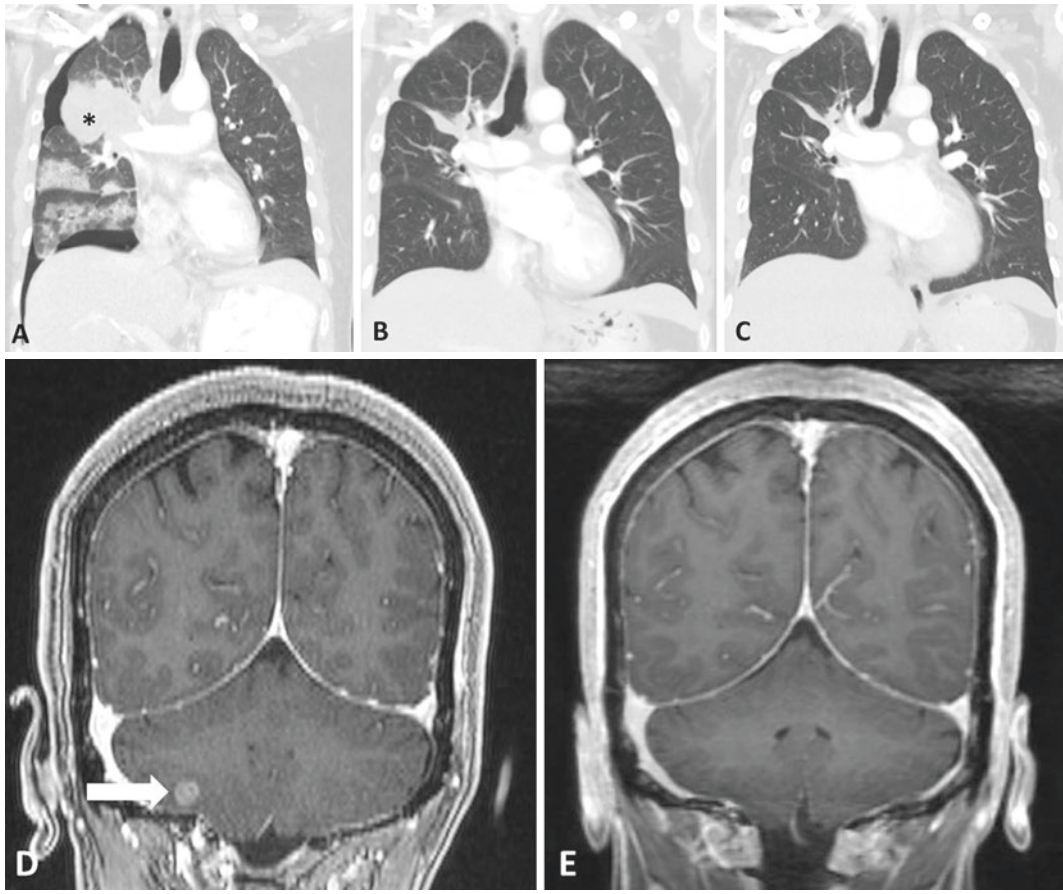

Fig. 4 A 56-year-old woman with *ALK*-rearranged advanced NSCLC patient treated initially with crizotinib, progressed in the brain and subsequently treated with alectinib. (**a**) Baseline chest CT showed a dominant mass in the right upper lobe (asterisk) extending from the right hilum. The patient also has pneumothorax from prior thoracentesis. (**b**) Patient showed marked response to crizotinib, with small residual tumor burden in the right upper lobe at 4 months of therapy. (**c**, **d**) The lung tumor burden showed continued response to therapy after 2 years of crizotinib therapy (**c**). However, the brain MRI demonstrated a new enhancing lesion in the right cerebellum (arrow, **d**), suggesting central nervous system (CNS) progression. (**e**) The patient discontinued crizotinib and started alectinib. Follow-up brain MRI at 1.5 months of alectinib therapy showed resolution of the brain metastasis, reflecting superior activity of alectinib for CNS lesions because of the better blood-brain-barrier penetration compared to crizotinib

(PD-1)/PD-ligand 1 (PD-L1) inhibitors, have shown marked efficacy in patients with advanced lung cancer and have added another dimension to treatment approaches to these patients. Of note, the introduction of immune-checkpoint inhibitors has added a promising treatment option for NSCLC patients without any targetable mutations. Marked and durable responses and prolonged clinical benefits to PD-1/PD-L1 inhibitor therapy are noted in a proportion of these patients (Fig. 5) (Rizvi et al. 2015; Gettinger et al. 2015; Garon et al. 2015; Brahmer et al. 2015; Borghaei et al. 2015). Immune-checkpoint inhibitors that are currently approved in the USA for treatment of advanced NSCLC include PD-1 inhibitors, nivolumab, and pembrolizumab (alone or in combination with chemotherapy), as well as PD-L1 inhibitor atezolizumab (alone or in combination with bevacizumab, paclitaxel, and carboplatin). In addition, PD-L1 inhibitor, durvalumab is also approved as a consolidation therapy after chemoradiation in stage III NSCLC, expanding the utility of immunotherapy (Antonia et al. 2017, 2018). Moreover, nivolumab also

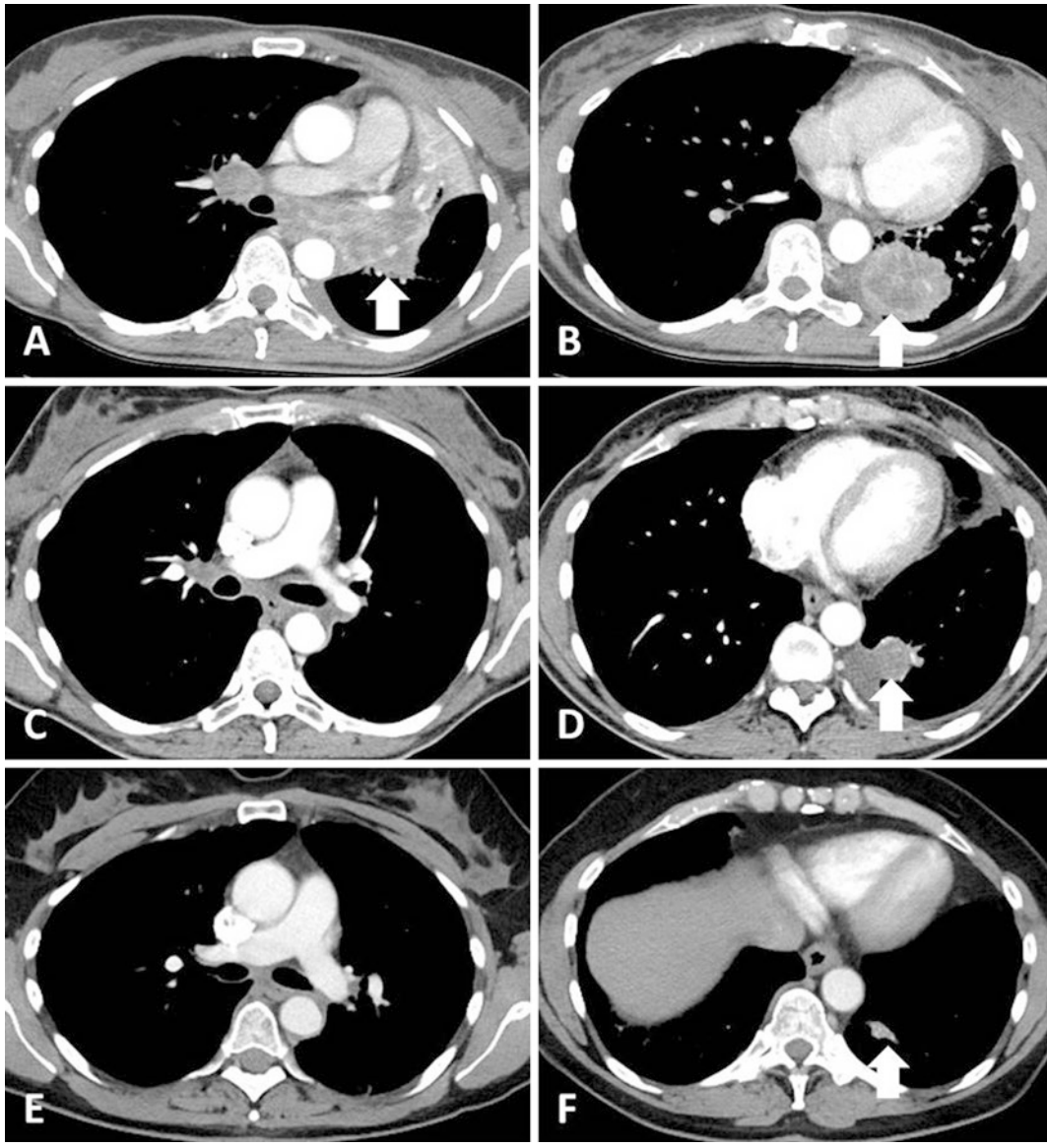

Fig. 5 A 42-year-old woman with advanced NSCLC treated with nivolumab. (**a**, **b**) Baseline CT shows an irregular mass (arrow, **a**) with post-obstructive atelectasis in the left upper lobe involving the subcarinal lymph nodes, and a dominant lobulated mass in the left lower lobe (arrow, **b**). Enlarged right hilar node was also noted. (**c**, **d**) At 2 months of nivolumab therapy, marked response was noted with reduction of tumor burden in the mediastinum and left upper lobe, as well as decrease in size of left lower lobe lesion (arrow). (**e**, **f**) CT scan after 1.5 years of therapy demonstrates continued response with further decrease of mediastinal and left lower lobe (arrow, **f**) tumor burden

showed durable response in patients with small cell lung cancer (SCLC) after progression on two or more chemotherapy regimens, where more effective therapies are sorely needed. Nivolumab was approved for the treatment of SCLC after disease progression following platinum-based chemotherapy and one other line of therapy in 2018, bringing a promising treatment option for SCLC patients (Ready et al. 2019).

When using immune-checkpoint inhibitors for advanced NSCLC, a patient selection based on biomarkers is important, because not all patients

respond to immune-checkpoint inhibitor therapy. Among various biomarkers under investigation, PD-L1 expression in tumor cells by immunohistochemistry (IHC) has been shown to be a useful and relatively practical marker to identify patients who benefit from PD-1/PD-L1 inhibitor therapy (Nishino et al. 2017a). A higher response rate as well as longer PFS and overall survival (OS) were noted in patients whose tumors showed high PD-L1 expression, defined as PD-L1 staining in ≥50% of tumor cells, in a phase III trial of pembrolizumab in advanced NSCLC patients (Reck et al. 2016). The results led to the approval of pembrolizumab as the first-line therapy for NSCLC patients without EGFR mutations and ALK rearrangements and with ≥50% PD-L1 staining in tumor cells, as an important step toward precision immunotherapy for lung cancer and expanding a subset of NSCLC patients who benefit from precision medicine approaches (Park et al. 2019; Johnson 2016). For patients with <50% PD-L1 staining, combination therapy with pembrolizumab and platinum doublet chemotherapy is an actively used treatment regimen, because it has shown to improve PFS and OS regardless of the levels of PD-L1 expression compared to chemotherapy alone, and has been approved for treatment of both nonsquamous and squamous NSCLC (Gandhi et al. 2018; Paz-Ares et al. 2018). PD-L1 testing is also included in the NCCN guideline for the management of advanced NSCLC patients as Category 1 recommendation (https://www.nccn.org/professionals/physician_gls/pdf/nscl.pdf).

2 Imaging for Treatment Monitoring for Lung Cancer in the Era of Precision Cancer Therapy

Discoveries of newer genomic abnormalities that can be treated effectively with specific targeting agents, as well as the successful clinical applications of immune-checkpoint inhibitors, continue to advance precision lung cancer therapy. Imaging plays a key role in therapeutic monitoring of these new therapeutic approaches for lung cancer. With the rapidly advancing landscape of treatment approaches to lung cancer patients, it is important to note the characteristics patterns of radiographic response and progression and pitfalls in these specific treatment settings.

2.1 Treatment Monitoring During Molecular Targeted Therapy for Lung Cancer

Patterns of tumor response and progression during molecular targeted therapy for lung cancer have been most extensively studied in EGFR-mutant NSCLC patients treated with EGFR inhibitors. Many patients experience initial tumor burden decrease, with the response rate of up to 70–80%. The tumor shrinkage can be dramatic in some patients, with the median value of maximal tumor size shrinkage of 40–56% (Takeda et al. 2014; Nishino et al. 2013a). Some studies indicated that RECIST response can be a marker for longer PFS and OS in EGFR-mutant NSCLC patients treated with EGFR inhibitors (Takeda et al. 2014; Salvador-Coloma et al. 2018). In 40 patients with EGFR-mutant NSCLC treated with EGFR inhibitors, responders (including those who with complete or partial response) by RECIST1.1 at 6–8 weeks of therapy had significantly longer PFS (10.9 vs. 2.4 months; HR: 0.42; 95% CI: 0.19–0.93; $P = 0.033$) and OS (23.2 vs. 11.9 months; HR: 0.3; 95% CI: 0.15–0.85; $P = 0.021$) compared to non-responders (with stable disease and progressive disease) at 6–8 weeks (Salvador-Coloma et al. 2018).

However, after initial response, tumors start to gradually grow back while on therapy and patients eventually experience disease progression by RECIST, typically around or after 12 months of therapy, due to the development of acquired resistance (Fig. 6) (Nishino et al. 2011a, 2013a, 2014). Characterization of tumor growth and progression on imaging is particularly important in detecting the development of acquired resistance and in providing guidance for treatment decisions. Of note, in these patients with sensitizing EGFR mutations, tumors tend to grow back slowly over the course of many months or

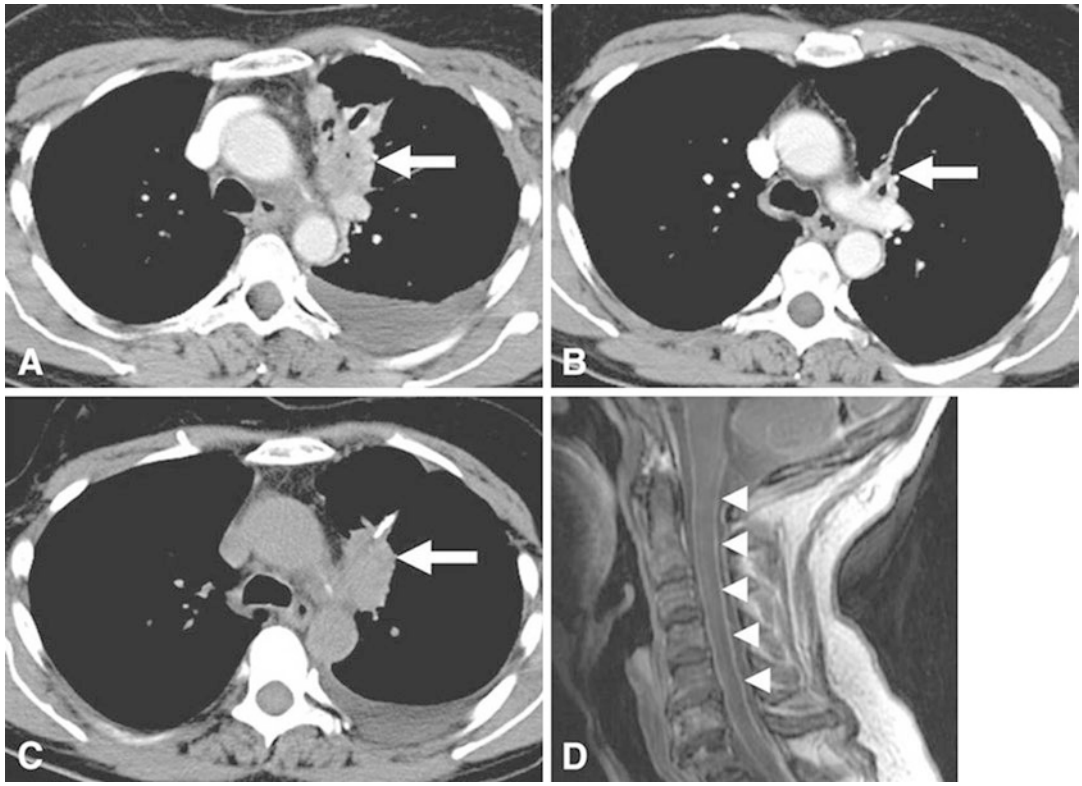

Fig. 6 A 50-year-old woman with lung adenocarcinoma harboring sensitizing EGFR mutation. (**a**) Baseline chest CT before therapy demonstrated an irregular mass in the left upper lobe, measuring 3.1 cm. (**b**) The patient started treatment with erlotinib and demonstrated marked tumor decrease as a response to therapy. After 11 months of therapy, the left upper lobe lesion measured 0.8 cm (arrow), which was the smallest measurement since the baseline. Subsequently, the lesion started to grow slowly, and at 15 months of therapy, the lesion measured 1.4 cm, meeting the criteria for progression by RECIST 1.1 (≥20% and ≥5-mm increase since the nadir). Given the small burden of the tumor, the patient continued to receive erlotinib without any additional agent. (**c**, **d**) At 22 months of therapy, the left upper lobe lesion further increased in size, measuring 4.1 cm (**c**, arrow). MRI of the cervical spine demonstrated diffuse leptomeningeal enhancement (**d**, arrowheads), representing new leptomeningeal metastasis. Erlotinib was discontinued, and the patient was subsequently enrolled in another investigational therapy. (Reprinted with permission from Am Soc Clin Oncol Educ Book. 2018 May 23;(38):1019–1029)

years (Nishino et al. 2013a, b, 2016; Nishino 2018). Slow growth during initially very effective EGFR inhibitor therapy suggest some tumor cells may still remain sensitive to EGFR inhibitors, and oncologists often continue to treat these patients with EGFR beyond RECIST progression (Nishino 2018; Riely et al. 2007; Mok 2010; Nishino et al. 2013c). In a report of 56 EGFR-mutant NSCLC patients treated with erlotinib or gefitinib, 88% of the patients continued their EGFR inhibitors after they experienced RECIST1.1 progression (Fig. 6) (Nishino 2018; Nishino et al. 2013c). In a phase 2 trial of EGFR-mutant patients treated with first-line erlotinib, continuation of therapy beyond RECIST progression is feasible and delayed salvage therapy with a median of 3.1 months (Park et al. 2016). Similar observations are noted in other subset of NSCLC with targetable genomic abnormalities, including ALK-rearranged NSCLC patients treated with ALK inhibitors (Nishino 2018; Camidge et al. 2012; Nishino et al. 2012a; Tani et al. 2016; Kim et al. 2015; Isozaki et al. 2016; Eberlein et al. 2015). The patterns of treatment decisions at RECIST progression in these patients may be changing with increasing availability of newer

targeting agents that are effective in patients with acquired resistance to conventional agents; however, emerging data suggest that further acquired resistance to these newer agents are inevitable, which indicate that the issue continues to be important in the new era of precision therapy for lung cancer.

To meet the increasing clinical demands for accurately characterizing slow progression and providing aids to determine when to consider alternate therapy, tumor volume analysis has been investigated. The advances of multi-detector row CT (MDCT) technology and increased availability of image-processing software and workstation allow for quantification of tumor volume burden in addition to size in a relatively practical manner especially in lung tumors. Using tumor volume has an advantage over tumor size, because tumor volume measurements have less measurement variability and are more reproducible compared to size measurements, and thus can accurately characterize small tumor burden changes (Nishino et al. 2014, 2011b; Zhao et al. 2009; Mozley et al. 2012). For the characterization of initial response, tumor volume decrease at 8 weeks of EGFR inhibitor therapy was associated with longer OS in EGFR-mutant advanced NSCLC patients, which was validated in the external cohort (Fig. 7) (Nishino et al. 2013a, 2016). Another study of tumor volume analysis in EGFR-mutant patients also showed the association between tumor volume decrease during EGFR inhibitor therapy and OS (Lee et al. 2016). In these studies, a distinct pattern of tumor volume dynamics of EGFR-mutant NSCLC patients was demonstrated based on the analysis of serial CT scans during therapy, which is characterized by marked initial decrease, followed by durable response and eventual regrowth (Nishino et al. 2013a, 2016).

Given its better reproducibility, tumor volume can be utilized to quantitatively characterize the rate of slow tumor progression after initial response to EGFR inhibitor therapy.

Contrary to RECIST that uses the simple percent changes without consideration of the length of time between scans or on therapy, tumor growth rate evaluates the changes in tumor burden over time, which can help to assess if the tumor is growing rapidly or slowly. In

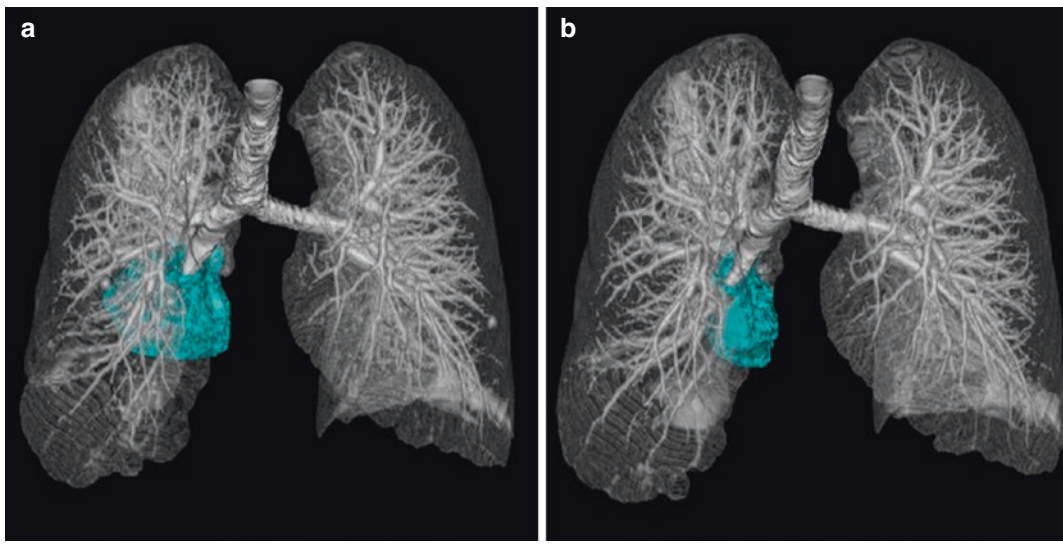

Fig. 7 A representative case of tumor volume decrease at 8-week scan with longer survival in a 66-year-old woman with stage IV NSCLC harboring EGFR L858R mutation treated with gefitinib. Baseline chest CT prior to therapy, (**a**) demonstrated a large dominant lung lesion in the right lower lobe, measuring 105,157 mm^3. The 8-week follow-up CT (**b**) showed a significant volume decrease of the lesion, measuring 42,914 mm^3, demonstrating 59.2% decrease in reference to the baseline scan. The patient had an overall survival of 45.4 months after the 8-week scan. *CT* computed tomography, *EGFR* epidermal growth factor receptor, *NSCLC* non-small cell lung cancer. (Reprinted with permission from Acad Radiol. 2016 Mar;23(3):329–36)

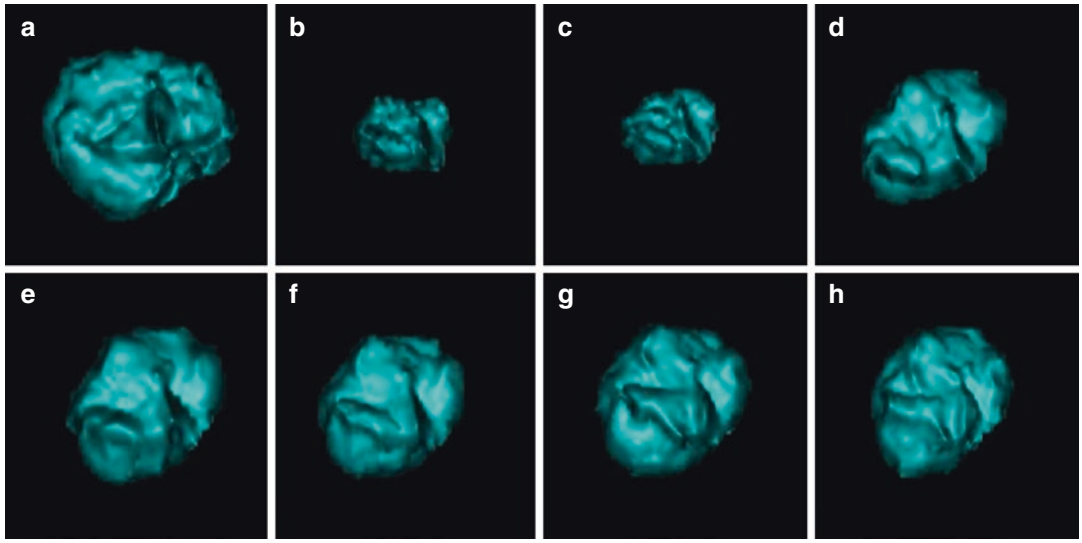

Fig. 8 Computed tomography (CT) images of a segmented lung tumor from a woman aged 52 years who had stage IV lung adenocarcinoma with slow tumor growth. (Reprinted with permission from Cancer. 2013 Nov 1;119(21):3761–8). (**a**) The baseline CT scan revealed a dominant right upper lobe lesion measuring 14,495 mm^3. (**b**) The patient received treatment with gefitinib, and her tumor volume significantly decreased, reaching the nadir, measuring 4121 mm^3, at 8 months. (**c**–**h**) The tumor started to grow back with a gradual increase in tumor volume over a course of 2 years observed after (**c**) 11 months, (**d**) 16 months, (**e**) 19 months, (**f**) 21 months, (**g**) 26 months, and (**h**) 28 months of therapy. The maximum tumor growth rate (measured using the logarithm of tumor volume [$\log_e V$]) between two consecutive scans since nadir was 0.09 mm^3 per month. Gefitinib was discontinued at 28 months, and the patient subsequently was treated on a trial with an irreversible EGFR inhibitor

EGFR-mutant advanced NSCLC patients treated with erlotinib or gefitinib, the growth rate of tumor volume after initial response was 0.12/month for the logarithm of the volume (which was originally measured in mm^3), proposing a reference value to define slow progression in this specific setting (Fig. 8) (Nishino et al. 2013b, 2016). Further investigations are ongoing to achieve clinical translation and technology transfer of the approach (Nishino et al. 2018).

2.2 Treatment Monitoring During Immune-Checkpoint Inhibitor Therapy for Lung Cancer

The unique mechanism of immune-checkpoint inhibitors that utilizes activation of T cell immunity against tumors may lead to unconventional tumor response patterns in some patients with lung cancer. Different sets of modified response criteria have been proposed to accurately characterize response and progression during immunotherapy, as discussed in detail in chapter "Response Evaluations for Precision Cancer Therapy and Immunotherapy". Among the several atypical response patterns noted during immune-checkpoint inhibitor therapy, pseudoprogression is well recognized among radiologists and treating providers. Pseudoprogression is noted as an immune-related response pattern on imaging when patients experience tumor burden reduction (1) after an initial increase of tumor burden, or (2) after or during the appearance of new lesions (Fig. 9) (Nishino et al. 2013d, 2017a, 2019; Wolchok et al. 2009). Though the concept is becoming better known, it is important to note that pseudoprogression is a relatively rare event, especially in NSCLC patients treated with immune-checkpoint inhibitor therapy (Nishino et al. 2017a, 2019). Pseudoprogression was noted in 5% (6/129) of the patients with advanced NSCLC patients treated with nivolumab in a phase 1 trial (Gettinger et al. 2015). In a study of advanced NSCLC patients treated with commercial PD-1 inhibitor monotherapy, only 1 out of

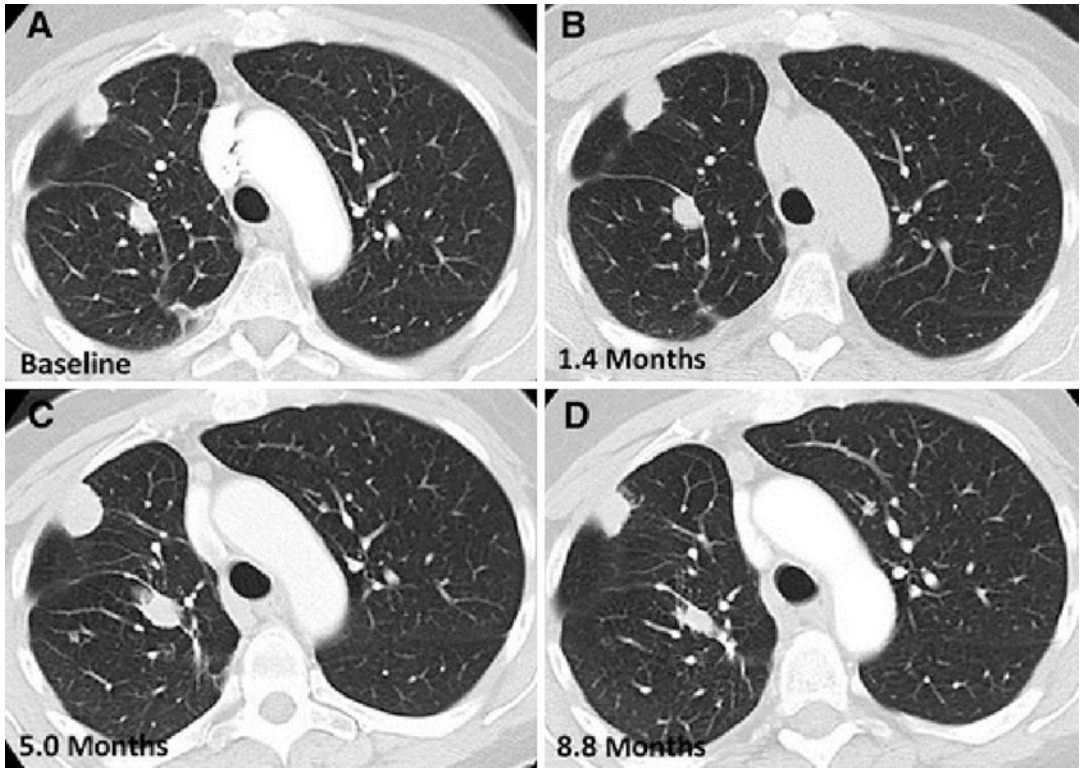

Fig. 9 Pseudoprogression followed by subsequent tumor reduction noted after confirmation of PD on a consecutive scan over the course of several months. (Reprinted with permission from Clin Cancer Res. 2017;23:5737–5744). A 63-year-old female with lung adenocarcinoma treated with nivolumab, who experienced pseudoprogression. Comparing to the baseline (**a**), the patient experienced tumor burden increase at 1.4 months of therapy (**b**), meeting the criteria for progressive disease, which was confirmed on the serial CT scans (**c**). Subsequently, tumor regression was noted at 8.8 months of therapy (**d**)

160 patients (0.6%) experienced pseudoprogression, emphasizing the rarity of the phenomenon in this setting (Nishino et al. 2017b). Though further data are accumulating, it should be noted that tumor burden increase in advanced NSCLC patients treated with immune-checkpoint inhibitor monotherapy much more likely indicates true progression than pseudoprogression.

Another important pattern noted during immunotherapy is hyperprogressive disease, which is an aggressive pattern of tumor growth after starting immunotherapy. It is originally defined as a RECIST progression at the first evaluation and a ≥2-fold increase of the tumor growth rate after starting PD-1/PD-L1 inhibitor therapy compared to the period before starting PD-1/PD-L1 inhibitor therapy (Champiat et al. 2017). In phase 1 clinical trials of PD-1/PD-L1 inhibitor monotherapy for various tumor types, 9% (12/131) of the patients experienced hyperprogressive disease (Champiat et al. 2017). A study focusing on advanced NSCLC patients used a slightly different definition of hyperprogressive disease, using >50% increase of tumor growth rate before and during PD-1/PD-L1 treatment. In this study, hyperprogressive disease was noted in 13.8% of NSCLC patients and was associated with shorter survival (Ferrara et al. 2018). Attention is needed to capture this aggressive pattern of tumor dynamics during immunotherapy. It is also necessary to identify biomarkers for this phenomenon for better patient selection (Nishino et al. 2019).

Emerging data also suggest the importance of evaluating overall tumor burden kinetics during immune-checkpoint inhibitor therapy (Nishino

et al. 2017b, c, 2019). In patients with advanced melanoma treated with pembrolizumab monotherapy, tumor burden increase <20% from baseline during therapy, noted in 55% of the cohort, was associated with longer overall survival (Nishino et al. 2017c). Similarly, in 160 patients with advanced NSCLC treated with nivolumab or pembrolizumab monotherapy, a significantly prolonged overall survival was noted in patients with <20% tumor burden increase throughout therapy compared to those who had tumor burden increase ≥20% (Nishino et al. 2017b). Though validation studies are required, the observations indicate imaging may provide a practical marker of treatment benefit of immune-checkpoint inhibitor therapy based on the serial CT scan evaluations (Nishino et al. 2019).

2.3 Treatment Monitoring During Antiangiogenic Therapy for Lung Cancer

Antiangiogenic therapy using vascular endothelial growth factor (VEGF) inhibitor is another approach that has been used to treat advanced NSCLC. VEGF inhibitor, bevacizumab, has been approved as the first-line treatment for advanced nonsquamous NSCLC in combination with carboplatin/paclitaxel chemotherapy since 2006 (Russo et al. 2017; Sandler et al. 2006). More recently, bevacizumab was also approved as a part of the combination regimen with PD-L1 inhibitor, atezolizumab, and chemotherapeutic agents, paclitaxel, and carboplatin (Socinski et al. 2018). Patients with lung cancer treated with antiangiogenic agents such as bevacizumab develop cavitation in their lung lesions during therapy, which occurs in 14–24% of the patients (Nishino et al. 2012a, b; Marom et al. 2008; Crabb et al. 2009). The phenomenon provides a challenge for accurate tumor response evaluations using RECIST that relies on the longest diameter of the lung lesions, because the tumor cavity is filled with air and does not contribute to the solid tumor burden. Alternative methods of response assessment for cavitary lung lesions were proposed, which subtract the central cavity diameter from the overall longest diameter of the lesion (Fig. 10) (Nishino et al.

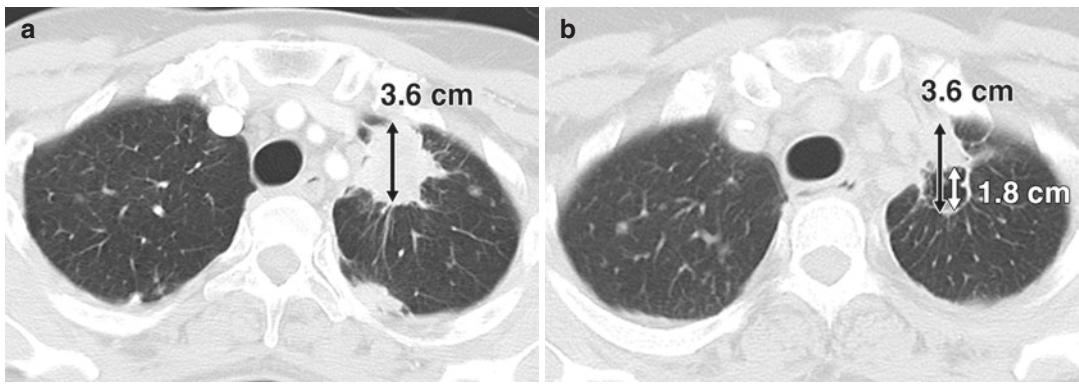

Fig. 10 A 53-year-old woman with stage IV adenocarcinoma of lung treated with paclitaxel, carboplatin, and concurrent vascular epidermal growth factor receptor inhibitor, bevacizumab. (Reprinted with permission from AJR Am J Roentgenol. 2012;198: 737–745). (**a**) Baseline CT scan of chest before bevacizumab therapy shows spiculated mass (double-ended arrow) in left upper lobe, which measured 3.6 cm in longest diameter. (**b**) Follow-up CT after 6 weeks of therapy reveals development of tumor cavitation. Measurement of lesion by Response Evaluation Criteria in Solid Tumors would be 3.6 cm (black double-ended arrow), which is not different compared with baseline, even though decrease of tumor volume is evident after bevacizumab therapy. Using alternate method incorporating cavitation, measurement of lesion would be 1.8 cm (white double-ended arrow) because diameter of cavity (1.8 cm) should be extracted from longest diameter of entire lesion (3.6 cm). Measurement by alternate method shows 50% decrease compared with baseline, meeting criteria for partial response

2012a). Though the approach intuitively makes sense, only a minority of patients experienced an alteration of the response assessment results using the alternate methods compared to those by RECIST (Crabb et al. 2009).

The concept was also applied to NSCLC patients treated with EGFR inhibitors, because these agents also have antiangiogenic activity. In a study by Lee et al., the modified method used the longest diameters of the solid component only, using the mediastinal window images, to exclude ground glass components, in addition to subtracting the diameter of the cavitary component. CT attenuation changes were also included in the response assessment, with the cut point of ≥15% decrease in tumor attenuation (HU). Responders by the modified methods had significantly longer OS, while RECIST response did not correlate with OS (Lee et al. 2011). Though both approaches need to be prospectively validated, it is important to note the tumor cavitation as a sign of response to antiangiogenic therapy, which is a pitfall of the conventional RECIST-based assessment.

3 Imaging and Treatment Monitoring of Thoracic Malignancies Other than Lung Cancer

3.1 Thymic Epithelial Tumors

Thymic epithelial tumors are rare malignant tumors accounting for 0.2–1.5% of all malignancies, and include thymoma, thymic carcinoma, and thymic neuroendocrine tumors (NET) (Carter et al. 2017; Nishino et al. 2006). These tumors have unique clinical characteristics, and are associated with clinical conditions and syndromes including myasthenia gravis, pure red cell aplasia in thymoma, and Cushing's syndrome, multiple endocrine neoplasia (MEN type 1) for thymic NET. Thymic epithelial tumors are also unique radiologically, given their propensity to spread along the pleura, and characteristically present with pleural seeding or "drop metastasis" (Fig. 11) (Carter et al. 2017; Nishino et al. 2006; Benveniste et al. 2011; Detterbeck et al. 2014). In a study of radiographic patterns of metastasis or recurrence of thymomas or thymic carcinomas

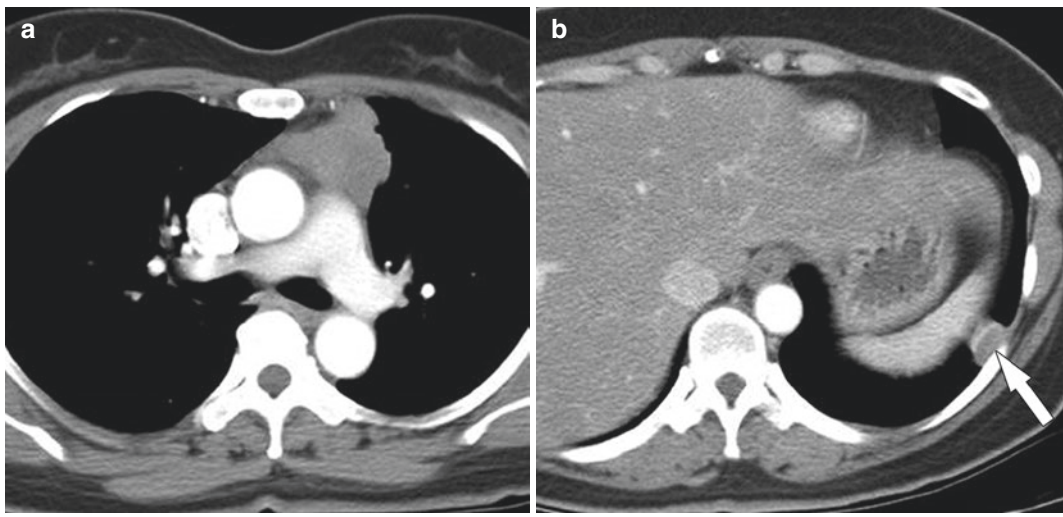

Fig. 11 Pleural seeding from a WHO type B2 (cortical) thymoma in a 40-year-old woman who presented with myasthenia gravis. (**a**) Contrast-enhanced CT scan shows a lobulated anterior mediastinal mass. (**b**) Contrast-enhanced CT scan obtained at the level of the upper abdomen shows an enhancing pleura-based nodule (arrow), a finding that represents pleural seeding. Pathologic analysis showed a predominance of lymphoid cells (type B2 tumor). (Reprinted with permission from Radiographics. 2006 Mar–Apr;26(2):335–48)

after surgery, metastasis or recurrence was most common in pleura, followed by lung and thoracic nodes particularly in supraclavicular or paraesophageal nodes (Khandelwal et al. 2016).

Given the unique pattern of tumor spread and metastasis with a propensity to involve pleura, the conventional tumor response evaluation approach using RECIST has a limitation in thymic epithelial tumors, because RECIST is based on unidimensional measurements which may not be suitable to accurately characterize pleural tumor burden. International Thymic Malignancy Interest Group (ITMG) has published recommendations for the modifications of tumor measurements and response assessments in thymic epithelial tumors (Table 2) (Benveniste et al. 2011). The ITMIG recommendations mostly follow RECIST1.1, except for pleural disease which should be measured using the short axis (thickness perpendicular to the chest wall or mediastinum). The pleural disease should be ≥15 mm in short axis to be considered as measurable (Fig. 12). In terms of the number of pleural target lesions, up to two sites at three separate axial levels can be measured for pleural disease, and the sum of the maximum six measurements included as one organ. The response categories are defined using the percent change of the sum of the measurable tumor burden including pleural disease, using the cutoff values according to RECIST1.1 (Table 2). While the value and utility of the recommendations need to be validated, this is an important first step for the response assessment of thymic epithelial tumors, as more effective treatments using precision medicine approaches are under active investigation for these tumors as well (Radovich et al. 2018).

Table 2 International Thymic Malignancy Interest Group (ITMIG) recommendations for response assessment in thymic epithelial tumors (Benveniste et al. 2014)

	RECIST version 1.1 (2009)	ITMIG recommendations for thymic tumors (2014)
Measurement	• Longest diameter (LD) for lesions other than lymph nodes • Short axis (SA) for lymph nodes	*Follows RECIST1.1 except:* • Short axis (thickness perpendicular to chest wall or mediastinum) for pleural disease
Minimum size for target lesions	• ≥10 mm in LD for non-nodal lesions • ≥15 mm in SA for lymph nodes	*Follows RECIST1.1 except:* • ≥15 mm in SA for pleural tumor burden
Number of target lesions	• Up to 2 per organ • Up to 5 in total	*Follows RECIST1.1 except:* • Up to two sites at three separate levels for pleural tumor burden • The sum of thickness of up to six pleural sites are included as one organ

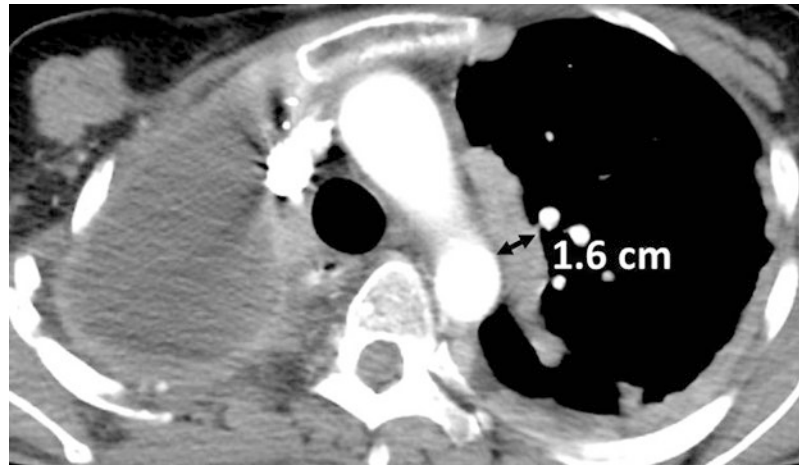

Fig. 12 Chest CT scan of a patient with metastatic thymic epithelial tumor demonstrates a pleural-based tumor burden on the left. According to the ITMG recommendation, the pleural tumor burden should be measured using the short axis, which is perpendicular to the chest wall or mediastinum (double-headed arrow)

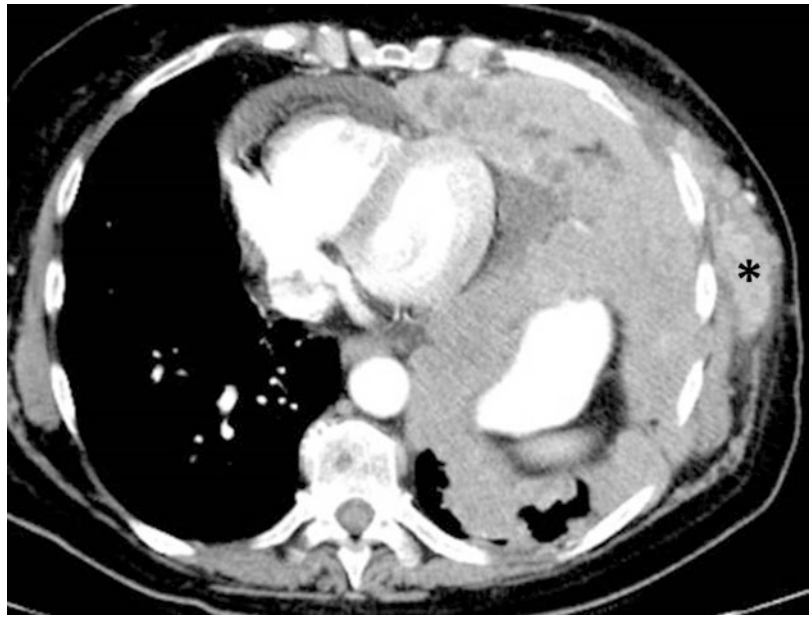

Fig. 13 Extensive pleural tumor involvement in a patient with malignant pleural mesothelioma. Chest CT demonstrates enhancing irregular pleural thickening that encases the pleura, with soft tissue extension to the chest wall on the left (asterisk). The pattern of pleural-based tumor involvement causes a difficulty in quantitative assessment of the tumor burden by RECIST guidelines

Fig. 14 Modified RECIST measurements in malignant pleural mesothelioma use short axis measurements for the pleural tumor burden, with measurements that are perpendicular to the chest wall or mediastinum (double-headed arrow)

3.2 Malignant Pleural Mesothelioma

Malignant pleural mesothelioma (MPM) is the most common primary malignancy of pleura with 3000 cases per year in the United States, and arises from mesothelial cells covering lung and chest wall. It is associated with asbestos exposure with latency periods of 20–50 years. Histologically, it is classified as epithelial, sarcomatoid, and biphasic subtypes (Nickell et al. 2014). MPM often presents with unilateral pleural effusion and circumferential and nodular pleural thickening. It may involve the entire pleura and interlobar space, with tumoral encasement of the lung. Tumor spread is primarily by local extension throughout the pleural cavity, invasion of the chest wall, mediastinum, and diaphragm, and into the abdomen (Fig. 13). Modified RECIST for MPM has also been proposed, using short axis (thickness) for the pleural tumor burden and including up to two sites at three separate levels as one organ for pleural disease (Fig. 14) (Armato and Nowak 2018). Volumetric and

functional approaches are also under investigation for this relatively rare thoracic malignancy with unique pattern of spread (Armato and Nowak 2018; Kindler et al. 2018).

4 Conclusions

Remarkable advances are made in the treatment approaches for thoracic malignancies, especially in the area of precision therapy and immunotherapy for lung cancer. Treatment monitoring strategies of thoracic tumors heavily relay on imaging, and radiographic response assessment methods should evolve in parallel with the advances of therapy. Attention to the mechanism of action of anticancer agents and the specific types and subtypes of the tumors are important for accurate interpretation of the imaging studies for treatment monitoring.

References

Antonia SJ, Villegas A, Daniel D et al (2017) Durvalumab after chemoradiotherapy in stage III non-small-cell lung cancer. N Engl J Med 377:1919–1929

Antonia SJ, Villegas A, Daniel D et al (2018) Overall survival with durvalumab after chemoradiotherapy in stage III NSCLC. N Engl J Med 379:2342–2350

Armato SG 3rd, Nowak AK (2018) Revised modified response evaluation criteria in solid tumors for assessment of response in malignant pleural mesothelioma (version 1.1). J Thorac Oncol 13:1012–1021

Benveniste MF, Korst RJ, Rajan A, Detterbeck FC, Marom EM (2014) A practical guide from the International Thymic Malignancy Interest Group (ITMIG) regarding the radiographic assessment of treatment response of thymic epithelial tumors using modified RECIST criteria. J Thorac Oncol 9:S119–S124

Benveniste MF, Rosado-de-Christenson ML, Sabloff BS, Moran CA, Swisher SG, Marom EM (2011) Role of imaging in the diagnosis, staging, and treatment of thymoma. Radiographics 31:1847–1861; discussion 1861–1843

Borghaei H, Paz-Ares L, Horn L et al (2015) Nivolumab versus docetaxel in advanced nonsquamous non-small-cell lung cancer. N Engl J Med 373:1627–1639

Brahmer J, Reckamp KL, Baas P et al (2015) Nivolumab versus docetaxel in advanced squamous-cell non-small-cell lung cancer. N Engl J Med 373:123–135

Breathnach OS, Freidlin B, Conley B et al (2001) Twenty-two years of phase III trials for patients with advanced non-small-cell lung cancer: sobering results. J Clin Oncol 19:1734–1742

Camidge DR, Bang YJ, Kwak EL et al (2012) Activity and safety of crizotinib in patients with ALK-positive non-small-cell lung cancer: updated results from a phase 1 study. Lancet Oncol 13:1011–1019

Carter BW, Benveniste MF, Madan R et al (2017) IASLC/ITMIG staging system and lymph node map for thymic epithelial neoplasms. Radiographics 37:758–776

Champiat S, Dercle L, Ammari S et al (2017) Hyperprogressive disease is a new pattern of progression in cancer patients treated by anti-PD-1/PD-L1. Clin Cancer Res 23:1920–1928

Costa DB, Shaw AT, Ou SH et al (2015) Clinical experience with crizotinib in patients with advanced ALK-rearranged non-small-cell lung cancer and brain metastases. J Clin Oncol 33:1881–1888

Crabb SJ, Patsios D, Sauerbrei E et al (2009) Tumor cavitation: impact on objective response evaluation in trials of angiogenesis inhibitors in non-small-cell lung cancer. J Clin Oncol 27:404–410

Detterbeck FC, Stratton K, Giroux D et al (2014) The IASLC/ITMIG thymic epithelial tumors staging project: proposal for an evidence-based stage classification system for the forthcoming (8th) edition of the TNM classification of malignant tumors. J Thorac Oncol 9:S65–S72

Eberlein CA, Stetson D, Markovets AA et al (2015) Acquired resistance to the mutant-selective EGFR inhibitor AZD9291 is associated with increased dependence on RAS signaling in preclinical models. Cancer Res 75:2489–2500

Ferrara R, Mezquita L, Texier M et al (2018) Hyperprogressive disease in patients with advanced non-small cell lung cancer treated with PD-1/PD-L1 inhibitors or with single-agent chemotherapy. JAMA Oncol 4:1543–1552

Gandhi L, Rodriguez-Abreu D, Gadgeel S et al (2018) Pembrolizumab plus chemotherapy in metastatic non-small-cell lung cancer. N Engl J Med 378:2078–2092

Garon EB, Rizvi NA, Hui R et al (2015) Pembrolizumab for the treatment of non-small-cell lung cancer. N Engl J Med 372:2018–2028

Gazdar AF (2009) Personalized medicine and inhibition of EGFR signaling in lung cancer. N Engl J Med 361:1018–1020

Gettinger SN, Horn L, Gandhi L et al (2015) Overall survival and long-term safety of nivolumab (anti-programmed death 1 antibody, BMS-936558, ONO-4538) in patients with previously treated advanced non-small-cell lung cancer. J Clin Oncol 33:2004–2012

Goss G, Tsai CM, Shepherd FA et al (2016) Osimertinib for pretreated EGFR Thr790Met-positive advanced non-small-cell lung cancer (AURA2): a multicentre, open-label, single-arm, phase 2 study. Lancet Oncol 17:1643–1652

Herbst RS, Heymach JV, Lippman SM (2008) Lung cancer. N Engl J Med 359:1367–1380

Isozaki H, Ichihara E, Takigawa N et al (2016) Non-small cell lung cancer cells acquire resistance to the ALK inhibitor alectinib by activating alternative receptor tyrosine kinases. Cancer Res 76(6):1506–1516

Janne PA, Gurubhagavatula S, Yeap BY et al (2004) Outcomes of patients with advanced non-small cell

lung cancer treated with gefitinib (ZD1839, "Iressa") on an expanded access study. Lung Cancer 44:221–230
Janne PA, Yang JC, Kim DW et al (2015) AZD9291 in EGFR inhibitor-resistant non-small-cell lung cancer. N Engl J Med 372:1689–1699
Johnson BE (2016) Divide and conquer to treat lung cancer. N Engl J Med 375:1892–1893
Khandelwal A, Sholl LM, Araki T, Ramaiya NH, Hatabu H, Nishino M (2016) Patterns of metastasis and recurrence in thymic epithelial tumours: longitudinal imaging review in correlation with histological subtypes. Clin Radiol 71:1010–1017
Kim TM, Song A, Kim DW et al (2015) Mechanisms of acquired resistance to AZD9291: a mutation-selective, irreversible EGFR inhibitor. J Thorac Oncol 10:1736–1744
Kindler HL, Ismaila N, Armato SG 3rd et al (2018) Treatment of malignant pleural mesothelioma: American Society of Clinical Oncology Clinical Practice Guideline. J Clin Oncol 36:1343–1373
Kwak EL, Bang YJ, Camidge DR et al (2010) Anaplastic lymphoma kinase inhibition in non-small-cell lung cancer. N Engl J Med 363:1693–1703
Lee HY, Lee KS, Ahn MJ et al (2011) New CT response criteria in non-small cell lung cancer: proposal and application in EGFR tyrosine kinase inhibitor therapy. Lung Cancer 73:63–69
Lee JH, Lee HY, Ahn MJ et al (2016) Volume-based growth tumor kinetics as a prognostic biomarker for patients with EGFR mutant lung adenocarcinoma undergoing EGFR tyrosine kinase inhibitor therapy: a case control study. Cancer Imaging 16:5
Lynch TJ, Bell DW, Sordella R et al (2004) Activating mutations in the epidermal growth factor receptor underlying responsiveness of non-small-cell lung cancer to gefitinib. N Engl J Med 350:2129–2139
Marom EM, Martinez CH, Truong MT et al (2008) Tumor cavitation during therapy with antiangiogenesis agents in patients with lung cancer. J Thorac Oncol 3:351–357
Mok TS (2010) Living with imperfection. J Clin Oncol 28:191–192
Mok TS, Wu YL, Thongprasert S et al (2009) Gefitinib or carboplatin-paclitaxel in pulmonary adenocarcinoma. N Engl J Med 361:947–957
Mozley PD, Bendtsen C, Zhao B et al (2012) Measurement of tumor volumes improves RECIST-based response assessments in advanced lung cancer. Transl Oncol 5:19–25
Nickell LT Jr, Lichtenberger JP 3rd, Khorashadi L, Abbott GF, Carter BW (2014) Multimodality imaging for characterization, classification, and staging of malignant pleural mesothelioma. Radiographics 34:1692–1706
Nishino M (2018) Tumor response assessment for precision cancer therapy: response evaluation criteria in solid tumors and beyond. Am Soc Clin Oncol Educ Book 38:1019–1029
Nishino M, Ashiku SK, Kocher ON, Thurer RL, Boiselle PM, Hatabu H (2006) The thymus: a comprehensive review. Radiographics 26:335–348
Nishino M, Cardarella S, Dahlberg SE et al (2013c) Radiographic assessment and therapeutic decisions at RECIST progression in EGFR-mutant NSCLC treated with EGFR tyrosine kinase inhibitors. Lung Cancer 79:283–288
Nishino M, Cryer SK, Okajima Y et al (2012b) Tumoral cavitation in patients with non-small-cell lung cancer treated with antiangiogenic therapy using bevacizumab. Cancer Imaging 12:225–235
Nishino M, Dahlberg SE, Adeni AE et al (2017b) Tumor response dynamics of advanced non-small cell lung cancer patients treated with PD-1 inhibitors: imaging markers for treatment outcome. Clin Cancer Res 23:5737–5744
Nishino M, Dahlberg SE, Cardarella S et al (2013a) Tumor volume decrease at 8 weeks is associated with longer survival in EGFR-mutant advanced non-small-cell lung cancer patients treated with EGFR TKI. J Thorac Oncol 8:1059–1068
Nishino M, Dahlberg SE, Cardarella S et al (2013b) Volumetric tumor growth in advanced non-small cell lung cancer patients with EGFR mutations during EGFR-tyrosine kinase inhibitor therapy: developing criteria to continue therapy beyond RECIST progression. Cancer 119:3761–3768
Nishino M, Dahlberg SE, Fulton LE et al (2016) Volumetric tumor response and progression in EGFR-mutant NSCLC patients treated with erlotinib or gefitinib. Acad Radiol 23:329–336
Nishino M, Giobbie-Hurder A, Gargano M, Suda M, Ramaiya NH, Hodi FS (2013d) Developing a common language for tumor response to immunotherapy: immune-related response criteria using unidimensional measurements. Clin Cancer Res 19:3936–3943
Nishino M, Giobbie-Hurder A, Manos MP et al (2017c) Immune-related tumor response dynamics in melanoma patients treated with pembrolizumab: identifying markers for clinical outcome and treatment decisions. Clin Cancer Res 23:4671–4679
Nishino M, Guo M, Jackman DM et al (2011b) CT tumor volume measurement in advanced non-small-cell lung cancer: performance characteristics of an emerging clinical tool. Acad Radiol 18:54–62
Nishino M, Hatabu H, Hodi FS (2019) Imaging of cancer immunotherapy: current approaches and future directions. Radiology 290:9–22
Nishino M, Hatabu H, Johnson BE, McLoud TC (2014) State of the art: response assessment in lung cancer in the era of genomic medicine. Radiology 271:6–27
Nishino M, Jackman DM, Hatabu H, Janne PA, Johnson BE, Van den Abbeele AD (2011a) Imaging of lung cancer in the era of molecular medicine. Acad Radiol 18:424–436
Nishino M, Jagannathan JP, Krajewski KM et al (2012a) Personalized tumor response assessment in the era of molecular medicine: cancer-specific and therapy-specific response criteria to complement pitfalls of RECIST. AJR Am J Roentgenol 198:737–745
Nishino M, Ramaiya NH, Hatabu H, Hodi FS (2017a) Monitoring immune-checkpoint blockade: response

evaluation and biomarker development. Nat Rev Clin Oncol 14:655–668

Nishino M, Wakai S, Hida T et al (2018) Automated image analysis tool for tumor volume growth rate to guide precision cancer therapy: EGFR-mutant non-small-cell lung cancer as a paradigm. Eur J Radiol 109:68–76

Ortiz-Cuaran S, Scheffler M, Plenker D et al (2016) Heterogeneous mechanisms of primary and acquired resistance to third-generation EGFR inhibitors. Clin Cancer Res 22:4837–4847

Ou SH, Ahn JS, De Petris L et al (2016) Alectinib in crizotinib-refractory ALK-rearranged non-small-cell lung cancer: a phase II global study. J Clin Oncol 34:661–668

Paez JG, Janne PA, Lee JC et al (2004) EGFR mutations in lung cancer: correlation with clinical response to gefitinib therapy. Science 304:1497–1500

Pao W, Miller V, Zakowski M et al (2004) EGF receptor gene mutations are common in lung cancers from "never smokers" and are associated with sensitivity of tumors to gefitinib and erlotinib. Proc Natl Acad Sci U S A 101:13306–13311

Park H, Sholl LM, Hatabu H, Awad MM, Nishino M (2019) Imaging of precision therapy for lung cancer: current state of the art. Radiology 293(1):15–29

Park K, Yu CJ et al (2016) First-line erlotinib therapy until and beyond response evaluation criteria in solid tumors progression in Asian patients with epidermal growth factor receptor mutation-positive non-small-cell lung cancer: the ASPIRATION study. JAMA Oncol 2(3):305–312

Paz-Ares L, Luft A, Vicente D et al (2018) Pembrolizumab plus chemotherapy for squamous non-small-cell lung cancer. N Engl J Med 379:2040–2051

Peters S, Camidge DR, Shaw AT et al (2017) Alectinib versus crizotinib in untreated ALK-positive non-small-cell lung cancer. N Engl J Med 377:829–838

Radovich M, Pickering CR, Felau I et al (2018) The integrated genomic landscape of thymic epithelial tumors. Cancer Cell 33:244–258. e210

Ready N, Farago AF, de Braud F et al (2019) Third-line nivolumab monotherapy in recurrent SCLC: CheckMate 032. J Thorac Oncol 14(2):237–244

Reck M, Rodriguez-Abreu D, Robinson AG et al (2016) Pembrolizumab versus chemotherapy for PD-L1-positive non-small-cell lung cancer. N Engl J Med 375(19):1823–1833

Riely GJ, Kris MG, Zhao B et al (2007) Prospective assessment of discontinuation and reinitiation of erlotinib or gefitinib in patients with acquired resistance to erlotinib or gefitinib followed by the addition of everolimus. Clin Cancer Res 13:5150–5155

Rizvi NA, Mazieres J, Planchard D et al (2015) Activity and safety of nivolumab, an anti-PD-1 immune checkpoint inhibitor, for patients with advanced, refractory squamous non-small-cell lung cancer (CheckMate 063): a phase 2, single-arm trial. Lancet Oncol 16:257–265

Russo AE, Priolo D, Antonelli G, Libra M, McCubrey JA, Ferrau F (2017) Bevacizumab in the treatment of NSCLC: patient selection and perspectives. Lung Cancer (Auckl) 8:259–269

Salvador-Coloma C, Lorente D, Palanca S et al (2018) Early radiological response as predictor of overall survival in non-small cell lung cancer (NSCLC) patients with epidermal growth factor receptor mutations. J Thorac Dis 10:1386–1393

Sandler A, Gray R, Perry MC et al (2006) Paclitaxel-carboplatin alone or with bevacizumab for non-small-cell lung cancer. N Engl J Med 355:2542–2550

Shaw AT, Gandhi L, Gadgeel S et al (2016) Alectinib in ALK-positive, crizotinib-resistant, non-small-cell lung cancer: a single-group, multicentre, phase 2 trial. Lancet Oncol 17:234–242

Shaw AT, Kim DW, Nakagawa K et al (2013) Crizotinib versus chemotherapy in advanced ALK-positive lung cancer. N Engl J Med 368:2385–2394

Siegel RL, Miller KD, Jemal A (2019) Cancer statistics, 2019. CA Cancer J Clin 69:7–34

Socinski MA, Jotte RM, Cappuzzo F et al (2018) Atezolizumab for first-line treatment of metastatic nonsquamous NSCLC. N Engl J Med 378: 2288–2301

Solomon BJ, Mok T, Kim DW et al (2014) First-line crizotinib versus chemotherapy in ALK-positive lung cancer. N Engl J Med 371:2167–2177

Soria JC, Ohe Y, Vansteenkiste J et al (2018) Osimertinib in untreated EGFR-mutated advanced non-small-cell lung cancer. N Engl J Med 378:113–125

Takeda M, Okamoto I, Nakagawa K (2014) Survival outcome assessed according to tumor response and shrinkage pattern in patients with EGFR mutation-positive non-small-cell lung cancer treated with gefitinib or erlotinib. J Thorac Oncol 9:200–204

Tani T, Yasuda H, Hamamoto J et al (2016) Activation of EGFR bypass signaling by TGFalpha overexpression induces acquired resistance to alectinib in ALK-translocated lung cancer cells. Mol Cancer Ther 15:162–171

Wolchok JD, Hoos A, O'Day S et al (2009) Guidelines for the evaluation of immune therapy activity in solid tumors: immune-related response criteria. Clin Cancer Res 15:7412–7420

Zhao B, James LP, Moskowitz CS et al (2009) Evaluating variability in tumor measurements from same-day repeat CT scans of patients with non-small cell lung cancer. Radiology 252:263–272

Zhou C, Wu YL, Chen G et al (2011) Erlotinib versus chemotherapy as first-line treatment for patients with advanced EGFR mutation-positive non-small-cell lung cancer (OPTIMAL, CTONG-0802): a multicentre, open-label, randomised, phase 3 study. Lancet Oncol 12:735–742

Therapy Response Imaging in Gastrointestinal Malignancy

Satomi Kawamoto

Contents

Abstract

Gastric and colorectal adenocarcinomas are common malignancies, and have been one of the major causes of cancer related death. Although gastrointestinal stromal tumor (GIST) is much less common compared to gastric or colorectal adenocarcinomas accounting for 0.2% of all gastrointestinal tumors, GIST is now considered a highly treatable tumor with the tyrosine kinase inhibitors (TKIs) imatinib mesylate, and became an important paradigm of molecular targeted therapy in solid tumors. Neoadjuvant and adjuvant chemotherapy is standard of care for operable gastric and colorectal adenocarcinomas, and has shown to improve survival. Target therapy and immunotherapy agents have shown survival benefit in subset of metastatic gastric and colorectal adenocarcinomas, for example, anti-HER2 trastuzumab for Her2-positive gastric cancers, and immune checkpoint inhibitors. Accurate assessment of treatment response is critical for planning of the optimal management. RECIST has been used for assessment of treatment response, but it can be insufficiently sensitive for evaluating response in targeted therapies. MDCT is the primary modality to assess treatment response of gastric cancer and GIST, and MRI is the primary modality to assess treatment response of rectal cancer. ^{18}F-FDG PET/CT has gained widespread acceptance as a modality for

S. Kawamoto (✉)
The Russell H. Morgan Department of Radiology and Radiological Science, Johns Hopkins School of Medicine, Baltimore, MD, USA
e-mail: skawamo1@jhmi.edu

M. Nishino (ed.), *Therapy Response Imaging in Oncology*, Medical Radiology, Diagnostic Imaging,
https://doi.org/10.1007/978-3-030-31171-1_7

therapy monitoring. Newer techniques including diffusion-weighted MRI, dynamic contrast-enhanced CT or MRI, and monochromatic CT using dual-energy CT potentially improve assessment of treatment response. Radiomics features extracted from CT, MRI, and PET may potentially provide information regarding treatment response and improve risk stratification.

1 Advances in Therapeutic Approaches

1.1 Gastric Cancer

Gastric cancer remains an important cancer worldwide and is the fifth most frequently diagnosed cancer and the third leading cause of cancer death worldwide (Bray et al. 2018). Although gastric cancers arising from non-cardia region have been steadily declining over the last one-half century in most populations, incidence of cancers arising from gastric cardia has been increasing particularly in high-income countries (Bray et al. 2018).

Most gastric cancers are adenocarcinoma. Histologically, gastric adenocarcinoma is classified by Lauren classification (Lauren 1965) and WHO classification (2017). By Lauren classification, gastric adenocarcinomas are classified into two major types, intestinal type (54%) and diffuse type (32%), with indeterminate type as uncommon variant (15%) (Hu et al. 2012). The intestinal type is often associated with intestinal metaplasia and Helicobacter pylori infection (Hu et al. 2012), and they are usually nodular, polypoid, or fungating (Hallinan and Venkatesh 2013). The diffuse type is more often seen in females and young individuals (Hu et al. 2012), and is grossly ill-defined and may have the appearance of linitis plastica (Hallinan and Venkatesh 2013).

Surgery is the standard treatment for gastric cancer (Lee et al. 2014). Complete resection of the primary tumor with safe margin and radical lymphadenectomy is considered curative treatment (Lee et al. 2014; Lim et al. 2006), although treatments tailored to individual cases has become increasingly utilized, such as endoscopic mucosal resection for selected mucosal cancers without evidence of lymph node involvement (Lee et al. 2014; Lim et al. 2006).

Preoperative or postoperative chemotherapy is the standard of care for operable gastric cancer (Ilson 2018). A meta-analysis of clinical trials showed that adjuvant chemotherapy increased the survival duration and that fluoropyrimidine-containing therapy lowered the risk of death (Lee et al. 2014; Coccolini et al. 2018). Morbidity and perioperative mortality rate are not influenced by neoadjuvant chemotherapy (Coccolini et al. 2018). In patients with advanced stage gastric cancer, chemotherapy alone or in combination with radiotherapy have been shown to improve survival (Hallinan and Venkatesh 2013).

For the first line of therapy of advanced gastric cancer, Fluoropyrimidine (5-fluorouracil [5-FU], S-1 [compounds of tegafur, gimeracil, and oteracil potassium], or capecitabine), platinum (cisplatin or oxaliplatin), taxane (docetaxel or paclitaxel), epirubicin, and irinotecan may be employed alone or in combination (Park and Chun 2013).

Human epithelial growth factor receptor 2 (HER2), a member of the human epidermal growth factor receptor (EGFR) family, is overexpressed in 15–25% of gastric adenocarcinoma (Hu et al. 2012; Bang et al. 2010), and more often noted in intestinal type carcinoma (Hu et al. 2012) and in the carcinomas located at proximal stomach or cardia and gastroesophageal junction (24–35%) (Hu et al. 2012). In ToGA trial, a phase 3 randomised clinical trial for HER2-positive advanced gastric or gastroesphageal (GE) junction cancer, the addition of trastuzumab (Herceptin) to first-line chemotherapy (capecitabine or 5-fluorouracil and cisplatin) significantly improved response and the median overall survival (13.5 versus 11.1 months) (Bang et al. 2010). In 2010, the US Food and Drug Administration (FDA) approved trastuzumab (Herceptin), a humanized monoclonal antibody against HER2 receptor, for the treatment of patients with HER2-positive metastatic

adenocarcinoma of the stomach and GE junction, and trastuzumab in combination with capecitabine or 5-FU and cisplatin is now the standard of care for HER2-positive gastric cancers (Bang et al. 2010).

Other target agents against the epidermal growth factor receptor (EGFR), vascular endothelial growth factor (VEGF), and the mammalian target of rapamycin (mTOR) have been evaluated for the antitumor efficacy for gastric cancer by many clinical trials (Park and Chun 2013). The VEGF recepter-2 (VEGFR-2) inhibitor ramucirumab was shown to confer a survival benefit in the second-line setting of advanced gastric and GE junction adenocarcinomas (Fuchs et al. 2014; Wilke et al. 2014).

HER2 protein expression or gene amplification tests are useful in the management of gastric cancer patients for selecting proper patients for targeted therapy (Lee et al. 2014).

In 2017, the US FDA approved pembrolizumab as the first immunotherapy agent for the third-line (or higher) treatment of advanced gastric and/or GE junction adenocarcinoma whose tumors express programmed cell death ligand 1 (PD-L1) (Joshi et al. 2018). Pembrolizumab has modest benefit in treating refractory metastatic esophagogastric adenocarcinoma when used either as monotherapy or in combination with other agents (Ilson 2018; Joshi et al. 2018). There are a number of other monoclonal antibody checkpoint inhibitors that are being investigated in gastroesophageal adenocarcinoma including nivolumab (anti-PD-1), avelumab (anti-PD-L1), durvalumab (anti-PD-L1), atezolizumab (anti-PD-L1), ipilimumab (anti-CTLA-4), and tremelimumab (anti-CTLA4) (Joshi et al. 2018).

1.2 Colorectal Cancer

Colorectal cancer is the third most common cancer worldwide (Bray et al. 2018), affecting 5% of the population in the United States and Western countries (Ben-Haim and Ell 2009). Of the colorectal cancers, 30% will arise in the rectum. Colorectal cancer is the second most common cause of cancer death worldswide (Bray et al. 2018). Although the overall incidence and survival rate of colorectal cancer is improving, the incidence of colorectal cancer in young adults is increasing in the United States (Bailey et al. 2015; Weinberg and Marshall 2019).

The treatments for colorectal cancer include surgery in the early stages, followed by chemo- and/or radiotherapy for patients in advanced stages (Yaghoubi et al. 2019). For stage T3 or T4 rectal cancer or disease involving the potential circumferential resection margin on preoperative MRI, chemoradiation therapy results in a decreased rate of postoperative local recurrence (Sauer et al. 2004; Arnoletti and Bland 2006; Patel et al. 2012; Kim et al. 2010) and improved overall survival (Roh et al. 2009; Jhaveri and Hosseini-Nik 2015). Also, preoperative chemoradiation therapy may downstage locally advanced disease and enable sphincter preserving resection for rectal cancer (Kim et al. 2010; Park et al. 2004).

Commonly used chemotherapeutic options for colorectal cancer include 5-FU, irinotecan, and oxaliplatin. Capecitabine is also commonly used oral chemotherapy drug which is metabolized to 5-FU. Development of molecular target agents contributes to prolonging survival of patients with metastatic colorectal cancer (Ohhara et al. 2016). Bevacizumab, targeting VEGF, and cetuximab and panitumumab, targeting EGFR, have demonstrated significant survival benefits in combination with cytotoxic chemotherapy in the first-line, second-line, or salvage setting (Ohhara et al. 2016).

Recently, immune checkpoint molecules such as PD-1 and PD-L1 have been identified as a possible target for immunotherapy in colorectal cancer (Xiao and Freeman 2015). Checkpoint inhibitors, nivolumab and pembrolizumab are now approved by US FDA for metastatic colorectal cancer after disease progression on oxaliplatin- and irinotecan-based regimens (Das et al. 2018). Microsatellite instability (MSI) is characterized by mutations in repetitive DNA sequence tracts caused by deficiency of mismatch repair enzymes, and seen in approximately 15% of sporadic colorectal cancer and most familial colorectal cancer (Xiao and Freeman 2015). Microsatellite instable colorectal cancer is a good

candidate for checkpoint immunotherapy (Xiao and Freeman 2015). For optimal selection of treatment approach for patients with metastatic colorectal cancer, assessment of genomic variables such as HER2, high microsatellite instability (MSI-H), and RSA mutation by next-generation sequencing from tumor tissue is beneficial to individualize treatment based on the findings (Das et al. 2018).

1.3 Gastrointestinal Stromal Tumor (GIST)

While GIST account for only 0.2% of all gastrointestinal tumors, 80% of all gastrointestinal sarcomas are GISTs (Choi 2008). The most common primary site is in the stomach (50–60%), followed by the small intestine (20%), colon/rectum (5%), and esophagus (5%) (Zhou et al. 2016). Gastric GIST consists of 2–3% of gastric tumors (Richman et al. 2017). GISTs have a complex biologic behavior and their malignant potential is difficult to predict, and different risk stratification methods have been proposed. National Institutes of Health (NIH) modified criteria published in 2008 (Joensuu 2008) have been commonly accepted as a risk stratification scheme for GIST. It uses four categories from very low to high risk to predict patient prognosis according to four risk stratification factors (tumor size, mitotic count, primary tumor site, and tumor rupture) (Joensuu 2008).

The vast majority of GISTs harbor unique activating mutations in *KIT* gene or *PDGFRA* gene (Liegl et al. 2009). Imatinib, a low-molecular-weight tyrosine kinase inhibitor that blocks the kinase activity of both KIT and PDGFRA, was first approved for treatment of advanced or metastatic GIST by the US FDA in 2002. Imatinib have substantially improved survival in patients with unresectable or metastatic GISTs (Joensuu 2008). Sunitinib is the second-line treatment for patients demonstrating primary or secondary resistance to imatinib (Demetri et al. 2006). Regorafenib can be used to treat GIST after failure of imatinib and resistant to sunitinib (Demetri et al. 2013).

2 Therapy Response Imaging Strategies and Pitfalls

2.1 Therapy Response Imaging Strategies

Although responses to treatment can be measured by multiple parameters, including the clinical and laboratory responses, imaging-based response assessment on cross-sectional imaging is essential. For locally advanced gastrointestinal tumors, assessment of local staging (T-staging) as well as N and M staging before and after chemoradiation therapy is critical for planning of the optimal management.

Traditional objective response evaluation criteria for solid tumors using quantitative CT data analysis is Response Evaluation Criteria in Solid Tumors (RECIST) criteria (Eisenhauer et al. 2009), which is widely considered the method of choice for the assessment of tumor response to treatment (Hallinan and Venkatesh 2013).

2.1.1 Gastric Cancer

For staging of gastric adenocarcinoma, endoscopic ultrasonography (EUS) can be used to evaluate the depth of invasion with a relatively good sensitivity and specificity for differentiating between T1 to 2 and T3 to 4 lesions (86% and 91%, respectively), although the sensitivity and specificity for detecting lymph node metastases were lower (69% and 84%, respectively) (Lee et al. 2014; Mocellin et al. 2011).

Multidetector CT (MDCT) is a widely accepted imaging modality for staging gastric adenocarcinoma that can assess tumor depth, local extension or tumor, regional lymph nodes, and metastases (Hallinan and Venkatesh 2013; Choi et al. 2014). Arterial-phase imaging allows easy detection of enhanced mucosal lesions, and portal venous-phase imaging provides more accurate information including the depth of invasion and the involvement of adjacent organs and lymph node metastases (Lee et al. 2014). Ingestion of 800–1000 mL of water or administration of aerogenic power before the scan is helpful to adequately distend the gastric lumen.

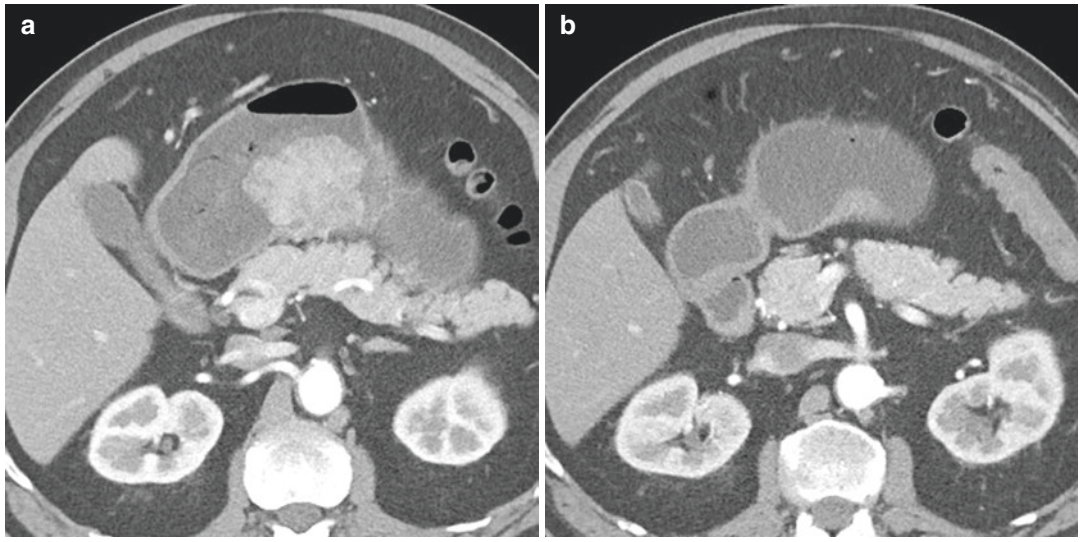

Fig. 1 A patient with gastric mass found by upper endoscopy. Biopsy revealed moderate to poorly differentiated adenocarcinoma. (**a**) Axial contrast-enhanced arteria phase CT shows an enhancing polypoid mass in the gastric body measuring 4.3 × 5.8 cm. (**b**) CT performed 2 months after chemotherapy with FLOT regimen (fluorouracil, leucovorin, oxaliplatin, and docetaxel) shows significant interval decrease in size of the gastric mass, measuring 2.8 × 1.5 cm. Surgical specimen after partial gastrectomy revealed 0.5 cm tubular (intestinal) adenocarcinoma (ypT1aN0)

MRI has not proven to be effective but development of high-speed sequences has made MRI a feasible tool (Choi et al. 2014). MRI is widely used for the evaluation of liver metastases (Lee et al. 2014). PET is useful in some patients for detecting and characterizing distant metastases (Hallinan and Venkatesh 2013; Lee et al. 2014).

Assessment of treatment response is currently performed with MDCT and/or ^{18}F-FDG PET/CT (Hallinan and Venkatesh 2013). MDCT has been the primary tool in determining response to therapeutic effect after anticancer therapy (Fig. 1). However, differentiate treatment-induced morphologic changes from tumor may be difficult to differentiate on conventional imaging modalities including CT and MRI (Lim et al. 2006). Reported accuracy of T-staging and N-staging of gastric cancer after neoadjuvant chemotherapy on MDCT is 42.7–57% and 37–44%, respectively (Park et al. 2008; Yoshikawa et al. 2014), which are lower than that of initially staging of gastric cancer before treatment (67.9–90.9% for T staging; median value 82.1%, and from 56.9% to 86% for N staging; median value 69.5%) (Lee et al. 2014).

2.1.2 Colorectal Cancer

In the local staging of rectal cancer, MRI and transerectal ultrasound (TRUS) are the modality of choice (Kekelidze et al. 2013). However, at higher disease stages, MRI is better than TRUS in the assessment of the primary tumor location and extension, involvement of mesorectal fascia, surrounding viscera, relationships to the sphincter complex, anterior peritoneal reflection and pelvic nodes (Kim et al. 2010; Jhaveri and Hosseini-Nik 2015; Kekelidze et al. 2013; Blazic and Campbell 2016). MRI is also widely used for the evaluation of liver metastases. CT is not suitable for T staging of rectal cancer because of its lower contrast resolution. However, CT is the preferred modality for detecting distant metastasis (Fig. 2), especially when combined with PET (Jhaveri and Hosseini-Nik 2015).

For response evaluation, T2-weighted MRI has been used as a standard tool for local restaging (Kekelidze et al. 2013). Evaluation of both the pre- and post-chemoradiation therapy for rectal cancer, MRI with side-by-side comparison of tumor location, tumor bulk, and change in

Fig. 2 A patient with metastatic colon cancer. (**a**) Axial contrast-enhanced CT shows a large mass measuring 13.2 cm in longest dimension in right anterior abdomen progressed despite treatment with FOLFOX (leucovorin, 5-FU and oxaliplatin) regimen. (**b**) Axial contrast-enhanced CT 2 months after the initiation of pembrolizumab monotherapy shows decreasing size of the mass (9.4 cm). (**c**) Axial contrast-enhanced CT 4 months after the initiation of pembrolizumab monotherapy shows further decreasing size of the mass (4.5 cm). (**d**) Axial contrast-enhanced CT 2 years after (**a**) shows complete disappearance of the mass

tumor signal intensity is essential (Kim et al. 2010). After chemoradiation therapy, areas of fibrosis have very low signal intensity which is similar to that of the muscularis propria (Patel et al. 2012) (Fig. 3). Similarly, low-signal intensity desmoplastic reaction can be seen as spicules or strands in the perirectal fat radiating from the residual tumor (Fig. 4), which does not contain tumor, whereas areas of residual tumor have intermediate signal-intensity on T2-weighted MRI that is similar to that of baseline tumor (Patel et al. 2012).

The accuracy of posttreatment rectal cancer restaging using conventional MRI sequences is generally lower than that of initial staging mainly due to overstaging of nodal disease, failure to differentiate tumor from desmoplastic reaction or radiation fibrosis, and misinterpretation of radiation proctitis as local invasion (Jhaveri and Hosseini-Nik 2015; Kekelidze et al. 2013; Blazic

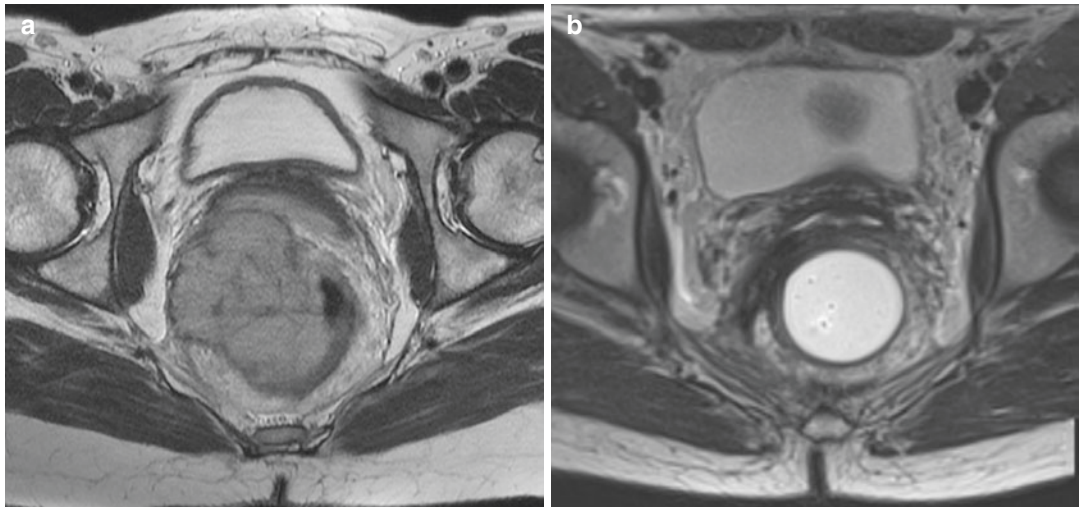

Fig. 3 A patient with rectal squamous cell cancer. (**a**) Initial T2-weighted axial MR image shows a large mass of intermediate signal intensity abutting the mesorectal fascia, posterior vaginal wall, and right levator muscle. (**b**) T2-weighted axial MR image performed 3 months after chemotherapy (5-FU and mitomycin) and radiation therapy shows no residual soft tissue mass compatible with complete radiological resolution. T2-hypointense soft tissue thickening in the area of previous mass is likely related to treatment change. Endoscopy and biopsy showed scarring, and were negative for residual tumor. The patient is followed up by MRI and endoscopy

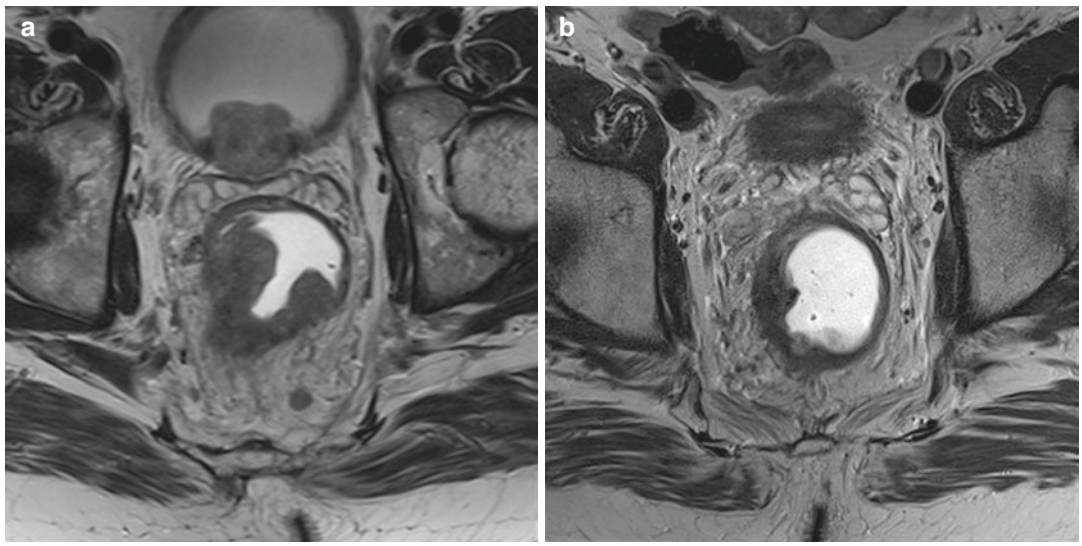

Fig. 4 A patient with rectal adenocarcinoma. (**a**) Initial T2-weighted axial MR image shows mass in the mid rectum from 4 to 10 o'clock with tumor extends up to 6 mm beyond muscularis propria with suspicious lymph nodes, with circumferential resection margin of 5 mm. Clinical stage T3N2M0. (**b**) T2-weighted axial MR image 3 months after radiation and 2 months after FOLFOX chemotherapy shows good response to therapy, and most (>75%) tumor become T2-hypointense dense fibrosis. Enlarged lymph nodes are no longer visualized. Although tumor extension beyond muscularis propria was suspected at 7 o'clock, surgical specimen showed rare small groups of invasive cancer cells to musucalis propria, but not beyond muscularis propria (ypT2N0)

and Campbell 2016) (Fig. 4). In addition, MRI is not reliable for confirming complete response because of its inability to detect microscopic foci of residual tumor or mucin lakes that can be detected at histopathology (Kim et al. 2010; Jhaveri and Hosseini-Nik 2015; Blazic and

Campbell 2016). Reported overall accuracy of MRI in predicting the pathologic stage of irradiated rectal cancer is 47–54% for T staging, 64–68% for N staging, and 66% in predicting circumferential resection margin involvement, which are lower than initial staging (71–91%, 43–85%, 92–95% respectively) (Kim et al. 2010).

An MRI-based tumor regression grading system has been developed based on the extent of visible fibrosis on MRI (Patel et al. 2012; Jhaveri and Hosseini-Nik 2015). MRI assessment of tumor regression grade was a significant independent predictor of overall survival and disease-free survival (Patel et al. 2012). A more extensive fibrosis in a postsurgical specimen is correlated with greater tumor regression and predicts a higher likelihood of survival (Jhaveri and Hosseini-Nik 2015).

For rectal cancer, MRI is the primary imaging modality for assessment of treatment response, however, CT may also be used to assess chemotherapy response to colon cancer. Reported accuracy of CT for T and N staging of locally advanced colon cancer after neoadjuvant chemotherapy was 62% and 87%, respectively, and accuracy for TN staging is 77%, with 13.6% of patients being understaged, and 9.1% of patients overstaged (Arredondo et al. 2014).

2.1.3 Gastrointestinal Stromal Tumor (GIST)

Contrast-enhanced CT is the most commonly used modality in monitoring GIST patients treated with imatinib (Choi 2008). Initial tumor response to imatinib treatment is often seen as decreased density of the lesion on contrast-enhanced CT as early as 1 week with decreased SUV_{max} values and no significant change in the bidimensional size at an early posttreatment stage on ^{18}F-FDG PET (Choi 2008; Richman et al. 2017). Tumors responding to imatinib also shows decreased number of intratumoral vessels, and the tumor becomes homogeneous and hypodense (Choi 2008) (Fig. 5). Specifically, Choi et al. evaluated 173 GIST tumors on contrast-enhanced CT and ^{18}F-FDG PET and found that the tumor density decreased by 16.5% and the SUV_{max} decreased by 64.9% (Choi et al. 2004). Size alone was not accurate in demonstrating treatment response (Choi et al. 2004). Choi et al. defined that "good response" on ^{18}F-FDG PET as a decrease in SUV <70% from baseline or a drop in the absolute value of SUV_{max} <2.5 (Choi 2008), and ≥10% decrease in tumor size or a ≥15% decrease in tumor density on contrast-enhanced CT at 8 weeks of imatinib treatment.

The decrease in attenuation on contrast-enhanced CT is also seen in metastatic lesions. Additionally, these findings can result in the unmasking of isoattenuating liver lesions as "new" metastases, which complicates the assessment of treatment response (Richman et al. 2017). In some responding tumors, the tumor size increases as a result of intratumoral hemorrhage, necrosis, or myxoid degeneration (Choi 2008).

PET is highly sensitive in detecting early response, and is useful in predicting long-term response to imatinib in patients with metastatic GISTs expressing c-Kit receptor tyrosine kinase (Choi 2008). MRI may also be useful especially in anorectal GISTs (Vernuccio et al. 2016).

2.2 Therapy Response Imaging Pitfalls

2.2.1 Nodal Status

Although the extent of nodal disease is important for planning preoperative chemoradiation therapy and surgery, prediction of the nodal status of gastric and colorectal cancers on conventional imaging studies remains problematic. A malignant node typically has morphologic features such as small short-to-long axis ratios, irregular outlines or mixed internal signal heterogeneity (Patel et al. 2012; Jhaveri and Hosseini-Nik 2015) and increased attenuation on contrast-enhanced images. However, it is difficult to differentiate a metastatic lymph node and irradiated lymph node change with MRI by using morphologic criteria, and may result in lymph node overstaging (Kim et al. 2010). Diffusion-weighted MR imaging (DW-MRI) has not been found to be helpful in distinguishing benign from malignant nodes (Blazic and Campbell 2016). Although FDG PET/CT

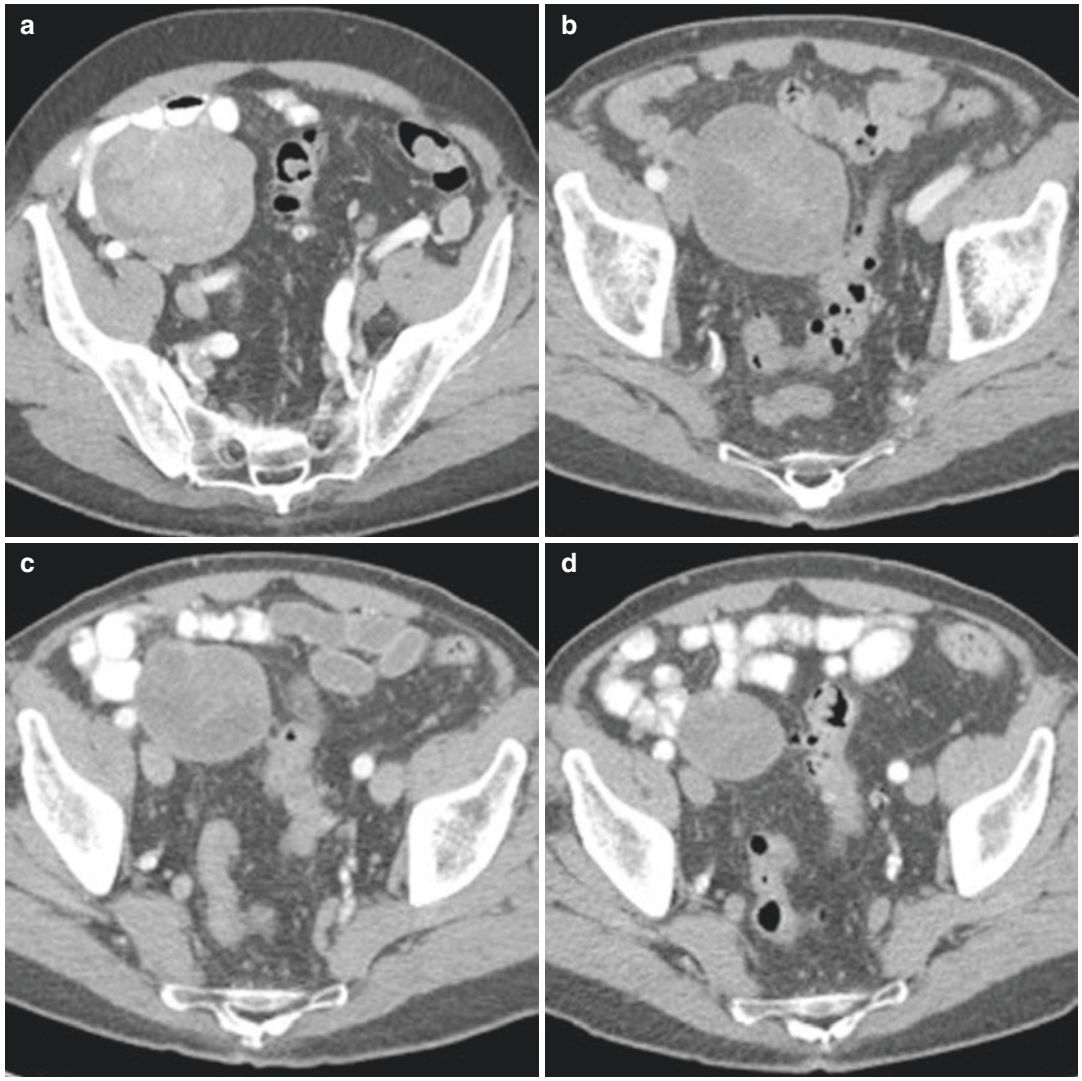

Fig. 5 A patient with incidentally diagnosed small bowel GIST with peritoneal metastases. (**a**) On initial axial contrast-enhanced CT image, the primary tumor in the right lower quadrant measures 8.4 cm in the longest dimension, and 92 HU. (**b**) Axial contrast-enhanced CT 2 months after the initiation of imatinib. The mass is unchanged in size (8.3 cm) but decreased in attenuation to 42 HU. (**c**) Axial contrast-enhanced CT 4 months after the initiation of imatinib. The mass decreased in size (6.6 cm) and attenuation (38 HU). (**d**) Axial contrast-enhanced CT 6 months after the initiation of imatinib. The mass further decreased in size (4.7 cm) and remains hypodense (38 HU)

may provide additional information for N staging, utilization of this modality is limited and cannot be applied broadly (Kekelidze et al. 2013).

2.2.2 Mucinous Tumors

Mucinous adenocarcinoma is a histological variant of gastric and colorectal adenocarcinomas, and is characterized by excess mucin production. Mucinous gastric carcinoma accounts for 2.6–6.6% of all gastric cancers, and has worse prognosis than that of nonmucinous tumors as the mucinous gastric carcinomas tend to present with more advanced tumor stages (Zhao et al. 2017; Isobe et al. 2015). Mucinous rectal adenocarcinoma is more aggressive than usual nonvariant adenocarcinoma (Kim et al. 2010), and have

higher metastatic tendency and often have a higher stage at the time of diagnosis (Jhaveri and Hosseini-Nik 2015). Mucinous rectal tumors comprise pools or lakes of extracellular mucin lined by columns of malignant cells, cords, and vessels seen as intermediate signal intensity within hyperintense mucin on T2-wieghted MR images (Patel et al. 2012). On post chemoradiation MRI, mucinous rectal tumors retains high signal intensity on T2-weighted images, making it difficult to distinguish between a true tumor or remaining mucin (Kim et al. 2010). When mucinous rectal tumors containing intermediate-signal-intensity components on T2-weighted MR images at baseline are unchanged on posttreatment imaging, these findings indicate nonresponse (Patel et al. 2012).

PET is less sensitive in the evaluation of mucinous tumors (≈50%), which uptake less tracer because of their lower cellular density (Jhaveri and Hosseini-Nik 2015). On DW-MRI, because mucinous tumors exhibit ADC hyperintensity even before treatment, their response to chemoradation therapy cannot be assessed using DW-MRI (Jhaveri and Hosseini-Nik 2015).

2.2.3 Tumor Size Measurement

Response Evaluation Criteria in Solid Tumors (RECIST) is widely considered the method of choice for the assessment of tumor response to treatment (Hallinan and Venkatesh 2013). However, in most studies, this measurement is focused on solid organ tumors with limited focus on response in gastrointestinal tumors (Hallinan and Venkatesh 2013).

One of the pitfalls in gastrointestinal tumor response monitoring is difficulty of accurate and reproducible measurements of the primary lesions owing to the irregular configuration (Kim et al. 2010). Cancers which cause diffuse concentric wall thickening such as linitis plastica of gastric cancer may be difficult or impossible to measure accurately (Ng et al. 1996).

For gastric cancer, Mazzei et al. obtained maximal tumor diameter (D-max) measured using a curved line through 2D multiplanar reconstructions in order to obtain the maximum tumor extension with D-max reduction rate at CT after neoadjuvant chemotherapy, and reported that there was a strong correlation between the radiological and histological D-max measurements (Mazzei et al. 2018). For rectal cancer, the change in maximum tumor length between baseline and posttreatment sagittal images has been investigated as a tool to evaluate tumor response (Patel et al. 2012). The EXPERT-C Trial, a phase 2 randomized clinical trial for rectal cancer, has shown good correlation between RECIST assessment and survival outcomes (Patel et al. 2012; Richman et al. 2017). But the CORE trial showed that the reproducibility of maximum tumor length between two readers measured on sagittal MR images was only slight (k = 0.13) despite good correlation between length assessment and histopathologic T stage (Patel et al. 2012; Joensuu et al. 2008; Patel and Brown et al. 2012). Therefore, length measurements are useful in the assessment of tumor response but central review may be needed in clinical trials because of the lack of interobserver reproducibility (Patel et al. 2012; Richman et al. 2017).

Tumor volumetry allows a more accurate and objective indicator of quantification in tumors than one-dimensional measurement in assessing changes in tumor size (Graser et al. 2008). Tumor volume may be measured automatically or semiautomatically with manual adjustment when necessary with the aid of segmentation software. Tumor volumetry has been clinically applied for assessment of response to treatment of GIST (Schramm et al. 2013), gastric cancer (Wang et al. 2017), and colorectal cancer (Kim et al. 2010; Arredondo et al. 2014; Lambregts et al. 2015).

2.2.4 Response Criteria

In contrast to cytotoxic conventional chemotherapeutics, targeted therapies demonstrate predominantly cytostatic effects, and may cause tumor necrosis without a marked decrease in tumor size. Therefore, RECIST criteria can be insufficiently sensitive for evaluating responses in targeted therapies. Choi et al. reported that RECIST significantly underestimated tumor response to imatinib in advanced GIST (Choi et al. 2004). Choi et al. proposed criteria to evaluate treatment

response of GIST to imatinib (Choi criteria) (Choi et al. 2007). Choi criteria use tumor attenuation in addition to tumor size. It defines ≥15% decrease in tumor density in Hounsfield unit (HU) or ≥10% decrease in size is defined as partial response (as opposed to 30% used in RECIST). Whereas nonresponder is defined as ≥10% increase in size and does not meet criteria of partial response by tumor density. Choi criteria correlated better with disease-specific survival in imatinib-treated GIST patients than RECIST (Choi 2008; Choi et al. 2007). Attempts have been made to adapt the Choi criteria in the assessment of other tumors (Tirkes et al. 2013).

For patients receiving immunotherapy, conventional and nonconventional responses have been reported. For example, patients may show a pseudoprogression secondary to inflammatory response that can simulate progression of the disease or the onset of new lesions subsequently followed by tumor shrinkage (Procaccio et al. 2017). Radiographic growth in pseudoprogression is secondary to the infiltration of immune cells such as cytotoxic T lymphocytes around tumors, edema, and necrosis (Chiou and Burotto 2015). RECIST criteria might not be adequate to assess immune response, and criteria considering immune-related response such as irRC (Wolchok et al. 2009) and irRECIST (Seymour et al. 2017) have been introduced. However, they are still not universally adopted especially in clinical trials on gastrointestinal tumor immunotherapy (Procaccio et al. 2017). A new, specific approach to evaluate responses to immunotherapy is needed in order to guide treatment with immunotherapy.

In a subset of patients who are treated with immunotherapy with PD-1 or PD-L1 blockades, an unexpected dramatic tumor surge may occur early after the initiation of immunotherapy (Fig. 6), known as hyperprogression (Fuentes-Antras et al. 2018; Wang et al. 2018). Unlike pseudoprogression, tumor growth is not prompted by increased inflammation but by a plausible idiosyncratic effect of immune checkpoint blockades as enhancers of tumor progression, and patients with hyperprogression present worse survival outcomes (Fuentes-Antras et al. 2018; Wang et al. 2018). Early diagnosis and careful monitoring of hyperprogression is necessary. Although no consistent definition of hyperprogression is determined, it may be depicted as a RECIST progression at the first on-treatment scan combined with the analysis of tumor growth kinetics, at least a doubling in growth rate (percent variation of tumor volume per time interval) when comparing pre- and posttreatment periods (Fuentes-Antras et al. 2018).

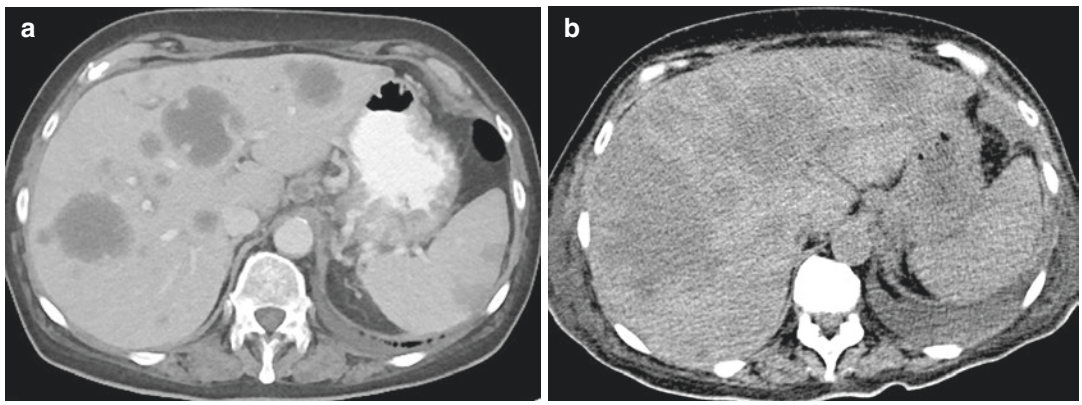

Fig. 6 A patient with history of metastatic gastric cancer, previously treated with FOLFOX. (**a**) Axial contrast-enhanced CT shows primary tumor in the gastric fundus with multiple liver metastases and gastrohepatic ligament adenopathy. Trace left pleural effusion is present. (**b**) Axial noncontrast CT obtained at emergency department due to deterioration of the patient's condition after recent initiation of a clinical trial with ipilimumab and nivolumab at outside institution. Increasing liver metastases and new small ascites are seen. New and enlarging pulmonary nodules and pleural effusions are also present (not shown), concerning for general progression of disease

3 Emerging Approaches/ Challenges for Therapy Response Imaging for GI Malignancies

3.1 FDG PET/CT

^{18}F-FDG PET/CT has gained widespread acceptance as a key to demonstrate early response to therapy of cancer (Ben-Haim and Ell 2009). For gastric cancer, several reports suggested that efficacy of therapeutic options can be determined by FDG PET/CT by evaluating early metabolic changes in addition to changes in size (Lim et al. 2006; Kitajima et al. 2017) and it may play an important role in the treatment algorithm (Ben-Haim and Ell 2009). The role of FDG PET/CT in management of gastrointestinal tumors will likely continue to expand in the future (Lee et al. 2014).

For colorectal cancer, PET has a high diagnostic performance for the interim assessment of response (sensitivity and specificity ≈ 80%) but is less specific in post-radiation therapy response assessment (≈60%) (Jhaveri and Hosseini-Nik 2015) because increased ^{18}F-FDG activity after radiation may also be due to inflammatory changes, and false-positive results may persist for 6 month after completion of radiotherapy (Ben-Haim and Ell 2009; Kekelidze et al. 2013). The role of ^{18}F-FDG PET in the prediction of response to therapy at earlier stages in treatment between responder and non-responder has been assessed by several studies. Large prospective trials are needed to validate the use of ^{18}F-FDG PET response criteria for individual patient management decisions to maximize tumor response before surgical resection (Ben-Haim and Ell 2009; Kekelidze et al. 2013).

^{18}F-FDG PET/CT is increasingly used in GIST for therapy monitoring, and it is generally accepted that FDG PET is more sensitive for the assessment of early therapy response than morphologic imaging modalities. However, several questions remain open, including the appropriate time to monitor a therapeutic protocol and the appropriate therapy response evaluation criteria (Dimitrakopoulou-Strauss et al. 2017).

3.2 Diffuse-Weighted MR Imaging (DW-MRI)

DW-MRI measures the mobility of water molecules within tissues. Water diffusion is restricted in highly cellular tissues such as tumors, and tissues with higher cellularity result in higher signal intensity on DW-MRI. It has been applied to investigate treatment response of the gastric cancer (Giganti et al. 2014; De Cobelli et al. 2013), colorectal cancer, and GIST (Vernuccio et al. 2016), but particularly well assessed in rectal cancer. Recent studies reported that DW-MRI may help in the assessment of response after chemoradiation therapy of colorectal cancer (Jhaveri and Hosseini-Nik 2015; Kekelidze et al. 2013; Lambregts et al. 2015). After chemoradiation therapy, the decrease in cellularity and the development of fibrosis or necrosis in responders result in an increase in diffusion and decrease in the ADC value (Park and Chun 2013; Bang et al. 2010; Fuchs et al. 2014; Wilke et al. 2014; Joshi et al. 2018; Jhaveri and Hosseini-Nik 2015). It is also shown to be feasible as early marker of treatment response because cell death and vascular alterations typically occur before size changes (Kekelidze et al. 2013).

It also has been proved that DW-MRI in addition to standard MRI significantly improves the performance of radiologists to select complete therapy responders compared to standard MRI only and preventing overstaging with MRI (Kim et al. 2010; Kekelidze et al. 2013; Blazic and Campbell 2016). A meta-analysis study showed that DW-MRI is more sensitive than (62–94%) and is almost as specific as (74–91%) conventional MRI in restaging rectal tumors after chemoradiation therapy (Jhaveri and Hosseini-Nik 2015; Chen et al. 2017); however nodal staging remained challenging (Kekelidze et al. 2013; Arredondo et al. 2014).

3.3 Dynamic Contrast-Enhanced (DCE) CT and MRI

Dynamic contrast-enhanced (DCE) CT and MRI with quantitative parameters have been

described as potential prognostic biomarkers in gastrointestinal tumors, and has been applied to assess treatment response of gastric cancer, colorectal cancer, and GIST (Consolino et al. 2017).

Regression of tumor microcirculation is considered an important early prognostic factor for treatment response, before reductions in tumor volume (Kim et al. 2010). The quantification of vascular permeability of the tumor tissue is represented as the K^{trans} (volume transfer constant, a measure of capillary permeability). Recent studies with DCE-MRI reported that a large decrease in the mean K^{trans} after chemoradiation therapy is associated with a good response for locally advanced rectal cancer, while persistent raised values indicate residual active disease (George et al. 2001; Kim et al. 2014; Intven et al. 2015). DCE-MRI may help in the prediction of response to chemoradiation therapy of rectal cancer. Rectal cancers with higher K^{trans} values at presentation appear to respond better to chemoradiation therapy than those with lower values (George et al. 2001; Tong et al. 2015).

Studies evaluated DCE-CT as a biomarker for treatment response of rectal cancer reported significant decrease in blood flow and blood volume after chemotherapy or chemoradiation therapy (Bellomi et al. 2007; Sahani et al. 2005). Bellomi et al. also reported that the baseline low perfusion values were associated with a poorer response (Bellomi et al. 2007). For gastric cancer and GE junction cancer, a study by Hanse et al. reported CT perfusion has only moderate sensitivity and specificity in response assessment of neoadjuvant chemotherapy, and as a single diagnostic test, it is insufficient for clinical decision purposes (Lundsgaard Hansen et al. 2014).

3.4 Monochromatic CT Using Dual-Energy CT

Dual-energy (DE) CT allows material decomposition on the bases of energy-dependent attenuation profiles of specific material by using two different energies. It allows quantitative iodine mapping which has been applied to oncologic imaging such as assessment of microvessel density of gastric cancers in different pathological subgroups (Chen et al. 2017; Liang et al. 2017).

Iodine quantification may also serves as a surrogate biomarker for monitoring effects of the tumor treatment (Agrawal et al. 2014). Several studies indicated that tumor iodine concentration measured by DE CT may benefit in predicting the response to neoadjuvant chemotherapy of locally advanced gastric cancer (Gao et al. 2018) and in assessment of treatment response to tyrosine-kinase inhibitors of GIST (Meyer et al. 2013; Apfaltrer et al. 2012). A study reported that the changes in iodine concentration of gastric carcinomas at baseline and after standard neoadjuvant chemotherapy can help predict pathological regression in gastric cancer better than that for tumor thickness, with iodine concentration on the arterial phase being a better predictor than iodine concentration on the venous phase (Tang et al. 2015).

3.5 Radiomics Features

Radiomics extract quantitative imaging features based on the intensity, shape, size or volume, and texture. Radiomics can be performed with tomographic images from CT, MRI, and PET, and its oncologic application can help in diagnosis, assessment of prognosis, and prediction of therapy response (Gillies et al. 2016; Lubner et al. 2017).

Recently, a growing number of studies are evaluating gastrointestinal tumors using radiomics features. Ng et al. evaluated colorectal tumors in 55 patients by CT texture features with 5-year overall survival, and reported that it may improve prognostication (Ng et al. 2013). Giganti et al. evaluated CT radiomics features of gastric adenocarcinoma in 56 patients before neoadjuvant therapy and correlated with tumor regression grade at the final surgical histology after treatment completion and reported promising result to potentially provide information regarding treatment response and improve risk stratification (Giganti et al. 2017). Jeng et al.

retrospectively analyzed CT radiomics features in 1591 consecutive patients with gastric adenocarcinoma to assess survival and chemotherapeutic benefits and reported that the radiomics features can effectively predict survival and add prognostic value to the TNM staging system (Jiang et al. 2018). These studies suggest that radiomics may be a powerful tool to predict patient survival and select patients who may have benefit from therapy.

4 Conclusions

Treatment response of gastrointestinal tumors is primarily assessed by conventional morphological parameters using CT or MRI with Response Evaluation Criteria in Solid Tumors (RECIST) criteria. However, ^{18}F-FDG PET/CT has also gained widespread acceptance as a key tool to assess early response to treatment. Newer imaging techniques such as diffusion-weighted MRI, dynamic contrast-enhanced CT or MRI, monochromatic CT using dual-energy CT system, and radiomics analysis of CT, MRI and PET may improve assessment and prediction of treatment response.

References

Agrawal MD, Pinho DF, Kulkarni NM, Hahn PF, Guimaraes AR, Sahani DV (2014) Oncologic applications of dual-energy CT in the abdomen. Radiographics 34(3):589–612

Apfaltrer P, Meyer M, Meier C, Henzler T, Barraza JM Jr, Dinter DJ et al (2012) Contrast-enhanced dual-energy CT of gastrointestinal stromal tumors: is iodine-related attenuation a potential indicator of tumor response? Investig Radiol 47(1):65–70

Arnoletti JP, Bland KI (2006) Neoadjuvant and adjuvant therapy for rectal cancer. Surg Oncol Clin N Am 15(1):147–157

Arredondo J, Gonzalez I, Baixauli J, Martinez P, Rodriguez J, Pastor C et al (2014) Tumor response assessment in locally advanced colon cancer after neoadjuvant chemotherapy. J Gastrointest Oncol 5(2):104–111

Bailey CE, Hu CY, You YN, Bednarski BK, Rodriguez-Bigas MA, Skibber JM et al (2015) Increasing disparities in the age-related incidences of colon and rectal cancers in the United States, 1975–2010. JAMA Surg 150(1):17–22

Bang YJ, Van Cutsem E, Feyereislova A, Chung HC, Shen L, Sawaki A et al (2010) Trastuzumab in combination with chemotherapy versus chemotherapy alone for treatment of HER2-positive advanced gastric or gastro-oesophageal junction cancer (ToGA): a phase 3, open-label, randomised controlled trial. Lancet 376(9742):687–697

Bellomi M, Petralia G, Sonzogni A, Zampino MG, Rocca A (2007) CT perfusion for the monitoring of neoadjuvant chemotherapy and radiation therapy in rectal carcinoma: initial experience. Radiology 244(2):486–493

Ben-Haim S, Ell P (2009) ^{18}F-FDG PET and PET/CT in the evaluation of cancer treatment response. J Nucl Med 50(1):88–99

Blazic IM, Campbell NM (2016) Gollub MJ**.** MRI for evaluation of treatment response in rectal cancer. Br J Radiol 89(1064):20150964

Bray F, Ferlay J, Soerjomataram I, Siegel RL, Torre LA, Jemal A (2018) Global cancer statistics 2018: GLOBOCAN estimates of incidence and mortality worldwide for 36 cancers in 185 countries. CA Cancer J Clin 68(6):394–424

Chen XH, Ren K, Liang P, Chai YR, Chen KS, Gao JB (2017) Spectral computed tomography in advanced gastric cancer: can iodine concentration noninvasively assess angiogenesis? World J Gastroenterol 23(9):1666–1675

Chiou VL, Burotto M (2015) Pseudoprogression and immune-related response in solid tumors. J Clin Oncol 33(31):3541–3543

Choi H (2008) Response evaluation of gastrointestinal stromal tumors. Oncologist 13(Suppl 2):4–7

Choi H, Charnsangavej C, de Castro Faria S, Tamm EP, Benjamin RS, Johnson MM et al (2004) CT evaluation of the response of gastrointestinal stromal tumors after imatinib mesylate treatment: a quantitative analysis correlated with FDG PET findings. AJR Am J Roentgenol 183(6):1619–1628

Choi H, Charnsangavej C, Faria SC, Macapinlac HA, Burgess MA, Patel SR et al (2007) Correlation of computed tomography and positron emission tomography in patients with metastatic gastrointestinal stromal tumor treated at a single institution with imatinib mesylate: proposal of new computed tomography response criteria. J Clin Oncol 25(13):1753–1759

Choi JI, Joo I, Lee JM (2014) State-of-the-art preoperative staging of gastric cancer by MDCT and magnetic resonance imaging. World J Gastroenterol 20(16):4546–4557

Coccolini F, Nardi M, Montori G, Ceresoli M, Celotti A, Cascinu S et al (2018) Neoadjuvant chemotherapy in advanced gastric and esophago-gastric cancer. Meta-analysis of randomized trials. Int J Surg 51: 120–127

Consolino L, Longo DL, Sciortino M, Dastru W, Cabodi S, Giovenzana GB et al (2017) Assessing tumor vascularization as a potential biomarker of imatinib resistance in gastrointestinal stromal tumors by dynamic contrast-enhanced magnetic resonance imaging. Gastric Cancer 20(4):629–639

Das S, Ciombor KK, Haraldsdottir S, Goldberg RM (2018) Promising new agents for colorectal cancer. Curr Treat Options in Oncol 19(6):29

De Cobelli F, Giganti F, Orsenigo E, Cellina M, Esposito A, Agostini G et al (2013) Apparent diffusion coefficient modifications in assessing gastro-oesophageal cancer response to neoadjuvant treatment: comparison with tumour regression grade at histology. Eur Radiol 23(8):2165–2174

Demetri GD, van Oosterom AT, Garrett CR, Blackstein ME, Shah MH, Verweij J et al (2006) Efficacy and safety of sunitinib in patients with advanced gastrointestinal stromal tumour after failure of imatinib: a randomised controlled trial. Lancet 368(9544): 1329–1338

Demetri GD, Reichardt P, Kang YK, Blay JY, Rutkowski P, Gelderblom H et al (2013) Efficacy and safety of regorafenib for advanced gastrointestinal stromal tumours after failure of imatinib and sunitinib (GRID): an international, multicentre, randomised, placebo-controlled, phase 3 trial. Lancet 381(9863):295–302

Dimitrakopoulou-Strauss A, Ronellenfitsch U, Cheng C, Pan L, Sachpekidis C, Hohenberger P et al (2017) Imaging therapy response of gastrointestinal stromal tumors (GIST) with FDG PET, CT and MRI: a systematic review. Clin Transl Imaging 5(3):183–197

Eisenhauer EA, Therasse P, Bogaerts J, Schwartz LH, Sargent D, Ford R et al (2009) New response evaluation criteria in solid tumours: revised RECIST guideline (version 1.1). Eur J Cancer 45(2):228–247

Fuchs CS, Tomasek J, Yong CJ, Dumitru F, Passalacqua R, Goswami C et al (2014) Ramucirumab monotherapy for previously treated advanced gastric or gastro-oesophageal junction adenocarcinoma (REGARD): an international, randomised, multicentre, placebo-controlled, phase 3 trial. Lancet 383(9911):31–39

Fuentes-Antras J, Provencio M, Diaz-Rubio E (2018) Hyperprogression as a distinct outcome after immunotherapy. Cancer Treat Rev 70:16–21

Gao X, Zhang Y, Yuan F, Ding B, Ma Q, Yang W et al (2018) Locally advanced gastric cancer: total iodine uptake to predict the response of primary lesion to neoadjuvant chemotherapy. J Cancer Res Clin Oncol 144(11):2207–2218

George ML, Dzik-Jurasz AS, Padhani AR, Brown G, Tait DM, Eccles SA et al (2001) Non-invasive methods of assessing angiogenesis and their value in predicting response to treatment in colorectal cancer. Br J Surg 88(12):1628–1636

Giganti F, De Cobelli F, Canevari C, Orsenigo E, Gallivanone F, Esposito A et al (2014) Response to chemotherapy in gastric adenocarcinoma with diffusion-weighted MRI and (18) F-FDG-PET/CT: correlation of apparent diffusion coefficient and partial volume corrected standardized uptake value with histological tumor regression grade. J Magn Reson Imaging 40(5):1147–1157

Giganti F, Marra P, Ambrosi A, Salerno A, Antunes S, Chiari D et al (2017) Pre-treatment MDCT-based texture analysis for therapy response prediction in gastric cancer: comparison with tumour regression grade at final histology. Eur J Radiol 90:129–137

Gillies RJ, Kinahan PE, Hricak H (2016) Radiomics: images are more than pictures, they are data. Radiology 278(2):563–577

Graser A, Becker CR, Reiser MF, Stief C, Staehler M (2008) Volumetry of metastases from renal cell carcinoma: comparison with the RECIST criteria. Radiologe 48(9):850–856

Hallinan JT, Venkatesh SK (2013) Gastric carcinoma: imaging diagnosis, staging and assessment of treatment response. Cancer Imaging 13:212–227

Hu B, El Hajj N, Sittler S, Lammert N, Barnes R, Meloni-Ehrig A (2012) Gastric cancer: classification, histology and application of molecular pathology. J Gastrointest Oncol 3(3):251–261

Ilson DH (2018) Advances in the treatment of gastric cancer. Curr Opin Gastroenterol 34(6):465–468

Intven M, Reerink O, Philippens ME (2015) Dynamic contrast enhanced MR imaging for rectal cancer response assessment after neo-adjuvant chemoradiation. J Magn Reson Imaging 41(6):1646–1653

Isobe T, Hashimoto K, Kizaki J, Matono S, Murakami N, Kinugasa T et al (2015) Characteristics and prognosis of mucinous gastric carcinoma. Mol Clin Oncol 3(1):44–50

Jhaveri KS, Hosseini-Nik H (2015) MRI of rectal cancer: an overview and update on recent advances. AJR Am J Roentgenol 205(1):W42–W55

Jiang Y, Chen C, Xie J, Wang W, Zha X, Lv W et al (2018) Radiomics signature of computed tomography imaging for prediction of survival and chemotherapeutic benefits in gastric cancer. EBioMedicine 36:171–182

Joensuu H (2008) Risk stratification of patients diagnosed with gastrointestinal stromal tumor. Hum Pathol 39(10):1411–1419

Joshi SS, Maron SB, Catenacci DV (2018) Pembrolizumab for treatment of advanced gastric and gastroesophageal junction adenocarcinoma. Future Oncol 14(5):417–430

Kekelidze M, D'Errico L, Pansini M, Tyndall A, Hohmann J (2013) Colorectal cancer: current imaging methods and future perspectives for the diagnosis, staging and therapeutic response evaluation. World J Gastroenterol 19(46):8502–8514

Kim DJ, Kim JH, Lim JS, Yu JS, Chung JJ, Kim MJ et al (2010) Restaging of rectal cancer with MR imaging after concurrent chemotherapy and radiation therapy. Radiographics 30(2):503–516

Kim SH, Lee JM, Gupta SN, Han JK, Choi BI (2014) Dynamic contrast-enhanced MRI to evaluate the therapeutic response to neoadjuvant chemoradiation therapy in locally advanced rectal cancer. J Magn Reson Imaging 40(3):730–737

Kitajima K, Nakajo M, Kaida H, Minamimoto R, Hirata K, Tsurusaki M et al (2017) Present and future roles of FDG-PET/CT imaging in the management of gastrointestinal cancer: an update. Nagoya J Med Sci 79(4):527–543

Lambregts DM, Rao SX, Sassen S, Martens MH, Heijnen LA, Buijsen J et al (2015) MRI and diffusion-weighted MRI volumetry for identification of complete tumor responders after preoperative chemoradiotherapy in patients with rectal cancer: a bi-institutional validation study. Ann Surg 262(6):1034–1039

Lauren P (1965) The two histological main types of gastric carcinoma: diffuse and so-called intestinal-type carcinoma. An attempt at a histo-clinical classification. Acta Pathol Microbiol Scand 64:31–49

Lee JH, Kim JG, Jung HK, Kim JH, Jeong WK, Jeon TJ et al (2014) Clinical practice guidelines for gastric cancer in Korea: an evidence-based approach. J Gastric Cancer 14(2):87–104

Liang P, Ren XC, Gao JB, Chen KS, Xu X (2017) Iodine concentration in spectral CT: assessment of prognostic determinants in patients with gastric adenocarcinoma. AJR Am J Roentgenol 209(5):1033–1038

Liegl B, Hornick JL, Lazar AJ (2009) Contemporary pathology of gastrointestinal stromal tumors. Hematol Oncol Clin North Am 23(1):49–68, vii–viii

Lim JS, Yun MJ, Kim MJ, Hyung WJ, Park MS, Choi JY et al (2006) CT and PET in stomach cancer: preoperative staging and monitoring of response to therapy. Radiographics 26(1):143–156

Lubner MG, Smith AD, Sandrasegaran K, Sahani DV, Pickhardt PJ (2017) CT texture analysis: definitions, applications, biologic correlates, and challenges. Radiographics 37(5):1483–1503

Lundsgaard Hansen M, Fallentin E, Lauridsen C, Law I, Federspiel B, Baeksgaard L et al (2014) Computed tomography (CT) perfusion as an early predictive marker for treatment response to neoadjuvant chemotherapy in gastroesophageal junction cancer and gastric cancer—a prospective study. PLoS One 9(5):e97605

Mazzei MA, Bagnacci G, Gentili F, Nigri A, Pelini V, Vindigni C et al (2018) Gastric cancer maximum tumour diameter reduction rate at ct examination as a radiological index for predicting histopathological regression after neoadjuvant treatment: a multicentre GIRCG study. Gastroenterol Res Pract 2018:1794524

Meyer M, Hohenberger P, Apfaltrer P, Henzler T, Dinter DJ, Schoenberg SO et al (2013) CT-based response assessment of advanced gastrointestinal stromal tumor: dual energy CT provides a more predictive imaging biomarker of clinical benefit than RECIST or Choi criteria. Eur J Radiol 82(6):923–928

Mocellin S, Marchet A, Nitti D (2011) EUS for the staging of gastric cancer: a meta-analysis. Gastrointest Endosc 73(6):1122–1134

Ng VW, Husband JE, Nicolson VM, Minty I, Bamias A (1996) CT evaluation of treatment response in advanced gastric cancer. Clin Radiol 51(3):215–220

Ng F, Ganeshan B, Kozarski R, Miles KA, Goh V (2013) Assessment of primary colorectal cancer heterogeneity by using whole-tumor texture analysis: contrast-enhanced CT texture as a biomarker of 5-year survival. Radiology 266(1):177–184

Ohhara Y, Fukuda N, Takeuchi S, Honma R, Shimizu Y, Kinoshita I et al (2016) Role of targeted therapy in metastatic colorectal cancer. World J Gastrointest Oncol 8(9):642–655

Park SC, Chun HJ (2013) Chemotherapy for advanced gastric cancer: review and update of current practices. Gut Liver 7(4):385–393

Park SR, Lee JS, Kim CG, Kim HK, Kook MC, Kim YW et al (2008) Endoscopic ultrasound and computed tomography in restaging and predicting prognosis after neoadjuvant chemotherapy in patients with locally advanced gastric cancer. Cancer 112(11):2368–2376

Park JH, Kim JH, Ahn SD, et al (2004). Prospective phase II study of preoperative chemoradiation with capecitabine in locally advanced rectal cancer. Cancer Res Treat 36:354–359

Patel UB, Blomqvist LK, Taylor F, George C, Guthrie A, Bees N et al (2012) MRI after treatment of locally advanced rectal cancer: how to report tumor response—the MERCURY experience. AJR Am J Roentgenol 199(4):W486–W495

Patel UB, Brown G, Rutten H, et al (2012). Comparison of magnetic resonance imaging and histopathological response to chemoradiotherapy in locally advanced rectal cancer. Ann Surg Oncol 19:2842–2852. https://www.ncbi.nlm.nih.gov/pubmed/22526897

Procaccio L, Schirripa M, Fassan M, Vecchione L, Bergamo F, Prete AA et al (2017) Immunotherapy in gastrointestinal cancers. Biomed Res Int 2017:4346576

Richman DM, Tirumani SH, Hornick JL, Fuchs CS, Howard S, Krajewski K et al (2017) Beyond gastric adenocarcinoma: multimodality assessment of common and uncommon gastric neoplasms. Abdom Radiol (NY) 42(1):124–140

Roh MS, Colangelo LH, O'Connell MJ, Yothers G, Deutsch M, Allegra CJ et al (2009) Preoperative multimodality therapy improves disease-free survival in patients with carcinoma of the rectum: NSABP R-03. J Clin Oncol 27(31):5124–5130

Sahani DV, Kalva SP, Hamberg LM, Hahn PF, Willett CG, Saini S et al (2005) Assessing tumor perfusion and treatment response in rectal cancer with multisection CT: initial observations. Radiology 234(3):785–792

Sauer R, Becker H, Hohenberger W, Rodel C, Wittekind C, Fietkau R et al (2004) Preoperative versus postoperative chemoradiotherapy for rectal cancer. N Engl J Med 351(17):1731–1740

Schramm N, Englhart E, Schlemmer M, Hittinger M, Ubleis C, Becker CR et al (2013) Tumor response and clinical outcome in metastatic gastrointestinal stromal tumors under sunitinib therapy: comparison of RECIST, Choi and volumetric criteria. Eur J Radiol 82(6):951–958

Seymour L, Bogaerts J, Perrone A, Ford R, Schwartz LH, Mandrekar S et al (2017) iRECIST: guidelines for response criteria for use in trials testing immunotherapeutics. Lancet Oncol 18(3):e143–ee52

Tang L, Li ZY, Li ZW, Zhang XP, Li YL, Li XT et al (2015) Evaluating the response of gastric carcinomas

to neoadjuvant chemotherapy using iodine concentration on spectral CT: a comparison with pathological regression. Clin Radiol 70(11):1198–1204

Tirkes T, Hollar MA, Tann M, Kohli MD, Akisik F, Sandrasegaran K (2013) Response criteria in oncologic imaging: review of traditional and new criteria. Radiographics 33(5):1323–1341

Tong T, Sun Y, Gollub MJ, Peng W, Cai S, Zhang Z et al (2015) Dynamic contrast-enhanced MRI: use in predicting pathological complete response to neoadjuvant chemoradiation in locally advanced rectal cancer. J Magn Reson Imaging 42(3):673–680

Vernuccio F, Taibbi A, Picone D, L LAG, Midiri M, Lagalla R et al (2016) Imaging of gastrointestinal stromal tumors: from diagnosis to evaluation of therapeutic response. Anticancer Res 36(6):2639–2648

Wang ZC, Wang C, Ding Y, Ji Y, Zeng MS, Rao SX (2017) CT volumetry can potentially predict the local stage for gastric cancer after chemotherapy. Diagn Interv Radiol 23(4):257–262

Wang Q, Gao J, Pseudoprogression WX (2018) Hyperprogression after checkpoint blockade. Int Immunopharmacol 58:125–135

Weinberg BA, Marshall JL (2019) Colon cancer in young adults: trends and their implications. Curr Oncol Rep 21(1):3

Wilke H, Muro K, Van Cutsem E, Oh SC, Bodoky G, Shimada Y et al (2014) Ramucirumab plus paclitaxel versus placebo plus paclitaxel in patients with previously treated advanced gastric or gastro-oesophageal junction adenocarcinoma (RAINBOW): a double-blind, randomised phase 3 trial. Lancet Oncol 15(11):1224–1235

Wolchok JD, Hoos A, O'Day S, Weber JS, Hamid O, Lebbe C et al (2009) Guidelines for the evaluation of immune therapy activity in solid tumors: immune-related response criteria. Clin Cancer Res 15(23):7412–7420

Xiao Y, Freeman GJ (2015) The microsatellite instable subset of colorectal cancer is a particularly good candidate for checkpoint blockade immunotherapy. Cancer Discov 5(1):16–18

Yaghoubi N, Soltani A, Ghazvini K, Hassanian SM, Hashemy SI (2019) PD-1/ PD-L1 blockade as a novel treatment for colorectal cancer. Biomed Pharmacother 110:312–318

Yoshikawa T, Tanabe K, Nishikawa K, Ito Y, Matsui T, Kimura Y et al (2014) Accuracy of CT staging of locally advanced gastric cancer after neoadjuvant chemotherapy: cohort evaluation within a randomized phase II study. Ann Surg Oncol 21(Suppl 3):S385–S389

Zhao J, Ren G, Cai R, Chen J, Li H, Guo C et al (2017) Mucinous adenocarcinoma and non-mucinous adenocarcinoma: differing clinicopathological characteristics and computed tomography features in gastric cancer. Oncotarget 8(28):45698–45709

Zhou C, Duan X, Zhang X, Hu H, Wang D, Shen J (2016) Predictive features of CT for risk stratifications in patients with primary gastrointestinal stromal tumour. Eur Radiol 26(9):3086–3093

Therapy Response Imaging in Hepatobiliary and Pancreatic Malignancies

Sanaz Ameli, Mohammadreza Shaghaghi, Ihab R. Kamel, and Atif Zaheer

Contents

Abstract

Hepatocellular carcinoma (HCC), cholangiocarcinoma, and pancreatic ductal adenocarcinoma (PDAC) are the most common primary hepatobiliary and pancreatic cancers and are associated with poor survival. With improvements in anticancer therapy during recent decades, assessment of treatment response has become more significant and different methods have been utilized in evaluating response to therapy. While conventional methods rely solely on size reduction, newer techniques

S. Ameli · M. Shaghaghi · I. R. Kamel · A. Zaheer (✉)
The Russell H. Morgan Department of Radiology and Radiological Science, Johns Hopkins School of Medicine, Baltimore, MD, USA
e-mail: sameli1@jhmi.edu; mshagha1@jhmi.edu; ikamel@jhmi.edu; azaheer1@jhmi.edu

M. Nishino (ed.), *Therapy Response Imaging in Oncology*, Medical Radiology, Diagnostic Imaging,
https://doi.org/10.1007/978-3-030-31171-1_8

focus on changes in tumor functional features as a response to treatment. In assessing HCC tumors response, WHO and RECIST only considered tumor shrinkage as a response to treatment. With the introduction of locoregional and molecular-targeted therapies in HCC treatment, the limitations of size-based criteria were addressed by development of new criteria that considered functional imaging parameters such as tumor enhancement. Functional criteria such as Choi, RECICL, EASL criteria, and mRECIST mostly focus on the viability/functionality of the tumor and are considered more accurate in assessing treatment response. In addition, new advanced technologies like CTPI, DWI, IVIM, MRS, MR-PWI, FDG-PET/CT, and PET/MRI can detect response at molecular level and can assess treatment response before any morphological changes take place. Similar to HCC, functional criteria using modalities like FDG-PET/CT, PET/MRI, DCE-MRI, and DWI are also being utilized in the evaluation of cholangiocarcinoma and PDAC in addition to conventional size criteria to detect early changes of treatment response.

Hepatocellular carcinoma (HCC), cholangiocarcinoma, and pancreatic ductal adenocarcinoma (PDAC) are the most common primary hepatobiliary and pancreatic cancers and are associated with poor survival, with 5-year survival rates of 31%,15%, 14%, respectively, at the best estimates (Liver Cancer Survival Rates n.d.; Pancreatic Cancer Survival Rates, by Stage n.d.; Survival Rates for Bile Duct Cancer 2018). With improvements in anticancer therapy during recent decades, assessment of treatment response has become significant. Tumor response was assessed for the first time in 1960s when reduction in tumor size was defined as a criterion for treatment response in several inoperable solid gastrointestinal (GI) tumors (Hurley and Ellison 1960). Since then, several other approaches have been considered to assess treatment response, until 1981 when the World Health Organization (WHO) attempted to standardize the treatment response criteria. Four categories of response were defined based on these criteria: complete response (CR), partial response (PR), stable disease (SD), and progressive disease (Miller et al. 1981). In addition to time intervals to response (TTR) or progression (TTP), many clinical trials have utilized WHO categories as the primary end point for treatment response assessment. As therapeutic methods advanced over time, several shortcomings have been recognized in the WHO criteria, leading to development of more accurate criteria. These include: Response Evaluation Criteria in Solid Tumors (RECIST), modified RECIST (mRECIST), RECIST 1.1, and European Association for the Study of the Liver (EASL) guidelines (Bruix et al. 2001; Therasse et al. 2000; Eisenhauer et al. 2009; Schwartz et al. 2016). Variation in treatment modalities demanded more advanced radiologic criteria to accurately assess response. For example, loco-regional therapy (LRT) may not necessarily cause any change in tumor size in the short term and this prompted the use of changes in tumor functional features in assessing treatment response (Kamel et al. 2007; Yaghmai et al. 2013). Functional imaging is a novel method which can evaluate posttreatment changes by investigating tissue metabolism, blood flow, or texture. Technologies like diffusion-weighted imaging (DWI), apparent diffusion coefficient (ADC) maps, dynamic contrast enhancement (DCE-MRI), perfusion computed tomography (pCT), and positron emission tomography CT (PET-CT) have been added to conventional magnetic resonance imaging (MRI) and computed topography (CT). These techniques are capable of investigating tissue characteristics on a molecular scale and can serve as novel biomarkers in tumor response (Minocha and Lewandowski 2015).

1 Hepatocellular Carcinoma

HCC is the most common primary tumor of the liver and is among the most common causes of cancer-related mortality worldwide (Di Bisceglie 1997). Liver transplantation is the only curative

option in treating HCC, but in many cases, the disease is already in an advanced stage and surgery or transplantation may not be applicable. The Milan criteria are usually used to select candidates with HCC for liver transplantation. Based on these criteria patient should have a single HCC lesion smaller than 5 cm or 3 lesions smaller than 3 cm without any vascular invasion or metastasis (Iwatsuki et al. 1985). Nonsurgical tumor ablative methods like trans-arterial chemoembolization (TACE), which locally delivers high concentration of chemotherapeutic agents to the targeted lesion, have shown improvement in survival of patients with unresectable HCC. Assessing tumor response to treatment is important as these therapies are used to downstage patients who are not candidates for liver transplantation due to the disease burden with tumor sizes beyond the Milan criteria. With increasing acceptance of loco-regional therapies (LRT), evaluation of early treatment response is becoming more important for predicting the success of treatment and planning for the next step in patient management (Kamel et al. 2006).

Overall, HCC is one of the most studied tumors in the field of functional imaging. Assessing response to treatment based on tumor size has been used routinely in clinical trials. On size-based criteria, only tumor shrinkage is considered as a favorable response. WHO, RESCIST 1.0, and RECIST 1.1 are three main size based. Contrast-enhanced CT (CECT) imaging has low accuracy in detecting viable residual tumor after chemoembolization as compared to contrast-enhanced MRI (CEMRI), due to its high sensitivity for the hyper-dense lipiodol deposition within the lesion after treatment which obscures the assessment of tumor enhancement (Hunt et al. 2009). Volumetric measurements have shown better association with tumor histopathology and these measurements can better address irregularities in tumor shape and response to treatment compared with axial measurements (Bonekamp et al. 2013). The best results can be achieved by combining these volumetric measurements with MRI functional imaging biomarkers like enhancement and diffusion-weighted sequences (Chapiro et al. 2014).

Table 1 Response categories based on WHO criteria

Response category	Criteria
Complete response (CR)	Complete disappearance of the target tumor 4 weeks after treatment
Partial response (PR)	≥50% decrease in tumor size within 4 weeks of treatment
Stable disease (SD)	Neither partial response nor progressive disease
Progressive disease (PD)	≥25% increase in size of one or more lesions Alternatively, the appearance of new lesions

1.1 WHO Criteria

WHO criteria, defined in 1979, assesses tumor response to treatment using bidimensional measurement of tumor size. Tumor size can be measured by multiplying the longest diameter (LD) of tumor by its greatest perpendicular diameter. In case of multiple target lesions, the products of LDs and longest perpendicular diameters are added (Sylvester 1980). Based on WHO criteria tumor response can be categorized into four groups and shown in Table 1.

There are limitations to these criteria including: (1) measurements may not be reproducible, (2) criteria are based on tumor size only as the metric and does not take into account other types of response like tumor necrosis, (3) no standard method regarding the minimum or maximum number of measurable lesions, and (4) no standard method for minimum and maximum size of measurable tumors (Therasse et al. 2000). Moreover, the difference in contrast timing can alter the appearance of the tumor in the liver and thus result in inconsistency in measurements (Hayano et al. 2015).

1.2 Response Evaluation Criteria in Solid Tumors (RECIST) 1.0

RECIST 1.0 was established in 2000 to address some of the limitations of WHO. Based on these criteria lesions must be at least 2 cm with conventional methods such as radiography or 1 cm with

spiral computed tomography (CT) scan to be considered as measurable, and up to 5 lesions per organ and 10 lesions in total can be measured. RECIST 1.0 is a one-dimensional measurement which calculates the sum of the LDs of all target lesions. CR and SD based on RECIST criteria are similar to WHO criteria; PR is defined as ≥30% decrease in sum of LDs after 4 weeks, and PD is defined as ≥20% increase in the sum of LDs (Therasse et al. 2000).

RECIST criteria has several advantages over WHO criteria; however, it still has some limitations including: (1) all measurements are bound to subjectivity and therefore hard to reproduce, (2) this method is unable to differentiate viable tumor from necrosis, (3) infiltrative tumor cannot be measured accurately because of ill-defined margins, (4) maximum number of 10 target lesion seems to be arbitrary, and (5) no well-defined method for lymph node evaluation (Gonzalez-Guindalini et al. 2013).

In some studies, WHO criteria were superior to RECIST 1.0 because WHO better addressed the nonspherical nature of HCC tumor. However, both criteria perform similar in assessing response to LRTs. WHO and RECIST 1.0 criteria can detect response to treatment as early as 7.7 months. This relatively long interval might not be suitable for patients listed for transplantation. However, these criteria can serve as reliable predictors for overall survival (Riaz et al. 2010).

1.3 Response Evaluation Criteria in Solid Tumors (RECIST) 1.1

A revised version of RECIST was released in 2009. Changes in the new guideline were as follow: (1) the total number of assessed lesions is 2 in the liver and a total of 5 in each patient, (2) lymph nodes with short axis greater than or equal to 15 mm were considered as target lesion, (3) for PD, in addition to ≥20% increase in the sum of LDs it requires at least a 5 mm absolute increase in the sum of LDs, (4) for CR, all lesions should disappear completely and all pathological lymph nodes must shrink to less than 10 mm in their short axis, and (5) revised RECIST also includes new guideline to use 18F-fluorodeoxyglucose (FDG) positron emission tomography (PET) for detecting new lesions (Eisenhauer et al. 2009).

Limitations of these criteria include: (1) RECIST 1.1 also provides unidimensional measurement and assumes all tumors as spherical, (2) as all previous guidelines, RECIST 1.1 considers the largest lesion as target lesion which may be affected by subjectivity. Different lesions can be targeted by LRT for treatment at different time points and based on their accessibility, (3) tumor necrosis is not still addressed as part of response criteria, (4) it does not specify the appropriate phase after intravenous contrast agent injection to measure lesion (Gonzalez-Guindalini et al. 2013).

With the introduction of locoregional and molecular-targeted therapies in HCC treatment, the limitations of size-based criteria became more apparent, since these treatments might not reduce the size of the tumor but induce necrosis instead and may even increase tumor size due to hemorrhage or inflammation (Atassi et al. 2008). Therefore, to address the shortcomings of previous methods new criteria were developed, which in addition to size, considered functional imaging parameters such as tumor enhancement. Using these imaging modalities, functional criteria such as Choi, Response Evaluation Criteria in Cancer of the Liver (RECICL), European Association for Study of the Liver Criteria (EASL criteria), and Modified RECIST (mRECIST) mostly focus on the viability/functionality of the tumor rather than just the size.

1.4 Modified CT Response Evaluation Criteria (Choi Criteria)

Choi criteria were developed in 2007 to assess GIST response to imatinib treatment. Imatinib is a tyrosine kinase inhibitor, which has a cytostatic effect without causing cytotoxic effects.

Since its introduction for treatment of gastrointestinal stromal tumor (GIST), the use of size-based tumor response methods has been questioned (Choi et al. 2007). In Choi criteria, CT attenuation coefficient is measured by region of interest (ROI) placement on lesions during the portal venous phase. Based on these criteria, CR and SD are the same as the previous criteria (WHO, RECISTs). However, PR is described as >10% decrease in LD and >15% decrease in tumor enhancement after treatment. Definition for PD is either a >10% increase in tumor diameter or the appearance of new lesions (Gonzalez-Guindalini et al. 2013). Although Choi criteria were intended for GIST treatment evaluation, it has been used in other hypervascular tumors like HCC (Boninsegna et al. 2017). Several studies showed superiority of Choi criteria to WHO and RECIST in predicting overall survival in HCC patients treated by sorafenib and transarterial radioembolization (TARE) (Ronot et al. 2014; Weng et al. 2013). Reproducibility is a limitation due to operator dependence. Three-dimensional (3D) semiautomated volumetric measurement can address this shortcoming and increase reproducibility of tumor measurements (Chalian et al. 2012).

1.5 Response Evaluation Criteria in Cancer of the Liver (RECICL)

RECICL evaluate HCC response to LRT. In contrast to previous methods, RECICL measure changes in necrotic parts of the tumor for assessing treatment efficacy. In addition, these criteria take into account the type of treatment in timing of follow-up evaluation. Posttreatment assessment by imaging is recommended 1 month after TACE and 6 months after TARE (Kudo et al. 2010). RECICL quantifies the necrotic parts using bidimensional measurements like WHO. This method is still in the experimental phase and its potential benefits are yet to be determined (Kudo et al. 2010). However, preliminary data suggests that in sorafenib-treated HCC patients, RECICL had good reproducibility and better performance in predicting overall survival compared to RECICT 1.1 or Modified RECIST (see below) (Arizumi et al. 2014; Tovoli et al. 2018).

1.6 European Association for Study of the Liver Criteria (EASL Criteria)

The European Association for Study of the Liver proposed new criteria (EASL criteria) in 2000 to address the limitations of size-based criteria in assessing tumor response to LRT. EASL criteria utilized the same method as WHO, but instead of applying the bidimensional measurements on the whole tumor it only focused on viable tumor tissue, which can be identified as the sum of arterially enhancing part of hepatocellular carcinoma. EASL criteria assess the development of necrosis after treatment based on percentage change in the enhancing tissue on cross-sectional images. Response grouping was also the same as WHO guideline (Bruix et al. 2001). EASL can detect tumor response as early as 1.6 months after therapy and is an independent predictor of survival in patients with HCC (Riaz et al. 2010; Gillmore et al. 2011).

1.7 Modified RECIST (mRECIST)

Although EASL criteria considered the functional aspect of HCC on imaging and focused on change in viable part of the tumor rather than entire tumor size, it still had some limitations including the complexity of bidimensional measurements and lack of comprehensive guideline for new lesions or nontarget lesions assessment. To address these limitations, the American Association for the Study of Liver Disease published a new guideline in 2010. They combined some features of EASL criteria with RECIST criteria and designed new guideline as modified RECIST (mRECIST). Based on

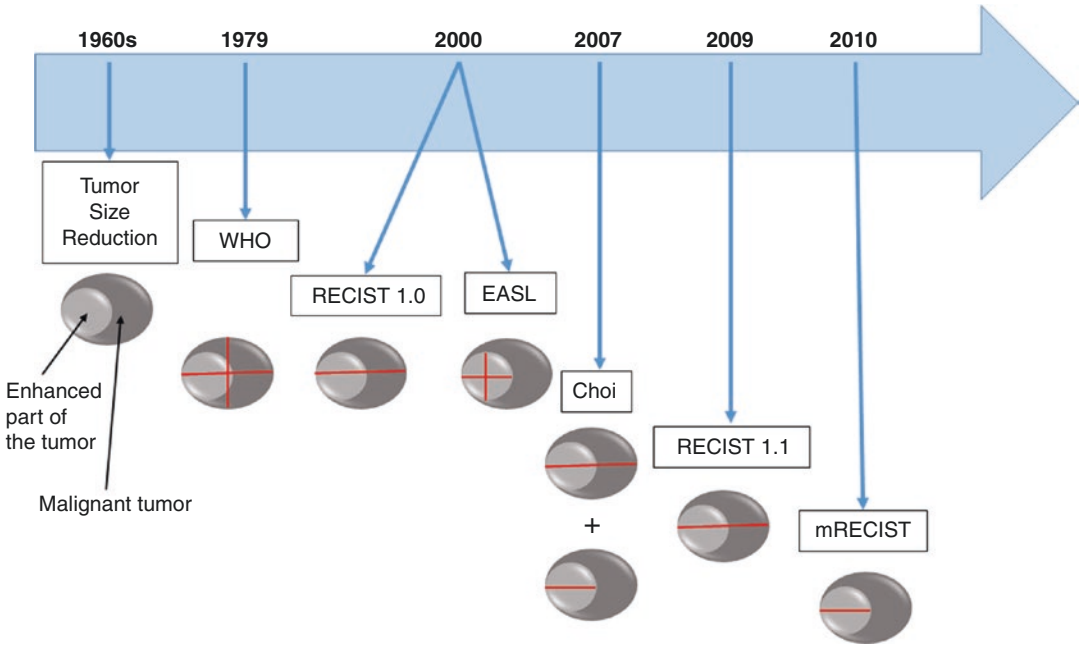

Fig. 1 Conventional criteria in assessing tumor response to treatment

mRECIST, the LD of the enhancing part of the tumor in arterial phase CT or MRI should be calculated without taking into account the necrotic part of the tumor. Poorly enhancing HCC and tumor with atypical enhancement cannot be selected as target lesions (Lencioni and Llovet 2010). Other aspects of mRECIST are as same as RECIST 1.1 criteria.

mRECIST and EASL perform almost identical in assessing tumor response by detecting changes as early as 2 months. In addition, both criteria can predict overall survival between 2 and 3 months after TACE (Gillmore et al. 2011; Lencioni et al. 2017).

The limitations include: (1) it assumes the viable part of tumor as a sphere, (2) there is no defined guideline to choose the target lesion, (3) with LRT, lesions can be treated at different time points so each lesion can be served as a targeted or nontargeted lesion.

Figure 1 shows the evolution of conventional methods through time. A summary of all conventional methods of assessing tumor response is shown in Table 2.

2 Advanced Methods of Assessing Tumor Response

2.1 Computed Tomography Perfusion Imaging (CTPI)

CTPI is a technique that uses dynamic CT to measure tissue perfusion and presents the results as a colored map (Fig. 2). CTPI can be acquired by performing rapid sequential imaging following an intravenous injection of iodinated contrast agent. The changes in contrast density over time is shown as a time-density curve (TDC), and then different mathematical methods are used to obtain different perfusion parameters. CTPI can measure hepatic arterial perfusion, hepatic portal perfusion, blood volume, and mean transit time (Yang et al. 2016a) and serve as an estimate of tumor angiogenesis to predict response to treatment and patients' overall survival (Chen et al. 2008). There has been significant progress in CT hardware and software for perfusion imaging. New multislice spiral CT scanners reconstruct liver perfusion map with

Table 2 Response categories based on conventional methods

Response	WHO criteria	RECIST 1.0	RECIST 1.1	Choi criteria	RECICL	EASL criteria	mRECIST
Complete response (CR)	Complete disappearance of the target tumor	Complete disappearance of the target tumor	In addition to disappearance of target tumor, all pathological lymph nodes must shrink to less than 10 mm in their short axis	Complete disappearance of all lesions	Complete tumor necrosis	Disappearance of enhancing tissue	Disappearance of arterial enhancement and disappearance of all pathological lymph node
Partial response (PR)	≥50% decrease in tumor size within 4 weeks of treatment	≥30% decrease in sum of LDs after 4 weeks	≥30% decrease in sum of LDs after 4 weeks	>10% decrease in LD and >15% decrease in tumor enhancement after treatment	Tumor necrosis between 50 and <100%	≥50% decrease in arterial-enhanced area	≥30% decrease in sum of diameter of enhancing area
Stable disease (SD)	Neither CR, PR nor PD	Neither CR, PR, nor PD	Neither CR, PR, nor PD	Neither CR, PR, nor PD	Neither CR, PR, nor PD	Neither CR, PR, nor PD	Neither CR, PR, nor PD
Progressive disease (PD)	≥25% increase in size of one or more lesions. Alternatively, the appearance of new lesions	≥20% increase in the sum of LDs	≥20% increase in the sum of LDs. Additionally it requires a 5 mm absolute increase in the sum of LDs	>10% increase in tumor diameter or appearance of new lesions	Tumor area growth >25% regardless of necrosis effect[a]	≥25% increase in arterial-enhanced area	≥20% increase in the sum of diameter of enhancing area

[a]Defined as tumor enlargement of ≥50% excluding the area of necrosis after treatment in RECICL 2015 revised version (Hepatology Research 2016; 46: 3–9)
LD longest diameter (modified from Radiographics. 2013;33(6):1781–800)

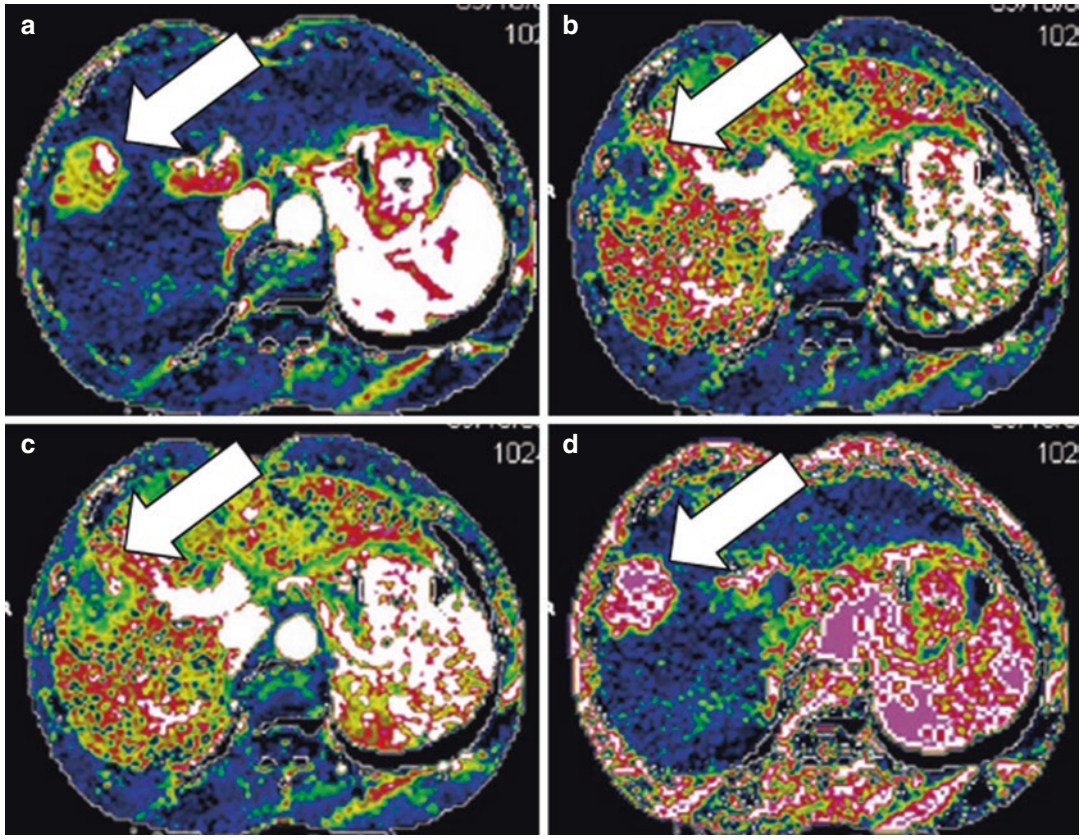

Fig. 2 70-year-old man with hepatocellular carcinoma. (**a**) Image of hepatic arterial perfusion; (**b**) image of hepatic portal perfusion; (**c**) image of total liver perfusion; (**d**) image of hepatic arterial perfusion index. Axial perfusion images of the tumor before transarterial chemoembolization were created by maximum slope method. The tumor (arrows) showed an increased hepatic arterial perfusion and decreased hepatic portal perfusion compared with the normal parenchyma. The values of hepatic arterial perfusion, hepatic portal perfusion, total liver perfusion, and hepatic arterial perfusion index were 0.512 mL/min mL, 0.226 mL/min mL, 0.738 mL/min mL, and 69.4%, respectively. (Reprinted with permission from World Journal of Gastroenterology 2016;22(20):4835–4847)

an enhanced resolution and provide more detailed information about tumor hemodynamics in a single scan (Yang et al. 2016a). The most recent advanced form of CTPI is C-arm CT technology, which assesses tumor blood volume and changes in perfusion. It can be utilized for detecting the tumor and identifying its blood supply, as well as assessing response to TACE (Syha et al. 2016).

Limitations include higher exposure to radiation, misregistration due to patient movement and variations due to flow changes induced by different contrast agents (Yang et al. 2016a; Miles et al. 1991).

2.2 Diffusion-Weighted Imaging (DWI)

DWI relies on random movement of water molecules, known as a Brownian movement, to differentiate types of tissues. Water diffusion can be altered based on tissue properties. Spin echo-echo planar imaging (SE-EPI) is the most commonly used technique to acquire this sequence. DWI can detect the slightest amount of diffusion and its sensitivity is influenced by the choice of *b*-value. Results are reported as a diffusion coefficient, shown as a map of apparent diffusion coefficient (ADC) over the region

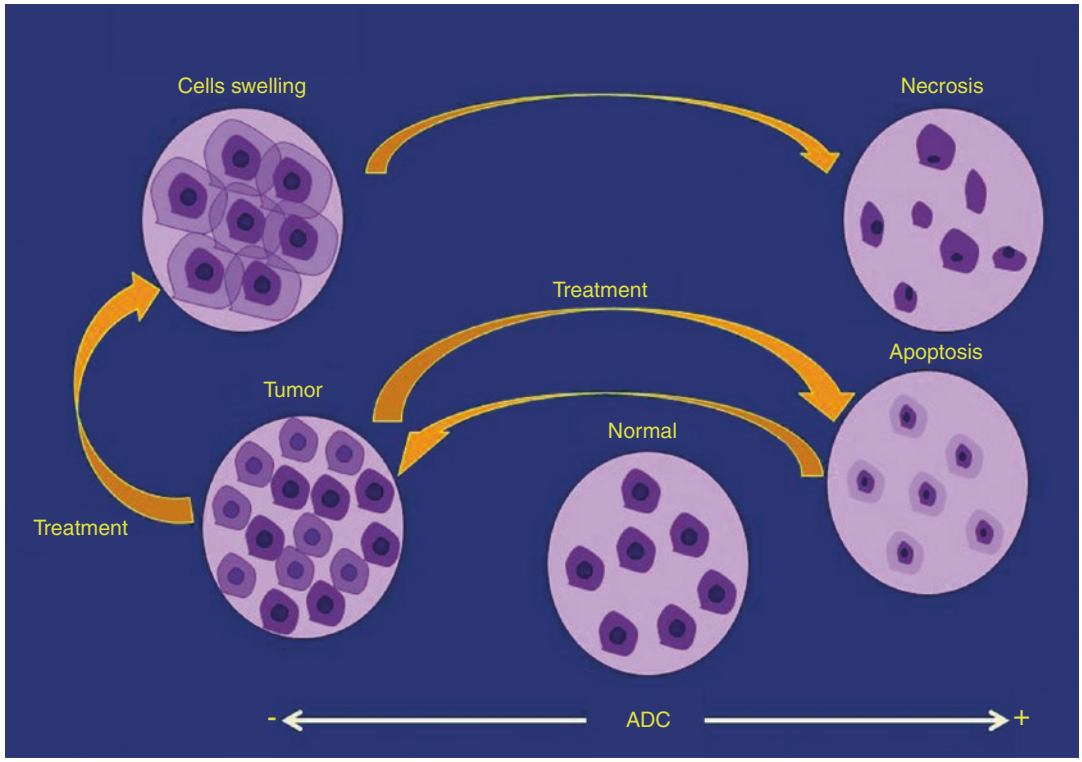

Fig. 3 Successful treatment causes necrosis/apoptosis in HCC tumor, makes water diffuse more freely and therefore increased ADC (modified from AJR 2007;188:1622–1635)

of interest. Cellularity and density of the tissue can be quantitatively calculated from the ADC map. As water diffusion becomes more restricted, such as in highly cellular tumors, the ADC value decreases. This feature makes ADC an excellent tool for the initial detection of HCC and for follow-up after LRT. HCCs have higher cellularity as compared to their surrounding liver parenchyma; therefore, the tumor ADC is lower compared to that of normal liver tissue. On the other hand, LRT can induce necrosis within the tumor and freely moving water within a necrotic tumor results in an increased ADC (Fig. 3). The ADC does not change in the absence of response to therapy, in the presence of residual tumor, or due to recurrence (Yang et al. 2016a).

Different studies reported different values for ADC in HCC tumors ranging from 0.95 to 3.84 × 10^{-3} mm^2/s. These discrepancies in results is due to the use of different scanners and b-values used to acquire DWI sequences (Kamel et al. 2006; Ichikawa et al. 1998; Sun et al. 2005).

A decrease in enhancement can be detected immediately after TACE. Additionally, ADC increases significantly in 1–2 weeks after TACE. These findings precede changes in RECIST which becomes apparent 6 months after TACE (Bonekamp et al. 2011a; Kamel et al. 2009). Similar changes in ADC can be detected in patients treated with Y-90 radioembolization, 1 month after treatment (Rhee et al. 2008).

There are limitations to this technique, including low signal-to-noise ratio, low imaging quality due to SE-EPI sequence associated artifacts, ADC overlap between benign and malignant lesions, ADC variability based on scanner type and *b*-value. Furthermore, ROI placement in this technique could be affected by readers' error

(Yang et al. 2016a; Kele and van der Jagt 2010). The latter has been addressed by the development of novel semiautomated volumetric techniques for ADC measurement, which increase the reliability and reproducibility of ADC measurements by 3D evaluation of the entire tumor (Bonekamp et al. 2014).

2.3 Intravoxel Incoherent Motion MRI (IVIM)

The quality of the ADC map is highly dependent on the *b*-value of the DWI. A higher *b*-value in DWI provides more accurate information on water diffusion within tissue by omitting signals from blood flow. However, this is associated with lower image quality. On the other hand, by decreasing *b*-value, DWI signal will be affected by blood perfusion in addition to water diffusion (Yang et al. 2016a).

IVIM calculates the micro translations occurring in each voxel. By combining low and high *b*-value, IVIM can distinguish water diffusion from blood perfusion. Several parameters can be obtained from IVIM, including true diffusion coefficient, perfusion-related diffusion coefficient, and perfusion fraction (Fig. 4). Thereby IVIM can better approximate true water diffusion in lesions, as compared to DWI, and is a better representative of tissue characteristics with higher accuracy in distinguishing benign from malignant liver lesions (Watanabe et al. 2014; Woo et al. 2014). It has also been used in assessing HCC response to antiangiogenesis and radiofrequency ablation therapies. The results in several animal study have shown that IVIM has the ability to detect tumor response immediately after treatment (Guo et al. 2015; Joo et al. 2014). Also Shirota et al. showed that IVIM at baseline can predict the response to treatment in HCC patients treated with sorafenib as the baseline diffusion coefficient (DC) value was higher in responders as compared to nonresponders group (Shirota et al. 2016).

2.4 Magnetic Resonance Spectroscopy (MRS)

MRS distinguishes different metabolites and their concentration in vivo by using a magnetic field to induce radiofrequency signals. Proton magnetic resonance spectroscopy (HMRS) detects choline concentration, which is part of the cell wall and can indirectly show cellular proliferation rate (Martín Noguerol et al. 2016). Several studies used this feature to assess HCC response to TACE as early as 2–5 days after treatment, in order to find any viable residual tissue in case of treatment failure (Chen et al. 2006; Kuo et al. 2004). A decrease in choline level after TACE correlates with size reduction few months later detected by RECIST. These early changes in MRS signals are also associated with increase in ADC. Combining MRS and DWI may help achieve better assessment of response to treatment (Bonekamp et al. 2011b). An important shortcoming of MRS is the effect of movements such as respiration and cardiac motility on image quality (ter Voert et al. 2011) and low resolution of spectra in small lesions, because of unfavorable voxel size and signal-to-noise ratio (Yang et al. 2016b).

2.5 Magnetic Resonance Perfusion-Weighted Imaging (MR-PWI)

Similar to CTPI, MR-PWI studies the blood supply within a tumor. It identifies micro-vessels by analyzing changes in signal intensity of intravenous contrast agent at different time intervals. The results are shown as time-intensity curve (TIC). Parameters such as initial enhancement rate and maximal enhancement are calculated. These parameters show changes in blood flow and vascular permeability, and indirectly represent tumor vasculature making it useful in determining tumor response to antiangiogenic treatments. Different sequences are used in MR-PWI technology for the assessment of HCC treatment response, most common being

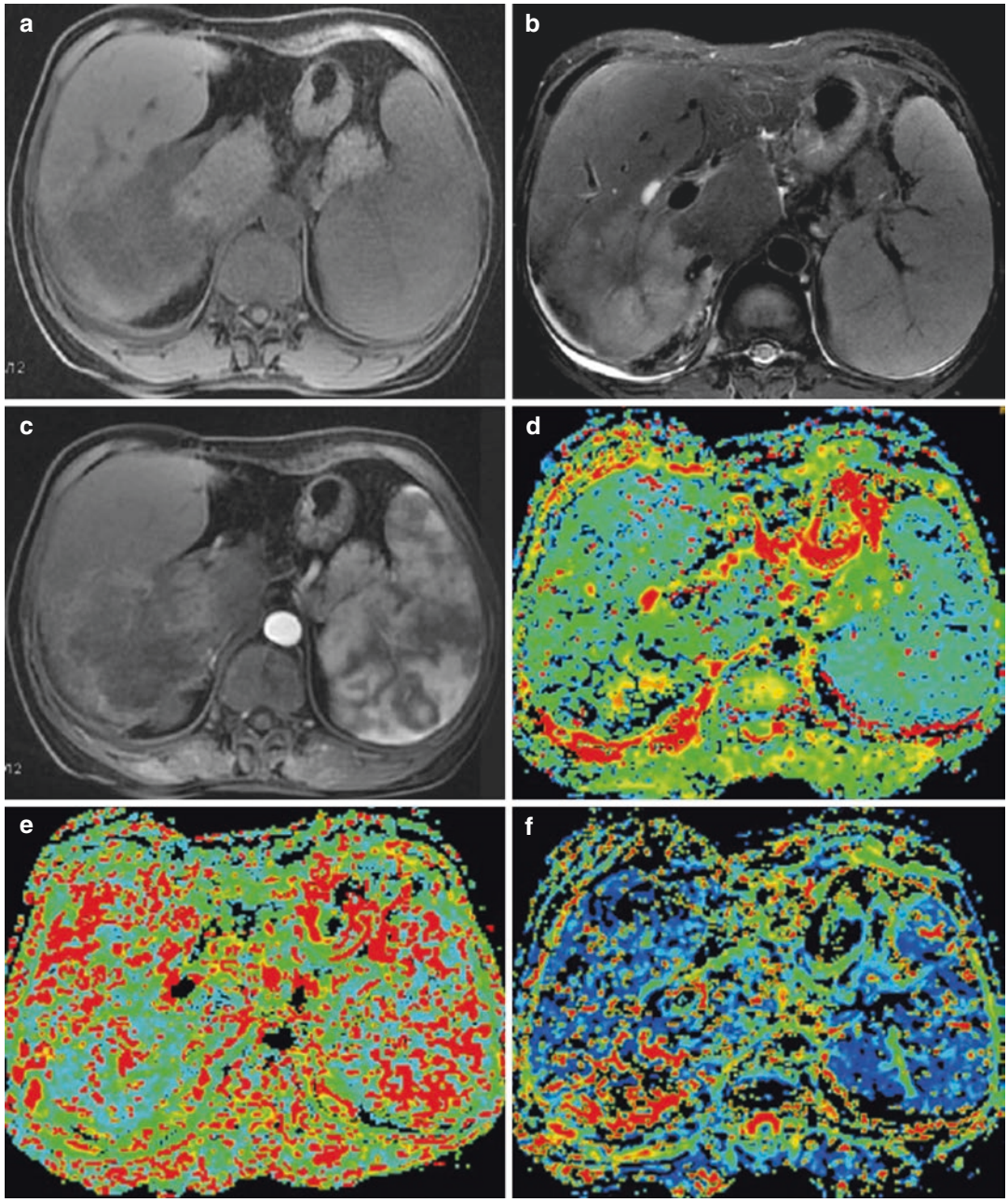

Fig. 4 53-year-old woman with hepatocellular carcinoma in the right lobe of the liver. (**a**) Axial T1-weighted image shows a hypointense mass in the posterior right lobe of the liver; (**b**) axial T2-weighted image shows a hyperintense mass; (**c**) contrast-enhanced MRI during the arterial phase showing lesion enhancement; (**d**) mapping of the estimated value of the true molecular-diffusion coefficient (*D* parameter). The average value in the lesion region of interest (ROI) was $D = 1.22 \times 10^{-3}$ mm²/s; (**e**) mapping of the estimated value of the perfusion-related diffusion coefficient ($D*$ parameter). The average value in the lesion ROI was $D* = 20.6 \times 10^{-3}$ mm²/s; (**f**) mapping of the perfusion fraction (*f*) with a value of 19.6%. (Reprinted with permission from World journal of gastroenterology 2016;22(20):4835–4847)

T1-weighted dynamic contrast-enhanced sequence (Yang et al. 2016a).

Several studies showed the additive value of MR-PWI in combination with DWI. As ADC increases after TACE due to tumor necrosis, MTD, K^{trans}, and K_{ep} decreases (Lin et al. 2016; Braren et al. 2011).

Although MR-PWI has some advantages over CTPI like higher resolution and lack of radiation exposure, its limitations include the need for a more customized scanner, longer scan times, and complex post-processing analysis, which makes it less suitable for clinical use (Yang et al. 2016a).

2.6 FDG-PET/CT and PET/MRI

FDG-PET/CT evaluates glucose metabolism, which indirectly estimates tumor activity. Although it has limited usefulness in the detection of HCC due to the increased background liver uptake, it can assess treatment failure earlier by detecting residual metabolism within a tumor following TACE before any structural changes occur by measuring the standardized uptake value (SUV) change in the lesion at baseline and after TACE treatment (Yang et al. 2016a). In a study by Kim et al., SUV ratio of tumor to normal liver was obtained on pretherapy PET/CT, and tumors with SUV ratio higher than 2.5 were associated with better response to radiotherapy (Kim et al. 2012a). Other studies have used high tumor-to-liver SUV ratio as a marker for aggressive disease and poor survival (Sung et al. 2018; Song et al. 2015). FDG-PET/CT should be performed at least 1 month after TACE to avoid false positive results due to treatment-induced inflammation. One study suggested tumor-to-liver SUV ratio lower than 1.9 after treatment as a predictor of good response (Ortega Lopez 2015).

Despite high accuracy of FDG-PET/CT in detecting metastasis, residual tumor, and disease recurrence, its use may be limited in patients requiring multiple follow-ups due to higher radiation exposure. Development of PET/MRI has resolved this limitation. In addition, PET/MRI provides improved soft tissue resolution and has the ability of combining functional data using DWI to serve as a good modality for assessing HCC response to treatment (Yang et al. 2016a).

3 Intrahepatic Cholangiocarcinoma (ICCA)

ICCA is the second most common primary tumor in the liver with increasing incidence likely attributed to improved molecular diagnostics (Saha et al. 2016). The only potentially curative treatment for ICCA is surgical resection. Since only patients with sufficient liver remnant after complete excision of margin-negative tumor, without extrahepatic disease or lymph node involvement, are considered for surgery, only a small fraction of patients are surgical candidates (Weber et al. 2015). However, systemic chemotherapy has shown minimal advantage in treatment (Fig. 5). The overall survival in this group remains between 3 and 6 months. However, new LRTs like TACE have shown improved survival up to 12–16 months (Seidensticker et al. 2016). Thus, assessing tumor response to treatment is of great importance for treatment planning (Vossen et al. 2006). Conventionally, size-based criteria like WHO, RECIST, mRECIST, and EASL have been used for this purpose (Fig. 6). However, they have several shortcomings like variability in measuring methods, low reproducibility, and reliance on the slow developing morphological changes as response indicators (Therasse et al. 2000). By contrast, new functional modalities like DWI can detect treatment response earlier by revealing changes in tumors microstructures (Corona-Villalobos and Kamel 2014). Several studies have shown that an increase in ADC 3–4 weeks after TACE can be an early indicator of successful therapy (Halappa et al. 2012; Pandey et al. 2018). In addition to ADC, changes in delayed phase enhancement (180 s after injection of contrast agent) can be considered another parameter in assessing treatment response, as ICCA is best detected on this phase (Camacho et al. 2014). Another approach for evaluating treatment

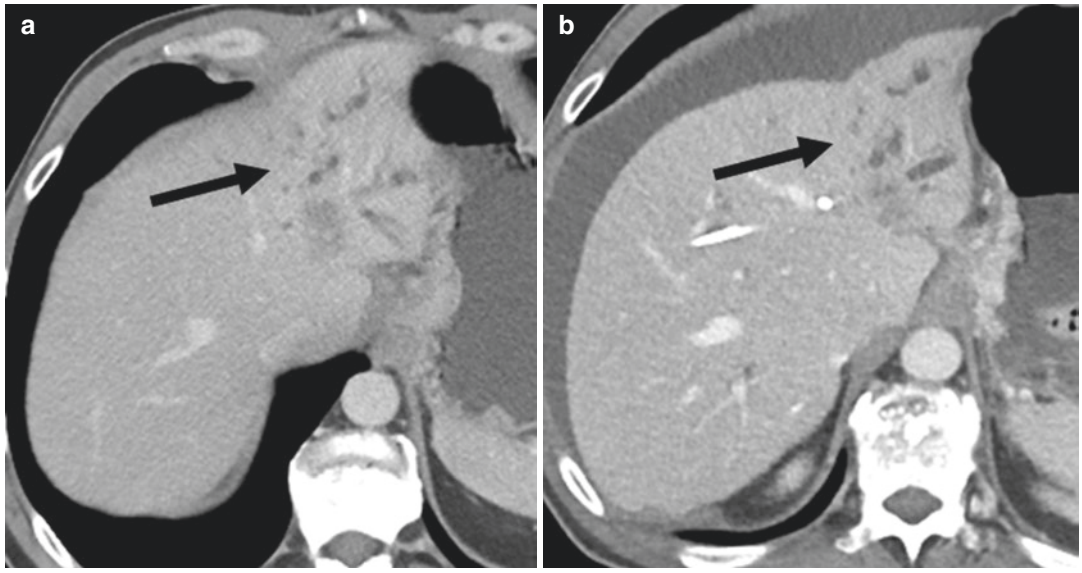

Fig. 5 Cholangiocarcinoma at baseline (arrows) (**a**) and 2 months after chemotherapy (**b**) on CT shows minimal change in tumor size and enhancement in response to chemotherapy

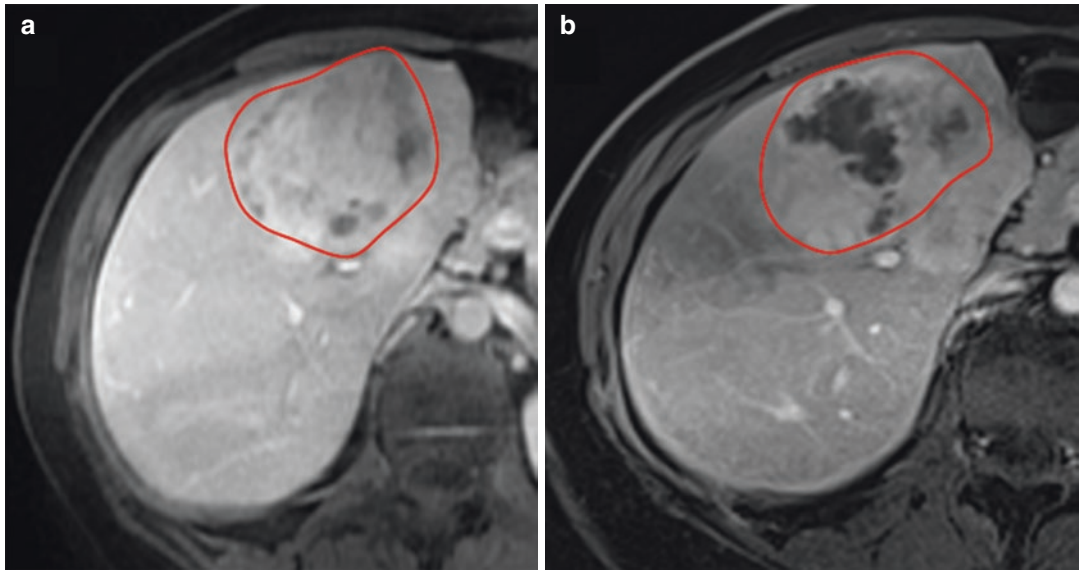

Fig. 6 Cholangiocarcinoma at baseline (red circle) (**a**) and 1 month after TACE (**b**) on MRI shows minimal change in tumor size but considerable decrease in enhancement in response to TACE

response is using DCE-MRI, which noninvasively estimates tumor microvasculature and perfusion. This approach relies on the fact that a decrease in tumor perfusion after treatment can be an indirect indicator of treatment success (Camacho et al. 2014).

4 Pancreatic Ductal Adenocarcinoma (PDAC)

PDAC is among the deadliest cancers worldwide with a very poor prognosis (Pancreatic Cancer Survival Rates, by Stage n.d.). It usually becomes

symptomatic in late stages of disease, and therefore distant metastasis and local invasion are often evident at the time of diagnosis (Li et al. 2004). The only curative treatment is resection of the primary tumor (Wray et al. 2005). However, new advances preoperative neoadjuvant therapy (combined chemo and radiation) have led to downstaging disease in up to 30% patients potentially increasing the pool of surgical candidates (Gillen et al. 2010).

CT and MRI are the most commonly used methods in response evaluation. Although multidetector row computed tomography (MDCT) is considered the best imaging modality in PDAC, its accuracy in assessing treatment response has been challenged due to the complex structure of the tumor and the presence of fibrosis (Trajkovic-Arsic et al. 2017). Different approaches for treatment evaluation are listed below.

4.1 Multi-detector Row Computed Tomography (MDCT)

MDCT is the most commonly used imaging modality early in the diagnosis of PDAC, because of its high spatial resolution. It also has a high accuracy in detecting vascular involvement, which helps decide the operability of tumor (Li et al. 2006). Thereby, MDCT is the preferred method to follow the tumor response after treatment. New MDT scanner have resolved the prior limitation of detecting lesions smaller than 2 cm. However, MDCT has decreased specificity in differentiating posttreatment fibrosis from residual tumor as size and attenuation after treatment do not serve as reliable markers for response to therapy (Katz et al. 2012).

4.2 Response Evaluation Criteria in Solid Tumors 1.1

Similar to HCC and other solid tumors, RECIST 1.1 criteria can be used to follow treatment response in PDAC, especially to assess response in the hepatic metastasis. However, its use is limited for the assessment of the primary tumor due to ill-defined and unclear borders and the absence of size change in many cases even after favorable response to therapy (Katz et al. 2012). On the other hand, decrease in tumor-vessel circumferential contact assessed on MDCT has been found to be associated with a negative resection margin with a specificity of 86%, sensitivity of 61%, positive predictive value of 91%, and negative predictive value of 48% (Cassinotto et al. 2014).

Additionally, RECIST 1.1 criteria assume all the tumors as spherical, which is not true in most cases of PDAC (Boninsegna et al. 2017).

4.3 Choi Criteria

As explained above, Choi criteria was defined based on enhancement attenuation. Although it is not a good choice for assessing response in PDAC because of its failure in differentiating residual tumor from fibro-inflammatory response to treatment, it has been shown to be better than RECIST in predicting response to treatment and overall survival (Cassinotto et al. 2014; Vecchiarelli et al. 2013). Vecchiarelli showed that Choi criteria can better stratify responders 3 months after treatment as compared to RECIST. Statistically significant difference was demonstrated in the overall survival of patients with PR, SD, and PD using the Choi criteria as compared to the RECIST criteria (Vecchiarelli et al. 2013).

4.4 FDG-PET/CT

FDG-PET/CT is a promising complementary modality to CT scan in assessing response to treatment or recurrence after chemotherapy/ surgery. It can detect recurrence after surgery earlier than CT, with the sensitivity as high as 96%. It can also detect decreased metabolism in responders before any morphological changes occur (Sahani et al. 2012). FDG-PET/CT can also be used to predict the prognosis and overall survival in PDAC patients (Epelbaum et al. 2013). The study is expensive and requires many adjustments for standardizing the protocol in assessing

tumor response. Despite these limitations, it is gaining more advantage over other methods and becoming the gold standard in treatment response assessment in PDAC (Boninsegna et al. 2017).

4.5 PET Response Criteria in Solid Tumors (PERCIST)

PERCIST is defined based on FDG-PET/CT scan. New chemotherapeutic agents mostly arrest cell growth rather than inducing cell necrosis; therefore, some tumors might show response to treatment by decreased metabolism rather than shrinkage. With PERCIST criteria, response to treatment can be assessed based on changes in the maximum accumulation of tracer in body or SUL (SUV adjusted for lean body mass) (Wahl et al. 2009). Response to treatment is categorized in four groups described in Table 3.

Two studies demonstrated the correlation of tumor response with SUV change. A drop in SUV after treatment from 5.7 to 1.6 and 7.2 to 4.5 were both associated with favorable tumor response and an improvement in CA 19.9 level (Patel et al. 2011; Alvarez et al. 2013).

4.6 PET/MR

Several studies have shown the advantages of PET/MR over FDG-PET/CT in detecting and staging pancreatic neoplasm and also predicting patient survival after resection (Chen et al. 2016; Nagamachi et al. 2013). Results show higher accuracy for PET/MRI (97.7% vs. 85.2%) and specificity (92.9% vs. 21.4%) in detecting pancreatic tumor of all size, as compared to FDG-PET/CT. In a study, combination of PET/MRI and DWI had shown to be the most powerful biomarker in predicting patient's survival. An increase in metabolic tumor volume (MTV), derived from PET, and decrease in ADC, 1 month after treatment, were associated with low progression-free survival in PDAC patients (Chen et al. 2016).

Table 3 Response categories based on PERCIST criteria

Response category	Description
Complete response (CR)	No metabolism in previously active lesions
Partial response (PR)	>30% decrease in SUL peak
Progressive disease (PD)	>30% increase in SUL peak or new lesion formation
Stable disease (SD)	Neither PR nor PD

4.7 Dynamic Contrast-Enhanced MRI (DCE-MRI)

DCE-MRI is a functional modality, and can assess tumor micro-structure. It can be a useful tool in differentiating PDAC from other pathologies. The slow gradual enhancement pattern of pancreatic cancer is quite different from the normal parenchyma, chronic pancreatitis, and pancreatic neuroendocrine tumors. While pancreatic cancer demonstrates slow gradual enhancement, chronic pancreatitis has gradual increase followed by decreasing enhancement. Pancreatic neuroendocrine tumors show rapidly increasing enhancement followed by a gradual decline (Kim et al. 2013).

DCE-MRI can be used to assess PDAC microvasculature, which makes it an excellent tool for evaluating response to chemotherapeutic agents targeting angiogenesis. Besides, DCE-MRI can quantitatively calculate PDAC fibrosis, which has been shown to be involved in tumor growth and resistance to therapy (Bali et al. 2011) and has the potential to both to predict and assess response to therapy. A reduction in K^{trans} and V_e was detected in responders 28 days after antiangiogenic therapy. Additionally, K^{trans} and K_{ep} higher than 0.78 mL/mL min and 1.43 min^{-1} pretreatment were associated with higher rate of response (Akisik et al. 2010).

4.8 DWI

Neoadjuvant therapy is frequently provided to patients with borderline resectable disease to increase the potential of downsizing the tumor grade for tumor negative surgery. It may cause

minimal structural changes, which can remain undetectable by anatomic imaging. This limitation highlights the significance of functional imaging protocols such as DWI or FDG-PET/CT. Generally, in malignant tumors with high cellularity (e.g., PDAC) diffusion coefficients will be lower than its background parenchyma. Several studies confirmed these hypotheses by detecting lower ADC in PDAC as compared to normal parenchyma (Fattahi et al. 2009; Lee et al. 2008). Recent studies have shown that cellular density in PDAC could contribute to tumors prognosis, and potentially be useful in treatment evaluation (Kim et al. 2012b). They suggested that high pretreatment ADC is significantly associated with better response to treatment with a mean ADC of 1.61×10^{-3} mm^2/s in responders vs. 1.25×10^{-3} mm^2/s in nonresponders (Cuneo et al. 2014). Additionally, patient with early progression after treatment had lower ADC before receiving gemcitabine as a treatment (Niwa et al. 2009).

DWI can be used to detect tumor remnants after chemotherapy or surgery (Choi et al. 2004). However, there are some limitations in using this modality. Several confounders can alter ADC results like the type of scanner and coil, tumor vasculature, and room temperature (Boninsegna et al. 2017).

4.9 Texture Analysis

Texture analysis includes a variety of image analysis techniques that assess variation in lesion characteristics that are imperceptible to the human eye using a variety of imaging techniques including CT, MRI, and PET. These features are calculated based on the shape of histogram after a region of interest analysis. Post-processing analysis can quantitatively determine tumor heterogeneity, and as a result predict the tumor appearance. CT texture analysis may have added value in downstaging patients after chemotherapy who otherwise show no evidence of downstaging on conventional CT interpretation (Ciaravino et al. 2018). In another study on assessing response to chemoradiation therapy in PDAC patients, several radiomics features of CT histogram distinguished responders from nonresponders. The change of mean CT number, decrease in volume and kurtosis, and increase in skewness could predict the good tumor response as early as 2 weeks after treatment (Chen et al. 2017). It has been shown that in PDAC patient, changes in mean, variance density values, and kurtosis of different MRI biomarkers are associated with response to FOLFIRINOX treatment. Textural feature of entropy on T2-weighted imaging has also shown to be significantly associated with overall survival in patients with PDAC (Choi et al. 2018). However, large sample studies are still needed. Yue et al. also showed that in PDAC patients who underwent FDG-PET/CT 6 weeks after radiotherapy, tumors were more homogeneous after likely due to decreased metabolic activity after treatment (Yue et al. 2017). Texture analysis is inexpensive and can be done on already available imaging, which makes it a valuable tool in assessing tumor response to treatment (Boninsegna et al. 2017).

5 Conclusion

In conclusion, in patients with hepatobiliary and pancreatic malignancy, early treatment response is becoming more important for predicting the success of treatment and planning for the next step in patient management and functional criteria have shown superiority over the conventional size-based criteria for such evaluations.

References

Akisik MF, Sandrasegaran K, Bu G, Lin C, Hutchins GD, Chiorean EG (2010) Pancreatic cancer: utility of dynamic contrast-enhanced MR imaging in assessment of antiangiogenic therapy. Radiology 256(2):441–449. https://doi.org/10.1148/radiol.10091733

Alvarez R, Musteanu M, Garcia-Garcia E, Lopez-Casas PP, Megias D, Guerra C, Muñoz M, Quijano Y, Cubillo A, Rodriguez-Pascual J, Plaza C, de Vicente E, Prados S, Tabernero S, Barbacid M, Lopez-Rios F, Hidalgo M (2013) Stromal disrupting effects of nab-paclitaxel in pancreatic cancer. Br J Cancer 109:926. https://doi.org/10.1038/bjc.2013.415. https://www.nature.com/articles/bjc2013415#supplementary-information

Arizumi T, Ueshima K, Takeda H, Osaki Y, Takita M, Inoue T, Kitai S, Yada N, Hagiwara S, Minami Y, Sakurai T, Nishida N, Kudo M (2014) Comparison of systems for assessment of post-therapeutic response to sorafenib for hepatocellular carcinoma. J Gastroenterol 49(12):1578–1587. https://doi.org/10.1007/s00535-014-0936-0

Atassi B, Bangash AK, Bahrani A, Pizzi G, Lewandowski RJ, Ryu RK, Sato KT, Gates VL, Mulcahy MF, Kulik L, Miller F, Yaghmai V, Murthy R, Larson A, Omary RA, Salem R (2008) Multimodality imaging following 90Y radioembolization: a comprehensive review and pictorial essay. Radiographics 28(1):81–99. https://doi.org/10.1148/rg.281065721

Bali MA, Metens T, Denolin V, Delhaye M, Demetter P, Closset J, Matos C (2011) Tumoral and nontumoral pancreas: correlation between quantitative dynamic contrast-enhanced MR imaging and histopathologic parameters. Radiology 261(2):456–466. https://doi.org/10.1148/radiol.11103515

Bonekamp S, Jolepalem P, Lazo M, Gulsun MA, Kiraly AP, Kamel IR (2011a) Hepatocellular carcinoma: response to TACE assessed with semiautomated volumetric and functional analysis of diffusion-weighted and contrast-enhanced MR imaging data. Radiology 260(3):752–761. https://doi.org/10.1148/radiol.11102330

Bonekamp S, Shen J, Salibi N, Lai HC, Geschwind J, Kamel IR (2011b) Early response of hepatic malignancies to locoregional therapy-value of diffusion-weighted magnetic resonance imaging and proton magnetic resonance spectroscopy. J Comput Assist Tomogr 35(2):167–173. https://doi.org/10.1097/RCT.0b013e3182004bfb

Bonekamp S, Halappa VG, Geschwind JF, Li Z, Corona-Villalobos CP, Reyes D, Bhagat N, Cosgrove DP, Pawlik TM, Mezey E, Eng J, Kamel IR (2013) Unresectable hepatocellular carcinoma: MR imaging after intraarterial therapy. Part II. Response stratification using volumetric functional criteria after intraarterial therapy. Radiology 268(2):431–439. https://doi.org/10.1148/radiol.13121637

Bonekamp D, Bonekamp S, Halappa VG, Geschwind JF, Eng J, Corona-Villalobos CP, Pawlik TM, Kamel IR (2014) Interobserver agreement of semi-automated and manual measurements of functional MRI metrics of treatment response in hepatocellular carcinoma. Eur J Radiol 83(3):487–496. https://doi.org/10.1016/j.ejrad.2013.11.016

Boninsegna E, Negrelli R, Zamboni GA, Avesani G, Manfredi R, Pozzi-Mucelli R (2017) Assessing treatment response in pancreatic cancer: role of different imaging criteria. In: ECR 2017

Braren R, Altomonte J, Settles M, Neff F, Esposito I, Ebert O, Schwaiger M, Rummeny E, Steingoetter A (2011) Validation of preclinical multiparametric imaging for prediction of necrosis in hepatocellular carcinoma after embolization. J Hepatol 55(5):1034–1040. https://doi.org/10.1016/j.jhep.2011.01.049

Bruix J, Sherman M, Llovet JM, Beaugrand M, Lencioni R, Burroughs AK, Christensen E, Pagliaro L, Colombo M, Rodes J (2001) Clinical management of hepatocellular carcinoma. Conclusions of the Barcelona-2000 EASL conference. European Association for the Study of the Liver. J Hepatol 35(3):421–430

Camacho JC, Kokabi N, Xing M, Prajapati HJ, El-Rayes B, Kim HS (2014) Modified response evaluation criteria in solid tumors and European Association for The Study of the Liver criteria using delayed-phase imaging at an early time point predict survival in patients with unresectable intrahepatic cholangiocarcinoma following yttrium-90 radioembolization. J Vasc Interv Radiol 25(2):256–265. https://doi.org/10.1016/j.jvir.2013.10.056

Cassinotto C, Mouries A, Lafourcade JP, Terrebonne E, Belleannee G, Blanc JF, Lapuyade B, Vendrely V, Laurent C, Chiche L, Wagner T, Sa-Cunha A, Gaye D, Trillaud H, Laurent F, Montaudon M (2014) Locally advanced pancreatic adenocarcinoma: reassessment of response with CT after neoadjuvant chemotherapy and radiation therapy. Radiology 273(1):108–116. https://doi.org/10.1148/radiol.14132914

Chalian H, Tochetto SM, Tore HG, Rezai P, Yaghmai V (2012) Hepatic tumors: region-of-interest versus volumetric analysis for quantification of attenuation at CT. Radiology 262(3):853–861. https://doi.org/10.1148/radiol.11110106

Chapiro J, Wood LD, Lin M, Duran R, Cornish T, Lesage D, Charu V, Schernthaner R, Wang Z, Tacher V, Savic LJ, Kamel IR, Geschwind JF (2014) Radiologic-pathologic analysis of contrast-enhanced and diffusion-weighted MR imaging in patients with HCC after TACE: diagnostic accuracy of 3D quantitative image analysis. Radiology 273(3):746–758. https://doi.org/10.1148/radiol.14140033

Chen CY, Li CW, Kuo YT, Jaw TS, Wu DK, Jao JC, Hsu JS, Liu GC (2006) Early response of hepatocellular carcinoma to transcatheter arterial chemoembolization: choline levels and MR diffusion constants—initial experience. Radiology 239(2):448–456. https://doi.org/10.1148/radiol.2392042202

Chen G, Ma DQ, He W, Zhang BF, Zhao LQ (2008) Computed tomography perfusion in evaluating the therapeutic effect of transarterial chemoembolization for hepatocellular carcinoma. World J Gastroenterol 14(37):5738–5743

Chen BB, Tien YW, Chang MC, Cheng MF, Chang YT, Wu CH, Chen XJ, Kuo TC, Yang SH, Shih IL, Lai HS, Shih TT (2016) PET/MRI in pancreatic and periampullary cancer: correlating diffusion-weighted imaging, MR spectroscopy and glucose metabolic activity with clinical stage and prognosis. Eur J Nucl Med Mol Imaging 43(10):1753–1764. https://doi.org/10.1007/s00259-016-3356-y

Chen X, Oshima K, Schott D, Wu H, Hall W, Song Y, Tao Y, Li D, Zheng C, Knechtges P, Erickson B, Li XA (2017) Assessment of treatment response during chemoradiation therapy for pancreatic cancer based on

quantitative radiomic analysis of daily CTs: an exploratory study. PLoS One 12(6):e0178961. https://doi.org/10.1371/journal.pone.0178961

Choi H, Charnsangavej C, de Castro Faria S, Tamm EP, Benjamin RS, Johnson MM, Macapinlac HA, Podoloff DA (2004) CT evaluation of the response of gastrointestinal stromal tumors after imatinib mesylate treatment: a quantitative analysis correlated with FDG PET findings. AJR Am J Roentgenol 183(6):1619–1628. https://doi.org/10.2214/ajr.183.6.01831619

Choi H, Charnsangavej C, Faria SC, Macapinlac HA, Burgess MA, Patel SR, Chen LL, Podoloff DA, Benjamin RS (2007) Correlation of computed tomography and positron emission tomography in patients with metastatic gastrointestinal stromal tumor treated at a single institution with imatinib mesylate: proposal of new computed tomography response criteria. J Clin Oncol 25(13):1753–1759. https://doi.org/10.1200/jco.2006.07.3049

Choi MH, Lee YJ, Yoon SB, Choi JI, Jung SE, Rha SE (2018) MRI of pancreatic ductal adenocarcinoma: texture analysis of T2-weighted images for predicting long-term outcome. Abdominal Radiol (New York). https://doi.org/10.1007/s00261-018-1681-2

Ciaravino V, Cardobi N, DER R, Capelli P, Melisi D, Simionato F, Marchegiani G, Salvia R, D'Onofrio M (2018) CT texture analysis of ductal adenocarcinoma downstaged after chemotherapy. Anticancer Res 38(8):4889–4895. https://doi.org/10.21873/anticanres.12803

Corona-Villalobos CP, Kamel IR (2014) Functional volumetric MRI in assessing treatment response to intra-arterial therapy of primary and secondary liver tumors. J Comput Assist Tomogr 38(4):513–517. https://doi.org/10.1097/rct.0000000000000072

Cuneo KC, Chenevert TL, Ben-Josef E, Feng MU, Greenson JK, Hussain HK, Simeone DM, Schipper MJ, Anderson MA, Zalupski MM, Al-Hawary M, Galban CJ, Rehemtulla A, Feng FY, Lawrence TS, Ross BD (2014) A pilot study of diffusion-weighted MRI in patients undergoing neoadjuvant chemoradiation for pancreatic cancer. Translational Oncol 7(5):644–649. https://doi.org/10.1016/j.tranon.2014.07.005

Di Bisceglie AM (1997) Hepatitis C and hepatocellular carcinoma. Hepatology 26(3 Suppl 1):34s–38s. https://doi.org/10.1002/hep.510260706

Eisenhauer EA, Therasse P, Bogaerts J, Schwartz LH, Sargent D, Ford R, Dancey J, Arbuck S, Gwyther S, Mooney M, Rubinstein L, Shankar L, Dodd L, Kaplan R, Lacombe D, Verweij J (2009) New response evaluation criteria in solid tumours: revised RECIST guideline (version 1.1). Eur J Cancer (Oxford, England: 1990) 45(2):228–247. https://doi.org/10.1016/j.ejca.2008.10.026

Epelbaum R, Frenkel A, Haddad R, Sikorski N, Strauss LG, Israel O, Dimitrakopoulou-Strauss A (2013) Tumor aggressiveness and patient outcome in cancer of the pancreas assessed by dynamic 18F-FDG PET/CT. J Nucl Med 54(1):12–18. https://doi.org/10.2967/jnumed.112.107466

Fattahi R, Balci NC, Perman WH, Hsueh EC, Alkaade S, Havlioglu N, Burton FR (2009) Pancreatic diffusion-weighted imaging (DWI): comparison between mass-forming focal pancreatitis (FP), pancreatic cancer (PC), and normal pancreas. J Magn Reson Imaging 29(2):350–356. https://doi.org/10.1002/jmri.21651

Gillen S, Schuster T, Meyer Zum Buschenfelde C, Friess H, Kleeff J (2010) Preoperative/neoadjuvant therapy in pancreatic cancer: a systematic review and meta-analysis of response and resection percentages. PLoS Med 7(4):e1000267. https://doi.org/10.1371/journal.pmed.1000267

Gillmore R, Stuart S, Kirkwood A, Hameeduddin A, Woodward N, Burroughs AK, Meyer T (2011) EASL and mRECIST responses are independent prognostic factors for survival in hepatocellular cancer patients treated with transarterial embolization. J Hepatol 55(6):1309–1316. https://doi.org/10.1016/j.jhep.2011.03.007

Gonzalez-Guindalini FD, Botelho MP, Harmath CB, Sandrasegaran K, Miller FH, Salem R, Yaghmai V (2013) Assessment of liver tumor response to therapy: role of quantitative imaging. Radiographics 33(6):1781–1800. https://doi.org/10.1148/rg.336135511

Guo Z, Zhang Q, Li X, Jing Z (2015) Intravoxel incoherent motion diffusion weighted MR imaging for monitoring the instantly therapeutic efficacy of radiofrequency ablation in rabbit VX2 tumors without evident links between conventional perfusion weighted images. PLoS One 10(5):e0127964. https://doi.org/10.1371/journal.pone.0127964

Halappa VG, Bonekamp S, Corona-Villalobos CP, Li Z, Mensa M, Reyes D, Eng J, Bhagat N, Pawlik TM, Geschwind JF, Kamel IR (2012) Intrahepatic cholangiocarcinoma treated with local-regional therapy: quantitative volumetric apparent diffusion coefficient maps for assessment of tumor response. Radiology 264(1):285–294. https://doi.org/10.1148/radiol.12112142

Hayano K, Lee SH, Sahani DV (2015) Imaging for assessment of treatment response in hepatocellular carcinoma: Current update. Indian J Radiol Imaging 25(2):121–128. https://doi.org/10.4103/0971-3026.155835

Hunt SJ, Yu W, Weintraub J, Prince MR, Kothary N (2009) Radiologic monitoring of hepatocellular carcinoma tumor viability after transhepatic arterial chemoembolization: estimating the accuracy of contrast-enhanced cross-sectional imaging with histopathologic correlation. J Vasc Interv Radiol 20(1):30–38. https://doi.org/10.1016/j.jvir.2008.09.034

Hurley JD, Ellison EH (1960) Chemotherapy of solid cancer arising from the gastro-intestinal tract. Ann Surg 152:568–582

Ichikawa T, Haradome H, Hachiya J, Nitatori T, Araki T (1998) Diffusion-weighted MR imaging with a single-shot echoplanar sequence: detection and characterization of focal hepatic lesions. Am J Roentgenol 170(2):397–402. https://doi.org/10.2214/ajr.170.2.9456953

Iwatsuki S, Gordon RD, Shaw BW Jr, Starzl TE (1985) Role of liver transplantation in cancer therapy. Ann Surg 202(4):401–407

Joo I, Lee JM, Han JK, Choi BI (2014) Intravoxel incoherent motion diffusion-weighted MR imaging for monitoring the therapeutic efficacy of the vascular disrupting agent CKD-516 in rabbit VX2 liver tumors. Radiology 272(2):417–426. https://doi.org/10.1148/radiol.14131165

Kamel IR, Bluemke DA, Eng J, Liapi E, Messersmith W, Reyes DK, Geschwind J-FH (2006) The role of functional MR imaging in the assessment of tumor response after chemoembolization in patients with hepatocellular carcinoma. J Vasc Interv Radiol 17(3):505–512. https://doi.org/10.1097/01.RVI.0000200052.02183.92

Kamel IR, Reyes DK, Liapi E, Bluemke DA, Geschwind JF (2007) Functional MR imaging assessment of tumor response after 90Y microsphere treatment in patients with unresectable hepatocellular carcinoma. J Vasc Interv Radiol 18(1 Pt 1):49–56. https://doi.org/10.1016/j.jvir.2006.10.005

Kamel IR, Liapi E, Reyes DK, Zahurak M, Bluemke DA, Geschwind J-FH (2009) Unresectable hepatocellular carcinoma: serial early vascular and cellular changes after transarterial chemoembolization as detected with MR imaging. Radiology 250(2):466–473. https://doi.org/10.1148/radiol.2502072222

Katz MH, Fleming JB, Bhosale P, Varadhachary G, Lee JE, Wolff R, Wang H, Abbruzzese J, Pisters PW, Vauthey JN, Charnsangavej C, Tamm E, Crane CH, Balachandran A (2012) Response of borderline resectable pancreatic cancer to neoadjuvant therapy is not reflected by radiographic indicators. Cancer 118(23):5749–5756. https://doi.org/10.1002/cncr.27636

Kele PG, van der Jagt EJ (2010) Diffusion weighted imaging in the liver. World J Gastroenterol 16(13):1567–1576

Kim JW, Seong J, Yun M, Lee IJ, Yoon HI, Cho HJ, Han KH (2012a) Usefulness of positron emission tomography with fluorine-18-fluorodeoxyglucose in predicting treatment response in unresectable hepatocellular carcinoma patients treated with external beam radiotherapy. Int J Radiat Oncol Biol Phys 82(3):1172–1178. https://doi.org/10.1016/j.ijrobp.2010.11.076

Kim SH, Won KS, Choi BW, Jo I, Zeon SK, Chung WJ, Kwon JH (2012b) Usefulness of F-18 FDG PET/CT in the evaluation of early treatment response after interventional therapy for hepatocellular carcinoma. Nucl Med Mol Imaging 46(2):102–110. https://doi.org/10.1007/s13139-012-0138-8

Kim JH, Lee JM, Park JH, Kim SC, Joo I, Han JK, Choi BI (2013) Solid pancreatic lesions: characterization by using timing bolus dynamic contrast-enhanced MR imaging assessment—a preliminary study. Radiology 266(1):185–196. https://doi.org/10.1148/radiol.12120111

Kudo M, Kubo S, Takayasu K, Sakamoto M, Tanaka M, Ikai I, Furuse J, Nakamura K, Makuuchi M (2010) Response Evaluation Criteria in Cancer of the Liver (RECICL) proposed by the Liver Cancer Study Group of Japan (2009 Revised Version). Hepatol Res 40(7):686–692. https://doi.org/10.1111/j.1872-034X.2010.00674.x

Kuo YT, Li CW, Chen CY, Jao J, Wu DK, Liu GC (2004) In vivo proton magnetic resonance spectroscopy of large focal hepatic lesions and metabolite change of hepatocellular carcinoma before and after transcatheter arterial chemoembolization using 3.0-T MR scanner. J Magn Reson Imaging 19(5):598–604. https://doi.org/10.1002/jmri.20046

Lee SS, Byun JH, Park BJ, Park SH, Kim N, Park B, Kim JK, Lee M-G (2008) Quantitative analysis of diffusion-weighted magnetic resonance imaging of the pancreas: usefulness in characterizing solid pancreatic masses. J Magn Reson Imaging 28(4):928–936. https://doi.org/10.1002/jmri.21508

Lencioni R, Llovet JM (2010) Modified RECIST (mRECIST) assessment for hepatocellular carcinoma. Semin Liver Dis 30(1):52–60. https://doi.org/10.1055/s-0030-1247132

Lencioni R, Montal R, Torres F, Park JW, Decaens T, Raoul JL, Kudo M, Chang C, Rios J, Boige V, Assenat E, Kang YK, Lim HY, Walters I, Llovet JM (2017) Objective response by mRECIST as a predictor and potential surrogate end-point of overall survival in advanced HCC. J Hepatol 66(6):1166–1172. https://doi.org/10.1016/j.jhep.2017.01.012

Li D, Xie K, Wolff R, Abbruzzese JL (2004) Pancreatic cancer. Lancet (London, England) 363(9414):1049–1057. https://doi.org/10.1016/s0140-6736(04)15841-8

Li H, Zeng MS, Zhou KR, Jin DY, Lou WH (2006) Pancreatic adenocarcinoma: signs of vascular invasion determined by multi-detector row CT. Br J Radiol 79(947):880–887. https://doi.org/10.1259/bjr/19684199

Lin M, Tian M-M, Zhang W-P, Xu L, Jin P (2016) Predictive values of diffusion-weighted imaging and perfusion-weighted imaging in evaluating the efficacy of transcatheter arterial chemoembolization for hepatocellular carcinoma. OncoTargets Ther 9:7029–7037. https://doi.org/10.2147/OTT.S112555

Liver Cancer Survival Rates (n.d.). https://www.cancer.org/cancer/liver-cancer/detection-diagnosis-staging/survival-rates.html

Martín Noguerol T, Sánchez-González J, Martínez Barbero JP, García-Figueiras R, Baleato-González S, Luna A (2016) Clinical imaging of tumor metabolism with ^{1}H magnetic resonance spectroscopy. Magnetic Resonance Imaging Clinics 24(1):57–86. https://doi.org/10.1016/j.mric.2015.09.002

Miles KA, Hayball M, Dixon AK (1991) Colour perfusion imaging: a new application of computed tomography. Lancet (London, England) 337(8742):643–645

Miller AB, Hoogstraten B, Staquet M, Winkler A (1981) Reporting results of cancer treatment. Cancer 47(1):207–214

Minocha J, Lewandowski RJ (2015) Assessing imaging response to therapy. Radiol Clin North Am 53(5):1077–1088. https://doi.org/10.1016/j.rcl.2015.05.010

Nagamachi S, Nishii R, Wakamatsu H, Mizutani Y, Kiyohara S, Fujita S, Futami S, Sakae T, Furukoji E, Tamura S, Arita H, Chijiiwa K, Kawai K (2013) The usefulness of (18)F-FDG PET/MRI fusion image in diagnosing pancreatic tumor: comparison with (18) F-FDG PET/CT. Ann Nucl Med 27(6):554–563. https://doi.org/10.1007/s12149-013-0719-3

Niwa T, Ueno M, Ohkawa S, Yoshida T, Doiuchi T, Ito K, Inoue T (2009) Advanced pancreatic cancer: the use of the apparent diffusion coefficient to predict response to chemotherapy. Br J Radiol 82(973):28–34. https://doi.org/10.1259/bjr/43911400

Ortega Lopez N (2015) PET/computed tomography in evaluation of transarterial chemoembolization. PET clinics 10(4):507–517. https://doi.org/10.1016/j.cpet.2015.05.006

Pancreatic Cancer Survival Rates, by Stage (n.d.). https://www.cancer.org/cancer/pancreatic-cancer/detection-diagnosis-staging/survival-rates.html

Pandey A, Pandey P, Aliyari Ghasabeh M, Najmi Varzaneh F, Shao N, Khoshpouri P, Zarghampour M, Fouladi DF, Liddell R, Kamel IR (2018) Unresectable intrahepatic cholangiocarcinoma: multiparametric MR imaging to predict patient survival. Radiology 288(1):109–117. https://doi.org/10.1148/radiol.2018171593

Patel M, Hoffe S, Malafa M, Hodul P, Klapman J, Centeno B, Kim J, Helm J, Valone T, Springett G (2011) Neoadjuvant GTX chemotherapy and IMRT-based chemoradiation for borderline resectable pancreatic cancer. J Surg Oncol 104(2):155–161. https://doi.org/10.1002/jso.21954

Rhee TK, Naik NK, Deng J, Atassi B, Mulcahy MF, Kulik LM, Ryu RK, Miller FH, Larson AC, Salem R, Omary RA (2008) Tumor response after yttrium-90 radioembolization for hepatocellular carcinoma: comparison of diffusion-weighted functional MR imaging with anatomic MR imaging. J Vasc Interv Radiol 19(8):1180–1186. https://doi.org/10.1016/j.jvir.2008.05.002

Riaz A, Miller FH, Kulik LM, Nikolaidis P, Yaghmai V, Lewandowski RJ, Mulcahy MF, Ryu RK, Sato KT, Gupta R, Wang E, Baker T, Abecassis M, Benson AB 3rd, Nemcek AA Jr, Omary R, Salem R (2010) Imaging response in the primary index lesion and clinical outcomes following transarterial locoregional therapy for hepatocellular carcinoma. JAMA 303(11):1062–1069. https://doi.org/10.1001/jama.2010.262

Ronot M, Bouattour M, Wassermann J, Bruno O, Dreyer C, Larroque B, Castera L, Vilgrain V, Belghiti J, Raymond E, Faivre S (2014) Alternative response criteria (Choi, European association for the study of the liver, and modified Response Evaluation Criteria in Solid Tumors [RECIST]) versus RECIST 1.1 in patients with advanced hepatocellular carcinoma treated with sorafenib. Oncologist 19(4):394–402. https://doi.org/10.1634/theoncologist.2013-0114

Saha SK, Zhu AX, Fuchs CS, Brooks GA (2016) Forty-year trends in cholangiocarcinoma incidence in the U.S.: intrahepatic disease on the rise. Oncologist 21(5):594–599. https://doi.org/10.1634/theoncologist.2015-0446

Sahani DV, Bonaffini PA, Catalano OA, Guimaraes AR, Blake MA (2012) State-of-the-art PET/CT of the pancreas: current role and emerging indications. Radiographics 32(4):1133–1158.; ; discussion 1158–1160. https://doi.org/10.1148/rg.324115143

Schwartz LH, Seymour L, Litiere S, Ford R, Gwyther S, Mandrekar S, Shankar L, Bogaerts J, Chen A, Dancey J, Hayes W, Hodi FS, Hoekstra OS, Huang EP, Lin N, Liu Y, Therasse P, Wolchok JD, de Vries E (2016) RECIST 1.1—standardisation and disease-specific adaptations: perspectives from the RECIST Working Group. Eur J Cancer (Oxford England: 1990) 62:138–145. https://doi.org/10.1016/j.ejca.2016.03.082

Seidensticker R, Seidensticker M, Doegen K, Mohnike K, Schutte K, Stubs P, Kettner E, Pech M, Amthauer H, Ricke J (2016) Extensive use of interventional therapies improves survival in unresectable or recurrent intrahepatic cholangiocarcinoma. Gastroenterol Res Pract 2016:8732521. https://doi.org/10.1155/2016/8732521

Shirota N, Saito K, Sugimoto K, Takara K, Moriyasu F, Tokuuye K (2016) Intravoxel incoherent motion MRI as a biomarker of sorafenib treatment for advanced hepatocellular carcinoma: a pilot study. Cancer Imaging 16(1). https://doi.org/10.1186/s40644-016-0059-3

Song HJ, Cheng JY, Hu SL, Zhang GY, Fu Y, Zhang YJ (2015) Value of 18F-FDG PET/CT in detecting viable tumour and predicting prognosis of hepatocellular carcinoma after TACE. Clin Radiol 70(2):128–137. https://doi.org/10.1016/j.crad.2014.09.020

Sun X-J, Quan X-Y, Huang F-H, Xu Y-K (2005) Quantitative evaluation of diffusion-weighted magnetic resonance imaging of focal hepatic lesions. World J Gastroenterol 11(41):6535–6537. https://doi.org/10.3748/wjg.v11.i41.6535

Sung PS, Park HL, Yang K, Hwang S, Song MJ, Jang JW, Choi JY, Yoon SK, Yoo IR, Bae SH (2018) (18)F-fluorodeoxyglucose uptake of hepatocellular carcinoma as a prognostic predictor in patients with sorafenib treatment. Eur J Nucl Med Mol Imaging 45(3):384–391. https://doi.org/10.1007/s00259-017-3871-5

Survival Rates for Bile Duct Cancer (2018). https://www.cancer.org/cancer/bile-duct-cancer/detection-diagnosis-staging/survival-by-stage.html. Published 2018

Syha R, Grozinger G, Grosse U, Maurer M, Zender L, Horger M, Nikolaou K, Ketelsen D (2016) Parenchymal blood volume assessed by C-arm-based computed tomography in immediate posttreatment evaluation of drug-eluting bead transarterial chemoembolization in hepatocellular carcinoma. Invest Radiol 51(2):121–126. https://doi.org/10.1097/rli.0000000000000215

Sylvester R (1980) WHO handbook for reporting results of cancer treatment: WHO offset publication #48 World Health Organization, Geneva, 1979, 45 pages, 6 Swiss Francs. Control Clin Trials 1(3):276–277. https://doi.org/10.1016/0197-2456(80)90009-4

Therasse P, Arbuck SG, Eisenhauer EA, Wanders J, Kaplan RS, Rubinstein L, Verweij J, Van Glabbeke M, van Oosterom AT, Christian MC, Gwyther SG (2000) New guidelines to evaluate the response to treatment in solid tumors. European Organization for Research and Treatment of Cancer, National Cancer Institute of the United States, National Cancer Institute of Canada. J Natl Cancer Inst 92(3):205–216

Tovoli F, Renzulli M, Negrini G, Brocchi S, Ferrarini A, Andreone A, Benevento F, Golfieri R, Morselli-Labate AM, Mastroroberto M, Badea RI, Piscaglia F (2018) Inter-operator variability and source of errors in tumour response assessment for hepatocellular carcinoma treated with sorafenib. Eur Radiol 28(9):3611–3620. https://doi.org/10.1007/s00330-018-5393-3

Trajkovic-Arsic M, Heid I, Steiger K, Gupta A, Fingerle A, Worner C, Teichmann N, Sengkwawoh-Lueong S, Wenzel P, Beer AJ, Esposito I, Braren R, Siveke JT (2017) Apparent Diffusion Coefficient (ADC) predicts therapy response in pancreatic ductal adenocarcinoma. Sci Rep 7(1):17038. https://doi.org/10.1038/s41598-017-16826-z

Vecchiarelli S, Macchini M, Grassi E, Ferroni F, Ciccarese F, Calculli L, Ricci C, Casadei R, Pezzilli R, Biasco G, Marco MD (2013) Comparing recist and Choi's criteria to evaluate radiological response to chemotherapy in patients with advanced pancreatic cancer. J Clin Oncol 31(15 Suppl):e15069. https://doi.org/10.1200/jco.2013.31.15_suppl.e15069

ter Voert EGW, Heijmen L, van Laarhoven HWM, Heerschap A (2011) In vivo magnetic resonance spectroscopy of liver tumors and metastases. World J Gastroenterol 17(47):5133–5149. https://doi.org/10.3748/wjg.v17.i47.5133

Vossen JA, Buijs M, Kamel IR (2006) Assessment of tumor response on MR imaging after locoregional therapy. Tech Vasc Interv Radiol 9(3):125–132. https://doi.org/10.1053/j.tvir.2007.02.004

Wahl RL, Jacene H, Kasamon Y, Lodge MA (2009) From RECIST to PERCIST: evolving considerations for PET response criteria in solid tumors. J Nucl Med 50(Suppl 1):122s–150s. https://doi.org/10.2967/jnumed.108.057307

Watanabe H, Kanematsu M, Goshima S, Kajita K, Kawada H, Noda Y, Tatahashi Y, Kawai N, Kondo H, Moriyama N (2014) Characterizing focal hepatic lesions by free-breathing intravoxel incoherent motion MRI at 3.0 T. Acta Radiol (Stockholm Sweden: 1987) 55(10):1166–1173. https://doi.org/10.1177/0284185113514966

Weber SM, Ribero D, O'Reilly EM, Kokudo N, Miyazaki M, Pawlik TM (2015) Intrahepatic cholangiocarcinoma: expert consensus statement. HPB (Oxford) 17(8):669–680. https://doi.org/10.1111/hpb.12441

Weng Z, Ertle J, Zheng S, Lauenstein T, Mueller S, Bockisch A, Gerken G, Yang D, Schlaak JF (2013) Choi criteria are superior in evaluating tumor response in patients treated with transarterial radioembolization for hepatocellular carcinoma. Oncol Lett 6(6):1707–1712. https://doi.org/10.3892/ol.2013.1612

Woo S, Lee JM, Yoon JH, Joo I, Han JK, Choi BI (2014) Intravoxel incoherent motion diffusion-weighted MR imaging of hepatocellular carcinoma: correlation with enhancement degree and histologic grade. Radiology 270(3):758–767. https://doi.org/10.1148/radiol.13130444

Wray CJ, Ahmad SA, Matthews JB, Lowy AM (2005) Surgery for pancreatic cancer: recent controversies and current practice. Gastroenterology 128(6):1626–1641

Yaghmai V, Besa C, Kim E, Gatlin JL, Siddiqui NA, Taouli B (2013) Imaging assessment of hepatocellular carcinoma response to locoregional and systemic therapy. AJR Am J Roentgenol 201(1):80–96. https://doi.org/10.2214/ajr.13.10706

Yang K, Zhang XM, Yang L, Xu H, Peng J (2016a) Advanced imaging techniques in the therapeutic response of transarterial chemoembolization for hepatocellular carcinoma. World J Gastroenterol 22(20):4835–4847. https://doi.org/10.3748/wjg.v22.i20.4835

Yang Z, Sun S, Chen Y, Li R (2016b) Application of single voxel 1H magnetic resonance spectroscopy in hepatic benign and malignant lesions. Med Sci Monit 22:5003–5010

Yue Y, Osipov A, Fraass B, Sandler H, Zhang X, Nissen N, Hendifar A, Tuli R (2017) Identifying prognostic intratumor heterogeneity using pre- and post-radiotherapy 18F-FDG PET images for pancreatic cancer patients. J Gastrointest Oncol 8(1):127–138. https://doi.org/10.21037/jgo.2016.12.04

Therapy Response Imaging in Genitourinary Malignancies

Katherine M. Krajewski

Contents

Abstract

Renal cell carcinoma, bladder cancer, and prostate cancer are each among the top ten causes of cancer death in men in the United States (American Cancer Society, Cancer Facts & Figures 2018, Atlanta: American Cancer Society, 2018). Fortunately, there are multiple therapies approved by the U.S. Food and Drug Administration (FDA) for each of these common cancers, several of which have been approved recently. In this context, imaging assessment of response to treatment will become increasingly important, as multiple options are available for patients who do not show evidence of response or benefit from a particular agent. Substantial efforts to optimize imaging response assessment in treatment-specific settings have been published in each of these genitourinary malignancies.

In this chapter, imaging response assessment methods in renal cell carcinoma, bladder cancer, and prostate cancer will be reviewed, including a discussion of current therapeutic approaches in each disease, response criteria and associated pitfalls, and emerging challenges.

K. M. Krajewski (✉)
Department of Imaging, Dana-Farber Cancer Institute, Harvard Medical School, Boston, MA, USA

Department of Radiology, Brigham and Women's Hospital, Harvard Medical School, Boston, MA, USA
e-mail: kmkrajewski@bwh.harvard.edu

M. Nishino (ed.), *Therapy Response Imaging in Oncology*, Medical Radiology, Diagnostic Imaging,
https://doi.org/10.1007/978-3-030-31171-1_9

1 Renal Cell Carcinoma Treatment Landscape

Currently approved agents for the treatment of advanced or metastatic renal cell carcinoma (mRCC) largely target either neoangiogenesis or immune surveillance escape, two drivers of this disease (Calvo et al. 2018; Mosillo et al. 2018). Vascular endothelial growth factor (VEGF) inhibitors, such as pazopanib or sunitinib, have been commonly used in the first-line treatment of metastatic clear cell RCC, though the recently approved immune checkpoint blocker (ICB) combination of nivolumab and ipilimumab has become the standard of care in patients with intermediate or poor risk disease (Motzer et al. 2018; Powles et al. 2017a, Fig. 1). Therapies combining immune checkpoint inhibition and multi-tyrosine kinase inhibitors are also recently approved, such as avelumab plus axitinib (Motzer et al. 2019). Since the treatment landscape in mRCC is rapidly evolving to include molecularly targeted agents, ICB and combination therapies, several new questions have arisen, including: (a) what is the optimal drug selection and sequencing for individual patients? (b) what are the relevant clinical, imaging, and/ or molecular biomarkers in drug selection and follow-up? and (c) what are the optimal treatment response assessment methods by imaging?

Additionally, other types of novel therapeutics remain under investigation, which have the potential to further complicate treatment algorithms and associated imaging response assessment. For example, radium-223 dichloride has been investigated in combination with VEGF-targeted therapy in mRCC patients with bone metastases (McKay et al. 2018a). Bone

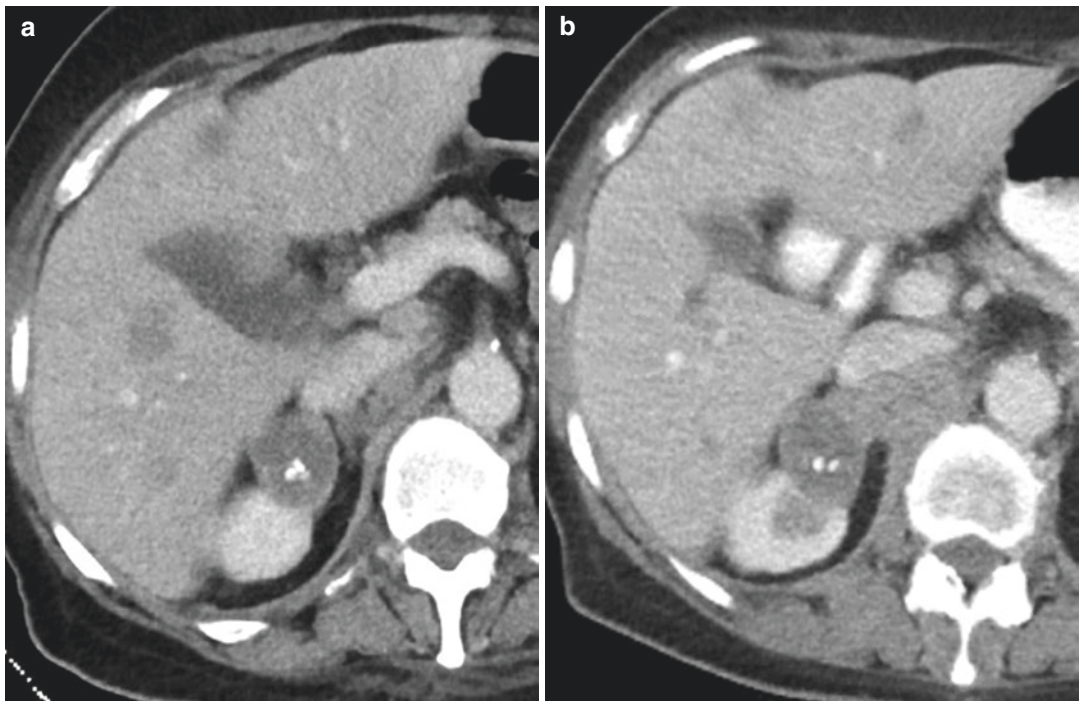

Fig. 1 68-year-old woman with poor risk, metastatic renal cell carcinoma treated with nivolumab and ipilimumab. Baseline contrast-enhanced CT (**a**) shows a right renal mass with calcification representing the primary tumor, retrocaval adenopathy, and multiple liver metastases. Follow-up contrast-enhanced CT after 12 weeks of treatment (**b**) demonstrates significantly decreased size of multiple liver metastases. The right renal mass is not significantly changed, while the retrocaval adenopathy is increased. Therapy was continued in this patient with partial response

metastases are associated with shorter survival in mRCC, with potential therapeutic implications (McKay et al. 2014). Computed tomography (CT) and [99mTc]-Technetium methylene diphosphate bone scans (BS) are usual means of bone metastasis assessment in mRCC, and overall response rate according to Response Evaluation Criteria in Solid Tumors (RECIST) version 1.1 and response according to M.D. Anderson Criteria (Fig. 2) were reported in this study (Eisenhauer et al. 2009a; Hamaoka et al. 2004). Another metabolic response assessment method, Positron Emission Tomography (PET) Response Criteria in Solid Tumors (PERCIST 1.0), has also been explored in this setting (Dibble et al. 2018), to overcome known limitations in bone metastasis response assessment using conventional methods (Padhani et al. 2017).

Adding further complexity, the advanced RCC treatment armamentarium also includes local treatments such as metastasectomy, thermal ablation, and radiotherapy in selected cases. Metastasectomy is feasible in patients with limited tumor burden and can afford patients with significant time off therapy (Karam et al. 2011). Radiotherapy of various types, including whole brain radiotherapy, stereotactic radiosurgery, and conventional and stereotactic body radiation may also be treatment options for patients with non-operable primary tumor or in selected cases of metastatic disease (Dabestani et al. 2014, Fig. 3). The potential synergistic effects of SBRT and ICB therapy are under active study (Francolini

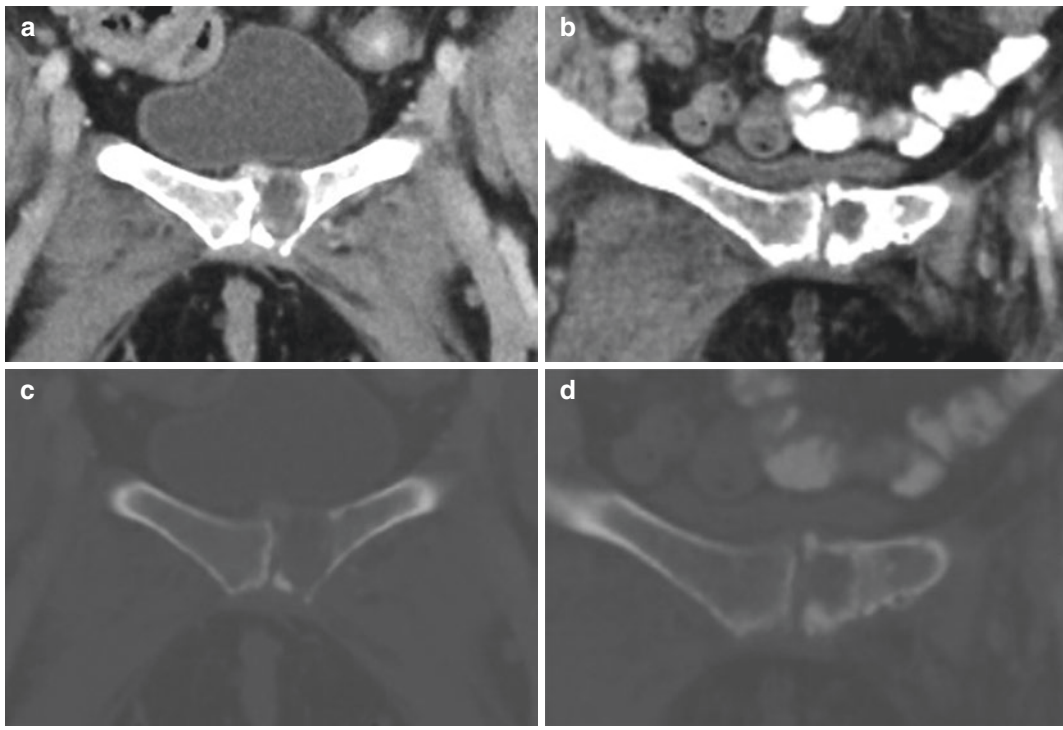

Fig. 2 68-year-old woman with metastatic renal cell carcinoma treated with nivolumab and ipilimumab, and denosumab. Baseline CT in soft tissue (**a**) and bone (**c**) windows demonstrates a lytic lesion in the left pubic bone with peripheral rim soft tissue. Follow-up CT in soft tissue (**b**) and bone (**d**) windows demonstrates peripheral rim sclerosis of this lesion, representing partial response according to M.D. Anderson bone criteria in this lesion. Partial response in this criteria is indicated by the development of a sclerotic rim around a previously lytic lesion, sclerosis of a previously undetected lesion, partial fill-in or sclerosis of a lytic lesion, or regression of a measurable lesion

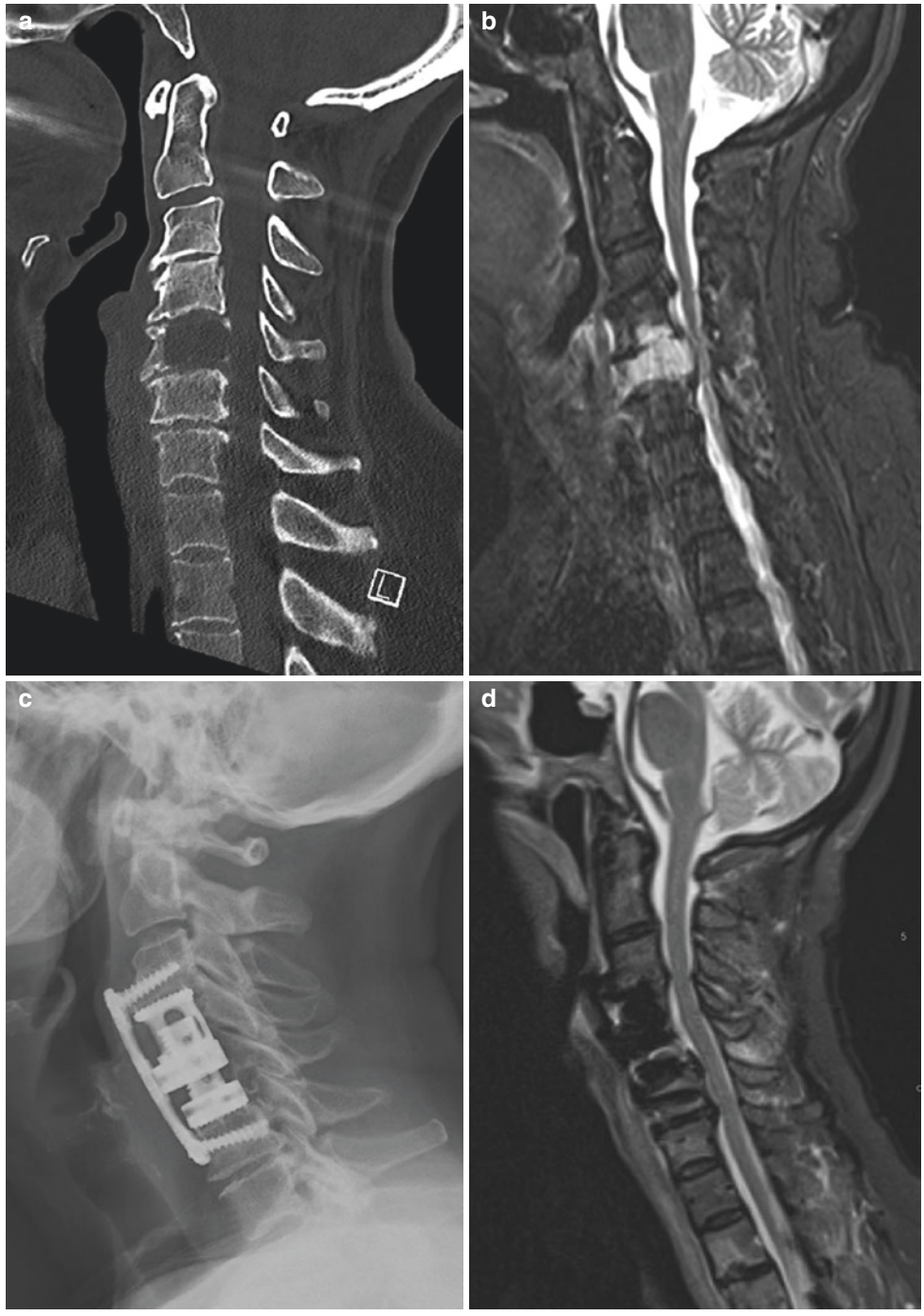

Fig. 3 68-year-old woman with metastatic renal cell carcinoma and neck pain. Baseline cervical spine CT (**a**) shows a large lytic metastasis destroying most of the C5 vertebral body. Baseline cervical spine short tau inversion recovery (STIR) MR image (**b**) shows the metastasis occupying the entire C5 vertebral body, extending superiorly to C4 and posteriorly into the left epidural space. On images not shown, the mass effaced the C4-C5 and C5-C6 left lateral recesses, narrowed neural foramina, and encased approximately 180 degrees of bilateral vertebral arteries. The patient was treated with C4 and C5 corpectomy and anterior fusion from C3 to C7 with cage reconstruction, as well as radiation to C3-C6. Follow-up radiograph (**c**) and STIR MR image (**d**) demonstrates the expected posttreatment changes

et al. 2018). It is important for radiologists to be aware of both local and systemic treatments, to best characterize response to each of these.

2 RCC Imaging Response Assessment

In clinical trials of patients with mRCC, imaging response to treatment has conventionally been assessed using the Response Evaluation Criteria In Solid Tumors (RECIST) criteria. RECIST is a common language to describe objective changes in tumor size and is widely applied across tumor and therapy types. RECIST version 1.1 has been employed in the most recent mRCC trials, though response assessments according to the original RECIST 1.0 and RECIST 1.1 have been shown to be highly concordant in RCC, when using the same target lesions or a subset by RECIST 1.1 (Krajewski et al. 2015). An important difference between RECIST 1.0 and 1.1 is the maximum number of reportable target lesions, with ten maximum and five per organ by RECIST 1.0 and five maximum and two per organ by RECIST 1.1 (Eisenhauer et al. 2009b). Interestingly, recent literature has shown that variation in target lesion selection using RECIST 1.1 may yield inconsistent or even conflicting response assessments in patients with metastatic cancer; thus, fewer target lesions according to RECIST 1.1 may not reflect overall tumor load and response (Kuhl et al. 2019).

In RECIST 1.0 and 1.1, partial response (PR) is indicated by 30% decrease in the sum diameter of target lesions compared to baseline, while progression of disease (PD) is indicated by new lesions or 20% increase in the sum diameter of target lesions compared to the nadir (Eisenhauer et al. 2009b). The stable disease designation includes patients not meeting criteria for partial response or progressive disease. Less than half of mRCC patients treated with modern therapies achieve partial response by RECIST 1.0/1.1, in the range of 10–40% of patients treated with VEGF-targeted therapies, <10% treated with mTOR inhibitors, and 25% treated with nivolumab (Motzer et al. 2008, 2013, 2015). Patients with a best response of stable disease on treatment are a heterogeneous group, including those with prolonged "clinical benefit" and prolonged time on treatment, and others who progress in the near term.

The arbitrary number of reportable target lesions, thresholds for partial response and progressive disease, and the lack of incorporated early response indicators are recognized limitations in RECIST response assessment in mRCC. In VEGF-targeted treatment, several class-specific alternative response criteria have been developed and evaluated in efforts to better separate responders and nonresponders to therapy. Some schemas have incorporated both size and density changes into the criteria (as in Choi or Morphology, Attenuation, Size and Structure {MASS} criteria), because changes in tumor vascularity/ enhancement are observed in patients treated with VEGF-targeted therapy (van der Veldt et al. 2010; Smith et al. 2010, Fig. 4). Clinical factors (such as Memorial Sloan Kettering Cancer Center Risk Factors and the International Metastatic Renal Cell Carcinoma Database Consortium model) have been combined with response assessments by RECIST and MASS to identify patients with progression-free survival of less than or greater than/equal to 1 year (Smith et al. 2013). Early modest size changes, including 10% tumor shrinkage on first follow-up imaging, have been associated with improved progression-free and overall survival outcomes (Thiam et al. 2010; Krajewski et al. 2011, 2014). While alternative criteria have shown utility in identifying patients with prolonged time to treatment failure and better outcomes, they have been less useful in optimizing progressive disease designations, thereby treatment changes.

With regard to ICB treatments in mRCC, numerous clinical trials have used and are using RECIST 1.1 to determine overall response rate and to characterize progressive disease. In the phase III study comparing nivolumab to everolimus, secondary endpoints of investigator-assessed overall response rate and progression-free survival were determined using RECIST 1.1 (Motzer et al. 2015). Of interest, patients were

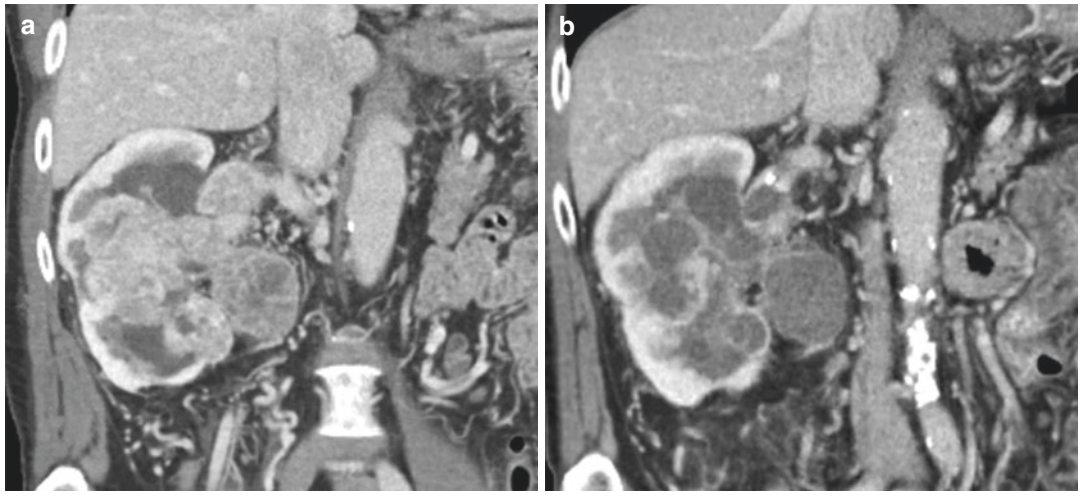

Fig. 4 72-year-old man with clear cell renal cell carcinoma, on pazopanib. Baseline coronal contrast-enhanced CT (**a**) demonstrates a large right renal mass with tumor thrombus extension to the renal vein and enlarged, heterogenous perinephric adenopathy which have moderately decreased in density (though little changed in size) on follow-up contrast-enhanced CT (**b**), representing response to treatment according to Choi criteria and favorable response according to MASS criteria

allowed to continue on treatment beyond RECIST PD if clinical benefit was assessed by the investigator and side effects were acceptable. Ongoing multicenter trials of ICBs combined with another ICB or another agent typically use RECIST 1.1 to characterize overall response rate and determine progression of disease on imaging. However, heterogeneous changes in tumor burden have been described in RCC patients treated with ICBs, and radiologic assessment of response in this treatment setting remains challenging (de Velasco et al. 2016). Atypical patterns have encountered, including increased before decreased tumor burden on treatment termed "pseudoprogression," mixed changes with new lesions, and even possible "hyperprogressive" disease (Champiat et al. 2018a). Given the unique mechanism of action of these agents which block inhibitory signals of the immune system to boost T-cell response to cancer cells, it is not surprising that differences in the underlying biology yield distinct radiologic changes and toxicities in treated patients.

The differing spectrum of patterns of response and progressive disease in patients with various malignancies treated with ICB as opposed to tyrosine kinase inhibitors has been known for greater than a decade, and modified ICB class-specific imaging response criteria have been developed. The first such criteria were termed the "immune-related response criteria" (irRC), published in 2009, which aimed to capture additional response patterns in melanoma treated with ipilimumab (Wolchok et al. 2009). These criteria employ bidirectional tumor measurements and the sum product diameters of the target lesions to quantify changes in tumor burden, with thresholds of partial response and progressive disease used in the WHO criteria, specifically ≥50% decrease in tumor burden from baseline and ≥25% increase in tumor burden from the nadir, respectively. Importantly, these criteria permitted new lesions to be incorporated into the sum product diameters of the targets rather than deeming patients with new lesions as having progressive disease. Furthermore, confirmatory scans at least 4 weeks after initial response assessment scans were advised to confirm complete response, PR and PD designations, the latter in the absence of rapid clinical

deterioration. Subsequently, immune-related RECIST (irRECIST) was developed, an adaptation using unidirectional measurements and PR/PD thresholds as in RECIST while maintaining elements of irRC pertaining to new lesions and confirmatory scans (Nishino et al. 2013). Subsequent iterations include immune RECIST (iRECIST) published by the RECIST working group and immune-modified RECIST (imRECIST) (Seymour et al. 2017; Hodi et al. 2018).

For the most part, despite the development of various immune-related criteria, primary endpoints in clinical trials of ICB continue to employ RECIST 1.1, including in RCC (Seymour et al. 2017). Alternative/adjunct immune-related criteria have been employed as secondary or exploratory endpoints in ongoing RCC trials at the author's institution and others. According to the RECIST working group, RECIST 1.1 should continue to be used as the primary criteria for response-based endpoints, at least while iRECIST is formally evaluated and validated (Seymour et al. 2017). Furthermore, use of iRECIST is recommended in the context of clinical trials rather than routine care, whereby treatment beyond RECIST 1.1- progression occurs in carefully selected instances.

3 Challenges and Emerging Approaches in RCC Response Assessment

Combination regimens, including two ICBs as well as ICB combined with VEGF-targeted agents, are being evaluated for RCC treatment in clinical trials. Five phase III trials of different combinations of ICB and VEGF-targeted agents are ongoing, most using progression-free survival as the primary study endpoint (McKay et al. 2018b). Assessing response to therapy in patients treated with combination regimens may certainly be achieved using RECIST, though it remains to be seen whether alternative immune-based response criteria better classify responders to treatment or predict outcomes, which remain questions in studies of single agent ICB. Interestingly, in a study of patients with metastatic melanoma treated with combined ipilimumab and bevacizumab, multiple imaging response assessments were studied, including size change and density change thresholds, and response according to RECIST, MASS, and Choi criteria; none of the investigated changes correlated with survival (Nishino et al. 2014). It seems useful to further study and compare RECIST and other alternative immune response assessments in mRCC treated with ICB and combination regimens, to determine whether response according to any of these correlates with outcomes. Ultimately, to help select the best candidates for ICB treatment, functional imaging with novel tracers such as zirconium-89-labeled atezolizumab (anti-PD-L1) may prove useful to predict and assess response. Future treatment algorithms may incorporate clinical, imaging-based, histologic, and genomic biomarkers at baseline, as well as changes in each of these over the course of treatment for personalized management of individual mRCC patients (Bensch et al. 2018).

Another opportunity for further refinement in RCC response assessment pertains to the optimal timing of treatment changes and "progressive disease" designations. With a number of therapies FDA-approved for mRCC, patients have many options for treatment. As such, it makes sense to better define whether patients are achieving treatment benefit early in the course of therapy, and also to more precisely determine whether a drug is still exerting a treatment effect at the time of RECIST defined progression. Measurement of tumor growth rate (TGR) has been advocated to achieve these goals (Ferté et al. 2014). In a study of mRCC patients enrolled in one of two phase III studies (sorafenib v. placebo, everolimus v. placebo), TGR was examined at four timepoints: before treatment introduction (wash-out), under (first cycle), progression (last cycle), and after treatment discontinuation (wash-out). TGR was associated with progression-free and overall survival, allowed for quantitative characterization of drug activity at the first evaluation, and TGR suggested that sorafenib still exerted antitumoral activity in patients at the time

of progression. Decreased TGR at the time of RECIST progression could provide a rationale for continuing a treatment, be it targeted therapy or an ICB.

TGR measurement may also be useful in further exploring the phenomenon termed hyperprogressive disease, or an apparent acceleration of disease pace postulated to occur in some patients treated with ICB (Champiat et al. 2018b). Multiple definitions of hyperprogression exist, including time-to-treatment failure (TTF) <2 months, >50% increase in tumor burden compared with pre-immunotherapy imaging, and >2-fold increase in progression pace; or disease progression at the first evaluation with a minimum increase in TGR of >50% (Kato et al. 2017; Champiat et al. 2017; Ferrara et al. 2018). It remains undetermined whether hyperprogression represents unresponsive, aggressive disease versus disease worsening related to the treatment, and furthermore it is challenging to differentiate pseudoprogression from true or hyperprogression on imaging (Elias et al. 2018). Additionally, the significance of new lesions has not been fully characterized, since tumor burden measurements for hyperprogression typically use target lesions according to RECIST 1.1, wherein new lesions are not added to the target lesions measurements. New lesions which develop on treatment are treated differently in the various immune response criteria; for example, added to the sum diameters in irRC, and measured and recorded separately in iRECIST. New lesions may impact survival outcomes differently than growth of existing target lesions, which may have implications for optimized response criteria (Hodi et al. 2018).

Much work remains in refining RCC response assessment, particularly in this era of immune-oncology. Consensus must be reached as to the optimal response criteria to employ for particular treatment settings. It will be helpful to further study the typical and atypical patterns of response to treatment and progression, to correlate these patterns with survival outcomes and to identify biomarkers predictive of early response, durable treatment benefit, pseudoprogression, and hyperprogression.

4 Urothelial Carcinoma of the Bladder Response Assessment

Urothelial carcinoma of the bladder is another common genitourinary malignancy in which imaging plays an important role in assessing response to treatment and guiding treatment decisions (American Cancer Society 2018). While most bladder cancer is non-muscle invasive and primarily diagnosed using a combination of cystoscopy and tissue sampling, patients with muscle-invasive and metastatic disease are commonly staged and followed-up with imaging. MRI is most frequently employed in staging muscle-invasive disease due to its superior soft tissue contrast, and MRI response to neoadjuvant treatment has been described in the literature, though post-neoadjuvant MRI prior to cystectomy may not be performed routinely (Barentsz et al. 1998; Schrier et al. 2006; Choueiri et al. 2014).

In a phase II study of dose-dense methotrexate, vinblastine, adriamycin, and cisplatin (MVAC) in muscle-invasive bladder cancer, radiologic response was assessed with pre- and post-neoadjuvant treatment MRI, and radiologic response correlated with disease-free survival (Choueiri et al. 2014). Radiologic response in this circumstance, indicated by >50% decrease in the product of the longest perpendicular diameters, delayed enhancement of residual tumor, and normalization of node size if enlarged nodes were present was felt to offer complimentary prognostic information to pathologic response, though the need for prospective validation was acknowledged (Fig. 5). Other MRI parameters have been explored as biomarkers of response in the neoadjuvant setting, including relative enhancement at venous phase imaging which was significantly different among pathologic responder types (Chakiba et al. 2015) and median plasma perfusion, which differed in patients with residual tumor versus areas of treatment effect (Donaldson et al. 2013). MRI predictors of response on pretreatment MRI have also been explored, including apparent diffusion coefficient values at diffusion-weighted imaging (Yoshida et al. 2012). The role of imaging in

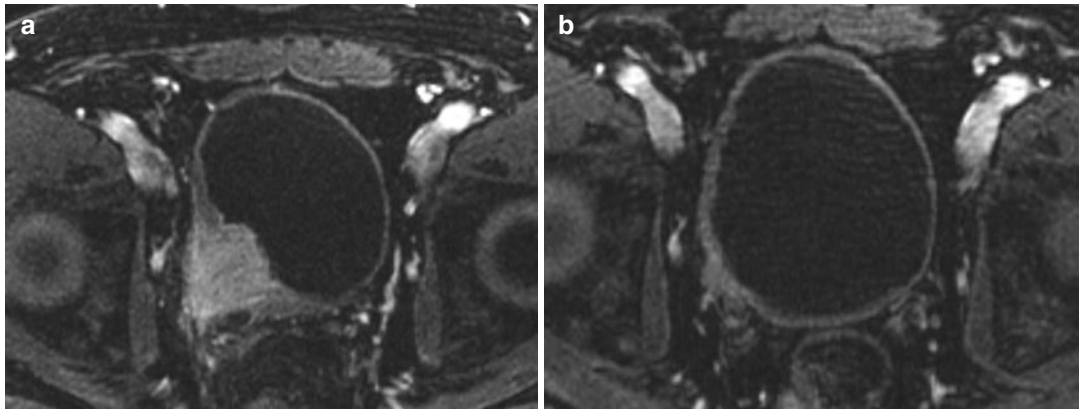

Fig. 5 60-year-old man with muscle-invasive bladder cancer treated with neoadjuvant, dose dense MVAC. Baseline fat-saturated T1W post contrast MRI of the pelvis (**a**) demonstrates a mass at the right vesicoureteral junction extending through the wall of the bladder and into the perivesical fat (T3b). Right hydroureteronephrosis was present (not shown). After neoadjuvant treatment with ddMVAC, 10 week follow-up fat-saturated T1W post contrast MRI of the pelvis follow-up MRI (**b**) significant decrease in size of the bladder mass with a residual small enhancing nodule. No residual carcinoma was identified at cystoprostatectomy

patient selection for bladder conserving therapies has not yet been defined.

In terms of recurrent/metastatic disease, few bladder cancer patients present with metastatic disease, though one third of patients with muscle-invasive disease treated with cystectomy relapse (Moschini et al. 2016). Metastasectomy may be useful for selected patients, but those with disseminated disease are generally treated with systemic therapy (National Comprehensive Cancer Network 2018a). Chemotherapy options depend on patient comorbidities, but combination regimens include gemcitabine and cisplatin, and dose-dense MVAC with growth factor support. For patients who are cisplatin ineligible, options include gemcitabine and carboplatin, atezolizumab or pembrolizumab (National Comprehensive Cancer Network 2018a). Atezolizumab and pembrolizumab are first-line considerations in patients whose tumors express PD-L1 or for patients not eligible for any platinum-containing chemotherapy (Balar et al. 2017a, b). For patients who have locally advanced or metastatic urothelial carcinoma that has progressed during or after platinum-based chemotherapy or that has progressed within 12 months of neoadjuvant/adjuvant therapy, several PD-1/PD-L1 inhibitors have been FDA approved, including pembrolizumab, nivolumab, atezolizumab, durvalumab, and avelumab (Rosenberg et al. 2016; Sharma et al. 2017; Powles et al. 2017b; Patel et al. 2018).

Response assessment in phase II clinical trials of these ICB in locally advanced and/ or metastatic urothelial carcinoma has largely been according to RECIST 1.1, with overall response rates in the range of 17–24%, including some complete and durable responses in the studies (Chakiba et al. 2015; Donaldson et al. 2013; Yoshida et al. 2012; Moschini et al. 2016; National Comprehensive Cancer Network 2018a; Balar et al. 2017a). Interestingly, co-primary endpoints in one report included independent review facility-assessed objective response rate according to RECIST 1.1 and investigator-assessed objective response rate according to irRECIST, analyzed by intention to treat; response rates were similar using the two criteria (Rosenberg et al. 2016; Nishino et al. 2015). In this study, patients were permitted to continue atezolizumab beyond RECIST progression if they met criteria for clinical benefit, and 20 (17%) of 121 patients treated beyond progression showed subsequent partial response. These data highlight the necessity of confirming suspected progression on two consecutive follow-up imag-

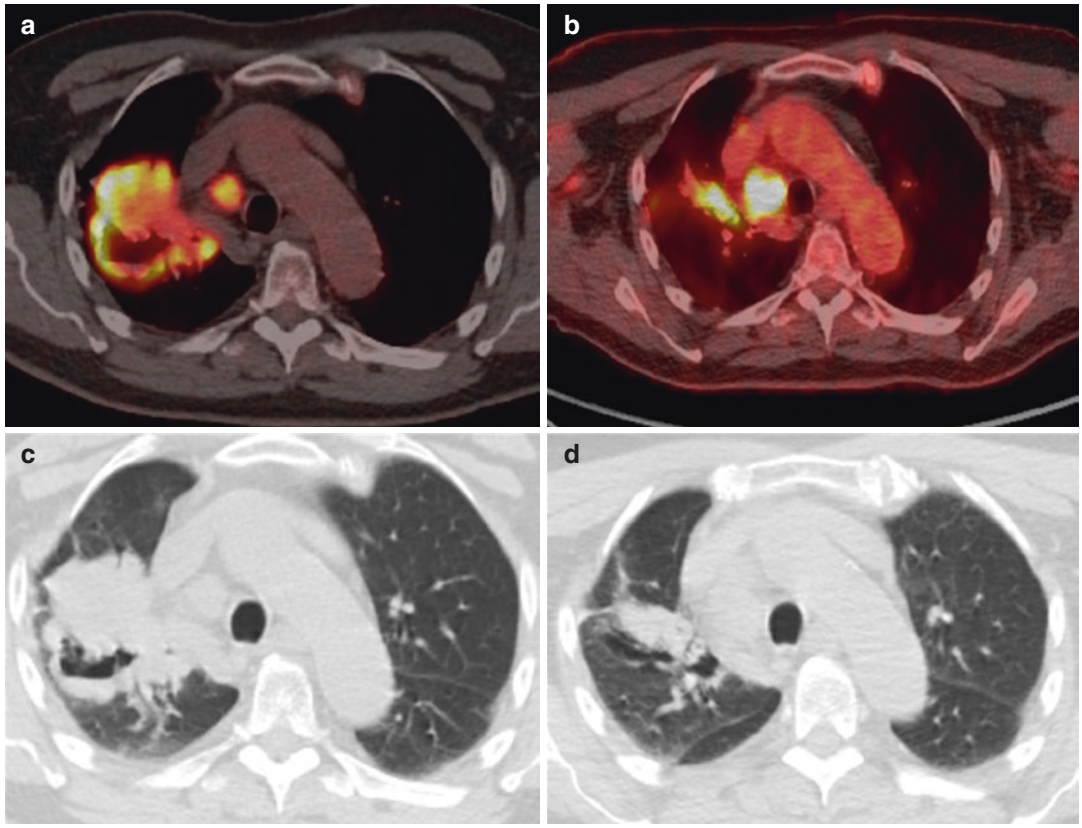

Fig. 6 81-year-old man with history of metastatic urothelial carcinoma of a solitary left kidney, treated with pembrolizumab. Pretreatment fused FDG PET-CT (**a**) and non-contrast CT of the lungs (**c**) show a large, FDG-avid right upper lobe mass and right paratracheal adenopathy. After 8 weeks of treatment, follow-up fused FDG PET-CT (**b**) and non-contrast CT of the lungs (**d**) show interval decrease in size and uptake of the dominant right upper lobe mass and decreased disease elsewhere (not shown), however with increased size and uptake of right paratracheal adenopathy, possibly sarcoid-like reaction given improvement of other sites, or less likely increased disease at this site. Short-term follow-up imaging was advised

ing studies performed at least 4 weeks apart, to capture potential pseudoprogression and permit patients the opportunity to continue effective treatment in this setting (Fig. 6).

5 Prostate Adenocarcinoma Response Assessment

Imaging response assessment in prostate cancer is challenging for several reasons (Hope et al. 2018). First, after definitive treatment with either surgery or radiation, patients may experience biochemical recurrence without imaging evidence of metastatic disease using traditional modalities (CT, MRI, and 99mTc-methyl-diphosphonate (MDP) bone scintigraphy). After prostatectomy, biochemical recurrence is evidenced by two consecutive prostate-specific antigen (PSA) levels greater than 0.2 ng/mL 6–8 weeks after surgery (Cookson et al. 2007), and after radiation, this is indicated by greater than 2.0-ng/mL increase in PSA level over the posttreatment nadir (Roach 3rd et al. 2006). Additionally, when metastases are identified they may be bone only, often sclerotic and without measurable soft tissue components necessary for measurable targets according to RECIST 1.1. Involved lymph nodes may also be small/ not measurable according to RECIST criteria. Thus,

utility of anatomic modalities and RECIST is limited in patients with bone-only and/or low volume metastatic prostate cancer, representing a substantial number of patients (Scher et al. 2008).

Nuclear imaging contributes significantly to response assessment in metastatic prostate cancer. Bone scintigraphy is routinely used to assess response to treatment/ progression in osseous metastatic disease, though flare phenomenon may create confusion, in which apparent increased uptake and/ or new lesions are detected soon after starting treatment due to healing and osteoblastic response in the lesions (Pollen et al. 1984, Fig. 7). The "2 + 2 rule" is aimed at better

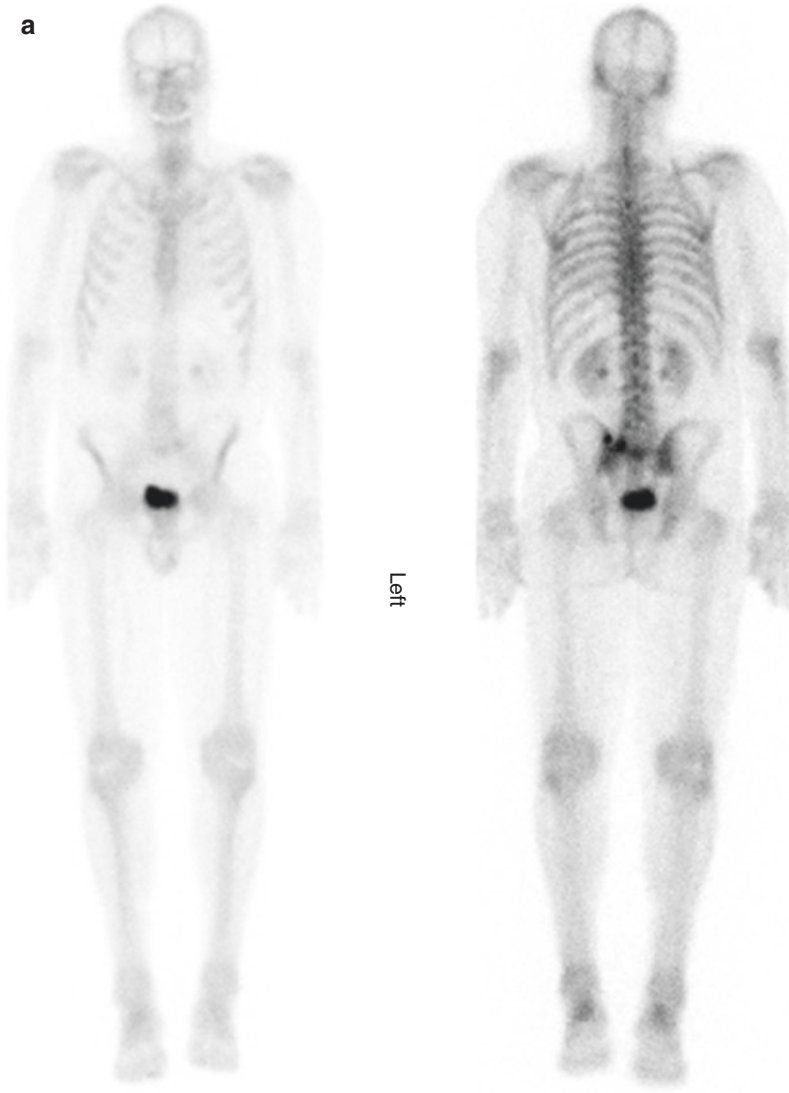

Fig. 7 63-year-old man with metastatic castrate-resistant prostate cancer, recently treated with enzalutamide and radiotherapy to the sacrum. Declining PSA. Tc-99 m-methylene diphosphonate (MDP) bone scan pre (**a**) and post (**b**) radiotherapy demonstrate new foci of uptake in the right lateral sixth rib, left fifth rib, left 11th rib, and increased extent of uptake in the left posterior iliac bone and sacrum. Given the context and decreasing PSA level, the findings were noted to be potentially related to osteoblastic response to therapy (flare) rather than progression, and follow-up was advised

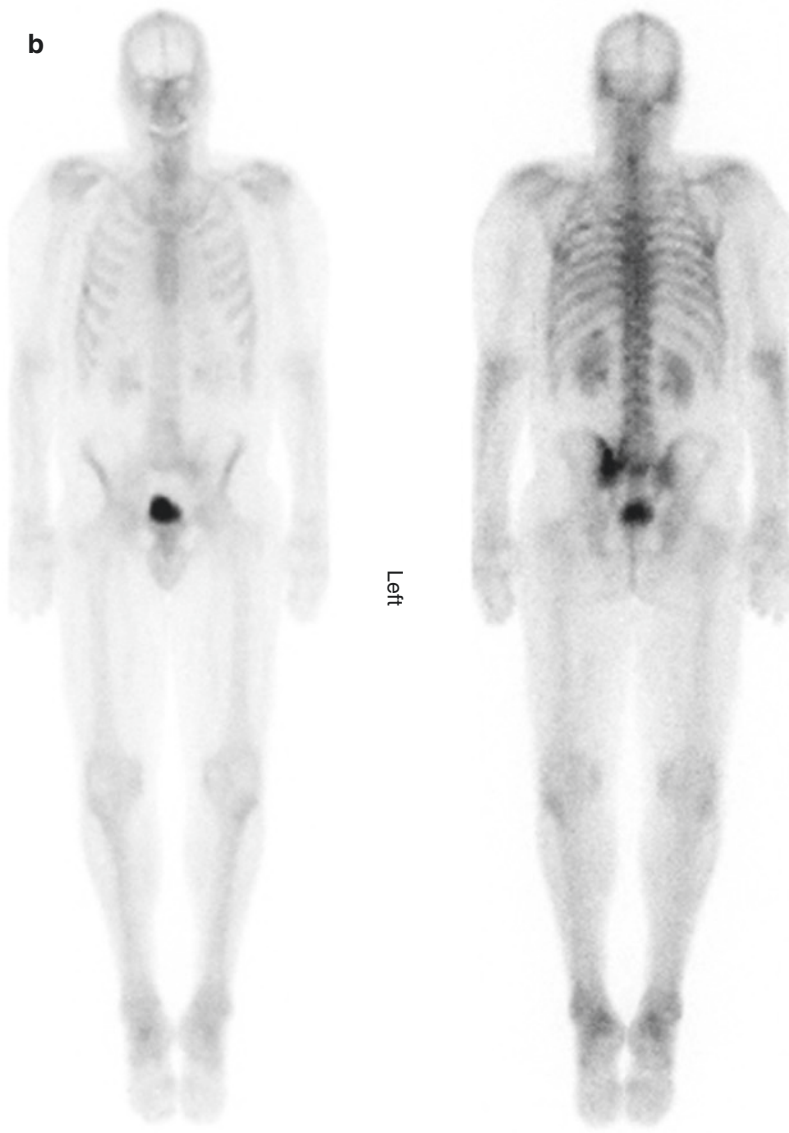

Fig. 9.7 (continued)

defining progressive osseous metastatic disease, whereby patients with new lesions/ possible flare phenomenon on initial posttreatment bone scan are further evaluated on a second bone scan ≥6 weeks later, deemed as having progressed if the second scan demonstrates ≥two additional new lesions (for a total of ≥four new lesions from baseline) (Scher et al. 2008; Morris et al. 2015). If the initial posttreatment bone scan is performed beyond the flare window of 12 weeks and 2 new bone lesions are detected, a confirmatory scan ≥6 weeks later should be performed to verify continued presence of the new lesions though no additional new lesions are required. Radiographic progression-free survival, assessed according to this definition for bone

disease and according to RECIST for soft tissue disease, has been correlated to overall survival in the context of clinical trials (Morris et al. 2015; Rathkopf et al. 2018).

Fluoro-[18F]-deoxy-2-D-glucose (FDG-PET/CT) is a modality which has limited utility in biochemically recurrent prostate cancer since disease may or may not be FDG-avid, though it has the potential to demonstrate bone and soft tissue metastases (Jadvar et al. 2012; Jadvar 2016). FDG-avidity has been correlated with biologically aggressive disease. Some studies have reported utility of FDG-PET/CT in assessing response to systemic treatments for metastatic prostate cancer, via changes in average SUVmax and other criteria (Morris et al. 2005; Zukotynski et al. 2014). Other "next-generation imaging" tracers may be sensitive and specific in biochemical recurrence, including [18F]-fluciclovine and bone metastasis-specific [18F]-sodium fluoride, both of which are FDA approved, and [68Ga]-prostate specific membrane antigen (PSMA) which is currently investigational in the United States (Crawford et al. 2018, Fig. 8). While low volume/oligometastatic disease detection using these techniques may make patients eligible for local treatments (e.g., metastasectomy, radiation) and systemic treatments requiring imaging evidence of metastatic disease, the role of next-generation imaging tracers in more disseminated disease and treatment response assessment is not yet defined.

A variety of treatment options exist for patients with recurrent and metastatic prostate cancer. Androgen deprivation therapy (ADT) is an option for patients with rising PSA without imaging evidence of metastases, and it is the gold standard for patients with metastatic disease (National Comprehensive Cancer Network 2018b). When patients develop resistance to initial ADT, this is termed castrate-resistant prostate cancer (CRPC). Onset of CRPC may be indicated by a PSA >2.0 ng/mL that rises >0.2 on two subsequent readings, any doubling of the PSA, progression in existing metastases or new lesions. Therapeutic options for CRPC depend on the presence or absence of metastatic disease on imaging and symptoms, and include secondary hormonal therapy (several, including but not limited to apalutamide, enzalutamide, abiraterone with prednisone), chemotherapy (docetaxel or cabazitaxel with steroids), and immunotherapy (sipuleucel-T, pembrolizumab) with various specific indications for each of these agents (National Comprehensive Cancer Network 2018b). In recent years, primary clinical trial endpoints have shifted from overall survival toward other clinically meaningful outcome measures including time to symptomatic skeletal event, time to first metastasis, and time to progression, to permit drug evaluation in patients with a variety of disease states, including those earlier in the disease continuum without measurable disease and/ or with low volume disease at baseline (Scher et al. 2016).

For predominantly bone metastases without visceral metastases, the alpha emitter radiopharmaceutical radium-223 dichloride is also a treatment option. Radium-223 dichloride binds to areas of increased bone turnover and thus targets osteoblastic metastases, acting over a short tissue range of <100 μm (Bruland et al. 2006). Radium-223 dichloride has been shown to improve overall survival and prolong the time to first symptomatic skeletal event (including radiation for bone pain palliation, new pathological fracture, spinal cord compression or tumor-related orthopedic surgery) in castrate-resistant prostate cancer patients with bone metastases (Parker et al. 2013; Sartor et al. 2014, Fig. 9). Of note, time to first symptomatic skeletal event was clinically assessed during the phase III trial study period and follow-up periods, did not include asymptomatic fractures detected radiographically, and radiographic response in bone lesions was not reported (Parker et al. 2013). Particularly in patients with osseous metastatic disease, clinical and imaging follow-up is often aimed at detecting progressive disease, as opposed to response. It remains undetermined whether nuclear techniques using novel tracers will be helpful to assess response in this setting.

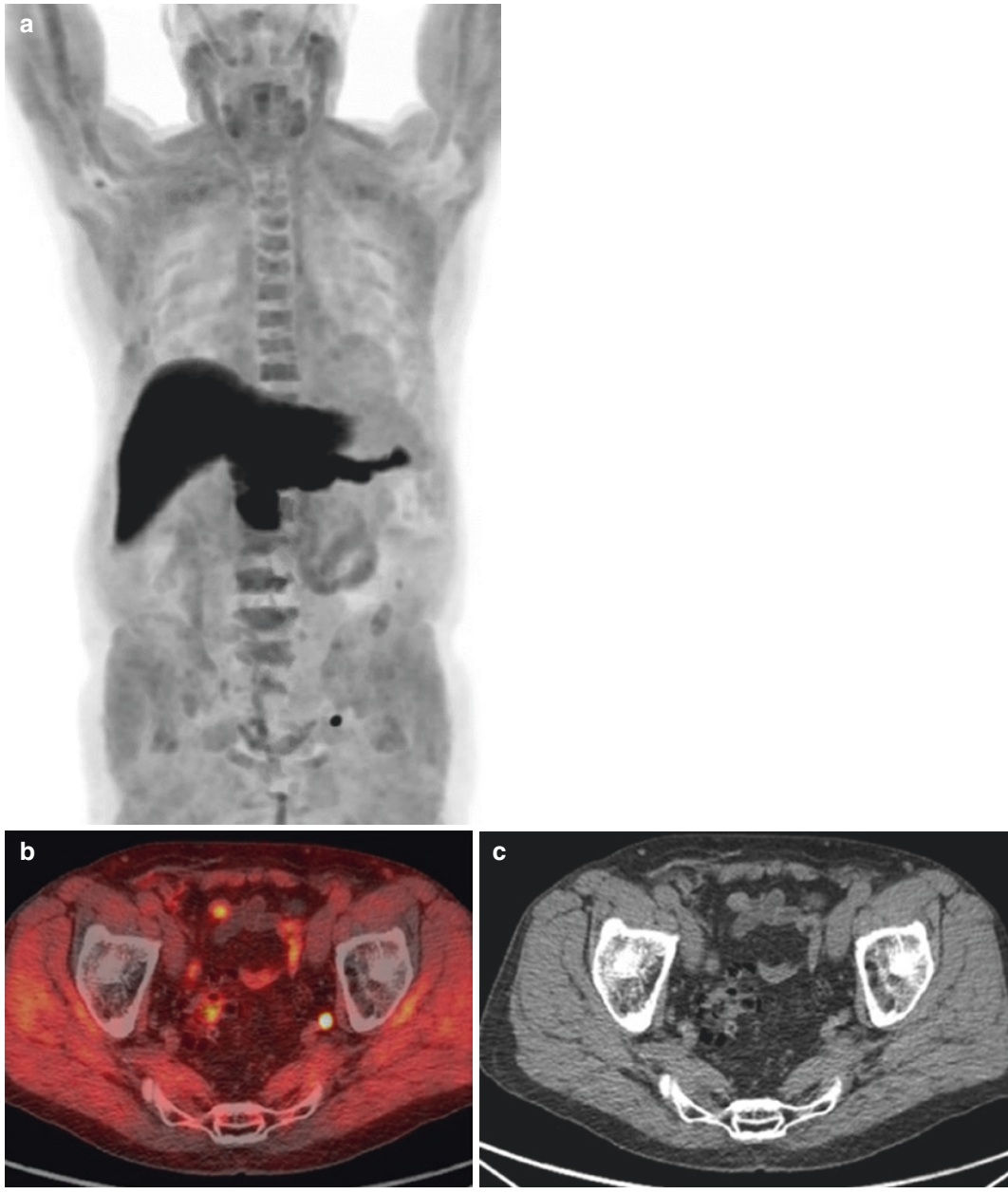

Fig. 8 76-year-old male with biochemically recurrent prostate cancer (PSA 0.4) after radical prostatectomy. Fluciclovine PET-CT maximum intensity projection (MIP) image (**a**), fused PET-CT (**b**) and non-contrast CT (**c**) images show a 10 × 8 mm radiotracer avid left internal iliac node with SUVmax of 9.5, representing the site of recurrent disease

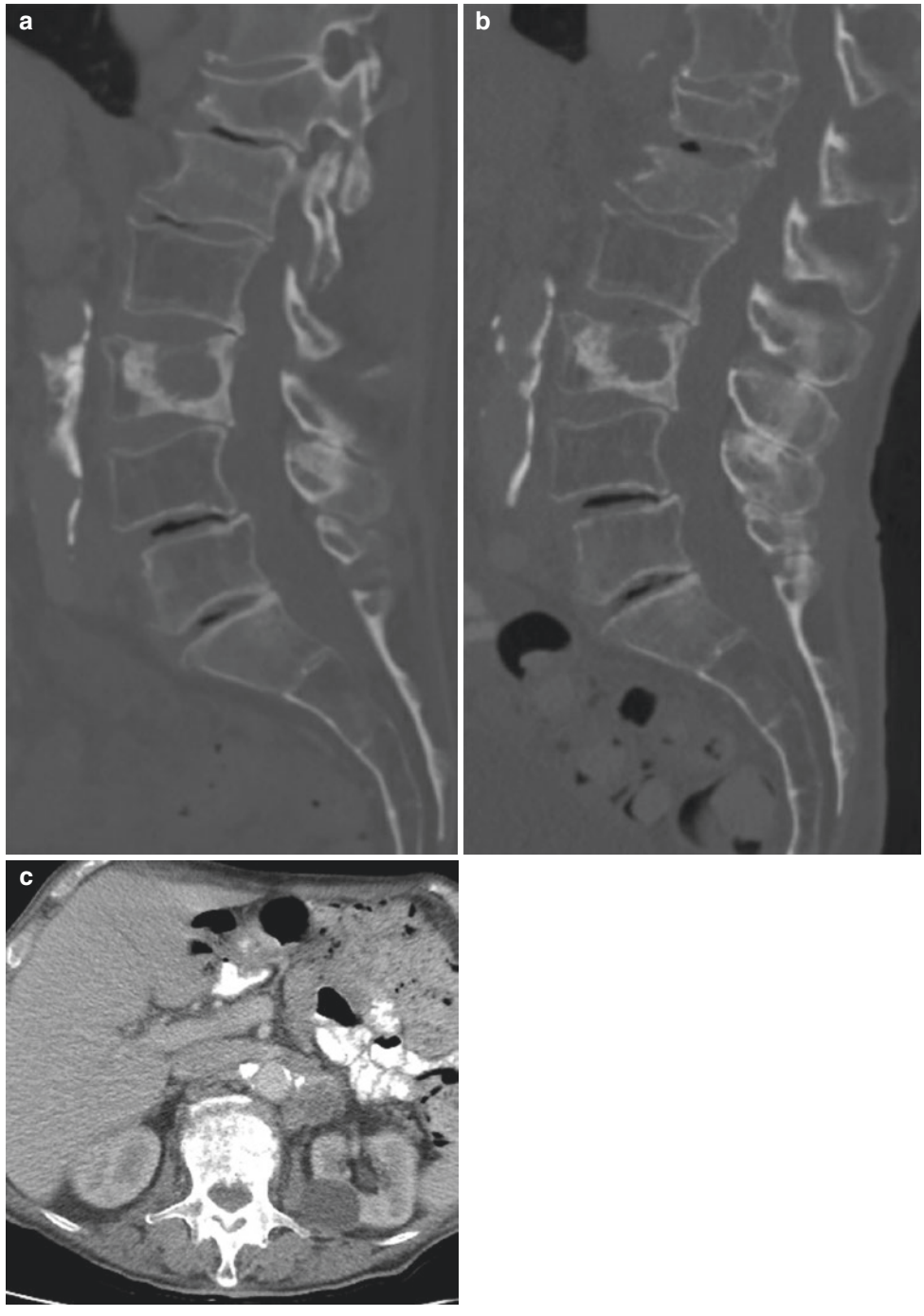

Fig. 9 79-year-old man with metastatic, castration-resistant prostate cancer. Baseline sagittal CT (**a**) demonstrates a lytic metastasis with surrounding sclerosis in L3 and moderate compression deformity of T12. Follow-up sagittal CT (**b**) 4 months after initiating treatment with Radium-223 demonstrates no significant change in the L3 lesion but new mild sclerosis, fragmentation, and mild height loss at L1, representing a new compression deformity which was symptomatic (symptomatic skeletal event). The patient also developed new multistation lymphadenopathy (axial CT, **c**), indicating the need for a change in treatment

6 Conclusion

In conclusion, there are a variety of anatomic and functional imaging modalities employed in assessing response to treatment in renal cell carcinoma, bladder cancer, and prostate cancer, including investigational techniques. Current themes in response assessment include the development of disease-specific and/ or treatment-specific approaches to guide treatment continuation and change decisions, taking into account the mechanisms of action of therapeutic agents, disease biology, and behavior. Multidisciplinary collaboration is necessary to refine imaging best practices, to further develop imaging techniques to predict and measure response, and to incorporate rational exploratory response assessment methods into prospective trials.

References

American Cancer Society (2018) Cancer facts & figures 2018. American Cancer Society, Atlanta

Balar AV, Castellano D, O'Donnell PH et al (2017a) First-line pembrolizumab in cisplatin-ineligible patients with locally advanced and unresectable or metastatic urothelial cancer (KEYNOTE-052): a multicentre, single-arm, phase 2 study. Lancet Oncol 18(11):1483–1492. https://doi.org/10.1016/S1470-2045(17)30616-2. [Epub 2017 Sep 26]

Balar AV, Galsky MD, Rosenberg JE et al (2017b) Atezolizumab as first-line treatment in cisplatin-ineligible patients with locally advanced and metastatic urothelial carcinoma: a single-arm, multicentre, phase 2 trial. Lancet 389(10064):67–76. https://doi.org/10.1016/S0140-6736(16)32455-2. [Epub 2016. Erratum in: Lancet. 2017 Aug 26;390(10097):848]

Barentsz JO, Berger-Hartog O, Witjes JA et al (1998) Evaluation of chemotherapy in advanced urinary bladder cancer with fast dynamic contrast-enhanced MR imaging. Radiology 207:791–797

Bensch F, van der Veen EL, Lub-de Hooge MN et al (2018) 89Zr-atezolizumab imaging as a non-invasive approach to assess clinical response to PD-L1 blockade in cancer. Nat Med 24(12):1852–1858. https://doi.org/10.1038/s41591-018-0255-8. [Epub 2018 Nov 26]

Bruland ØS, Nilsson S, Fisher DR, Larsen RH (2006) High-linear energy transfer irradiation targeted to skeletal metastases by the alpha-emitter 223Ra: adjuvant or alternative to conventional modalities? Clin Cancer Res 12(20 Pt 2):6250s–6257s

Calvo E, Porta C, Grünwald V, Escudier B (2018) The current and evolving landscape of first-line treatments for advanced renal cell carcinoma. Oncologist. https://doi.org/10.1634/theoncologist.2018-0267. [Epub ahead of print]

Chakiba C, Cornelis F, Descat E et al (2015) Dynamic contrast enhanced MRI-derived parameters are potential biomarkers of therapeutic response in bladder carcinoma. Eur J Radiol 84(6):1023–1028. https://doi.org/10.1016/j.ejrad.2015.02.026. [Epub 2015 Mar 6]

Champiat S, Dercle L, Ammari S et al (2017) Hyperprogressive disease is a new pattern of progression in cancer patients treated by anti-PD-1/PD-L1. Clin Cancer Res 23(8):1920–1928

Champiat S, Ferrara R, Massard C et al (2018a Dec) Hyperprogressive disease: recognizing a novel pattern to improve patient management. Nat Rev Clin Oncol 15(12):748–762. https://doi.org/10.1038/s41571-018-0111-2

Champiat S, Ferrara R, Massard C et al (2018b) Hyperprogressive disease: recognizing a novel pattern to improve patient management. Nat Rev Clin Oncol. https://doi.org/10.1038/s41571-018-0111-2. [Epub ahead of print]

Choueiri TK, Jacobus S, Bellmunt J et al (2014) Neoadjuvant dose-dense methotrexate, vinblastine, doxorubicin, and cisplatin with pegfilgrastim support in muscle-invasive urothelial cancer: pathologic, radiologic, and biomarker correlates. J Clin Oncol 32(18):1889–1894. https://doi.org/10.1200/JCO.2013.52.4785. [Epub 2014 May 12]

Choueiri TK, Larkin J, Oya M et al (2018) Preliminary results for avelumab plus axitinib as first-line therapy in patients with advanced clear-cell renal-cell carcinoma (JAVELIN Renal 100): an open-label, dose-finding and dose-expansion, phase 1b trial. Lancet Oncol 19(4):451–460. https://doi.org/10.1016/S1470-2045(18)30107-4. [Epub 2018 Mar 9]

Cookson MS, Aus G, Burnett AL et al (2007) Variation in the definition of biochemical recurrence in patients treated for localized prostate cancer: the American Urological Association prostate guidelines for localized prostate cancer update panel report and recommendations for a standard in the reporting of surgical outcomes. J Urol 177:540–545

Crawford ED, Koo PJ, Shore N et al (2018) A clinician's guide to next generation imaging in patients with advanced prostate cancer (Prostate Cancer Radiographic Assessments for Detection of Advanced Recurrence [RADAR] III). J Urol. https://doi.org/10.1016/j.juro.2018.05.164 [Epub ahead of print]

Dabestani S, Marconi L, Hofmann F et al (2014) Local treatments for metastases of renal cell carcinoma: a systematic review. Lancet Oncol 15(12):e549–e561. https://doi.org/10.1016/S1470-2045(14)70235-9. [Epub 2014 Oct 26]

de Velasco G, Krajewski KM, Albiges L et al (2016) Radiologic heterogeneity in responses to anti-PD-1/PD-L1 therapy in metastatic renal cell carcinoma. Cancer Immunol Res 4(1):12–17. https://doi.org/10.1158/2326-6066.CIR-15-0197. [Epub 2015 Nov 20]

Dibble EH, Krajewski KM, Kravets S, et al (2018) FDG-PET/CT versus 99mTc-MDP bone scan and contrast-enhance CT in patients with metastatic renal cell cancer receiving a combination of vascular endothelial growth factor (VEGF)-targeted therapy and a radiopharmaceutical. Poster presentation at the 2018 annual meeting of the Society of Nuclear Medicine and Molecular Imaging, Philadelphia, PA, June 2018

Donaldson SB, Bonington SC, Kershaw LE et al (2013) Dynamic contrast-enhanced MRI in patients with muscle-invasive transitional cell carcinoma of the bladder can distinguish between residual tumour and post-chemotherapy effect. Eur J Radiol 82:2161–2168

Eisenhauer EA, Therasse P, Bogaerts J et al (2009a) New response evaluation criteria in solid tumours: revised RECIST guideline (version 1.1). Eur J Cancer 45:228–247

Eisenhauer EA, Therasse P, Bogaerts J et al (2009b Jan) New response evaluation criteria in solid tumours: revised RECIST guideline (version 1.1). Eur J Cancer 45(2):228–247. https://doi.org/10.1016/j.ejca.2008.10.026

Elias R, Kapur P, Pedrosa I, Brugarolas J (2018) Renal cell carcinoma pseudoprogression with clinical deterioration: to hospice and back. Clin Genitourin Cancer. https://doi.org/10.1016/j.clgc.2018.07.015. [Epub ahead of print]

Ferrara R, Mezquita L, Texier M et al (2018) Hyperprogressive disease in patients with advanced non-small cell lung cancer treated with PD-1/PD-L1 inhibitors or with single-agent chemotherapy. JAMA Oncol 4(11):1543–1552. https://doi.org/10.1001/jamaoncol.2018.3676

Ferté C, Koscielny S, Albiges L et al (2014) Tumor growth rate provides useful information to evaluate sorafenib and everolimus treatment in metastatic renal cell carcinoma patients: an integrated analysis of the TARGET and RECORD phase 3 trial data. Eur Urol 65(4):713–720. https://doi.org/10.1016/j.eururo.2013.08.010. [Epub 2013 Aug 15]

Francolini G, Detti B, Ingrosso G et al (2018) Stereotactic body radiation therapy (SBRT) on renal cell carcinoma, an overview of technical aspects, biological rationale and current literature. Crit Rev Oncol Hematol 131:24–29. https://doi.org/10.1016/j.critrevonc.2018.08.010. [Epub 2018 Aug 28]

Hamaoka T, Madewell JE, Podoloff DA, Hortobagyi GN, Ueno NT (2004) Bone imaging in metastatic breast cancer. J Clin Oncol 22:2942–2953

Hodi FS, Ballinger M, Lyons B, Soria JC, Nishino M, Tabernero J, Powles T, Smith D, Hoos A, McKenna C, Beyer U, Rhee I, Fine G, Winslow N, Chen DS, Wolchok JD (2018) Immune-Modified Response Evaluation Criteria In Solid Tumors (imRECIST): refining guidelines to assess the clinical benefit of cancer immunotherapy. J Clin Oncol 36(9):850–858. https://doi.org/10.1200/JCO.2017.75.1644. [Epub 2018 Jan 17]

Hope TA, Afshar-Oromieh A, Eiber M et al (2018) Imaging prostate cancer with prostate-specific membrane antigen PET/CT and PET/MRI: current and future applications. AJR Am J Roentgenol 211(2):286–294. https://doi.org/10.2214/AJR.18.19957. [Epub 2018 Jun 27]

Jadvar HI (2016) There use for FDG-PET in prostate cancer? Semin Nucl Med 46(6):502–506. https://doi.org/10.1053/j.semnuclmed.2016.07.004. [Epub 2016 Sep 3]

Jadvar H, Desai B, Ji L et al (2012) Prospective evaluation of 18F-NaF and 18F-FDG PET/CT in detection of occult metastatic disease in biochemical recurrence of prostate cancer. Clin Nucl Med 37(7):637–643. https://doi.org/10.1097/RLU.0b013e318252d829

Karam JA, Rini BI, Varella L et al (2011) Metastasectomy after targeted therapy in patients with advanced renal cell carcinoma. J Urol 185(2):439–444. https://doi.org/10.1016/j.juro.2010.09.086. [Epub 2010 Dec 17]

Kato S, Goodman A, Walavalkar V et al (2017) Hyperprogressors after immunotherapy: analysis of genomic alterations associated with accelerated growth rate. Clin Cancer Res 23(15):4242–4250. https://doi.org/10.1158/1078-0432.CCR-16-3133. [Epub 2017 Mar 28]

Krajewski KM, Guo M, Van den Abbeele AD et al (2011) Comparison of four early posttherapy imaging changes (EPTIC; RECIST 1.0, tumor shrinkage, computed tomography tumor density, Choi criteria) in assessing outcome to vascular endothelial growth factor-targeted therapy in patients with advanced renal cell carcinoma. Eur Urol 59(5):856–862

Krajewski KM, Franchetti Y, Nishino M et al (2014) 10% tumor diameter shrinkage on the first follow-up computed tomography predicts clinical outcome in patients with advanced renal cell carcinoma treated with angiogenesis inhibitors: a follow-up validation study. Oncologist 19:507

Krajewski KM, Nishino M, Ramaiya NH, Choueiri TK (2015) RECIST 1.1 compared with RECIST 1.0 in patients with advanced renal cell carcinoma receiving vascular endothelial growth factor-targeted therapy. AJR Am J Roentgenol 204(3):W282–W288

Kuhl CK, Alparslan Y, Schmoee J, Sequeira B, Keulers A, Brümmendorf TH, Keil S (2019) Validity of RECIST Version 1.1 for response assessment in metastatic cancer: a prospective, multireader study. Radiology 290(2):349–356. https://doi.org/10.1148/radiol.2018180648. [Epub ahead of print]

McKay RR, Kroeger N, Xie W et al (2014) Impact of bone and liver metastases on patients with renal cell carcinoma treated with targeted therapy. Eur Urol 65(3):577–584. https://doi.org/10.1016/j.eururo.2013.08.012. [Epub 2013 Aug 15]

McKay RR, Bossé D, Gray KP et al (2018a) Radium-223 dichloride in combination with vascular endothelial growth factor-targeting therapy in advanced renal cell carcinoma with bone metastases. Clin Cancer Res 24(17):4081–4088. https://doi.org/10.1158/1078-0432.CCR-17-3577. [Epub 2018 May 30]

McKay RR, Bossé D, Choueiri TK (2018b) Evolving systemic treatment landscape for patients with advanced

renal cell carcinoma. J Clin Oncol 29:JCO2018790253. https://doi.org/10.1200/JCO.2018.79.0253. [Epub ahead of print]

Morris MJ, Akhurst T, Larson SM et al (2005) Fluorodeoxyglucose positron emission tomography as an outcome measure for castrate metastatic prostate cancer treated with antimicrotubule chemotherapy. Clin Cancer Res 11:3210–3216

Morris MJ, Molina A, Small EJ et al (2015) Radiographic progression-free survival as a response biomarker in metastatic castration-resistant prostate cancer: COU-AA-302 results. J Clin Oncol 33(12):1356–1363

Moschini M, Karnes RJ, Sharma V et al (2016) Patterns and prognostic significance of clinical recurrences after radical cystectomy for bladder cancer: a 20-year single center experience. Eur J Surg Oncol 42(5):735–743. https://doi.org/10.1016/j.ejso.2016.02.011. [Epub 2016 Feb 18]

Mosillo C, Ciccarese C, Bimbatti D et al (2018) Renal cell carcinoma in one year: going inside the news of 2017—a report of the main advances in RCC cancer research. Cancer Treat Rev 67:29–33. https://doi.org/10.1016/j.ctrv.2018.02.009. [Epub 2018 May 2]

Motzer RJ, Escudier B, Oudard S et al (2008) Efficacy of everolimus in advanced renal cell carcinoma: a double-blind, randomised, placebo-controlled phase III trial. Lancet 372(9637):449–456

Motzer RJ, Hutson TE, Cella D et al (2013) Pazopanib versus sunitinib in metastatic renal-cell carcinoma. N Engl J Med 369(8):722–731

Motzer RJ, Escudier B, McDermott DF (2015) Nivolumab versus everolimus in advanced renal-cell carcinoma. N Engl J Med 373(19):1803–1813. https://doi.org/10.1056/NEJMoa1510665. [Epub 2015 Sep 25]

Motzer RJ, Tannir NM, McDermott DF et al (2018) Nivolumab plus Ipilimumab versus Sunitinib in advanced renal-cell carcinoma. N Engl J Med 378(14):1277–1290. https://doi.org/10.1056/NEJMoa1712126. [Epub 2018 Mar 21]

Motzer RJ et al (2019) Avelumab plus axitinib versus sunitinib for advanced renal cell carcinoma. N Engl J Med 380(12):1103–1115

National Comprehensive Cancer Network (2018a) NCCN Clinical Practice Guidelines in Oncology (NCCN guidelines) Bladder Cancer (version 5.2018)

National Comprehensive Cancer Network (2018b) NCCN Clinical Practice Guidelines in Oncology (NCCN guidelines) Prostate Cancer (version 4.2018)

Nishino M, Giobbie-Hurder A, Gargano M, Suda M, Ramaiya NH, Hodi FS (2013) Developing a common language for tumor response to immunotherapy: immune-related response criteria using unidimensional measurements. Clin Cancer Res 19(14):3936–3943. https://doi.org/10.1158/1078-0432.CCR-13-0895. [Epub 2013 June 6]

Nishino M, Giobbie-Hurder A, Ramaiya NH, Hodi FS (2014) Response assessment in metastatic melanoma treated with ipilimumab and bevacizumab: CT tumor size and density as markers for response and outcome. J Immunother Cancer 2(1):40. https://doi.org/10.1186/s40425-014-0040-2. eCollection 2014.

Nishino M, Tirumani SH, Ramaiya NH, Hodi FS (2015) Cancer immunotherapy and immune-related response assessment: the role of radiologists in the new arena of cancer treatment. Eur J Radiol 84(7):1259–1268. https://doi.org/10.1016/j.ejrad.2015.03.017. [Epub 2015 Mar 23]

Padhani AR, Lecouvet FE, Tunariu N et al (2017) Rationale for modernising imaging in advanced prostate cancer. Eur Urol Focus 3(2–3):223–239. https://doi.org/10.1016/j.euf.2016.06.018. [Epub 2016 Jul 15]

Parker C, Nilsson S, Heinrich D et al (2013) Alpha emitter radium-223 and survival in metastatic prostate cancer. N Engl J Med 369(3):213–223

Patel MR, Ellerton J, Infante JR et al (2018) Avelumab in metastatic urothelial carcinoma after platinum failure (JAVELIN Solid Tumor): pooled results from two expansion cohorts of an open-label, phase 1 trial. Lancet Oncol 19(1):51–64. https://doi.org/10.1016/S1470-2045(17)30900-2. [Epub 2017 Dec 5]

Pollen JJ, Witztum KF, Ashburn WL (1984) The flare phenomenon on radionuclide bone scan in metastatic prostate cancer. AJR Am J Roentgenol 142(4):773–776

Powles T, Albiges L, Staehler M et al (2017a) Updated European Association of Urology guidelines recommendations for the treatment of first-line metastatic clear cell renal cancer. Eur Urol. https://doi.org/10.1016/j.eururo.2017.11.016. [Epub ahead of print]

Powles T, O'Donnell PH, Massard C et al (2017b) Efficacy and safety of durvalumab in locally advanced or metastatic urothelial carcinoma: updated results from a phase 1/2 open-label study. JAMA Oncol 3(9):e172411. https://doi.org/10.1001/jamaoncol.2017.2411. [Epub 2017 Sep 14]

Rathkopf DE, Beer TM, Loriot Y et al (2018) Radiographic progression-free survival as a clinically meaningful end point in metastatic castration-resistant prostate cancer: the PREVAIL Randomized Clinical Trial. JAMA Oncol 4(5):694–701

Roach M 3rd, Hanks G, Thames H et al (2006) Defining biochemical failure following radiotherapy with or without hormonal therapy in men with clinically localized prostate cancer: recommendations of the RTOG-ASTRO Phoenix Consensus Conference. Int J Radiat Oncol Biol Phys 65:965–974

Rosenberg JE, Hoffman-Censits J, Powles T et al (2016) Atezolizumab in patients with locally advanced and metastatic urothelial carcinoma who have progressed following treatment with platinum-based chemotherapy: a single-arm, multicentre, phase 2 trial. Lancet 387(10031):1909–1920. https://doi.org/10.1016/S0140-6736(16)00561-4. [Epub 2016 Mar 4]

Sartor O, Coleman R, Nilsson S et al (2014) Effect of radium-223 dichloride on symptomatic skeletal events in patients with castration-resistant prostate cancer and bone metastases: results from a phase 3, double-blind, randomised trial. Lancet Oncol 15(7):738–746

Scher HI, Halabi S, Tannock I et al (2008) Design and end points of clinical trials for patients with progressive prostate cancer and castrate levels of testoster-

one: recommendations of the Prostate Cancer Clinical Trials Working Group. J Clin Oncol 26(7):1148–1159. https://doi.org/10.1200/JCO.2007.12.4487

Scher HI, Morris MJ, Stadler WM et al (2016) Trial design and objectives for castration-resistant prostate cancer: updated recommendations from the Prostate Cancer Clinical Trials Working Group 3. J Clin Oncol 34(12):1402–1418. https://doi.org/10.1200/JCO.2015.64.2702. [Epub 2016 Feb 22]

Schrier BP, Peters M, Barentsz JO, Witjes JA (2006) Evaluation of chemotherapy with magnetic resonance imaging in patients with regionally metastatic or unresectable bladder cancer. Eur Urol 49:698–703

Seymour L, Bogaerts J, Perrone A, Ford R, Schwartz LH, Mandrekar S, Lin NU, Litière S, Dancey J, Chen A, Hodi FS, Therasse P, Hoekstra OS, Shankar LK, Wolchok JD, Ballinger M, Caramella C, De Vries EG, RECIST Working Group (2017) iRECIST: guidelines for response criteria for use in trials testing immunotherapeutics. Lancet Oncol 18(3):e143–e152. https://doi.org/10.1016/S1470-2045(17)30074-8. [Epub 2017 Mar 2]. Review

Sharma P, Retz M, Siefker-Radtke A et al (2017) Nivolumab in metastatic urothelial carcinoma after platinum therapy (CheckMate 275): a multicentre, single-arm, phase 2 trial. Lancet Oncol 18(3):312–322. https://doi.org/10.1016/S1470-2045(17)30065-7. [Epub 2017 Jan 26]

Smith AD, Shah SN, Rini BI, Lieber ML, Remer EM (2010) Morphology, Attenuation, Size, and Structure (MASS) criteria: assessing response and predicting clinical outcome in metastatic renal cell carcinoma on antiangiogenic targeted therapy. AJR Am J Roentgenol 194(6):1470–1478

Smith AD, Shah SN, Rini BI, Lieber ML, Remer EM (2013) Utilizing pre-therapy clinical schema and initial CT changes to predict progression-free survival in patients with metastatic renal cell carcinoma on VEGF-targeted therapy: a preliminary analysis. Urol Oncol 31(7):1283–1291

Thiam R, Fournier LS, Trinquart L et al (2010) Optimizing the size variation threshold for the CT evaluation of response in metastatic renal cell carcinoma treated with sunitinib. Ann Oncol 21(5):936–941

van der Veldt AA, Meijerink MR, van den Eertwegh AJ, Haanen JB, Boven E (2010) Choi response criteria for early prediction of clinical outcome in patients with metastatic renal cell cancer treated with sunitinib. Br J Cancer 102(5):803–809

Wolchok JD, Hoos A, O'Day S et al (2009) Guidelines for the evaluation of immune therapy activity in solid tumors: immune-related response criteria. Clin Cancer Res 15(23):7412–7420. https://doi.org/10.1158/1078-0432.CCR-09-1624. [Epub 2009 Nov 24]

Yoshida S, Koga F, Kobayashi S et al (2012) Role of diffusion-weighted magnetic resonance imaging in predicting sensitivity to chemoradiotherapy in muscle-invasive bladder cancer. Int J Radiat Oncol Biol Phys 83(1):e21–e27. https://doi.org/10.1016/j.ijrobp.2011.11.065. [Epub 2012 Mar 11]

Zukotynski KA, Kim CK, Gerbaudo VH et al (2014) (18) F-FDG-PET/CT and (18)F-NaF-PET/CT in men with castrate-resistant prostate cancer. Am J Nucl Med Mol Imaging 5(1):72–82. eCollection 2015

Therapy Response Imaging in Gynecologic Malignancies

Aki Kido

Contents

Abstract

The three most common malignancies in gynecological oncology are cervical cancer, endometrial cancer, and ovarian cancer. Studies related to treatment response and prognosis of these cancers have mainly examined magnetic resonance (MR) imaging factors, which include tumor size, diffusion-weighted image (DWI), and perfusion image, followed by positron emission tomography/computed tomography (PET/CT) and CT images. To study cervical cancer, imaging modalities and factors have been combined variously with clinical factors, and DWI and derived apparent diffusion coefficient (ADC) values playing important roles. Because endometrial cancer diagnosed at an early stage exhibits favorable overall survival, many studies have specifically examined relations with clinical factors such as stage, histology, depth of myometrial invasion, lymphovascular invasion, and lymph node (LN) metastasis. Ovarian cancer is diagnosed at a high stage with tumor spread in the abdomen and thoracic cavity. Then PET/CT is more emphasized than MRI for the evaluation of treatment response. The latest analytic methods using radiogenomics and texture analysis are also applied to evaluate cervical cancer and ovarian cancer.

A. Kido (✉)
Department of Diagnostic Radiology and Nuclear Medicine, Graduate School of Medicine, Kyoto University, Kyoto, Japan
e-mail: akikido@kuhp.kyoto-u.ac.jp

M. Nishino (ed.), *Therapy Response Imaging in Oncology*, Medical Radiology, Diagnostic Imaging,
https://doi.org/10.1007/978-3-030-31171-1_10

1 Introduction

The International Federation of Gynecology and Obstetrics (FIGO) staging system provides fundamental and important criteria for developing treatment strategies and for estimating the prognoses of gynecological cancers. However, FIGO staging alone might not be satisfactory for accurately providing prognostic evaluation. Clinical need exists for noninvasive prognostic biomarkers to provide more detailed tumor characterization at the baseline and/or during early therapy, which might permit personalized treatment and which might support improved outcomes because traditional clinical and morphological predictors include tumor volume, histology, performance status, and nodal status (Barwick et al. 2013; Katanyoo et al. 2011; Kristensen et al. 1999). Radiological imaging, especially MR imaging, has long played an important role for tumor measurements in 2D or 3D sections in gynecological tumors. Recent development of MR imaging with functional imaging has led to tumor biology work for the assessment of biomarkers indicating tumor response, such as glucose metabolism, hypoxia, and cellularity. Debate continues as to which imaging biomarker is more robust for the accurate prediction of individual prognosis in pretreatment assessment of patients with gynecological cancers. This review presents details related to the current evidence and future potential of functional imaging to predict tumor response in gynecological cancers.

2 Cervical Cancer

Uterine cervical cancer, the third most commonly diagnosed cancer, is the fourth leading cause of cancer death among women worldwide, although its incidence has decreased in economically developed countries because of improved public health measures and wider implementation of Pap-smear screening (Jemal et al. 2011; Kurman et al. 2014a). Fifty percent of patients are diagnosed at stage 1; their five-year survival rate is over 90%. Nevertheless, cervical cancer has a high rate of recurrence after the end of therapy: about 35% (Zola et al. 2015; Salani et al. 2011). The most common histopathology subtypes are squamous cell carcinoma (SCC), accounting for almost 80%, followed by adenocarcinoma (Intaraphet et al. 2013). Actually, the FIGO stage is the most important prognostic factor, but tumor size, depth of invasion, parametrial invasion, and nodal status are also related to prognosis (Wright et al. 2002). Treatment might vary within stages because the individual stages are currently defined by the FIGO stage. Main treatment modalities include surgery, chemotherapy, and radiation therapy, but concurrent chemoradiation therapy (CCRT) is applied for advanced tumors (Wright et al. 2002). Identification of patients at higher risk of recurrence before treatment or in an early stage of chemoradiation therapy might give rise to more personalized or stratified treatment. In addition to basic morphological assessment of tumors using CT and conventional MRI sequences, functional MRI and FDG-PET CT are anticipated to reveal functional aspects of tumors, including tumor metabolism, water diffusion, perfusion, and tumor heterogeneity, and to facilitate the early detection of tumor response (Fig. 1). As described in this section explaining cervical cancer, various imaging factors were introduced: from observation of morphological change to recent techniques.

Fundamental assessment of treatment response depends on the tumor volume. Mayr et al. compared overall survival (OS) according to the respective volumes of residual tumors during and after radiation therapy (Mayr et al. 2010). Results indicate that OS is significantly higher in the group with rapidly regressing tumors with proportional tumor volumes of less than 20% at 40–50 Gy and 10% at 1–2 months postradiation therapy (Mayr et al. 2010). Regarding the risk assessment of tumor recurrence, volumes of areas of high signal intensity involving the uterine cervix on T2-weighted MR images after radiation therapy were used (Saida et al. 2010). Greater volume of areas of high signal intensity on

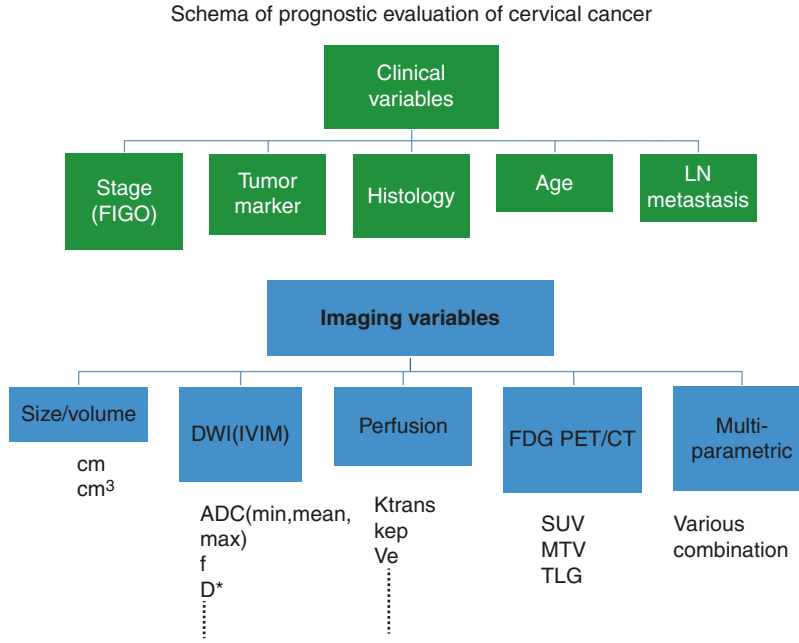

Fig. 1 The schema shows the list of clinical and imaging variables for treatment response and prognostic evaluation for cervical cancer. FIGO staging is the most important in clinical factors. Regarding imaging variables, DWI, FDG PET/CT and those combinations were mainly used for the research. *LN* lymph node, *ADC* apparent, diffusion coefficient, *IVIM* intravoxel incoherent motion, *f* perfusion fraction, *D*∗ pseudodiffusion coefficient, K^{trans} volume transfer constant between the blood plasma and the extracellular–extravascular space (EES)), k^{ep} rate constant between the EES and the blood plasma, *Ve* fractional volume of EES, *SUV* standardized uptake values, *MTV* metabolic tumor volume, *TLG* total lesion glycolysis

T2-weighted images (WI) obtained immediately before and after completion of irradiation therapy is associated with higher risk of recurrence (Saida et al. 2010). The salient difficulty of T2WI has been identified as acute radiation change of inflammation and edema. An additional shortcoming of volume measurement is delay in the onset of treatment effects.

Diffusion-weighted imaging (DWI), which provides information about the random (Brownian) motion of water molecules in tissues (Padhani et al. 2009), is expected to provide early response when using chemotherapy and to elucidate the patient prognosis. Reduced motion of water in malignant tumors is probably related to a combination of higher cellularity, tissue disorganization, and increased extracellular space tortuosity (Padhani et al. 2009). Therefore, many researchers have pursued effective and proper evaluation timing of ADC value measurement reflecting treatment response or prognosis. Numerous reports have described the evaluation of treatment response or prognosis using DWI and ADC values. However, their respective study designs have differed widely. In fact, numerous and diverse imaging modalities exist, involving the timing of image acquisition or evaluation and the combination of therapies. Variations also exist in the measurement of ADC values, including the minimum, mean, maximum, the change of ADC, and histogram analysis. Placement of ROIs also presents various alternatives: 2D or 3D ROI, single or multiple ROIs, oval or square ROI, and manual or automatic. Discussion has continued as to which approach is appropriate for prognosis evaluation. Although automatic measurements of the whole tumor probably can elicit information of the tumor without bias, the accessibility of such methods is also an important issue for consideration. Further development of both

hardware and software might be necessary to resolve those various difficulties.

In their study, Himoto et al. included stages IB through IIIB, irrespective of treatment, and analyzed squamous cell carcinoma (SCC) separately from other histologies (Himoto et al. 2015). Multivariate analysis revealed that mean ADC values at preoperation were a significant factor related to event-free survival (HR 3.34, $P = 0.03$) in the SCC group along with LN metastases and definitive surgery, but not in all cases (Himoto et al. 2015). From these results, consideration of histological types is recommended when using ADC values as a prognostic imaging marker. Nakamura et al. compared the three ADC values of minimum, mean, and maximum ADC values as predictive markers of recurrence after operation (Nakamura et al. 2012a). Multivariate analysis of variance (ANOVA) indicated only the mean ADC value and histology remained as independent prognostic factors for disease-free survival ($P = 0.01$) (Nakamura et al. 2012a). The change of ADC values is used to detect early response of CCRT. In studies of cervical cancer patients with CCRT, significant positive correlation was found between the tumor response and the change in ADC values at 2 and 4 weeks after the start of CCRT (Harry et al. 2008; Kim et al. 2013). Nevertheless, no correlation was found between pretreatment ADC values and tumor size. Recent data also demonstrate the usefulness of change in ADC between pre-CRT and post-CRT (Onal et al. 2016). Results demonstrate that the ADC change was lower in patients with recurrence (25.7% vs. 42.8%, $P < 0.001$) than in patients without recurrence (Onal et al. 2016). Multivariate analysis of pelvic lymph node metastasis and pretreatment mean ADC values revealed prognostic factors affecting OS and disease-free survival (DFS) (Onal et al. 2016). Larger change of ADC value was a positive prognostic factor for OS, although lower pretreatment ADC and positive LN metastases have been identified as negative prognostic factors for both OS and DFS (Onal et al. 2016).

Histogram analysis of DWI is another means of predicting tumor response. A histogram analysis can provide additional parameters to ADC values, such as percentile analysis, skewness, and kurtosis reflecting the biologic heterogeneity of a tumor (Rosenkrantz 2013). The salient benefit of using histogram analysis is that it can incorporate all voxels within the lesion, thereby avoiding the subjectivity of placing an ROI within a small lesion (Rosenkrantz 2013). This benefit engenders improved reproducibility as well as enhanced evaluation of heterogeneity and other additional textures of the tumor. Downey et al. compared histogram analysis results for stage I cervical cancer between SCC and adenocarcinoma (Downey et al. 2013). No significant difference was found at any percentile among 10th, 25th, 50th, 75th, and 90th percentiles. In fact, only skewness was found to have a significant difference between the two histologies, indicating that adenocarcinoma shows a more heterogeneous mixture of cellular architecture than SCC (Downey et al. 2013). Gladwish et al. included patients treated by radiation therapy (RT) or CCRT and analyzed their cases to investigate DFS using histogram analysis with volumetric ADC values (Gladwish et al. 2016). Multivariate analysis showed that absolute and normalized 95th percentile ADC remained associated with DFS (hazard ratio (HR), 0.90–0.98; $P < 0.05$) (Gladwish et al. 2016). For the ROC curve, the AUC is increased by adding 95th percentile ADC values for other clinical variables (Gladwish et al. 2016).

In a meta-analysis conducted in 2015 to ascertain the role of DWI in evaluating response to CCRT, DWI was found to be useful for monitoring treatment response after treatment, but the limited number of reports was insufficient to verify its usefulness for monitoring of early response (Schreuder et al. 2015). A multicenter study of local control evaluation after radiotherapy in Europe found that DWI significantly increases the specificity of MR imaging for the detection of local residual tumors (Thomeer et al. 2019). For 107 cervical cancer patients, the addition of MR imaging with DWI to clinical response evaluation by gynecologists was

found to have a statistically significant incremental value for identifying residual tumors (Thomeer et al. 2019).

Intravoxel incoherent motion (IVIM) of water molecules in vivo includes tissue microenvironments with perfusion in addition to Brownian motion obtained using DWI (Le Bihan et al. 1986, 1989). Zhu et al. applied IVIM methods to advanced cervical cancer patients for prediction of the effects of CCRT (Zhu et al. 2017). The ADC, pure diffusion coefficient (D), and f values change significantly as early as the second week after the initiation of CCRT. In addition, the most dramatic change within 2 weeks is observed for f values (Zhu et al. 2017). Beyond the resources necessary to measure ADC values, the requirement of specific software for analysis of IVIM might represent an obstacle to overcome.

Dynamic contrast-enhanced (DCE) MRI might be useful to assess microvascular structure and perfusion (Zahra et al. 2007). One of several pharmacokinetic models, the so-called Tofts model, posits the extracellular–extravascular space (EES) and plasma as two compartments. Transport between these two compartments is determined using K^{trans} (volume transfer constant between the blood plasma and the EES) and K^{ep} (rate constant between the EES and the blood plasma); many other factors influence enhancement patterns in both tumors and blood vessels (Zahra et al. 2007). The first report describing the prediction of treatment response using DCE-MR parameters was presented by Zahra et al. (2009). The report described that DCE-MR images were acquired at pretreatment and at two points during CCRT, 2 and 5 weeks after the start of RT. Good response to RT was associated with increased perfusion and higher contrast-enhancement ratio and K^{trans} values (Zahra et al. 2009). Mayr's team has long examined tumor perfusion. After they reported histographic analysis of the perfusion of cervical cancer (Mayr et al. 2010), they followed the change of histogram patterns of perfusion during radiation therapy. Their findings show that persistently low perfusion before and during radiation therapy indicates a high risk of treatment failure, although outcomes are favorable in patients with initially high perfusion or subsequent improvement of initially low perfusion (Mayr et al. 2010). These findings suggest that blood supply and oxygenation profoundly influence the radiation response in cervical cancer (Mayr et al. 2010). Coudray et al. used both perfusion and IVM for predicting the risk of local recurrence after preoperative CCRT and operation (Jalaguier-Coudray et al. 2017). Their results show that dynamic enhancement patterns reflect the tumor response for CCRT compared to IVIM factors. Incomplete response was associated significantly with early strong enhancement of the tumor and low signal intensity on the ADC map (Jalaguier-Coudray et al. 2017).

Increasingly, PET/CT has played an important role for predicting prognosis with several quantitative factors such as standardized uptake values (SUV), metabolic tumor volume (MTV), and total lesion glycolysis (TLG) (Barwick et al. 2013). A meta-analysis conducted using data of 12 studies including 660 patients evaluated the predictive value of ^{18}F-FDG PET/CT, showing worse prognosis with high MTV and TLG for both EFS and OS (Han et al. 2018a). In multiple subgroup analyses, the prognostic values of MTV and TLG for EFS were consistently significant (pooled HRs of 5.08–7.30 and 4.80–15.83, respectively) (Han et al. 2018a). The Mallinckrodt Institute of Radiology group developed FDG-PET-based prognostic nomograms from their retrospective database of 234 cervical cancer patients to evaluate recurrence-free survival (Kidd et al. 2012). In this nomogram, only the PET values are used, but combining clinical factors and other modalities is anticipated as the next step.

Texture analysis is a recent technique used to assess tumor heterogeneity by analyzing the distribution and relation of pixel or voxel gray levels in the image (Ganeshan and Miles 2013). It can provide an objective, quantitative assessment of tumor heterogeneity using statistically based methods (Ganeshan and Miles 2013). Ho et al. analyzed the heterogeneity of intratumoral FDG

distribution using texture analysis with grey-level run length encoding matrix (GLRLM) and grey-level size zone matrix (GLSZM) (Ho et al. 2016). Results obtained for 44 patients with bulky tumors revealed high intratumoral metabolic heterogeneity and early temporal change in TLG as a high-risk group with worse survival outcome (Ho et al. 2016).

Quantitative, functional parameters from multiparametric MRI and FDG PET/CT have been investigated as prognostic and predictive biomarkers. Each report combined those parameters variously. However, debate continues as to which imaging biomarker is more robust for accurately predicting individual prognosis in the pretreatment assessment of patients with cervical cancer. Sala et al. evaluated the incremental prognostic values of MRI and FDG-PET/CT compared to clinical histopathologic factors (Sala et al. 2015). They designed three models for predicting PFS: FIGO stage only, clinical factors including age at diagnosis and tumor grade, and a combined model of clinical and imaging parameters including age at diagnosis, tumor grade, parametrial invasion on MRI and para-aortic/distant metastasis on PET (Sala et al. 2015). Among those three models, the combined model of clinical and imaging parameters had significantly higher concordance for predicting PFS than the model including only clinical parameters (Sala et al. 2015). The prognostic model combining imaging parameters and clinical-pathological factors provides information that complements clinical-pathological factors.

3 Endometrial Cancer

Endometrial carcinoma is the most common gynecologic malignancy in the United States and economically developed countries (Morice et al. 2016). Most patients with endometrial cancer will present with symptoms of abnormal or postmenopausal bleeding that allows for early tumor detection (Morice et al. 2016). Therefore, most patients are diagnosed at an early stage, when a tumor is confined to the uterus, resulting in favorable overall survival of more than 80% (Rose 1996; Amant et al. 2005; Odagiri et al. 2011). However, recurrence rates for patients with early stage disease are 2–15%, reaching as high as 50% in advanced stages or in patients with aggressive histologic condition (Sorbe et al. 2014; Fung-Kee-Fung et al. 2006). Many local recurrences are curable. For that reason, early detection and proper diagnostic factors for screening are critically important for patients' prognosis (Salani et al. 2011).

The reported prognostic factors for endometrial cancer are age, stage, histology, depth of myometrial invasion, lymphovascular space invasion, and LN metastasis (Larson et al. 1996) (Fig. 2). Among those factors, many reports have examined relations with histology and the depth of myometrial invasion. Among the many histologies of endometrial cancer, such as endometrioid carcinoma, mucinous carcinoma, and serous carcinoma, 70–80% of uterine corpus cancer were of endometrioid type (Kurman et al. 2014b). Endometrioid carcinoma is graded by the pathological architecture: grade 1 has 5% or less solid growth; grade 2 has 6–50%; and grade 3 has more than 50% (Kurman et al. 2014b). Recurrence develops in 7.7% of grade 1 tumors, 10.5% of grade 2 tumors, and 36.1% of grade 3 tumors (Lurain 2002). Overall 5-year-survival is 86–92% for grades 1 and 2, but 64% for grade 3. It is 50% for clear cell carcinoma and 36% for serous carcinoma (Rose 1996; Lurain 2002). Because these grades are strongly correlated with prognosis, many researchers have tried to assess the relations between these grades and imaging factors, especially ADC values (Tamai et al. 2007; Rechichi et al. 2011; Seo et al. 2013), with varying results. Tamai et al. reported a significant difference between mean ADCs of grade 1 and grade 3 tumors, but considerable overlap was found in that study (Tamai et al. 2007). Other reports describe no significant difference found, but some tendency of decreased ADC value in higher grade (Rechichi et al. 2011). It might not be easy to estimate the precise histological grade based on mean ADC values. Other histological classifications are used for endometrial carcinoma types I and II. Types I and II were suggested by Bokhman in 1983, with classification

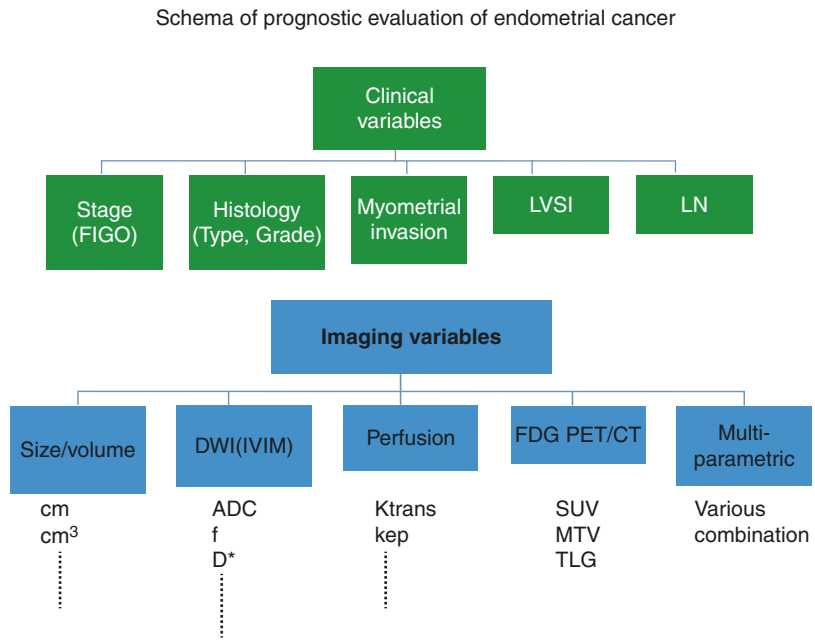

Fig. 2 The schema shows the list of clinical and imaging variables for treatment response and prognostic evaluation for corpus cancer. In endometrial cancer, the trials evaluating the relation of imaging factors with clinical variables, especially histology and myometrial invasion have been performed. Lymphovascular space invasion is characteristic for this cancer. *LVSI* lymphovascular space invasion

according to clinicopathologic, immunohistochemical, and molecular genetic studies (Bokhman 1983; Ronnet et al. 2002). In fact, 89–90% of endometrial carcinoma is classified as Type I with favorable prognosis, including grade 1 and 2 endometrioid carcinoma associated with hyperestrogenism and genetic alterations of PTEN mutation, microsatellite instability, and KRAS mutation (Ronnet et al. 2002). Type II carcinoma is unrelated to estrogen. It includes aggressive histologic subtypes such as grade 3 endometrioid adenocarcinoma, serous carcinoma, and clear cell carcinoma (Ronnet et al. 2002). Genetic mutation of p53 has been suggested (Ronnet et al. 2002). From an imaging perspective, analysis of semiquantitative enhancement pattern on DCE-MRI has revealed that unfavorable Type II tumors show stronger enhancement than that of Type I tumors (Fukunaga et al. 2015).

The depth of myometrial invasion is one important prognostic factor (Larson et al. 1996). Regarding the relation with imaging factors, SUV_{max} and minimum ADC values have been reported as related factors (Inoue et al. 2015; Nakamura et al. 2012b; Kitajima et al. 2012). Inoue et al. showed that the minimum ADC was significantly lower for patients with deep myometrial invasion, although mean ADC did not differ significantly: 0.84 for superficial and 0.78 for deep myometrial invasion ($P = 0.081$) (Inoue et al. 2015). Actually, their results accord well with those reported by Nakamura et al., which showed a utility minimum ADC value with the relation of myometrial invasion (Nakamura et al. 2012b). Histogram analysis of ADC values indicates that the higher the quartile ADC (qADC) value is, the deeper the myometrial invasion and higher the frequency of LVSI and cervical invasion are (Cao et al. 2012). Their results suggest that high tumor heterogeneity might be related with tumor invasiveness (Cao et al. 2012). Recently, simple MR volumetric assessment of tumors is suggested as an easy and accurate method for predicting lymphovascular and myometrial invasion (Nougaret et al. 2015). A total tumor volume ratio (TVR = total tumor volume/total uterine volume × 100) greater than or equal to 25% allows prediction of deep myometrial invasion with sensitivity of 100% and specificity of 93% (area under the curve, 0.96; 95% confidence interval, 0.86,

0.99) at axial oblique diffusion-weighted imaging (Nougaret et al. 2015).

The following studies were undertaken to assess the relation between prognosis and imaging factors directly. Using minimum ADC values and the CA125 tumor marker, Nakamura et al. examined disease-free survival in 111 patients (Nakamura et al. 2012b). Results show that the FIGO stage was the independent prognostic factor for DFS (P = 0.013), followed by the minimum ADC value among other factors of FIGO stage, depth of myometrial invasion, cervical involvement, lymph node metastasis, ovarian metastasis, peritoneal cytology, and tumor maximum size (Nakamura et al. 2012b). No correlation was found between serum CA125 levels and biological parameters for endometrial cancer (Nakamura et al. 2012b). Kuwahara et al. included only patients after complete tumor resection and examined the prediction of tumor recurrence (Kuwahara et al. 2018). Among 210 patients with stages IA to IIIC endometrial cancer who had undergone complete resection of the tumor, minimum and mean ADC values of tumors and those normalized by urine ADC (minimum, mean) were calculated for 210 patients (Kuwahara et al. 2018). Results showed that lower mean ADC and normalized mean ADC values were associated independently with shorter RFS (Kuwahara et al. 2018). By stepwise variable selection, results showed that tumor histology, cervical stromal invasion, and T3 factor were independently associated with shorter RFS (Kuwahara et al. 2018). Even after adding mean ADC values to these three factors, mean ADC values (both with and without normalization) remained useful as independent prognostic factors (Kuwahara et al. 2018) (Fig. 3).

Two studies have been undertaken to evaluate prognosis solely on the basis of SUV_{max} obtained from PET/CT. Results of both studies showed that high SUV_{max} primary tumors had significantly lower DFS and OS rates than low SUV_{max} tumors (Kitajima et al. 2012; Nakamura et al. 2011). Nakamura et al. used multivariate analysis to demonstrate SUV_{max} of the primary tumor as an independent prognostic factor only for OS (P = 0.025), but showed the FIGO stage as the strongest independent prognostic factor for both DFS and OS (P = 0.039 and P = 0.001, respectively) (Nakamura et al. 2011). Chung et al. used metabolic tumor volume (MTV) for the estimation of progression-free survival (PFS) (Chung et al. 2013). Actually, MTV is the estimated volume of tumor tissues with increased tracer uptake measured from a PET/CT image. They calculated the tumor volumes by MRI and MTV as independent significant factors of recurrence (HR 5.795, P = 0.032, 95% CI 1.160–28.958) in Cox regression analysis.

Nakamura et al. tried to combine minimum ADC and SUV_{max} for prognosis prediction (Nakamura et al. 2013). In univariate analysis, both minimum ADC value and SUV_{max} showed significance, but only FIGO stage and high SUV values were found to be independent prognostic factors from multivariate analysis for DFS and OS (Nakamura et al. 2013). Analyses using Kaplan–Meier curves showed that higher SUV had poorer DFS and OS than lower SUV; also, high SUV_{max} with low ADC_{min} was significantly shorter DFS, but was not associated with OS (Nakamura et al. 2013).

Haldorsen et al. examined prognoses using perfusion analysis using a two compartment model of DCE-MRI in addition to ADC values (Haldorsen et al. 2013). Combining several perfusion factors, they examined recurrence-free/progression-free survival (Haldorsen et al. 2013). Low blood flow (Fb) significantly reduced recurrence-free/progression-free survival (Haldorsen et al. 2013). Because low tumor blood flow (Fb) might reflect the tumor's hypoxic capacity, their results indicated that a hypoxic tumor indicates unfavorable prognosis (Haldorsen et al. 2013). Other results of high tumor extraction fraction (E) and vessel heterogeneity (capillary transit time (T_c)) value also support their hypothesis (Haldorsen et al. 2013). Tumors with low perfusion might be less oxygenated and might be therefore less sensitive to radiation or chemotherapeutics delivered by the vascular system and caused unfavorable results in cases with an unresected tumor of high stage.

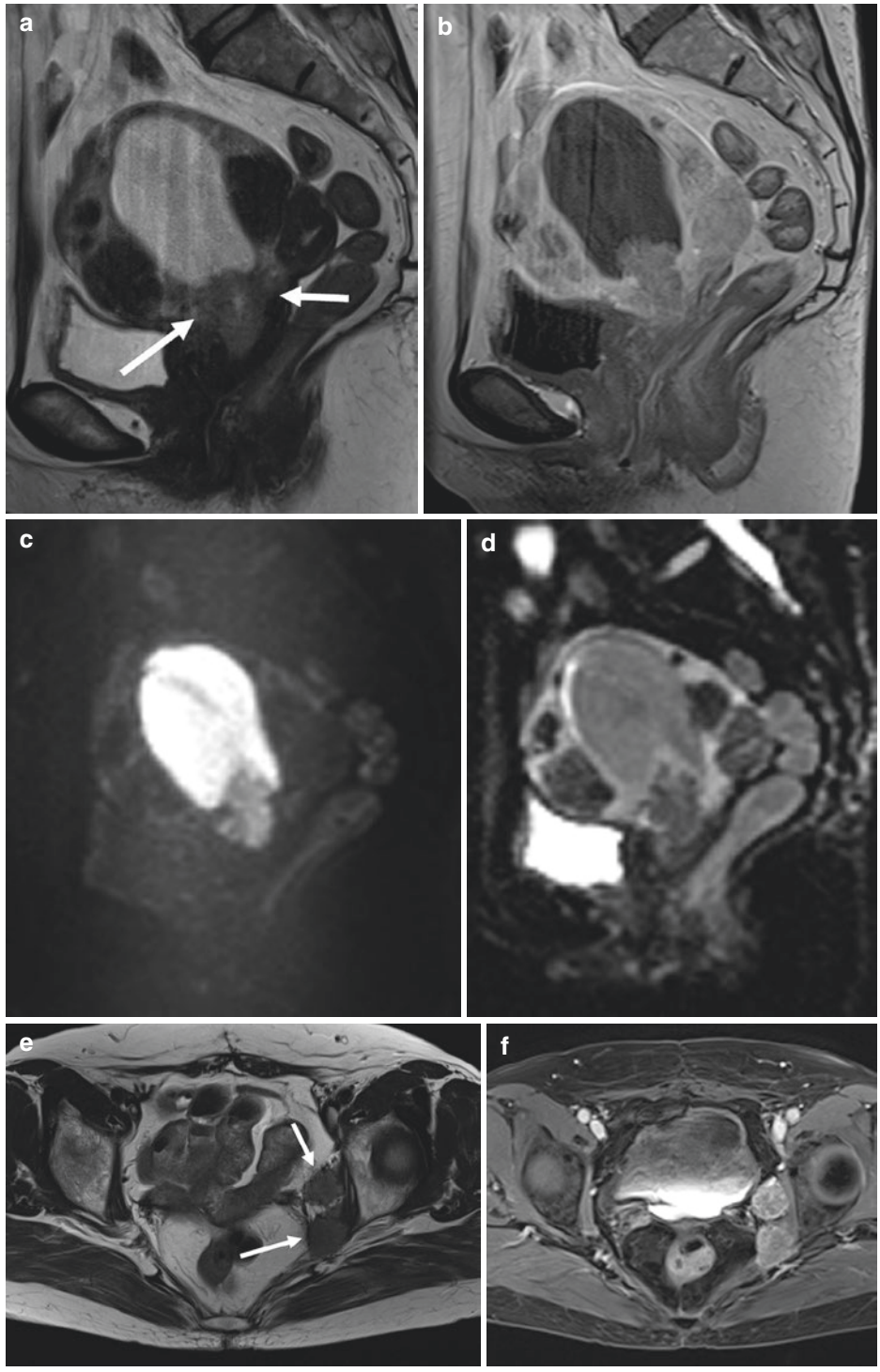

Fig. 3 63-year-old woman with hematometra. Sagittal (**a**) T2WI, (**b**) gadlinium-enhanced T1WI, (**c**) DWI, (**d**) ADC map. Tumor was located at the cervical OS and invaded to myometrium and cervical stroma (arrows). The tumor was diagnosed as endometrioid adenocarcinoma, Grade 2, stage IIb and treat by surgery. Mean ADC values of the tumor was 0.54×10^{-3} mm^2/s and it was lower than cutoff value of mean ADC value for recurrence in the report of Kuwahara et al. (2018). Axial (**e**) T2WI, (**f**) gadlinium-enhanced T1WI of 4 years later, lymph node metastases was recognized at the left pelvic wall (arrows) and treated by concurrent chemoradiation therapy

4 Ovarian Cancer

Ovarian cancer includes many histologic subtypes of malignancies that vary in etiology, molecular biology, and various characteristics. Ninety percent of ovarian cancers are epithelial, the most common being serous carcinoma (75%) followed by mucinous carcinoma (20%), endometrioid carcinoma (2%), clear cell carcinoma, and others (Torre et al. 2018; Berek 2002). Most ovarian carcinomas are diagnosed at an advanced stage of FIGO stage III or IV; their five-year survival was low about 10–30% (Cannistra 2004). Although platinum-based chemotherapy is effective for high-grade serous carcinoma, relapse rates are also high (Siegel et al. 2013). Regarding the treatment of ovarian cancer, primary debulking surgery (PDS), which removes the primary tumor as well as the associated metastatic disease, is an important factor for the prognosis of the patients and treatment of ovarian cancer because removal of bulky tumor reduces the volume of ascites and eliminates areas that are somewhat resistant to treatment (Berek 2002). Therefore, in addition to the FIGO stage, the extent of residual disease after primary surgery, the volume of ascites, patient age, and performance status are all independent prognostic variables (Berek 2002). Regarding imaging findings, examination using PET/CT is dominant over examinations using CT and MRI, probably because ovarian cancer is diagnosed at high stage with tumor spread in the abdomen and thoracic cavity (Figs. 4 and 5).

For treatment in advanced stages, neoadjuvant chemotherapy (NACT) is performed before PDS. The response for the chemotherapy is estimated using PET-CT or MRI (Avril et al. 2005). Avil et al. evaluated sequential FDG-PET uptake to predict treatment response after the first and third cycle of NACT in advanced-stage (FIGO stages IIIC and IV) ovarian cancer (Avril et al. 2005). Responders were defined those who showed decreased SUV more than 20% after the first cycle of NACT and more than 55% after the third cycle of NACT (Avril et al. 2005). As a criterion for treatment response, 20% of decrease in FDG uptake was proposed by Weber et al. (1999, 2003). Overall survival was found to be correlated significantly with the FDG-PET response after chemotherapy. Regarding the MR imaging factors, Sala et al. attempted to predict the treatment response to NACT using multiparametric MRI including diffusion, perfusion, and MR

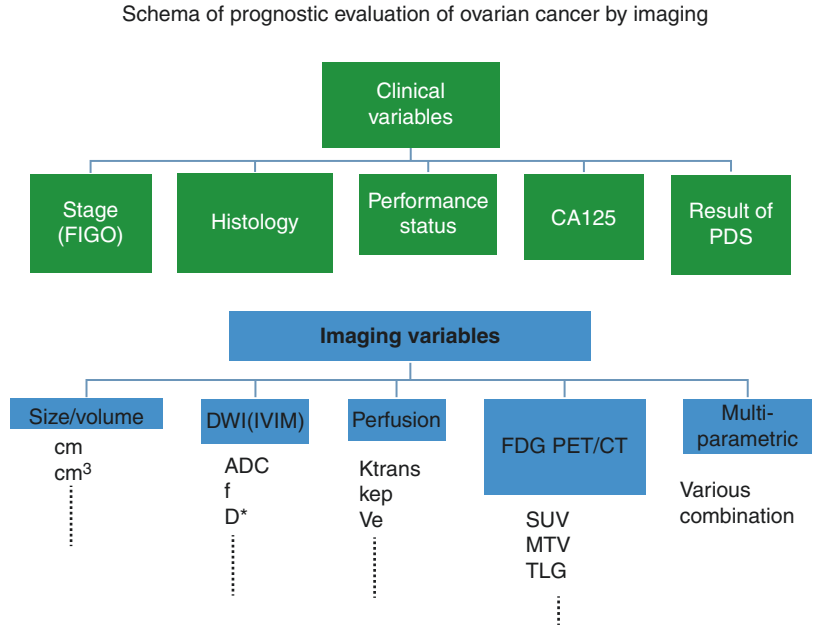

Fig. 4 The schema shows the list of clinical and imaging variables for treatment response and prognostic evaluation for ovarian cancer. CA125 and the result of primary debulking surgery are important factor as clinical variables in ovarian cancer. In imaging variables, FDG-PET/CT occupy most of the reports because ovarian cancer disseminate in both thoracic and abdominal cavity widely. *PDS* primary debulking surgery

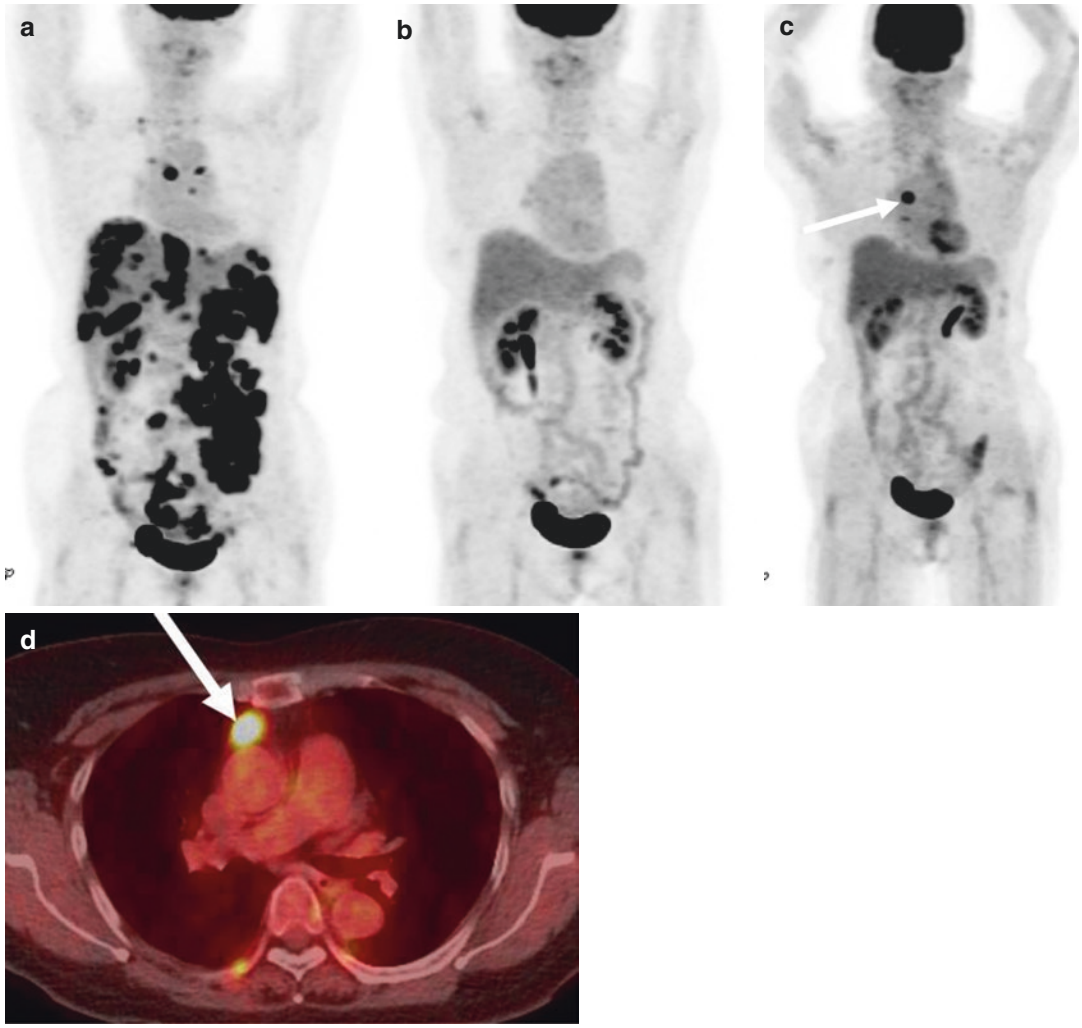

Fig. 5 69-year-old female. The patient was diagnosed high-grade serous carcinoma, FIGO stage IV. (**a**) Maximum intensity projection (MIP) image of PET. At the time of diagnosis, multiple lymph node metastases in both mediastinum and abdomen were found in addition to multiple dissemination in the abdominal cavity. (**b**) After three course of platinum-based chemotherapy, PET image showed prominent response. CA 125 also reduced dramatically from over 16,000 to 15 U/mL. The operation was performed and resulted in optimal surgery. (**c**, **d**) After 3 years, lymph node metastasis at anterior mediastinum (arrow) was found at FDG/PET/CT

spectroscopy (Sala et al. 2012). They evaluated multi-parametric MR imaging factors derived of both original tumor and dissemination (Sala et al. 2012). After treatment, responders showed a significantly greater increase in ADC value (P = 0.021) of ovarian lesions than shown by nonresponders (Sala et al. 2012). Significant decrease in K^{ep} values (P = 0.006) and increase in V_e values (P = 0.025) were observed only in ovarian lesions after chemotherapy, but not other sites of omental or peritoneal deposits (Sala et al. 2012). Those results show the different effects of chemotherapy among primary tumors and disseminations. They have speculated that peritoneal disease has more densely packed cells that might be more resistant against delivery of platinum-based chemotherapy (Sala et al. 2012).

The next two reports explained herein described evaluation of survival using parameters from pretreatment primary ovarian tumors. Lee

et al. assessed the prognostic value of intratumoral FDG uptake heterogeneity (IFH) derived from PET/CT at pretreatment ovarian cancer (Lee et al. 2017). Tumor heterogeneity was calculated statistically using the coefficient of variation (CV), a representative parameter of the global level (Bundschuh et al. 2014). High tumor heterogeneity (IFH) was associated with higher incidence of recurrence ($P = 0.005$, hazard ratio 4.504, 95% CI 1.572–12.902). Kaplan–Meier survival graphs show DFS that is significantly longer in groups with IFH ($P = 0.002$). Diaz-Gil et al. used the peritoneal carcinomatosis index, as detected by CT (CT-PCI) to evaluate correlation with five-year survival combined with ECOG score reflecting patients performance status (Diaz-Gil et al. 2016). This index was determined by the number and location of pretreatment peritoneal dissemination detected by CT as described by Sugarbaker (Jacquet and Sugarbaker 1996). Whole abdomen was divided into nine regions and dissemination was scored at each region. Results obtained for 82 patients with stage III or stage IV ovarian cancer showed that multivariate binary logistic regression suggested significantly improved five-year survival with lower CT-PCI and lower ECOG performance scores, which indicate good daily activity and physical ability (Diaz-Gil et al. 2016). Simple evaluation merely using pretreatment CT and performance status might be beneficial to both clinicians and patients. Kyriazi et al. evaluated the prediction of chemotherapy response in patients with primary ovarian or peritoneal cancer using an ADC histogram (Kyriazi et al. 2011). In addition, DW imaging was performed through the abdomen and pelvis before and after 1 and 3 cycles of chemotherapy with newly diagnosed or recurrent disease. Results reveal that pretreatment ADCs were not predictive of response (Jacquet and Sugarbaker 1996). In responders, all ADCs increased after the first and third cycle ($P < 0.001$), whereas skew and kurtosis decreased after the third ($P < 0.001$ and $P = 0.006$, respectively) (Jacquet and Sugarbaker 1996). The best discriminant parameter of response after both the first and third cycles was the percentage change of the 25th percentile (% delta C25) (Jacquet and Sugarbaker 1996). In nonresponders, no parameter changed significantly.

Most patients with newly diagnosed ovarian carcinoma are initially treated with a combination of platinum-based chemotherapy and surgical debulking of abdominal tumors. Several trials have assessed predicted prognosis using residual disease on CT after PDS. Evaluation of the results of PDS was classified into “optimal surgery” for which the visually residual tumor is less than 1 cm and “suboptimal surgery” with visually residual tumor size greater than 1 cm. A noteworthy point is that there is considerable discrepancy about the judgment of PDS, about 52%, between gynecologist judgment and imaging findings by CT scan (Chi et al. 2010; Lakhman et al. 2012). The locations of residual tumors larger than 1 cm on CT were the perihepatic region, large-bowel serosa, upper abdominal lymph nodes, and supradiaphragmatic lymph node (Lakhman et al. 2012). Those locations were areas for which radiologists must take care to observe at CT after PDS. Chi et al. analyzed prognostic factors for PFS and OS after PDS (Chi et al. 2010). Multivariate analysis revealed that age ($P = 0.040$), stage III vs. stage IV ($P = 0.038$), and residual disease of 0.5 mm or less vs. 0.6–1.0 cm ($P = 0.018$) were significant for favorable OS. Later, Lakhman strove to clarify the correlation between suboptimally debulked residual disease on CT and patients’ prognosis (Lakhman et al. 2012). Patients with suboptimally debulked residual disease on CT had significantly worse median progression-free survival ($P = 0.001$) and overall survival ($P \leq 0.010$). Multivariate analysis showed that residual disease larger than 1 cm on CT remained an important predictor of overall survival, after adjustment for stage and days between surgery and postoperative CT.

Distinction between perihepatic dissemination and hematogenous hepatic metastases is important because FIGO staging classifies perihepatic capsular metastases as stage III and hematogenous hepatic metastases as stage IV (Prat and FCoG 2015). O’Neill et al. compared the prognosis between liver metastasis and dissemination (O’Neill et al. 2017). They divided liver tumors into disseminations with or without liver

parenchymal invasion and hematogenous metastases. Results demonstrate that OS with and without liver parenchymal invasion were similar (median, 80 months; $P = 0.6$), but hematogenous metastases were associated with significantly shorter survival by univariate (median 63 months) and multivariate analyses ($P = 0.03$; HR, 1.88; 95% CI: 1.14, 3.28) (O'Neill et al. 2017).

For ovarian cancers, PET/CT is used widely for detecting widely disseminating tumors both before and after first-line treatment. Yamamoto et al. used pretreatment PET/CT values for predicting prognosis (Yamamoto et al. 2016). In multivariate analysis, only TLG showed a significant difference ($P = 0.038$) among MTV, TLG, SUV_{max}, tumor size, and CA125 (Yamamoto et al. 2016). Both lower MTV and lower TLG showed poorer PFS and could serve as potential surrogate biomarkers for recurrence in patients who undergo primary cytoreductive surgery followed by platinum-based chemotherapy (Yamamoto et al. 2016). Caobelli et al. used PET images after first-line treatment as multi-institutional center study (Caobelli et al. 2016). Prognosis was compared by the presence or absence of FDG uptake after first-line treatment for both whole body and lymph nodes. Results demonstrate that PFS and OS were significantly longer in patients with a negative than a positive uptake after 4 years of follow-up. In addition, this multicenter study stratified the same FIGO stage patients according to the prognosis evaluated by PET (Caobelli et al. 2016). Patients with the same FIGO stage I–II or III–IV, but with negative PET had a significantly better four-year OS than patients with the same FIGO stage group but positive PET (Caobelli et al. 2016). This result might indicate that prognosis is favorable if FDG uptake disappeared after the treatment even in advanced stage cancer than in patients with early stage but poor treatment response. According to the meta-analysis evaluating prognostic value of volume-based metabolic parameters of 18F-FDG PET/CT, eight papers with 473 patients were included (Han et al. 2018b). Results demonstrate that the MTV and TLG for PFS were associated significantly with PFS (Han et al. 2018b). SUV was not included in this study.

The following two reports described evaluation of prognoses using the latest analytical methods. The emerging discipline of "radiogenomics" is described by Ruthman et al.: 'Imaging features could serve as molecular surrogates that contribute to the diagnosis, prognosis, and likely gene-expression-associated treatment response of various forms of human cancer' (Rutman and Kuo 2009). Recently, high-grade serous ovarian cancer (HGSOC) was classified into four types based on analysis by TCGA research network and called Classification of Ovarian Cancer (CLOVAR) (Tothill et al. 2008; Verhaak et al. 2013). Four prognostically relevant CLOVAR subtypes of HGSOC were identified and designated as differentiated, immunoreactive, mesenchymal, and proliferative (Tothill et al. 2008; Verhaak et al. 2013). Vargas investigated associations among imaging traits observed on CT images, CLOVAR gene signatures, and survival in women with HGSOC (Vargas et al. 2015). Results obtained from 46 patients before surgery, the presence of mesenteric infiltration, and diffuse peritoneal involvement by tumor at CT were associated significantly with CLOVAR mesenchymal subtype (Vargas et al. 2015). Mesenteric infiltration was defined as "diffuse thickening or tethering along the mesentery" (Fig. 6). It was associated with CLOVAR mesenchymal subtype. Patients with mesenteric

Fig. 6 65-year-old female, diagnosed as peritonitis carcinomatosa of peritoneal origin, high-grade serous carcinoma, diagnosed by omental resection. Contrast-enhanced CT image showed diffuse thickening and nodularity along mesentery (arrows) with massive ascites. Gene expression was clarified as mesenchymal transition type

infiltration had shorter median PFS than patients without mesenteric involvement (14.7 vs. 25.6 months) or OS (49.0 vs. 58.2 months) (Vargas et al. 2015). Other imaging features were not significantly associated with CLOVAR subtype or survival (Vargas et al. 2015). Intratumoral heterogeneity was examined in both MRI and PET-CT, but few studies have evaluated inter-site heterogeneity (Soslow 2008; Khalique et al. 2007). A novel experiment using pretreatment CT texture analysis to evaluate inter-site tumor heterogeneity in ovarian cancer was reported by Vargas et al. It classified ovarian cancers by clinical outcome (Vargas et al. 2017). In 38 patients with HGSOC, all lesions of tumor involvement were included; 12 inter-site texture heterogeneity metrics were evaluated using a Gaussian Mixture Model and inter-site similarity matrix (ISM) (Vargas et al. 2017). Differences in texture similarities across HGSOC sites were associated with shorter overall survival (inter-site similarity entropy, similarity level cluster shade, and inter-site similarity level cluster prominence; $P \leq 0.05$) (Vargas et al. 2017). Heterogeneity metrics were also associated with incomplete surgical resection of HGSOC (similarity level cluster shade, inter-site similarity level cluster prominence and inter-site cluster variance; $P \leq 0.05$) (Vargas et al. 2017). Neither the total number of disease sites per patient nor the overall tumor volume per patient was associated with overall survival (Vargas et al. 2017).

5 Conclusion

It has been already 10 years since ADC value is expected to be an imaging biomarker (Padhani et al. 2009). Since then, many researchers have tried to investigate quantitative, functional parameters as prognostic and predictive biomarkers from multiparametric MRI and FDG PET/CT. However, there is continued debate as to which imaging biomarker is more robust for accurately predicting individual prognosis in the pretreatment assessment of patients with gynecological cancers. Emerging new analytic methods dealing with large amount of data and radiogenomics are expected to obtain more detailed tumor characterization which might permit personalized treatment and support improved outcomes.

References

Amant F, Moerman P, Neven P, Timmerman D, Van Limbergen E, Vergote I (2005) Endometrial cancer. Lancet 366(9484):491–505. https://doi.org/10.1016/S0140-6736(05)67063-8

Avril N, Sassen S, Schmalfeldt B, Naehrig J, Rutke S, Weber WA et al (2005) Prediction of response to neoadjuvant chemotherapy by sequential F-18-fluorodeoxyglucose positron emission tomography in patients with advanced-stage ovarian cancer. J Clin Oncol Off J Am Soc Clin Oncol 23(30):7445–7453. https://doi.org/10.1200/JCO.2005.06.965.

Barwick TD, Taylor A, Rockall A (2013) Functional imaging to predict tumor response in locally advanced cervical cancer. Curr Oncol Rep 15(6):549–558. https://doi.org/10.1007/s11912-013-0344-2

Berek JS (2002) Ovarian cancer. In: Berek JS (ed) Novak's gynecology, 13th edn. Lippincott Williams and Wilkins, Philadelphia, pp 1245–1320

Bokhman JV (1983) Two pathogenetic types of endometrial carcinoma. Gynecol Oncol 15(1):10–17

Bundschuh RA, Dinges J, Neumann L, Seyfried M, Zsoter N, Papp L et al (2014) Textural parameters of tumor heterogeneity in (1)(8)F-FDG PET/CT for therapy response assessment and prognosis in patients with locally advanced rectal cancer. J Nucl Med 55(6):891–897. https://doi.org/10.2967/jnumed.113.127340.

Cannistra SA (2004) Cancer of the ovary. N Engl J Med 351(24):2519–2529. https://doi.org/10.1056/NEJMra041842

Cao K, Gao M, Sun YS, Li YL, Sun Y, Gao YN et al (2012) Apparent diffusion coefficient of diffusion weighted MRI in endometrial carcinoma—relationship with local invasiveness. Eur J Radiol 81(8):1926–1930. https://doi.org/10.1016/j.ejrad.2011.04.019

Caobelli F, Alongi P, Evangelista L, Picchio M, Saladini G, Rensi M et al (2016) Predictive value of (18) F-FDG PET/CT in restaging patients affected by ovarian carcinoma: a multicentre study. Eur J Nucl Med Mol Imaging 43(3):404–413. https://doi.org/10.1007/s00259-015-3184-5

Chi DS, Barlin JN, Ramirez PT, Levenback CF, Mironov S, Sarasohn DM et al (2010) Follow-up study of the correlation between postoperative computed tomographic scan and primary surgeon assessment in patients with advanced ovarian, tubal, or peritoneal carcinoma reported to have undergone primary surgical cytoreduction to residual disease of 1 cm or smaller. Int J Gynecol Cancer 20(3):353–357. https://doi.org/10.1111/IGC.0b013e3181d09fd6.

Chung HH, Lee I, Kim HS, Kim JW, Park NH, Song YS et al (2013) Prognostic value of preoperative metabolic tumor volume measured by (1)(8)F-FDG PET/CT and MRI in patients with endometrial cancer. Gynecol Oncol 130(3):446–451. https://doi.org/10.1016/j.ygyno.2013.06.021

Diaz-Gil D, Fintelmann FJ, Molaei S, Elmi A, Hedgire SS, Harisinghani MG (2016) Prediction of 5-year survival in advanced-stage ovarian cancer patients based on computed tomography peritoneal carcinomatosis index. Abdom Radiol (NY) 41(11):2196–2202. https://doi.org/10.1007/s00261-016-0817-5

Downey K, Riches SF, Morgan VA, Giles SL, Attygalle AD, Ind TE et al (2013) Relationship between imaging biomarkers of stage I cervical cancer and poor-prognosis histologic features: quantitative histogram analysis of diffusion-weighted MR images. AJR Am J Roentgenol 200(2):314–320. https://doi.org/10.2214/AJR.12.9545

Fukunaga T, Fujii S, Inoue C, Kato A, Chikumi J, Kaminou T et al (2015) Accuracy of semiquantitative dynamic contrast-enhanced MRI for differentiating type II from type I endometrial carcinoma. J Magn Reson Imaging 41(6):1662–1668. https://doi.org/10.1002/jmri.24730

Fung-Kee-Fung M, Dodge J, Elit L, Lukka H, Chambers A, Oliver T et al (2006) Follow-up after primary therapy for endometrial cancer: a systematic review. Gynecol Oncol 101(3):520–529. https://doi.org/10.1016/j.ygyno.2006.02.011

Ganeshan B, Miles KA (2013) Quantifying tumour heterogeneity with CT. Cancer Imaging 13:140–149. https://doi.org/10.1102/1470-7330.2013.0015.

Gladwish A, Milosevic M, Fyles A, Xie J, Halankar J, Metser U et al (2016) Association of apparent diffusion coefficient with disease recurrence in patients with locally advanced cervical cancer treated with radical chemotherapy and radiation therapy. Radiology 279(1):158–166. https://doi.org/10.1148/radiol.2015150400

Haldorsen IS, Gruner R, Husby JA, Magnussen IJ, Werner HMJ, Salvesen OO et al (2013) Dynamic contrast-enhanced MRI in endometrial carcinoma identifies patients at increased risk of recurrence. Eur Radiol 23(10):2916–2925. https://doi.org/10.1007/s00330-013-2901-3

Han S, Kim H, Kim YJ, Suh CH, Woo S (2018a) Prognostic value of volume-based metabolic parameters of (18)F-FDG PET/CT in uterine cervical cancer: a systematic review and meta-analysis. AJR Am J Roentgenol 211(5):1112–1121. https://doi.org/10.2214/AJR.18.19734

Han S, Kim H, Kim YJ, Suh CH, Woo S (2018b) Prognostic value of volume-based metabolic parameters of (18) F-FDG PET/CT in ovarian cancer: a systematic review and meta-analysis. Ann Nucl Med 32(10):669–677. https://doi.org/10.1007/s12149-018-1289-1

Harry VN, Semple SI, Gilbert FJ, Parkin DE (2008) Diffusion-weighted magnetic resonance imaging in the early detection of response to chemoradiation in cervical cancer. Gynecol Oncol 111(2):213–220. https://doi.org/10.1016/j.ygyno.2008.07.048

Himoto Y, Fujimoto K, Kido A, Baba T, Tanaka S, Morisawa N et al (2015) Pretreatment mean apparent diffusion coefficient is significantly correlated with event-free survival in patients with International Federation of Gynecology and Obstetrics stage Ib to IIIb cervical cancer. Int J Gynecol Cancer 25(6):1079–1085. https://doi.org/10.1097/IGC.0000000000000445.

Ho KC, Fang YH, Chung HW, Yen TC, Ho TY, Chou HH et al (2016) A preliminary investigation into textural features of intratumoral metabolic heterogeneity in (18)F-FDG PET for overall survival prognosis in patients with bulky cervical cancer treated with definitive concurrent chemoradiotherapy. Am J Nucl Med Mol Imaging 6(3):166–175

Inoue C, Fujii S, Kaneda S, Fukunaga T, Kaminou T, Kigawa J et al (2015) Correlation of apparent diffusion coefficient value with prognostic parameters of endometrioid carcinoma. J Magn Reson Imaging 41(1):213–219. https://doi.org/10.1002/jmri.24534

Intaraphet S, Kasatpibal N, Siriaunkgul S, Sogaard M, Patumanond J, Khunamornpong S et al (2013) Prognostic impact of histology in patients with cervical squamous cell carcinoma, adenocarcinoma and small cell neuroendocrine carcinoma. Asian Pac J Cancer Prev 14(9):5355–5360

Jacquet P, Sugarbaker PH (1996) Clinical research methodologies in diagnosis and staging of patients with peritoneal carcinomatosis. Cancer Treat Res 82:359–374

Jalaguier-Coudray A, Villard-Mahjoub R, Delouche A, Delarbre B, Lambaudie E, Houvenaeghel G et al (2017) Value of dynamic contrast-enhanced and diffusion-weighted MR imaging in the detection of pathologic complete response in cervical cancer after neoadjuvant therapy: a retrospective observational study. Radiology 284(2):432–442. https://doi.org/10.1148/radiol.2017161299

Jemal A, Bray F, Center MM, Ferlay J, Ward E, Forman D (2011) Global cancer statistics. CA Cancer J Clin 61(2):69–90. https://doi.org/10.3322/caac.20107

Katanyoo K, Tangjitgamol S, Chongthanakorn M, Tantivatana T, Manusirivithaya S, Rongsriyam K et al (2011) Treatment outcomes of concurrent weekly carboplatin with radiation therapy in locally advanced cervical cancer patients. Gynecol Oncol 123(3):571–576. https://doi.org/10.1016/j.ygyno.2011.09.001

Khalique L, Ayhan A, Weale ME, Jacobs IJ, Ramus SJ, Gayther SA (2007) Genetic intra-tumour heterogeneity in epithelial ovarian cancer and its implications for molecular diagnosis of tumours. J Pathol 211(3):286–295. https://doi.org/10.1002/path.2112

Kidd EA, El Naqa I, Siegel BA, Dehdashti F, Grigsby PW (2012) FDG-PET-based prognostic nomograms for locally advanced cervical cancer. Gynecol Oncol 127(1):136–140. https://doi.org/10.1016/j.ygyno.2012.06.027

Kim HS, Kim CK, Park BK, Huh SJ, Kim B (2013) Evaluation of therapeutic response to concurrent

chemoradiotherapy in patients with cervical cancer using diffusion-weighted MR imaging. J Magn Reson Imaging 37(1):187–193. https://doi.org/10.1002/jmri.23804

Kitajima K, Kita M, Suzuki K, Senda M, Nakamoto Y, Sugimura K (2012) Prognostic significance of SUVmax (maximum standardized uptake value) measured by [(1)(8)F]FDG PET/CT in endometrial cancer. Eur J Nucl Med Mol Imaging 39(5):840–845. https://doi.org/10.1007/s00259-011-2057-9

Kristensen GB, Abeler VM, Risberg B, Trop C, Bryne M (1999) Tumor size, depth of invasion, and grading of the invasive tumor front are the main prognostic factors in early squamous cell cervical carcinoma. Gynecol Oncol 74(2):245–251. https://doi.org/10.1006/gyno.1999.5420

Kurman RJ, Carcangiu ML, Herrington DS, Young HR (2014a) Tumours of the uterine cervix. In: Kuraman RJ, Carcangiu ML, Herrington DS, Young HR (eds) WHO classification of Tumours of Female Reproductive Organas, 4th edn. International Agency for Research on Cancer (IARC), Lyon, pp 169–206

Kurman RJ, Carcangiu ML, Herrington DS, Young RH (2014b) Tumours of the uterine corpus. In: Kuramn RJ, Carcangiu ML, Herrington DS, Young RH (eds) WHO classification of Tumours of Female Reproductive Organas, 4th edn. International Agency for Research on Cancer (IARC), Lyon, pp 121–154

Kuwahara R, Kido A, Tanaka S, Abiko K, Nakao K, Himoto Y et al (2018) A predictor of tumor recurrence in patients with endometrial carcinoma after complete resection of the tumor: the role of pretreatment apparent diffusion coefficient. Int J Gynecol Cancer 28(5):861–868. https://doi.org/10.1097/IGC.0000000000001259.

Kyriazi S, Collins DJ, Messiou C, Pennert K, Davidson RL, Giles SL et al (2011) Metastatic ovarian and primary peritoneal cancer: assessing chemotherapy response with diffusion-weighted MR imaging—value of histogram analysis of apparent diffusion coefficients. Radiology 261(1):182–192. https://doi.org/10.1148/radiol.11110577

Lakhman Y, Akin O, Sohn MJ, Zheng J, Moskowitz CS, Iyer RB et al (2012) Early postoperative CT as a prognostic biomarker in patients with advanced ovarian, tubal, and primary peritoneal cancer deemed optimally debulked at primary cytoreductive surgery. AJR Am J Roentgenol 198(6):1453–1459. https://doi.org/10.2214/AJR.11.7257

Larson DM, Connor GP, Broste SK, Krawisz BR, Johnson KK (1996) Prognostic significance of gross myometrial invasion with endometrial cancer. Obstet Gynecol 88(3):394–398. https://doi.org/10.1016/0029-7844(96)00161-5

Le Bihan D, Breton E, Lallemand D, Grenier P, Cabanis E, Laval-Jeantet M (1986) MR imaging of intravoxel incoherent motions: application to diffusion and perfusion in neurologic disorders. Radiology 161(2):401–407

Le Bihan D, Turner R, MacFall JR (1989) Effects of intravoxel incoherent motions (IVIM) in steady-state free precession (SSFP) imaging: application to molecular diffusion imaging. Magn Reson Med 10(3):324–337

Lee M, Lee H, Cheon GJ, Kim HS, Chung HH, Kim JW et al (2017) Prognostic value of preoperative intratumoral FDG uptake heterogeneity in patients with epithelial ovarian cancer. Eur Radiol 27(1):16–23. https://doi.org/10.1007/s00330-016-4368-5

Lurain JR (2002) Uterine cancer. In: Berek JS (ed) Novak's gynecology. Lippincott Williams and Wilkins, Philadelphia, pp 1143–1198

Mayr NA, Wang JZ, Lo SS, Zhang D, Grecula JC, Lu L et al (2010) Translating response during therapy into ultimate treatment outcome: a personalized 4-dimensional MRI tumor volumetric regression approach in cervical cancer. Int J Radiat Oncol Biol Phys 76(3):719–727. https://doi.org/10.1016/j.ijrobp.2009.02.036

Morice P, Leary A, Creutzberg C, Abu-Rustum N, Darai E (2016) Endometrial cancer. Lancet 387(10023):1094–1108. https://doi.org/10.1016/S0140-6736(15)00130-0

Nakamura K, Hongo A, Kodama J, Hiramatsu Y (2011) The measurement of SUVmax of the primary tumor is predictive of prognosis for patients with endometrial cancer. Gynecol Oncol 123(1):82–87. https://doi.org/10.1016/j.ygyno.2011.06.026

Nakamura K, Imafuku N, Nishida T, Niwa I, Joja I, Hongo A et al (2012b) Measurement of the minimum apparent diffusion coefficient (ADCmin) of the primary tumor and CA125 are predictive of disease recurrence for patients with endometrial cancer. Gynecol Oncol 124(2):335–339. https://doi.org/10.1016/j.ygyno.2011.10.014

Nakamura K, Joja I, Fukushima C, Haruma T, Hayashi C, Kusumoto T et al (2013) The preoperative SUVmax is superior to ADCmin of the primary tumour as a predictor of disease recurrence and survival in patients with endometrial cancer. Eur J Nucl Med Mol Imaging 40(1):52–60. https://doi.org/10.1007/s00259-012-2240-7

Nakamura K, Joja I, Nagasaka T, Fukushima C, Kusumoto T, Seki N et al (2012a) The mean apparent diffusion coefficient value (ADCmean) on primary cervical cancer is a predictive marker for disease recurrence. Gynecol Oncol 127(3):478–483. https://doi.org/10.1016/j.ygyno.2012.07.123

Nougaret S, Reinhold C, Alsharif SS, Addley H, Arceneau J, Molinari N et al (2015) Endometrial cancer: combined MR volumetry and diffusion-weighted imaging for assessment of myometrial and lymphovascular invasion and tumor grade. Radiology 276(3):797–808. https://doi.org/10.1148/radiol.15141212

O'Neill AC, Somarouthu B, Tirumani SH, Braschi-Amirfarzan M, Van den Abbeele AD, Ramaiya NH et al (2017) Patterns and prognostic importance of hepatic involvement in patients with serous ovarian cancer: a single-institution experience with 244

patients. Radiology 282(1):160–170. https://doi.org/10.1148/radiol.2016152595

Odagiri T, Watari H, Hosaka M, Mitamura T, Konno Y, Kato T et al (2011) Multivariate survival analysis of the patients with recurrent endometrial cancer. J Gynecol Oncol 22(1):3–8. https://doi.org/10.3802/jgo.2011.22.1.3

Onal C, Erbay G, Guler OC (2016) Treatment response evaluation using the mean apparent diffusion coefficient in cervical cancer patients treated with definitive chemoradiotherapy. J Magn Reson Imaging 44(4):1010–1019. https://doi.org/10.1002/jmri.25215

Padhani AR, Liu G, Koh DM, Chenevert TL, Thoeny HC, Takahara T et al (2009) Diffusion-weighted magnetic resonance imaging as a cancer biomarker: consensus and recommendations. Neoplasia 11(2):102–125

Prat J, FCoG O (2015) Staging classification for cancer of the ovary, fallopian tube, and peritoneum: abridged republication of guidelines from the International Federation of Gynecology and Obstetrics (FIGO). Obstet Gynecol 126(1):171–174. https://doi.org/10.1097/AOG.0000000000000917

Rechichi G, Galimberti S, Signorelli M, Franzesi CT, Perego P, Valsecchi MG et al (2011) Endometrial cancer: correlation of apparent diffusion coefficient with tumor grade, depth of myometrial invasion, and presence of lymph node metastases. AJR Am J Roentgenol 197(1):256–262. https://doi.org/10.2214/AJR.10.5584

Ronnet BM, Zaino RJ, Ellenson LH, Kurman RJ (2002) Endometrial carcinoma. In: Kurman RJ (ed) Blaustein's pathology of the female genital tract. Springer, New York, pp 501–560

Rose PG (1996) Endometrial carcinoma. N Engl J Med 335(9):640–649. https://doi.org/10.1056/NEJM199608293350907

Rosenkrantz AB (2013) Histogram-based apparent diffusion coefficient analysis: an emerging tool for cervical cancer characterization? AJR Am J Roentgenol 200(2):311–313. https://doi.org/10.2214/AJR.12.9926

Rutman AM, Kuo MD (2009) Radiogenomics: creating a link between molecular diagnostics and diagnostic imaging. Eur J Radiol 70(2):232–241. https://doi.org/10.1016/j.ejrad.2009.01.050

Saida T, Tanaka YO, Ohara K, Oki A, Sato T, Yoshikawa H et al (2010) Can MRI predict local control rate of uterine cervical cancer immediately after radiation therapy? Magn Reson Med Sci 9(3):141–148. JST.JSTAGE/mrms/9.141 [pii]

Sala E, Kataoka MY, Priest AN, Gill AB, McLean MA, Joubert I et al (2012) Advanced ovarian cancer: multiparametric MR imaging demonstrates response- and metastasis-specific effects. Radiology 263(1):149–159. https://doi.org/10.1148/radiol.11110175

Sala E, Micco M, Burger IA, Yakar D, Kollmeier MA, Goldman DA et al (2015) Complementary prognostic value of pelvic magnetic resonance imaging and whole-body Fluorodeoxyglucose positron emission tomography/computed tomography in the pretreatment assessment of patients with cervical cancer. Int J Gynecol Cancer 25(8):1461–1467. https://doi.org/10.1097/IGC.0000000000000519.

Salani R, Backes FJ, Fung MF, Holschneider CH, Parker LP, Bristow RE et al (2011) Posttreatment surveillance and diagnosis of recurrence in women with gynecologic malignancies: Society of Gynecologic Oncologists recommendations. Am J Obstet Gynecol 204(6):466–478. https://doi.org/10.1016/j.ajog.2011.03.008

Schreuder SM, Lensing R, Stoker J, Bipat S (2015) Monitoring treatment response in patients undergoing chemoradiotherapy for locally advanced uterine cervical cancer by additional diffusion-weighted imaging: a systematic review. J Magn Reson Imaging 42(3):572–594. https://doi.org/10.1002/jmri.24784

Seo JM, Kim CK, Choi D, Kwan Park B (2013) Endometrial cancer: utility of diffusion-weighted magnetic resonance imaging with background body signal suppression at 3T. J Magn Reson Imaging 37(5):1151–1159. https://doi.org/10.1002/jmri.23900

Siegel R, Naishadham D, Jemal A (2013) Cancer statistics, 2013. CA Cancer J Clin 63(1):11–30. https://doi.org/10.3322/caac.21166

Sorbe B, Juresta C, Ahlin C (2014) Natural history of recurrences in endometrial carcinoma. Oncol Lett 8(4):1800–1806. https://doi.org/10.3892/ol.2014.2362

Soslow RA (2008) Histologic subtypes of ovarian carcinoma: an overview. Int J Gynecol Pathology 27(2):161–174. https://doi.org/10.1097/PGP.0b013e31815ea812.

Tamai K, Koyama T, Saga T, Umeoka S, Mikami Y, Fujii S et al (2007) Diffusion-weighted MR imaging of uterine endometrial cancer. J Magn Reson Imaging 26(3):682–687. https://doi.org/10.1002/jmri.20997

Thomeer MG, Vandecaveye V, Braun L, Mayer F, Franckena-Schouten M, de Boer P et al (2019) Evaluation of T2-W MR imaging and diffusion-weighted imaging for the early post-treatment local response assessment of patients treated conservatively for cervical cancer: a multicentre study. Eur Radiol 29(1):309–318. https://doi.org/10.1007/s00330-018-5510-3

Torre LA, Trabert B, DeSantis CE, Miller KD, Samimi G, Runowicz CD et al (2018) Ovarian cancer statistics, 2018. CA Cancer J Clin 68(4):284–296. https://doi.org/10.3322/caac.21456

Tothill RW, Tinker AV, George J, Brown R, Fox SB, Lade S et al (2008) Novel molecular subtypes of serous and endometrioid ovarian cancer linked to clinical outcome. Clin Cancer Res 14(16):5198–5208. https://doi.org/10.1158/1078-0432.CCR-08-0196.

Vargas HA, Micco M, Hong SI, Goldman DA, Dao F, Weigelt B et al (2015) Association between morphologic CT imaging traits and prognostically relevant gene signatures in women with high-grade serous ovarian cancer: a hypothesis-generating study. Radiology 274(3):742–751. https://doi.org/10.1148/radiol.14141477

Vargas HA, Veeraraghavan H, Micco M, Nougaret S, Lakhman Y, Meier AA et al (2017) A novel

representation of inter-site tumour heterogeneity from pre-treatment computed tomography textures classifies ovarian cancers by clinical outcome. Eur Radiol 27(9):3991–4001. https://doi.org/10.1007/s00330-017-4779-y

Verhaak RG, Tamayo P, Yang JY, Hubbard D, Zhang H, Creighton CJ et al (2013) Prognostically relevant gene signatures of high-grade serous ovarian carcinoma. J Clin Invest 123(1):517–525. https://doi.org/10.1172/JCI65833

Weber WA, Ziegler SI, Thodtmann R, Hanauske AR, Schwaiger M (1999) Reproducibility of metabolic measurements in malignant tumors using FDG PET. J Nucl Med 40(11):1771–1777

Weber WA, Petersen V, Schmidt B, Tyndale-Hines L, Link T, Peschel C et al (2003) Positron emission tomography in non-small-cell lung cancer: prediction of response to chemotherapy by quantitative assessment of glucose use. J Clin Oncol Off J Am Soc Clin Oncol 21(14):2651–2657. https://doi.org/10.1200/JCO.2003.12.004.

Wright TC, Frenczy A, Kurman RJ (2002) Carcinoma and other tumors of the cervix. In: Kurman RJ (ed) Blaustein's pathology of the female genital tract. Springer, New York, pp 325–382

Yamamoto M, Tsujikawa T, Fujita Y, Chino Y, Kurokawa T, Kiyono Y et al (2016) Metabolic tumor burden predicts prognosis of ovarian cancer patients who receive platinum-based adjuvant chemotherapy. Cancer Sci 107(4):478–485. https://doi.org/10.1111/cas.12890

Zahra MA, Hollingsworth KG, Sala E, Lomas DJ, Tan LT (2007) Dynamic contrast-enhanced MRI as a predictor of tumour response to radiotherapy. Lancet Oncol 8(1):63–74. https://doi.org/10.1016/S1470-2045(06)71012-9

Zahra MA, Tan LT, Priest AN, Graves MJ, Arends M, Crawford RA et al (2009) Semiquantitative and quantitative dynamic contrast-enhanced magnetic resonance imaging measurements predict radiation response in cervix cancer. Int J Radiat Oncol Biol Phys 74(3):766–773. https://doi.org/10.1016/j.ijrobp.2008.08.023

Zhu L, Zhu L, Wang H, Yan J, Liu B, Chen W et al (2017) Predicting and early monitoring treatment efficiency of cervical cancer under concurrent chemoradiotherapy by intravoxel incoherent motion magnetic resonance imaging. J Comput Assist Tomogr 41(3):422–429. https://doi.org/10.1097/RCT.0000000000000550

Zola P, Macchi C, Cibula D, Colombo N, Kimmig R, Maggino T et al (2015) Follow-up in gynecological malignancies: a state of art. Int J Gynecol Cancer 25(7):1151–1164. https://doi.org/10.1097/IGC.0000000000000498.

Therapy Response Imaging in Lymphoma and Hematologic Malignancies

Hina Shah and Heather Jacene

Contents

H. Shah · H. Jacene (✉)
Dana-Farber Cancer Institute and Brigham and Women's Hospital, Boston, MA, USA
e-mail: hina_shah@dfci.harvard.edu; hjacene@bwh.harvard.edu

Abstract

Hematologic malignancies are a heterogeneous group of disorders characterized by a clonal proliferation of abnormal cells in the bone marrow and lymphoid tissues and are divided into two major categories, lymphoid and myeloid. Imaging is most commonly used for staging and response evaluations in lymphoid malignancies, of which there are over 90 subtypes (Swerdlow SH, Campo E, Pileri SA, Blood 127:2375–2390, 2016).

The history of staging and therapy response for hematologic malignancies can be traced to the Ann Arbor staging classification for Hodgkin lymphoma (HL) (Carbone PP, Kaplan HS, Musshoff K, Smithers DW, Tubiana M, Cancer Res 31:1860–1, 1971; Rosenberg SA, Boiron M, DeVita VT, Jr., et al. Cancer Res 31:1862–3, 1971). Numerous therapeutic advances for HL and non-Hodgkin lymphoma (NHL) in the 1980s prompted revisions of existing staging systems and the Cotswold meeting report was the first to introduce specific definitions for posttreatment evaluations (Lister TA, Crowther D, Sutcliffe SB, J Clin Oncol 7:1630–1636, 1989). In the past 20 years, multiple updates to response criteria have occurred due to the recognition of the predictive power of 2-deoxy-2-[18F]-fluoro-D-glucose positron emission tomography/computed tomography (FDG-PET/CT), the

M. Nishino (ed.), *Therapy Response Imaging in Oncology*, Medical Radiology, Diagnostic Imaging,
https://doi.org/10.1007/978-3-030-31171-1_11

subsequent widespread use of FDG-PET/CT, and the introduction of biologic therapeutic agents, like immune checkpoint inhibitors.

This chapter is structured to provide an update for lymphoma (~50% of all hematologic malignancies) and multiple myeloma (~12%) on (1) therapeutic advances, (2) current therapy response criteria and challenges, and (3) emerging approaches for therapy response imaging.

1 Therapeutic Advances in Lymphoma

HL and NHL are each further subdivided based on distinct morphologic and molecular features (Swerdlow et al. 2016). HL, ~10% of lymphomas, has two major subclasses: classical HL (cHL) and lymphocyte-predominant HL (lpHL). NHL has over 30 subtypes grouped by lineage (B cell vs. T cell) and maturity of the cell from which the abnormal clonal population is derived. Clinically, NHL behaves either aggressively or indolently. Diffuse large B cell lymphoma (DLBCL) and follicular lymphoma (FL) are the most common NHL subtypes in the United States. Classical HL is grouped with aggressive NHL while lpHL behaves like an indolent NHL. Treatment choices for patients with lymphoma are dependent on specific subtype, and a complete review is beyond the scope of this chapter. There are, however, commonalities in treatment mainstays and recent therapeutic advances.

1.1 Brief Review of First-Line Therapeutic Approaches and Advances for Lymphoma

For aggressive lymphoma, chemotherapy remains the backbone of first-line therapy. The most common first-line regimen for HL is ABVD (adriamycin, bleomycin, vinblastine, dacarbazine) (Carde et al. 1993; Connors et al. 1997; Duggan et al. 2003; Klimm et al. 2005; Sieber et al. 2002; Bartlett and Foyil 2008). Stanford V and BEACOPP (bleomycin, etoposide, doxorubicin, cyclophosphamide, vincristine, prednisone, and procarbazine) are alternatives. For DLBCL, the preferred first-line regimen is CHOP (cyclophosphamide, doxorubicin, vincristine, and prednisone) and anti-CD20 immunotherapy (Pfreundschuh et al. 2006). Shorter courses of chemotherapy or chemoimmunotherapy combined with involved-field radiation are typically given for early stage disease while longer courses of chemotherapy are given for advanced disease.

For early stage HL and DLBCL, a major objective is balancing cure with risk of recurrence and late toxicity. In recent years, radiation field sizes have been reduced to involved-site or involved-nodal radiation to decrease toxicity to normal organs in early stage HL (Kamran et al. 2018). For non-bulky limited stage DLBCL, no significant difference in 5-year event-free and overall survival (OS) was found between patients who received R-CHOP ($n = 165$) versus R-CHOP plus radiotherapy ($n = 169$) (Lamy et al. 2018).

Treatment options for FL depend on the tumor's clinical behavior and ranges from watch and wait to involved-site radiation for early stage disease to single-agent or combination chemoimmunotherapy regimens for disease rapidly progressing or causing organ dysfunction. Combination of bendamustine and rituximab (BR) was shown in a prospective randomized trial to provide longer progression-free survival (PFS) and less toxicity compared to R-CHOP (Rummel et al. 2013).

Second-generation anti-CD20 antibodies are now approved or under investigation with similar efficacy and toxicity profiles to rituximab. Obinutuzumab is a fully humanized antibody approved by the Food and Drug Administration (FDA) in 2013 for treatment of previously untreated FL, relapsed/refractory (to rituximab) FL, and chronic lymphocytic leukemia (CLL) (Genentech 2013). Ofatumumab is another human anti-CD20 monoclonal antibody that binds a different CD20 epitope than rituximab with modest antitumor activity in patients with heavily pretreated rituximab-refractory follicular NHL (Czuczman et al. 2012; Teeling et al. 2006).

1.2 Therapeutic Advances Beyond the First-Line Setting

Beyond the first-line setting, advances in therapy for lymphoma can be grouped into the general categories of lymphoma-specific targeted therapy, including antibodies and small-molecule inhibitors, and immunotherapy (Table 1).

1.2.1 Lymphoma-Specific Antibodies and Small Molecules

Brentuximab Vedotin (BrV) is an antibody-drug conjugate targeting CD30, an overexpressed cytokine receptor in HL (Falini et al. 1995). BrV is approved for treatment of untreated stage III/IV HL in combination with chemotherapy, in high-risk HL for consolidation after autologous

Table 1 Recently approved and novel therapies for lymphoma

	Target		Approved indications	Investigational indications
Lymphoma-specific antibodies	CD20 (next generation)	Obinutuzumab	FL: Relapsed/refractory with bendamustine; untreated stage II bulky, III, IV with chemotherapy CLL: Untreated with chlorambucil	
		Ofatumumab	CLL	FL
	CD80	Galiximab		HL
Antibody-drug conjugate	CD30	Brentuximab vedotin	HL: Relapsed post ASCT or 2 systemic regimens if ineligible for ASCT Anaplastic large-cell NHL: Relapse after 1 multi-agent regimen	
Small molecule inhibitors	Bruton's tyrosine kinase	Ibrutinib	Mantle cell after 1 prior therapy Marginal zone after 1 anti-CD20 therapy CLL/SLL Waldenstrom's macroglobulinemia	FL DLBCL
	NF-κB	Bortezomib	Mantle cell NHL	HL
	PI3 kinase	Idelalisib	Relapsed/refractory FL ≥2 regimens	HL
	PI3 kinase	Copanlisib		Indolent and aggressive NHL
	Histone deacetylase	Panobinostat		HL
Immunotherapy	PD1	Nivolumab	Classical HL relapsed/progressed after ASCT and brentuximab or after ≥3 lines systemic therapy including ASCT	
	PD1	Pembrolizumab	Relapsed/refractory classical HL after ≥3 prior therapies Relapsed/refractory primary mediastinal large B cell NHL after ≥2 prior therapies	
	PD1	Pidilizumab		Various lymphoma subtypes
	CTLA-4	Ipilimumab		Various lymphoma subtypes
CAR-T cell	CD19	Tisagenlecleucel	Relapsed/refractory DLBCL after ≥2 prior therapies	
	CD19	Axicabtagene ciloleucel	Relapsed/refractory DLBCL after ≥2 prior therapies	

HL Hodgkin lymphoma, *NHL* non-Hodgkin lymphoma, *FL* follicular lymphoma, *CLL/SLL* chronic lymphocytic leukemia/small lymphocytic lymphoma, *MM* multiple myeloma, *ASCT* autologous stem cell transplant, *DLBCL* diffuse large B cell lymphoma

stem cell transplant (ASCT) and in relapsed disease after ASCT or for those who are ineligible for transplant (de Claro et al. 2012). A meta-analysis of 17 studies showed an estimated overall complete remission rate of 33.3% for BrV and 11.1% for other therapies in patients with relapsed/refractory HL post ASCT (Bonthapally et al. 2015). In the phase III multicenter randomized ECHELON-1 trial in patients with untreated stage III/IV cHL, 2-year modified PFS was higher for the BrV + AVD group (82.1%, $n = 664$) compared to the ABVD group (77.2%, $n = 670$, $p = 0.04$) (Connors et al. 2018). BrV as a single agent or in combination with chemotherapy has been shown to be tolerable with antitumor activity in multiple other settings of HL (Bazarbachi et al. 2019; Chen et al. 2015; LaCasce et al. 2018) and is also now approved for treatment of untreated or relapsed anaplastic large-cell lymphoma and adult peripheral T cell lymphoma expressing CD30. Other monoclonal antibodies have also been tested, for example, galiximab against CD80 on Reed-Sternberg cells in relapsed HL, but with less encouraging results (Smith et al. 2013; Suvas et al. 2002).

Targeted therapy with small molecule inhibitors has been tested in multiple lymphoma subtypes. Ibrutinib inhibits Bruton's tyrosine kinase (BTK), a kinase important for B cell development (Lee et al. 2016), and is approved for treating marginal zone and mantle cell lymphoma, CLL/SLL and Waldenstrom's macroglobulinemia. Ibrutinib also has activity in combination with rituximab for untreated and relapsed/refractory follicular NHL (Fowler et al. 2016), with response rates ranging from 20 to 38% in the relapsed/refractory setting (Bartlett et al. 2018; Gopal et al. 2018). Ibrutinib can be considered for DLBCL but may be more effective in certain subsets of DLBCL (Wilson et al. 2015; Younes et al. 2019).

Other small molecular inhibitors for treatment of lymphoma target phosphatidyl inositol-3-kinase delta (PI3K), JAK/STAT, NF-κB, and MEK/ERK pathways, some with promising and others with less promising results (i.e., NF-κB inhibitor bortezomib for HL (Younes et al. 2006)). Idelalisib is a PI3K inhibitor approved for relapsed/refractory follicular NHL after 2 or more systemic chemotherapy regimens. For heavily pretreated HL, Gopal et al. found only modest activity with idelalisib alone (Gopal et al. 2017). Copanlisib, another PI3K inhibitor, has shown promising efficacy in heavily treated patients with indolent and aggressive lymphoma, with an objective response rate of 43.7% in relapsed/refractory indolent lymphoma and manageable toxicity (Dreyling et al. 2017). Panobinostat and other histone deacetylase inhibitors are being studied in translational and clinical trials in HL (Batlevi and Younes 2013).

1.2.2 Immunotherapy

Immune checkpoint inhibitors are associated with durable responses and improved survival in many cancers. The initial studies of these agents were in solid tumors, but checkpoint inhibitors are not "cancer-type" specific and have also been approved or are being investigated in hematologic malignancies. Although the specific targets for checkpoint inhibitors are different, the overall conceptual mechanism of action is similar across agents. When tumor antigen is presented to a naïve T cell and binds a T cell receptor, inhibitory interactions on T cell function occur between PD-1 and PD-L1 and CTLA-4 and B7. The checkpoint inhibitors bind to PD-1, PD-L1, or CTLA-4 and block these inhibitory interactions resulting in amplification of the T cell immune response against tumor.

Nivolumab (Bristol-Myers Squibb n.d.) and pembrolizumab (Merck 2014) are both anti-PD-1 antibodies approved for treatment of cHL in 2016 and 2017, respectively. A pivotal study of nivolumab for cHL enrolled 23 patients with relapse after ASCT (78%) and BrV (78%). Nivolumab was given every 2 weeks until complete response, progression, or excessive toxicity. The objective response rate was 87%, with 17% complete responses, and 24-week PFS was 86% (Ansell et al. 2015). Similar results were seen in another multicenter phase 2 trial including 80

patients with recurrent cHL after ASCT and relapsed or nonresponsive to BrV. Radiographic objective responses were seen in 53/80 with median follow-up of 8.9 months (Younes et al. 2016). In both studies, nivolumab had antitumor activity against cHL and acceptable toxicity profiles (Ansell et al. 2015; Younes et al. 2016).

Pembrolizumab has also been shown to have high activity in relapsed/refractory cHL. KEYNOTE-087 was a single-arm phase 2 study of pembrolizumab in the setting of relapsed or refractory HL defined as ≥3 lines of prior therapy. Patients (n = 210) were enrolled into and response rates were reported for three cohorts depending on prior treatment. For those with disease after ASCT and subsequent BrV (n = 69), overall response rate (ORR) was 74%; after salvage chemotherapy and BrV and ineligible for ASCT (n = 81), ORR was 64%; and after ASCT but no BrV, ORR was 70%. The duration of response was greater than 6 months for 31 patients (Chen et al. 2017). Long-term efficacy of single-agent pembrolizumab given as part of the KEYNOTE-13 study was also demonstrated in the cohort of 31 patients with cHL who were heavily pretreated and had failed BrV therapy (Armand et al. 2016).

Ipilimumab blocks cytotoxic T lymphocyte antigen-4 (CTLA-4), a negative regulator of T cells (O'Day et al. 2007). Ipilimumab has been studied in liquid tumors, alone and in combination with other targeted agents and immune checkpoint inhibitors but is not currently approved for these indications. Phase I studies demonstrated safety of these combinations and responses as well as graft-versus-malignancy effect after allo-transplant.

Several immune checkpoint inhibitors have or are being studied for follicular NHL. An open-label phase II study of pidilizumab, a PD1inhibitor, in combination with rituximab was performed in 32 patients with relapsed rituximab-sensitive follicular NHL. No autoimmune or treatment-related grade 3 or 4 adverse events were reported. Response could be assessed in 29 patients; 15 had a complete response and 4 had a partial response demonstrating activity of the combination against relapsed follicular NHL (Westin et al. 2014). Other early phase studies of other anti-PD1 and PDL1 agents alone and in combination with chemotherapy and targeted therapies also show activity in NHL and future work will likely continue to define the optimal combinations for specific subsets of lymphoma (Lesokhin et al. 2016).

Another recent successful approach to immune-modulatory therapy has been to manipulate a patient's own T cells to recognize tumor antigen. The prime example is chimeric antigen receptor (CAR) T cell therapy for DLBCL. In this approach, individual patients' T cells are collected and then genetically modified ex vivo to recognize antigens on lymphoma cells. Upon re-infusion, the genetically modified cells attack tumor antigen expressing cells. In the case of recurrent/refractory DLBCL and B cell precursor acute lymphoblastic leukemia (ALL), CAR-T cells targeting CD19 on B cells are currently available. Multicenter trials in patients with recurrent/refractory DLBCL after ASCT (or ineligible for transplant) have reported complete response rates in the 40–58% range, with durable remissions reported (Schuster et al. 2017; Locke et al. 2019). A study by Schuster et al. included 14 patients with follicular NHL and 10 had a CR, 89% of which was a continued response with median follow-up 28.6 months (Schuster et al. 2017). The toxicity of CAR-T cells can be substantial, including fatal neurologic complications, cytokine release syndrome, fever, and flu-like illness.

Other genetic mutations can also be used to modify T cells and serve as targets for therapy. For example, HVEM (herpes virus entry mediator) is a receptor gene frequently mutated in follicular NHL leading to increased B cell activation and survival. HVEM ectodomain protein binds B and T lymphocyte attenuator and tumor suppression is restored. CAR-T cells can be used to locally produce the HVEM protein, called solHVEM. This type of CAR-T cell therapy showed enhanced activity in a xenograft follicular lymphoma model (Boice et al. 2016).

CAR-T cells for HL are being explored. In a phase I study of anti-CD30-CAR-T cells for relapsed/refractory HL, 7 of 18 had a partial response and 6 of 18 had stable disease (Ramos et al. 2017). Another study testing anti-CD30-CAR-T cell therapy included 7 patients with HL and found the therapy to be safe with some clinical responses (Wang et al. 2017).

Lenalidomide, an immunomodulatory drug used for years to treat multiple myeloma, works by modulating cytokine production and stimulating T cells and NK cell cytotoxicity (Kotla et al. 2009). Lenalidomide has been shown to have antitumor activity against follicular NHL alone, in combination with rituximab (Leonard et al. 2015; Martin et al. 2017) and in combination with rituximab and ibrutinib (Ujjani et al. 2016; Chanan-Khan and Cheson 2008). Lenalidomide may be considered as a late line of therapy for cHL (Hoppe et al. 2017).

In summary, therapies for lymphoma are continually being modified, including chemotherapy regimens and approaches to radiation therapy for limited stage disease. Multiple new therapeutic combinations, novel targeted drugs and CAR-T cells are being developed to move from a generalized to a more personalized approach.

2 Brief History of Response Criteria for Lymphoma

Standardization of staging evaluations for lymphoma appeared in the early 1970s for HL (Carbone et al. 1971; Rosenberg et al. 1971). Radiologic evaluations played an important role and comprised available techniques at the time. In 1971, this included X-ray, intravenous pyelogram, and bilateral lower extremity lymphogram. Skeletal scintigraphy was considered useful for selected patients with bone pain and whole body (Cheson et al. 2014) Gallium scans were considered experimental (Even-Sapir and Israel 2003). Staging evaluations were updated, and response criteria were added in the 1989 Cotswold meting report (Lister et al. 1989; Crowther and Lister 1990). CT scanning of the chest, abdomen, and pelvis with intravenous contrast was added to the staging studies for HL. Functional imaging with (Cheson et al. 2014) Gallium or technetium was considered useful in certain, but not all, situations for staging and (Cheson et al. 2014) Gallium scanning was suggested to resolve whether residual radiologic abnormalities represented active HL post-therapy.

Ten years later, the International Working Group (IWG) published criteria for standardizing response of NHL to therapy (Cheson et al. 1999). IWG criteria were based on changes in tumor size on CT. The new category complete response unconfirmed (CRu) was introduced and defined as the presence of a residual mass after treatment but at least a 75% decrease in lymphoma burden. It was also around this time that investigations demonstrating the prognostic and predictive value of (Cheson et al. 2014) Gallium for post-therapy assessment of aggressive lymphoma were emerging (Devizzi et al. 1997; Israel et al. 1988; Kaplan et al. 1990; Vose et al. 1996). Several studies demonstrated a worse prognosis for patients with HL and large-cell lymphoma with a positive (Cheson et al. 2014) Gallium scans after initial therapy (Devizzi et al. 1997; Kaplan et al. 1990; Cheson et al. 2014). Gallium imaging with single-photon emission computed tomography (SPECT) scans was encouraged, but not mandated for large-cell lymphoma.

FDG-PET/CT has become the standard imaging modality in the present day for staging and response assessment of lymphoma. FDG-PET/CT was integrated into the 2007 revision of the IWG criteria for post-therapy response assessment of aggressive lymphomas (HL and DLBCL) as numerous studies showed the predictive value of the post-therapy FDG-PET (Cheson et al. 2007; Juweid et al. 2007). This included an important retrospective study of 54 patients with aggressive NHL that demonstrated a more favorable prognosis in a subset of PET negative, but partial responders by IWG criteria (Juweid et al. 2005) (Fig. 1). The 2007 IWG criteria (Cheson et al. 2007) and the accompanying imaging

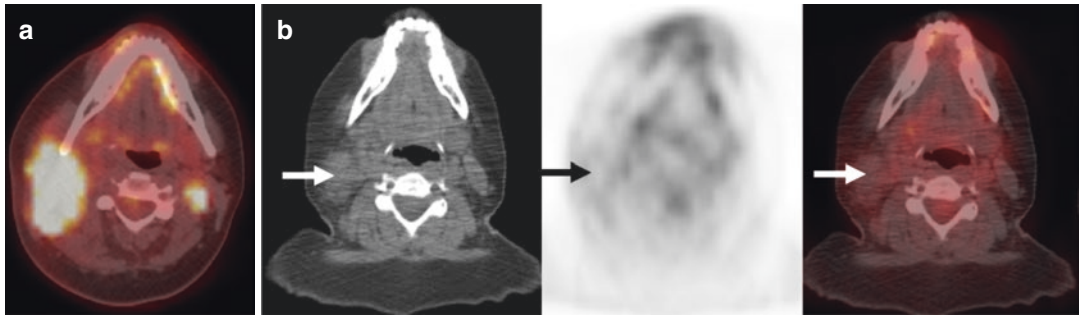

Fig. 1 (**a**) Baseline FDG-PET/CT in a patient with diffuse large B cell lymphoma showed intensely FDG-avid right cervical adenopathy. (**b**) End of therapy PET/CT demonstrated a residual mass in the right neck with FDG uptake similar to mediastinal blood pool (arrows). A negative end of therapy FDG-PET/CT portends a good prognosis despite the residual mass on CT

subcommittee consensus (Juweid et al. 2007) recommended that FDG-PET be performed at least 3 weeks post chemotherapy, preferably at 6–8 weeks and at least 8–12 weeks after radiation therapy. Visual assessment of tumor FDG uptake post-therapy was considered adequate using mediastinal blood pool activity as reference background. Uptake greater than mediastinal blood pool in residual mass >2 cm on CT was considered a marker of residual active disease. In these guidelines, end of therapy FDG-PET was recommended for consistently FDG-avid subtypes like HL and DLBCL. In other non-avid lymphomas or those with variable FDG uptake, FDG-PET was not recommended in the clinical setting. End of therapy PET scan was suggested in clinical practice, but interim PET scan only in the setting of clinical trial (Cheson et al. 2007).

3 Current Response Criteria for Lymphoma

Subsequent experience with the 2007 revised IWG criteria revealed its limitations. This included application of post-therapy criteria in the interim setting. The 2014 modifications in the Lugano classification expanded the role of FDG-PET/CT from the post-therapy setting and as of this writing is the current version of the criteria (Cheson et al. 2014). The 2007 consensus report from the imaging subcommittee of the International Harmonization Project in Lymphoma on the acquisition and interpretation of PET scans was also updated (Barrington et al. 2014).

The Deauville 5-point scale was adopted in the Lugano classification for the interpretation of both post-therapy and interim PET/CT scans (Tables 2 and 3). Tumor uptake is qualitatively compared to reference background uptake in the mediastinal blood pool and liver. The interpretation of the scoring assigned is similar for post-therapy and interim scans for scores 1 and 2 (Figs. 2 and 3), but varies for scores 3, 4, and 5. Scores of 4 or 5 are considered positive for active lymphoma at the end of therapy (Figs. 4 and 5). On interim scans, although there may be prognostic implications, a score of 4 or 5 is considered a partial response if the uptake is

Table 2 Deauville 5-point scale

1	No uptake
2	Uptake less than or equal to mediastinum
3	Uptake more than mediastinum but less than or equal to liver
4	Uptake moderately more than liver uptake, at any site
5	Markedly increased uptake at any site and new sites of disease
X	New area of uptake unlikely to be related to lymphoma

Table 3 Lugano criteria for response assessment in lymphoma (Juweid et al. 2007)

Response category	PET/CT[a]	CT
Complete response	Score 1, 2, 3 with or without residual mass in nodes or extra-nodal sites	Complete resolution of all disease sites or decrease in node size to ≤1.5 cm in LDi
Partial response	Score 4 or 5 with decreased FDG uptake versus baseline with residual masses of any size	≥50% decline product of PPD (single lesion) or SPD of 6 measurable target nodes and/or extra-nodal sites (multiple lesions); decline spleen size >50%
No response/stable disease	Score 4 or 5 with no obvious change in FDG uptake versus baseline	<50% decrease in PPD (single lesion) or SPD of 6 measurable target nodes and/or extra-nodal sites (multiple lesions) and no criteria for progressive disease
Progressive disease	Score 4 or 5 with increase in intensity of FDG uptake versus baseline or new foci of FDG uptake consistent with lymphoma	New or increased adenopathy (nodes 1.5 cm >longest transverse, PPD ≥ 50% from nadir, LDi or SDi increase from nadir by 0.5 cm for lesions ≤2 cm and by >1.0 cm for lesions >2.0 cm), increase in spleen size by >50% of its prior increase from baseline or 2 cm from baseline if no prior splenomegaly, new or recurrent splenomegaly, new nodal or extra-nodal sites; increase of preexisting non-measurable lesions

[a]Deauville 5-point scale

FDG-PET/CT: Score interpretation depends on whether interim or end of therapy scan and clinical scenario. Score 1 or 2: complete response on both interim and end of therapy scans. Score of 4 or 5: partial response on interim scans if FDG uptake is less than baseline or as progressive disease if the FDG uptake is greater than baseline; end of therapy: treatment failure. Score 3: usually negative on both interim and end of therapy scans, but as an inadequate response in risk-adapted trials evaluating de-escalation strategies

CT: A measurable node should be 1.5 cm in longest transverse diameter (LDi) and a measurable extra-nodal site should be 1.0 cm in longest diameter. Longest and shortest (SDi) diameters on the transverse plane of each lesion are multiplied to obtain product of the perpendicular diameters (PPD). Six largest measurable (in two dimensions) nodes and extra-nodal sites are identified from different body regions. Sum of products of the diameters (SPD): adding product of the diameters of the six measurable lesions

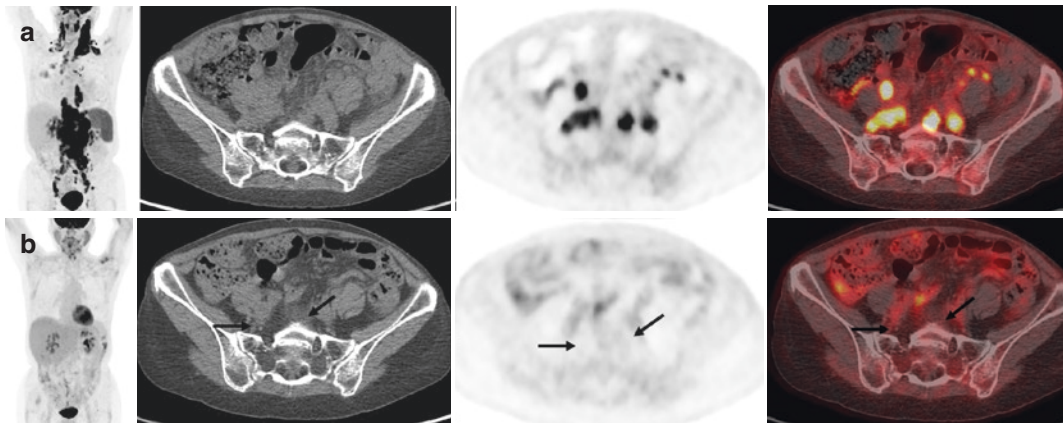

Fig. 2 60-year-old woman with diffuse large B cell lymphoma. (**a**) Baseline FDG-PET/CT scans showed intensely FDG-avid lymphadenopathy above and below the diaphragm and moderately increased FDG uptake diffusely in the spleen. (**b**) After 6 cycles of R-CHOP chemotherapy, the size of the lymph nodes decreased to normal and the FDG uptake in the lymphadenopathy and spleen resolved (arrows). This pattern is consistent with Deauville score 1

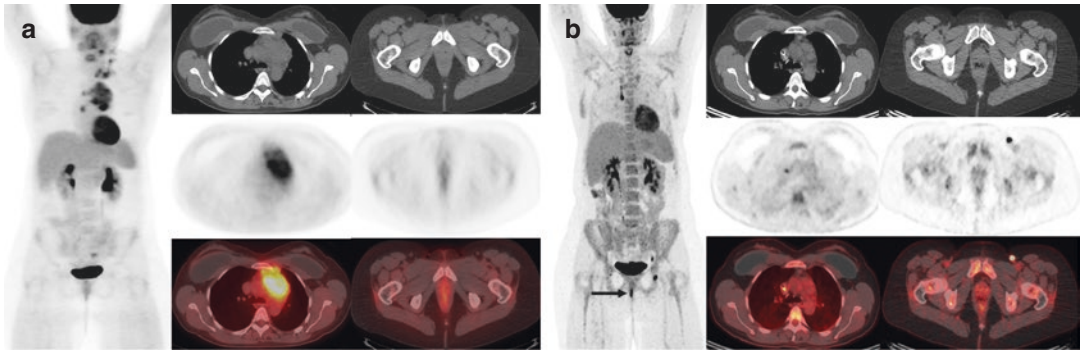

Fig. 3 34-year-old woman with classical Hodgkin lymphoma. (**a**) Baseline FDG-PET/CT scan showed metabolically active left lower cervical, supraclavicular, and mediastinal lymph nodes, consistent with Stage II disease. (**b**) After 2 cycles of ABVD chemotherapy, the lymph nodes decreased in size and residual nodes had FDG uptake similar to mediastinal blood pool; Deauville 2. There was also a new enlarged and intensely FDG-avid left inguinal lymph node (Deauville X). This was felt to most likely be related to inflamed hemorrhoids (arrow). Residual FDG activity was seen in the right chest port catheter used for injection

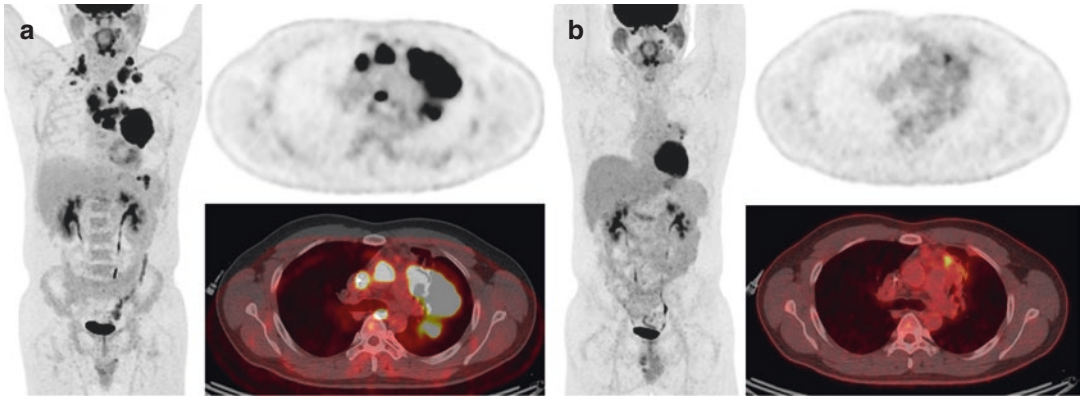

Fig. 4 32-year-old man with classical Hodgkin lymphoma. (**a**) Baseline FDG-PET/CT showed intensely FDG-avid bilateral cervical and mediastinal lymph nodes consistent with metabolically active lymphoma. (**b**) After 2 cycles of ABVD chemotherapy, several focal areas of residual increased FDG uptake greater than the liver were seen in residual mediastinal soft tissue (Deauville 4). At an interim time-point, Deauville 4 may represent treatment response with the presence of residual active disease. At the end of therapy, Deauville 4 is considered treatment failure

decreased versus baseline but as progressive disease if the uptake is greater than baseline. A score of 3 may be considered negative on post-therapy and interim PET/CT scans, but action based on this score may vary in risk-adapted clinical trials depending on the clinical scenario (Fig. 6). For non-FDG avid lymphomas, CT criteria for response are like the original (1999) and revised (2007) IWG criteria (Table 3).

One limitation of the Lugano classification is that the sensitivity and specificity of the criteria to predict outcome is not 100% and varies depending on specific lymphoma subtype. The ability to predict outcome in HL at the end of first-line therapy is more robust, with reported negative predictive values in the 95–100% range and positive predictive values >90% (Engert et al. 2012). In contrast, the positive and negative predictive values of post-therapy FDG-PET/CT in DLBCL are lower and more variable (Cashen et al. 2011; Micallef et al. 2011; Mikhaeel et al. 2000). In a meta-analysis of 7 studies including

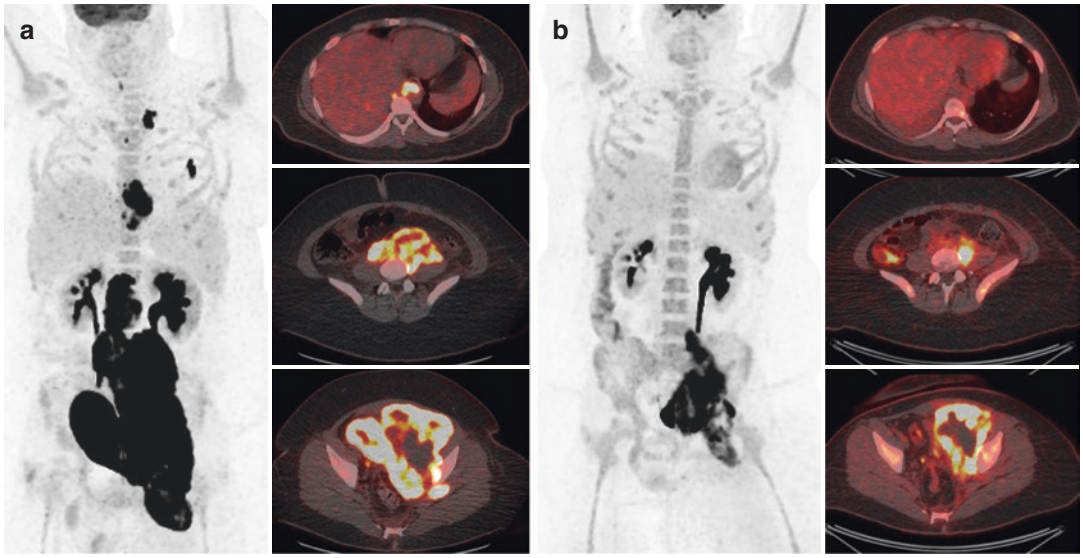

Fig. 5 23-year-old man with T cell histiocyte-rich B cell lymphoma. (**a**) Baseline FDG–PET/CT scan showed extensive intensely FDG-avid left supraclavicular, posterior mediastinal, and retroperitoneal lymphadenopathy and lung nodules. The maximum standardized uptake value (SUV) of the hottest lymph node was 46. (**b**) After 2 cycles of R-CHOP chemotherapy, intensely FDG-avid lymphadenopathy remained in the retroperitoneum with SUVmax of 29 (Deauville Score 5). The sum of the products of target lesions decreased by approximately 60% between the baseline and post cycle 2 scans. As this was an interim FDG–PET/CT scan, Deauville score 5 with decline SUVmax and accompanying decrease of tumor size represents a response; although probably with worse prognosis. At the end of therapy, the Deauville score 5 would have represented treatment failure

737 patients with DLBCL treated with R-CHOP, the relapse rate in patients achieving a PET complete response at the end of treatment ranged from 7 to 20% (Adams et al. 2015). In another study integrating PET response and the National Comprehensive Cancer Network-International Prognostic Index (NCCN-IPI) for DLBCL, Bishton et al. found the PET response provided more information for distinguishing outcomes in patients with NCCN-IPI scores 1–5, compared to those with scores >6. In the later setting, the outcome was poor regardless of response to R-CHOP by FDG-PET (Bishton et al. 2016). Large prospective studies with homogeneous populations are needed to better understand the interplay of current prognostic indicators.

Interim PET/CT scan is one performed early or at the midpoint of treatment to define tumor chemosensitivity, a known prognostic marker. The prognostic value of the Deauville 5-point scale criteria for interim PET/CT assessment was validated in both HL and NHL (Biggi et al. 2013; Itti et al. 2013). Itti et al. studied 114 patients with newly diagnosed DLBCL who received rituximab containing regimens (Itti et al. 2013). With 39 months median follow-up and using Deauville 4 (> liver) as a threshold for positive, 3-year PFS was 81% for PET-negative patients after 2 cycles and 59% for those who were PET positive (Itti et al. 2013). The interobserver agreement was optimal when liver was used as background rather than mediastinal blood pool (Itti et al. 2013). Similarly, a validation study in 260 patients with advanced HL showed accurate and reproducible results using the Deauville 5-point scale. Using scores of 4 or 5 of positive, FDG-PET scan was found to have sensitivity of 73%, specificity of 94%, accuracy of 91%, negative predictive value of 94%, and positive predictive value of 73% for predicating failure-free survival. The interobserver agreement for assigning Deauville scores was good or very good by Kappa analysis among 6 international nuclear medicine experts (Biggi et al. 2013).

Data from prospective studies of risk-adapted therapy using the Deauville 5-point scale are

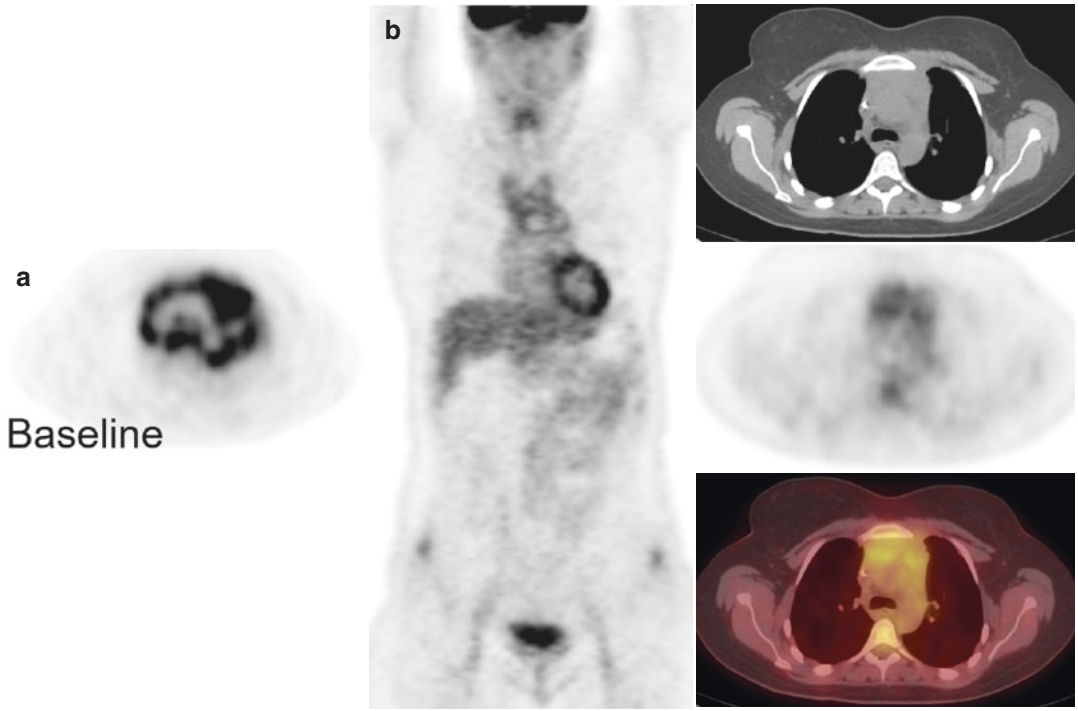

Fig. 6 (**a**) Intensely FDG-avid primary mediastinal large B cell lymphoma in the neck and mediastinum prior to therapy. (**b**) End of therapy PET/CT scan showed FDG uptake greater than blood pool but similar to the liver in the residual mediastinal mass. This is a Deauville 3 response. The level of FDG uptake in the blood and liver is often similar and visualizing the difference between Deauville 2 and 3 scores is challenging. Review of coronal images may be helpful in these cases

emerging. The value of interim PET is better established in HL compared to DLBCL. A review of all these studies is beyond the scope of this review, but a few are described next. In CALGB506, 149 patients with non-bulky early stage HL underwent interim PET after 2 cycles of ABVD. Only 14 patients were PET2 positive and subsequently received escalated BEACOPP and involved-field radiation therapy. The 135 patients with PET2 negative received 2 additional cycles of ABVD without RT. 3-year PFS in this group was 91%. This met the primary endpoint of 3-year PFS > 85% (Straus et al. 2018).

The Southwest Oncology Group performed a prospective study of 336 patients with stage III/IV HL (S0816). After 2 cycles of ABVD chemotherapy, interim PET was performed (PET2). Those with a negative PET2 (i.e., Deauville 1–3) received 4 additional cycles of ABVD, and those with a positive PET2 (i.e., Deauville 4–5) switched to escalated BEACOPP. The estimated 2-year PFS for the 60 PET2 positive patients was 64%, higher than the expected 15–30% (Press et al. 2016). Johnson et al. reported that omission of bleomycin after 2 cycles of ABVD for advanced stage HL resulted in lower pulmonary toxicity without significantly altering efficacy, although the results were just short of the planned noninferiority margin (Johnson et al. 2016). In summary, interim PET-driven switch of therapy is probably feasible and safe for HL.

Studies of risk-adapted therapy based on interim PET in DLBCL have yielded more mixed results. An International Atomic Energy Agency (IAEA) sponsored a multinational prospective study in 327 patients with DLBCL (Carr et al. 2014). Interim FDG-PET/CT was performed after 2 (n = 251), 3 (n = 73) or 4 (n = 3) cycles of chemotherapy. Two-year OS was lower for those with a positive (72%) vs. negative (93%) interim

PET. They also found that among those with positive interim PET, 54% became PET negative at the end of treatment. The 2-year EFS was lower in the interim positive, post-therapy negative patients but some had durable responses and less of a difference in 2-year OS. In contrast, a study from France showed that a negative interim PET in DLBCL can effectively predict better OS and PFS, with 3-year OS of 88% in PET-negative patients and 62% in PET-negative patients (Safar et al. 2012).

4 Challenges of Current Lymphoma Criteria for Response

Response assessment using the Lugano classification, and its earlier versions, were designed based on data using chemotherapeutic drugs and monoclonal antibodies. One early observation and challenge of interpreting end of therapy FDG-PET/CT was visualization of newly FDG-avid lesions in the setting of good response in areas of known disease. A common example of this inflammatory lung lesions (Figs. 3 and 7) and is noted as Deauville X (Table 2).

Immune checkpoint inhibitors have changed the landscape of how tumor response is monitored with imaging. The phenomenon of pseudoprogression (i.e., false worsening) on imaging was first described in patients with melanoma receiving ipilimumab but was also observed in early studies of immune checkpoint inhibitors in lymphoma. A need to address a standardized approach for assessing response of lymphoma to immune checkpoint inhibitors became evident. In addition, the role of FDG-PET/CT for prognostication after CAR-T cell therapy has not been systematically studied (Fig. 8).

Lymphoma response to immunomodulatory therapy criteria (LYRIC) was published to provide guidance for response assessment of lymphoma to immune checkpoint inhibitors (Cheson et al. 2016). In LYRIC, the authors introduced an "indeterminate category" (IR) of response to

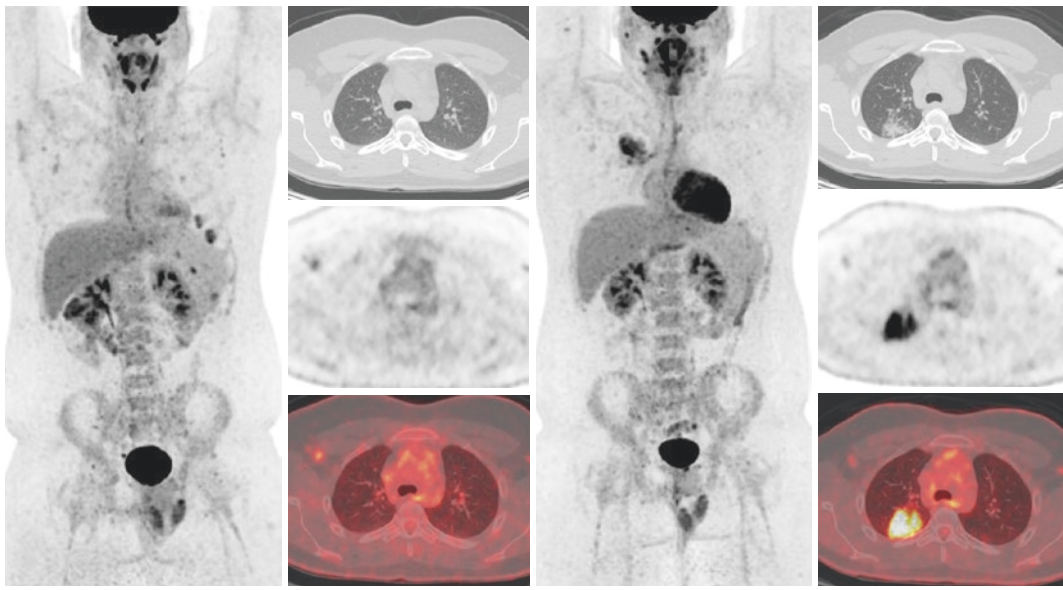

Fig. 7 (**a**) Baseline FDG-PET/CT in a patient with Hodgkin lymphoma showed left epiphrenic and splenic hilar lymph nodes but no lymphoma in the lungs. (**b**) End of therapy FDG-PET/CT shows interval resolution of FDG-avid left epiphrenic and splenic hilar lymph nodes as well as a new FDG-avid consolidative opacity in the right apex. This is classified as Deauville X, since the lung was not a site of disease at baseline and was most likely inflammatory. The findings in the lungs should be correlated with clinical symptoms and followed up with chest computed tomography to assure resolution

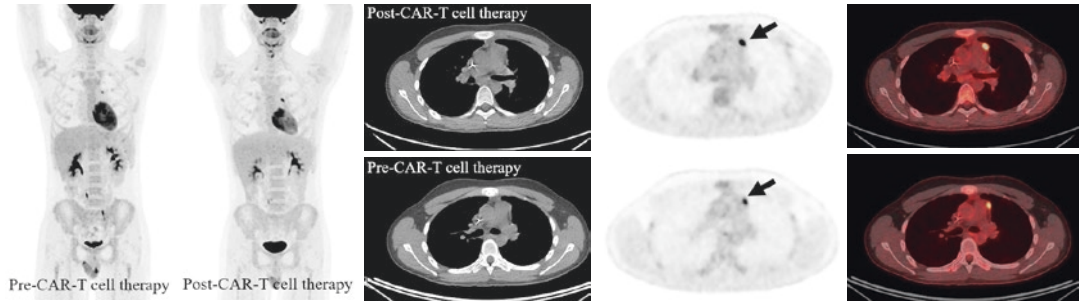

Fig. 8 46-year-old man with diffuse large B cell lymphoma. Prior to CAR-T cell therapy, FDG-avid lymphoma was seen in a 1.3 × 0.5 cm anterior mediastinal soft tissue density with SUVmax 5.2 (arrow). Post-CAR-T cell therapy, the FDG-avid anterior mediastinal soft tissue nodule remained (arrow), measuring 1.4 × 0.8 cm with SUVmax 10.6 (Deauville 5). After CAR-T cell therapy, the significance of a Deauville 5 response at the site of disease is not clear and further investigations are needed

Table 4 LYRIC Indeterminate Response (IR) categories and follow-up (Carr et al. 2014)

IR type	Definition at first follow-up scan	Follow-up of IR findings—definitions of progressive disease[a]
1	Increase in overall tumor burden[b] by ≥50% of up to 6 measurable lesions in the first 12 weeks of therapy and no clinical deterioration	Comparison between current and the scan which showed IR1 response ≥10% increase SPD and increase in size of ≥5 mm of for lesions ≤2 cm and ≥10 mm for lesions >2 cm
2	New lesions at any time or increase 50% any 1 lesion, but not overall progressive disease	New or growing lesions should be added to target lesion(s); up 6 lesions total Newly defined target lesions increase in increase ≥50% nadir value
3	Increase FDG uptake only without concomitant size increase	Increase in size or new lesion defined above

[a]Defined by sum of the products of the diameters (SPD) of measurable target lesions
[b]Patients with IR response on first follow-up should be rescanned 12 weeks later or sooner if clinically indicated

avoid early discontinuation of effective therapy in the setting of pseudo-progression. The definitions of IR are shown in Table 4 (Figs. 9, 10, and 11). While a paucity of evidence supporting the definitions was recognized, the authors emphasized that these criteria are likely to be modified in the future as more data emerges. Importantly, these provisional criteria provide backbone guidance for investigators to incorporate imaging endpoints into clinical trials to assess response of lymphoma to immune checkpoint inhibitors.

Immune-related adverse events may be detected on response assessment scans for lymphoma and may be seen on FDG-PET/CT prior to anatomic imaging. A variety of patterns of immune-related adverse events were reviewed by Kwak et al. (2015) and can be seen in nearly every organ (Fig. 12).

Most recently, RECIL guidelines were published to try to align lymphoma response assessments with those for solid tumors, namely RECIST 1.1(Table 5) (Younes et al. 2017). The Lugano classification, and prior criteria for assessing response in lymphoma, has used bidimensional tumor measurements, whereas RECIST 1.1 is based on changes in unidimensional tumor size. The hypothesis of the RECIL study was that unidimensional measurements could be used for lymphoma response assessment and would produce similar results to the Lugano classification criteria for assigning response (Younes et al. 2017). In this

Fig. 9 Classical Hodgkin lymphoma. (**a**) Baseline CT chest showed abnormal soft tissue in the superior mediastinum around the aortic arch. (**b**) The first restaging scan 12 weeks after starting nivolumab showed increase in tumor burden (sum of the products of the diameter) by greater than 50%. This would be classified as IR1 according to LYRIC. (**c**) On the second restaging scan 24 weeks after starting nivolumab, the tumor burden significantly decreased in size, now classifying as a partial response

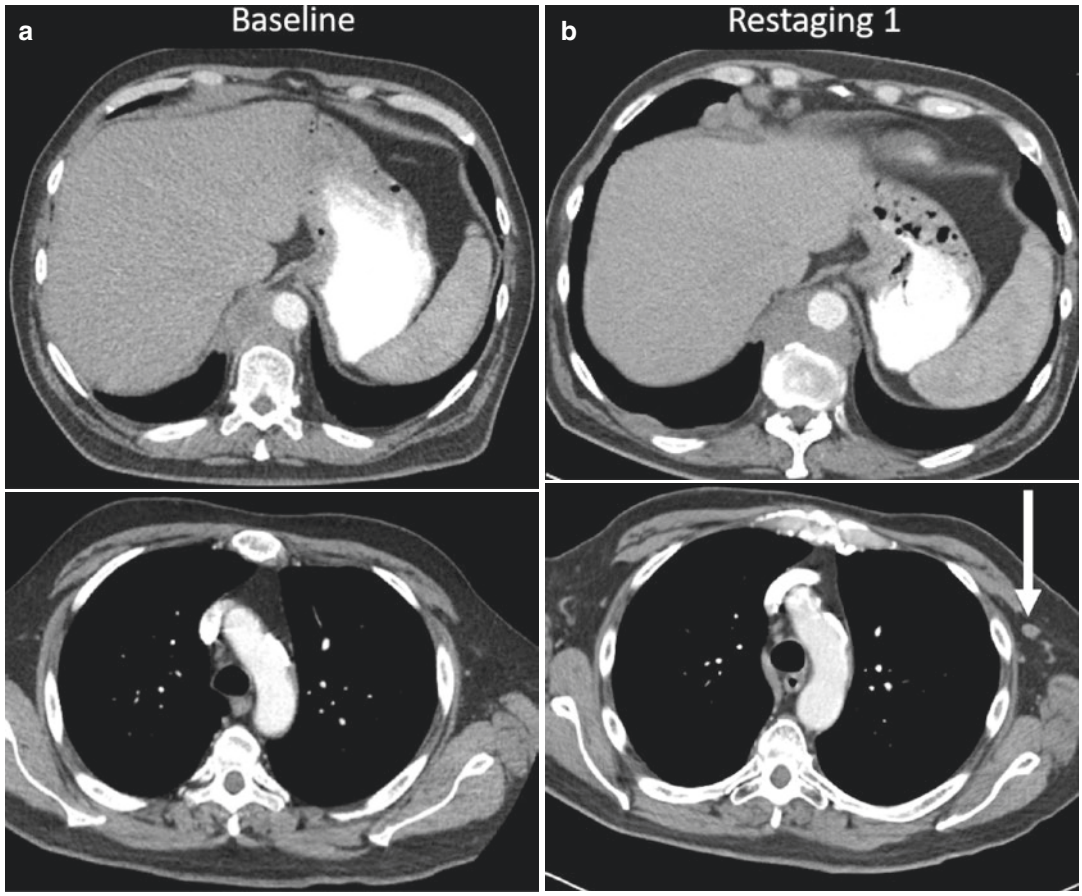

Fig. 10 Diffuse large B cell lymphoma. (**a**) Baseline CT scan prior to starting nivolumab showed abnormal soft tissue surrounding the descending aorta. No abnormal axillary lymph nodes were seen. (**b**) On the first restaging CT scan 12 weeks after starting nivolumab, the soft tissue around the aorta increased slightly, but not more than 50%. A new enlarged left axillary node was seen (arrow). This classifies as IR2 response according to LYRIC. The patient progressed and died shortly after without additional imaging

multicenter study, 47, 828 imaging measurements were made from 2983 patients participating in adult and pediatric clinical trials. The authors showed that PFS curves were similar for assigning response comparing bidimensional and unidimensional measurements. There was

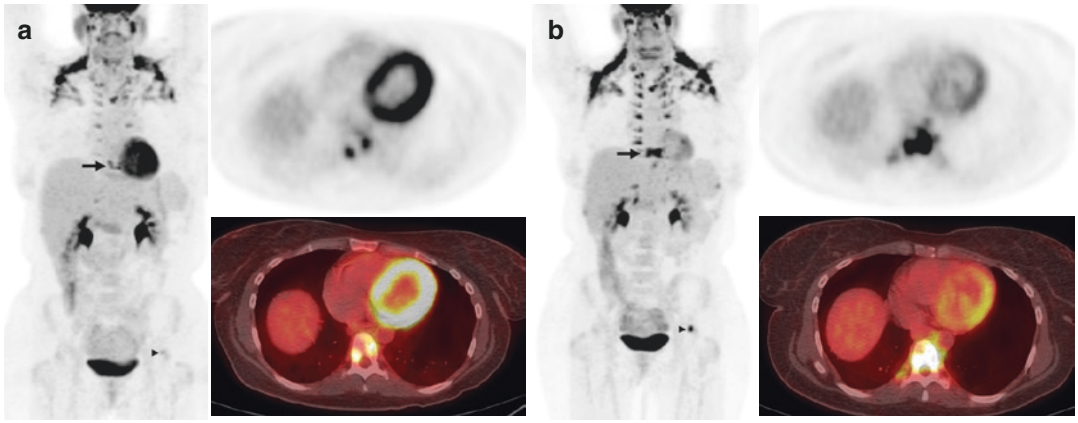

Fig. 11 Classical Hodgkin lymphoma. (**a**) Baseline FDG-PET/CT showed abnormal FDG uptake in a mid-thoracic vertebra (SUVmax 5, arrow) and the left proximal femur (SUVmax 3, arrowhead) representing metabolically active lymphoma. (**b**) FDG-PET/CT scan 12 weeks after starting nivolumab showed increasing FDG uptake in the lesions in the mid-thoracic vertebrae (SUVmax 11.9, arrow) and left proximal femur (SUVmax 5, arrowhead). There was no anatomic progression. This represents an IR3 response according to LYRIC. Physiologic brown fat uptake is seen at baseline and post-nivolumab in the neck and paraspinal regions

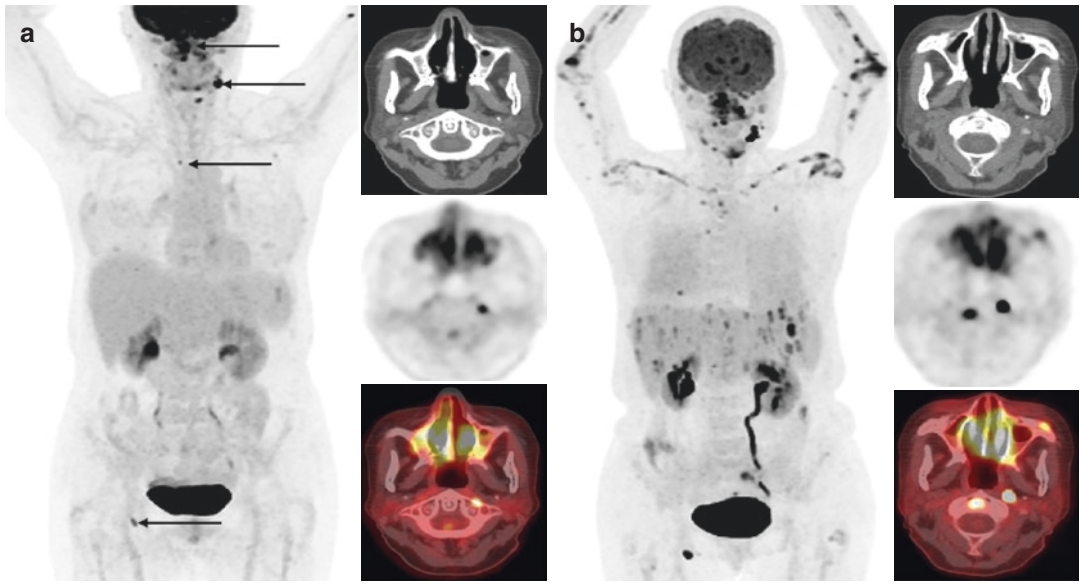

Fig. 12 A 47-year-old woman with recurrent NHL. (**a**) Baseline FDG-PET/CT scan prior to starting pembrolizumab demonstrated FDG-avid lymphoma in the sinonasal regions bilaterally, left neck, and few scattered lymph nodes (e.g., right inguinal and mediastinum, arrows). (**b**) FDG-PET/CT after 2 cycles of pembrolizumab showed increasing FDG uptake in the areas of known disease, but there was also new FDG uptake in the bilateral clavicles and upper extremities, lungs, liver, and spleen. The pattern of the new uptake in the bilateral clavicles and upper extremities, lungs, liver, and spleen favored multi-organ immune-related adverse events rather than new lymphoma involvement. Unfortunately, the patient clinically deteriorated and died and confirmation of progression vs. pseudo-progression in the known tumor could not be obtained

also agreement in response categories assigned using the 6, 5, or 3 largest lesions. RECIL distinguished patients with a complete response on PET with greater and less than a 30% change in the sum of the longest diameter (Younes et al. 2017); however, the publication did not appear to include differences in PFS between these two groups.

Table 5 Comparison of RECIL and Lugano classifications of response

	RECIL (Safar et al. 2012)	Lugano (Juweid et al. 2007)
Measurement	Sum of longest diameters	Sum of products of longest perpendicular diameters
Number of target lesions	Three	Six
RECIL Response Categories	Percentage change in lesion	
Complete	≥30% decrease in sum of diameter with negative FDG PET Complete resolution of target lesions <1 cm size of all lymph nodes	
Partial	≥30% decrease in sum of diameter but not fitting in complete response	
Minimal response (proposed)	≥10% decrease in sum of diameter but <30%	
Stable disease	<10% decrease in sum of diameter of target lesions 20% increase in sum of diameter of target lesions	
Progressive disease	Appearance of a new lesion >20% increase in the sum of diameters of target lesions Lymph node—diameter exceeding 1.5 cm with an increase in size by 0.5 cm	

Table 6 Recently approved and novel therapies for multiple myeloma

Drug type	Target	Drug name (FDA approval)	Indication for multiple myeloma
Antibodies	CD38	Daratumumab (2015)	Relapsed/refractory
	SLAMF7	Elotuzumab (2015)	Relapsed/refractory in combination with lenalidomide or pomalidomide and dexamethasone
		Isatuximab	Investigational (Phase III trials): relapsed/refractory
Proteasome inhibitors	NF-κB	Bortezomib (2003)	Initial, relapsed/refractory
	20S proteasome	Carfilzomib (2012)	Relapsed/refractory
	20S proteasome	Ixazomib (2015)	Relapsed/refractory
	20S proteasome	Marizomib	Investigational: relapsed/refractory
	20S proteasome	Oporozomib	Investigational: relapsed/refractory
Bcl-2 inhibitors	Bcl-2	Venetoclax (2013)	Relapsed/refractory
Histone deacetylase inhibitors	Histone deacetylase	Panobinostat (2015)	Relapsed/refractory in combination with bortezomib and dexamethasone
Kinesin spindle protein inhibitor	kinesin spindle protein	Filanesib	Investigational: relapsed/refractory
Immune modulators		Thalidomide (1998)	Initial, relapsed/refractory
		Lenalidomide (2005)	Initial, relapsed/refractory
		Pomalidomide (2013)	Relapsed/refractory
Checkpoint inhibitors	PD1	Pembrolizumab	Investigational: combination with lenalidomide and dexamethasone; combination with pomalidomide

Others have also suggested that combining PET and CT criteria would better predict response compared to either modality alone. Kostakoglu et al. evaluated interim FDG-PET in 88 patients with stage I/II non-bulky HL (CALGB 50203) (Kostakoglu et al. 2012). FDG-PET was obtained at baseline and after 2 cycles of AVG chemotherapy and response was assessed using 1999 IWG criteria. Using a cutoff of 65% for change in tumor size, there was some suggestion that the combined criteria provided additional predictive information. Definitive conclusions were limited by small numbers in each subgroup.

Another current challenge is how to integrate the quantitative information and volumetrics that can be obtained from FDG-PET/CT into response

criteria. Itti et al. reported that greater than 65.7% decline in SUVmax after 2 cycles of front-line therapy for DLBCL decreased the false-positive rate for separating those with better vs. worse outcomes (Itti et al. 2013). In a follow-up study, however, the addition of semiquantitative data (i.e., change in SUVmax) did not add additional information to visual assessments after 4 cycles of therapy (Itti et al. 2009). These studies highlight the challenges in creating a "one-size-fits-all" response criteria for the various lymphoma subtypes at different times of assessment.

5 Potential Emerging Approaches for Therapy Response Assessments

The use of metabolic tumor volume (MTV) or total lesion glycolysis (TLG) for response assessment in lymphoma was recently reviewed in detail by Kostakoglu and Chauvie (2018). The advantages of MTV and TLG over SUVmax and SUVpeak include that these values are less affected by image noise and represent the total tumor volume, which can have prognostic implications. A major disadvantage is that these methods are time consuming to perform. The data across the different lymphoma subtypes and time during therapy (baseline versus interim versus end of therapy) are variable. Larger studies in homogeneous populations with prospectively set thresholds are needed to further investigate the promising early results using quantitative PET assessment thus far.

Radiomics is a feature of extracting quantification information from the images and using this for characterization of tumor (Lambin et al. 2012) and is a bridge between imaging and personalized medicine. It is especially important in cancer research and is likely to provide important diagnostic, prognostic, accurate tool in clinical decision-making (Lambin et al. 2017). It provides a unique in vivo technology to obtain phenotyping information and has features parallel and overlapping to genomics, thus helping to achieve the aim of precision oncology by using radio-genomics (Castiglioni and Gilardi 2018).

Radiomics in various types of lymphoma has been attempted by various imaging modalities like CT, MRI, and FDG-PET. CT-derived radiomics data has been found to be useful in distinguishing Borrmann Type IV gastric cancer from gastric lymphoma (Ma et al. 2017). Large-scale MRI derived radiomics in combination with machine learning algorithm has a potential to differentiate primary CNS lymphoma from non-necrotic atypical glioblastoma multiforme (Suh et al. 2018). Researchers have studied role of metabolic tumor volume and radiomics parameters obtained from FDG PET/CT in aggressive B cell lymphoma and found that metabolic tumor volume has correlation with response to therapy. Some radiomic features like skewness, entropy, short-run emphasis (SRE), short-run high gray-level emphasis (SRHGE), low gray-level run emphasis (LGRE), short-zone high gray-level emphasis (SZHGE), low gray-level zone emphasis (*LGZE)*, gray-level nonuniformity for zone (GLNU), and zone length nonuniformity (ZLNU) showed correlation with residual tumor and some others like long zone emphasis (LZE), long-zone low gray-level emphasis (LZLGE), and gray-level nonuniformity for run (GLNU) showed correlation with disease-free status and Kurtosis showed correlation with OS (Clavagnier 2018; Vessel et al. 2018).

Parametric imaging, imaging derived mathematically by dividing one image by other or a technique to trace physiological activity, has not been studied in lymphoma according to the best of our knowledge. However, parametric imaging using ultrasound has been studied using contrast-enhanced ultrasound in characterization of lymph nodes (Yin et al. 2019).

6 Therapeutic Advances in Multiple Myeloma

Multiple myeloma is a plasma cell neoplasm diagnosed based on clinical, biochemical, and pathologic findings and using the International Myeloma Working Group criteria (Kumar et al. 2016). The pathogenesis of multiple myeloma was reviewed by Palumbo and Anderson (2011)

and is a multistep process from monoclonal gammopathy of unknown significance (MGUS) to multiple myeloma (Rajkumar et al. 2014).

MGUS can be further subdivided based on type of immunoglobulin secreted as IgM, non-IgM and light chain MGUS with progression rates to MM decreasing, respectively (Rajkumar 2012). Smoldering MM is an intermediate stage. The International Myeloma Working Group (IMWG) criteria focuses on the presence of end-organ damage when there is >10% clonal involvement of the marrow, but currently one or more of the following biomarkers of malignancy also qualify for the diagnosis of MM: clonal bone marrow involvement ≥60%, involved:uninvolved serum-free light chain ratio ≥100; and/or >1 focal lesions on MRI measuring >5 mm in size (Kumar et al. 2016).

Choice of therapy for MM is influenced by risk stratification. The presence of one or more of the following features indicates high-risk disease: certain genetic mutations including t(4;14), t(14;16), t(14;20), del17p13, or gain 1q by fluorescence in situ hybridization (FISH), lactate dehydrogenase levels two times normal and/or features of plasma cell leukemia (Kumar et al. 2012; Rajan and Rajkumar 2015; Rajkumar 2016), and all others are standard risk. Autologous stem cell transplant has been shown to prolong OS and is an important early treatment goal. Various combinations of different drug types are used for initial therapy and therapy in the relapsed/refractory setting (Table 6).

Immunotherapy combinations with checkpoint inhibitors are underway for MM, including pembrolizumab in combination with lenalidomide and dexamethasone. The combination of pembrolizumab and pomalidomide has shown anti-MM activity (Hoyos and Borrello 2016). Multiple targets are under investigation for CAR-T cells in MM including B cell maturation antigen (BCMA), CD19, CD38, CD138, and SLAMF7 with promising results seen with BCMA (Cohen 2018). Multiple vaccines have also been using dendritic cells, granulocyte-macrophage colony stimulating factor, myeloma derived proteins like cancer-testis antigen MAGE-A3 (Garfall and Stadtmauer 2016).

7 Imaging Multiple Myeloma for Disease Detection and Therapy Response

Imaging in multiple myeloma is usually used to detect end-organ defining events, like bone lesions. Prior to 2014, the imaging modality of choice for bone lesions was X-ray (skeletal survey). In 2014, the IMWG expanded the definition of a myeloma defining event to include visualization of bone lesions on advanced imaging, including CT, FDG- PET/CT, and a focal lesion 5 mm or greater more on MRI (Rajkumar et al. 2014; Hillengass et al. 2010). The Durie-Salmon Plus myeloma staging system also considers the imaging features of PET or MRI for disease staging (Durie 2006). PET or MRI may upstage disease based on the number of lesions present. Imaging-based staging offers early identification of disease in those with a clinical and biochemical diagnosis of MGUS or smoldering MM and distinction between stage II and III for prognostication (Durie 2006).

Whole body low dose CT scan is an initial imaging modality of choice for assessing lytic lesions in multiple myeloma (Terpos et al. 2015). A disadvantage of CT is non-visualization of lesions in appendicular skeleton due to the typically limited field of view (Hillengass et al. 2017). MRI is considered the gold standard for demonstrating bone marrow infiltration of MM (Zamagni et al. 2018). Hillengass et al. studied whole-body MRI in patients with smoldering multiple myeloma and found that patients with >1 lesion on MRI have a worse prognosis compared to those with ≤1 lesion (Chantry et al. 2017). MRI demonstrable myeloma is categorized into five types (Dimopoulos et al. 2015): (1) normal; (2) focal lesions; (3) Diffuse homogenous involvement; (4) combination of 2 and 3; and (5) variegated inhomogeneous involvement, also known as salt and pepper appearance. Diffusion-weighted MRI sequences are found to be most useful for identifying myelomatous deposits (Attariwala and Picker 2013). Dimopouolos et al. recommended repeat an MRI after 3–6 months if findings are equivocal (Dimopoulos et al. 2015). Another MRI

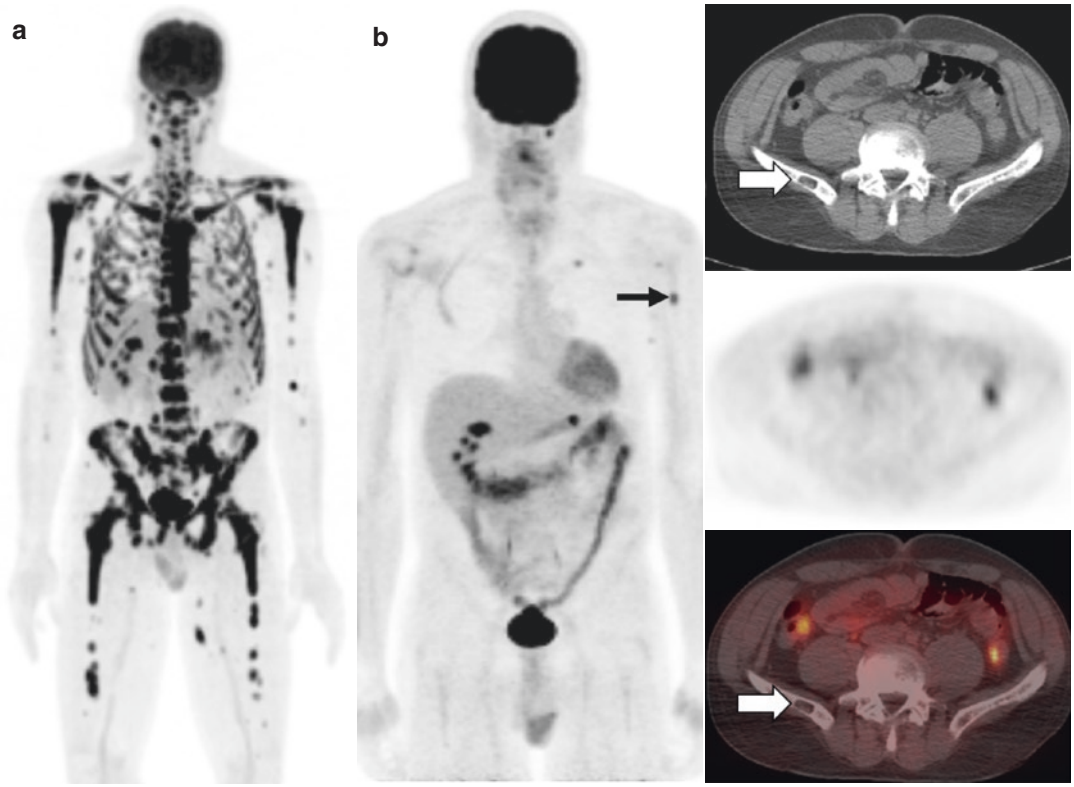

Fig. 13 53-year-old gentleman with IgG kappa multiple myeloma complicated by lytic bone disease, anemia, and fevers, post 4 cycles of lenalidomide, bortezomib, and dexamethasone, 2 cycles of dexamethasone, cyclophosphamide, etoposide, and cisplatin chemotherapy and stem cell transplant. He presented to clinic with malaise, anorexia, and jaw pain. (**a**) Restaging FDG-PET/CT scan showed extensive FDG uptake throughout the bone marrow. He subsequently received 4 cycles of bortezomib, cyclophosphamide, and dexamethasone. (**b**) Follow-up FDG-PET/CT scan showed resolution of FDG uptake in the bone marrow and most of the lytic lesions on CT (white arrow); however, there was residual FDG uptake in the left humerus (black arrow), likely representing residual metabolically active disease. FDG-PET/CT can show metabolic response or residual disease in the setting of stable anatomic abnormalities. The patient had progressive disease within 4 months

technique which is employed is contrast-enhanced dynamic sequences; this sequence depicts marrow angiogenesis; however, it is not routinely used in clinical routine (Huang et al. 2012).

IMWG recommends FDG-PET/CT to confirm the diagnosis of solitary plasmacytoma and to distinguish smoldering myeloma from multiple myeloma if skeletal survey is negative and whole-body MRI cannot be performed/unavailable (Cavo et al. 2017). The negative predictive FDG-PET/CT for active myeloma in the setting of MGUS is high (Durie et al. 2002). Uptake alone without a lytic lesion on CT scan is not considered sufficient to diagnose MM (Rajkumar et al. 2014); however, this is a limitation as CT may be negative in the setting of infiltrating marrow disease (Nakamoto et al. 2005). One prospective study found similarly sensitivity of FDG-PET/CT and whole-body MRI for detecting untreated MM (Sachpekidis et al. 2015).

Response assessment for myeloma is based on the IMWG criteria and includes clinical assessment and laboratory evaluations including SPEP, UPEP, free light chain assay, and bone marrow biopsy in some patients. Imaging may be used for response assessment for those with suspected complete response and/or extramedullary disease, and FDG-PET/CT is the preferred modality (Fig. 13) (Zamagni et al. 2019). Comparative

studies of advanced imaging modalities for monitoring response of MM to therapy are limited. MRI was found to have higher sensitivity in patients treated with ASCT, which the author suggested could be due to FDG-PET becoming negative earlier than MRI in the posttreatment setting and false-positive MRI findings (Sachpekidis et al. 2015). Persistence of FDG uptake posttransplant has been shown to correlate with early relapse (Durie et al. 2002). There may be role of PET/MRI for detection and monitoring of MM. This modality has the advantage of combining the sensitivity of MRI and the specificity of FDG for detecting active disease in the presence of residual morphologic abnormalities (Sachpekidis et al. 2015).

References

Adams HJ, Nievelstein RA, Kwee TC (2015) Prognostic value of complete remission status at end-of-treatment FDG-PET in R-CHOP-treated diffuse large B-cell lymphoma: systematic review and meta-analysis. Br J Haematol 170:185–191

Ansell SM, Lesokhin AM, Borrello I et al (2015) PD-1 blockade with nivolumab in relapsed or refractory Hodgkin's lymphoma. N Engl J Med 372:311–319

Armand P, Shipp MA, Ribrag V et al (2016) Programmed Death-1 blockade with Pembrolizumab in patients with classical Hodgkin lymphoma after Brentuximab Vedotin failure. J Clin Oncol 34:3733–3739

Attariwala R, Picker W (2013) Whole body MRI: improved lesion detection and characterization with diffusion weighted techniques. J Magn Reson Imaging 38:253–268

Barrington SF, Mikhaeel NG, Kostakoglu L et al (2014) Role of imaging in the staging and response assessment of lymphoma: consensus of the international conference on malignant lymphomas imaging working group. J Clin Oncol 32:3048–3058

Bartlett NL, Foyil KV (2008) Hodgkin's lymphoma. In: Abeloff M, Armitage J, Niederhuber JE, Kastan MB, McKenna WG (eds) Abeloff's clinical oncology, 4th edn. Churchill Livingstone Elsevier, Philadelphia

Bartlett NL, Costello BA, LaPlant BR et al (2018) Single-agent ibrutinib in relapsed or refractory follicular lymphoma: a phase 2 consortium trial. Blood 131:182–190

Batlevi CL, Younes A (2013) Novel therapy for Hodgkin lymphoma. Hematology Am Soc Hematol Educ Program 2013:394–399

Bazarbachi A, Boumendil A, Finel H et al (2019) Brentuximab vedotin for recurrent Hodgkin lymphoma after allogeneic hematopoietic stem cell transplantation: a report from the EBMT lymphoma working party. Cancer 125:90–98

Biggi A, Gallamini A, Chauvie S et al (2013) International validation study for interim PET in ABVD-treated, advanced-stage Hodgkin lymphoma: interpretation criteria and concordance rate among reviewers. J Nucl Med 54:683–690

Bishton MJ, Hughes S, Richardson F et al (2016) Delineating outcomes of patients with diffuse large b cell lymphoma using the national comprehensive cancer network-international prognostic index and positron emission tomography-defined remission status; a population-based analysis. Br J Haematol 172:246–254

Boice M, Salloum D, Mourcin F et al (2016) Loss of the HVEM tumor suppressor in lymphoma and restoration by modified CAR-T cells. Cell 167:405–18 e13

Bonthapally V, Wu E, Macalalad A et al (2015) Brentuximab vedotin in relapsed/refractory Hodgkin lymphoma post-autologous transplant: meta-analysis versus historical data. Curr Med Res Opin 31:993–1001

Bristol-Myers Squibb (n.d.) Accessed 4 July 2019

Carbone PP, Kaplan HS, Musshoff K, Smithers DW, Tubiana M (1971) Report of the committee on Hodgkin's disease staging classification. Cancer Res 31:1860–1861

Carde P, Hagenbeek A, Hayat M et al (1993) Clinical staging versus laparotomy and combined modality with MOPP versus ABVD in early-stage Hodgkin's disease: the H6 twin randomized trials from the European Organization for Research and Treatment of Cancer lymphoma cooperative group. J Clin Oncol 11:2258–2272

Carr R, Fanti S, Paez D et al (2014) Prospective international cohort study demonstrates inability of interim PET to predict treatment failure in diffuse large B-cell lymphoma. J Nucl Med 55:1936–1944

Cashen AF, Dehdashti F, Luo J, Homb A, Siegel BA, Bartlett NL (2011) 18F-FDG PET/CT for early response assessment in diffuse large B-cell lymphoma: poor predictive value of international harmonization project interpretation. J Nucl Med 52:386–392

Castiglioni I, Gilardi MC (2018) Radiomics: is it time to compose the puzzle? Clin Transl Imaging 6:411–413

Cavo M, Terpos E, Nanni C et al (2017) Role of (18) F-FDG PET/CT in the diagnosis and management of multiple myeloma and other plasma cell disorders: a consensus statement by the international myeloma working group. Lancet Oncol 18:e206–ee17

Chanan-Khan AA, Cheson BD (2008) Lenalidomide for the treatment of B-cell malignancies. J Clin Oncol 26:1544–1552

Chantry A, Kazmi M, Barrington S et al (2017) Guidelines for the use of imaging in the management of patients with myeloma. Br J Haematol 178:380–393

Chen R, Palmer JM, Martin P et al (2015) Results of a multicenter phase II trial of Brentuximab Vedotin as second-line therapy before autologous transplantation

in relapsed/refractory Hodgkin lymphoma. Biol Blood Marrow Transplant 21:2136–2140
Chen R, Zinzani PL, Fanale MA et al (2017) Phase II study of the efficacy and safety of Pembrolizumab for relapsed/refractory classic Hodgkin lymphoma. J Clin Oncol 35:2125–2132
Cheson BD, Horning SJ, Coiffier B et al (1999) Report of an international workshop to standardize response criteria for non-Hodgkin's lymphomas. NCI Sponsored International Working Group. J Clin Oncol 17:1244
Cheson BD, Pfistner B, Juweid ME et al (2007) Revised response criteria for malignant lymphoma. J Clin Oncol 25:579–586
Cheson BD, Fisher RI, Barrington SF et al (2014) Recommendations for initial evaluation, staging, and response assessment of Hodgkin and non-Hodgkin lymphoma: the Lugano classification. J Clin Oncol 32:3059–3068
Cheson BD, Ansell S, Schwartz L et al (2016) Refinement of the Lugano classification lymphoma response criteria in the era of immunomodulatory therapy. Blood 128:2489–2496
de Claro RA, McGinn K, Kwitkowski V et al (2012) U.S. Food and Drug Administration approval summary: brentuximab vedotin for the treatment of relapsed Hodgkin lymphoma or relapsed systemic anaplastic large-cell lymphoma. Clin Cancer Res 18:5845–5849
Clavagnier I (2018) Rev Infirm 67:15
Cohen AD (2018) CAR T cells and other cellular therapies for multiple myeloma: 2018 update. Am Soc Clin Oncol Educ Book 38:e6–e15
Connors JM, Klimo P, Adams G et al (1997) Treatment of advanced Hodgkin's disease with chemotherapy—comparison of MOPP/ABV hybrid regimen with alternating courses of MOPP and ABVD: a report from the National Cancer Institute of Canada clinical trials group. J Clin Oncol 15:1638–1645
Connors JM, Jurczak W, Straus DJ et al (2018) Brentuximab Vedotin with chemotherapy for stage III or IV Hodgkin's lymphoma. N Engl J Med 378:331–344
Crowther D, Lister TA (1990) The Cotswolds report on the investigation and staging of Hodgkin's disease. Br J Cancer 62:551–552
Czuczman MS, Fayad L, Delwail V et al (2012) Ofatumumab monotherapy in rituximab-refractory follicular lymphoma: results from a multicenter study. Blood 119:3698–3704
Devizzi L, Maffioli L, Bonfante V et al (1997) Comparison of gallium scan, computed tomography, and magnetic resonance in patients with mediastinal Hodgkin's disease. Ann Oncol 8(Suppl 1):53–56
Dimopoulos MA, Hillengass J, Usmani S et al (2015) Role of magnetic resonance imaging in the management of patients with multiple myeloma: a consensus statement. J Clin Oncol 33:657–664
Dreyling M, Morschhauser F, Bouabdallah K et al (2017) Phase II study of copanlisib, a PI3K inhibitor, in relapsed or refractory, indolent or aggressive lymphoma. Ann Oncol 28:2169–2178
Duggan DB, Petroni GR, Johnson JL et al (2003) Randomized comparison of ABVD and MOPP/ABV hybrid for the treatment of advanced Hodgkin's disease: report of an intergroup trial. J Clin Oncol 21:607–614
Durie BG (2006) The role of anatomic and functional staging in myeloma: description of Durie/Salmon plus staging system. Eur J Cancer 42:1539–1543
Durie BG, Waxman AD, D'Agnolo A, Williams CM (2002) Whole-body (18)F-FDG PET identifies high-risk myeloma. J Nucl Med 43:1457–1463
Engert A, Haverkamp H, Kobe C et al (2012) Reduced-intensity chemotherapy and PET-guided radiotherapy in patients with advanced stage Hodgkin's lymphoma (HD15 trial): a randomised, open-label, phase 3 non-inferiority trial. Lancet 379:1791–1799
Even-Sapir E, Israel O (2003) Gallium-67 scintigraphy: a cornerstone in functional imaging of lymphoma. Eur J Nucl Med Mol Imaging 30(Suppl 1):S65–S81
Falini B, Pileri S, Pizzolo G et al (1995) CD30 (Ki-1) molecule: a new cytokine receptor of the tumor necrosis factor receptor superfamily as a tool for diagnosis and immunotherapy. Blood 85:1–14
Fowler NNL, de Vos S et al (2016) Ibrutinib combined with rituximab in treatment-naive patients with follicular lymphoma: arm 1 + arm 2 results from a multicenter, open-label phase 2 study. Blood 128:1804
Garfall AL, Stadtmauer EA (2016) Cellular and vaccine immunotherapy for multiple myeloma. Hematology Am Soc Hematol Educ Program 2016:521–527
Genentech (2013) Obinutuzumab prescribing information
Gopal AK, Fanale MA, Moskowitz CH et al (2017) Phase II study of idelalisib, a selective inhibitor of PI3Kdelta, for relapsed/refractory classical Hodgkin lymphoma. Ann Oncol 28:1057–1063
Gopal AK, Schuster SJ, Fowler NH et al (2018) Ibrutinib as treatment for patients with relapsed/refractory follicular lymphoma: results from the open-label, multicenter, phase II DAWN study. J Clin Oncol 36:2405–2412
Hillengass J, Fechtner K, Weber MA et al (2010) Prognostic significance of focal lesions in whole-body magnetic resonance imaging in patients with asymptomatic multiple myeloma. J Clin Oncol 28:1606–1610
Hillengass J, Moulopoulos LA, Delorme S et al (2017) Whole-body computed tomography versus conventional skeletal survey in patients with multiple myeloma: a study of the international myeloma working group. Blood Cancer J 7:e599
Hoppe RT, Advani RH, Ai WZ et al (2017) Hodgkin lymphoma version 1.2017, NCCN clinical practice guidelines in oncology. J Natl Compr Cancer Netw 15:608–638
Hoyos V, Borrello I (2016) The immunotherapy era of myeloma: monoclonal antibodies, vaccines, and adoptive T-cell therapies. Blood 128:1679–1687

Huang SY, Chen BB, Lu HY et al (2012) Correlation among DCE-MRI measurements of bone marrow angiogenesis, microvessel density, and extramedullary disease in patients with multiple myeloma. Am J Hematol 87:837–839

Israel O, Front D, Lam M et al (1988) Gallium 67 imaging in monitoring lymphoma response to treatment. Cancer 61:2439–2443

Itti E, Lin C, Dupuis J et al (2009) Prognostic value of interim 18F-FDG PET in patients with diffuse large B-cell lymphoma: SUV-based assessment at 4 cycles of chemotherapy. J Nucl Med 50:527–533

Itti E, Meignan M, Berriolo-Riedinger A et al (2013) An international confirmatory study of the prognostic value of early PET/CT in diffuse large B-cell lymphoma: comparison between Deauville criteria and DeltaSUVmax. Eur J Nucl Med Mol Imaging 40:1312–1320

Johnson P, Federico M, Kirkwood A et al (2016) Adapted treatment guided by interim PET-CT scan in advanced Hodgkin's lymphoma. N Engl J Med 374:2419–2429

Juweid ME, Wiseman GA, Vose JM et al (2005) Response assessment of aggressive non-Hodgkin's lymphoma by integrated international workshop criteria and fluorine-18-fluorodeoxyglucose positron emission tomography. J Clin Oncol 23:4652–4661

Juweid ME, Stroobants S, Hoekstra OS et al (2007) Use of positron emission tomography for response assessment of lymphoma: consensus of the imaging Subcommittee of International Harmonization Project in lymphoma. J Clin Oncol 25:571–578

Kamran SC, Jacene HA, Chen YH, Mauch PM, Ng AK (2018) Clinical outcome of patients with early stage favorable Hodgkin lymphoma treated with ABVD x two cycles followed by FDG-PET/CT restaging and 20 Gy of involved-site radiotherapy. Leuk Lymphoma 59:1384–1390

Kaplan WD, Jochelson MS, Herman TS et al (1990) Gallium-67 imaging: a predictor of residual tumor viability and clinical outcome in patients with diffuse large-cell lymphoma. J Clin Oncol 8:1966–1970

Klimm B, Diehl V, Pfistner B, Engert A (2005) Current treatment strategies of the German Hodgkin study group (GHSG). Eur J Haematol Suppl 75:125–134

Kostakoglu L, Chauvie S (2018) Metabolic tumor volume metrics in lymphoma. Semin Nucl Med 48:50–66

Kostakoglu L, Schoder H, Johnson JL et al (2012) Interim [(18)F]fluorodeoxyglucose positron emission tomography imaging in stage I-II non-bulky Hodgkin lymphoma: would using combined positron emission tomography and computed tomography criteria better predict response than each test alone? Leuk Lymphoma 53:2143–2150

Kotla V, Goel S, Nischal S et al (2009) Mechanism of action of lenalidomide in hematological malignancies. J Hematol Oncol 2:36

Kumar S, Fonseca R, Ketterling RP et al (2012) Trisomies in multiple myeloma: impact on survival in patients with high-risk cytogenetics. Blood 119:2100–2105

Kumar S, Paiva B, Anderson KC et al (2016) International myeloma working group consensus criteria for response and minimal residual disease assessment in multiple myeloma. Lancet Oncol 17:e328–ee46

Kwak JJ, Tirumani SH, Van den Abbeele AD, Koo PJ, Jacene HA (2015) Cancer immunotherapy: imaging assessment of novel treatment response patterns and immune-related adverse events. Radiographics 35:424–437

LaCasce AS, Bociek RG, Sawas A et al (2018) Brentuximab vedotin plus bendamustine: a highly active first salvage regimen for relapsed or refractory Hodgkin lymphoma. Blood 132:40–48

Lambin P, Rios-Velazquez E, Leijenaar R et al (2012) Radiomics: extracting more information from medical images using advanced feature analysis. Eur J Cancer 48:441–446

Lambin P, Leijenaar RTH, Deist TM et al (2017) Radiomics: the bridge between medical imaging and personalized medicine. Nat Rev Clin Oncol 14:749–762

Lamy T, Damaj G, Soubeyran P et al (2018) R-CHOP 14 with or without radiotherapy in nonbulky limited-stage diffuse large B-cell lymphoma. Blood 131:174–181

Lee CS, Rattu MA, Kim SS (2016) A review of a novel, Bruton's tyrosine kinase inhibitor, ibrutinib. J Oncol Pharm Pract 22:92–104

Leonard JP, Jung SH, Johnson J et al (2015) Randomized trial of Lenalidomide alone versus Lenalidomide plus rituximab in patients with recurrent follicular lymphoma: CALGB 50401 (Alliance). J Clin Oncol 33:3635–3640

Lesokhin AM, Ansell SM, Armand P et al (2016) Nivolumab in patients with relapsed or refractory hematologic malignancy: preliminary results of a phase Ib study. J Clin Oncol 34:2698–2704

Lister TA, Crowther D, Sutcliffe SB et al (1989) Report of a committee convened to discuss the evaluation and staging of patients with Hodgkin's disease: Cotswolds meeting. J Clin Oncol 7:1630–1636

Locke FL, Ghobadi A, Jacobson CA et al (2019) Long-term safety and activity of axicabtagene ciloleucel in refractory large B-cell lymphoma (ZUMA-1): a single-arm, multicentre, phase 1-2 trial. Lancet Oncol 20:31–42

Ma Z, Fang M, Huang Y et al (2017) CT-based radiomics signature for differentiating Borrmann type IV gastric cancer from primary gastric lymphoma. Eur J Radiol 91:142–147

Martin P, Jung SH, Pitcher B et al (2017) A phase II trial of lenalidomide plus rituximab in previously untreated follicular non-Hodgkin's lymphoma (NHL): CALGB 50803 (Alliance). Ann Oncol 28:2806–2812

Merck (2014) Pembrolizumab prescribing information

Micallef IN, Maurer MJ, Wiseman GA et al (2011) Epratuzumab with rituximab, cyclophosphamide, doxorubicin, vincristine, and prednisone chemotherapy in patients with previously untreated diffuse large B-cell lymphoma. Blood 118:4053–4061

Mikhaeel NG, Timothy AR, Hain SF, O'Doherty MJ (2000) 18-FDG-PET for the assessment of residual masses on CT following treatment of lymphomas. Ann Oncol 11(Suppl 1):147–150

Nakamoto Y, Cohade C, Tatsumi M, Hammoud D, Wahl RL (2005) CT appearance of bone metastases detected with FDG PET as part of the same PET/CT examination. Radiology 237:627–634

O'Day SJ, Hamid O, Urba WJ (2007) Targeting cytotoxic T-lymphocyte antigen-4 (CTLA-4): a novel strategy for the treatment of melanoma and other malignancies. Cancer 110:2614–2627

Palumbo A, Anderson K (2011) Multiple myeloma. N Engl J Med 364:1046–1060

Pfreundschuh M, Trumper L, Osterborg A et al (2006) CHOP-like chemotherapy plus rituximab versus CHOP-like chemotherapy alone in young patients with good-prognosis diffuse large-B-cell lymphoma: a randomised controlled trial by the MabThera international trial (MInT) group. Lancet Oncol 7:379–391

Press OW, Li H, Schoder H et al (2016) US intergroup trial of response-adapted therapy for stage III to IV Hodgkin lymphoma using early interim Fluorodeoxyglucose-positron emission tomography imaging: southwest oncology group S0816. J Clin Oncol 34:2020–2027

Rajan AM, Rajkumar SV (2015) Interpretation of cytogenetic results in multiple myeloma for clinical practice. Blood Cancer J 5:e365

Rajkumar SV (2012) Preventive strategies in monoclonal gammopathy of undetermined significance and smoldering multiple myeloma. Am J Hematol 87:453–454

Rajkumar SV (2016) Multiple myeloma: 2016 update on diagnosis, risk-stratification, and management. Am J Hematol 91:719–734

Rajkumar SV, Dimopoulos MA, Palumbo A et al (2014) International myeloma working group updated criteria for the diagnosis of multiple myeloma. Lancet Oncol 15:e538–e548

Ramos CA, Ballard B, Zhang H et al (2017) Clinical and immunological responses after CD30-specific chimeric antigen receptor-redirected lymphocytes. J Clin Invest 127:3462–3471

Rosenberg SA, Boiron M, DeVita VT Jr et al (1971) Report of the committee on Hodgkin's disease staging procedures. Cancer Res 31:1862–1863

Rummel MJ, Niederle N, Maschmeyer G et al (2013) Bendamustine plus rituximab versus CHOP plus rituximab as first-line treatment for patients with indolent and mantle-cell lymphomas: an open-label, multicentre, randomised, phase 3 non-inferiority trial. Lancet 381:1203–1210

Sachpekidis C, Mosebach J, Freitag MT et al (2015) Application of (18)F-FDG PET and diffusion weighted imaging (DWI) in multiple myeloma: comparison of functional imaging modalities. Am J Nucl Med Mol Imaging 5:479–492

Safar V, Dupuis J, Itti E et al (2012) Interim [18F] fluorodeoxyglucose positron emission tomography scan in diffuse large B-cell lymphoma treated with anthracycline-based chemotherapy plus rituximab. J Clin Oncol 30:184–190

Schuster SJ, Svoboda J, Chong EA et al (2017) Chimeric antigen receptor T cells in refractory B-cell lymphomas. N Engl J Med 377:2545–2554

Sieber M, Tesch H, Pfistner B et al (2002) Rapidly alternating COPP/ABV/IMEP is not superior to conventional alternating COPP/ABVD in combination with extended-field radiotherapy in intermediate-stage Hodgkin's lymphoma: final results of the German Hodgkin's lymphoma study group trial HD5. J Clin Oncol 20:476–484

Smith SM, Schoder H, Johnson JL et al (2013) The anti-CD80 primatized monoclonal antibody, galiximab, is well-tolerated but has limited activity in relapsed Hodgkin lymphoma: cancer and leukemia group B 50602 (Alliance). Leuk Lymphoma 54:1405–1410

Straus DJ, Jung SH, Pitcher B et al (2018) CALGB 50604: risk-adapted treatment of nonbulky early-stage Hodgkin lymphoma based on interim PET. Blood 132:1013–1021

Suh HB, Choi YS, Bae S et al (2018) Primary central nervous system lymphoma and atypical glioblastoma: differentiation using radiomics approach. Eur Radiol 28:3832–3839

Suvas S, Singh V, Sahdev S, Vohra H, Agrewala JN (2002) Distinct role of CD80 and CD86 in the regulation of the activation of B cell and B cell lymphoma. J Biol Chem 277:7766–7775

Swerdlow SH, Campo E, Pileri SA et al (2016) The 2016 revision of the World Health Organization classification of lymphoid neoplasms. Blood 127:2375–2390

Teeling JL, Mackus WJ, Wiegman LJ et al (2006) The biological activity of human CD20 monoclonal antibodies is linked to unique epitopes on CD20. J Immunol 177:362–371

Terpos E, Kleber M, Engelhardt M et al (2015) European myeloma network guidelines for the management of multiple myeloma-related complications. Haematologica 100:1254–1266

Ujjani CS, Jung SH, Pitcher B et al (2016) Phase 1 trial of rituximab, lenalidomide, and ibrutinib in previously untreated follicular lymphoma: Alliance A051103. Blood 128:2510–2516

Vessel EA, Maurer N, Denker AH, Starr GG (2018) Stronger shared taste for natural aesthetic domains than for artifacts of human culture. Cognition 179:121–131

Vose JM, Bierman PJ, Anderson JR et al (1996) Single-photon emission computed tomography gallium imaging versus computed tomography: predictive value in patients undergoing high-dose chemotherapy and autologous stem-cell transplantation for non-Hodgkin's lymphoma. J Clin Oncol 14:2473–2479

Wang CM, Wu ZQ, Wang Y et al (2017) Autologous T cells expressing CD30 chimeric antigen receptors for relapsed or refractory Hodgkin lymphoma: an open-label phase I trial. Clin Cancer Res 23:1156–1166

Westin JR, Chu F, Zhang M et al (2014) Safety and activity of PD1 blockade by pidilizumab in combination with rituximab in patients with relapsed follicular

lymphoma: a single group, open-label, phase 2 trial. Lancet Oncol 15:69–77

Wilson WH, Young RM, Schmitz R et al (2015) Targeting B cell receptor signaling with ibrutinib in diffuse large B cell lymphoma. Nat Med 21:922–926

Yin SS, Cui QL, Fan ZH, Yang W, Yan K (2019) Diagnostic value of arrival time parametric imaging using contrast-enhanced ultrasonography in superficial enlarged lymph nodes. J Ultrasound Med 38(5):1287–1298

Younes A, Pro B, Fayad L (2006) Experience with bortezomib for the treatment of patients with relapsed classical Hodgkin lymphoma. Blood 107:1731–1732

Younes A, Santoro A, Shipp M et al (2016) Nivolumab for classical Hodgkin's lymphoma after failure of both autologous stem-cell transplantation and brentuximab vedotin: a multicentre, multicohort, single-arm phase 2 trial. Lancet Oncol 17:1283–1294

Younes A, Hilden P, Coiffier B et al (2017) International working group consensus response evaluation criteria in lymphoma (RECIL 2017). Ann Oncol 28:1436–1447

Younes A, Sehn LH, Johnson P et al (2019) Randomized phase III trial of ibrutinib and rituximab plus cyclophosphamide, doxorubicin, vincristine, and prednisone in non-germinal center B-cell diffuse large B-cell lymphoma. J Clin Oncol 37(15):1285–1295

Zamagni E, Cavo M, Fakhri B, Vij R, Roodman D (2018) Bones in multiple myeloma: imaging and therapy. Am Soc Clin Oncol Educ Book 38:638–646

Zamagni E, Tacchetti P, Cavo M (2019) Imaging in multiple myeloma: how? When? Blood 133:644–651

Therapy Response Imaging in Sarcoma and Musculoskeletal Malignancies

Sree Harsha Tirumani

Contents

Abstract

Imaging plays an important role in assessing response to treatment in both primary and metastatic sarcomas. The response of sarcomas to targeted therapies is best exemplified by response of gastrointestinal stromal tumor (GIST) to imatinib. Alternate tumor response criteria, namely Choi criteria, were proposed to overcome limitations of Response Evaluation Criteria In Solid Tumors (RECIST) in interpreting response of GIST to imatinib. These alternate tumor response criteria were subsequently found to have a role in assessing response of non-GIST sarcomas including those treated with conventional chemoradiation therapy. In this chapter, we will discuss in detail the pros and cons of various response criteria in GIST and non-GIST sarcomas.

1 Introduction

Sarcomas are a complex, heterogenous group of tumors which arise from the mesenchymal tissues. There are more than 50 histologic subtypes of sarcomas with widely variable biologic behavior (Doyle 2014). The major histologic subtypes of sarcomas described in the 2013 revised WHO classification are: adipocytic tumors, fibroblastic/myofibroblastic tumors, fibrohistocytic tumors, smooth muscle tumors, pericytic tumors, skeletal

S. H. Tirumani (✉)
Department of Imaging, Dana-Farber Cancer Institute/Brigham and Women's Hospital, Boston, MA, USA

Department of Radiology, University Hospitals Cleveland Medical Center, Case Western Reserve University School of Medicine, Cleveland, OH, USA
e-mail: sreeharsha.tirumani@uhhospitals.org; sht27@case.edu

M. Nishino (ed.), *Therapy Response Imaging in Oncology*, Medical Radiology, Diagnostic Imaging,
https://doi.org/10.1007/978-3-030-31171-1_12

muscle tumors, vascular tumors, gastrointestinal stromal tumor (GIST), chondro-osseous tumors, nerve-sheath tumors, tumors of uncertain differentiation, and undifferentiated/unclassified sarcomas. Broadly, sarcomas can be divided into soft tissue sarcomas (sarcomas arising from muscles, nerves, fat, and other connective tissues) and sarcomas of the bone (Doyle 2014). The anatomic site of origin of sarcomas influences treatment decision and prognosis of sarcomas. The most common sites of origin of sarcomas include extremities (43%), trunk (10%), viscera (19%), retroperitoneum (15%), and head and neck (9%) (NCCN Clinical Practice Guidelines in Oncology Soft Tissue Sarcoma Version 2 2018). Sarcomas are uncommon in adults accounting for 1% of all malignancies but much more common in pediatric population (15% of all pediatric malignancies) (NCCN Clinical Practice Guidelines in Oncology Soft Tissue Sarcoma Version 2 2018). The most common types of sarcomas are undifferentiated pleomorphic sarcoma, GIST, liposarcoma, and leiomyosarcoma.

2 Management of Sarcomas

Management of bone and soft tissue sarcomas requires multidisciplinary approach (Siegel et al. 2015). The definitive treatment for most patients with localized sarcomas is surgical resection with negative margins. Sarcomas occurring in the abdomen, especially in the retroperitoneum, often involve multiple viscera, and their resection often entails resection of contiguous abdominal viscera. Sarcomas occurring in the extremities are managed by limb-sparing, function-preserving surgery with negative margins and often require complex soft tissue and neurovascular reconstruction (Papagelopoulos et al. 2008). Preoperative radiotherapy is used in many centers to down-stage tumors to achieve adequate surgical margin and to decrease local recurrences and improve overall survival (Al-Absi et al. 2010; Albertsmeier et al. 2018). Postoperative radiotherapy can similarly help in decreasing local recurrences when surgical margins are either close or positive at histopathology (Zhao et al. 2016). Preoperative chemotherapy or chemoradiation is used in many centers for high-grade tumors though the results of such strategy are inconsistent (Gronchi et al. 2017; Look Hong et al. 2013; Mullen et al. 2012). Postoperative chemotherapy with or without radiotherapy, on the other hand, has been shown to consistently increase the recurrence-free survival (Pervaiz et al. 2008).

Advanced, unresectable, and metastatic sarcomas are challenging to manage. Single agent (doxorubicin, dacarbazine, or ifosfamide) or combination (doxorubicin with ifosfamide) anthracycline-based regimens are widely used in this setting (Bramwell et al. 2003; Lorigan et al. 2007). Gemcitabine, docetaxel, liposomal doxorubicin, vinorelbine, and temozolomide are other chemotherapeutic that have been shown to be active in metastatic sarcomas (Garcia del Muro et al. 2005, 2011; Judson et al. 2001; Seddon et al. 2017). Trabectedin is a DNA-binding agent which has shown to be effective in few phase II and III trials for sarcomas like leiomyosarcoma, liposarcoma, and translocation-related sarcoma (Demetri et al. 2009, 2016). Eribulin is a microtubule inhibitor which has been found to have some activity as a single agent in leiomyosarcoma, liposarcoma, and synovial sarcoma (Schoffski et al. 2016).

Several novel targeted therapies in the last two decades have shown promising results in sarcomas and some of them have been approved for certain histologic types of sarcomas. The most notable examples in this category are imatinib and sunitinib which are first- and second-line therapies for metastatic GIST (Demetri et al. 2002, 2006). Other targeted therapies approved for treatment of sarcomas include regorafenib for GIST, pazopanib, sunitinib, and olaratumab (in combination with doxorubicin) for non-GIST soft tissue sarcomas (Demetri et al. 2013; Kollar et al. 2017; Stacchiotti et al. 2011; Tap et al. 2016). Immunotherapeutic agents like CTLA4 and PD-1/PDL-1 inhibitors are under investigation for treatment of bone and soft tissue sarcomas.

3 Imaging of Treatment Response in Sarcomas

Imaging plays an important role in assessing response to treatment in both primary and metastatic sarcomas (Levy et al. 2017a, b; Robinson et al. 2008). CT scan of the chest is essential for the staging and also assessing response to sarcomas as most sarcomas undergo hematogenous spread to lung. CT of the abdomen and pelvis is the modality of choice for response assessment of primary tumors and metastatic disease in the abdomen and pelvis (NCCN Clinical Practice Guidelines in Oncology Soft Tissue Sarcoma Version 2 2018; Levy et al. 2017a, b). MRI is preferred for assessing response in primary tumors in the extremities. Whole body MRI is preferred for evaluating metastasis from myxoid/round cell liposarcoma (Schwab et al. 2007). Brain MRI is recommended for evaluating sarcomas like alveolar soft part sarcoma which have high propensity for brain metastasis (Sood et al. 2014). 18F-Fluorodeoxy glucose (FDG) positron emission tomography (PET)/CT (FDG-PET/CT) can be used for evaluating response in the preoperative and metastatic setting as it detects response early and the response on PET correlates better with histopathologic response than Response Evaluation Criteria In Solid Tumors (RECIST) (Evilevitch et al. 2008; Schuetze 2006; Schuetze et al. 2005).

In the subsequent sections, we will discuss assessment of treatment response in GIST and non-GIST sarcomas.

3.1 Response Assessment in GIST

The response of sarcomas to targeted therapies is best exemplified by GIST which is the prototype for response of solid tumors to targeted therapies. Following the first report of imatinib response in a 50-year-old woman with advanced metastatic GIST in 2001 (Joensuu et al. 2001) and success in the phase II B2222 trial, imatinib was granted accelerated approved by the US FDA in 2002 (Demetri et al. 2002; Cohen et al. 2009; Dagher et al. 2002). Currently imatinib is the first-line agent in metastatic GIST and also used in the neoadjuvant and adjuvant setting. When there is primary or secondary resistance to imatinib, second-line sunitinib is the treatment of choice (Demetri et al. 2006). Resistance to first- and second-line therapies is managed with third-line regorafenib (Demetri et al. 2013). Rechallenge with imatinib is reserved for patients who are refractory to all lines of treatment as it can slow the disease progression (Kang et al. 2013).

3.1.1 RECIST vs. Alternate Tumor Response Criteria in GIST: Imatinib

Liver and peritoneal cavity are the most common sites of metastasis in GIST. Contrast-enhanced CT of the abdomen and pelvis is the imaging modality of choice for monitoring the response of GIST. Both primary and metastatic GIST have a unique morphologic response to imatinib on contrast-enhanced CT scans (Choi et al. 2004). The heterogeneously enhancing primary and metastatic lesions show a dramatic decrease in the enhancing component after treatment with or without change in lesion size (Fig. 1). The treated lesions appear as cystic lesions with homogeneous decrease in attenuation. This appearance on CT correlates with myxoid degeneration instead of necrosis (as seen with conventional chemotherapy) at histopathology. There may be a transient increase in size in some cases due to intratumoral edema or hemorrhage which can mask the actual morphologic response. As per RECIST such lesions can be labeled as either stable or progressive disease if size alone is used for interpreting response. Choi et al. in 36 GIST patients with 173 lesions found that 70% patients responding on PET were labeled as partial response by change in tumor density but nearly 75% were labeled as stable disease by RECIST (Choi et al. 2004).

In a subsequent study, Choi et al. proposed alternate tumor response criteria incorporating changes in tumor attenuation along with size reduction (Choi et al. 2007). In this study of 40 patients with GIST treated with imatinib and

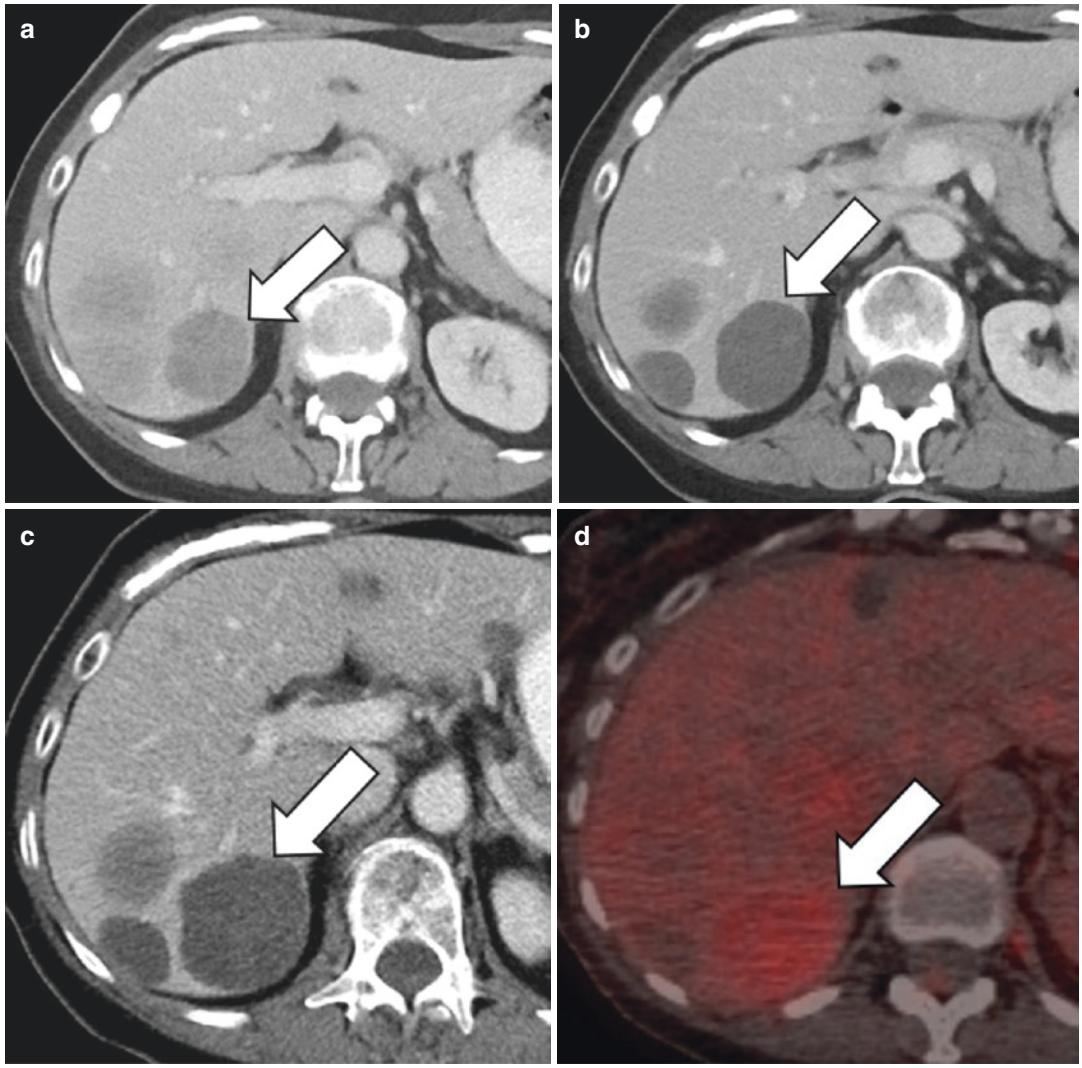

Fig. 1 68-year-old woman with GIST metastatic to the liver treated with imatinib. (**a**) Baseline contrast-enhanced CT of the abdomen demonstrates multiple heterogeneously enhancing liver metastases (arrow). (**b**) Follow-up CT scan 3 months after treatment with imatinib demonstrates typical response to therapy, with homogeneously decreased density and enhancement of the liver metastases. There is apparent increase in size of the index liver lesion (arrow). (**c**) Subsequent follow-up CT scan 6 months after treatment shows mild increase in the size of the index lesion with increase in density which was suspected to be recurrence. To confirm the recurrence, 18F-FDG-PET/CT was performed. (**d**) Axial fused image from 18F-FDG PET/CT demonstrates increase in uptake in the index liver lesion confirming recurrence

evaluated with pre- and posttreatment CT and FDG-PET/CT, 97% responders by PET (defined as decrease in SUV by more than 70% from baseline or absolute SUV_{max} of <2.5) showed 15% decrease in CT attenuation or 10% decrease in unidimensional size at 8 weeks of imatinib treatment. Using these modified criteria identified greater number of responders compared to RECIST (Choi et al. 2007). In a subsequent validation study, Benjamin et al. in 58 patients with imatinib-treated GIST found that Choi criteria correlated better with time to progression and disease-specific survival compared to RECIST (Benjamin et al. 2007).

Primary and metastatic GIST treated with imatinib tend to become cyst-like during follow-up. Detection of recurrence or disease progression in such cyst-like treated metastases

can be challenging with RECIST. Disease progression by RECIST is suspected when there is increase in size of tumor or when new lesions appear. However, recurrence in treated GIST metastasis can be seen as increase in tumor attenuation or appearance of new intratumoral nodules without change in tumor size (Shankar et al. 2005) (Fig. 2). Desai et al. found that 23

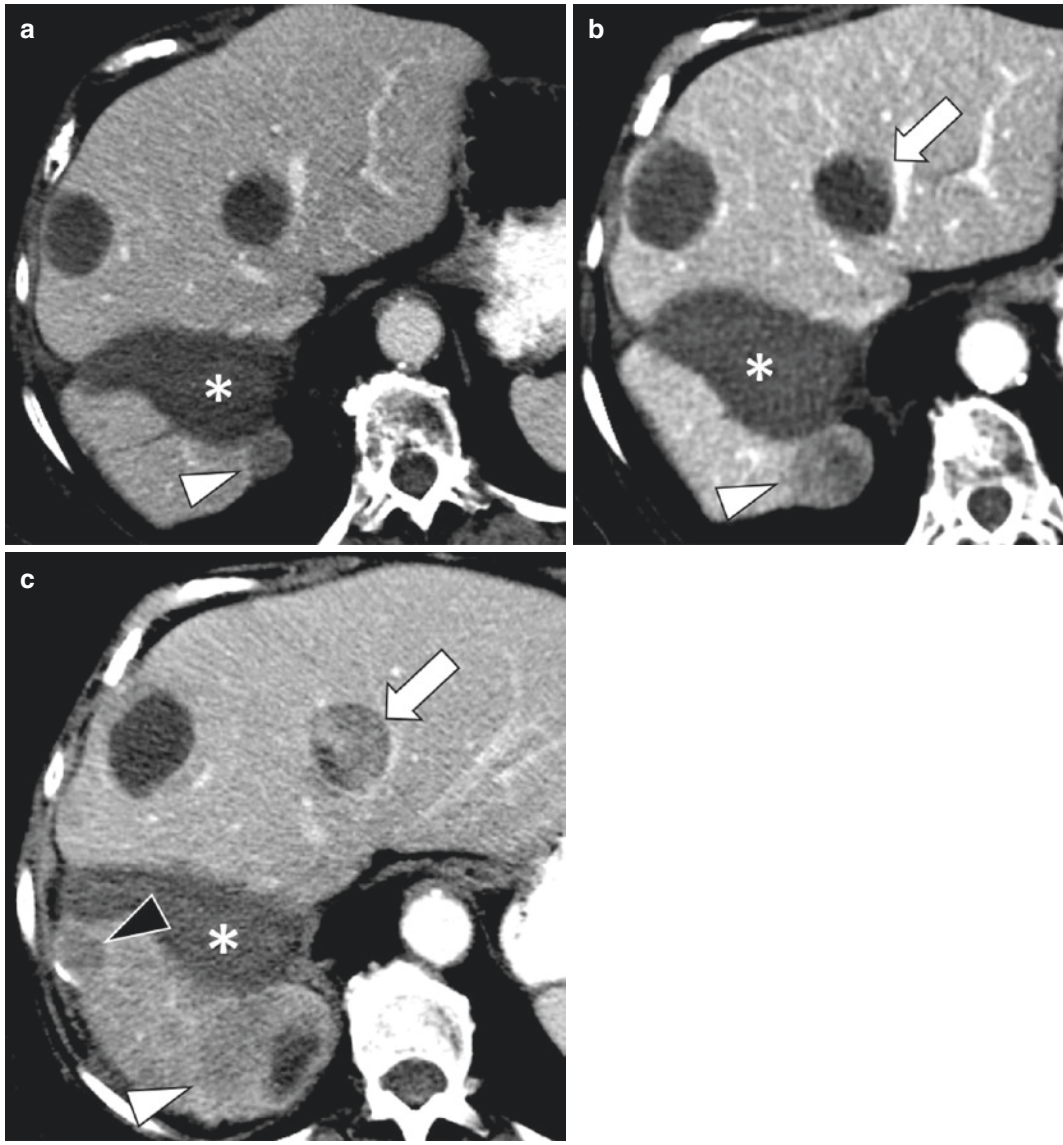

Fig. 2 76-year-old female with history of GIST metastatic to liver, previously treated with hepatic resection and ablation, currently off therapy. (**a**) Axial contrast-enhanced CT image obtained during surveillance demonstrates a cystic-appearing lesion in the liver which likely represent treated metastases. A large ablation zone is seen in the right lobe (asterisk). A hypodense lesion posterior to the ablation zone (white arrowhead) was suspicious for recurrence. (**b**) Follow-up CT obtained 1 month later shows enlargement of the lesion posterior to the ablation zone (white arrowhead) confirming new metastasis. In addition, one of the previously cystic lesions (arrow) now shows a nodule within the wall without change in size suggestive of typical "nodule-within-cyst" pattern of recurrence within this treated metastatic lesion. (**c**) Subsequent follow-up 1 month later shows increase in the internal heterogeneity within the index liver metastasis confirming recurrence. There are also new (black arrowhead) and enlarging liver metastasis (white arrowhead)

out of 48 patients who progressed during follow-up after imatinib therapy developed a "resistant clonal nodule" at a median of 5 months earlier than progression by RECIST (Desai et al. 2007). In a prospective study of 107 patients, Mabille et al. found that 70 patients showed cyst-like transformation of the metastases which remained stable in size per RECIST (Mabille et al. 2009). However, recurrence was seen as new peripheral nodules in 28 patients and thick peripheral enhancement in 17 patients without change in size. Based on evidence from these studies, morphologic changes are also incorporated into Choi criteria in defining disease progression.

A few researchers have compared RECIST and Choi criteria with volumetric criteria. RECIST assumes tumors to be spherical and therefore uses longest diameters in assessing response. However, it is often argued that volume is a better representation of the actual number of tumor cells than single longest diameter. Both primary and metastatic tumors in GIST are irregular in shape rather than spherical as assumed by RECIST (Rezai et al. 2013). Accordingly moderate changes in size can be better captured by using volumetric analysis rather than single dimension-based RECIST (Tirumani et al. 2016). Schiavon et al. studied the concept of volume in response assessment in two independent studies in hepatic metastasis from GIST. In the first study of liver metastasis from GIST in 84 patients treated with imatinib, volume more frequently identified >20% change in size than RECIST and was able to identify more number of partial responders than RECIST and correlated better with overall survival. Volume was comparable to Choi for identifying partial responders. In a subsequent study of 78 patients with hepatic metastases from GIST who were treated with imatinib (Schiavon et al. 2012, 2014), they concluded that GIST metastasis should be conceptualized mathematically as ellipsoidal lesions rather than spheroidal and found that the metastatic lesions demonstrated a change in morphology (from ellipsoidal to spheroidal and vice versa) after treatment which RECIST may not capture (Schiavon et al. 2012, 2014).

3.1.2 RECIST vs. Alternate Tumor Response Criteria in GIST: Sunitinib and Regorafenib

Patients who fail to respond or develop resistance to imatinib are treated with second- and third-line tyrosine kinase inhibitors (TKIs). It is not known if the dramatic density changes seen with imatinib occur when challenged with new TKIs. Few recent studies have attempted to study the various treatment response criteria in metastatic GIST patients treated with second- and third-line TKIs and correlate them with survival (Schramm et al. 2013; Shinagare et al. 2014, 2016). Schramm et al. analyzed response of metastatic GIST in 20 patients treated with second-line sunitinib. 68 target lesions were assessed using RECIST, Choi, and volumetric criteria at 3-month and 1-year intervals after start of treatment. The results were correlated with disease-specific survival (DSS) (Schramm et al. 2013). The authors found that responses by volumetric criteria were more in agreement with RECIST than Choi criteria both at 3-month and 1-year intervals. Though Choi criteria classified more number of patients as partial responders on 3-month and 1-year scans, partial responders by Choi criteria at 1-year follow-up had shorter DSS than patients with stable disease (SD) or progressive disease (PD) (Schramm et al. 2013). The best correlation of DSS was with RECIST. Partial responders as per RECIST had the longest DSS and patients with progressive disease (PD) per RECIST had the shortest survival on both 3-month and 1-year scans (Schramm et al. 2013). The study concludes that further studies are required to demonstrate the value of alternate criteria like Choi criteria in predicting long-term survival (Schramm et al. 2013). Shinagare et al. studied 62 patients derived from two clinical trials evaluating response of metastatic GIST response to second-line sunitinib. In this study, response derived by RECIST 1.0, RECIST 1.1, Choi criteria, and modified Choi criteria (progressive disease defined as >20% increase in sum of the longest dimension instead of 10% increase per Choi criteria) were compared in terms of clinical benefit ratio (CBR: complete response, partial response or stable disease ≥12 weeks) and progression-free survival. Similar

to prior studies, this study found more number of partial responders with shorter time to best response by Choi criteria and modified Choi criteria. However, RECIST, RECIST1.1, and modified Choi criteria resulted in similar progression-free survival whereas Choi criteria had shorter progression-free survival. The CBR was similar with all the response criteria. The study concluded that RECIST 1.1 should be used as the primary response criteria reserving Choi criteria to detect early responses.

In a similar study Shinagare et al. studied response in 20 patients with advanced GIST treated with third-line regorafenib in a phase II trial using Choi criteria, RECIST, RECIST 1.1, and WHO criteria (Shinagare et al. 2014). Similar to other studies, Choi criteria again identified more number of partial responders. CBR was similar among all tumor response criteria (Shinagare et al. 2014) but the PFS was longest for RECIST 1.1 and shortest for Choi criteria. Furthermore, the PFS was strongly concordant with overall survival by RECIST, RECIST 1.1, and WHO criteria but not by Choi criteria (Shinagare et al. 2014). The study arrived at a similar conclusion that using RECIST 1.1 is recommended especially in clinical trial setting as patients would progress sooner with Choi criteria than RECIST (Shinagare et al. 2014).

3.1.3 Role of PET/CT and MRI in Response Assessment in GIST

Most GISTs show high metabolic activity due to intense glycolysis and therefore intensely FDG-avid on 18F-FDG-PET (Van den Abbeele 2008). Initial studies evaluating the response of GIST to imatinib found that metabolic activity in GIST declines dramatically on FDG-PET/CT and the response can be seen as early as 24 h after initiation of treatment whereas response by CT lags by weeks to months (Van den Abbeele 2001). A baseline scan obtained prior to initiating treatment can help in assessing metabolic changes overtime. The prognostic value of metabolic response on PET has been variably reported in different studies. While some studies have shown that PET responders had longer progression-free survival, others did not. In a study of 63 patients with GIST treated with imatinib by Holdsworth et al., absolute SUVmax of 2.5 at 1 month or EORTC criteria for partial response (25% decline in SUVmax) at 1 month were associated with durable response (Holdsworth et al. 2007). Stroobants et al. reported longer one-year progression-free survival in PET responders using EORTC criteria (Stroobants et al. 2003). On the contrary, McAuliffe et al., in a study of 19 patients, found that response by PET was not predictive of progression-free survival (McAuliffe et al. 2009). Similar conclusion was obtained by Chacon et al. in a study of 16 patients (Chacon et al. 2015). PET/CT has also been shown to be useful in detecting primary and secondary resistance to imatinib. However the routine use of FDG-PET/CT in clinical practice does not have additional advantages over CT scan (NCCN Clinical Practice Guidelines in Oncology Soft Tissue Sarcoma Version 2 2018). The National Comprehensive Cancer Network (NCCN) guidelines do not recommend FDG-PET/CT in the routine management of GIST (NCCN Clinical Practice Guidelines in Oncology Soft Tissue Sarcoma Version 2 2018). The European Society for Medical Oncology (ESMO) guidelines recommend FDG-PET/CT when targeted therapy is under investigation (ESMO / European Sarcoma Network Working Group 2012). Because of its ability to detect response or resistance to new therapy earlier than CT scan, FDG-PET/CT can be used for determining efficacy of drugs early in the treatment course (Van den Abbeele 2001, 2003, 2008). FDG-PET/CT can be used to evaluate ambiguous findings encountered on CT or magnetic resonance imaging (MRI) but has no role in surveillance (Fig. 1).

MRI has limited role in response assessment of GIST and is not used routinely in the clinical practice (Dimitrakopoulou-Strauss et al. 2017). A few studies evaluated the utility of MRI in response assessment of GIST. Stroszczynski et al. performed MRI in 45 patients at 2-, 4-, and 6-month intervals after starting imatinib (Stroszczynski et al. 2005). While there was significant decrease in size of several lesions, the authors found that responders showed increase in signal-to-noise ratio on T2-weighted

images at 2 months and showed decrease in enhancing areas at 4 and 6 months compared to nonresponders. In another study, Tan et al. used diffusion-weighted imaging in 32 patients with GIST treated with imatinib to show that increase in ADC at 1 week after therapy was significantly different between good and poor-response groups (Tang et al. 2011). Overall MRI is not considered a primary imaging modality in GIST response assessment. As recommended by the German GIST Working Group (Kalkmann et al. 2012), MRI can be used as a problem-solving tool for clarifying liver-specific questions and when CT is contraindicated. Increase in tumor density in some GIST metastasis due to hemorrhage (especially with sunitinib) can mimic progression. MRI due to better soft tissue resolution can help in such scenarios (Tirumani et al. 2013).

3.2 Response Assessment in Non-GIST Sarcomas

Similar to GIST, response of both primary and metastatic non-GIST sarcomas can be better evaluated by personalized tumor response criteria by taking into account morphologic changes with or without change in size. Primary non-GIST sarcomas are frequently treated with neoadjuvant chemoradiation therapy. MRI is frequently used for assessing response in this setting. The European Organization for Research and Treatment of Cancer—Soft Tissue and Bone Sarcoma Group (EORTC—STBSG) and Imaging Group guidelines recommend MRI for response assessment as close to the surgical date as possible usually at least 4–6 weeks after radiotherapy (Messiou et al. 2016). Chemoradiation therapy results in histopathological changes like necrosis, hemorrhage, cystic change, and fibrosis which can in turn change tumor dimensions. Several studies have shown that decrease in tumor size is a rare event in sarcomas treated with radiation except for myxoid liposarcomas (Look Hong et al. 2013; Canter et al. 2010; Miki et al. 2010; Roberge et al. 2010) (Fig. 3). If a tumor increases in size following therapy, careful assessment should be made for changes in tumor density (on CT) or contrast enhancement on MRI, to ensure that this does not represent pseudoprogression. Miki et al. in their study found that nearly one-third tumors increased by >10% size following radiation therapy and that there was no correlation between RECIST and eventual outcome (Miki et al. 2010) (Fig. 3).

Stacchiotti et al. prospectively compared RECIST and Choi criteria in a cohort of 37 patients with high-grade soft tissue sarcomas treated with preoperative chemoradiation therapy (Stacchiotti et al. 2009). The authors adapted Choi criteria for MR imaging and used two pathologic cutoffs for response if tumors showed at least 10% treatment-related changes (good response if 50% residual tumor was present and very good response if less than 10% residual tumor was present). The study found that RECIST (32% and 41% for good and very good response) was less sensitive than Choi criteria (82 and 88% for good and very good response) in predicting pathologic response in 28 soft tissue sarcomas other than synovial sarcomas (Stacchiotti et al. 2009). In synovial sarcomas, the response assessment was more challenging due to the presence of nontreatment-related neoplastic cystic areas which can be confused on imaging with treatment-related necrosis. The study concluded that Choi criteria is more predictive of pathologic response and tumor size itself may be insufficient for response assessment. In a follow-up study, Stacchiotti et al. compared the prognostic relevance of RECIST and Choi criteria in a larger cohort (Stacchiotti et al. 2012). A subgroup analysis of 69 patients who received chemotherapy alone showed that Choi criteria correlated better with overall survival and freedom from progression whereas RECIST correlated with only freedom from progression (Stacchiotti et al. 2012). The study also found that histology had significant correlation with outcome: undifferentiated pleomorphic sarcoma had a better response rate than leiomyosarcoma.

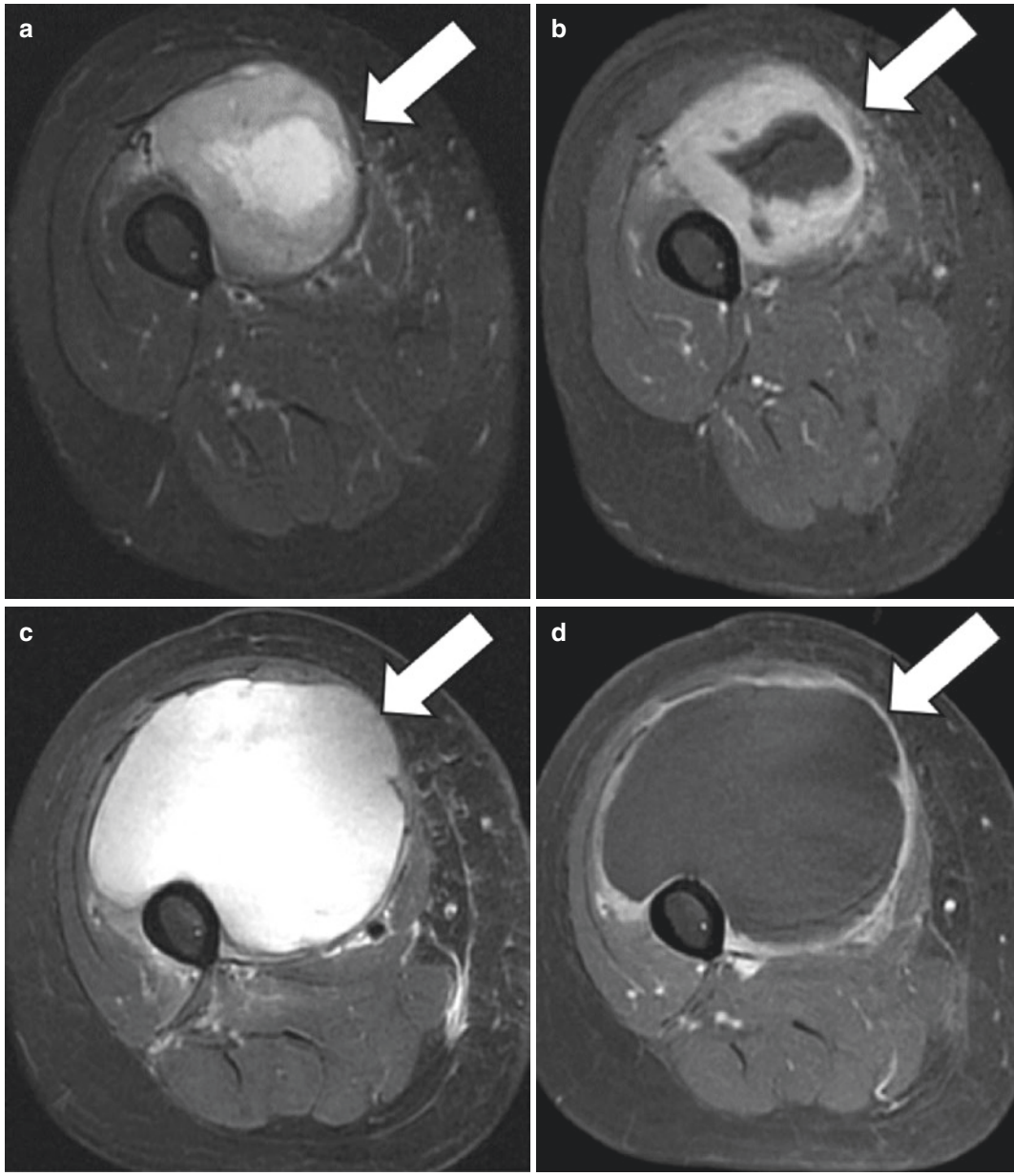

Fig. 3 69-year-old woman with high-grade pleomorphic sarcoma of the right thigh treated with neoadjuvant chemoradiation therapy. (**a**, **b**) Axial short-tau inversion recovery (STIR) and post-gadolinium fat-suppressed T1-weighted images demonstrate a T2 hyperintense mass (arrow) in the anterior thigh with central necrosis and peripheral thick enhancement. (**c**, **d**) Following neoadjuvant chemoradiation therapy, there is a significant increase in tumor size, with increased necrosis seen on T2-weighted images, and post-contrast T1-weighted images. Surgical histopathology demonstrated greater than 75% necrosis in the tumor

3.2.1 Response Assessment in Specific Subtypes of Non-GIST Sarcomas

Certain subtypes of sarcomas have unique patterns of response that must be taken into account by the radiologist. Synovial sarcomas are often multilobulated or septated masses on imaging. They tend to have heterogeneous signal intensity on both T1- and T2-weighted images. The heterogeneity is secondary to areas of cystic change, necrosis, calcification, and hemorrhage within the tumor, and maybe manifest as "triple sign" on T2-weighted images (consisting of hypo-, iso-, and hyperintense signal). Similarly, "fluid–fluid levels" secondary to layering hemorrhage and "bowl of grapes" appearance from T2 hyperintense lobulated areas and T2 hypointense septa may be present in some cases (Baheti et al. 2015; Murphey et al. 2006; O'Sullivan et al. 2008). As discussed previously, in synovial sarcomas the presence of neoplastic cystic component can confound response assessment: increase in cystic component following therapy could potentially be confused with necrosis which can be seen with treatment response. Because of this, modified response criteria may not be appropriate for synovial sarcomas (Stacchiotti et al. 2009).

Myxoid/round cell liposarcoma has a unique translocation t(12; 16)(q13; q11) which is encountered in nearly 90% cases and results in a chimeric fusion protein FUS-CHOP (Recine et al. 2017). This chimeric protein is responsible for tumorigenesis by blocking the PPARɣ pathway necessary for adipocytic maturation. Trabectedin (ET-743) is a novel drug which has been shown to be highly effective in myxoid liposarcoma due to its ability to block the FUS-CHOP protein. In a retrospective multicenter analysis of 51 patients with metastatic myxoid liposarcoma treated with trabectedin, two patients had complete radiologic response and 24 had partial response by RECIST with an overall response of 51% (Grosso et al. 2007). Interestingly, 17 patients showed decrease in tumor density on CT and decrease in enhancement on MRI well before tumor shrinkage. Some of these patients showed monovacuolated lipoblasts indicating adipocytic maturation (Fig. 4). The basis for this radiologic and pathologic response pattern is hypothesized to be related to removal of the block in cell maturation by trabectedin-induced inactivation of the FUS-CHOP protein (Grosso et al. 2007). This manifests at histopathology as replacement of cellular tumor with acellular stroma and radiologically as decrease in density. A similar response pattern has been reported following chemotherapy and radiation therapy. In a study of 22 patients with

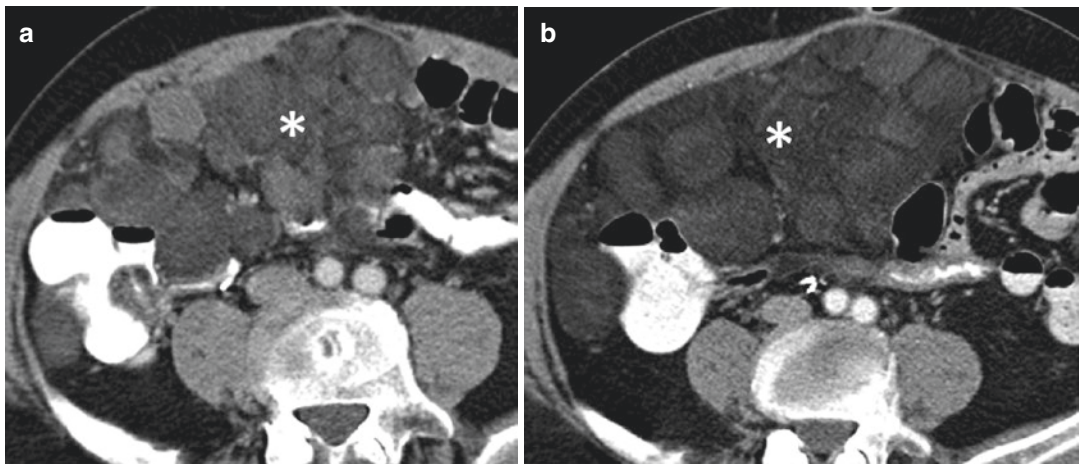

Fig. 4 62-year-old man with myxoid liposarcoma treated with trabectedin. (**a**, **b**) Axial contrast-enhanced CT images at baseline and 12 months after start of treatment demonstrate increase in the fatty attenuation within the intraabdominal masses (asterisk) consistent with adipocytic maturation

myxoid liposarcoma treated with neoadjuvant chemoradiation therapy, Wang et al. noted extensive hyalinization in 16 patients and adipocytic maturation in 6 patients (Wang et al. 2012). Of the 6 patients with adipocytic maturation at pathology in this study, four patients showed increased fat on MRI (Wang et al. 2012).

Dramatic decrease in size is seen with myxoid liposarcoma, in contrast to other sarcomas which tend to increase in size following radiation therapy (Fig. 5). Piston et al. in their study of 15 patients with myxoid LPS and 16 patients with malignant fibrous histiocytoma (MFH) treated with radiotherapy found that myxoid LPS showed statistically significant decrease in tumor volume and maximal dimension compared to MFH, some of the MFH increasing in size following radiotherapy (Pitson et al. 2004). Wortman et al. in a

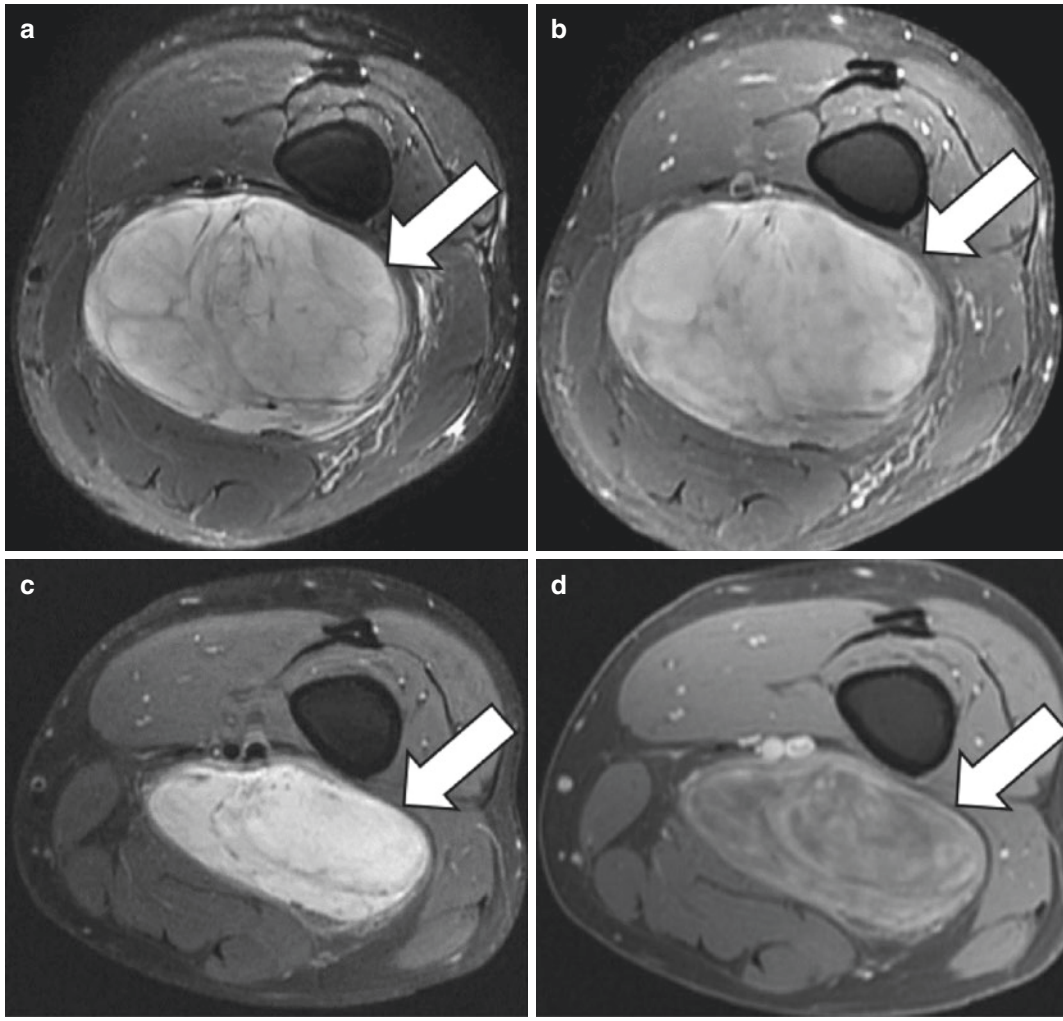

Fig. 5 51-year-old man with myxoid liposarcoma of the left thigh treated with neoadjuvant chemoradiation therapy. (**a**, **b**). Axial short-tau inversion recovery (STIR) and post-gadolinium fat-suppressed T1-weighted images demonstrate T2 hyperintense mass in the posterior compartment of the thigh (arrow) which shows intense homogeneous enhancement after contrast administration. (**c**, **d**) Following neoadjuvant chemoradiation therapy, there was a significant decrease in tumor size, as well as decrease in overall degree of enhancement in the mass. No significant hemorrhage or necrosis was seen. Surgical histopathology demonstrated large volume (95%) hyalinization and fibrosis

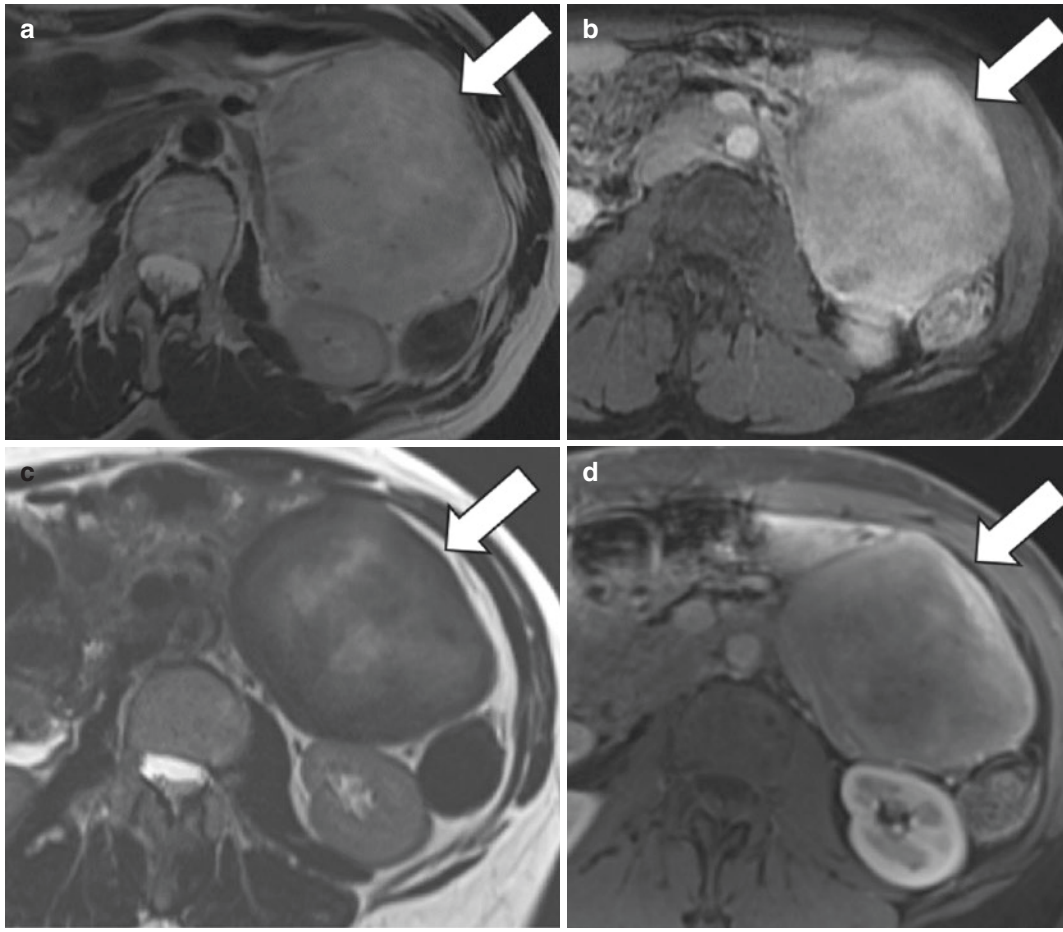

Fig. 6 53-year-old woman with mesenteric desmoid tumor treated with systemic therapy. (**a**, **b**) Axial T2-weighted and post-gadolinium fat-suppressed T1-weighted MR images demonstrate a well-circumscribed mildly heterogenous T2 hyperintense mass within the mesentery which shows intense enhancement (arrow) after contrast administration. (**c**, **d**) Follow-up MRI after 6 months of treatment shows mild decrease in size of the lesion but marked decrease in T2 signal (arrow) and decrease in enhancement consistent with treatment response

study of 18 patients consisting of 5 pleomorphic liposarcomas and 13 myxoid liposarcomas showed that pleomorphic liposarcoma increased in size with increase in peritumoral edema, hemorrhage, and necrosis (Wortman et al. 2016). This contrasted sharply with myxoid liposarcoma in which none of the cases showed increase in size but instead showed decreases in size and enhancement. De Vreeze et al. in their study of sarcomas treated with radiation therapy including 10 myxoid liposarcomas concluded that the sensitivity of myxoid liposarcoma to radiation therapy is related to damage to the medium-sized arterioles which retain the typical crow-feet pattern of vascular architecture but show thrombosis and fibrosis leading to tumor hypoxia and cell death leading to decrease in the production of myxoid stroma by the tumor cells (de Vreeze et al. 2008). At pathology the radiographic change mirrored in form of large volume of hyalinization/fibrosis.

Desmoid fibromatosis is a benign mesenchymal neoplasm which is locally aggressive but non-metastasizing. Histologically it is composed of clonal proliferation of fibroblasts and

myofibroblasts which produce collagen. Desmoid tumors are managed by surgical resection but have a high chance (>30% in some studies) of local recurrence (He et al. 2015; Wang et al. 2015). Local radiation has shown to decrease recurrence rate. Recent studies have shown that systemic medical therapies like hormonal therapy, anti-inflammatory drugs, conventional chemotherapy, and targeted therapies are effective in desmoid fibromatosis. Response of desmoid tumors to such systemic therapies tends to be different from other sarcomas (Braschi-Amirfarzan et al. 2016). Active desmoid tumors have heterogeneously hyperintense signal on T2-weighted images and isointense signal on T1-weighted images. Bands of low signal can be seen interspersed within the high signal areas on T2-weighted images and represent densely packed collagen stroma. Intense enhancement after contrast administration typically involves the high T2 signal areas which represent increased cellularity and active disease. Following systemic treatment, desmoid tumors show increase in the T2 hypointense signal and decrease in enhancement independent of size change (Fig. 6). The increase in hypointense signal correlates with increased collagenization at histopathology indicating maturation. Due to this unique response pattern, like other sarcomas, RECIST 1.1 may be suboptimal for response assessment in desmoid tumors. In a study of 23 patients with desmoid fibromatosis treated with various therapies, Sheth et al. showed that volumetric criteria detected more number of partial responders than RECIST 1.1 and that change in T2 hyperintensity correlated well with volume change (Sheth et al. 2016). In another study of 32 patients with desmoid fibromatosis treated with tamoxifen with or without anti-inflammatory drugs, Libertini et al. found that there was no correlation between symptomatic benefit and RECIST 1.1 response (Libertini et al. 2018). Gounder et al. studied the response of desmoid tumors to sorafenib in 26 patients and found that 12 out of 13 patients (92%) evaluated by MRI showed >30% decrease in T2 signal whereas by RECIST 1.1 25% showed partial response and 70% showed stable disease (Gounder et al. 2011).

4 Summary and Conclusions

In the era of precision medicine, interpreting therapeutic response of sarcomas, especially to novel molecular targeted therapies, can be challenging. Response of both primary and metastatic GIST or non-GIST sarcomas can be better evaluated by personalized tumor response criteria by taking into account morphologic changes with or without change in size. Though RECIST 1.1 is widely used for assessing response of sarcomas in clinical trials, in the opinion of the author, knowledge of alternate response patterns can be useful in both clinical and research settings to identify unusual response patterns of sarcomas to both conventional and novel therapies.

References

Al-Absi E, Farrokhyar F, Sharma R, Whelan K, Corbett T, Patel M et al (2010) A systematic review and meta-analysis of oncologic outcomes of pre-versus post-operative radiation in localized resectable soft-tissue sarcoma. Ann Surg Oncol 17(5):1367–1374

Albertsmeier M, Rauch A, Roeder F, Hasenhutl S, Pratschke S, Kirschneck M et al (2018) External beam radiation therapy for resectable soft tissue sarcoma: a systematic review and meta-analysis. Ann Surg Oncol 25(3):754–767

Baheti AD, Tirumani SH, Sewatkar R, Shinagare AB, Hornick JL, Ramaiya NH et al (2015) Imaging features of primary and metastatic extremity synovial sarcoma: a single institute experience of 78 patients. Br J Radiol 88(1046):20140608

Benjamin RS, Choi H, Macapinlac HA, Burgess MA, Patel SR, Chen LL et al (2007) We should desist using RECIST, at least in GIST. J Clin Oncol 25(13):1760–1764

Bramwell VH, Anderson D, Charette ML (2003) Sarcoma disease site G. Doxorubicin-based chemotherapy for the palliative treatment of adult patients with locally advanced or metastatic soft tissue sarcoma. Cochrane Database Syst Rev (3):CD003293

Braschi-Amirfarzan M, Keraliya AR, Krajewski KM, Tirumani SH, Shinagare AB, Hornick JL et al (2016) Role of imaging in management of desmoid-type fibromatosis: a primer for radiologists. Radiographics 36(3):767–782

Canter RJ, Martinez SR, Tamurian RM, Wilton M, Li CS, Ryu J et al (2010) Radiographic and histologic response to neoadjuvant radiotherapy in patients with soft tissue sarcoma. Ann Surg Oncol 17(10):2578–2584

Chacon M, Eleta M, Espindola AR, Roca E, Mendez G, Rojo S et al (2015) Assessment of early response to

imatinib 800 mg after 400 mg progression by (1)(8) F-fluorodeoxyglucose PET in patients with metastatic gastrointestinal stromal tumors. Future Oncol 11(6):953–964

Choi H, Charnsangavej C, de Castro Faria S, Tamm EP, Benjamin RS, Johnson MM et al (2004) CT evaluation of the response of gastrointestinal stromal tumors after imatinib mesylate treatment: a quantitative analysis correlated with FDG PET findings. AJR Am J Roentgenol 183(6):1619–1628

Choi H, Charnsangavej C, Faria SC, Macapinlac HA, Burgess MA, Patel SR et al (2007) Correlation of computed tomography and positron emission tomography in patients with metastatic gastrointestinal stromal tumor treated at a single institution with imatinib mesylate: proposal of new computed tomography response criteria. J Clin Oncol 25(13):1753–1759

Cohen MH, Farrell A, Justice R, Pazdur R (2009) Approval summary: imatinib mesylate in the treatment of metastatic and/or unresectable malignant gastrointestinal stromal tumors. Oncologist 14(2):174–180

Dagher R, Cohen M, Williams G, Rothmann M, Gobburu J, Robbie G et al (2002) Approval summary: imatinib mesylate in the treatment of metastatic and/or unresectable malignant gastrointestinal stromal tumors. Clin Cancer Res 8(10):3034–3038

Demetri GD, von Mehren M, Blanke CD, Van den Abbeele AD, Eisenberg B, Roberts PJ et al (2002) Efficacy and safety of imatinib mesylate in advanced gastrointestinal stromal tumors. N Engl J Med 347(7):472–480

Demetri GD, van Oosterom AT, Garrett CR, Blackstein ME, Shah MH, Verweij J et al (2006) Efficacy and safety of sunitinib in patients with advanced gastrointestinal stromal tumour after failure of imatinib: a randomised controlled trial. Lancet 368(9544):1329–1338

Demetri GD, Chawla SP, von Mehren M, Ritch P, Baker LH, Blay JY et al (2009) Efficacy and safety of trabectedin in patients with advanced or metastatic liposarcoma or leiomyosarcoma after failure of prior anthracyclines and ifosfamide: results of a randomized phase II study of two different schedules. J Clin Oncol 27(25):4188–4196

Demetri GD, Reichardt P, Kang YK, Blay JY, Rutkowski P, Gelderblom H et al (2013) Efficacy and safety of regorafenib for advanced gastrointestinal stromal tumours after failure of imatinib and sunitinib (GRID): an international, multicentre, randomised, placebo-controlled, phase 3 trial. Lancet 381(9863):295–302

Demetri GD, von Mehren M, Jones RL, Hensley ML, Schuetze SM, Staddon A et al (2016) Efficacy and safety of trabectedin or dacarbazine for metastatic liposarcoma or leiomyosarcoma after failure of conventional chemotherapy: results of a phase III randomized multicenter clinical trial. J Clin Oncol 34(8):786–793. Pubmed Central PMCID: 5070559 online at www.jco.org. Author contributions are found at the end of this article

Desai J, Shankar S, Heinrich MC, Fletcher JA, Fletcher CD, Manola J et al (2007) Clonal evolution of resistance to imatinib in patients with metastatic gastrointestinal stromal tumors. Clin Cancer Res 13(18 Pt 1):5398–5405

Dimitrakopoulou-Strauss A, Ronellenfitsch U, Cheng C, Pan L, Sachpekidis C, Hohenberger P et al (2017) Imaging therapy response of gastrointestinal stromal tumors (GIST) with FDG PET, CT and MRI: a systematic review. Clin Transl Imaging 5(3):183–197

Doyle LA (2014) Sarcoma classification: an update based on the 2013 World Health Organization classification of tumors of soft tissue and bone. Cancer 120(12):1763–1774

ESMO/European Sarcoma Network Working Group (2012) Gastrointestinal stromal tumors: ESMO Clinical Practice Guidelines for diagnosis, treatment and follow-up. Ann Oncol 23(Suppl 7):vii49–vii55

Evilevitch V, Weber WA, Tap WD, Allen-Auerbach M, Chow K, Nelson SD et al (2008) Reduction of glucose metabolic activity is more accurate than change in size at predicting histopathologic response to neoadjuvant therapy in high-grade soft-tissue sarcomas. Clin Cancer Res 14(3):715–720

Garcia del Muro X, Lopez-Pousa A, Martin J, Buesa JM, Martinez-Trufero J, Casado A et al (2005) A phase II trial of temozolomide as a 6-week, continuous, oral schedule in patients with advanced soft tissue sarcoma: a study by the Spanish Group for Research on Sarcomas. Cancer 104(8):1706–1712

Garcia-Del-Muro X, Lopez-Pousa A, Maurel J, Martin J, Martinez-Trufero J, Casado A et al (2011 Jun 20) Randomized phase II study comparing gemcitabine plus dacarbazine versus dacarbazine alone in patients with previously treated soft tissue sarcoma: a Spanish Group for Research on Sarcomas study. J Clin Oncol 29(18):2528–2533

Gounder MM, Lefkowitz RA, Keohan ML, D'Adamo DR, Hameed M, Antonescu CR et al (2011) Activity of Sorafenib against desmoid tumor/deep fibromatosis. Clin Cancer Res 17(12):4082–4090

Gronchi A, Ferrari S, Quagliuolo V, Broto JM, Pousa AL, Grignani G et al (2017) Histotype-tailored neoadjuvant chemotherapy versus standard chemotherapy in patients with high-risk soft-tissue sarcomas (ISG-STS 1001): an international, open-label, randomised, controlled, phase 3, multicentre trial. Lancet Oncol 18(6):812–822

Grosso F, Jones RL, Demetri GD, Judson IR, Blay JY, Le Cesne A et al (2007) Efficacy of trabectedin (ecteinascidin-743) in advanced pretreated myxoid liposarcomas: a retrospective study. Lancet Oncol 8(7):595–602

He XD, Zhang YB, Wang L, Tian ML, Liu W, Qu Q et al (2015) Prognostic factors for the recurrence of sporadic desmoid-type fibromatosis after macroscopically complete resection: analysis of 114 patients at a single institution. Eur J Surg Oncol 41(8):1013–1019

Holdsworth CH, Badawi RD, Manola JB, Kijewski MF, Israel DA, Demetri GD et al (2007) CT and PET: early prognostic indicators of response to imatinib mesylate in patients with gastrointestinal stromal tumor. AJR Am J Roentgenol 189(6):W324–W330

Joensuu H, Roberts PJ, Sarlomo-Rikala M, Andersson LC, Tervahartiala P, Tuveson D et al (2001) Effect of the tyrosine kinase inhibitor STI571 in a patient with a metastatic gastrointestinal stromal tumor. N Engl J Med 344(14):1052–1056

Judson I, Radford JA, Harris M, Blay JY, van Hoesel Q, le Cesne A et al (2001) Randomised phase II trial of pegylated liposomal doxorubicin (DOXIL/CAELYX) versus doxorubicin in the treatment of advanced or metastatic soft tissue sarcoma: a study by the EORTC Soft Tissue and Bone Sarcoma Group. Eur J Cancer 37(7):870–877

Kalkmann J, Zeile M, Antoch G, Berger F, Diederich S, Dinter D et al (2012) Consensus report on the radiological management of patients with gastrointestinal stromal tumours (GIST): recommendations of the German GIST Imaging Working Group. Cancer Imaging 12:126–135

Kang YK, Ryu MH, Yoo C, Ryoo BY, Kim HJ, Lee JJ et al (2013) Resumption of imatinib to control metastatic or unresectable gastrointestinal stromal tumours after failure of imatinib and sunitinib (RIGHT): a randomised, placebo-controlled, phase 3 trial. Lancet Oncol 14(12):1175–1182

Kollar A, Jones RL, Stacchiotti S, Gelderblom H, Guida M, Grignani G et al (2017) Pazopanib in advanced vascular sarcomas: an EORTC Soft Tissue and Bone Sarcoma Group (STBSG) retrospective analysis. Acta Oncol 56(1):88–92

Levy AD, Manning MA, Al-Refaie WB, Miettinen MM (2017a) Soft-tissue sarcomas of the abdomen and pelvis: radiologic-pathologic features, Part 1—common sarcomas: from the radiologic pathology archives. Radiographics 37(2):462–483

Levy AD, Manning MA, Miettinen MM (2017b) Soft-tissue sarcomas of the abdomen and pelvis: radiologic-pathologic features, Part 2—uncommon sarcomas. Radiographics 37(3):797–812

Libertini M, Mitra I, van der Graaf WTA, Miah AB, Judson I, Jones RL et al (2018) Aggressive fibromatosis response to tamoxifen: lack of correlation between MRI and symptomatic response. Clin Sarcoma Res 8:13

Look Hong NJ, Hornicek FJ, Harmon DC, Choy E, Chen YL, Yoon SS et al (2013) Neoadjuvant chemoradiotherapy for patients with high-risk extremity and truncal sarcomas: a 10-year single institution retrospective study. Eur J Cancer 49(4):875–883

Lorigan P, Verweij J, Papai Z, Rodenhuis S, Le Cesne A, Leahy MG et al (2007) Phase III trial of two investigational schedules of ifosfamide compared with standard-dose doxorubicin in advanced or metastatic soft tissue sarcoma: a European Organisation for Research and Treatment of Cancer Soft Tissue and Bone Sarcoma Group Study. J Clin Oncol 25(21):3144–3150

Mabille M, Vanel D, Albiter M, Le Cesne A, Bonvalot S, Le Pechoux C et al (2009) Follow-up of hepatic and peritoneal metastases of gastrointestinal tumors (GIST) under Imatinib therapy requires different criteria of radiological evaluation (size is not everything!!!). Eur J Radiol 69(2):204–208

McAuliffe JC, Hunt KK, Lazar AJ, Choi H, Qiao W, Thall P et al (2009) A randomized, phase II study of preoperative plus postoperative imatinib in GIST: evidence of rapid radiographic response and temporal induction of tumor cell apoptosis. Ann Surg Oncol 16(4):910–919

Messiou C, Bonvalot S, Gronchi A, Vanel D, Meyer M, Robinson P et al (2016) Evaluation of response after pre-operative radiotherapy in soft tissue sarcomas; the European Organisation for Research and Treatment of Cancer-Soft Tissue and Bone Sarcoma Group (EORTC-STBSG) and Imaging Group recommendations for radiological examination and reporting with an emphasis on magnetic resonance imaging. Eur J Cancer 56:37–44

Miki Y, Ngan S, Clark JC, Akiyama T, Choong PF (2010) The significance of size change of soft tissue sarcoma during preoperative radiotherapy. Eur J Surg Oncol 36(7):678–683

Mullen JT, Kobayashi W, Wang JJ, Harmon DC, Choy E, Hornicek FJ et al (2012) Long-term follow-up of patients treated with neoadjuvant chemotherapy and radiotherapy for large, extremity soft tissue sarcomas. Cancer 118(15):3758–3765

Murphey MD, Gibson MS, Jennings BT, Crespo-Rodriguez AM, Fanburg-Smith J, Gajewski DA (2006) From the archives of the AFIP: imaging of synovial sarcoma with radiologic-pathologic correlation. Radiographics 26(5):1543–1565

NCCN Clinical Practice Guidelines in Oncology Soft Tissue Sarcoma Version 2 (2018) NCCN; 2018 [12.02.2018]. http://www.nccn.org/professionals/physician_gls/f_guidelines.asp#site

O'Sullivan PJ, Harris AC, Munk PL (2008) Radiological features of synovial cell sarcoma. Br J Radiol 81(964):346–356

Papagelopoulos PJ, Mavrogenis AF, Mastorakos DP, Patapis P, Soucacos PN (2008) Current concepts for management of soft tissue sarcomas of the extremities. J Surg Orthopaedic Adv 17(3):204–215

Pervaiz N, Colterjohn N, Farrokhyar F, Tozer R, Figueredo A, Ghert M (2008) A systematic meta-analysis of randomized controlled trials of adjuvant chemotherapy for localized resectable soft-tissue sarcoma. Cancer 113(3):573–581

Pitson G, Robinson P, Wilke D, Kandel RA, White L, Griffin AM et al (2004) Radiation response: an additional unique signature of myxoid liposarcoma. Int J Radiat Oncol Biol Phys 60(2):522–526

Recine F, Bongiovanni A, Riva N, Fausti V, De Vita A, Mercatali L et al (2017) Update on the role of trabectedin in the treatment of intractable soft tissue sarcomas. OncoTargets Ther 10:1155–1164

Rezai P, Pisaneschi MJ, Feng C, Yaghmai V (2013) A radiologist's guide to treatment response criteria in oncologic imaging: anatomic imaging biomarkers. AJR Am J Roentgenol 201(2):237–245

Roberge D, Skamene T, Nahal A, Turcotte RE, Powell T, Freeman C (2010) Radiological and pathological response following pre-operative radiotherapy for soft-tissue sarcoma. Radiotherapy Oncol 97(3):404–407

Robinson E, Bleakney RR, Ferguson PC, O'Sullivan B (2008) Oncodiagnosis panel: 2007: multidisciplinary management of soft-tissue sarcoma. Radiographics 28(7):2069–2086

Schiavon G, Ruggiero A, Schoffski P, van der Holt B, Bekers DJ, Eechoute K et al (2012) Tumor volume as an alternative response measurement for imatinib treated GIST patients. PloS one 7(11):e48372

Schiavon G, Ruggiero A, Bekers DJ, Barry PA, Sleijfer S, Kloth J et al (2014) The effect of baseline morphology and its change during treatment on the accuracy of Response Evaluation Criteria in Solid Tumours in assessment of liver metastases. Eur J Cancer 50(5):972–980

Schoffski P, Chawla S, Maki RG, Italiano A, Gelderblom H, Choy E et al (2016) Eribulin versus dacarbazine in previously treated patients with advanced liposarcoma or leiomyosarcoma: a randomised, open-label, multicentre, phase 3 trial. Lancet 387(10028):1629–1637

Schramm N, Englhart E, Schlemmer M, Hittinger M, Ubleis C, Becker CR et al (2013) Tumor response and clinical outcome in metastatic gastrointestinal stromal tumors under sunitinib therapy: comparison of RECIST, Choi and volumetric criteria. Eur J Radiol 82(6):951–958

Schuetze SM (2006) Utility of positron emission tomography in sarcomas. Curr Opin Oncol 18(4):369–373

Schuetze SM, Rubin BP, Vernon C, Hawkins DS, Bruckner JD, Conrad EU 3rd et al (2005) Use of positron emission tomography in localized extremity soft tissue sarcoma treated with neoadjuvant chemotherapy. Cancer 103(2):339–348

Schwab JH, Boland PJ, Antonescu C, Bilsky MH, Healey JH (2007) Spinal metastases from myxoid liposarcoma warrant screening with magnetic resonance imaging. Cancer 110(8):1815–1822

Seddon B, Strauss SJ, Whelan J, Leahy M, Woll PJ, Cowie F et al (2017) Gemcitabine and docetaxel versus doxorubicin as first-line treatment in previously untreated advanced unresectable or metastatic soft-tissue sarcomas (GeDDiS): a randomised controlled phase 3 trial. Lancet Oncol 18(10):1397–1410

Shankar S, vanSonnenberg E, Desai J, Dipiro PJ, Van Den Abbeele A, Demetri GD (2005) Gastrointestinal stromal tumor: new nodule-within-a-mass pattern of recurrence after partial response to imatinib mesylate. Radiology 235(3):892–898

Sheth PJ, Del Moral S, Wilky BA, Trent JC, Cohen J, Rosenberg AE et al (2016) Desmoid fibromatosis: MRI features of response to systemic therapy. Skelet Radiol 45(10):1365–1373

Shinagare AB, Jagannathan JP, Kurra V, Urban T, Manola J, Choy E et al (2014) Comparison of performance of various tumour response criteria in assessment of regorafenib activity in advanced gastrointestinal stromal tumours after failure of imatinib and sunitinib. Eur J Cancer 50(5):981–986

Shinagare AB, Barysauskas CM, Braschi-Amirfarzan M, O'Neill AC, Catalano PJ, George S et al (2016) Comparison of performance of various tumor response criteria in assessment of sunitinib activity in advanced gastrointestinal stromal tumors. Clin Imaging 40(5):880–884

Siegel GW, Biermann JS, Chugh R, Jacobson JA, Lucas D, Feng M et al (2015) The multidisciplinary management of bone and soft tissue sarcoma: an essential organizational framework. J Multidiscip Healthc 8:109–115

Sood S, Baheti AD, Shinagare AB, Jagannathan JP, Hornick JL, Ramaiya NH et al (2014) Imaging features of primary and metastatic alveolar soft part sarcoma: single institute experience in 25 patients. Br J Radiol 87(1036):20130719

Stacchiotti S, Collini P, Messina A, Morosi C, Barisella M, Bertulli R et al (2009) High-grade soft-tissue sarcomas: tumor response assessment—pilot study to assess the correlation between radiologic and pathologic response by using RECIST and Choi criteria. Radiology 251(2):447–456

Stacchiotti S, Negri T, Zaffaroni N, Palassini E, Morosi C, Brich S et al (2011) Sunitinib in advanced alveolar soft part sarcoma: evidence of a direct antitumor effect. Ann Oncol 22(7):1682–1690

Stacchiotti S, Verderio P, Messina A, Morosi C, Collini P, Llombart-Bosch A et al (2012) Tumor response assessment by modified Choi criteria in localized high-risk soft tissue sarcoma treated with chemotherapy. Cancer 118(23):5857–5866

Stroobants S, Goeminne J, Seegers M, Dimitrijevic S, Dupont P, Nuyts J et al (2003) 18FDG-positron emission tomography for the early prediction of response in advanced soft tissue sarcoma treated with imatinib mesylate (Glivec). Eur J Cancer 39(14): 2012–2020

Stroszczynski C, Jost D, Reichardt P, Chmelik P, Gaffke G, Kretzschmar A et al (2005) Follow-up of gastrointestinal stromal tumours (GIST) during treatment with imatinib mesylate by abdominal MRI. Eur Radiol 15(12):2448–2456

Tang L, Zhang XP, Sun YS, Shen L, Li J, Qi LP et al (2011) Gastrointestinal stromal tumors treated with imatinib mesylate: apparent diffusion coefficient in the evaluation of therapy response in patients. Radiology 258(3):729–738

Tap WD, Jones RL, Van Tine BA, Chmielowski B, Elias AD, Adkins D et al (2016) Olaratumab and doxorubicin versus doxorubicin alone for treatment of soft-tissue sarcoma: an open-label phase 1b and randomised phase 2 trial. Lancet 388(10043):488–497

Tirumani SH, Jagannathan JP, Krajewski KM, Shinagare AB, Jacene H, Ramaiya NH (2013) Imatinib and beyond in gastrointestinal stromal tumors: a radiologist's perspective. AJR Am J Roentgenol 201(4):801–810

Tirumani SH, Shinagare AB, O'Neill AC, Nishino M, Rosenthal MH, Ramaiya NH (2016) Accuracy and feasibility of estimated tumour volumetry in primary gastric gastrointestinal stromal tumours: validation using semiautomated technique in 127 patients. Eur Radiol 26(1):286–295

Van den Abbeele AD (ed) (2001) F18-FDG-PET provides early evidence of biological response to STI571 in patients with malignant gastrointestinal stromal tumors (GIST). Proc Am Soc Clin Oncol 20:362a

Van den Abbeele AD (2008) The lessons of GIST—PET and PET/CT: a new paradigm for imaging. Oncologist 13(Suppl 2):8–13

Van den Abbeele A, Badawi R, Tetrault R, Cliche J, Manola J, Spangler T et al (eds) (2003) FDG-PET as a surrogate marker for response to Gleevec (TM)(imatinib mesylate) in patients with advanced gastrointestinal stromal tumors (GIST). J Nucl Med 44:24–25

de Vreeze RS, de Jong D, Haas RL, Stewart F, van Coevorden F (2008) Effectiveness of radiotherapy in myxoid sarcomas is associated with a dense vascular pattern. Int J Radiat Oncol Biol Phys 72(5):1480–1487

Wang WL, Katz D, Araujo DM, Ravi V, Ludwig JA, Trent JC et al (2012) Extensive adipocytic maturation can be seen in myxoid liposarcomas treated with neoadjuvant doxorubicin and ifosfamide and pre-operative radiation therapy. Clin Sarcoma Res 2(1):25

Wang YF, Guo W, Sun KK, Yang RL, Tang XD, Ji T et al (2015) Postoperative recurrence of desmoid tumors: clinical and pathological perspectives. World J Surg Oncol 13:26

Wortman JR, Tirumani SH, Tirumani H, Shinagare AB, Jagannathan JP, Hornick JL et al (2016) Neoadjuvant radiation in primary extremity liposarcoma: correlation of MRI features with histopathology. Eur Radiol 26(5):1226–1234

Zhao RP, Yu XL, Zhang Z, Jia LJ, Feng Y, Yang ZZ et al (2016) The efficacy of postoperative radiotherapy in localized primary soft tissue sarcoma treated with conservative surgery. Radiat Oncol 11:25

Part IV

Emerging Approaches and Future Directions

Radiomics and Imaging Genomics for Evaluation of Tumor Response

Geewon Lee, So Hyeon Bak, Ho Yun Lee, Joon Young Choi, and Hyunjin Park

Geewon Lee and So Hyeon Bak contributed equally.

G. Lee
Department of Radiology and Center for Imaging Science, Samsung Medical Center, Sungkyunkwan University School of Medicine, Seoul, South Korea

Department of Radiology and Medical Research Institute, Pusan National University Hospital, Pusan National University School of Medicine, Busan, South Korea

S. H. Bak
Department of Radiology and Center for Imaging Science, Samsung Medical Center, Sungkyunkwan University School of Medicine, Seoul, South Korea

Department of Radiology, Kangwon National University Hospital, Kangwon National University School of Medicine, Chuncheon, South Korea
e-mail: sohyeon.bak@kangwon.ac.kr

H. Y. Lee (✉)
Department of Radiology and Center for Imaging Science, Samsung Medical Center, Sungkyunkwan University School of Medicine, Seoul, South Korea

Department of Health Sciences and Technology, SAIHST, Sungkyunkwan University, Seoul, South Korea
e-mail: hoyunlee@skku.edu

J. Y. Choi
Departments of Nuclear Medicine, Samsung Medical Center, Sungkyunkwan University School of Medicine, Seoul, South Korea
e-mail: gyrus@skku.edu

H. Park
School of Electronic and Electrical Engineering, Sungkyunkwan University, Suwon, South Korea

Center for Neuroscience Imaging Research, Institute for Basic Science, Suwon, South Korea
e-mail: hyunjinp@skku.edu

Contents

Abstract

During the past two decades, response evaluation criteria in solid tumors (RECIST) has been established as the standard guideline for measuring tumor burden and confirming tumor response. According to the RECIST criteria, the therapeutic effectiveness of anticancer treatment is evaluated by unidimensional

M. Nishino (ed.), *Therapy Response Imaging in Oncology*, Medical Radiology, Diagnostic Imaging,
https://doi.org/10.1007/978-3-030-31171-1_13

measurement of the tumor diameter. However, limitations have been observed when using this traditional response criteria alone. Multiple factors, including reader measurement variability and different technical scanning parameters, may cause errors in tumor measurement and response assessment to result in inappropriate anticancer treatment decisions. Furthermore, conventional response criteria may not accurately evaluate the latest cancer treatment options such as molecular therapy and immunotherapy. In this context, radiomics and imaging genomics may provide comprehensive information on tumor phenotypes and has shown potential for quantifying lung cancer biology and evaluating treatment response. In this review, we describe the measurement variability of the tumor burden according to different modalities of CT, PET, and MRI. In addition, we discuss the promising role of radiomics and imaging genomics in treatment response evaluation of lung cancer patients.

1 Limitations of RECIST

Since its publication in 2000 and revision in 2009, response evaluation criteria in solid tumors (RECIST) has been established as the standard guideline for measuring tumor burden and confirming tumor response (Eisenhauer et al. 2009; Therasse et al. 2000). According to the RECIST criteria, the therapeutic effectiveness of anticancer treatment is evaluated by unidimensional measurement of tumor diameter. However, limitations have been observed when using the traditional response criteria alone. Multiple factors, including reader measurement variability and different technical scanning parameters, may cause errors in tumor measurement and response assessment to result in inappropriate anticancer treatment decisions.

Traditional cytotoxic chemotherapy usually aims to kill rapidly dividing tumor cells, leading to promptly decreased tumor size that is readily assessed by the RECIST criteria. A large number of molecular targeted therapies have been developed in recent years, ushering in a new era of systemic cancer treatment. Molecular therapy targets transmembranous receptors and intracellular molecules that are responsible for tumor cell survival and proliferation. In addition, cancer immunotherapy aims to activate the immune system to fight cancer. Unlike traditional cytotoxic chemotherapy, these new anticancer treatments demonstrate new response patterns without concurrent tumor size reduction. Therefore, the tumor response may not be accurately evaluated by conventional response criteria such as RECIST.

2 Radiomics Application to Treatment Response

2.1 Introduction

Radiomics, the process of extracting large amounts of advanced quantitative information from radiological images, has shown potential for quantifying lung cancer biology and evaluating treatment response (Lee et al. 2017). Although radiomics demonstrates promising results for measuring tumor burden, a great deal of variability exists. Radiologists should be familiar with the technical variations, benefits, and drawbacks of radiomics regarding treatment response.

2.2 Volumetry

Precise measurement of tumor burden between interval studies is the foundation of accurate tumor response evaluation leading to appropriate treatment decisions. However, discordant unidimensional measurement has been reported previously (Erasmus et al. 2003). According to this study, variability of manual measurements is largely responsible for variability in tumor measurement. In other words, each reviewer may measure the tumor at different image slices, resulting in different unidimensional measurements. To resolve this problem, many publications have shown that measurement of the entire

tumor volume is advantageous compared to unidimensional measurement (Goldmacher and Conklin 2012; Jennings et al. 2004; Mozley et al. 2012; Nishino et al. 2011, 2013; Zhao et al. 2006). First, volumetric measurement has better reproducibility and repeatability (Han et al. 2017). Second, volumetric measurement is more sensitive than unidimensional measurement in detecting even small changes. For instance, in a 10-mm spherical nodule, a 1-mm increase in unidimensional diameter corresponds to a 10% increase in cross-sectional diameter and a 33% increase in volume (Plathow et al. 2006). Third, due to increasing use of post-processing computer software, tumor volumetric measurements are more convenient than ever. Oncology trials are beginning to use whole tumor volume as the clinical endpoint (Zhao et al. 2010); thus, it is important to understand variability in measurements of tumor volume (Zhao et al. 2010; Altorki et al. 2010; Hayes et al. 2016).

By definition, segmentation is delineating tumor boundaries and separating tumor from the neighboring anatomy. Typically, the whole tumor is selected as the volume of interest (VOI), which is feasible in most cases. However, when lung cancer is surrounded by pathological abnormalities, including atelectasis, pneumonia, or lung injury, accurate tumor segmentation becomes more challenging due to obscured tumor margins that may lead to variability in tumor measurement (Rios Velazquez et al. 2012; van Dam et al. 2010).

2.3 Texture Analysis

In contrast to histogram features, higher-order texture features retain spatial information about each voxel, thus showing the textural characteristics of cancers. A gray level co-occurrence matrix (GLCM) is constructed using the number, distance, and angle of a combination of gray levels in the image. From the GLCM, features of cluster, correlation, contrast, energy, and entropy can be extracted. A gray-level run-length matrix (GLRL) characterizes continuous voxels with the same gray level in any direction. From the GLRL, features such as long run emphasis, short run emphasis, run length non-uniformity, gray level non-uniformity, and run percentage can be extracted. The neighborhood gray-tone difference matrix (NGTDM) uses the intensity values of a neighborhood instead of one voxel to represent how similar or dissimilar voxel intensities are within a neighborhood. Features of busyness, complexity, and texture strength can be extracted from the NGTDM.

Based on the literature, texture features have shown promising results for predicting tumor stage, metastasis, treatment response, survival, and molecular genetic profiles in lung cancer (Al-Kadi and Watson 2008; Cook et al. 2013; Fried et al. 2014; Ganeshan et al. 2010, 2012). In a study of 127 NSCLC patients, pretreatment radiomics features including texture features could predict pathological gross residual disease (Coroller et al. 2016). According to a recent study, a radiomics signature score including higher levels of long gray-level run emphasis could discriminate indolent and invasive lung cancers (She et al. 2018).

2.4 Functional Imaging Analysis Regarding Tumor Hallmarks

Dynamic contrast-enhanced (DCE) and diffusion-weighted (DW) MRI can be used to evaluate functional changes in tumor microenvironment (Fig. 1) (Bains et al. 2012). DW-MRI allows mapping of water diffusion to reflect tissue cellularity, fluid viscosity, integrity of cell membranes, and tortuosity of extracellular spaces (Coche 2016). DW-MRI also allows calculation of the decay of the diffusion-weighted signal to provide an estimate of the apparent diffusion coefficient (ADC). The ADC typically decreases in highly cellular tissues (including tumor) and increases in necrotic regions and tissues with damaged or permeable cell membranes (Bains et al. 2012). ADC also increases after successful anticancer therapies because tumor cell death by necrosis or apoptosis decreases cell density and increases tumor extracellular volume (Yabuuchi et al. 2011). Therefore, ADC value is widely used

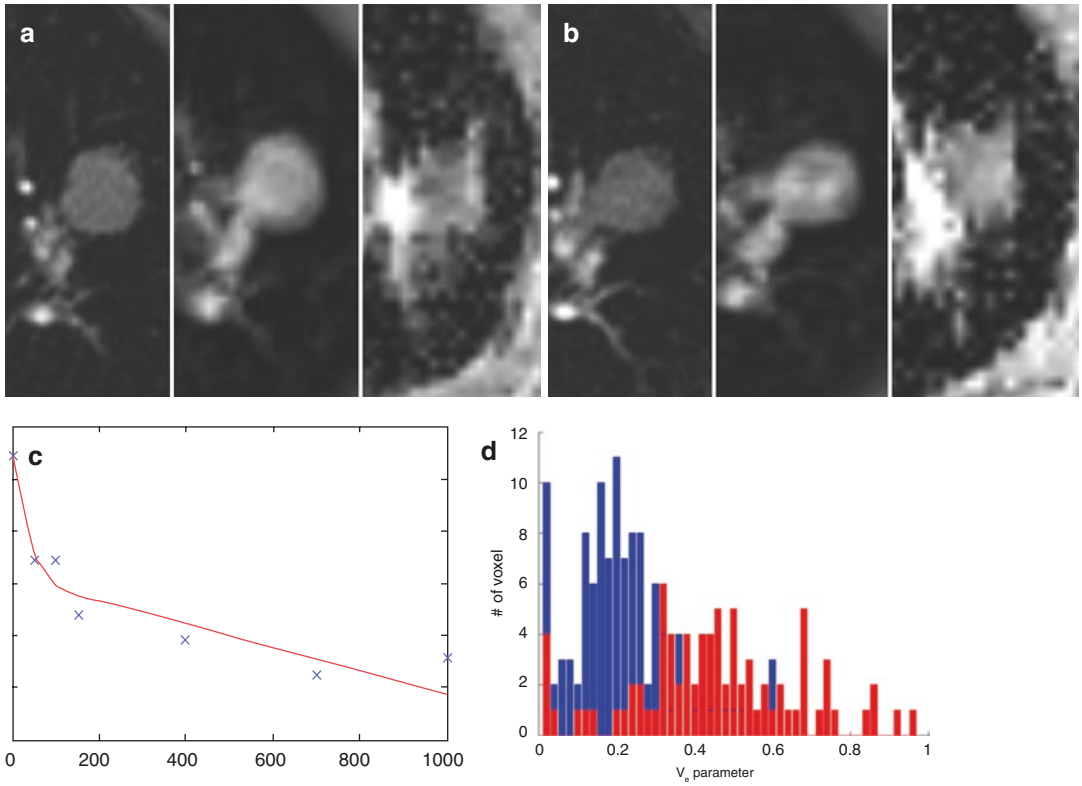

e

	Pre-chemotherapy	Post-chemotherapy	% change
Size (cm)	1.8	1.8	0%
Volume (cm^3)	0.45	0.42	-7%
Mean ADC ($10^{-3}mm^2$)	1.21	1.42	+17%
D ($10^{-3}mm^2$)	1.19	1.35	+13%
D* ($10^{-3}mm^2$)	25.3	30.4	+13%
f (%)	0.07	0.14	+100%
Mean Ve ($10^{-3}mm^{-1}$)	0.004	0.025	+500%

Fig. 1 Lung cancer patient treated with chemotherapy. Serial T2, enhanced-MR, and ADC maps obtained before (**a**) and 5 weeks after (**b**) chemotherapy. There are no significant interval changes in the maximum tumor diameter (1.8 cm); however, ADC value increases by 17% after targeted therapy. (**c**) The bi-exponential fitting of the diffuse signal decay. (**d**) Combined DCE MR-derived V_e (extracellular extravascular space volume per unit tissue volume) histogram representing tumor perfusion before (red) and after (blue) first cycle of chemotherapy. (**e**) Table showing changes in MR parameters before and after treatment

as a quantitative imaging biomarker to assess lung cancer and predict therapeutic effects because cell death and vascular change take precedence over changes in lesion size during anticancer therapy.

Angiogenesis is an important factor related to tumor growth, metastasis, and prognosis of lung cancer. Poorly differentiated tumors may have disorganized and permeable vessels that are inefficient in oxygen delivery, resulting in tumor hypoxia (Gaddikeri et al. 2016). Targeted therapy for angiogenesis may result in regression or normalization of neovasculature and inhibition of new blood vessel growth. DCE MRI provides

pharmacokinetic information to assess sensitive pathophysiological characteristics and detect changes in tumor vasculature and the peritumoral microenvironment. DCE-MRI is mainly performed using a two-compartment Tofts model. During targeted therapy, tumors decrease K^{trans}, which characterizes the diffusive transport of gadolinium chelates across the capillary endothelium, DCE-MRI measurements have been shown to have a significant correlation with effective tumor control and vascular inhibition (Chen et al. 2017).

3 Imaging Genomics Application to Treatment Response

Imaging genomics is the study of correlating imaging characteristics with underlying gene expression patterns, gene mutations, and other genome-related characteristics (Leithner et al. 2018; Vardhanabhuti and Kuo 2018). Imaging genomics has many advantages in oncology, including speed, cost-effectiveness, and capturing tumor genetic heterogeneity given that it is a noninvasive method that can be performed repeatedly, thus making it suitable for assessing treatment response (Jansen et al. 2018).

According to a pilot study by Aerts et al., radiomics data before treatment was able to predict mutation status and associated gefitinib response noninvasively, showing the potential of imaging genomics for treatment stratification and response assessment (Aerts et al. 2016). In another study, a prediction model based on multiple radiomics features could predict ALK fusion and ROS1/RET fusion in patients with lung cancer (Yoon et al. 2015).

In a recent study by Sun et al., a radiomics signature was able to assess CD8 cell tumor infiltration, which is promising for the prediction of immune phenotype in tumors and inferring clinical outcomes in patients treated with immunotherapy (Sun et al. 2018). Although still in the very early stages, imaging genomics has great potential for predicting treatment response and should be further investigated through large cohort studies.

4 Technical Considerations of Radiomics and Radiogenomics Approach

4.1 Volumetry

There are various segmentation methods, including manual, semiautomatic, and automatic methods. First, manual segmentation may be considered the "gold standard" when drawn by experienced experts. However, it has major disadvantages as it is a time-consuming and labor-intensive task with inevitable variability. Second, semiautomatic and automatic methods using post-processing software are more reproducible than manual segmentation (Rios Velazquez et al. 2012; Heye et al. 2013). In a study comparing manual and semiautomatic segmentation, the radiomics features derived from semiautomatic segmentation demonstrated significantly higher reproducibility and were more robust than those derived from manual contouring (Parmar et al. 2014). In cases of part-solid adenocarcinomas with a ground-glass opacity (GGO) component, there is decreased contrast between the GGO component and surrounding lung parenchyma, and fully automatic segmentation may exhibit inaccurate results (Ko et al. 2003). Hence, semiautomatic segmentation with tumor margin editing performed by an expert is currently the optimal choice for accurate tumor volume measurement of part-solid adenocarcinomas (Lassen et al. 2015; Oda et al. 2010). Advanced lung cancers with irregular margins, heterogeneous intratumoral texture, and surrounding atelectasis or effusions often require semiautomatic segmentation with expert radiologist manual editing (Nishino et al. 2011). Thus, tumor volumes obtained by semiautomatic segmentation are considered markers for prolonged survival in the setting of molecular targeted therapy in genomically defined cohorts, solidifying the potential of tumor volumes in precision medicine (Nishino et al. 2013, 2016).

The advantages of fully automatic segmentation methods based on deep learning include rapid and accurate tumor segmentation. Several

investigators have trained convolutional neural networks and demonstrated that deep learning can accurately localize and segment tumors in multiple organs (Havaei et al. 2017; Trebeschi et al. 2017; Wang et al. 2017; Zhao and Jia 2016). Although most of these articles were based on MRI scans of the brain, prostate, and rectum, deep learning technologies have shown potential to improve the accuracy and robustness of tumor segmentation. One last point that needs to be mentioned is the utilization of different volumetry software. Considerable variation was noted in studies that compared multiple volumetry software packages, implying that software packages should not be used interchangeably (Ashraf et al. 2010; de Hoop et al. 2009; Devaraj et al. 2017; Zhao et al. 2014a).

4.2 Bin Number

Radiomics analysis extracts hundreds or sometimes thousands of features from the underlying imaging modalities and their ROIs. The features are different from semantic features and are agnostic computational features whose formulae are defined by various parameters (Gillies et al. 2016). Thus, for a given radiomics feature, if the associated parameter changes, the ensuing radiomics feature might change as well. The majority of radiomics features, noted as histogram-based features, are calculated from intensity histograms using underlying imaging data within the ROI. Histograms are affected by binning parameters of bin width and range (Fig. 2). Range is application dependent, and 4096 is typically used for CT. Many people also use a number of bins, and range is divided by bin width for the binning parameter. The use of many bins allows fine differentiation between intensity values, but the use of too many bins leads to very narrow bin width. A narrow bin width leads to unreliable histogram estimates, and there may not be enough samples for some bins. The Freedman-Diaconis rule can be used to set bin width (Parekh and Jacobs 2016; Szigeti et al. 2016).

4.3 Texture Features

Texture features are widely recognized radiomics features (Aerts et al. 2014; Ganeshan et al. 2013; Tixier et al. 2011). The most representative texture features are computed from the gray-level co-occurrence matrix (GLCM) and intensity size zone matrix (ISZM). These matrices are constructed from 2D histograms that measure the frequency of a pair of observations compared to a 1D histogram, and researchers consider the frequency of one observation (e.g., intensity). GLCM measures the frequency of intensity pairs in the neighborhood, while ISZM measures the frequency of blobs with

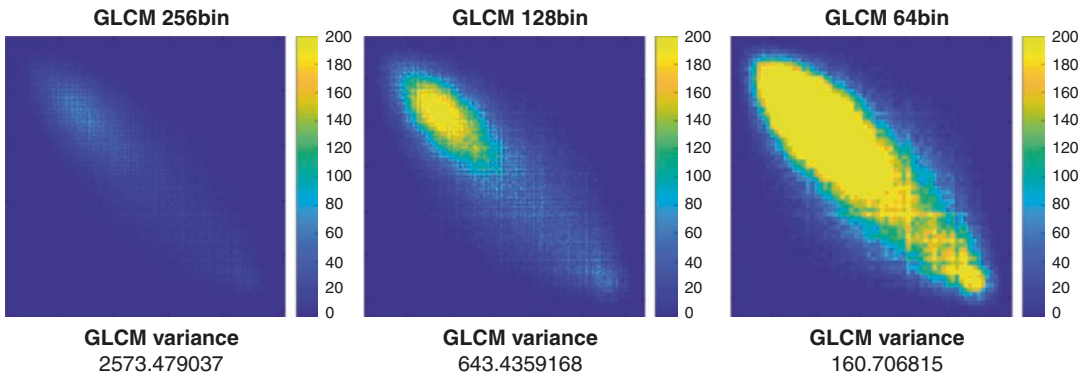

Fig. 2 Three gray-level co-occurrence matrix (GLCM) variance values according to the number of bins in the same tumor

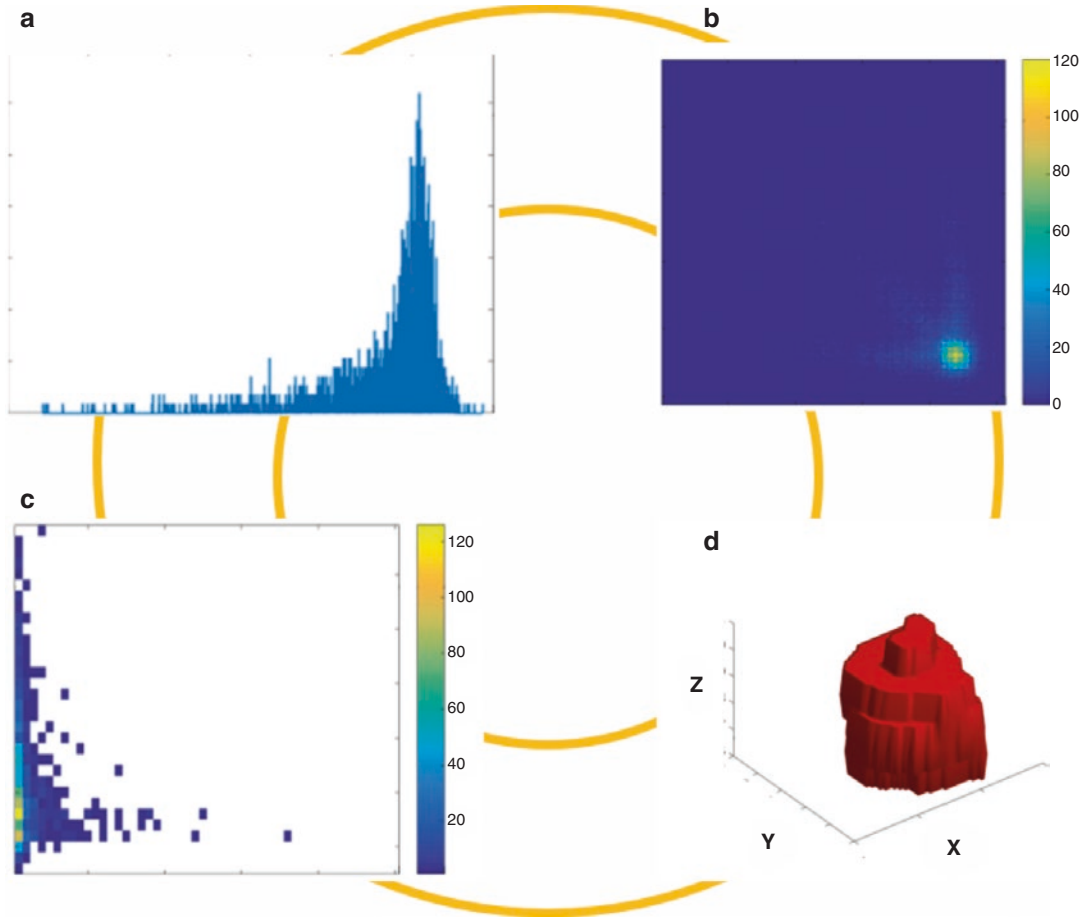

Fig. 3 Histogram features. (**a**) 1D Histogram of the tumor ROI demonstrates the entire distribution of HU value. (**b**) Gray-level co-occurrence matrix (GLCM). The 2D histogram of GLCM is created using intensity of given voxel as the first axis and intensity of the neighboring voxel as the second axis. (**c**) Intensity size zone matrix (ISZM). The horizontal axis represents intensity and the vertical axis represents size of a given blob. (**d**) 3D rendering image of the tumor

certain size and intensity (Fig. 3). For GLCM, 2D histograms are built using the intensity of the given voxel as the first axis and the intensity of the neighboring voxel as the second axis. The GLCM quantifies how intensity pairs occur in a neighbor and hence reflect textural information. Similar to 1D histograms, the number of bins is a major parameter in 2D histograms. In general, there are far fewer samples in the 2D histogram because voxels need to fill bins spanning the 2D space compared to 1D histograms. Due to this sparsity in 2D histograms, researchers typically use 128/256 bins for GLCM (Shafiq-Ul-Hassan et al. 2017).

The size of the ROI also affects 1D/2D histogram measures. If the ROI is large enough to contain thousands of voxels, then the above approaches are suitable. If a ROI has a very small number of voxels (perhaps around 100), then researchers need to significantly reduce the number of bins to ensure there are enough voxels occupying the bins.

4.4 Shape Features

Shape features are important aspects of radiomics analysis (Aerts et al. 2014; Kumar et al. 2012).

The shape of a ROI is quantified with various formulae. The ROI is composed of voxels that can be isotropic or non-isotropic. In many cases, there is good in-plane resolution and poor out-of-plane resolution (i.e., non-isotropic voxels). For non-isotropic voxels, shape features are more sensitive to shape change occurring in-plane and they are less sensitive to shape change occurring out-of-plane. For isotropic voxels, the shape features are equally sensitive to all directions. The shape of the target ROI may change in any direction; thus, isotropic voxels are preferable over non-isotropic voxels. If imaging data is non-isotropic, the imaging data can be interpolated to make it isotropic. This interpolation makes the data smoother but reduces shape variability.

4.5 Filter and Wavelet

Some researchers apply an edge enhancement filter, such as Laplacian of Gaussian (LoG), to imaging data and extract radiomics features from the filtered image (Aerts et al. 2016). The LoG filter has a scale parameter that controls the scale at which enhancement occurs. Researchers need to specify the scale parameter to suit their intended application. The scale should be set based on image quality and size of the ROI. If researchers have poor-quality image with large ROIs, large-scale operations are recommended.

Some studies also apply wavelet decomposition to imaging data (Aerts et al. 2014). The imaging data are decomposed into many output data, and radiomics features are computed from the decomposed data. There are many wavelet transforms to choose from, and each has a plethora of parameters. Coiflets are widely used for their simplicity. Researchers can decompose one 3D scan into 8 3D decomposed scans in the simplest version. Different wavelet transforms lead to different decomposed data and thus affect radiomics features. Researchers should fully consider the various parameters of wavelets before use in projects.

4.6 Particular Technical Considerations According to Modality

Although CT is the main imaging modality in lung cancer response evaluation, additional imaging modalities such as magnetic resonance imaging (MRI) and positron emission tomography (PET) may depict different aspects of the same tumor biological process (Padhani and Miles 2010). Thus, a combination of metabolic and functional information with conventional anatomical data may provide more comprehensive understanding of complex tumor biology and more accurate assessment of tumor response.

4.6.1 CT

Quantification of CT data gives accurate information about cancer burden. In addition to the variability introduced earlier, multiple technical factors influence objective CT measurements in clinical practice, including the reconstruction algorithm, slice thickness, and interscanner differences (Kemerink et al. 1995; Stoel et al. 1999, 2008). A combination of these factors may lead to considerable measurement variability of the tumor, making tumor response assessment difficult for radiologists.

4.6.1.1 Reconstruction Algorithm, Radiation Dose, and Reconstruction Kernel

Many investigators have explored the effect of reconstruction algorithm and radiation dose on lung nodule diameter or volume using chest phantoms (Kim et al. 2014, 2015; Ohno et al. 2016; Siegelman et al. 2015). According to these studies, various iterative reconstruction algorithms (e.g., adaptive statistical iterative reconstruction or model-based iterative reconstruction) showed no significant difference in nodule diameter or volume measurement compared to conventional filtered back projection (Kim et al. 2014, 2015; Ohno et al. 2016; Siegelman et al. 2015). Some studies even reported that iterative reconstruction algorithms demonstrated better

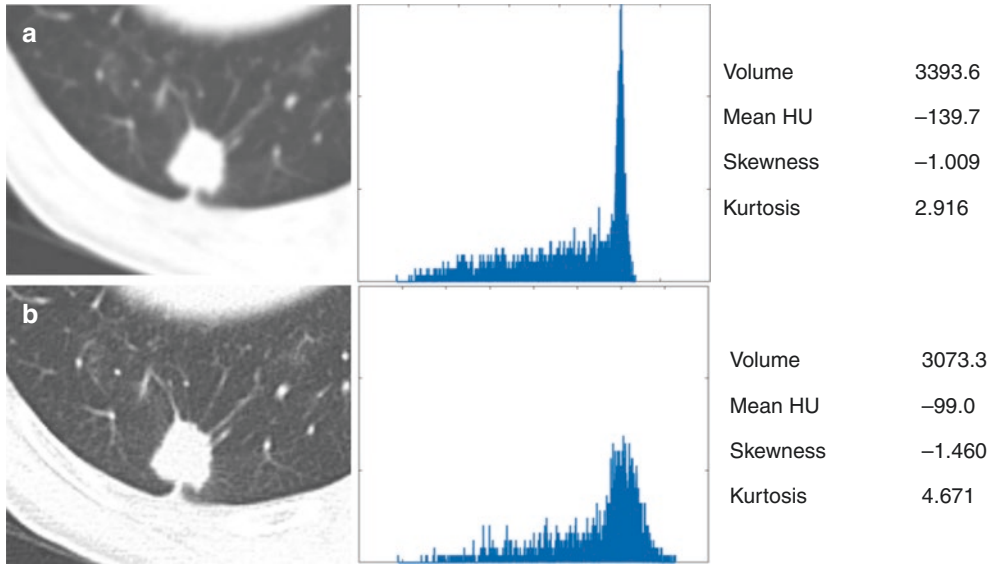

Fig. 4 Influence of reconstruction kernels. Low-frequency soft algorithms (**a**) shows larger volume compared to high-frequency bone algorithms (**b**). Reconstruction kernels could also affect the values of histogram features

measurement accuracy at a lower radiation dose (Kim et al. 2015; Ohno et al. 2016; Doo et al. 2014; Sakai et al. 2015). They assumed that iterative reconstruction algorithms reduced noise or increased image quality, thus leading to fewer measurement errors (Kim et al. 2015; Ohno et al. 2016; Doo et al. 2014; Sakai et al. 2015). According to a clinical study involving subsolid nodules reconstructed by both model-based iterative reconstruction and filtered back projection, semiautomatic measurements of diameter, volume, and solid components of subsolid nodules were within the range of measurement variability (Cohen et al. 2017). Therefore, in reference to these prior phantom and clinical studies, lung nodule volumetric measurements may be reliably compared regardless of the type of reconstruction algorithm used.

Considering the influence of reconstruction kernels on tumor volumes, investigations demonstrate conflicting results (Fig. 4). One study showed that soft tissue reconstructions demonstrated more repeatable volumetric measurements than sharp kernels (Wang et al. 2010). In another study, low-frequency soft algorithms demonstrated larger volumes compared to high-frequency bone algorithms (Devaraj et al. 2017; Christe et al. 2014).

4.6.1.2 Slice Thickness

Previous investigators have studied the effect of slice thickness on tumor measurement for lung cancer screening or tumor response evaluation (Petrou et al. 2007; Tan et al. 2012; Winer-Muram et al. 2003; Zhao et al. 2005, 2013). Theoretically, a thicker CT slice contains larger partial volume artifacts than a thinner CT slice. Therefore, the true details of a tumor are more suppressed on thicker CT slices, which disturbs accurate tumor segmentation and extracted radiomics features (Fig. 5) (Zhao et al. 2014b). Significant differences in lung nodule volume according to CT slice thickness are reported in the literature, especially for smaller lung nodules, and thicker slices introduce greater measurement variability (Petrou et al. 2007; Tan et al. 2012; Zhao et al. 2013). In cases of subcentimeter nodules, which have very small VOI, a partial volume artifact substantially influences volume measurement (Plathow et al. 2006).

Likewise, thinner CT slice images worked better than thicker slice images for extracting

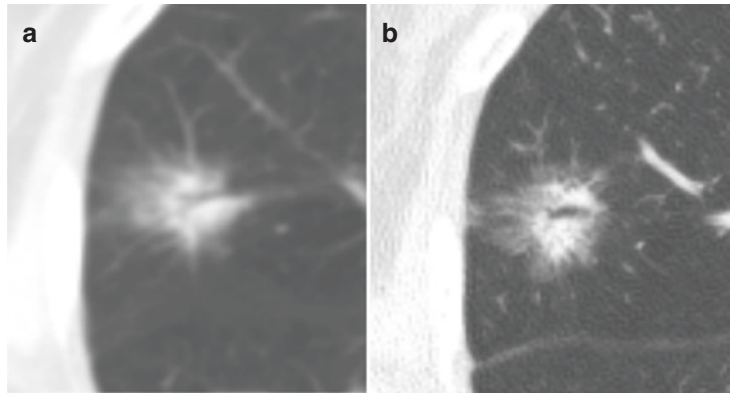

Fig. 5 Effect of CT section thickness on lung adenocarcinoma. In the thicker section (**a**, 5 mm slice thickness), the partial volume average effect increases more than the thin section (**b**, 1 mm slice thickness), which could affect the shape features. Thin sections have an advantage in evaluating morphologic nodule characteristics such as shape and spiculation and could refine subtle morphologic changes over time

radiomics features (Zhao et al. 2014b; He et al. 2016). In patients with lung cancer, a radiomics signature based on thinner CT slices (1.25 mm) demonstrated better diagnostic performance than the same signature applied to thicker CT slices (5 mm) (He et al. 2016). According to a chest phantom study, thinner (1.25 and 2.5 mm) slices are better for radiomics features quantifying tumor size, shape, and density (Zhao et al. 2014b). To minimize the measurement variability dependent upon CT slice thickness, we recommend using thinner slice images. In addition, different slice thicknesses should not be used interchangeably.

4.6.1.3 Effects of Respiration and Intravenous Contrast

Regarding differences in lung inflation due to an elastic chest wall, the influence of respiratory motion should not be underestimated when measuring tumors in the lung. Alveoli collapse with expiration and stretching of the tumor parenchyma with inspiration may both affect tumor burden assessment. Thus, motion artifacts during respiration can significantly affect the true outline of tumors, rendering their outline and volume assessment unreliable (Fig. 6). In addition, the presence of pleural effusion or pneumothorax may also influence tumor volume (Mansoor et al. 2015). Regarding radiomics, Oliver et al. suggested that almost 75% of CT radiomics features are susceptible to respiration (Oliver et al. 2015).

Meanwhile, intravenous contrast material may also influence lung nodule volumetry. Due to increased attenuation of the peripheral portion of a nodule at post-contrast scans, the contrast difference between the parenchyma and the nodule increases; thus, volume segmentation may include a greater area of the peripheral lung nodule (Devaraj et al. 2017). Studies show that although the precise increase was small, radiologists should be aware of the influence of contrast material on lung nodule volume (Honda et al. 2007; Rampinelli et al. 2010).

4.6.2 MRI

Owing to its complexity and lack of radiation exposure, MRI may play an important role for tumor categorization, therapeutic response assessment, and as a prognostic and predictive biomarker, either alone or combined with clinical and genomic oncology information (Gourtsoyianni et al. 2017; Incoronato et al. 2017). MRI is more reproducible for identifying lesions with superior soft tissue contrast than CT. MRI-based volumes are smaller than

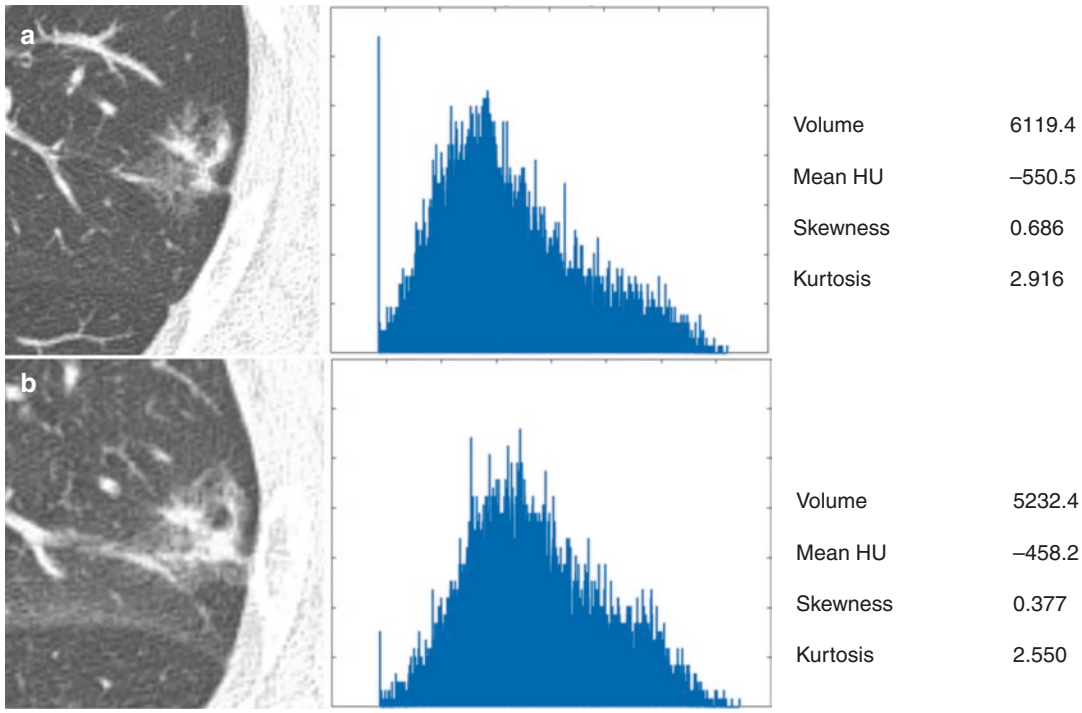

Fig. 6 Inspiration level is one of the factors contributing to measurement variability (**a**, inspiration; **b**, expiration)

CT-based volumes due to exclusion of other soft tissue structures with higher resolution (Rasch et al. 1999; Usmani et al. 2011). For quantitative analysis, MRI should all have the same field of view and acquisition matrix, field strength, and slice thickness, which have a strong effect on signal-to-noise ratio (Incoronato et al. 2017). However, complex acquisition of MRI has several parameters that affect the image quality and appearance, which eventually affects features extracted from the images (Saha et al. 2017).

4.6.2.1 Magnetic Field Strengths

As MR field strength increases, signal-to-noise (SNR) increases, leading to increased spatial and/or temporal resolution and significantly improved anatomical identification (Usmani et al. 2011; Soher et al. 2007). The use of higher MR field strength showed significant improvement in contouring variability with increased image quality (Usmani et al. 2011). However, higher MR field strength have potential disadvantages, including increased power deposition, image artifacts related to susceptibility, and signal heterogeneity (Ullrich et al. 2017). B1 inhomogeneity results in systematic error for T1 measurement (Leach et al. 2012). DW-MRI has been a powerful imaging tool for characterizing tumors and predicting treatment response in oncology. The objective image quality of DWI on 3T was significantly better compared to image quality on 1.5T because of increased SNR and CNR (Ullrich et al. 2017). Depending on the magnetic field strengths, the measured ADC is significantly different on phantom study. However, the ADC reproducibility is excellent (Lavdas et al. 2014). In addition, measured ADC values were higher at 3T than at 1.5T for liver, but there was no difference in pancreas and spleen (Dale et al. 2010). Therefore, the signal intensities, including ADC values, should be used to evaluate therapeutic response by considering the effect of field strength.

Furthermore, field strength-related changes of the relaxivity values of MR contrast media should be considered. The relaxivity of MR contrast media increased from 5 to 10% when changing from 1.5T to 3T (Soher et al. 2007). The individual dependencies of relaxivities on

field strength for different types of MR gadolinium contrast agent were significantly different (Rohrer et al. 2005). Successful response to anticancer treatment resulted in a decreased degree of enhancement. Therefore, administration of contrast agent to detect tumor enhancement should be modified according to field strength.

4.6.2.2 Acquisition Parameter

Since the signal intensity of MRI is derived from complex interactions between acquisition parameters and intrinsic tissue characteristics, it is difficult to derive information on the physical characteristics of the tissue only from MRI signal intensity. MRI acquisition protocols are very diverse among different studies or institutions, and variation in MR protocol leads to considerable differences in the results of quantitative image analysis. The reliability and reproducibility of quantitative information of DCE-MRI depends on contrast dose, administration method, acquisition parameters, and analysis method used (Kumar et al. 2012). Poor inter-scanner reproducibility of ADC, widely used for tumor evaluation, limits its use as a biomarker in clinical trials. Even when using the same scanner, inconsistent tumor position within the B0 field can distort the value of ADC (Weller et al. 2017), which negatively impacts reproducibility. Given a wide variety of acquisition protocols, assessment of the robustness of the quantitative matrix is essential (Horvat et al. 2018). Recently, Quantitative Imaging Biomarker Aliance (QIBA) attempted to standardize the protocol for DCE-MRI (Kumar et al. 2012).

The values of extracted features are mainly sensitive to scanner manufacturer and slice thickness. The effect of magnetic field strength is relatively small (Saha et al. 2017). Radiomics features increase sensitivity to variation acquisition as spatial resolution increases. The effects of acquisition parameter variations on pixel signal intensities are masked because of blurring and partial volume effects, thus reducing the effect on radiomics features. Nevertheless, as long as the clinically available spatial resolution is sufficiently high, variations in the number of acquisitions, repetition time, echo time, and sampling bandwidth have little effect on radiomics results (Mayerhoefer et al. 2009). The reproducibility of quantitative MRI features is better for global features such as first-order statistical histogram and model-based fractal features than for local-regional texture parameters (Gourtsoyianni et al. 2017).

4.6.2.3 Effect of Respiration

One of the main challenges using MRI to evaluate lung cancer is sensitivity to motion caused by cardiac pulsation and respiration, and breath-holds are widely used to overcome respiratory motion in routine practice (Chen et al. 2018). However, breath-hold techniques are time consuming and may fail in patients who cannot tolerate repeated breath-holds (Bak et al. 2017). Tumor volumes change significantly with the respiratory cycle; they increase during inspiration because of stretching of the tumor parenchyma (Plathow et al. 2006). The tumor volume change with respiration may affect current therapeutic response evaluation based on size. In addition, the degree of contrast enhancement with pulmonary perfusion MRI depends on different inspiratory levels. Perfusion during expiration is higher than perfusion during inspiration because expiration results in decreased pulmonary vascular resistance and increased venous return to the heart (Fink et al. 2005). However, evaluations of perfusion are less reproducible because it is difficult to similarly control the breathing level during breath-holds. On the other hand, evaluation of pulmonary hemodynamics with free breathing pulmonary MRI could be assessed more reproducibly due to intrinsic averaging over the breathing cycle and increased patient compliance (Ingrisch et al. 2014).

4.6.3 PET

Given its quantitative ability, PET usage has continuously increased for assessment of treatment response in patients with lung cancer. A variety of standardized uptake value (SUV)-based quantitative PET parameters are used as radiomics

features and treatment response criteria. However, multiple biological and technical factors may affect the measurement of SUV as follows below (Adams et al. 2010).

4.6.3.1 Normalization Method for SUV Calculation

SUV is calculated by activity concentration in tissue adjusted by the administered dose of radiopharmaceuticals and body size. Body size usually corresponds to the patient's body weight (SUV_{bw}). Nevertheless, other indexes such as lean body mass (SUV_{lbm}) or body surface area (SUV_{bsa}) can be used, which affects the measurement of SUV. A disadvantage of SUV_{bw} is that it may result in overestimation in obese patients. On the other hand, both SUV_{bw} and SUV_{bsa} are less sensitive to patient weight (Kim et al. 1994; Zasadny and Wahl 1993).

4.6.3.2 PET/CT Scanner Models and Image Acquisition/Reconstruction Protocol

PET/CT scanner models and image acquisition and reconstruction protocols also affect quantitative measurement of PET. Considering the performance of PET/CT scanners, the most important factors are intrinsic resolution and sensitivity, which affect image resolution and partial volume effect and, subsequently, SUV variability.

In the image acquisition protocol, one of the most important factors is uptake time. Uptake time refers to the interval time between injection of PET radiopharmaceutical and start time of PET scanning, which also influences SUV measurement. For ^{18}F-fluorodeoxyglucose (FDG), the most common uptake time is 60 min. After FDG injection, SUV continuously increases as metabolically active cells take up and subsequently trap the glucose analogue (Lowe et al. 1995). Hence, the use of a fixed uptake time is mandatory for consistency of SUV measurements. Conversely, scan duration or scan mode (2D vs. 3D) does not have a significant effect on SUV accuracy (Kinahan and Fletcher 2010).

In the reconstruction protocols, the attenuation correction method, reconstruction method (analytical vs. statistical/iterative methods), and smoothing filter are major factors affecting SUV measurement. For example, increased smoothing results in decreased noise and increased bias. Increased bias results in reduced SUV (Doot et al. 2010).

4.6.3.3 Patient Status

Even with the same PET/CT protocols and the same patient, SUV can vary due to biological processes such as different blood glucose and insulin levels, a phenomenon referred to as test-retest variability (Hofheinz et al. 2017). Serum blood glucose level is inversely correlated with SUVs (Huang 2000).

4.6.3.4 Types of Quantitative PET Parameters

Most quantitative PET parameters are related to measurement variability, including clinically used PET parameters such as maximum SUV, average SUV, peak SUV, metabolic tumor volume, and total lesion glycolysis (Moon et al. 2013). Although maximum SUV is usually not affected by determination of lesion ROI or volume-of-interest (VOI), ROI/VOI has significant influence on other PET parameters. However, there is continuous concern that maximum SUV, which represents a single pixel value, may not represent the whole metabolic picture of the lesion.

4.6.3.5 Harmonization of PET Parameters

Based on literature, the measurement variability of maximum SUV, average SUV, and peak SUV expressed as a coefficient of variation is approximately 10% (Lodge 2017). Due to the measurement variabilities of PET parameters, harmonization of PET response criteria has been studied. For example, image reconstruction-related variability can be solved using a standardized filter such as EQ.PET (Quak et al. 2016). Nevertheless, further efforts are necessary to standardize quantitative measurement of PET parameters.

5 Conclusions and Future Directions

Radiomics features show clear benefits for quantification of tumor biology and response to therapeutic treatment. Thus, many researchers are now paying close attention to the clinical usefulness of radiomics in assessing lung cancer treatment response. However, given the abundance of radiomics studies, it should be clearly noted that extracted radiomics features are inherently subject to variability. In an attempt to homogenize evaluation criteria and reporting guidelines for radiomics, Lambin et al. proposed the radiomics quality score (RQS) (Lambin et al. 2017). The RQS evaluates the necessary steps in radiomics analysis including 16 key components that are each given a number of points corresponding to their importance (Lambin et al. 2017). Major checkpoints in the RQS are data selection, medical imaging, features extraction, exploratory analysis, and modeling. The highest possible total RQS for quantification of the overall methodology and analysis of radiomics practice is 36 points. Thus, efforts should be made to consider RQS in future studies and to establish collaborative foundations to control and fully realize the potential of radiomics.

Another issue that should be highlighted is the role of delta radiomics in tumor response evaluation (Lambin et al. 2017; Fave et al. 2017). While the majority of radiomics studies extract features from a single time point (usually at the time of diagnosis), delta radiomics evaluates changes in radiomics features between interval studies. Delta-radiomics features have shown potential in predicting response or survival in patients with colorectal cancer liver metastasis, metastatic renal cell, and lung cancer (Fave et al. 2017; Goh et al. 2011; Rao et al. 2016). Nevertheless, if delta radiomics are incorporated into clinical practice, standardization of technical factors and high reproducibility of the features remain prerequisites.

Last, reducing the plethora of extracted radiomics features to a practical number is a major challenge in the field of radiomics. The abundance of radiomics features may lead to over-fitting and limited use in clinical practice. However, among hundreds of reported radiomics features, it remains unknown which features may truly reflect tumor biology and have clinical impact. Therefore, feature selection and modeling is an important process to incorporate radiomics into clinical practice and solidify its status as a powerful tool for tumor response.

In this era of precision medicine, tumor volumetry and radiomics in lung cancer surpass the limitations of current RECIST version 1.1 due to their advantages in quantitative measurements. Nevertheless, considerable variability can be introduced in the process of measuring tumor burden due to various technical factors. Furthermore, the increasing role of post-processing software and radiomics support the need for increased awareness of technical factors among radiologists. In the future, the traditional role of radiological practice in lung cancer studies is likely to change, and the concepts and knowledge described in this review will support radiologists with a new perspective for tumor response evaluations in cutting edge cancer patient care.

Acknowledgements *Conflict of interest and financial support.* This research was supported by the Korea Health Technology R&D Project through the Korea Health Industry Development Institute (KHIDI), which was funded by the Ministry of Health & Welfare (HI17C0086) and the National Research Foundation of Korea (NRF) grant funded by the Korean government (MSIP; Ministry of Science, ICT & Future Planning) (Nos. NRF-2016R1A2B4013046 and NRF-2017M2A2A7A02018568).

Declarations of interest: none

References

Adams MC, Turkington TG, Wilson JM et al (2010) A systematic review of the factors affecting accuracy of SUV measurements. AJR Am J Roentgenol 195:310–320

Aerts HJ, Velazquez ER, Leijenaar RT et al (2014) Decoding tumour phenotype by noninvasive imaging using a quantitative radiomics approach. Nat Commun 5:4006

Aerts HJ, Grossmann P, Tan Y et al (2016) Defining a radiomic response phenotype: a pilot study using targeted therapy in NSCLC. Sci Rep 6:33860

Al-Kadi OS, Watson D (2008) Texture analysis of aggressive and nonaggressive lung tumor CE CT images. IEEE Trans Biomed Eng 55:1822–1830

Altorki N, Lane ME, Bauer T et al (2010) Phase II proof-of-concept study of pazopanib monotherapy in treatment-naive patients with stage I/II resectable non-small-cell lung cancer. J Clin Oncol 28:3131–3137

Ashraf H, de Hoop B, Shaker SB et al (2010) Lung nodule volumetry: segmentation algorithms within the same software package cannot be used interchangeably. Eur Radiol 20:1878–1885

Bains LJ, Zweifel M, Thoeny HC (2012) Therapy response with diffusion MRI: an update. Cancer Imaging 12:395–402

Bak SH, Kim SH, Park S-J et al (2017) Assessment of left ventricular function with single breath-hold magnetic resonance cine imaging in patients with arrhythmia. Investig Magn Reson Imaging 21:20–27

Chen YF, Yuan A, Cho KH et al (2017) Functional evaluation of therapeutic response of HCC827 lung cancer to bevacizumab and erlotinib targeted therapy using dynamic contrast-enhanced and diffusion-weighted MRI. PLoS One 12:e0187824

Chen L, Liu D, Zhang J et al (2018) Free-breathing dynamic contrast-enhanced MRI for assessment of pulmonary lesions using golden-angle radial sparse parallel imaging. J Magn Reson Imaging 48:459–468

Christe A, Bronnimann A, Vock P (2014) Volumetric analysis of lung nodules in computed tomography (CT): comparison of two different segmentation algorithm softwares and two different reconstruction filters on automated volume calculation. Acta Radiol 55:54–61

Coche E (2016) Evaluation of lung tumor response to therapy: current and emerging techniques. Diagn Interv Imaging 97:1053–1065

Cohen JG, Kim H, Park SB et al (2017) Comparison of the effects of model-based iterative reconstruction and filtered back projection algorithms on software measurements in pulmonary subsolid nodules. Eur Radiol 27:3266–3274

Cook GJ, Yip C, Siddique M et al (2013) Are pretreatment 18F-FDG PET tumor textural features in non-small cell lung cancer associated with response and survival after chemoradiotherapy? J Nucl Med 54:19–26

Coroller TP, Agrawal V, Narayan V et al (2016) Radiomic phenotype features predict pathological response in non-small cell lung cancer. Radiother Oncol 119:480–486

Dale BM, Braithwaite AC, Boll DT et al (2010) Field strength and diffusion encoding technique affect the apparent diffusion coefficient measurements in diffusion-weighted imaging of the abdomen. Investig Radiol 45:104–108

van Dam IE, Van Sornsen de Koste JR, Hanna GG et al (2010) Improving target delineation on 4-dimensional CT scans in stage I NSCLC using a deformable registration tool. Radiother Oncol 96:67–72

Devaraj A, van Ginneken B, Nair A et al (2017) Use of volumetry for lung nodule management: theory and practice. Radiology 284:630–644

Doo KW, Kang EY, Yong HS et al (2014) Accuracy of lung nodule volumetry in low-dose CT with iterative reconstruction: an anthropomorphic thoracic phantom study. Br J Radiol 87:20130644

Doot RK, Scheuermann JS, Christian PE et al (2010) Instrumentation factors affecting variance and bias of quantifying tracer uptake with PET/CT. Med Phys 37:6035–6046

Eisenhauer EA, Therasse P, Bogaerts J et al (2009) New response evaluation criteria in solid tumours: revised RECIST guideline (version 1.1). Eur J Cancer 45:228–247

Erasmus JJ, Gladish GW, Broemeling L et al (2003) Interobserver and intraobserver variability in measurement of non-small-cell carcinoma lung lesions: implications for assessment of tumor response. J Clin Oncol 21:2574–2582

Fave X, Zhang L, Yang J et al (2017) Delta-radiomics features for the prediction of patient outcomes in non-small cell lung cancer. Sci Rep 7:588

Fink C, Ley S, Risse F et al (2005) Effect of inspiratory and expiratory breathhold on pulmonary perfusion: assessment by pulmonary perfusion magnetic resonance imaging. Investig Radiol 40:72–79

Fried DV, Tucker SL, Zhou S et al (2014) Prognostic value and reproducibility of pretreatment CT texture features in stage III non-small cell lung cancer. Int J Radiat Oncol Biol Phys 90:834–842

Gaddikeri S, Gaddikeri RS, Tailor T et al (2016) Dynamic contrast-enhanced MR imaging in head and neck cancer: techniques and clinical applications. AJNR Am J Neuroradiol 37:588–595

Ganeshan B, Abaleke S, Young RC et al (2010) Texture analysis of non-small cell lung cancer on unenhanced computed tomography: initial evidence for a relationship with tumour glucose metabolism and stage. Cancer Imaging 10:137–143

Ganeshan B, Panayiotou E, Burnand K et al (2012) Tumour heterogeneity in non-small cell lung carcinoma assessed by CT texture analysis: a potential marker of survival. Eur Radiol 22:796–802

Ganeshan B, Goh V, Mandeville HC et al (2013) Non-small cell lung cancer: histopathologic correlates for texture parameters at CT. Radiology 266:326–336

Gillies RJ, Kinahan PE, Hricak H (2016) Radiomics: images are more than pictures, they are data. Radiology 278:563–577

Goh V, Ganeshan B, Nathan P et al (2011) Assessment of response to tyrosine kinase inhibitors in metastatic renal cell cancer: CT texture as a predictive biomarker. Radiology 261:165–171

Goldmacher GV, Conklin J (2012) The use of tumour volumetrics to assess response to therapy in anticancer clinical trials. Br J Clin Pharmacol 73:846–854

Gourtsoyianni S, Doumou G, Prezzi D et al (2017) Primary rectal cancer: repeatability of global and local-regional MR imaging texture features. Radiology 284: 552–561

Han D, Heuvelmans MA, Oudkerk M (2017) Volume versus diameter assessment of small pulmonary nodules

in CT lung cancer screening. Transl Lung Cancer Res 6:52–61
Havaei M, Davy A, Warde-Farley D et al (2017) Brain tumor segmentation with deep neural networks. Med Image Anal 35:18–31
Hayes SA, Pietanza MC, O'Driscoll D et al (2016) Comparison of CT volumetric measurement with RECIST response in patients with lung cancer. Eur J Radiol 85:524–533
He L, Huang Y, Ma Z et al (2016) Effects of contrast-enhancement, reconstruction slice thickness and convolution kernel on the diagnostic performance of radiomics signature in solitary pulmonary nodule. Sci Rep 6:34921
Heye T, Merkle EM, Reiner CS et al (2013) Reproducibility of dynamic contrast-enhanced MR imaging. Part II. Comparison of intra- and interobserver variability with manual region of interest placement versus semi-automatic lesion segmentation and histogram analysis. Radiology 266:812–821
Hofheinz F, Apostolova I, Oehme L et al (2017) Test-retest variability in lesion SUV and lesion SUR in (18) F-FDG PET: an analysis of data from two prospective multicenter trials. J Nucl Med 58:1770–1775
Honda O, Johkoh T, Sumikawa H et al (2007) Pulmonary nodules: 3D volumetric measurement with multidetector CT—effect of intravenous contrast medium. Radiology 245:881–887
de Hoop B, Gietema H, van Ginneken B et al (2009) A comparison of six software packages for evaluation of solid lung nodules using semi-automated volumetry: what is the minimum increase in size to detect growth in repeated CT examinations. Eur Radiol 19:800–808
Horvat N, Veeraraghavan H, Khan M et al (2018) MR imaging of rectal cancer: radiomics analysis to assess treatment response after neoadjuvant therapy. Radiology 287:833–843
Huang SC (2000) Anatomy of SUV. Standardized uptake value. Nucl Med Biol 27:643–646
Incoronato M, Aiello M, Infante T et al (2017) Radiogenomic analysis of oncological data: a technical survey. Int J Mol Sci 18:805
Ingrisch M, Maxien D, Schwab F et al (2014) Assessment of pulmonary perfusion with breath-hold and free-breathing dynamic contrast-enhanced magnetic resonance imaging: quantification and reproducibility. Investig Radiol 49:382–389
Jansen RW, van Amstel P, Martens RM et al (2018) Non-invasive tumor genotyping using radiogenomic biomarkers, a systematic review and oncology-wide pathway analysis. Oncotarget 9:20134–20155
Jennings SG, Winer-Muram HT, Tarver RD et al (2004) Lung tumor growth: assessment with CT—comparison of diameter and cross-sectional area with volume measurements. Radiology 231:866–871
Kemerink GJ, Lamers RJ, Thelissen GR et al (1995) Scanner conformity in CT densitometry of the lungs. Radiology 197:749–752
Kim CK, Gupta NC, Chandramouli B et al (1994) Standardized uptake values of FDG: body surface area correction is preferable to body weight correction. J Nucl Med 35:164–167
Kim H, Park CM, Song YS et al (2014) Influence of radiation dose and iterative reconstruction algorithms for measurement accuracy and reproducibility of pulmonary nodule volumetry: a phantom study. Eur J Radiol 83:848–857
Kim H, Park CM, Chae HD et al (2015) Impact of radiation dose and iterative reconstruction on pulmonary nodule measurements at chest CT: a phantom study. Diagn Interv Radiol 21:459–465
Kinahan PE, Fletcher JW (2010) Positron emission tomography-computed tomography standardized uptake values in clinical practice and assessing response to therapy. Semin Ultrasound CT MR 31:496–505
Ko JP, Rusinek H, Jacobs EL et al (2003) Small pulmonary nodules: volume measurement at chest CT—phantom study. Radiology 228:864–870
Kumar V, Gu Y, Basu S et al (2012) Radiomics: the process and the challenges. Magn Reson Imaging 30:1234–1248
Lambin P, Leijenaar RTH, Deist TM et al (2017) Radiomics: the bridge between medical imaging and personalized medicine. Nat Rev Clin Oncol 14:749–762
Lassen BC, Jacobs C, Kuhnigk JM et al (2015) Robust semi-automatic segmentation of pulmonary subsolid nodules in chest computed tomography scans. Phys Med Biol 60:1307–1323
Lavdas I, Miquel ME, McRobbie DW et al (2014) Comparison between diffusion-weighted MRI (DW-MRI) at 1.5 and 3 tesla: a phantom study. J Magn Reson Imaging 40:682–690
Leach MO, Morgan B, Tofts PS et al (2012) Imaging vascular function for early stage clinical trials using dynamic contrast-enhanced magnetic resonance imaging. Eur Radiol 22:1451–1464
Lee G, Lee HY, Park H et al (2017) Radiomics and its emerging role in lung cancer research, imaging biomarkers and clinical management: state of the art. Eur J Radiol 86:297–307
Leithner D, Horvat JV, Ochoa-Albiztegui RE et al (2018) Imaging and the completion of the omics paradigm in breast cancer. Radiologe 58:7
Lodge MA (2017) Repeatability of SUV in oncologic (18) F-FDG PET. J Nucl Med 58:523–532
Lowe VJ, DeLong DM, Hoffman JM et al (1995) Optimum scanning protocol for FDG-PET evaluation of pulmonary malignancy. J Nucl Med 36: 883–887
Mansoor A, Bagci U, Foster B et al (2015) Segmentation and image analysis of abnormal lungs at CT: current approaches, challenges, and future trends. Radiographics 35:1056–1076
Mayerhoefer ME, Szomolanyi P, Jirak D et al (2009) Effects of MRI acquisition parameter variations and protocol heterogeneity on the results of texture analysis and pattern discrimination: an application-oriented study. Med Phys 36:1236–1243

Moon SH, Hyun SH, Choi JY (2013) Prognostic significance of volume-based PET parameters in cancer patients. Korean J Radiol 14(1):12

Mozley PD, Bendtsen C, Zhao B et al (2012) Measurement of tumor volumes improves RECIST-based response assessments in advanced lung cancer. Transl Oncol 5:19–25

Nishino M, Guo M, Jackman DM et al (2011) CT tumor volume measurement in advanced non-small-cell lung cancer: Performance characteristics of an emerging clinical tool. Acad Radiol 18:54–62

Nishino M, Dahlberg SE, Cardarella S et al (2013) Tumor volume decrease at 8 weeks is associated with longer survival in EGFR-mutant advanced non-small-cell lung cancer patients treated with EGFR TKI. J Thorac Oncol 8:1059–1068

Nishino M, Dahlberg SE, Fulton LE et al (2016) Volumetric tumor response and progression in EGFR-mutant NSCLC patients treated with erlotinib or gefitinib. Acad Radiol 23:329–336

Oda S, Awai K, Murao K et al (2010) Computer-aided volumetry of pulmonary nodules exhibiting ground-glass opacity at MDCT. AJR Am J Roentgenol 194:398–406

Ohno Y, Yaguchi A, Okazaki T et al (2016) Comparative evaluation of newly developed model-based and commercially available hybrid-type iterative reconstruction methods and filter back projection method in terms of accuracy of computer-aided volumetry (CADv) for low-dose CT protocols in phantom study. Eur J Radiol 85:1375–1382

Oliver JA, Budzevich M, Zhang GG et al (2015) Variability of image features computed from conventional and respiratory-gated PET/CT images of lung cancer. Transl Oncol 8:524–534

Padhani AR, Miles KA (2010) Multiparametric imaging of tumor response to therapy. Radiology 256: 348–364

Parekh V, Jacobs MA (2016) Radiomics: a new application from established techniques. Expert Rev Precis Med Drug Dev 1:207–226

Parmar C, Rios Velazquez E, Leijenaar R et al (2014) Robust radiomics feature quantification using semiautomatic volumetric segmentation. PLoS One 9:e102107

Petrou M, Quint LE, Nan B et al (2007) Pulmonary nodule volumetric measurement variability as a function of CT slice thickness and nodule morphology. AJR Am J Roentgenol 188:306–312

Plathow C, Schoebinger M, Fink C et al (2006) Quantification of lung tumor volume and rotation at 3D dynamic parallel MR imaging with view sharing: preliminary results. Radiology 240:537–545

Quak E, Le Roux PY, Lasnon C et al (2016) Does PET SUV harmonization affect PERCIST response classification? J Nucl Med 57:1699–1706

Rampinelli C, Raimondi S, Padrenostro M et al (2010) Pulmonary nodules: contrast-enhanced volumetric variation at different CT scan delays. AJR Am J Roentgenol 195:149–154

Rao SX, Lambregts DM, Schnerr RS et al (2016) CT texture analysis in colorectal liver metastases: a better way than size and volume measurements to assess response to chemotherapy? United European Gastroenterol J 4:257–263

Rasch C, Barillot I, Remeijer P et al (1999) Definition of the prostate in CT and MRI: a multi-observer study. Int J Radiat Oncol Biol Phys 43:57–66

Rios Velazquez E, Aerts HJ, Gu Y et al (2012) A semiautomatic CT-based ensemble segmentation of lung tumors: comparison with oncologists' delineations and with the surgical specimen. Radiother Oncol 105:167–173

Rohrer M, Bauer H, Mintorovitch J et al (2005) Comparison of magnetic properties of MRI contrast media solutions at different magnetic field strengths. Investig Radiol 40:715–724

Saha A, Yu X, Sahoo D et al (2017) Effects of MRI scanner parameters on breast cancer radiomics. Expert Syst Appl 87:384–391

Sakai N, Yabuuchi H, Kondo M et al (2015) Volumetric measurement of artificial pure ground-glass nodules at low-dose CT: comparisons between hybrid iterative reconstruction and filtered back projection. Eur J Radiol 84:2654–2662

Shafiq-Ul-Hassan M, Zhang GG, Latifi K et al (2017) Intrinsic dependencies of CT radiomic features on voxel size and number of gray levels. Med Phys 44:1050–1062

She Y, Zhang L, Zhu H et al (2018) The predictive value of CT-based radiomics in differentiating indolent from invasive lung adenocarcinoma in patients with pulmonary nodules. Eur Radiol 28:5121–5128

Siegelman JW, Supanich MP, Gavrielides MA (2015) Pulmonary nodules with ground-glass opacity can be reliably measured with low-dose techniques regardless of iterative reconstruction: results of a phantom study. AJR Am J Roentgenol 204:1242–1247

Soher BJ, Dale BM, Merkle EM (2007) A review of MR physics: 3T versus 1.5T. Magn Reson Imaging Clin N Am 15:277–290, v

Stoel BC, Vrooman HA, Stolk J et al (1999) Sources of error in lung densitometry with CT. Investig Radiol 34:303–309

Stoel BC, Bode F, Rames A et al (2008) Quality control in longitudinal studies with computed tomographic densitometry of the lungs. Proc Am Thorac Soc 5:929–933

Sun R, Limkin EJ, Vakalopoulou M et al (2018) A radiomics approach to assess tumour-infiltrating CD8 cells and response to anti-PD-1 or anti-PD-L1 immunotherapy: an imaging biomarker, retrospective multicohort study. Lancet Oncol 19:1180–1191

Szigeti K, Szabo T, Korom C et al (2016) Radiomics-based differentiation of lung disease models generated by polluted air based on X-ray computed tomography data. BMC Med Imaging 16:14

Tan Y, Guo P, Mann H et al (2012) Assessing the effect of CT slice interval on unidimensional, bidimensional and volumetric measurements of solid tumours. Cancer Imaging 12:497–505

Therasse P, Arbuck SG, Eisenhauer EA et al (2000) New guidelines to evaluate the response to treatment in solid tumors. European Organization for Research and Treatment of Cancer, National Cancer Institute of the United States, National Cancer Institute of Canada. J Natl Cancer Inst 92:205–216

Tixier F, Le Rest CC, Hatt M et al (2011) Intratumor heterogeneity characterized by textural features on baseline 18F-FDG PET images predicts response to concomitant radiochemotherapy in esophageal cancer. J Nucl Med 52:369–378

Trebeschi S, van Griethuysen JJM, Lambregts DMJ et al (2017) Deep learning for fully-automated localization and segmentation of rectal cancer on multiparametric MR. Sci Rep 7:5301

Ullrich T, Quentin M, Oelers C et al (2017) Magnetic resonance imaging of the prostate at 1.5 versus 3.0T: a prospective comparison study of image quality. Eur J Radiol 90:192–197

Usmani N, Sloboda R, Kamal W et al (2011) Can images obtained with high field strength magnetic resonance imaging reduce contouring variability of the prostate? Int J Radiat Oncol Biol Phys 80:728–734

Vardhanabhuti V, Kuo MD (2018) Lung cancer radiogenomics: the increasing value of imaging in personalized management of lung cancer patients. J Thorac Imaging 33:17–25

Wang Y, de Bock GH, van Klaveren RJ et al (2010) Volumetric measurement of pulmonary nodules at low-dose chest CT: effect of reconstruction setting on measurement variability. Eur Radiol 20:1180–1187

Wang S, Zhou M, Liu Z et al (2017) Central focused convolutional neural networks: developing a data-driven model for lung nodule segmentation. Med Image Anal 40:172–183

Weller A, Papoutsaki MV, Waterton JC et al (2017) Diffusion-weighted (DW) MRI in lung cancers: ADC test-retest repeatability. Eur Radiol 27:4552–4562

Winer-Muram HT, Jennings SG, Meyer CA et al (2003) Effect of varying CT section width on volumetric measurement of lung tumors and application of compensatory equations. Radiology 229:184–194

Yabuuchi H, Hatakenaka M, Takayama K et al (2011) Non-small cell lung cancer: detection of early response to chemotherapy by using contrast-enhanced dynamic and diffusion-weighted MR imaging. Radiology 261:598–604

Yoon HJ, Sohn I, Cho JH et al (2015) Decoding tumor phenotypes for ALK, ROS1, and RET fusions in lung adenocarcinoma using a radiomics approach. Medicine (Baltimore) 94:e1753

Zasadny KR, Wahl RL (1993) Standardized uptake values of normal tissues at PET with 2-[fluorine-18]-fluoro-2-deoxy-D-glucose: variations with body weight and a method for correction. Radiology 189:847–850

Zhao L, Jia K (2016) Multiscale CNNs for brain tumor segmentation and diagnosis. Comput Math Methods Med 2016:8356294

Zhao B, Schwartz LH, Moskowitz CS et al (2005) Pulmonary metastases: effect of CT section thickness on measurement—initial experience. Radiology 234:934–939

Zhao B, Schwartz LH, Moskowitz CS et al (2006) Lung cancer: computerized quantification of tumor response—initial results. Radiology 241:892–898

Zhao B, Oxnard GR, Moskowitz CS et al (2010) A pilot study of volume measurement as a method of tumor response evaluation to aid biomarker development. Clin Cancer Res 16:4647–4653

Zhao B, Tan Y, Bell DJ et al (2013) Exploring intra- and inter-reader variability in uni-dimensional, bi-dimensional, and volumetric measurements of solid tumors on CT scans reconstructed at different slice intervals. Eur J Radiol 82:959–968

Zhao YR, van Ooijen PM, Dorrius MD et al (2014a) Comparison of three software systems for semi-automatic volumetry of pulmonary nodules on baseline and follow-up CT examinations. Acta Radiol 55:691–698

Zhao B, Tan Y, Tsai WY et al (2014b) Exploring variability in CT characterization of tumors: a preliminary phantom study. Transl Oncol 7:88–93

Evolution of Clinical Trial Imaging and Co-clinical Imaging

Amy Junghyun Lee, Chong Hyun Suh, and Kyung Won Kim

Contents

A. J. Lee
Department of Medical Science and Asan Image Metrics, Asan Medical Institute of Convergence Science and Technology, Asan Medical Center, University of Ulsan College of Medicine, Seoul, Republic of Korea
e-mail: junghyun.lee@aim-aicro.com

C. H. Suh
Department of Radiology and Research Institute of Radiology, Asan Medical Center, University of Ulsan College of Medicine, Seoul, Republic of Korea

K. W. Kim (✉)
Department of Medical Science and Asan Image Metrics, Asan Medical Institute of Convergence Science and Technology, Asan Medical Center, University of Ulsan College of Medicine, Seoul, Republic of Korea

Department of Radiology and Research Institute of Radiology, Asan Medical Center, University of Ulsan College of Medicine, Seoul, Republic of Korea
e-mail: kyungwon_kim@amc.seoul.kr

Abstract

During the last two decades, imaging in drug development has been greatly advanced in a diversity of therapeutic fields, especially in the oncology field. As regulatory agencies seek robust evidence for primary endpoints, as much as possible, medical imaging usage is rapidly increased to support the primary endpoints in clinical trials. The addition of medical imaging in the clinical trials requires logistical and technical considerations, as follows: (1) selection of appropriate qualified imaging biomarker, (2) standardization of imaging acquisition, archive, and analysis, (3)

M. Nishino (ed.), *Therapy Response Imaging in Oncology*, Medical Radiology, Diagnostic Imaging,
https://doi.org/10.1007/978-3-030-31171-1_14

independent blinded image review, and (4) system for complex workflow and regulatory compliance. In 2018, US FDA issued "Clinical Trial Imaging Endpoint Process Standards Guidance for Industry" so that pharmaceutical companies, imaging scientists, and clinical trial professionals can utilize imaging in a clinical trial as an appropriate manner. In addition, preclinical imaging usage has been also increased in drug development, and recently incorporated in the clinical trial process, so-called co-clinical trial. The co-clinical trials, hence, enable bidirectional translation research between bench and bedside. Therefore, imaging professionals should be aware of these global trends in imaging for drug development.

1 Introduction

The medical imaging modalities generally visualize anatomy with or without physiology, which is very efficient in diagnosis, staging, and treatment response assessment of cancers (Yankeelov et al. 2016). The benefits of using imaging technologies such as computed tomography (CT), magnetic resonance imaging (MRI), and positron emission tomography (PET) are well established in clinical trials. Imaging is noninvasive and can yield surrogate endpoints quickly compared to others, decreasing the time and expense of drug development. The present medical imaging routinely incorporated in the standard-of-care and clinical trial. The most common imaging modality in oncology field is routine contrast-enhanced CT or MRI scan for anatomical information. With advances in therapeutic agents such as molecular targeted and immunotherapeutic agents, the use of quantitative imaging modality to measure physiology of disease as quantitative imaging biomarker has been increased in the clinical trial (Murphy and Koh 2010).

In order to use medical imaging in clinical trials, there are several significant considerations as follows: (1) selection of appropriate qualified imaging biomarker, (2) standardization of imaging acquisition, archive, and analysis, (3) independent blinded image review, and (4) system for complex workflow and regulatory compliance. In 2018, the US Food and Drug Administration (FDA) issued a "Clinical Trial Imaging Endpoint Process Standards Guidance for Industry" (hereafter referred to as the 2018 FDA Imaging Guidance) which provides current optimal procedures to use imaging in clinical trials, so that pharmaceutical companies, imaging scientists, and clinical trial professionals can use imaging in an appropriate manner (US Food and Drug Administration 2018). In this chapter, we discuss the details of these logistical and technical considerations based on the 2018 FDA Imaging Guidance.

Medical imaging, in addition, has been greatly used in the preclinical trial, and recently integrated with the clinical trial process, so-called co-clinical trial. The co-clinical trials using both mouse model and human subject simultaneously may enable to explore further the mechanism of drug response and resistance, or the predictive values of several biomarkers (Nishino et al. 2017). Co-clinical trials could empower bidirectional translation research between bench and bedside. As a result, the related parties, especially imaging professionals, with the clinical trial should focus on these global trends in imaging for drug development.

2 History of Clinical Trial Imaging

The clinical trial imaging has rapidly developed in less than two decades. Indeed, the concept of clinical trial imaging might be unfamiliar with very short history. The major milestones and events in clinical trial imaging are illustrated in Fig. 1.

2.1 Rapid Growth of CT/MRI Use in Cancer Imaging

When multi-detector CT (aka multi-slice CT) was developed, and became popular all over the world in around 2000, the oncology was the most active field to utilize multi-detector CT in the clinical trial (O'Connor et al. 2016). The MRI technology was also rapidly developed and well known in the cancer clinical trial. Furthermore,

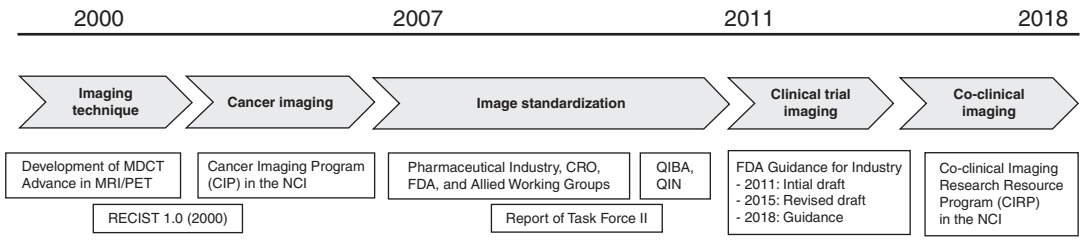

Fig. 1 History of clinical trial imaging. The major milestones of clinical trial imaging includes development of imaging technique, emergence of cancer imaging field, efforts for imaging standardization, and emergence of clinical trial imaging and co-clinical imaging fields. Several important events are listed in the boxes (*Abbreviations*: *CRO* contract research organization, *FDA* Food and Drug Administration, *MDCT* multi-detector computed tomography, *MRI* magnetic resonance imaging, *NCI* National Cancer Institute, *PET* positron emission tomography, *QIBA* Quantitative Imaging Biomarker Alliance, *QIN* Quantitative Imaging Network)

the Response Evaluation Criteria in Solid Tumors (RECIST) 1.0 issued in 2000 has highly facilitated the use of MDCT and MRI for treatment response in the vast majority of cancer trials (Therasse et al. 2000). In those days, the National Institute of Health (NIH) and FDA regarded imaging biomarkers as important surrogate endpoints in a clinical trial and started to put efforts to establish the infrastructure to use imaging endpoints appropriately. In 2003, the National Cancer Institute (NCI) of NIH established the Cancer Imaging Program (CIP) in order to foster advances in medical imaging through the support of basic and clinical research in a cancer study, which opened a new field of "Cancer Imaging" (Shankar 2012).

2.2 Efforts for Imaging Standardization

As the use of CT/MRI extremely increased during early 2000, standardization issues were also raised because critical variability was noticed among imaging machines, acquisition protocols, image quality, and analysis methods. In 2006, the FDA, thus, met face-to-face with a group of imaging stakeholders from imaging core lab, contract research organization (CRO), pharmaceutical industry, academia, and imaging device/software vendors. This was because the FDA discovered that medical imaging in clinical trials had been variously and widely used (Ford and Mozley 2008). Thereafter, the FDA and imaging stakeholders organized task force teams, and issued a consensus statement entitled "Report of Task Force II: Best Practices in the Use of Medical Imaging Techniques in Clinical Trials Consensus from a Public Meeting, October 16–17, 2007 The Medical Imaging Stakeholders Call for Action: Harmonization Across Key Elements and Integration of Imaging in Therapeutic Development—Pharmaceutical Industry, CRO, FDA, and Allied Working Groups Collaborate for Regulatory Guidance" (Ford and Mozley 2008).

In 2007, the Quantitative Imaging Biomarkers Alliance (QIBA) was also established by the Radiological Society of North America (RSNA) to facilitate quantitative imaging techniques and biomarkers in clinical trials by engaging imaging researchers and industry. The purpose of QIBA is to improve the value and practicality of quantitative imaging biomarkers by reducing variability across devices, patients, and time. So far, QIBA has closely cooperated with FDA, NIH, NCI, and other imaging organizations, and showed great achievements in standardization and industrialization of imaging biomarkers (Shukla-Dave et al. 2019; Nakahara et al. 2017; Sullivan et al. 2015).

2.3 New Regulation Compliance

During the 2000s, FDA had continuously raised concerns for objectivity and validity of imaging endpoints since there were several crucial biases, which could be highly effective towards the outcomes of clinical trial, such as validation of

imaging biomarker in technical characteristics (e.g., precision and accuracy), biological/clinical utility (linkage of imaging biomarker and biologic/pathologic process), and appropriateness of imaging data management based on good clinical practice (GCP), various FDA guidelines, and Health Insurance Portability and Accountability Act (HIPPA). The FDA, therefore, started to develop "Clinical Trial Imaging Endpoint Process Standards Guidance for Industry," was issued the first draft guidance in 2011, the revised draft guidance in 2015, and the final guidance in 2018 (US Food and Drug Administration 2018).

After the issue of the 2018 FDA Imaging Guidance, various imaging stakeholders including imaging core lab, pharmaceutical companies, and imaging vendors should follow the guidance in order to conduct precise and standardized clinical trials. To support imaging procedures in the trial and comply with this new regulation appropriately, special imaging professionals and institutions are required, which begin a new field of "Clinical Trial Imaging" (Murphy and Koh 2010).

2.4 Integration of Preclinical Trial and Clinical Trial

Generally, in cancer drug development, there is a huge gap between preclinical trial and clinical trial processes. To increase efficiency in drug development, "translation from preclinical to clinical" concept has been emphasized, and imaging is a high valuable method for such translational research due to the use of imaging in both animal and human. Furthermore, in 2011, Dr. Pier Paolo Pandolfi (Professor in Dana-Farber/Harvard Cancer Center) proposed to conduct preclinical trials in parallel with clinical trials, emphasizing bidirectional translation from mouse to human as well as from human to mouse (Nardella et al. 2011). Thereafter, several co-clinical trials were performed, and the results of these trials reported the beneficial effects of co-clinical trials (Chen et al. 2012; Lunardi et al. 2013; Kwong et al. 2015). In 2015, the NCI established the Co-clinical Imaging Research Resource Program (CIRP) in order to promote the development of quantitative imaging resources for therapeutic or prevention co-clinical trials (Colen et al. 2014). In near future, the value of co-clinical trial imaging would be more investigated.

3 Selection of Appropriate Imaging Biomarker

The FDA–NIH Biomarker Working Group defined a biomarker as "an indicator of normal biological processes, pathogenic processes or responses to exposure or intervention, including therapeutic interventions," and also stated that "molecular, histologic, radiographic or physiologic characteristics are examples of biomarkers" (O'Connor et al. 2016; FDA-NIH Biomarker Working Group 2016; Biomarkers, Definitions, Working, Group 2001). Not all the imaging biomarker can be used in the clinical trials. The approval of the medical imaging device and software does not completely guarantee to adapt all the imaging biomarker derived from the imaging device/software (Suh et al. 2018). In order to use an appropriate imaging biomarker in the clinical trial, the regulatory agency should restrict the selection of imaging biomarker based on biomarker qualification, which is processed by the FDA Center for Drug Evaluation and Research (CDER) (Amur et al. 2015). The use of qualified biomarker, as a result, is especially important in the late phase of the clinical trial (phase III or IIb) when the imaging biomarker is used as primary endpoints.

In the clinical trial of oncology, the RECIST 1.1 is the most widely used qualified biomarkers based on anatomical medical imaging and is adapted as a primary endpoint by the FDA (Eisenhauer et al. 2009). Nevertheless, RECIST 1.1 has its own limitation in treatment response assessment, specifically in the brain tumor, lymphoma, and bone lesions. The NCI's Cancer Imaging Program, therefore, allows to utilize other various imaging response criteria as summarized in Table 1 (Young et al. 1999; Wahl et al. 2009; Macdonald et al. 1990; Wen et al. 2010;

Table 1. Imaging response criteria commonly used in cancer clinical trials

Imaging response criteria	Comments
For [18F]FDG-PET scan	
European Organization for Research and Treatment of Cancer (EORTC) (Young et al. 1999)	Published in 1999, these set of recommendations are for measuring clinical and subclinical tumor response using FDG-PET scans
PET Response Criteria in Solid Tumors (PERCIST) (Wahl et al. 2009)	Published in 2009, PERCIST is a comprehensive set of response criteria for use with [18F]FDG-PET scans
For brain tumor	
McDonald Criteria (Macdonald et al. 1990)	Published in 1990 for use with contrast-enhanced CT and MRI scans of the head, response is based on changes in tumor size and interpreted in light of steroid use and neurologic findings
Response Assessment in Neuro-Oncology (RANO) (Wen et al. 2010)	Published in 2010, RANO is an update to the McDonald Criteria which also takes into consideration enhancing components of the tumor and non-contrast CT/MRI findings seen on the T2-weighted and FLAIR sequences
RANO—Brain Metastases (Lin et al. 2015)	Published in 2015, RANO-BM was developed by the RANO-BM Working Group as a standard response and progression criteria for use in clinical trials dealing with metastatic lesions to the brain
RANO—Leptomeningeal metastases (Chamberlain et al. 2017)	Published in 2017, RANO-leptomeningeal metastases was developed by the RANO Working Group and they proposed three basic elements: a standardized neurological examination, cerebral spinal fluid (CSF) cytology or flow cytometry, and radiographic evaluation
For lymphoma	
International Working Group (Cheson) Criteria (Cheson et al. 2007)	Published in 2007, the Cheson criteria defines standardized response criteria for Hodgkin's and non-Hodgkin's lymphoma using [18F]FDG PET, immunohistochemistry, and flow cytometry
Deauville Criteria (Meignan et al. 2009)	Published in 2009, Deauville Criteria describes a simplified 5 point scale to standardize interpretation of FDG-PET for lymphoma
Lugano Recommendations (Cheson et al. 2014)	Published in 2014 as a result of a workshop at the 12th International Conference on Malignant Lymphoma, the Lugano Recommendations represent a set of revised recommendations regarding the use of the Cheson and Deauville Criteria and formally incorporated [18F]FDG PET into standard staging and response evaluation for FDG-avid lymphomas
For bone lesions	
MD Anderson Bone Response Criteria (MDA) (Hamaoka et al. 2004)	Published in 2004, the MDA defines response in bone lesions based on anatomic imaging such as XR, CT, and MRI
Prostate Cancer Working Group 2 (PCWG2) (Scher et al. 2008)	Published in 2008, PCWG2 defines progression by imaging in prostate cancer but does not provide standardized definitions for treatment response by imaging
For immunotherapy	
iRECIST (Seymour et al. 2017)	Published in 2017, revised from the RECIST 1.1 for immunotherapy in solid tumor patients
iRANO (Okada et al. 2015)	Published in 2015, revised from the RANO for immunotherapy in brain tumor patients
LYRIC (Cheson et al. 2016)	Published in 2016, revised from the Lugano criteria for immunomodulatory therapy in lymphoma patients

Imaging response criteria are listed in the NCI's Cancer imaging program (assessed at https://imaging.cancer.gov/clinical_trials/imaging_response_criteria.htm)

Lin et al. 2015; Chamberlain et al. 2017; Cheson et al. 2007; Meignan et al. 2009; Cheson et al. 2014; Hamaoka et al. 2004; Scher et al. 2008). In recent years, new imaging response criteria have been developed for a treatment response of new immunotherapeutic agents (Seymour et al. 2017; Okada et al. 2015; Cheson et al. 2016). These imaging response criteria are contributed by the conventional anatomical CT/MRI imaging or FDG-PET/CT imaging.

Diffusion-weight image (DWI) or dynamic contrast-enhanced MRI (DCE-MRI) are commonly used nowadays as other functional quantitative imaging biomarkers in the clinical trials (Yankeelov et al. 2016; Murphy and Koh 2010; O'Connor et al. 2016). On the other hand, these functional quantitative imaging biomarkers have not fully qualified yet by the FDA, and it should be used as exploratory endpoints rather than primary endpoints. For instance, the DCE-MRI has been used in more than 80 cancer clinical trials of antiangiogenic and molecular targeted agents; however, the variability in DCE-MRI parameters and response criteria were very heterogeneous across studies (O'Connor et al. 2012).

4 Imaging Standardization

In order to accept medical imaging in clinical trials, minimization of imaging process variability is one of the main critical perspectives to generate reliable imaging outcomes. In the clinical practice, each hospital has its own institutional policy for imaging acquisition/analysis. The utilization of imaging for diagnosis and treatment response tends to be optimized by the hospital own setting, which can result in variability across hospitals. A hospital with specialized cancer center, for example, optimizes imaging setup for cancer patients; in contrast, a hospital with a lot of trauma patients optimizes imaging setup for trauma patients. However, in multicenter clinical trials, such variability among hospitals may hamper data reliability and reduce statistical power. Indeed, standardization of imaging acquisition, display, anonymization/transfer, analysis, and report are mandatory in clinical trials. At least, the standards of trial-specific imaging process should be achieved and detailed in a trial protocol or imaging charter, which is called "Trial-Specific Standardization" (Ford and Mozley 2008; Gillam et al. 2017).

The extent of trial-specific standardization is determined by the purpose of the clinical trial and imaging endpoints. The considering factors in the 2018 FDA Imaging Guidance are represented in Table 2. In general, a sponsor (e.g., pharmaceutical company) delegates trial-specific standardization process to specialized imaging teams such as

Table 2 Items for trial-specific imaging standardization based on the 2018 FDA imaging guidance

Items
• Imaging modality availability and the modality's technical performance variation across trial site
• Performance features of the imaging modality at the trial sites or any other locations where subjects may undergo imaging
• Qualifications of the imaging technologists and any special technological needs for the trial
• Proposed imaging measures' reliance on phantoms and/or calibration standards to ensure consistency and imaging quality control among clinical sites
• Any unique image acquisition features of the trial design, including subject positioning, anatomical coverage of imaging, use of contrast, timing of imaging, importance of subject sedation, and scanner settings for image acquisition
• Image quality control standards, including those specifying the need for repeat imaging to obtain interpretable images
• Procedures for imaging display and interpretation, including technical variations in reader display stations
• Nature of the primary endpoint image measurement, including the importance of training image readers in trial-specific quantification methods
• Extent that image archiving could be important to the trial's conduct, monitoring, and data auditing
• Potential for imaging modality upgrades or modality failures, as well as the potential variation in imaging drugs (such as contrast agents) across trial sites
• Precedent for use of the imaging-based primary endpoint measure in investigational drug development, especially previously observed imaging methodological problems

These items are listed in the FDA's Clinical Trial Imaging Endpoints Process Standards Guidance for Industry issued in 2018 (assessed at https://www.fda.gov/downloads/drugs/guidances/ucm268555.pdf)

imaging core lab or CRO. The imaging team establishes trial-specific standardized imaging protocols. To achieve appropriate trial-specific standardization, information of imaging policy and protocol from each hospital should be collected. For these information, each hospital or site is requested to fully complete a pre-study survey, which basically includes imaging modality and protocol information of the trial such as the number and type of scanners, desired mode of image transmittal, image storage capability, and the ability of sites to follow the trial-specific standardized imaging acquisition/analysis plan. If the usual institutional policy of a hospital/site is acceptable, it would be recommended to use during the clinical trial. If not, the trial-specific imaging protocol should be generated by imaging specialist in the hospital/site (Bae et al. 2018). Furthermore, the use of phantoms could also be significant to evaluate image acquisition standards, depending on the nature of the imaging endpoint.

Not only the standardization of imaging protocol but also integrated imaging management system to control image protocols, quality control, anonymization/transfer, and analysis enhance the efficiency of the overall imaging process. When a well-prepared imaging team and a technology-driven imaging management system are well performed together, the medical imaging would demonstrate more accurate and consistent results in the clinical trials.

5 Central Independent Blinded Image Review

In clinical trials, images can be interpreted either at each hospital/site or at a central image review team (hereafter referred to as site reading and central reading, respectively) (Beaumont et al. 2018). The interpretation of the medical image is generally subjective, and several image response criteria are products of efforts to convert subjective interpretation into the quantitative or semi-quantitative measure. Inter-reader variability of image interpretation, therefore, is inevitable. Especially, when a large number of sites are involved in large-scale trials, the variability between site readers may influence on the reliability of imaging endpoints. Site readers, moreover, are not blinded to the clinical and laboratory information which also may cause the objective imaging interpretation (Ford et al. 2009).

In order to overcome these drawbacks, central independent image review has gained emphasis in that it may increase the credibility and consistency of image assessments (Ford et al. 2009). In addition, the image quality check performed by the central imaging team might be better to reduce imaging defects or violation (Gierada et al. 2009). The extent of blinding image readers from clinical and laboratory information relies on the purpose and phase of clinical trials. In general, image review with blinding to the demographic information of the patient, site markings, clinical and laboratory information, and indicators of treatment arm ensure the objective image interpretation. According to the 2018 FDA Imaging Guidance, the central independent blinded image review is not mandatory but recommended in clinical trials, especially in the large-scale multicenter and randomized controlled trial (US Food and Drug Administration 2018).

There are several prerequisites to conduct successful central reading. The standardized imaging interpretation methods should be carefully designed in accordance with primary endpoints and documented in the imaging charter. The central readers should be satisfied with qualification of reader's skill, experience, conflict of interest, and availability. Reader training is also a very important step to minimize inter-reader variability, and ensure consistent and reproducible interpretation. The training manual for central readers and several sample cases for the specific trial should be prepared in advance, and mock tests for central readers are also recommended (Ford et al. 2009). During the central reading process, the reader performance and discrepancy rate between readers should be monitored continuously. Further detailed process of central readers are represented in the operation of clinical trial imaging.

6 Operation of Clinical Trial Imaging

As we discussed the above, the operation of imaging process for a clinical trial according to the 2018 FDA Imaging Guidance is very difficult and frequently requiring an imaging core lab and a computerized imaging system (US Food and Drug Administration 2018). Releasing guideline could be meant that regulation for imaging data collection, transfer, and analysis is strengthened to obligate. The guideline is the primary point to increase assurance for a clinical trial to analyze remedial effects. The standard procedure during image processing, for example, could minimize change or deviation. Imaging core lab, thus, is a necessity of system to perform optimized processes for imaging in the clinical trials based on the strengthened regulations and guidelines to standardize. The overall scheme to operate clinical trial imaging is summarized in Fig. 2 and a sample project is illustrated in Fig. 3.

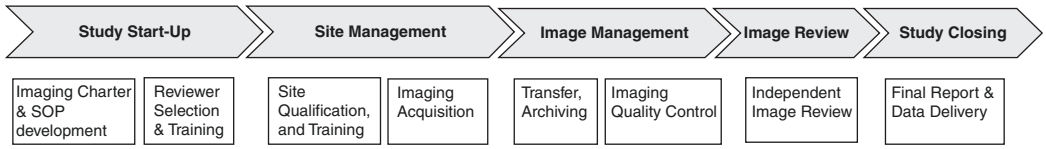

Fig. 2 Stepwise operation of clinical trial imaging. The operation of clinical trial imaging can be divided into five categories including study start-up, site management, image data management, image review, and study closing. In each category, there are several steps to perform following a stepwise and integrative approach

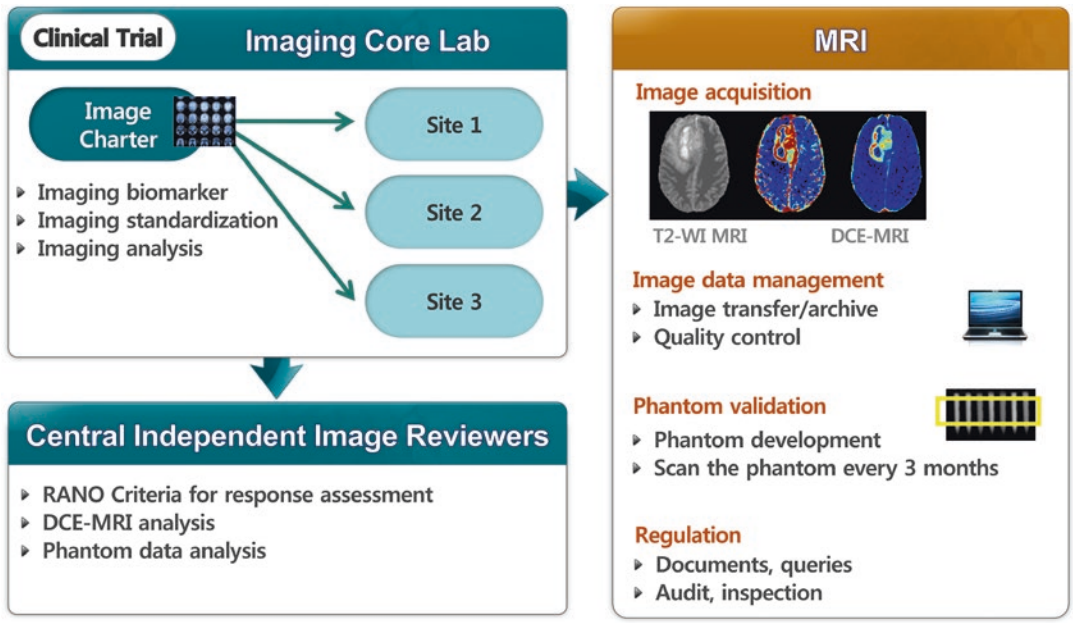

Fig. 3 Example of operation of clinical trial imaging. In a clinical trial which uses brain MRI for treatment assessment of brain tumors, an imaging core lab develops image charter which determines imaging biomarkers/endpoints and standardized imaging acquisition/analysis methods. Based on image charter, the imaging core lab manages multiple sites to get appropriate images acquired according to the predetermined imaging protocols. The image data are transferred and archived in the central server. Quality control of all acquired MRI images is performed. For the purpose of standardization and quality assurance, phantoms are developed and distributed to each site. The phantom MRI images are scanned every 3 months and analyzed. Imaging core lab also organizes a central independent image review team and trains each central reviewer to follow standardized imaging analysis methods

6.1 Image Charter and Standard Operation Procedures

An imaging charter is referred to either a single or a series of document(s) to describe all essential processes of imaging for the clinical trial, including imaging methodology, imaging modality with technical details, image interpretation, and the procedures for image archiving (US Food and Drug Administration 2018). This is simply indicated as a protocol for only imaging parts of the trial as same as the clinical trial protocol, and it could be attached to the clinical trial protocol as an appendix. The purpose of imaging charter is also related to the standardization of imaging processes during the whole clinical trial. Imaging charter contents are organized as three main categories: (1) image acquisition, (2) image interpretation, and (3) imaging data transfer and archiving. In these categories, image acquisition standard contains specific descriptions as imaging endpoints, imaging modality and operation, and imaging drugs such as contrast or radiology medicine.

In addition, development of the standard operating procedures (SOPs) provides a better quality of clinical trial management since it maintains appropriate procedures for the trial. Imaging Core Lab should be familiar with both imaging charter and SOPs for imaging is able to guide to conduct and manage the imaging process in the trial.

6.2 Site Qualification/Training

After imaging charter development, clinical research associate (CRA) of imaging core lab trains personnel of each site/hospital, and confirms physically the validation of imaging protocol and modalities through imaging modality calibration report for the clinical trial. Every trial has different imaging protocols, are developed based on the study type. During the site training, the main process is to confirm the imaging protocol settings, calibration report for modalities, and imaging site binder to retain every document related with imaging. Not only for these processes but also for quantitative imaging procedures, maintaining and controlling imaging hardware and software changes, including software versions, are also significant procedure to check the quality of site before and during the trial.

6.3 Image Acquisition

Based on imaging protocol in the imaging charter, every site is recommended to set up the protocol with selected modalities for minimizing variability. To minimize variability of imaging data is a critical issue, the 2018 FDA Imaging Guidance indicates "the use of a tabular listing of the acceptable imaging equipment, including the key characteristics, of the acquisition, processing, and display components of each scanner or review workstation." As standards for image acquisition, moreover, the imaging charter should describe vendor-specific equipment/platform, equipment technical settings at each site, the role of site imaging technicians in equipment operation, phantoms use for site qualification, subject preparation, positioning, and comfort measures, imaging schedule, off-protocol imaging, and imaging risks (US Food and Drug Administration 2018). Besides the above lists, the most important part of image acquisition is to maintain technical consistency across each site during the clinical trial.

6.4 Image Quality Control

During the ongoing clinical trial, all images from the site/hospital are performed for quality control (QC). Quality control is another critical step of the imaging process in the trial by imaging analysts, and the procedure should be written in the imaging charter, as well. As QC process, imaging analyst performs to assess images whether it is appropriate image quality based on image protocol, including image sequence, scan manual, document, and approved device usage. In addition, an imaging data query is generated during the QC process, and analyst has a responsibility

to resolve the query before the image interpretation. The reason for QC importance is that it controls the images across sites based on imaging protocols, which is another point to reduce variability.

6.5 Central Reader Management

Before image interpretation, central readers are selected on the basis of their background qualification and experiences. Reader training is performed once they are chosen, and the training session contains characteristics of the primary endpoint of the trial, the methodology of specific image acquisition, or quantitative analysis. Moreover, the timing of image reads and the read process should also be described in the imaging charter. The typical central reading process is that two primary readers independently review each case. However, if there is any discrepancy in the overall assessment between them, a third reader, adjudicator, joins to review the case. In this case, adjudicator only agrees with the result from one of the primary readers, and if it is necessary to re-review by primary readers, adjudicator enables to request. Through "double read with adjudication," the validity of the outcome could be improved. Even though the design of the central reading process could be differed by the clinical trial, this process is mainly suggested at first point.

6.6 Imaging Data Management

One of the general workflows in the clinical trial is to manage imaging data. Imaging data contains demographic information, the imaging modalities, and protocols for the study, and the result of imaging analysis, including RECIST, RANO, or LYRIC. Data standardization is an essential point in the clinical trial because it makes easier to understand and communicate data from the multicenters, including different countries, among a diversity of parties with the uniform data. Not only for understanding but also for the purpose of the future study, data scientists review data efficiently from multiple studies. Furthermore, in order to submit the data to the FDA for new drug approval, all terminology of the document is guided to be a standardized formats such as the National Drug File (NDF), Clinical Data Interchange Standards Consortium (CDISC) controlled terminology, and Medical Dictionary for Regulatory Activities (MedDRA). The FDA indicates, "The use of controlled terminology standards, also knowns as vocabularies, is an important component of achieving semantically interoperable data exchange" (U.S. Department of Health and Human Services FDA 2014). In this case, CDISC terminology for imaging of clinical trial represents imaging protocol and analysis criteria. As a result, using the standardized data leads that all researchers and data scientists are on the same page to share the clinical trial information over the world.

7 Clinical Trial Imaging Management System

Increased number of multicenter clinical trials in the world results in data integration and management issue. For instance, related parties for the trials such as sponsor (pharmaceutical company), CRO, principal investigator, and clinical research coordinator of site could track the status and data of trial using case report form (CRF) in real time. Since paper CRF is not efficient to maintain, update, and share real-time information, Clinical Trial Management System (CTMS) has been developed in recent years. Building an IT system as CTMS is another main perspective to support the process of standardized clinical trial, following the relevant compliances. This is because the responsibility of the academic medical center is to retain sufficiently a high level of quality during the clinical trial.

As the CTMS is implemented to the site/hospitals or research institutions, Clinical Trial Imaging Management System (CTIMS) has also been introduced, and it is primarily optimized for the medical images from the trials. The basic scheme of the CTIMS is illustrated in Fig. 4. Integrated imaging management system to

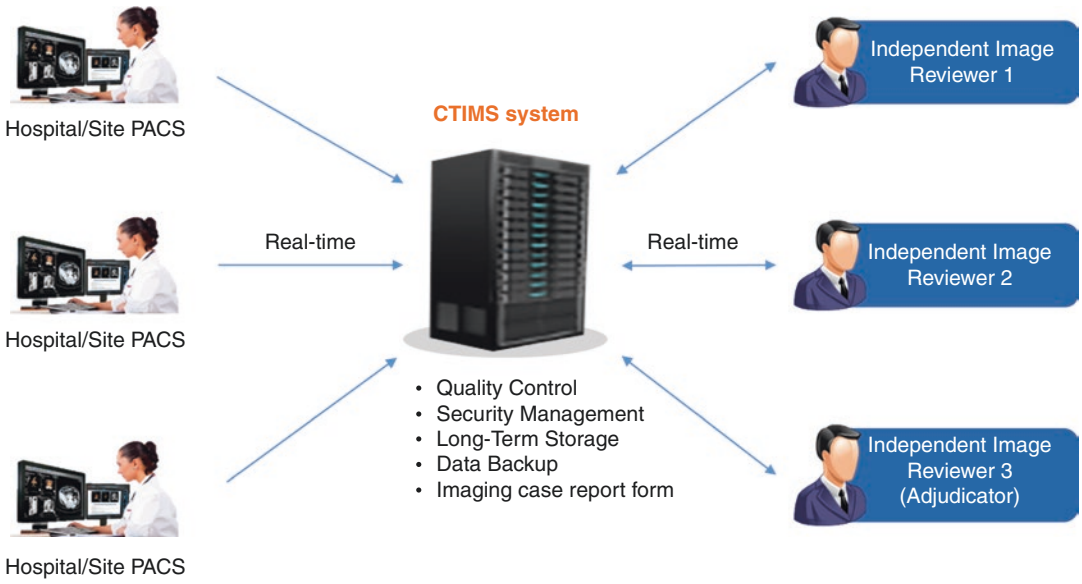

Fig. 4 Basic scheme of clinical trial imaging management system (CTIMS). In a multicenter clinical trial, the CTIMS enables each hospital/site to anonymize and transfer image data to the central server. CTIMS also enables independent image reviewers to view the images and analyze them. In addition, CTIMS can provide many functions to enhance image data management

control image anonymization/transfer, central reading, and analysis enhance the efficiency of the whole imaging process. In general, the larger the study and the more complex the therapeutic indication, the more sponsors risk an overwhelming number of imaging data points and measurements from many sites. The CTIMS, hence, could affect productive data management and integration in real time during the whole clinical trial period.

8 Co-clinical Trial Imaging

During the cancer drug discovery and development, data obtained from preclinical trial usually provide valuable insights for the new drug candidate such as proof of concept, drug toxicity/tolerability profiling, drug formulation and administration routes optimization, pharmacokinetics and pharmacodynamics information, determination of target tumors, drug efficacy evaluation, and drug resistance and its mechanism (Damia and D'Incalci 2009). However, it is difficult to translate or incorporate these preclinical data into the clinical drug development period. One of the main reasons is that the preclinical trials are usually performed separately (i.e., in advance) from the clinical trials conducted by the different team (Nishino et al. 2017).

To enhance translatability and bridging the gap between preclinical and clinical drug development process, several efforts have gained emphasis including the use of an appropriate animal models such as patient-derived xenograft model and use of translatable biomarkers such as medical imaging (Grassi et al. 2009). The recent co-clinical trial concept has been proposed, and the value of imaging in the co-clinical trial is actively being investigated (Nardella et al. 2011; Chen et al. 2012; Lunardi et al. 2013; Kwong et al. 2015).

The potential goals of co-clinical trials indicate (Yankeelov et al. 2016) the rapid optimization of therapy in patients based on concomitant mouse experiment of efficacy and tolerability/toxicity, (Murphy and Koh 2010) the rapid identification of resistant populations and mechanism of resistance through quick experiment using animal model, and (US Food and Drug

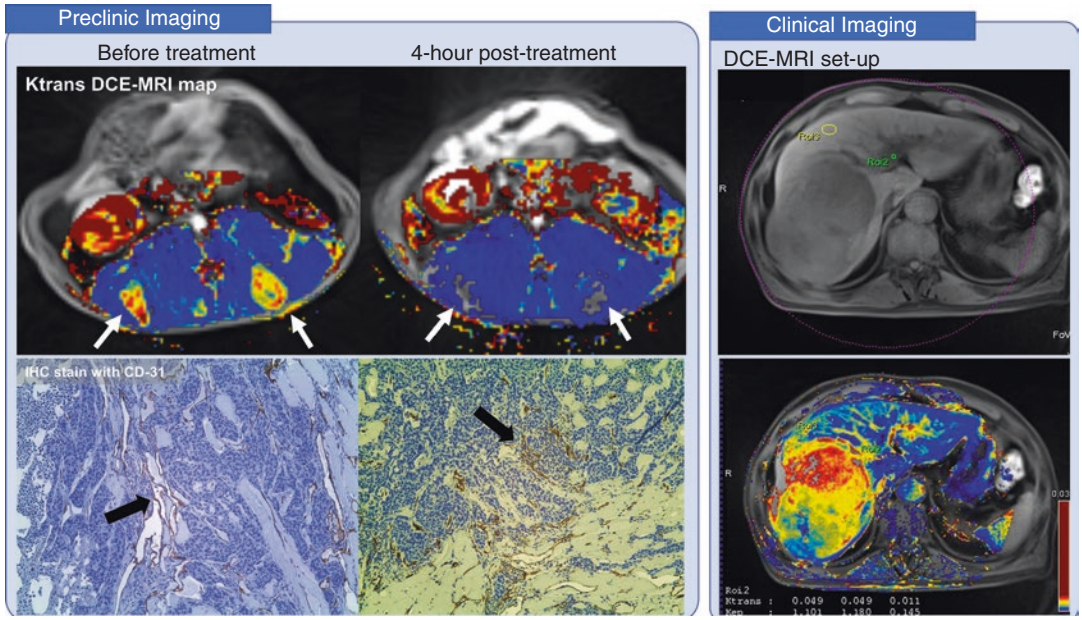

Fig. 5 Integration of preclinical and clinical imaging. In a drug development process of a vascular-disrupting agent, dynamic contrast-enhanced (DCE) MRI is used to evaluate anti-vascular effect of the drug. In a preclinical imaging using a rabbit tumor model, investigators are able to identify the optimal DCE-MRI biomarker, Ktrans, to reflect anti-vascular effect and histopathological change. Based on these data, clinical DCE-MRI can be analyzed efficiently

Administration 2018) better identification of molecular and imaging biomarker as illustrated in Fig. 5.

Important factors for successful co-clinical trial include to conduct a quick animal experiment during the clinical trial process, and to use an appropriate animal model recapitulating human disease. In order to conduct a mouse experiment quickly, we have to use a small number of animals and use appropriate biomarkers, which are able to monitor the animal and tumor easily and noninvasively. Imaging is valuable to monitor animal repeatedly in a noninvasive manner, and to detect any changes in tumor and body in a sensitive manner. Therefore, the majority of co-clinical trials for cancer drug development have used medical imaging (Nardella et al. 2011; Chen et al. 2012; Lunardi et al. 2013; Kwong et al. 2015).

Like clinical trial imaging, preclinical trial imaging also requires standards in imaging acquisition, reconstruction, display, data management, and interpretation. To establish these standards, the NCI established the Co-clinical Imaging Research Resource Program (assessed at https://nciphub.org/groups/cirphub) in 2015 to promote the development of quantitative imaging resources for co-clinical trials. Its mission is "to advance the practice of precision medicine by establishing consensus-based best practices for co-clinical imaging and developing optimized state-of-the-art translational quantitative imaging methodologies in order to enable disease detection, risk stratification, and assessment/prediction of response to therapy." A multidisciplinary team should be involved, including imaging scientists, engineers, animal model specialists, and radiologists (Colen et al. 2014). Radiologists can play a critical role in animal imaging and in the bidirectional translation of imaging results between animal and human study.

In order to facilitate the co-clinical trial, a special institution that can integrate the preclinical and clinical research including infrastructure and human resources is required. In several academic

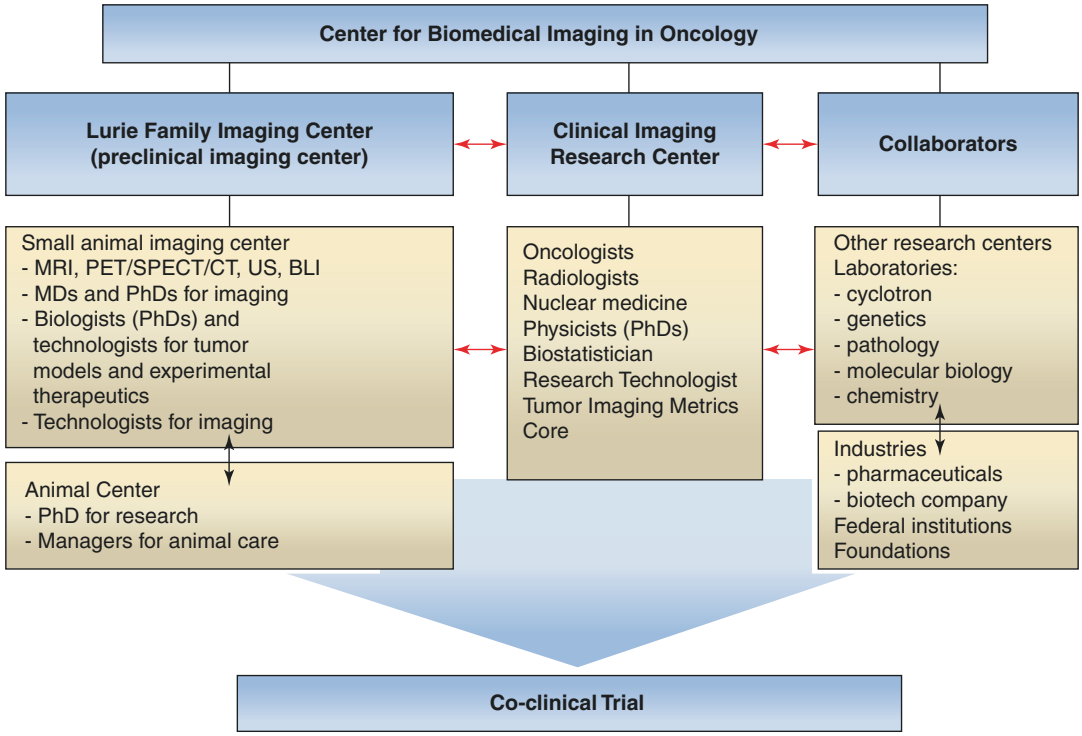

Fig. 6 Structure of the Center for Biomedical Imaging in Oncology (CBIO) in Dana-Farber/Harvard cancer center. The CBIO is composed of preclinical imaging center and clinical imaging research center, and works very closely with collaborators. These infrastructures facilitate a bidirectional translational multidisciplinary imaging researches and enable co-clinical trials

hospitals in the USA, they have both small animal imaging facilities and clinical trial centers. The co-clinical trial is possibly conducted when the small animal imaging facility and clinical trial center work together very closely. For example, Dana-Farber/Harvard cancer center established the Center for Biomedical Imaging in Oncology (CBIO), which is a seamless preclinical/clinical integrated imaging research program. This program facilitates the bidirectional translation of imaging research and imaging for cancer research and serves as a resource to basic scientists and clinical investigators by enabling translational cancer research and drug development. The CBIO might be an example of a translational multidisciplinary preclinical/clinical imaging facility which is optimized for co-clinical trial (Fig. 6). Indeed, the majority of previously reported co-clinical trials was conducted in the Dana-Farber/Harvard cancer center (Nishino et al. 2017; Nardella et al. 2011; Chen et al. 2012; Lunardi et al. 2013).

9 Conclusions

In recent years, the role of medical imaging in the drug development process from preclinical to clinical trial has greatly evolved, and it leads to rising of new research fields of clinical trial imaging and co-clinical imaging. The clinical trial imaging and co-clinical imaging are truly translational and multidisciplinary fields, requiring the participation of various academic researchers, clinicians, pharmaceutical industry, CRO, academic societies, and regulatory agencies. To derive precise results of the clinical trial using medical images, complying with a diversity of standardizations from the agencies, including FDA, NIH, and NCI, is the critical point. Without

following the compliances, the outcomes of the trial could be resulted in negative effect towards drug development due to variabilities. Therefore, we, imaging professionals, should be aware of these global trends in imaging, and study to generate better quality of imaging interpretation for future drug development.

References

Amur S, LaVange L, Zineh I, Buckman-Garner S, Woodcock J (2015) Biomarker qualification: toward a multiple stakeholder framework for biomarker development, regulatory acceptance, and utilization. Clin Pharmacol Ther 98(1):34–46

Bae H, Tsuchiya J, Okamoto T, Ito I, Sonehara Y, Nagahama F et al (2018) Standardization of [F-18] FDG PET/CT for response evaluation by the radiologic Society of North America-Quantitative Imaging Biomarker Alliance (RSNA-QIBA) profile: preliminary results from the Japan-QIBA (J-QIBA) activities for Asian international multicenter phase II trial. Jpn J Radiol 36(11):686–690

Beaumont H, Evans TL, Klifa C, Guermazi A, Hong SR, Chadjaa M et al (2018) Discrepancies of assessments in a RECIST 1.1 phase II clinical trial—association between adjudication rate and variability in images and tumors selection. Cancer Imaging 18(1):50

Biomarkers, Definitions, Working, Group (2001) Biomarkers and surrogate endpoints: preferred definitions and conceptual framework. Clin Pharmacol Ther 69(3):89–95

Chamberlain M, Junck L, Brandsma D, Soffietti R, Ruda R, Raizer J et al (2017) Leptomeningeal metastases: a RANO proposal for response criteria. Neuro-Oncology 19(4):484–492

Chen Z, Cheng K, Walton Z, Wang Y, Ebi H, Shimamura T et al (2012) A murine lung cancer co-clinical trial identifies genetic modifiers of therapeutic response. Nature 483(7391):613–617

Cheson BD, Pfistner B, Juweid ME, Gascoyne RD, Specht L, Horning SJ et al (2007) Revised response criteria for malignant lymphoma. J Clin Oncol 25(5):579–586

Cheson BD, Fisher RI, Barrington SF, Cavalli F, Schwartz LH, Zucca E et al (2014) Recommendations for initial evaluation, staging, and response assessment of Hodgkin and non-Hodgkin lymphoma: the Lugano classification. J Clin Oncol 32(27):3059–3068

Cheson BD, Ansell S, Schwartz L, Gordon LI, Advani R, Jacene HA et al (2016) Refinement of the Lugano classification lymphoma response criteria in the era of immunomodulatory therapy. Blood 128(21):2489–2496

Colen R, Foster I, Gatenby R, Giger ME, Gillies R, Gutman D et al (2014) NCI workshop report: clinical and computational requirements for correlating imaging phenotypes with genomics signatures. Transl Oncol 7(5):556–569

Damia G, D'Incalci M (2009) Contemporary preclinical development of anticancer agents—what are the optimal preclinical models? Eur J Cancer 45(16):2768–2781

Eisenhauer EA, Therasse P, Bogaerts J, Schwartz LH, Sargent D, Ford R et al (2009) New response evaluation criteria in solid tumours: revised RECIST guideline (version 1.1). Eur J Cancer (Oxford, England: 1990) 45(2):228–247

FDA-NIH Biomarker Working Group (2016) BEST (Biomarkers, EndpointS, and other Tools) Resource. Silver Spring: Food and Drug Administration. https://www.ncbi.nlm.nih.gov/books/NBK326791

Ford R, Mozley PD (2008) Report of Task Force II: best practices in the use of medical imaging techniques in clinical trials. Drug Inf J 42(5):515–523

Ford R, Schwartz L, Dancey J, Dodd LE, Eisenhauer EA, Gwyther S et al (2009) Lessons learned from independent central review. Eur J Cancer (Oxford England: 1990) 45(2):268–274

Gierada DS, Garg K, Nath H, Strollo DC, Fagerstrom RM, Ford MB (2009) CT quality assurance in the lung screening study component of the National Lung Screening Trial: implications for multicenter imaging trials. AJR Am J Roentgenol 193(2):419–424

Gillam LD, Leipsic J, Weissman NJ (2017) Use of imaging endpoints in clinical trials. JACC Cardiovasc Imaging 10(3):296–303

Grassi R, Cavaliere C, Cozzolino S, Mansi L, Cirillo S, Tedeschi G et al (2009) Small animal imaging facility: new perspectives for the radiologist. Radiol Med 114(1):152–167

Hamaoka T, Madewell JE, Podoloff DA, Hortobagyi GN, Ueno NT (2004) Bone imaging in metastatic breast cancer. J Clin Oncol 22(14):2942–2953

Kwong LN, Boland GM, Frederick DT, Helms TL, Akid AT, Miller JP et al (2015) Co-clinical assessment identifies patterns of BRAF inhibitor resistance in melanoma. J Clin Invest 125(4):1459–1470

Lin NU, Lee EQ, Aoyama H, Barani IJ, Barboriak DP, Baumert BG et al (2015) Response assessment criteria for brain metastases: proposal from the RANO group. Lancet Oncol 16(6):e270–e278

Lunardi A, Ala U, Epping MT, Salmena L, Clohessy JG, Webster KA et al (2013) A co-clinical approach identifies mechanisms and potential therapies for androgen deprivation resistance in prostate cancer. Nat Genet 45(7):747–755

Macdonald DR, Cascino TL, Schold SC Jr, Cairncross JG (1990) Response criteria for phase II studies of supratentorial malignant glioma. J Clin Oncol 8(7):1277–1280

Meignan M, Gallamini A, Meignan M, Gallamini A, Haioun C (2009) Report on the first international workshop on interim-PET-scan in lymphoma. Leuk Lymphoma 50(8):1257–1260

Murphy P, Koh DM (2010) Imaging in clinical trials. Cancer Imaging. 10(Spec no A):S74–S82

Nakahara T, Daisaki H, Yamamoto Y, Iimori T, Miyagawa K, Okamoto T et al (2017) Use of a digital phantom developed by QIBA for harmonizing SUVs obtained from the state-of-the-art SPECT/CT systems: a multicenter study. EJNMMI Res 7(1):53

Nardella C, Lunardi A, Patnaik A, Cantley LC, Pandolfi PP (2011) The APL paradigm and the "co-clinical trial" project. Cancer Discov 1(2):108–116

Nishino M, Sacher AG, Gandhi L, Chen Z, Akbay E, Fedorov A et al (2017) Co-clinical quantitative tumor volume imaging in ALK-rearranged NSCLC treated with crizotinib. Eur J Radiol 88:15–20

O'Connor JP, Jackson A, Parker GJ, Roberts C, Jayson GC (2012) Dynamic contrast-enhanced MRI in clinical trials of antivascular therapies. Nat Rev Clin Oncol 9(3):167–177

O'Connor JPB, Aboagye EO, Adams JE, Aerts HJWL, Barrington SF, Beer AJ et al (2016) Imaging biomarker roadmap for cancer studies. Nat Rev Clin Oncol 14:169

Okada H, Weller M, Huang R, Finocchiaro G, Gilbert MR, Wick W et al (2015) Immunotherapy response assessment in neuro-oncology: a report of the RANO working group. Lancet Oncol 16(15):e534–ee42

Scher HI, Halabi S, Tannock I, Morris M, Sternberg CN, Carducci MA et al (2008) Design and end points of clinical trials for patients with progressive prostate cancer and castrate levels of testosterone: recommendations of the Prostate Cancer Clinical Trials Working Group. J Clin Oncol 26(7):1148–1159

Seymour L, Bogaerts J, Perrone A, Ford R, Schwartz LH, Mandrekar S et al (2017) iRECIST: guidelines for response criteria for use in trials testing immunotherapeutics. Lancet Oncol 18(3):e143–ee52

Shankar LK (2012) The clinical evaluation of novel imaging methods for cancer management. Nat Rev Clin Oncol 9:738

Shukla-Dave A, Obuchowski NA, Chenevert TL, Jambawalikar S, Schwartz LH, Malyarenko D et al (2019) Quantitative imaging biomarkers alliance (QIBA) recommendations for improved precision of DWI and DCE-MRI derived biomarkers in multicenter oncology trials. J Magn Reson Imaging 49(7):e101–e121

Suh CH, Kim KW, Park SH, Lee SS, Kim HS, Tirumani SH et al (2018) Shear wave elastography as a quantitative biomarker of clinically significant portal hypertension: a systematic review and meta-analysis. AJR Am J Roentgenol 210(5):W185–WW95

Sullivan DC, Obuchowski NA, Kessler LG, Raunig DL, Gatsonis C, Huang EP et al (2015) Metrology standards for quantitative imaging biomarkers. Radiology 277(3):813–825

Therasse P, Arbuck SG, Eisenhauer EA, Wanders J, Kaplan RS, Rubinstein L et al (2000) New guidelines to evaluate the response to treatment in solid tumors. J Natl Cancer Inst 92(3):205–216

U.S. Department of Health and Human Services FDA (2014) Providing regulatory submissions in electronic format—standardized study data guidance for industry

US Food and Drug Administration (2018) Clinical trial imaging endpoint process standards guidance for industry

Wahl RL, Jacene H, Kasamon Y, Lodge MA (2009) From RECIST to PERCIST: evolving considerations for PET response criteria in solid tumors. J Nucl Med 50(Suppl 1):122S–150S

Wen PY, Macdonald DR, Reardon DA, Cloughesy TF, Sorensen AG, Galanis E et al (2010) Updated response assessment criteria for high-grade gliomas: response assessment in neuro-oncology working group. J Clin Oncol 28(11):1963–1972

Yankeelov TE, Mankoff DA, Schwartz LH, Lieberman FS, Buatti JM, Mountz JM et al (2016) Quantitative imaging in cancer clinical trials. Clin Cancer Res 22(2):284–290

Young H, Baum R, Cremerius U, Herholz K, Hoekstra O, Lammertsma AA et al (1999) Measurement of clinical and subclinical tumour response using [18F]-fluorodeoxyglucose and positron emission tomography: review and 1999 EORTC recommendations. Eur J Cancer 35(13):1773–1782

Molecular and Functional Imaging in Oncology Therapy Response

Katherine A. Zukotynski, Phillip H. Kuo, Chun K. Kim, and Rathan M. Subramaniam

Contents

K. A. Zukotynski (✉)
Departments of Medicine and Radiology, McMaster University, Hamilton, ON, Canada
e-mail: katherine.zukotynski@utoronto.ca

P. H. Kuo
Departments of Medical Imaging, Medicine, and Biomedical Engineering, University of Arizona, Tucson, AZ, USA
e-mail: pkuo@radiology.arizona.edu

C. K. Kim
Hanyang University College of Medicine, Seoul, South Korea
e-mail: chunkikim@hanyang.ac.kr

R. M. Subramaniam
Radiology, UT Southwestern Medical Center, Dallas, TX, USA
e-mail: Rathan.Subramaniam@UTSouthwestern.edu

Abstract

Molecular and functional imaging aims to assess oncologic therapy response by integrating molecular and functional tumor biology in order to assess therapeutic efficacy and improve patient outcome. Most oncologic processes reflect heterogeneous disease both functionally and morphologically. Further, clonal proliferations of cells may evolve with time becoming resistant to specific therapies. It is important to identify those cancer patients who derive benefit from therapy, such that expensive, toxic, or futile treatment is avoided in those who will not respond. The ultimate goal is to offer the right treatment to the right patient over time. Molecular and functional imaging either using positron emission tomography (PET) or gamma cameras often through hybrid scanners that also include computed tomography (CT) and/or magnetic resonance imaging (MRI) are sensitive techniques with a major role in the precision medicine algorithm

M. Nishino (ed.), *Therapy Response Imaging in Oncology*, Medical Radiology, Diagnostic Imaging,
https://doi.org/10.1007/978-3-030-31171-1_15

of oncology patients. These modalities provide insight prior to, during, and following therapy. Further, they often serve as a biomarker of tumoral heterogeneity helping to direct the selection of appropriate treatment, and detect early response to therapy. Also, molecular and functional imaging is a powerful prognostic biomarker in oncology that can suggest patient outcome based on treatment response.

1 Introduction

Cancer is a spectrum of disease that is morphologically and functionally heterogeneous. Further, the genetic profile of the disease can evolve with time leading to the development of resistance, and this evolution is not uniform throughout the body. Although localized disease may be cured following resection, metastatic disease is a leading cause of cancer-related death. Over the past few years, several new therapies have become available for oncology patients. Today, there is a suite of therapies available including surgery, radiation, chemotherapy, immunotherapy, and radionuclide therapy, among others. Further, technological advances have led to the creation of hybrid scanners such as positron emission tomography (PET)/ computed tomography (CT), single photon computed tomography(SPECT)/CT, and PET/magnetic resonance imaging (MRI). These scanners noninvasively assess morphological and functional tumor heterogeneity throughout the body, evaluate disease extent and biologic behavior before and after therapy, and identify sites of disease that are developing resistance. Multi-modality imaging is helpful, not only for staging but also to suggest the most appropriate ongoing therapy at a metabolic-molecular level. Understanding the genetic underpinnings and imaging signature of cancer is key if we wish to develop treatment algorithms that use the most effective therapy tailored to individual patients while limiting futile, toxic treatment.

2 A Bird's Eye View of Radiopharmaceuticals

There are many radionuclides, such as ^{99m}Tc, ^{111}In, ^{123}I, ^{131}I, ^{18}F, ^{11}C, ^{68}Ga, ^{64}Cu, and ^{89}Zr, among others, that can be used to label pharmaceuticals and create radiopharmaceuticals. Once all legal requirements and regulatory issues have been met (Schwarz et al. 2019), these radiopharmaceuticals can be administered to patients and the patients can be imaged to determine functional and molecular information. Radiopharmaceuticals labeled with positron-emitting radionuclides are imaged with PET, while those labeled with single photon-emitting radionuclides are typically imaged using gamma cameras with SPECT capability. Malignant cells often demonstrate increased glucose metabolism compared with normal tissue (Warburg et al. 1927; Warburg 1956), and ^{18}F-labeled 2-fluoro-2-deoxy-D-glucose (^{18}F-FDG), a radioactive glucose analogue that decays by positron emission, is the most ubiquitous PET radiopharmaceutical used in oncology today. Since glucose metabolism changes faster than tumor size, ^{18}F-FDG PET often shows therapy response much earlier than anatomic imaging with CT or MRI. Of course, it is important to recall that the intensity of ^{18}F-FDG uptake is affected by several factors including cellular histology, density, aggressiveness, and technical parameters, among others. Thus, imaging should be performed with standardized techniques, and evaluated in the correct clinical context. There are many radiopharmaceuticals used in oncology, often designed to target a cellular process, metabolism, receptor, or cell trafficking. For example: 3′-deoxy-3′-[^{18}F] fluorothymidine (FLT) is used to study proliferation by imaging the DNA salvage pathway, [^{18}F] fluoromisonidazole(1-(2-nitroimidazolyl)-2-hydroxy-3-fluoropropane (FMISO) and [^{18}F]fluoroazomycin arabinofuranoside (FAZA) are used to assess tumor hypoxia, and O-[^{18}F]fluoromethyl-L-tyrosine (FMT) is used to study amino acid transport. The idea is that through the use of different PET radiopharmaceuticals, imaging signatures will detail disease phenotype, genotype, and heterogeneity (Gerbaudo and Garcia 2016).

What is becoming evident is that more than one biomarker may be needed to determine the effectiveness of therapy and for the assessment of treatment response.

3 Functional and Molecular Imaging for Therapy Assessment in Oncology

Functional and molecular imaging has been used in therapy assessment for many years. Two examples are: (1) ^{99m}Tc-labeled methylene diphosphonate (^{99m}Tc-MDP) bone scans to assess response across a spectrum of oncologic disease and therapies (Fig. 1) (Scher et al. 2016) and (2) Iodine (^{123}I or ^{131}I) labeled metaiodobenzylguanidine (MIBG) in neuroblastoma (Fig. 2) (Ady et al. 1995). Depending on the radionuclide chosen and the amount of activity administered, radiolabeled MIBG can serve as an imaging agent and/or a therapeutic agent. For imaging, ^{123}I is preferred because of the shorter half-life, ideal gamma photon energy (159 keV), lack of beta emission, and lower radiation dose to the patient; however, access may be limited and expense is higher. For therapy, ^{131}I is required. In general, planar imaging is standard of care. The addition of SPECT increases the contrast of the planar scintigraphic images, thus providing improved functional information. The CT portion of the SPECT/CT, if performed, provides improved anatomical information by pinpointing the location of the abnormal activity seen on the SPECT images. Therefore, the addition of SPECT/CT usually provides a more accurate diagnosis than planar imaging alone. However, due to the increased time of acquisition and image interpretation as well as the radiation exposure from the CT component of the study, SPECT/CT is often done as needed on an ad hoc basis.

When interpreting functional and molecular imaging, it is important to recall the underlying mechanism that leads to the imaging obtained. On ^{99m}Tc-MDP bone scans, radiopharmaceutical uptake correlates with increased osteoblastic activity and findings suggestive of osseous disease reflect bone reaction to malignant cells, not the presence of the malignant cells themselves. Osteoblastic activity from healing following therapy is difficult to distinguish from progressive metastatic disease, confounding image interpretation. The flare phenomenon is

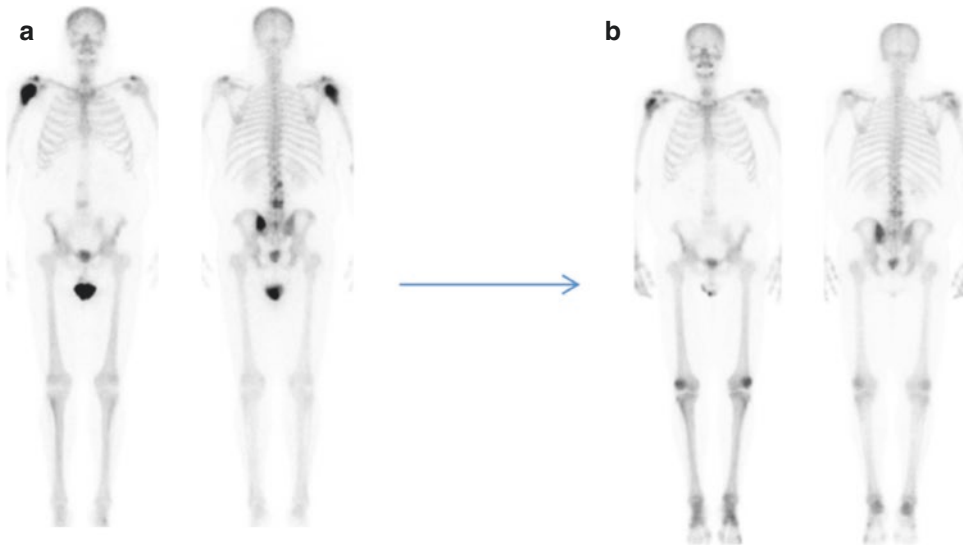

Fig. 1 Whole body planar ^{99m}Tc-MDP bone scan images in a man with symptomatic castration resistant prostate cancer bone metastases obtained prior to (**a**) and following (**b**) therapy with $^{223}RaCl_2$ show decrease in intensity of osseous disease in the right proximal humerus, lumbar spine, and left iliac bone following therapy

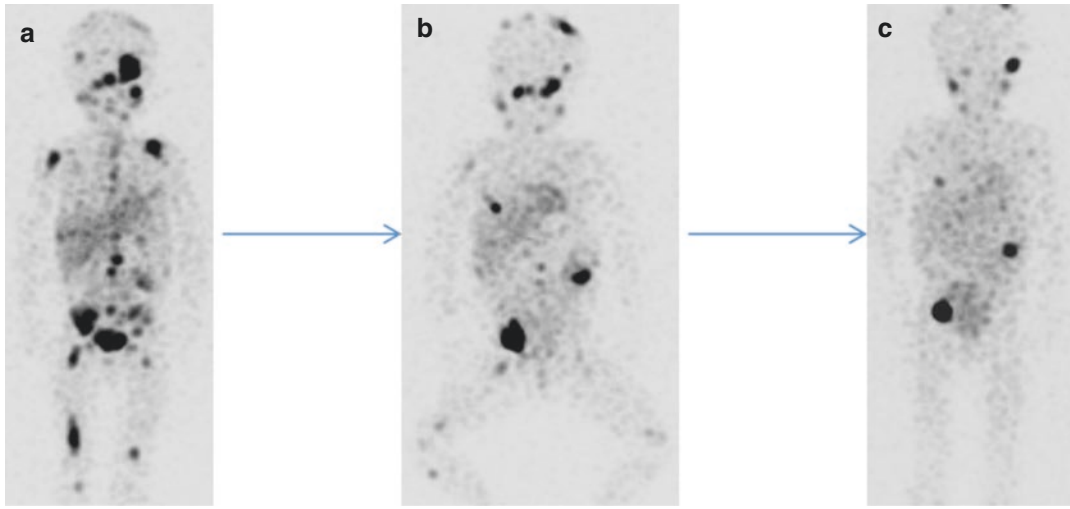

Fig. 2 Whole body planar ^{131}I-MIBG images in a child with metastatic neuroblastoma prior to (**a**), during (**b**) and following (**c**) therapy show multifocal disease that is decreasing in intensity and extent with therapy consistent with response

defined as apparent "disease progression" occurring until approximately 3 months of therapy due to increased lesion intensity or number in the context of improved clinical findings and stability or improvement of bone scan findings on repeat bone scan after 6 months of therapy (Cook et al. 2011; Pollen et al. 1984; Coleman et al. 1988). Also, it is challenging to accurately quantify the burden of osseous metastatic disease on ^{99m}Tc-MDP bone scans. Larson et al. proposed the Bone Scan Index (BSI) as a method to measure total skeletal disease by summing the product of the weight and fractional involvement of each of 158 individual bones, where each bone is expressed as a percentage of the entire skeleton (Dennis et al. 2012). However, this is time consuming and rarely used in clinical practice. Quantitative analysis is easier with PET, and ^{18}F-labeled sodium fluoride (^{18}F-NaF) is a high-affinity bone-seeking agent with higher affinity for osteoblastic activity and superior imaging characteristics than ^{99m}Tc-MDP (Grant et al. 2008). Even-Sapir et al. compared MDP bone scans and ^{18}F-NaF PET/CT in patients with localized high-risk or metastatic prostate cancer and found the sensitivity and specificity of ^{99m}Tc-MDP planar bone scans was 70% and 57%, respectively, whereas for ^{18}F-NaF PET/CT it was 100% and 100%, respectively (Even-Sapir et al. 2006). Similar to ^{99m}Tc-MDP bone scans, ^{18}F-NaF PET/CT detects bone turnover, not malignant cells themselves, and thus generate an indirect marker of osseous malignancy. ^{18}F-FDG is used to image glucose metabolism and has been compared with ^{18}F-NaF in the evaluation of therapy response, for example, in men with prostate cancer. ^{18}F-FDG is taken up at sites of disease, while ^{18}F-NaF is taken up at sites of osteoblastic reaction to the disease (Fig. 3). However, ^{18}F-FDG uptake is variable and may be low at sites of specific cancer histology. Recently, there has been growing interest in radiopharmaceuticals targeting the prostate-specific membrane antigen (PSMA), a cell surface transmembrane glycoprotein that is overexpressed on prostate cancer cells (Bouchelouche et al. 2010; Evans et al. 2011; Barrett et al. 2013). This has potential for detection of disease, therapy planning as well as for the assessment of therapy response (Rowe et al. 2016; Koerber et al. 2018; Emmett et al. 2018). Early results suggest response assessment may

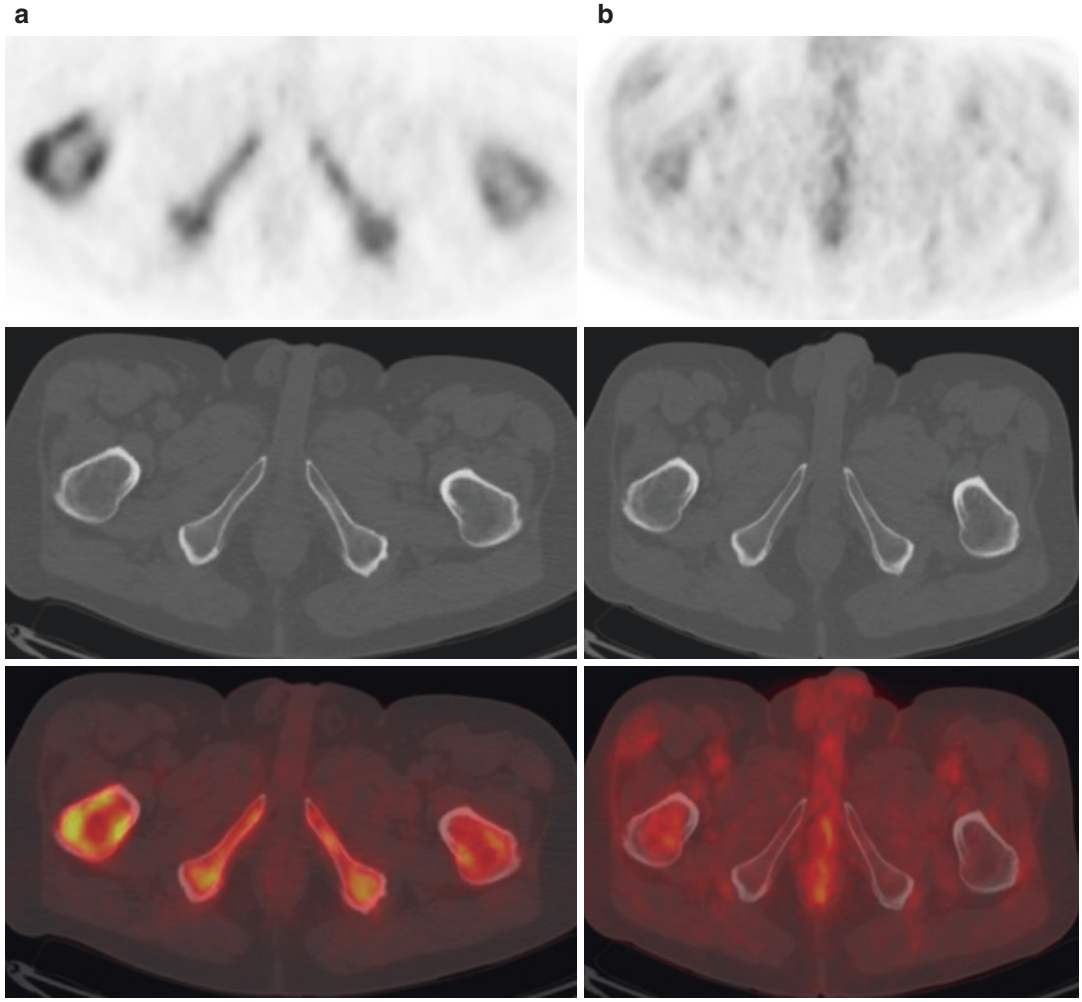

Fig. 3 Mechanism of radiopharmaceutical uptake. Axial PET, CT, and fused PET/CT images from an ^{18}F-NaF PET/CT shows radiotracer uptake at the periphery of a site of prostate cancer due to osteoblastic turnover (**a**), while axial PET, CT, and fused PET/CT images from an ^{18}F-FDG PET/CT show subtle radiotracer uptake within the tumor, likely involving the bone marrow (**b**)

be confounded by flare (Zacho and Petersen 2018; Zukotynski et al. 2018) and mixed interval change following therapy. Also, not all sites of disease show uptake of PSMA targeting radiopharmaceuticals, and the most helpful radiopharmaceutical to assess therapy response may be case specific (Figs. 4 and 5).

There are numerous cell-surface receptors involved in cell-signaling pathways and radiopharmaceuticals targeting cell receptors have become powerful imaging and therapy tools. The somatostatin receptor (SSTR)-binding radiopharmaceutical [^{68}Ga-DOTA^{0},Tyr^{3}] octreotate (^{68}Ga-DOTATATE) and peptide receptor radionuclide therapy (PRRT) with SSTR-binding peptide [^{177}Lu-DOTA^{0},Tyr^{3}] octreotate (^{177}Lu-DOTATATE) have been used to image and treat neuroendocrine disease, respectively (Figs. 6 and 7). Since radiopharmaceutical uptake is affected by tumor heterogeneity, volumes of interest obtained from imaging done prior to therapy can be used to compute the fraction of administered radiopharmaceutical sequestered in normal parenchyma as well as at sites of

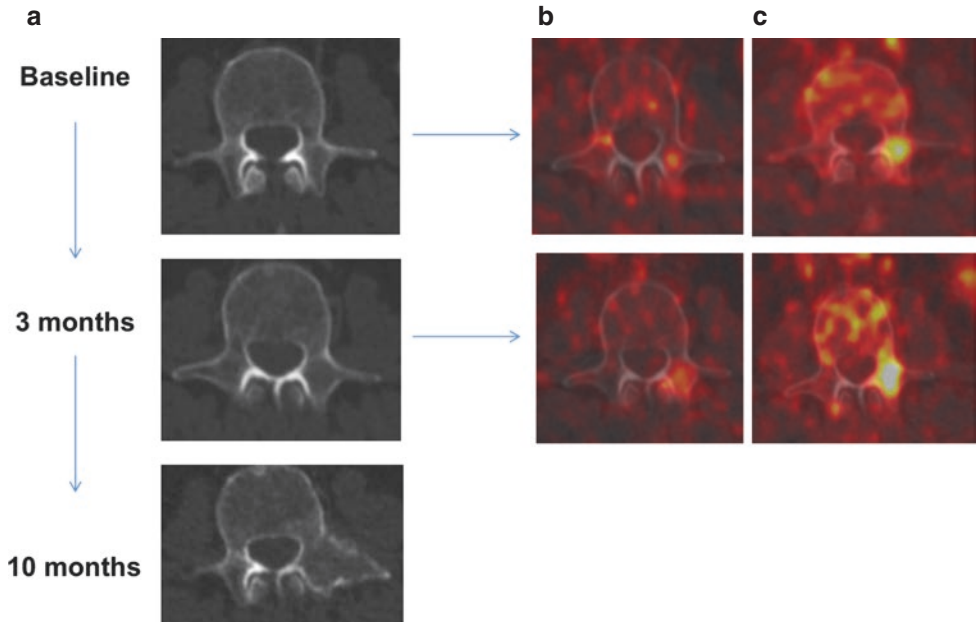

Fig. 4 More than one radiopharmaceutical may be helpful to assess therapy response in oncology. Change in radiopharmaceutical uptake is more pronounced on the ^{18}F-FDG PET/CT than on ^{18}F-DCFPyL PET/CT at a site of lytic metastatic prostate cancer. Axial CT at baseline, 3 months and 10 months of therapy (**a**), axial fused ^{18}F-DCFPyL PET/CT (**b**) and ^{18}F-FDG PET/CT (**c**) at baseline and 3 months of therapy

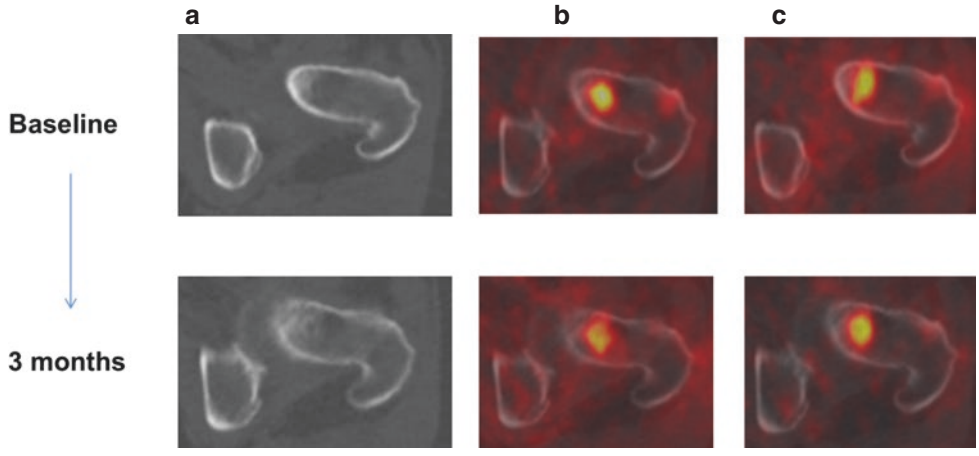

Fig. 5 More than one radiopharmaceutical may be helpful to assess therapy response in oncology. Change in radiopharmaceutical uptake is more pronounced on ^{18}F-DCFPyL PET/CT than on ^{18}F-FDG PET/CT at a site of lytic metastatic prostate cancer. Axial CT images at baseline and 3 months of therapy (**a**), axial fused ^{18}F-DCFPyL PET/CT (**b**) and ^{18}F-FDG PET/CT (**c**) images at baseline and 3 months of therapy

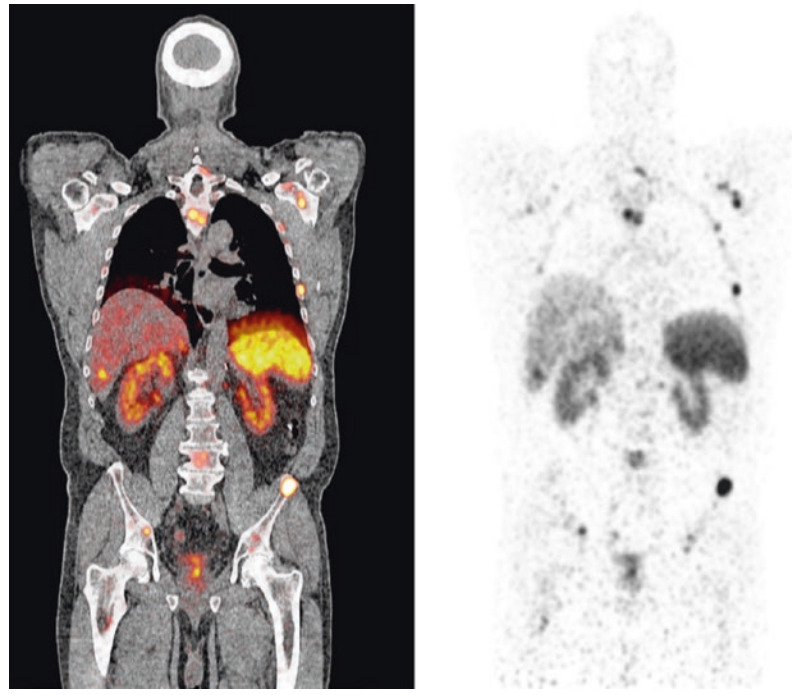

Fig. 6 Coronal fused and PET images from a ^{68}Ga-DOTATATE PET/CT show multifocal osseous and soft tissue disease prior to ^{177}Lu-DOTATATE therapy

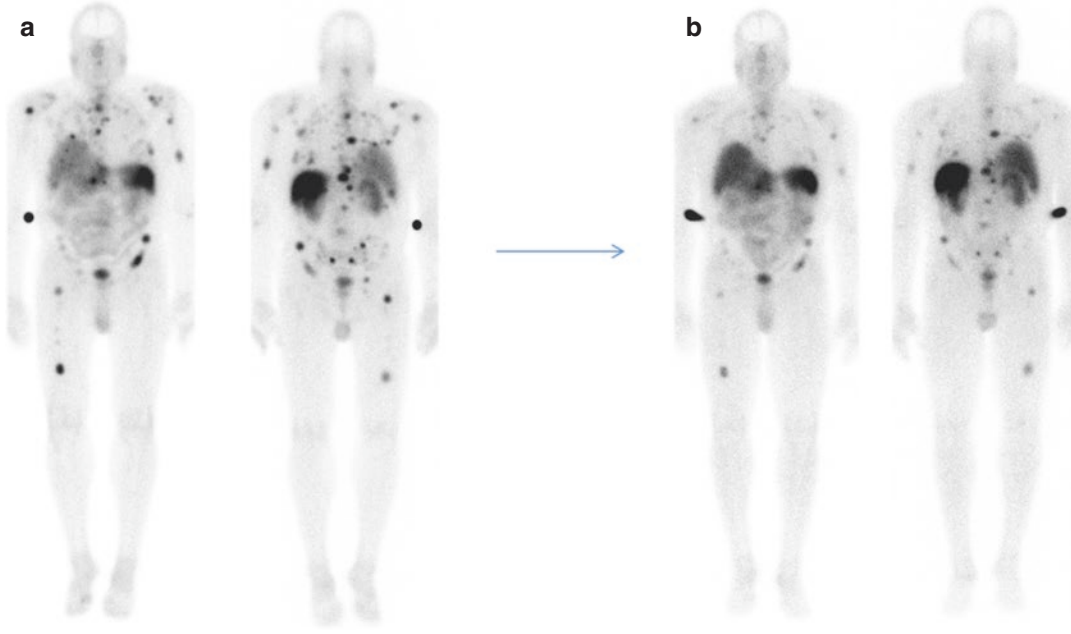

Fig. 7 Whole body planar images of the subject from Fig. 6 show multifocal osseous and soft tissue disease immediately following cycle 1 (**a**) and cycle 2 (**b**) of ^{177}Lu-DOTATATE therapy with interval decrease in intensity and extent of radiopharmaceutical uptake at sites of disease following therapy

disease (Beauregard et al. 2012). This can then be used to adjust the amount of administered therapeutic radiopharmaceutical to minimize toxicity while maximizing patient benefit.

4 Prognostic Value of Functional and Molecular Imaging Oncologic Imaging Response

Molecular and functional imaging response assessment has been studied across the spectrum of oncologic disease. Since metabolic and pathophysiological changes often precede alterations in morphology, PET is helpful to assess response to cytotoxic and cytostatic therapy and often predicts response before morphologic imaging (i.e., CT and MRI). In general, the earlier the response, the better the progression-free survival (PFS) and overall survival (OS) of the oncology patient. Thus, there is a concept of prognostic value of the reduction in FDG uptake related to treatment. For example, Weber et al. showed that in stage IIIB and IV non-small cell lung cancer (NSCLC), a reduction in tumor FDG uptake of more than 20% after one cycle of platinum-based chemotherapy was predictive of long-term survival (Weber et al. 2003). Vansteenkiste et al. found that in stage IIIA-N2 NSCLC, a reduction in tumor uptake by more than 50% on FDG-PET after 3 cycles of neoadjuvant chemotherapy was predictive of longer survival (Vansteenkiste et al. 2004). Hoekstra et al. reported that in stage IIIA-N2 NSCLC, a 35% reduction in tumor FDG uptake after one cycle of induction therapy showed prolonged overall survival (Hoekstra et al. 2005). MacManus and colleagues showed that tumor metabolic response predicts outcome following radiation therapy (Mac Manus et al. 2005). Complete metabolic responders had a 1-year survival rate of 93% compared to 47% for nonresponders, and 2-year survival rate of 62% versus 30%, respectively. Although imaging patients 3–4 months after radiotherapy minimizes false-positive FDG uptake in radiation-induced inflammation, a shorter time frame may be acceptable in certain cases (Hicks et al. 2004).

5 The Development of Molecular and Functional Therapy Response Assessment Criteria

Determining the effectiveness of cancer therapy requires a standardized, reproducible, and objective method for evaluating therapy response. Over the years several efforts were made to meet this clinical need resulting in the creation of multiple guidelines. The history of therapy response assessment in oncology is complex. As imaging techniques developed, so too did criteria for therapy response assessment. Morphologic imaging therapy response assessment criteria such as Response Evaluation Criteria In Solid Tumors (RECIST 1.1 (Eisenhauer et al. 2009)) are effective to monitor cytolytic therapy effect, in which clinical efficacy typically translates into tumor mass reduction. However, targeted cytostatic therapies (e.g., tyrosine kinase inhibitors such as erlotinib and gefitinib) primarily slow or stop tumor cell proliferation and may not result in a significant change in tumor mass, limiting size-based criteria for therapy response assessment. Initial ^{18}F-FDG-PET studies showed that successful response to erlotinib and gefitinib could be predicted within days of therapy (Sunaga et al. 2008; Takahashi et al. 2012). Also, metabolic treatment response was linked with survival and quality of life (Sunaga et al. 2008; Takahashi et al. 2012; van Gool et al. 2014a, b; Benz et al. 2011; Hachemi et al. 2014).

In 1999, the European Organization for Research and Treatment of Cancer (EORTC) published criteria for tumor response classification which were among the first to include the assessment of tumor metabolism using functional imaging with FDG PET (Young et al. 1999). These criteria used the standardized uptake value (SUV) as a metric for quantifying radiopharmaceutical uptake at sites of disease, a metric that reflects radiopharmaceutical uptake corrected for total body mass (patient weight) and injected radiopharmaceutical activity. According to EORTC criteria: (1) A complete metabolic response (CMR) was when there was no site of

disease distinguishable from adjacent background activity; (2) progressive metabolic disease (PMD) was an increase in maximum SUV (SUVmax) of 25% or more from baseline or the appearance of new disease sites; (3) a partial metabolic response (PMR) was a reduction in SUVmax between 15 and 25% after one or more cycles of chemotherapy; and (4) stable metabolic disease (SMD) was disease response that could not be classified into another category. The number of lesions to measure and minimum measurable lesion activity was not defined. Anatomic information was not included.

In 2009, Wahl et al. proposed Positron Emission Tomography Response Criteria In Solid Tumors (PERCIST) for FDG PET (Wahl et al. 2009). Main differences between EORTC and PERCIST were (Table 1, Aide et al. 2018): (1) use of SULpeak (radiopharmaceutical activity measured in a 1 cm^3 sphere at the site of highest tumor activity corrected for lean body mass) rather than SUVmax, (2) specification of five sites of disease (up to two per organ) or *target lesions* to be measured, and (3) definition of a measurable lesion as having at least 1.5 times the mean SUL of liver.

With the advent of standardized criteria for molecular and functional imaging therapy response assessment, debate flourished concerning the value of using a qualitative (visual) versus a quantitative (objective) approach. A study by Lin et al. comparing qualitative and quantitative FDG PET analysis in patients with diffuse large B cell lymphoma DLBCL (Lin et al. 2007) found the qualitative analysis predicted event-free survival with an accuracy of 65.2%, whereas the quantitative SUV-based analysis had an accuracy of 76.1%. However, quantitative analyses have limitations: (1) There are several methods for calculating and reporting radiopharmaceutical uptake at disease sites e.g., correcting for total body mass versus lean body mass, reporting maximal activity (SUVmax) versus average activity in a defined region (SUVpeak, SUVmean), use of metabolically active tumor bulk defined by indices of metabolic tumor volume (MTV) and total lesion glycolysis (TLG) as well as tumor metabolic heterogeneity estimated through texture analysis, among others. (2) Differences in scanner hardware, image reconstruction, and patient characteristics, among other factors, affect radiopharmaceutical uptake at disease sites and can impact metrics of response assessment (Ziai et al. 2016).

In an effort to achieve repeatability and reproducibility of response assessment metrics, guidelines were produced detailing how oncologic PET/CT scans should be performed (Boellaard et al. 2015; Fendler et al. 2017). Recommendations include the use of a standardized protocol for scan acquisition and maintenance of consistency between scanners, image acquisition and reconstruction parameters, dose of radiopharmaceutical administered and uptake time between baseline and follow-up imaging, among others. Also phantom derived parameters may help align quantification metrics between scanners and image reconstructions (Lasnon et al. 2013, 2017; Quak et al. 2016). Finally, inclusion of activity in a reference region of interest (ROI) such as liver or aortic blood pool is suggested in an oncologic PET/CT report to serve as an alert for potential technical issues if/when this is outside the expected range.

Currently, therapy response assessment criteria often include a combination of anatomic, molecular, and functional imaging. There are criteria for response assessment that are used in clinical trials and are not specific to cancer histology. In most cases there are no clinical guidelines or standards directing the use of these measurements in patient care and these criteria (such as PERCIST) are rarely used in routine clinical practice. A few criteria for molecular and functional disease response classification are specific to cancer histology (e.g., Deauville/Lugano). These criteria are incorporated into clinical guidelines (e.g., NCCN [National Comprehensive Cancer Network]) and included in clinical PET/CT reporting. Although the clinical and research communities remain fragmented in their use of molecular and functional imaging therapy response assessment criteria, there is momentum

Table 1 Comparison of different molecular and functional imaging response assessment criteria

Response	European Organisation for Research and Treatment of Cancer (EORTC)[a]	PET Response Criteria in Solid Tumors (PERCIST)[b]	PET/CT Criteria for Early Prediction of Response to Immune Checkpoint Inhibitor Therapy (combines RECIST 1.1 and PERCIST) (PECRIT)[c]			PET Response Evaluation Criteria for Immunotherapy (PERCIMT)[d]	
Complete response (CR)	Complete resolution of FDG uptake	Disappearance of all metabolically active tumors	RECIST 1.1 (disappearance of all target lesions; reduction in short axis of target lymph nodes to <1 cm; no new lesions)		Clinical benefit	Complete resolution of all preexisting ^{18}F-FDG-avid lesions; no new ^{18}F-FDG-avid lesions	Clinical benefit
Partial response (PR)	Minimum reduction of ±15–25% in tumor SUV after one cycle of chemotherapy, and >25% after more than one treatment cycle	Decline in SULpeak by 0.8 unit (>30%) between the most intense lesion before treatment and the most intense lesion after treatment	RECIST 1.1 (decrease in target lesion diameter sum ≥30%)		Clinical benefit	Complete resolution of some preexisting ^{18}F-FDG-avid lesions. No new, ^{18}F-FDG avid lesions	Clinical benefit
Stable disease (SD)	Increase in SUV of <25% or a decrease of less than 15%	Does not meet other criteria	Does not meet other criteria	Change in SULpeak of the hottest lesion of >15%	Clinical benefit	Neither PD nor PR/CR	Clinical benefit
				Change in SULpeak of the hottest lesion of ≤15%	No clinical benefit		
Progressive disease (PD)	Increase in tumor FDG uptake of >25%; increase in maximum tumor of >20%; new metastases	Increase in SULpeak of >30% or the appearance of a new metabolically active lesion	RECIST 1.1 (increase in target lesion diameter sum of ≥20% and at least 5 mm or new lesions)		No clinical benefit	Four or more new lesions of <1 cm in functional diameter or three or more new lesions of >1.0 cm in functional diameter or two or more new lesions of more than 1.5 cm in functional diameter	No clinical benefit

Content based on Table 1 from Aide et al. (2018)

SUV standardized uptake value and *SUL* SUV normalized by lean body mass

[a]Measurable lesions: the most FDG-avid lesions in terms of SUVs normalized by body surface area. New lesions: as progressive disease. Number of lesions: not specified

[b]Measurable lesions: minimum tumor SUL 1.5 times the mean SUL of the liver. New lesions: as progressive disease. Number of lesions: changes in the sum of up to five lesions as secondary measure to assess response

[c]Measurable lesions: RECIST 1.1 (1 cm on CT; longest diameter, except in lymph nodes); PERCIST (minimum tumor SUL 1.5 times the mean SUL of the liver). New lesions: as progressive disease. Number of lesions: RECIST 1.1 (up to five, maximum two per organ); PERCIST (changes in the sum of up to five lesions as secondary measure to assess response)

[d]Measurable lesions: FDG-avid lesions considered with regard to their absolute number and functional size (>1.0 cm or >1.5 cm) measured in centimeters on the fused PET/CT images. New lesions: as progressive disease, based on number and functional diameter. Number of lesions: up to five target lesions per patient before and after treatment

to converge on a common approach for the purposes of PET/CT reporting and the most illustrative example of this is lymphoma.

6 Molecular and Functional Imaging Response Assessment in Lymphoma

Lymphoma is a heterogeneous spectrum of lymphoproliferative disease classified as Hodgkin's lymphoma (HL) or non-Hodgkin's lymphoma (NHL) that encompasses a spectrum of disease of variable metabolic activity. It is estimated that approximately 40% of non-Hodgkin's lymphoma patients and 20% of Hodgkin's lymphoma patients have a residual mediastinal or abdominal mass following therapy, and that most are non-malignant on pathology (Orlandi et al. 1990; Aisner and Wiernik 1982; Mikhaeel et al. 2000). It is difficult to distinguish inflammatory, necrotic, or fibrotic tissue from residual lymphoma based on anatomic evaluation alone (Canellos 1988; Reske 2003; Lewis et al. 1982; Surbone et al. 1988). Molecular and functional imaging with PET can distinguish metabolically active from non-metabolically active disease and helps overcome the limitation of anatomically based response assessment for lymphoma. Molecular and functional response criteria have been used in the evaluation of patients with lymphoma for many years.

Following a workshop held in Deauville, France, in 2009 (Meignan et al. 2009), the Deauville 5-point scoring system was created based on FDG PET, with treatment response assessed qualitatively on a 5-point scale according to the intensity of uptake at sites of disease relative to reference activity in mediastinal blood pool and liver. Scores of 3 or below (comparable to liver activity or less) are considered negative for metabolically active residual disease (Fig. 8). Scores of 4–5 (above liver activity) are considered positive for residual metabolically active disease. Several studies have shown interobserver agreement of this system. For example, Barrington

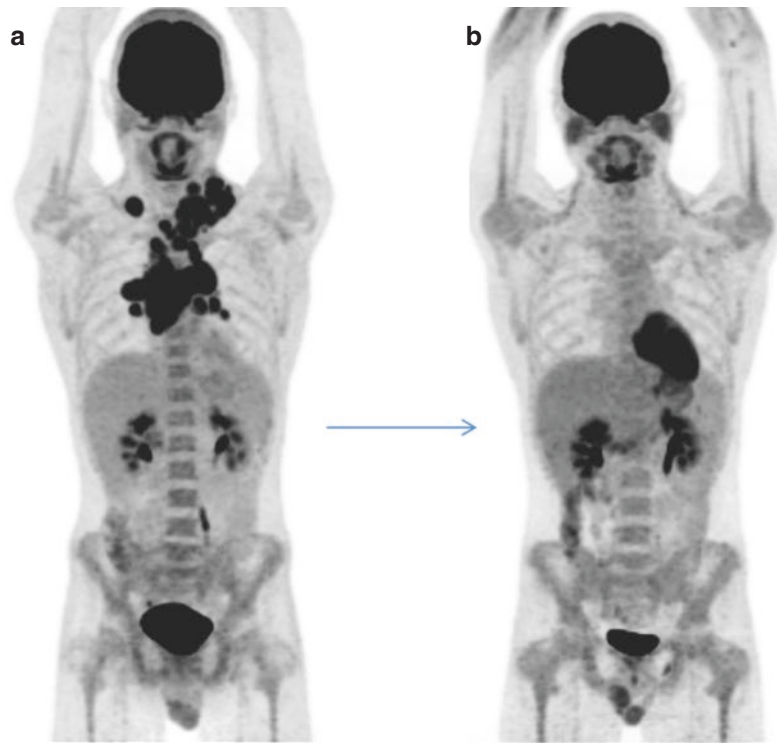

Fig. 8 Baseline ^{18}F-FDG PET/CT MIP image in a young man with Hodgkin's lymphoma shows metabolically active lymph nodes above the diaphragm (**a**). Interim ^{18}F-FDG PET/CT MIP image shows response to therapy, Deauville score 2 (**b**)

et al., Furth et al., and Gallamini et al. comparing interobserver agreement in HL reported κ values of 0.79–0.85, 0.748, and 0.69–0.84, respectively (Barrington et al. 2010; Furth et al. 2011; Gallamini et al. 2009, 2014). The system was easy to apply and was the first molecular and functional response criteria to become part of routine clinical oncologic PET/CT reporting for patients with HL (Meignan et al. 2010, 2012; Le Roux et al. 2011). In 2014, following the 12th International Conference on Malignant Lymphomas (ICML) in Lugano, Switzerland, the Lugano classification system was created (Barrington et al. 2014; Cheson et al. 2014). The Lugano classification includes both PET and CT response assessment as well as a combination of qualitative and quantitative metrics. The PET criteria are based on the Deauville 5-point scoring system, while the inclusion of CT criteria overcame the limitation of response in lymphomas with low or variable FDG avidity. Reproducibility of the Lugano classification system is being determined.

Among the advantages of a standardized response assessment in lymphoma is the predictive value and ability to modify treatment early in the disease course to improve outcome. In limited HL, the prognosis is excellent and so characterization of functional and molecular imaging therapy response on interim FDG PET/CT (typically after 2 or 4 chemotherapy cycles) has failed to distinguish between patients in terms of outcome. However, as the disease becomes more extensive, an interim positive PET suggests poorer outcome (Moghbel et al. 2017). Further, inclusion of both PET and CT response assessment typically show improved patient stratification and clinical outcome. For example, a study of interim PET and CT in HL reported 2-year PFS of 95%, 78%, 71%, and 36% with PET−/CT−, PET−/CT+, PET+/CT−, and PET+/CT+ patients, respectively (Kostakoglu et al. 2012). Further, the results of interim PET can show complications of therapy (Fig. 9) and enable early treatment modification resulting in improved outcome. For example, in a study of patients with HL and positive interim PET after 2 cycles of ABVD, escalating therapy (2 cycles of BEACOPP + involved node radiotherapy) resulted in improved PFS (90.6% versus 77.4%) (André et al. 2017).

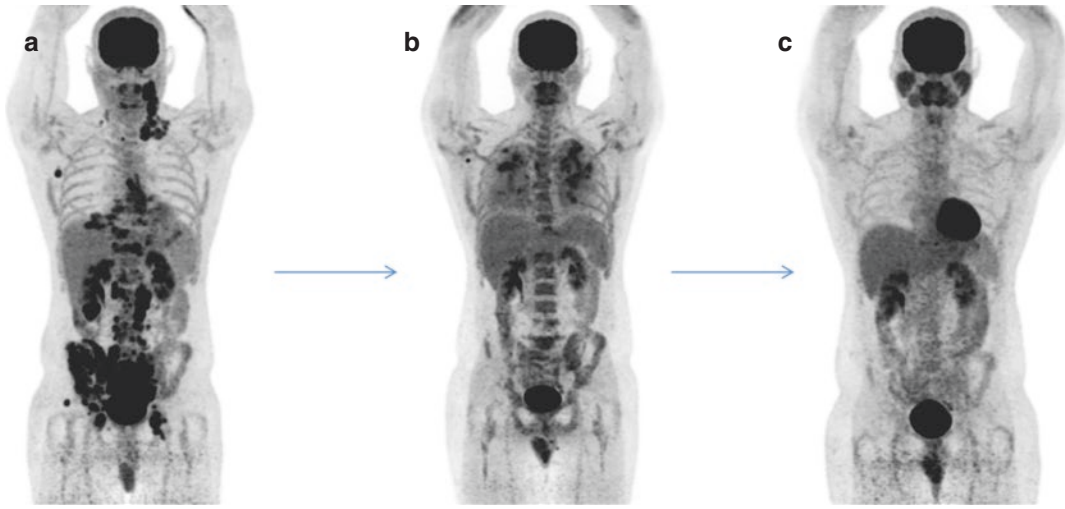

Fig. 9 Baseline ^{18}F-FDG PET/CT MIP image in a man with Hodgkin's lymphoma shows metabolically active lymph nodes above and below the diaphragm as well as osseous and right renal disease (**a**). Interim ^{18}F-FDG PET/CT MIP image shows response to therapy; however, there was development of pneumonitis likely related to drug toxicity (**b**). ^{18}F-FDG PET/CT MIP image at the completion of therapy shows response to therapy with resolution of the pneumonitis

Of course, in specific scenarios such as patients on immunotherapy, certain modifications to the criteria must be considered. In 2016, modification to the Lugano criteria (LYRIC criteria) was suggested to account for immunotherapy response assessment. The main change compared with the Lugano criteria was the addition of an indeterminate response category (Cheson et al. 2016).

7 Molecular and Functional Therapy Response Assessment and Immune Therapy

In recent years, there has been investigation into immunotherapy (Popovic et al. 2018). Today, the most ubiquitous agents include: (1) T lymphocyte-associated protein 4 (CTLA-4) inhibitors (e.g., ipilimumab) and (2) programmed cell death protein 1 (PD1) or PD1/programmed cell death protein ligand 1 (PD1/PD-L1) axis inhibitors (e.g., pembrolizumab and nivolumab). The idea is that CTLA-4 is a protein recruited to the surface of regulatory T cells where it interacts with B7 receptors on antigen-presenting cells resulting in T cell downregulation. Thus, inhibition of CTLA-4 results in enhanced T cell activation and immune response expansion. PD1 is a transmembrane glycoprotein expressed on immune cells and PD-L1 is a ligand for PD1 that may be expressed on tumor cells. When PD1 is bound by PD-L1, it inhibits kinases involved in T cell activation. Thus, inhibition of this process can also enhance immunity. Current research in the area is focused, at least in part, on blocking additional immune regulatory checkpoints, inducing immune responses with vaccines or increasing tumor traffic of lymphocytes. The literature suggests ipilimumab monotherapy results in overall benefit for about 20% of patients with melanoma (Hodi et al. 2010) and that this can be improved to over 50% using a combination of ipilimumab and nivolumab (Fig. 10), albeit with higher risk of toxicity (Larkin et al. 2015). Interestingly, radiation provides immune co-stimulatory signals, hence the rationale for combining external beam or radionuclide therapy with immunotherapy. It has been postulated that PET may noninvasively provide information of the tumor

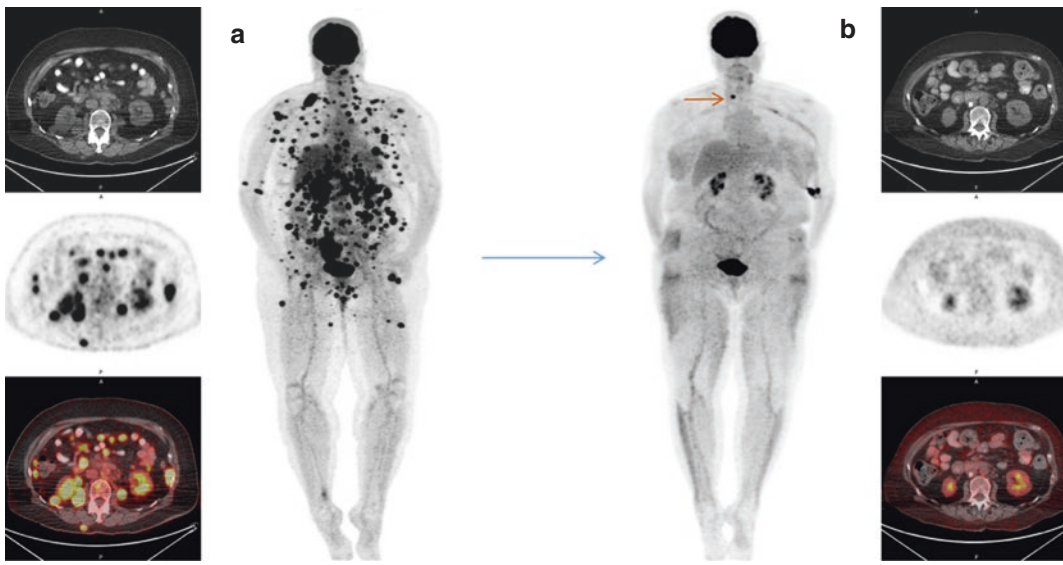

Fig. 10 ^{18}F-FDG PET/CT images in a woman with metabolically active melanoma. Axial CT, PET, fused and MIP images obtained prior to (**a**) and following (**b**) ipilimumab and nivolumab therapy show complete response. The focal radiopharmaceutical uptake in the right central neck (orange arrow) was in a thyroid nodule and likely reflects primary thyroid pathology (results of biopsy pending)

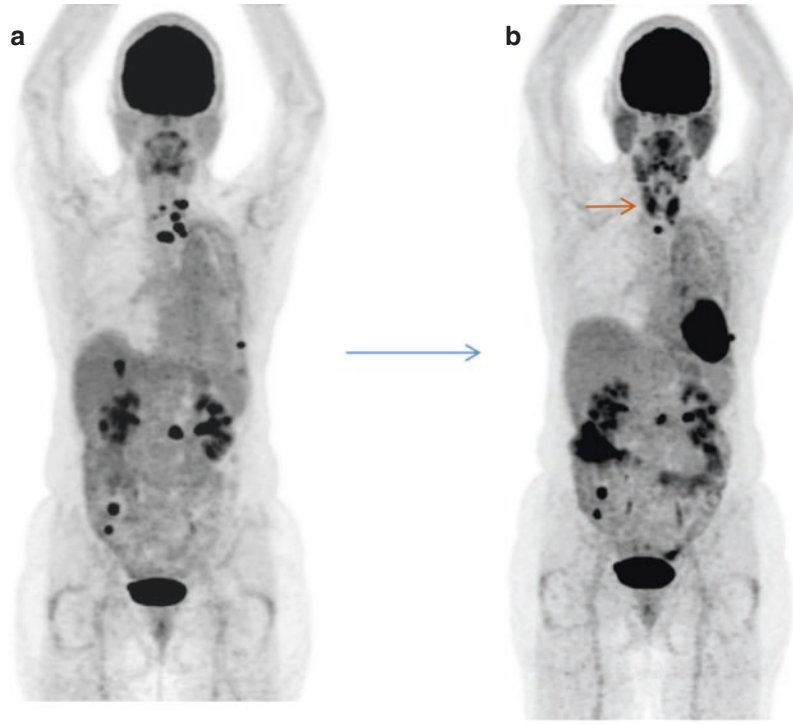

Fig. 11 ^{18}F-FDG PET/CT MIP images in a woman with chemotherapy refractory non-small cell lung cancer obtained prior to (**a**) and following (**b**) immunotherapy show partial metabolic response as well as development of thyroiditis (orange arrow)

microenvironment predictive of response; however, this remains to be rigorously proven.

By enhancing the immune response, immune-related adverse events may be induced (e.g., dermatitis (pruritus/rash/vitiligo), endocrine disorders (hypophysitis, thyroiditis, etc.), pneumonitis, gastrointestinal symptoms (diarrhea, colitis, etc.), hepatitis, pancreatitis, and myalgia among other things). Following immunotherapy, reactive splenic enlargement and reactive lymph node enlargement in the tumor drainage basin are also common. Since inflammation is typically FDG-avid, PET can detect immune-related adverse events, sometimes weeks before these become clinically apparent (Fig. 11) (Kwak et al. 2015). Although this is helpful since rapid initiation of systemic therapy (e.g., systemic corticosteroids) can improve patient outcome, it can make the disease response difficult to assess.

Clinical and imaging response to immunotherapy is variable. Often an early response is seen. Inflammatory reactions can occur at tumor sites within days of therapy (Reusch et al. 2006). In some cases a response can be delayed for weeks or months (Le et al. 2013). Further, tumor flare cannot be distinguished from progression based on morphologic, imaging or even on FDG PET/CT. It is estimated that approximately 15% of patients with melanoma on ipilimumab show increasing disease burden on imaging despite clinical benefit (e.g., pseudoprogression or flare), although this is lower (less than 3%) with other agents (Wolchok et al. 2009). In a small number of cases, immunotherapy can provoke rapid disease progression or *hyperprogression* (Champiat et al. 2017; Saâda-Bouzid et al. 2017). As such it is key to correlate imaging findings with the patient's clinical condition: (1) those patients with improving or stable clinical condition and progression on imaging may be experiencing pseudoprogression and, in this case, treatment may be continued with response confirmed by follow-up imaging; (2) those patients who are deteriorating are most likely progressing and discontinuing therapy may be warranted since waiting for imaging confirmation could lead to deterioration rendering a new therapy nonviable.

Recently, two new molecular and functional imaging response assessment criteria have been proposed in the setting of immunotherapy: (1) PET/CT Criteria for Early Prediction of Response to Immune Checkpoint Inhibitor Therapy (PECRIT) (Cho et al. 2017) and (2) PET Response Evaluation Criteria for Immunotherapy (PERCIMT) (Anwar et al. 2018; Sachpekidis et al. 2018). In both cases, the evaluation of clinical benefit is incorporated as well as the use of morphologic and functional metrics (Table 1). Currently, it is suggested that a baseline PET be performed prior to immunotherapy with follow-up 8–9 weeks or more after immunotherapy initiation (typically after 2 or 3 cycles of therapy) and at therapy completion. It is thought that the value of FDG PET is most pronounced in patients with limited morphological response on anatomic imaging, or who develop signs/ symptoms of immune-related adverse events. Further, clinical benefit and the presence of a metabolic response despite morphologic progression can be helpful for clinical decision-making.

Functional and molecular response assessment imaging in oncologic patients receiving immunotherapy remains imperfect, and research into more specific imaging biomarkers is ongoing, including clinical trials using ^{89}Zr-labeled immune checkpoint inhibitors as well as investigation into the use of radiolabeled antibody fragments.

8 Conclusion

We have come a long way from the crude manual disease assessment of yesterday to the standardized staging and response assessment criteria of today. Further, as our technology improves, so too does the possibility of more advanced imaging assessment including complex structural and functional data acquisition with parametric mapping and kinetic modeling allowing evaluation of tumor heterogeneity throughout the body. Also, the recent proliferation of hybrid scanners that include anatomic, functional, and molecular imaging capabilities has enhanced our ability to assess disease response, adjust therapy regimens, and develop an accurate measure of patient prognosis. It has been recognized that standardization of image acquisition and analysis parameters as well as harmonization of criteria used for response assessment across the clinical and research landscape is important. As our understanding of the biological effects of therapeutic interventions improves, so too does our understanding of the best time-points for therapy response assessment. Although further studies are necessary we are starting to converge on a universal system, particularly in certain tumors such as lymphoma.

References

Ady N, Zucker JM, Asselain B et al (1995) A new ^{123}I-MIBG whole body scan scoring method-application to the prediction of the response of metastases to induction chemotherapy in stage IV neuroblastoma. Eur J Cancer 31A(2):256–261

Aide N, Hicks RJ, Le Tourneau C, Lheureux S, Fanti S, Lopci E (2018) FDG PET/CT for assessing tumour response to immunotherapy—report on the EANM symposium n immune modulation nd recent review of the literature. Eur J Nucl Med Mol Imaging 46:238–250

Aisner J, Wiernik PH (1982) Restaging laparotomy in the management of the non-Hodgkin lymphomas. Med Pediatr Oncol 10:429–438

André MPE, Girinsky T, Federico M et al (2017) Early positron emission tomography response-adapted treatment in stage I and II Hodgkin lymphoma: final results of the randomized EORTC/LYSA/FIL H10 trial. J Clin Oncol 35:1786–1794

Anwar H, Sachpekidis C, Winkler J et al (2018) Absolute number of new lesions on ^{18}F-FDG PET/CT is more predictive of clinical response than SUV changes in metastatic melanoma patients receiving ipilimumab. Eur J Nucl Med Mol Imaging 45:376–383

Barrett JA, Coleman RE, Goldsmith SJ et al (2013) First-in-man evaluation of 2 high-affinity PSMA-avid small molecules for imaging prostate cancer. J Nucl Med 54:380–387

Barrington SF, Qian W, Somer EJ et al (2010) Concordance between four European centres of PET reporting criteria designed for use in multicentre trials in Hodgkin lymphoma. Eur J Nucl Med Mol Imaging 37:1824–1833

Barrington SF, Mikhaeel NG, Kostakoglu L et al (2014) Role of imaging in the staging and response assessment of lymphoma: consensus of the international conference on malignant lymphomas imaging working group. J Clin Oncol 32:3048–3058

Beauregard JM, Hodman MS, Kong GK et al (2012) The tumor sink effect on the biodistribution of ^{68}Ga-DOTA-octreotate: implications for peptide receptor radionuclide therapy. Eur J Nucl Med Mol Imaging 39:50–56

Benz MR, Herrmann K, Walter F et al (2011) ^{18}F-FDG PET/CT for monitoring treatment responses to the epidermal growth factor receptor inhibitor erlotinib. J Nucl Med 52(11):1684–1689

Boellaard R, Delgado-Bolton R, Oyen WJG et al (2015) FDG PET/CT: EANM procedure guidelines for tumour imaging: version 2.0. Eur J Nucl Med Mol Imaging 42:328–354

Bouchelouche K, Choyke PL, Capala J (2010) Prostate specific membrane antigen—a target for imaging and therapy with radionuclides. Discov Med 9:55–61

Canellos G (1988) Residual mass in lymphoma may not be residual disease. J Clin Oncol 6:931–933

Champiat S, Dercle L, Ammari S et al (2017) Hyperprogressive disease is a new pattern of progression in cancer patients treated by anti-PD-1/PD-L1. Clin Cancer Res 23:1920–1928

Cheson BD, Fisher RI, Barrington SF et al (2014) Recommendations for initial evaluation, staging, and response assessment of Hodgkin and non-Hodgkin lymphoma: the Lugano classification. J Clin Oncol 32:3059–3068

Cheson BD, Ansell S, Schwartz L et al (2016) Refinement of the Lugano classification lymphoma response criteria in the era of immunomodulatory therapy. Blood 128:2489–2496

Cho SY, Lipson EJ, Im HJ et al (2017) Prediction of response to immune checkpoint inhibitor therapy using early-time-point ^{18}F-FDG PET/CT imaging in patients with advanced melanoma. J Nucl Med 58:1421–1428

Coleman RE, Mashiter G, Whitaker KB, Moss DW, Rubens RD, Fogelman I (1988) Bone scan flare predicts successful systemic therapy for bone metastases. J Nucl Med 29:1354–1359

Cook GJR, Venkitaraman R, Sohaib AS (2011) The diagnostic utility of the flare phenomenon on bone scintigraphy in staging prostate cancer. Eur J Nucl Med Mol Imaging 38:7–13

Dennis ER, Jia X, Mezheritskiy IS et al (2012) Bone scan index: a quantitative treatment response biomarker for castration-resistant metastatic prostate cancer. J Clin Oncol 30:519–524

Eisenhauer EA, Therasse P, Bogaerts J et al (2009) New response evaluation criteria in solid tumours: revised RECIST guideline (version 1.1). Eur J Cancer 45:228–247

Emmett L, Crumbaker M, Ho B et al (2018) Metastatic castration-resistant prostate cancer including imaging predictors of treatment response and patterns of progression. Clin Genitourin Cancer. [Epub ahead of print]

Evans MJ, Smith-Jones PM, Wongvipat J et al (2011) Noninvasive measurement of androgen receptor signaling with positron emitting radiopharmaceutical that targets prostate-specific membrane antigen. Proc Natl Acad Sci U S A 108:9578–9582

Even-Sapir E, Metser U, Mishani E et al (2006) The detection of bone metastases in patients with high-risk prostate cancer: ^{99m}Tc-MDP Planar bone scintigraphy, single- and multi-field-of-view SPECT, ^{18}F-fluoride PET, and ^{18}F-fluoride PET/CT. J Nucl Med 47:287–297

Fendler W, Eiber M, Beheshti M et al (2017) ^{68}Ga-PSMA PET/CT: joint EANM and SNMMI procedure guideline for prostate cancer imaging: version 1.0. Eur J Nucl Med Mol Imaging 44:1014–1024

Furth C, Amthauer H, Hautzel H et al (2011) Evaluation of interim PET response criteria in paediatric Hodgkin's lymphoma—results for dedicated assessment criteria in a blinded dual-centre read. Ann Oncol 22:1198–1203

Gallamini A, Fiore F, Sorasio R, Meignan M (2009) Interim positron emission tomography scan in Hodgkin lymphoma: definitions, interpretation rules, and clinical validation. Leuk Lymphoma 50:1761–1764

Gallamini A, Barrington SF, Biggi A et al (2014) The predictive role of interim positron emission tomography for Hodgkin lymphoma treatment outcome is confirmed using the interpretation criteria of the Deauville five-point scale. Haematologica 99:1107–1113

Gerbaudo VH, Garcia CA (2016) PET/CT of lung cancer. Springer, Cham

van Gool MH, Aukema TS, Schaake EE et al (2014a) NEL Study Group. Timing of metabolic response monitoring during erlotinib treatment in non-small cell lung cancer. J Nucl Med 55(7):1081–1086

van Gool MH, Aukema TS, Schaake EE et al (2014b) ^{18}F-fluorodeoxyglucose positron emission tomography versus computed tomography in predicting histopathological response to epidermal growth factor receptor-tyrosine kinase inhibitor treatment in resectable non-small cell lung cancer. Ann Surg Oncol 21(9):2831–2837

Grant FD, Fahey FH, Packard AB et al (2008) Skeletal PET with ^{18}F-fluoride: applying a new technology to an old tracer. J Nucl Med 49:68–78

Hachemi M, Couturier O, Vervueren L et al (2014) [^{18}F] FDG positron emission tomography within two weeks of starting erlotinib therapy can predict response in non-small cell lung cancer patients. PLoS One 9(2):e87629

Hicks RJ, Mac Manus MP, Matthews JP et al (2004) Early FDG-PET imaging after radical radiotherapy for non-small-cell lung cancer: inflammatory changes in normal tissues correlate with tumor response and do not confound therapeutic response evaluation. Int J Radiat Oncol Biol Phys 60(2):412–418

Hodi FS, O'Day SJ, McDermott DF et al (2010) Improved survival with ipilimumab in patients with metastatic melanoma. N Engl J Med 363:711–723

Hoekstra CJ, Stroobants SG, Smit EF et al (2005) Prognostic relevance of response evaluation using [^{18}F]-2-fluoro-2-deoxy-D-glucose positron emission tomography in patients with locally advanced non-small-cell lung cancer. J Clin Oncol 23(33): 8362–8370

Koerber SA, Will L, Kratochwil C et al (2018) ^{68}Ga-PSMA-11 PET/CT in Primary and recurrent prostate carcinoma: implications for radiotherapeutic management in 121 patients. J Nucl Med [Epub ahead of print]

Kostakoglu L, Schöder H, Johnson JL et al (2012) Interim FDG PET imaging in stage I–II non-bulky Hodgkin lymphoma: would using combined positron emission tomography and computed tomography criteria better predict response than each test alone? Leuk Lymphoma 53:2143–2150

Kwak JJ, Tirumani SH, Van den Abbeele AD, Koo PJ, Jacene HA (2015) Cancer immunotherapy: imaging assessment of novel treatment response patterns and immune-related adverse events. Radiographics 35:424–437

Larkin J, Hodi FS, Wolchok JD (2015) Combined nivolumab and ipilimumab or monotherapy in untreated melanoma. N Engl J Med 373:1270–1271

Lasnon C, Desmonts C, Quak E et al (2013) Harmonizing SUVs in multicentre trials when using different generation PET systems: prospective validation in non-small cell lung cancer patients. Eur J Nucl Med Mol Imaging 40:985–996

Lasnon C, Quak E, Le Roux PY et al (2017) EORTC response criteria are more influenced by reconstruction inconsistencies than PERCIST but both benefit from the EARL harmonization program. EJNMMI Phys 4:17

Le Roux P-Y, Gastinne T, Le Gouill S et al (2011) Prognostic value of interim FDG PET/CT in Hodgkin's lymphoma patients treated with interim response-adapted strategy: comparison of International Harmonization Project (IHP), Gallamini and London criteria. Eur J Nucl Med Mol Imaging 38:1064–1071

Le DT, Lutz E, Uram JN et al (2013) Evaluation of ipilimumab in combination with allogeneic pancreatic tumor cells transfected with a GM-CSF gene in previously treated pancreatic cancer. J Immunother 36:382–389

Lewis E, Bernardino ME, Salvador PG, Cabanillas FF, Barnes PA, Thomas JL (1982) Post-therapy CT-detected mass in lymphoma patients: is it viable tissue? J Comput Assist Tomogr 6:792–795

Lin C, Itti E, Haioun C et al (2007) Early ^{18}F-FDG PET for prediction of prognosis in patients with diffuse large B-cell lymphoma: SUV-based assessment versus visual analysis. J Nucl Med 48:1626–1632

Mac Manus MP, Hicks RJ, Matthews JP, Wirth A, Rischin D, Ball DL (2005) Metabolic (FDG-PET) response after radical radiotherapy/chemoradiotherapy for non-small cell lung cancer correlates with patterns of failure. Lung Cancer 49(1):95–108

Meignan M, Gallamini A, Meignan M, Gallamini A, Haioun C (2009) Report on the first international workshop on interim-PET scan in lymphoma. Leuk Lymphoma 50:1257–1260

Meignan M, Gallamini A, Haioun C, Polliack A (2010) Report on the Second International Workshop on interim positron emission tomography in lymphoma held in Menton, France, 8–9 April 2010. Leuk Lymphoma 51:2171–2180

Meignan M, Gallamini A, Itti E, Barrington S, Haioun C, Polliack A (2012) Report on the third international workshop on interim positron emission tomography in lymphoma held in Menton, France, 26-27 September 2011 and Menton 2011 consensus. Leuk Lymphoma 53:1876–1881

Mikhaeel N, Timothy A, Hain S, O'Doherty M (2000) 18-FDG-PET for the assessment of residual masses on CT following treatment of lymphomas. Ann Oncol 11:S147–S150

Moghbel MC, Mittra E, Gallamini A et al (2017) Response assessment criteria and their applications in lymphoma: Part 2. J Nucl Med 58(1):13–22

Orlandi E, Lazzarino M, Brusamolino E et al (1990) Residual mediastinal widening following therapy in Hodgkin's disease. Hematol Oncol 8:125–131

Pollen JJ, Witztum KF, Ashburn WL (1984) The flare phenomenon on radionuclide bone scan in metastatic prostate cancer. AJR Am J Roentgenol 142: 773–776

Popovic A, Jaffee EM, Zaidi N (2018) Emerging strategies for combination checkpoint modulators in cancer immunotherapy. J Clin Invest 128:3209–3218

Quak E, Le Roux PY, Lasnon C et al (2016) Does PET SUV harmonization affect PERCIST response classification? J Nucl Med 57:1699–1706

Reske S (2003) PET and restaging of malignant lymphoma including residual masses and relapse. Eur J Nucl Med Mol Imaging 30(Suppl 1):S89–S96

Reusch U, Sundaram M, Davol PA et al (2006) Anti-CD3 × anti-epidermal growth factor receptor (EGFR) bispecific antibody redirects T-cell cytolytic activity to EGFR-positive cancers in vitro and in an animal model. Clin Cancer Res 12:183–190

Rowe SP, Macura KJ, Blackford AL et al (2016) PSMA-based [^{18}F]DCFPyL PET/CT is superior to conventional imaging for lesion detection in patients wit metastatic prostate cancer. Mol Imaging Biol 18(3):411–419

Saâda-Bouzid E, Defaucheux C, Karabajakian A et al (2017) Hyperprogression during anti-PD-1/PD-L1 therapy in patients with recurrent and/or metastatic head and neck squamous cell carcinoma. Ann Oncol 28:1605–1611

Sachpekidis C, Anwar H, Winkler J et al (2018) The role of interim ^{18}F-FDG PET/CT in prediction of response to ipilimumab treatment in metastatic melanoma. Eur J Nucl Med Mol Imaging 45:1289–1296

Scher HI, Morris MJ, Stadler WM et al (2016) Trial design and objectives for castration-resistant prostate cancer: updated recommendations from the prostate cancer clinical trials working group 3. J Clin Oncol 34:1402–1418

Schwarz SW, Decristoforo C, Goodbody AE et al (2019) Harmonization of United States, European Union and Canadian first-in-human regulatory requirements for radiopharmaceuticals—is this possible? J Nucl Med [Epub ahead of print]

Sunaga N, Oriuchi N, Kaira K et al (2008) Usefulness of FDG-PET for early prediction of the response to gefitinib in non-small cell lung cancer. Lung Cancer 59(2):203–210

Surbone A, Longo DL, DeVita V et al (1988) Residual abdominal masses in aggressive non-Hodgkin's lymphoma after combination chemotherapy: significance and management. J Clin Oncol 6:1832–1837

Takahashi R, Hirata H, Tachibana I et al (2012) Early [^{18}F] fluorodeoxyglucose positron emission tomography at two days of gefitinib treatment predicts clinical outcome in patients with adenocarcinoma of the lung. Clin Cancer Res 18(1):220–228

Vansteenkiste J, Fischer BM, Dooms C, Mortensen J (2004) Positron-emission tomography in prognostic and therapeutic assessment of lung cancer: systematic review. Lancet Oncol 5:531–540

Wahl RL, Jacene H, Kasamon Y, Lodge MA (2009) From RECIST to PERCIST: evolving considerations for PET response criteria in solid tumors. J Nucl Med 50(Suppl 1):122S–150S

Warburg O (1956) On respiratory impairment in cancer cells. Science 124(3215):269–270

Warburg O, Wind F, Negelein E (1927) The metabolism of tumours in the body. J Gen Physiol 8(6):519–530

Weber WA, Petersen V, Schmidt B et al (2003) Positron emission tomography in non-small-cell lung cancer: prediction of response to chemotherapy by quantitative assessment of glucose use. J Clin Oncol 21:2651–2657

Wolchok JD, Hoos A, O'Day S et al (2009) Guidelines for the evaluation of immune therapy activity in solid tumors: immune-related response criteria. Clin Cancer Res 15:7412–7420

Young H, Baum R, Cremerius U et al (1999) Measurement of clinical and subclinical tumour response using [^{18}F]-fluorodeoxyglucose and positron emission tomography: review and 1999 EORTC recommendations. European Organization for Research and Treatment of Cancer (EORTC) PET Study Group. Eur J Cancer 35:1773–1782

Zacho HD, Petersen LJ (2018) Bone flare to androgen deprivation therapy in metastatic, hormone-sensitive prostate cancer on ^{68}Ga-prostate-specific membrane antigen PET/CT. Clin Nucl Med 43(11): e404–e406

Ziai P, Hayeri MR, Salei A et al (2016) Role of optimal quantification of FDG PET imaging in the clinical practice of radiology. Radiographics 36:481–496

Zukotynski KA, Valliant J, Benard F et al (2018) Flare on serial prostate-specific membrane antigen-targeted 18F-DCFPyL PET/CT examinations in castration-resistant prostate cancer: first observations. Clin Nucl Med 43(3):213–216